XENOPUS MODELS OF ORGANOGENESIS AND DISEASE

EDITED BY: John Noel Griffin, Emily Sempou and Karen Liu
PUBLISHED IN: Frontiers in Physiology

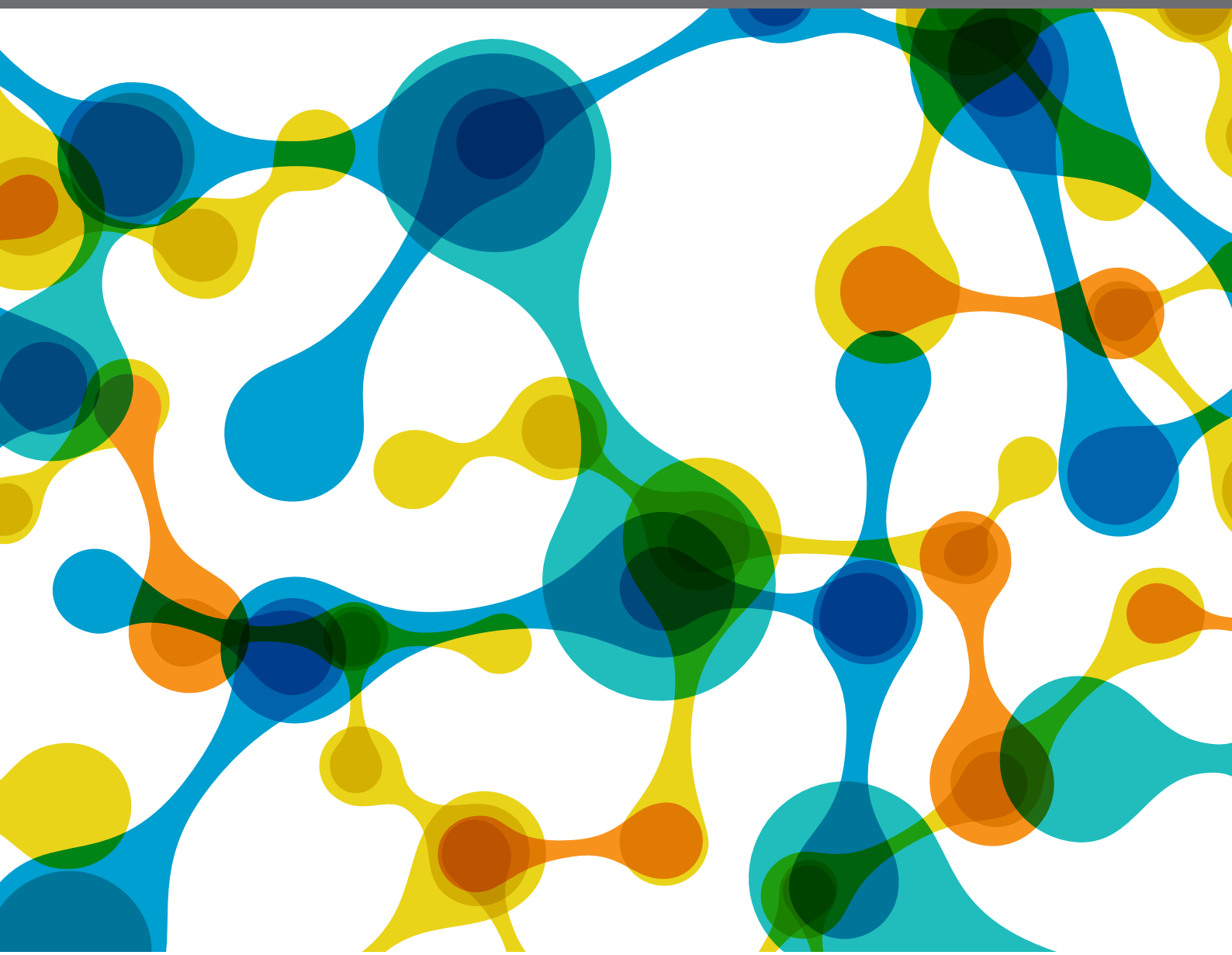

frontiers Research Topics

frontiers

ISSN 1664-8714
ISBN 978-2-88963-844-4
DOI 10.3389/978-2-88963-844-4

About Frontiers

Frontiers is more than just an open-access publisher of scholarly articles: it is a pioneering approach to the world of academia, radically improving the way scholarly research is managed. The grand vision of Frontiers is a world where all people have an equal opportunity to seek, share and generate knowledge. Frontiers provides immediate and permanent online open access to all its publications, but this alone is not enough to realize our grand goals.

Frontiers Journal Series

The Frontiers Journal Series is a multi-tier and interdisciplinary set of open-access, online journals, promising a paradigm shift from the current review, selection and dissemination processes in academic publishing. All Frontiers journals are driven by researchers for researchers; therefore, they constitute a service to the scholarly community. At the same time, the Frontiers Journal Series operates on a revolutionary invention, the tiered publishing system, initially addressing specific communities of scholars, and gradually climbing up to broader public understanding, thus serving the interests of the lay society, too.

Dedication to Quality

Each Frontiers article is a landmark of the highest quality, thanks to genuinely collaborative interactions between authors and review editors, who include some of the world's best academicians. Research must be certified by peers before entering a stream of knowledge that may eventually reach the public - and shape society; therefore, Frontiers only applies the most rigorous and unbiased reviews.
Frontiers revolutionizes research publishing by freely delivering the most outstanding research, evaluated with no bias from both the academic and social point of view. By applying the most advanced information technologies, Frontiers is catapulting scholarly publishing into a new generation.

What are Frontiers Research Topics?

Frontiers Research Topics are very popular trademarks of the Frontiers Journals Series: they are collections of at least ten articles, all centered on a particular subject. With their unique mix of varied contributions from Original Research to Review Articles, Frontiers Research Topics unify the most influential researchers, the latest key findings and historical advances in a hot research area! Find out more on how to host your own Frontiers Research Topic or contribute to one as an author by contacting the Frontiers Editorial Office: researchtopics@frontiersin.org

XENOPUS MODELS OF ORGANOGENESIS AND DISEASE

Topic Editors:
John Noel Griffin, University of East Anglia, United Kingdom
Emily Sempou, Yale University, United States
Karen Liu, King's College London, United Kingdom

Citation: Griffin, J. N., Sempou, E., Liu, K., eds. (2020). Xenopus Models of Organogenesis and Disease. Lausanne: Frontiers Media SA.
doi: 10.3389/978-2-88963-844-4

Table of Contents

05 ***Editorial:* Xenopus *Models of Organogenesis and Disease***
John N. Griffin, Karen J. Liu and Emily Sempou

08 **Xenopus *Models of Cancer: Expanding the Oncologist's Toolbox***
Laura J. A. Hardwick and Anna Philpott

15 ***Candidate Heterotaxy Gene FGFR4 is Essential for Patterning of the Left-Right Organizer in Xenopus***
Emily Sempou, Osaamah Ali Lakhani, Sarah Amalraj and Mustafa K. Khokha

24 **Xenopus *Hybrids Provide Insight Into Cell and Organism Size Control***
Romain Gibeaux, Kelly Miller, Rachael Acker, Taejoon Kwon and Rebecca Heald

35 **Xenopus tropicalis*: Joining the Armada in the Fight Against Blood Cancer***
Dionysia Dimitrakopoulou, Dieter Tulkens, Pieter Van Vlierberghe and Kris Vleminckx

44 ***Corrigendum: Xenopus tropicalis: Joining the Armada in the Fight Against Blood Cancer***
Dionysia Dimitrakopoulou, Dieter Tulkens, Pieter Van Vlierberghe and Kris Vleminckx

45 ***More Than Just a Bandage: Closing the Gap Between Injury and Appendage Regeneration***
Anneke D. Kakebeen and Andrea E. Wills

56 ***The Frog* Xenopus *as a Model to Study Joubert Syndrome: The Case of a Human Patient With Compound Heterozygous Variants in* PIBF1**
Tim Ott, Lilian Kaufmann, Martin Granzow, Katrin Hinderhofer, Claus R. Bartram, Susanne Theiß, Angelika Seitz, Nagarajan Paramasivam, Angela Schulz, Ute Moog, Martin Blum and Christina M. Evers

69 ***Dynamin Binding Protein is Required for* Xenopus laevis *Kidney Development***
Bridget D. DeLay, Tanya A. Baldwin and Rachel K. Miller

83 ***Xenbase: Facilitating the Use of* Xenopus *to Model Human Disease***
Mardi J. Nenni, Malcolm E. Fisher, Christina James-Zorn, Troy J. Pells, Virgilio Ponferrada, Stanley Chu, Joshua D. Fortriede, Kevin A. Burns, Ying Wang, Vaneet S. Lotay, Dong Zhou Wang, Erik Segerdell, Praneet Chaturvedi, Kamran Karimi, Peter D. Vize and Aaron M. Zorn

96 ***Liver Specification in the Absence of Cardiac Differentiation Revealed by Differential Sensitivity to Wnt/β Catenin Pathway Activation***
Kim Haworth, Lee Samuel, Sarah Black, Pavel Kirilenko and Branko Latinkic

106 ***A YWHAZ Variant Associated With Cardiofaciocutaneous Syndrome Activates the RAF-ERK Pathway***
Ivan K. Popov, Susan M. Hiatt, Sandra Whalen, Boris Keren, Claudia Ruivenkamp, Arie van Haeringen, Mei-Jan Chen, Gregory M. Cooper, Bruce R. Korf and Chenbei Chang

119 ***Wolf-Hirschhorn Syndrome-Associated Genes are Enriched in Motile Neural Crest Cells and Affect Craniofacial Development in* Xenopus laevis**
Alexandra Mills, Elizabeth Bearce, Rachael Cella, Seung Woo Kim, Megan Selig, Sangmook Lee and Laura Anne Lowery

135 **Xenopus** ***Resources: Transgenic, Inbred and Mutant Animals, Training Opportunities, and Web-Based Support***
Marko Horb, Marcin Wlizla, Anita Abu-Daya, Sean McNamara, Dominika Gajdasik, Takeshi Igawa, Atsushi Suzuki, Hajime Ogino, Anna Noble, Centre de Ressource Biologique Xenope Team in France, Jacques Robert, Christina James-Zorn and Matthew Guille

145 ***Cdc42 Effector Protein 3 Interacts With Cdc42 in Regulating Xenopus Somite Segmentation***
Mary Kho, Hongyu Shi and Shuyi Nie

154 ***Using the*** **Xenopus** ***Developmental Eye Regrowth System to Distinguish the Role of Developmental Versus Regenerative Mechanisms***
Cindy X. Kha, Dylan J. Guerin and Kelly Ai-Sun Tseng

169 ***The Many Faces of Xenopus: Xenopus laevis as a Model System to Study Wolf–Hirschhorn Syndrome***
Micaela Lasser, Benjamin Pratt, Connor Monahan, Seung Woo Kim and Laura Anne Lowery

181 **Xenopus*: Driving the Discovery of Novel Genes in Patient Disease and Their Underlying Pathological Mechanisms Relevant for Organogenesis***
Woong Y. Hwang, Jonathan Marquez and Mustafa K. Khokha

188 ***Quantitative Phenotyping of*** **Xenopus** ***Embryonic Heart Pathophysiology Using Hemoglobin Contrast Subtraction Angiography to Screen Human Cardiomyopathies***
Engin Deniz, Stephan Jonas, Mustafa K. Khokha and Michael A. Choma

197 ***Modeling Bainbridge-Ropers Syndrome in*** **Xenopus laevis** ***Embryos***
Hava Lichtig, Artyom Artamonov, Hanna Polevoy, Christine D. Reid, Stephanie L. Bielas and Dale Frank

frontiers in Physiology

EDITORIAL
published: 29 May 2020
doi: 10.3389/fphys.2020.00534

Editorial: *Xenopus* Models of Organogenesis and Disease

John N. Griffin[1]*, *Karen J. Liu*[2]* and *Emily Sempou*[3]*

[1] School of Biological Sciences, University of East Anglia, Norwich, United Kingdom, [2] Centre for Craniofacial and Regenerative Biology, King's College London, London, United Kingdom, [3] Pediatric Genomics Discovery Program, Departments of Pediatrics and Genetics, Yale University School of Medicine, New Haven, CT, United States

Keywords: *Xenopus*, development, organogenesis, disease model, oncology, patterning, regeneration

Editorial on the Research Topic

Xenopus Models of Organogenesis and Disease

We have long extrapolated from animal models to better understand our own biology and health. Amongst such models, amphibia, and in particular *Xenopus*, have emerged as a powerhouse of biological discovery, providing startling insights into fundamental processes in embryology, cell biology, genetics, physiology, toxicology, evolution, ecology, and disease. Indeed, research in amphibians has consistently thrown open new fields of discovery, a fact reflected in contributions to numerous Nobel prizes in Physiology or Medicine, beginning with August (Lindstedt, 2014) prize for discovery of capillary motor-regulating mechanism and most recently with John Gurdon's 2012 award for reprogramming mature cells to pluripotency (Krogh, 1919; Gurdon et al., 1958; Gurdon and Hopwood, 2000; Burggren and Warburton, 2007; Blum and Ott, 2018). Over the last 70 years, *Xenopus* has emerged as the predominant amphibian model and one of most widely used model systems globally, making a tremendous impact on biological research.

Native to south and central Africa, *Xenopus laevis* initially expanded into European and North American laboratories in the 1930's and 40's as the leading pregnancy test of the time; one injection of human urine containing gonadotrophic hormone is sufficient to induce egg laying within hours (Gurdon and Hopwood, 2000). However, this ability to produce thousands of eggs and externally developing embryos on demand year-round by simple hormone injection gave *Xenopus* a distinct advantage over other available experimental models. This, combined with its large oocytes and embryos that are well-suited to biochemical, cell biological and embryological manipulations, its ease of genomic manipulation, its relative evolutionary proximity to humans, low maintenance, short life cycle, and low cost, continue to make *Xenopus* an exceptionally valuable model. In the past two decades, the establishment of *X. tropicalis*, a diploid species, as a laboratory model has added additional powerful genetic tools (Grainger, 2012; Tandon et al., 2017). Together, *X. laevis* and *X. tropicalis* allow us to rapidly investigate fundamental biological processes both *in vivo* and *ex vivo*. This makes *Xenopus* an ideal system in the genomic era, where we are in need of efficient models suitable for testing human disease gene function.

The purpose of this Research Topic is to highlight the outstanding versatility and utility of *Xenopus* as a model system in which to investigate human development, disease, and pathology. It comprises 18 primary research and review articles exploring a diverse array of topics, including development, regeneration, cancer, biological scaling, and human disease modeling, as well as providing an overview of the extensive resources available to support *Xenopus* research. It is our hope that it will be a resource both for established *Xenopus* researchers, and *Xenopus* newcomers looking to identify the appropriate model system and approach for their research.

OPEN ACCESS

Edited and reviewed by:
Martin Blum,
University of Hohenheim, Germany

***Correspondence:**
John N. Griffin
john.griffin@uea.ac.uk
Karen J. Liu
karen.liu@kcl.ac.uk
Emily Sempou
emily.sempou@yale.edu

Specialty section:
This article was submitted to Embryonic and Developmental Physiology, a section of the journal Frontiers in Physiology

Received: *13 March 2020*
Accepted: *30 April 2020*
Published: *29 May 2020*

Citation:
Griffin JN, Liu KJ and Sempou E (2020) Editorial: Xenopus Models of Organogenesis and Disease. Front. Physiol. 11:534. doi: 10.3389/fphys.2020.00534

Several articles in this Research Topic illustrate the power of *Xenopus* in modeling and investigating a broad variety of inherited human diseases. For example, Mills et al. investigate the genetic and developmental causes of Wolf-Hirschhorn Syndrome (WHS), a multigenic disorder that results in characteristic facial abnormalities. In particular, they determine requirements for four distinct WHS candidate genes during cranial neural crest migration and facial morphogenesis. Depletion of these genes in frog can disrupt facial morphogenesis, recapitulating much of the patient phenotype. Importantly, this work demonstrates the relative ease with which complex multigenic syndromes can be dissected in *Xenopus*. Expanding upon this point, Lasser et al. contribute a complementary review of WHS and discuss how *Xenopus* might be exploited to further investigate the ontogeny of this and other multigenic conditions. Ott et al. identify and functionally analyze novel compound heterozygous variants of *PIBF1* that were identified in a Joubert syndrome patient. Importantly, they discover that these disease variants affect cilia function and discuss their likely contribution to the disease. In other examples, Sempou et al. report an unexpected role for the heterotaxy candidate gene, *Fgfr4*, in gastrulation and development of the left—right body axis, providing insight into the origin of the patient phenotype, while Popov et al. use *Xenopus laevis* to determine the functional consequence of a candidate disease variant in *YWHAZ*, and investigate the molecular mechanisms underlying its contribution to the RASopathy, Cardiofaciocutaneous syndrome. Lichtig et al. develop a *Xenopus* model of Bainbridge-Ropers syndrome and reveal that depletion of the *asxl3* disease gene perturbs early neural development. In doing so they produce a powerful tool for further investigation of the condition. Finally, Hwang et al. review recent methodological advances that allow organ specific phenotypic investigations in *Xenopus* and discuss their utility in modeling genetic disease. Together, these articles add a wealth of knowledge to our understanding of congenital disease.

Technological advances are rapidly augmenting the *Xenopus* experimental repertoire and opening innovative new avenues of investigation. This is strongly evident in the field of oncology, where the marriage of classical *Xenopus* attributes and modern gene editing tools is creating efficacious new experimental platforms. In this Research Topic, Hardwick and Philpott review *Xenopus*' many contributions to our knowledge of tumor biology and discuss how genome editing technologies are revolutionizing its utility in oncology research. In addition, Dimitrakopoulou et al. highlight the untapped potential of *Xenopus* as an emerging system in which to study hematologic malignancies, and outline their experimental pipeline for generating leukemia models in *Xenopus* using CRISPR/Cas9. Deniz et al. provide another example of technological application, by demonstrating the power of hemoglobin contrast subtraction angiography as a non-destructive and efficient method to quantify cardiac function, a technique that greatly facilitates high throughput investigation of candidate congenital heart disease genes.

Several articles showcase *Xenopus*' unrivaled power for studying fundamental processes in early vertebrate development and organogenesis. For example, despite being an integral biological process, we have little understanding of how size and scaling are controlled at the cell and organism levels. Gibeaux et al. exploit the size difference between the *Xenopus* species, and the ability to generate viable intermediately sized hybrids, to investigate this mystery. Based on their findings, they propose a model whereby cell and organism size are regulated through a combination of genome size and transcriptional regulation in *Xenopus*. Haworth et al. use the ease with which embryonic tissue can be isolated and manipulated in *Xenopus* to create *ex vivo* models of cardiac and liver induction, and use these systems to explore the differential requirements for Wnt, FGF, and BMP signaling in liver formation, information critical to the refinement of protocols for liver cell differentiation from pluripotent stem cells. DeLay et al. advance our understanding of kidney development by demonstrating that the CDC42-GEF, dynamin binding protein (Dnmbp/Tuba), is essential for pronephric patterning and nephrogenesis in *Xenopus*, while Kho et al. reveal that CEP3 regulates the coordinated cell shape changes and movements required in somite segmentation.

The regenerative abilities of amphibians have long captivated biologists and inspired hope that these healing mechanisms could be applied to human injuries. While *Xenopus* tadpoles can readily regenerate damaged tissues, this ability is lost during metamorphosis, making them an ideal system for studying both the mechanisms that promote and prevent regeneration. Furthermore, as developmental processes have been extensively studied in *Xenopus*, it is an ideal model in which to examine regeneration. In this collection, Kha et al., take advantage of *Xenopus* tadpoles' ability to regrow a functional and morphologically normal eye, to investigate how similarly developmental processes are employed during embryogenesis and regrowth following injury, while Kakebeen and Wills review the biophysical, biochemical, and epigenetic processes that underlie regeneration.

Xenopus research is supported by powerful resources, including Xenbase, an extensive online bioinformatics and research database. Three *Xenopus* resource centers also exist to support and encourage research in *Xenopus*. In this collection, Horb et al. provide an overview of these centralized resources and the support available to both specialist and non-specialist researchers, including the availability of transgenic, inbread, and mutant animals, molecular resources, training, and experimental support. Nenni et al. add a complimentary description of advancements in Xenbase, highlighting its application to the study of disease. They also report a very fitting meta-analysis of *Xenopus* research which provides a fascinating snapshot of the breath of human diseases being investigated using *Xenopus* and the diverse experimental approaches taken by the community to understand them.

We hope that this collection of articles will be of interest to the storied *Xenopus* community as well as to clinicians and investigators working in the broader field of developmental biology and disease research.

AUTHOR CONTRIBUTIONS

All authors listed have made a substantial, direct and intellectual contribution to the work, and approved it for publication.

ACKNOWLEDGMENTS

We are very grateful to the many authors and reviewers who contributed to this collection.

REFERENCES

Blum, M., and Ott, T. (2018). Xenopus: an undervalued model organism to study and model human genetic disease. *Cells Tissues Organs* 205, 303–313. doi: 10.1159/000490898

Burggren, W. W., and Warburton, S. (2007). Amphibians as animal models for laboratory research in physiology. *ILAR J.* 48, 260–269. doi: 10.1093/ilar.48.3.260

Grainger, R. M. (2012). *Xenopus tropicalis* as a model organism for genetics and genomics: past, present, and future. *Methods Mol. Biol.* 917, 3–15. doi: 10.1007/978-1-61779-992-1_1

Gurdon, J. B., Elsdale, T. R., and Fischberg, M. (1958). Sexually mature individuals of *Xenopus laevis* from the transplantation of single somatic nuclei. *Nature* 182, 64–65. doi: 10.1038/182064a0

Gurdon, J. B., and Hopwood, N. (2000). The introduction of *Xenopus laevis* into developmental biology: of empire, pregnancy testing and ribosomal genes. *Int. J. Dev. Biol.* 44, 43–50. Available online at: http://www.ijdb.ehu.es/web/paper.php?doi=10761846

Krogh, A. (1919). The supply of oxygen to the tissues and the regulation of the capillary circulation. *J. Physiol.* 52, 457–474.

Lindstedt, S. (2014). Krogh 1929 or 'The Krogh Principle'. *J. Exp. Biol.* 217, 1640–1641. doi: 10.1242/jeb.095505

Tandon, P., Conlon, F., Furlow, J. D., and Horb, M. E. (2017). Expanding the genetic toolkit in *Xenopus*: approaches and opportunities for human disease modeling. *Dev. Biol.* 426, 325–335. doi: 10.1016/j.ydbio.2016.04.009

Conflict of Interest: The authors declare that the research was conducted in the absence of any commercial or financial relationships that could be construed as a potential conflict of interest.

frontiers in Physiology

MINI REVIEW
published: 27 November 2018
doi: 10.3389/fphys.2018.01660

Xenopus Models of Cancer: Expanding the Oncologist's Toolbox

Laura J. A. Hardwick[1,2,3] *and Anna Philpott*[1,2]*

[1] Philpott Lab, Hutchison/MRC Research Centre, Department of Oncology, University of Cambridge, Cambridge, United Kingdom, [2] Wellcome MRC Stem Cell Institute, University of Cambridge, Cambridge, United Kingdom, [3] Peterhouse, University of Cambridge, Cambridge, United Kingdom

The use of the *Xenopus* model system has provided diverse contributions to cancer research, not least because of the striking parallels between tumour pathogenesis and early embryo development. Cell cycle regulation, signalling pathways, and cell behaviours such as migration are frequently perturbed in cancers; all have been investigated using *Xenopus*, and these developmental events can additionally act as an assay for drug development studies. In this mini-review, we focus our discussion primarily on whole embryo *Xenopus* models informing cancer biology; the contributions to date and future potential. Insights into tumour immunity, oncogene function, and visualisation of vascular responses during tumour formation have all been achieved with naturally occurring tumours and induced-tumour-like-structures in *Xenopus*. Finally, as we are now entering the era of genetically modified *Xenopus* models, we can harness genome editing techniques to recapitulate human disease through creating embryos with analogous genetic abnormalities. With the speed, versatility and accessibility that epitomise the *Xenopus* system, this new range of pre-clinical *Xenopus* models has great potential to advance our mechanistic understanding of oncogenesis and provide an early *in vivo* model for chemotherapeutic development.

Keywords: *Xenopus*, cancer, tumour, oncogene, transgenic

OPEN ACCESS

Edited by:
Karen Liu,
King's College London,
United Kingdom

Reviewed by:
Amy Katherine Sater,
University of Houston, United States
Jacques Robert,
University of Rochester, United States

***Correspondence:**
Anna Philpott
ap113@cam.ac.uk

Specialty section:
This article was submitted to Embryonic and Developmental Physiology, a section of the journal Frontiers in Physiology

Received: *12 September 2018*
Accepted: *02 November 2018*
Published: *27 November 2018*

Citation:
Hardwick LJA and Philpott A (2018) Xenopus Models of Cancer: Expanding the Oncologist's Toolbox. Front. Physiol. 9:1660. doi: 10.3389/fphys.2018.01660

INTRODUCTION

Cancer is a prominent cause of death worldwide and numbers of cases are predicted to increase as populations grow and age (Torre et al., 2016). Oncology research is also expanding in parallel and a wealth of discoveries have provided insight from a social level to intricate details of molecular pathogenesis. These advances would not be possible without the use of research models, but there is increasing pressure to reduce the use of mammalian animals in biomedical research, and there is still a gap for relevant translational models for high-throughput screening for therapeutic development (Naert et al., 2017). The articles in this special issue are testament to the versatility of the *Xenopus* system, and in keeping, the full repertoire of *in vitro* biochemistry, oocytes, explants, embryos, and adult frogs have all provided diverse contributions to cancer research, from understanding biological processes that are deranged in cancer to modelling using a new

age of genetically engineered transgenic animals. Here, we summarise the breadth of *Xenopus*' contribution to cancer research (see also Hardwick and Philpott, 2015), focusing our discussion on the development and application of whole embryos and adult *Xenopus* frogs as *in vivo* models informing cancer biology.

PARALLELS BETWEEN DEVELOPMENT AND DISEASE

The wide-ranging application of *Xenopus* to the field of oncology is built on the striking parallels between tumour pathogenesis and early embryo development. The "hallmarks of cancer" are now widely recognised as abnormal and tumorigenic properties (Hanahan and Weinberg, 2000, 2011), yet they often arise from inappropriate re-activation or de-regulation of normal physiological processes, many of which are instrumental to embryogenesis when precisely executed in space and time (Aiello and Stanger, 2016). Considerable literature now documents the similarities between early development and tumorigenesis in terms of gene expression, proteasome, signalling pathways, and cell behaviours (Ma et al., 2010). A greater understanding of the physiological processes in the embryo, both in terms of molecular components and regulatory mechanisms, may therefore give insight into tumour pathogenesis and potential therapeutic targets, as illustrated below.

To summarise the diverse application of the *Xenopus* system to cancer research, **Figure 1** illustrates contributions made to understanding each of the cancer hallmarks. This includes the use of *in vitro* extract systems, oocytes and developing *Xenopus* embryos to study fundamental aspects of cell biology such as DNA replication (Blow and Laskey, 2016), genome maintenance (Hoogenboom et al., 2017), DNA damage response (Cupello et al., 2016), cell cycle control (Philpott and Yew, 2008), metabolism (Ureta et al., 2001), and signalling pathways (Hill, 2001; Kuhl, 2002; Smith et al., 2008; Pera et al., 2014). Natural tumour immunity in amphibians has also elucidated immune system interactions (Banach and Robert, 2017), and together with *in vitro* experiments using extracts (Deming and Kornbluth, 2006), morphogenesis of embryos provides a physiological setting for study of apoptosis (Ishizuya-Oka, 2011; Ito et al., 2012). Similarly, key stromal interactions during tumour growth and metastasis have been informed by intra-vital imaging in *Xenopus* tadpoles (Haynes-Gimore et al., 2015) and by the study of developmental epithelial-to-mesenchymal transition (EMT) events (Pegoraro and Monsoro-Burq, 2013) that are key to malignant tumour invasion (Tanaka et al., 2016). Finally, tadpoles and adult frogs contribute to our understanding of genetic influences on tumorigenesis through induced-tumour-like-structures (ITLSs) (Wallingford, 1999) and the use of a new era of genetically engineered *Xenopus* models (GEXM) (Naert et al., 2017).

Increasingly oncologists have harnessed and applied aspects of the developmental biology toolbox, for example utilising lineage tracing technologies to investigate tumour cell origin and evolution (Aiello and Stanger, 2016). Similarly, given that developmental and oncogenic processes often depend on the same underlying pathways, it is perhaps not surprising that embryonic events provide an *in vivo* assay system for discovery and development of new therapeutics targeting these pathways. For example, aberrant Wnt signalling can contribute to all stages of tumorigenesis with a particularly prominent driving role in intestinal cancers, yet it has proved difficult to target therapeutically (Krishnamurthy and Kurzrock, 2018). Axis duplication can be induced in *Xenopus* embryos by injection of RNA encoding β-catenin into a ventral cell of a four cell embryo (Kuhl and Pandur, 2008), and preventing this Wnt-dependent secondary axis is a rapid and efficient screen for potential Wnt inhibitors (Waaler et al., 2011; De Robertis et al., 2013). Furthermore, monitoring developmental events such as tadpole blood and lymphatic formation can be used to screen chemical libraries for anti-angiogenic activity (Kalin et al., 2009), and a transgenic *Xenopus* reporter model now exists with expression of GFP in both blood and lymphatic vasculature under the xFlk1 promoter (Ny et al., 2005, 2013) simplifying such analysis even further. Additionally, gastrulation and neural crest migration critically require transient EMT events, and inhibition of the associated cell movements provides an initial *in vivo* assay to identify compounds that may also inhibit invasion and proliferation of several types of cancer (Tanaka et al., 2016). The large numbers, accessibility and rapid and robust development of embryos have earned *Xenopus* worldwide credibility in developmental biology; these same attributes are now valid for novel pharmacological screening approaches and are likely be utilised further in the future (Schmitt et al., 2014).

NATURALLY OCCURRING *XENOPUS* TUMOURS AND ANTI-CANCER DEFENCES

Naturally occurring tumours in *Xenopus* are believed to be rare, and potent carcinogens known in mammals have limited ability to induce tumours in amphibians, proving an intriguing insight into mechanisms of relative resistance and/or altered sensitivity to carcinogens. These may include control mechanisms present that regulate adult tissue regeneration, altered self-tolerance post-metamorphosis resulting in cancer cell rejection, ready induction of apoptosis and a reduced sensitivity to DNA damage; reviewed in Ruben et al. (2007). Amphibian skin also secretes a vast array of antibiotic peptides but some of these have inhibitory activity against human cancer cell growth, fuelling interest in defining more of these natural peptide secretions (Li et al., 2016).

Mechanisms of Tumour Immunity

Inflammation and evading the immune system are two hallmarks of cancer (Hanahan and Weinberg, 2011), and immune-based therapy is already employed in both human (Zhang and Chen, 2018) and veterinary cancer patients (Klingemann, 2018). However, a complex array of tumour and immune cell interactions can have disparate effects, leading to the concept of "immune-editing" of a heterogenous mix of tumour clones

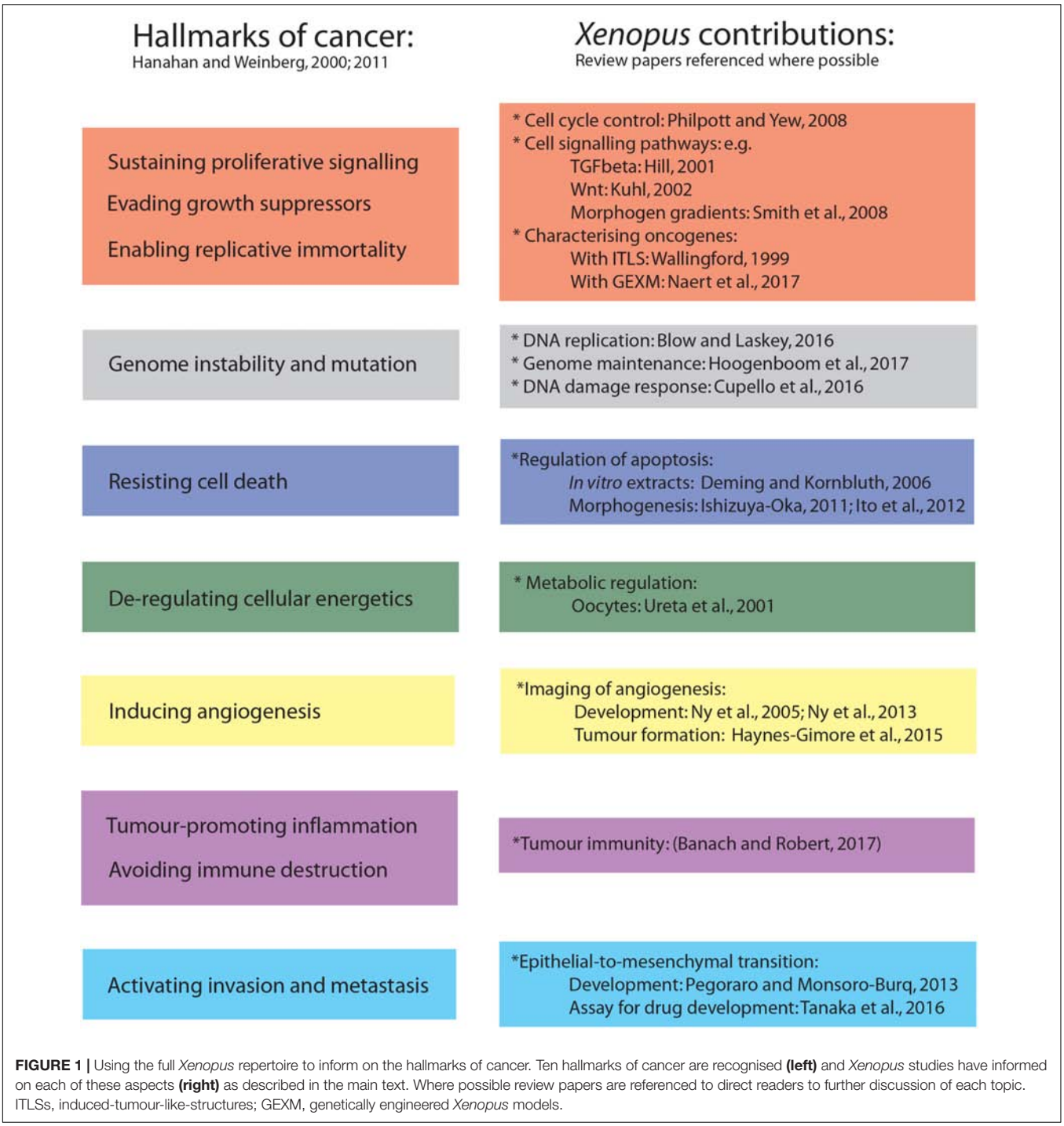

FIGURE 1 | Using the full *Xenopus* repertoire to inform on the hallmarks of cancer. Ten hallmarks of cancer are recognised **(left)** and *Xenopus* studies have informed on each of these aspects **(right)** as described in the main text. Where possible review papers are referenced to direct readers to further discussion of each topic. ITLSs, induced-tumour-like-structures; GEXM, genetically engineered *Xenopus* models.

(Bui and Schreiber, 2007). While some clones may be completely destroyed by the host immune system, selection pressure can create the persistence of clones with anti-immune defences or reduced immunogenicity, promoting tumour growth (Bui and Schreiber, 2007). Components of the innate and adaptive immune systems are highly conserved between *Xenopus* and mammals; readers are directed to Banach and Robert (2017) for a recent and in-depth review. With the derivation of defined immunogenic *Xenopus* cancer cell lines (see below), together with in-bred MHC-defined strains of *Xenopus* that permit tumour grafts without rejection, *Xenopus* is a highly valuable model for dissecting the roles of various immune system components; comprehensively reviewed in Goyos and Robert (2009); Robert (2010), and Banach and Robert (2017).

Original reports of highly malignant lymphosarcoma in *Xenopus* were subsequently demonstrated to be an infectious

granuloma in response to mycobacterium marinum (Asfari, 1988; Asfari and Thiebaud, 1988), but a range of genuine neoplastic and sometimes metastatic diseases are documented, including hepatoma, teratoma, renal carcinoma, fibrosarcoma, ovarian dysgerminoma, lymphoma, and pancreatic carcinoma (Banach and Robert, 2017). In the 1990s, five thymic lymphomas were reported in genetically different adult frogs, and these have provided five different and now extensively characterised lymphoid cell lines (B3B7, 15/0, 15/40, ff-2, and ff-2.64) (Robert and Cohen, 1998). Features such as high levels of myc expression, aneuploidy and genetic instability indicate their relevance to mammalian cancers, and mixed expression of T and B cell markers indicates resemblance to rare human leukocytic leukaemias (Robert and Cohen, 1998). These different thymic tumour cell lines arise in differing MHC immune backgrounds and display differing behaviours and invasiveness on transplantation, dependent on the immune status of the recipient tadpole or adult (Robert et al., 1994). These transplantation experiments coupled with the ease of genetic manipulation in *Xenopus* have allowed dissection of the mechanisms behind tumour and immune system interactions, including a key role of adult T cells for defence (Robert et al., 1997), and tumour expression of non-classical MHC class1b molecules for escaping immune recognition (Haynes-Gilmore et al., 2014).

Recent Advances Using Natural Tumour Grafts

Transplantation studies using the aggressive 15/0 tumour cell line and MHC compatible LG6 and LG15 tadpoles have also led to the recent development of a semi-solid tumour model by embedding tumour cells in a collagen matrix prior to subcutaneous engrafting (Haynes-Gimore et al., 2015). By fluorescently labelling tumour cells and infusing intra-cardiac labelled dextran, neoangiogenesis is visualised by intra-vital imaging to reveal a network of convoluted tumour vessels with slow laminar blood flow, recapitulating features of mammalian tumour vasculature. Utilising the natural transparency of *Xenopus* tadpoles, the semi-solid nature of the graft also enables visualisation of collagen rearrangements and infiltrating melanophores, characterising in real-time the tumour interaction with stroma and immune components (Haynes-Gimore et al., 2015). Just as developmental angiogenesis or neural crest formation can provide an *in vivo* screen for inhibitory drugs (see above), this accessible and well-characterised tumour model will surely attract further attention for chemotherapeutic development.

INDUCED TUMOUR-LIKE-STRUCTURES (ITLS) AS EARLY *XENOPUS* MODELS OF CANCER

Whilst there has been limited success in inducing tumours in *Xenopus* by carcinogens, simple genetic manipulation by RNA injection has been a cornerstone of the *Xenopus* system to study key developmental proteins, and this approach has also yielded early tumour models allowing characterisation of the role of various oncogenes or tumour suppressor proteins. These cancer models further emphasise the closely entwined features of both development and cancer, with developmental factors having influence on tumorigenesis, and the discovery that known oncogenic proteins may originally have a physiological role in development (Wallingford, 1999).

Developmental Regulators Influencing Oncogenesis

One of the first tumour phenotypes in *Xenopus* was reported through the study of tumour suppressor protein p53 in normal embryo development (Wallingford et al., 1997). Observations in tissue culture experiments and mouse models have long demonstrated the oncogenic effects of mutant p53, in part arising through a loss of cell cycle control and genomic instability. To investigate its role in embryogenesis and tumorigenesis, researchers turned to *Xenopus* where the rapid development of embryos allows analysis without the complicating effects of *de novo* mutations from inherent genomic instability. Human p53 alterations are the most common genetic abnormality in human cancers, often due to dominant-negative effects, and the human protein is biochemically similar to the *Xenopus* homolog, making *Xenopus* a relevant oncological model (Wallingford, 1999). Accordingly, targeted over-expression of dominant-negative human p53 in *Xenopus* embryos inhibits differentiation in multiple germ layers and produces cellular masses of undifferentiated cells with abnormal nuclear morphologies (Wallingford et al., 1997). This essential role of p53 in normal differentiation, beyond its roles in cell cycle control, is now well-documented in aspects of neurogenesis (Hardwick et al., 2014) and supports the notion that certain cancers may arise from a failure of differentiation rather than overt proliferation defects *per se*; a concept also suggested using a *Xenopus* developmental model for paediatric cancer Neuroblastoma (Wylie et al., 2015).

Oncogenic Regulators Influencing Development

Oncogenes can often directly influence aspects of cell fate and development. For example, over-expression of the viral oncogene polyoma middle T in *Xenopus* animal cap explants results in re-specification of prospective ectoderm to mesoderm, suggesting common signal transduction pathways between early inductive signals and oncogenic stimuli (Whitman and Melton, 1989). This is also supported by investigations in *Xenopus* using dominant inhibitory ras mutants, revealing a role for proto-oncogene $p21^{ras}$ in transduction of FGF and activin signalling in mesoderm induction (Whitman and Melton, 1992). Additionally, the Rel family of transcriptional activators are a diverse group including oncoprotein c-Rel. The *Xenopus* homolog Xrel3 is a distinct

rel protein expressed in two phases of early development, and its over-expression induces tumour formation (Yang et al., 1998). It his highly plausible that a protein with a physiological role in regulating the balance between cell proliferation and differentiation may become subverted and contribute to cancer formation, or alternatively there may be a convergence of oncogenic stimuli on the same developmental signalling pathways.

Characterising Oncogenes With Induced Tumour Models

Consistent with this theme of aberrant use of signalling pathways in oncogenesis, a *Xenopus* model of human basal cell carcinoma (BCC) has revealed the importance of Gli1 as a target and mediator of sonic hedgehog (Shh) signalling in BCC development. Over-expression of Gli1 in *Xenopus* embryos results in focal epidermal lesions with marker expression resembling that of human BCC and highlighting Gli1 as a potential early biomarker for diagnosis of BCC (Dahmane et al., 1997). Thus, ITLSs have been produced by over-expression of a range of proteins relevant to human cancers, and these tumours demonstrate disorganised and undifferentiated cells, high mitotic indicies, stromal interactions and neovascularisation (Chernet and Levin, 2013).

These same *Xenopus* models have also been used to extensively explore membrane depolarisation as a bioelectric marker predictive of ITLS foci (Chernet and Levin, 2013). Transmembrane potential itself may be an oncogenic driver and depolarisation of native neural crest cells can non-cell autonomously induce neoplastic changes in surrounding melanocytes (Blackiston et al., 2011; Lobikin et al., 2012). Similarly, formation of ITLS can be suppressed by hyperpolarisation of tumour or surrounding cells, suggested to be mediated through enhanced tumour uptake of butyrate with HDAC inhibitory properties, resulting in reduced cellular proliferation (Chernet and Levin, 2013, 2014). For further discussion (see Levin et al., 2017; Silver and Nelson, 2018).

GENETICALLY ENGINEERED *XENOPUS* MODELS (GEXM)

From the preceding discussion, *Xenopus* models have already assisted with investigation of both cancer pathogenesis and therapeutic development. These models are being expanded to a new dimension by using genome editing technology with TALENs or CRISPR/Cas9; methodology discussed in Naert et al. (2017). Genetically engineered mouse models are well-established in the Oncology toolbox, but aquatic models like zebrafish and *Xenopus* offer extra-uterine development of large embryos and simple injection set-ups for delivery of targeted nucleases, also usually lacking inherent complications of highly inbred genetic backgrounds (Naert et al., 2017). In addition to rapid development, high embryo number, and detailed fate maps for tissue-specific targeting, *Xenopus* also presents several advantages over zebrafish, such as reduced evolutionary distance to humans. Moreover, *Xenopus tropicalis* has a true diploid genome with substantial shared synteny with the human genome; in zebrafish whole genome duplication leads to redundancy and complications identifying human orthologs (Naert et al., 2017).

The first GEXM was established to phenocopy Familial Adenomatous Polyposis (FAP) by TALEN-mediated targeting of the *apc* gene in *Xenopus tropicalis*, replicating the human frame-shifting mutations and complementing models such as the Apc^{min} mouse and ENU-induced *apc* zebrafish mutant (Van Nieuwenhuysen et al., 2015). FAP is an autosomal dominant disease due to truncating mutations of the *apc* gene, resulting in 100s to 1000s of adenomatous polyps in the colon, potentially progressing to adenocarcinoma and sometimes accompanied by extra-colonic manifestations. Although F0 tadpoles do not develop genuine intestinal adenomas, they do display abnormal histological architecture of the intestine and the lack of adenomas may be explained by the distinct *Xenopus* intestinal folding pattern that allows proliferating cells to spread rather than form polyps (Van Nieuwenhuysen et al., 2015). Additionally, retinal hyperplasia and external tumours such as subcutaneous desmoid tumours resemble extra-colonic disease reported in humans, each displaying increased Wnt signalling and only mutant *apc* alleles. Thus, the *Xenopus apc* model provides high penetrance and rapid and reproducible tumour formation that is comparable to the human disease (Van Nieuwenhuysen et al., 2015).

A second model by the same group used CRISPR/Cas9-mediated knockout of *rb1* and *rbl1* genes in *Xenopus tropicalis* to phenocopy Retinoblastoma, a paediatric tumour of the developing retina (Naert et al., 2016). While mouse models exist, they show variable latency to tumour development and rely on conditional deletion as complete knock-out is embryonic lethal, while a zebrafish model relies on orthotopic retinoblastoma transplantation. As in mice, *Xenopus* tumours require inactivation of both *rb1* and *rbl1* genes, achieved by co-injection of independent pairs of guide RNAs and editing by CRISPR-Cas9; these mosaic double knock-out tadpoles develop a rapid and penetrant retinoblastoma in as little as 35 days, with histopathology and disease progression conserved with the human tumour (Naert et al., 2016). Efficiency of genome editing is reported at 25–30% for each locus, thus neoplasias develop in F0 mosaic mutants without high genome editing efficiencies, and given that an entire experiment can be conducted within 3 months, this technology using the *Xenopus* system has huge potential for future application (Naert et al., 2016).

FUTURE PERSPECTIVES

Building on the extensive history of *Xenopus* in exploring fundamental cell and developmental biology, we are now entering a new era where modern genome editing technology is being combined with all the classical attributes of the *Xenopus* system to generate clinically relevant cancer models that are rapid,

penetrant and highly suited to high-throughput screening. This is an important step allowing reduction of the number of mammals in pre-clinical research, and provides a range of platforms for therapeutic development, either using developmental events to screen for drugs targeting the same signalling pathways or as relevant *in vivo* tumour models. Furthermore, the aquatic nature of *Xenopus* permits fast and efficient preclinical screening of water-soluble compounds (Naert et al., 2017). There is also potential for characterising disease modifying genes by multiplexed biallelic targeting in *Xenopus* and proof of principle is already shown for dual target genes with TALENs (Naert et al., 2017) and triplex gene editing with CRISPR (Naert et al., 2016). Next steps will involve deletion of large chromosomal regions or replicating chromosomal translocations and relocations (Naert et al., 2017). Thus, *Xenopus* has rightfully earned a place in the Oncologist's toolbox and is likely to achieve even more prominence as the unique advantages of the *Xenopus* system become widely acknowledged in the oncology field.

AUTHOR CONTRIBUTIONS

LH wrote the manuscript and prepared the figure. AP reviewed and edited the manuscript.

FUNDING

Work in AP's lab was supported by a project grant from Neuroblastoma UK and by core support from the Wellcome Trust and MRC Cambridge Stem Cell. LH was supported by a Peterhouse Research Fellowship.

REFERENCES

Aiello, N. M., and Stanger, B. Z. (2016). Echoes of the embryo: using the developmental biology toolkit to study cancer. *Dis. Models Mech.* 9, 105–114. doi: 10.1242/dmm.023184

Asfari, M. (1988). Mycobacterium-induced infectious granuloma in Xenopus: histopathology and transmissibility. *Cancer Res.* 48, 958–963.

Asfari, M., and Thiebaud, C. H. (1988). Transplantation studies of a putative lymphosarcoma of Xenopus. *Cancer Res.* 48, 954–957.

Banach, M., and Robert, J. (2017). Tumor immunology viewed from alternative animal models-the Xenopus story. *Curr. Pathobiol. Rep.* 5, 49–56. doi: 10.1007/s40139-017-0125-y

Blackiston, D., Adams, D. S., Lemire, J. M., Lobikin, M., and Levin, M. (2011). Transmembrane potential of GlyCl-expressing instructor cells induces a neoplastic-like conversion of melanocytes via a serotonergic pathway. *Dis. Models Mech.* 4, 67–85. doi: 10.1242/dmm.005561

Blow, J. J., and Laskey, R. A. (2016). Xenopus cell-free extracts and their contribution to the study of DNA replication and other complex biological processes. *Int. J. Dev. Biol.* 60, 201–207. doi: 10.1387/ijdb.160142jb

Bui, J. D., and Schreiber, R. D. (2007). Cancer immunosurveillance, immunoediting and inflammation: independent or interdependent processes? *Curr. Opin. Immunol.* 19, 203–208. doi: 10.1016/j.coi.2007.02.001

Chernet, B. T., and Levin, M. (2013). Transmembrane voltage potential is an essential cellular parameter for the detection and control of tumor development in a Xenopus model. *Dis. Models Mech.* 6, 595–607. doi: 10.1242/dmm.010835

Chernet, B. T., and Levin, M. (2014). Transmembrane voltage potential of somatic cells controls oncogene-mediated tumorigenesis at long-range. *Oncotarget* 5, 3287–3306. doi: 10.18632/oncotarget.1935

Cupello, S., Richardson, C., and Yan, S. (2016). Cell-free Xenopus egg extracts for studying DNA damage response pathways. *Int. J. Dev. Biol.* 60, 229–236. doi: 10.1387/ijdb.160113sy

Dahmane, N., Lee, J., Robins, P., Heller, P., and Ruiz i Altaba, A. (1997). Activation of the transcription factor Gli1 and the Sonic hedgehog signalling pathway in skin tumours. *Nature* 389, 876–881. doi: 10.1038/39918

De Robertis, A., Valensin, S., Rossi, M., Tunici, P., Verani, M., De Rosa, A., et al. (2013). Identification and characterization of a small-molecule inhibitor of Wnt signaling in glioblastoma cells. *Mol. Cancer Ther.* 12, 1180–1189. doi: 10.1158/1535-7163.mct-12-1176-t

Deming, P., and Kornbluth, S. (2006). Study of apoptosis in vitro using the Xenopus egg extract reconstitution system. *Methods Mol. Biol.* 322, 379–393. doi: 10.1007/978-1-59745-000-3_27

Goyos, A., and Robert, J. (2009). Tumorigenesis and anti-tumor immune responses in Xenopus. *Front. Biosci.* 14, 167–176. doi: 10.2741/3238

Hanahan, D., and Weinberg, R. A. (2000). The hallmarks of cancer. *Cell* 100, 57–70. doi: 10.1016/S0092-8674(00)81683-9

Hanahan, D., and Weinberg, R. A. (2011). Hallmarks of cancer: the next generation. *Cell* 144, 646–674. doi: 10.1016/j.cell.2011.02.013

Hardwick, L. J., Ali, F. R., Azzarelli, R., and Philpott, A. (2014). Cell cycle regulation of proliferation versus differentiation in the central nervous system. *Cell Tissue Res.* 359, 187–200. doi: 10.1007/s00441-014-1895-8

Hardwick, L. J., and Philpott, A. (2015). An oncologists friend: how Xenopus contributes to cancer research. *Dev. Biol.* 408, 180–187. doi: 10.1016/j.ydbio.2015.02.003

Haynes-Gilmore, N., Banach, M., Edholm, E. S., Lord, E., and Robert, J. (2014). A critical role of non-classical MHC in tumor immune evasion in the amphibian Xenopus model. *Carcinogenesis* 35, 1807–1813. doi: 10.1093/carcin/bgu100

Haynes-Gimore, N., Banach, M., Brown, E., Dawes, R., Edholm, E. S., Kim, M., et al. (2015). Semi-solid tumor model in *Xenopus laevis/gilli* cloned tadpoles for intravital study of neovascularization, immune cells and melanophore infiltration. *Dev. Biol.* 408, 205–212. doi: 10.1016/j.ydbio.2015.01.003

Hill, C. S. (2001). TGF-beta signalling pathways in early Xenopus development. *Curr. Opin. Genet. Dev.* 11, 533–540. doi: 10.1016/S0959-437X(00)00229-X

Hoogenboom, W. S., Klein Douwel, D., and Knipscheer, P. (2017). Xenopus egg extract: a powerful tool to study genome maintenance mechanisms. *Dev. Biol.* 428, 300–309. doi: 10.1016/j.ydbio.2017.03.033

Ishizuya-Oka, A. (2011). Amphibian organ remodeling during metamorphosis: insight into thyroid hormone-induced apoptosis. *Dev. Growth Differ.* 53, 202–212. doi: 10.1111/j.1440-169X.2010.01222.x

Ito, M., Tamura, K., Mawaribuchi, S., and Takamatsu, N. (2012). Apoptotic and survival signaling mediated through death receptor members during metamorphosis in the African clawed frog *Xenopus laevis*. *Gen. Comp. Endocrinol.* 176, 461–464. doi: 10.1016/j.ygcen.2011.12.037

Kalin, R. E., Banziger-Tobler, N. E., Detmar, M., and Brandli, A. W. (2009). An in vivo chemical library screen in *Xenopus tadpoles* reveals novel pathways involved in angiogenesis and lymphangiogenesis. *Blood* 114, 1110–1122. doi: 10.1182/blood-2009-03-211771

Klingemann, H. (2018). Immunotherapy for dogs: running behind humans. *Front. Immunol.* 9:133. doi: 10.3389/fimmu.2018.00133

Krishnamurthy, N., and Kurzrock, R. (2018). Targeting the Wnt/beta-catenin pathway in cancer: update on effectors and inhibitors. *Cancer Treat. Rev.* 62, 50–60. doi: 10.1016/j.ctrv.2017.11.002

Kuhl, M. (2002). Non-canonical Wnt signaling in Xenopus: regulation of axis formation and gastrulation. *Semin. Cell Dev. Biol.* 13, 243–249. doi: 10.1016/S1084-9521(02)00050-2

Kuhl, M., and Pandur, P. (2008). Dorsal axis duplication as a functional readout for Wnt activity. *Methods Mol. Biol.* 469, 467–476. doi: 10.1007/978-1-60327-469-29

Levin, M., Pezzulo, G., and Finkelstein, J. M. (2017). Endogenous bioelectric signaling networks: exploiting voltage gradients for control of growth and form. *Annu. Rev. Biomed. Eng.* 19, 353–387. doi: 10.1146/annurev-bioeng-071114-040647

Li, S., Hao, L., Bao, W., Zhang, P., Su, D., Cheng, Y., et al. (2016). A novel short anionic antibacterial peptide isolated from the skin of *Xenopus laevis* with broad antibacterial activity and inhibitory activity against breast cancer cell. *Arch. Microbiol.* 198, 473–482. doi: 10.1007/s00203-016-1206-8

Lobikin, M., Chernet, B., Lobo, D., and Levin, M. (2012). Resting potential, oncogene-induced tumorigenesis, and metastasis: the bioelectric basis of cancer in vivo. *Phys. Biol.* 9:065002. doi: 10.1088/1478-3975/9/6/065002

Ma, Y., Zhang, P., Wang, F., Yang, J., Yang, Z., and Qin, H. (2010). The relationship between early embryo development and tumourigenesis. *J. Cell. Mol. Med.* 14, 2697–2701. doi: 10.1111/j.1582-4934.2010.01191.x

Naert, T., Colpaert, R., Van Nieuwenhuysen, T., Dimitrakopoulou, D., Leoen, J., Haustraete, J., et al. (2016). CRISPR/Cas9 mediated knockout of rb1 and rbl1 leads to rapid and penetrant retinoblastoma development in *Xenopus tropicalis*. *Sci. Rep.* 6:35264. doi: 10.1038/srep35264

Naert, T., Van Nieuwenhuysen, T., and Vleminckx, K. (2017). TALENs and CRISPR/Cas9 fuel genetically engineered clinically relevant *Xenopus tropicalis* tumor models. *Genesis* 55:e23005. doi: 10.1002/dvg.23005

Ny, A., Koch, M., Schneider, M., Neven, E., Tong, R. T., Maity, S., et al. (2005). A genetic *Xenopus laevis* tadpole model to study lymphangiogenesis. *Nat. Med.* 11, 998–1004. doi: 10.1038/nm1285

Ny, A., Vandevelde, W., Hohensinner, P., Beerens, M., Geudens, I., Diez-Juan, A., et al. (2013). A transgenic *Xenopus laevis* reporter model to study lymphangiogenesis. *Biol. Open* 2, 882–890. doi: 10.1242/bio.20134739

Pegoraro, C., and Monsoro-Burq, A. H. (2013). Signaling and transcriptional regulation in neural crest specification and migration: lessons from *xenopus embryos*. *Wiley Interdiscip. Rev. Dev. Biol.* 2, 247–259. doi: 10.1002/wdev.76

Pera, E. M., Acosta, H., Gouignard, N., Climent, M., and Arregi, I. (2014). Active signals, gradient formation and regional specificity in neural induction. *Exp. Cell Res.* 321, 25–31. doi: 10.1016/j.yexcr.2013.11.018

Philpott, A., and Yew, P. R. (2008). The Xenopus cell cycle: an overview. *Mol. Biotechnol.* 39, 9–19. doi: 10.1007/s12033-008-9033-z

Robert, J. (2010). Comparative study of tumorigenesis and tumor immunity in invertebrates and nonmammalian vertebrates. *Dev. Comp. Immunol.* 34, 915–925. doi: 10.1016/j.dci.2010.05.011

Robert, J., and Cohen, N. (1998). Evolution of immune surveillance and tumor immunity: studies in Xenopus. *Immunol. Rev.* 166, 231–243. doi: 10.1111/j.1600-065X.1998.tb01266.x

Robert, J., Guiet, C., Cohen, N., and Du Pasquier, L. (1997). Effects of thymectomy and tolerance induction on tumor immunity in adult *Xenopus laevis*. *Int. J. Cancer* 70, 330–334. doi: 10.1002/(SICI)1097-0215(19970127)70:3<330::AID-IJC14>3.0.CO;2-J

Robert, J., Guiet, C., and Du Pasquier, L. (1994). Lymphoid tumors of *Xenopus laevis* with different capacities for growth in larvae and adults. *Dev. Immunol.* 3, 297–307. doi: 10.1155/1994/37392

Ruben, L. N., Clothier, R. H., and Balls, M. (2007). Cancer resistance in amphibians. *Altern. Lab. Anim.* 35, 463–470.

Schmitt, S. M., Gull, M., and Brandli, A. W. (2014). Engineering *Xenopus embryos* for phenotypic drug discovery screening. *Adv. Drug Deliv. Rev.* 6, 225–246. doi: 10.1016/j.addr.2014.02.004

Silver, B. B., and Nelson, C. M. (2018). The bioelectric code: reprogramming cancer and aging from the interface of mechanical and chemical microenvironments. *Front. Cell. Dev. Biol.* 6:21. doi: 10.3389/fcell.2018.00021

Smith, J. C., Hagemann, A., Saka, Y., and Williams, P. H. (2008). Understanding how morphogens work. *Philos. Trans. R. Soc. Lond. B Biol. Sci.* 363, 1387–1392. doi: 10.1098/rstb.2007.2256

Tanaka, M., Kuriyama, S., Itoh, G., Kohyama, A., Iwabuchi, Y., Shibata, H., et al. (2016). Identification of anti-cancer chemical compounds using *Xenopus embryos*. *Cancer Sci.* 107, 803–811. doi: 10.1111/cas.12940

Torre, L. A., Siegel, R. L., Ward, E. M., and Jemal, A. (2016). Global cancer incidence and mortality rates and trends–an update. *Cancer Epidemiol. Biomarkers Prev.* 25, 16–27. doi: 10.1158/1055-9965.epi-15-0578

Ureta, T., Preller, A., and Kessi, E. (2001). Frog oocytes: a living test tube for studies on metabolic regulation. *IUBMB Life* 51, 5–10. doi: 10.1080/15216540117404

Van Nieuwenhuysen, T., Naert, T., Tran, H. T., Van Imschoot, G., Geurs, S., Sanders, E., et al. (2015). TALEN-mediated apc mutation in *Xenopus tropicalis* phenocopies familial adenomatous polyposis. *Oncoscience* 2, 555–566. doi: 10.18632/oncoscience.166

Waaler, J., Machon, O., von Kries, J. P., Wilson, S. R., Lundenes, E., Wedlich, D., et al. (2011). Novel synthetic antagonists of canonical Wnt signaling inhibit colorectal cancer cell growth. *Cancer Res.* 71, 197–205. doi: 10.1158/0008-5472.CAN-10-1282

Wallingford, J. B. (1999). Tumors in tadpoles: the *Xenopus embryo* as a model system for the study of tumorigenesis. *Trends Genet.* 15, 385–388. doi: 10.1016/S0168-9525(99)01800-4

Wallingford, J. B., Seufert, D. W., Virta, V. C., and Vize, P. D. (1997). p53 activity is essential for normal development in Xenopus. *Curr. Biol.* 7, 747–757. doi: 10.1016/S0960-9822(06)00333-2

Whitman, M., and Melton, D. A. (1989). Induction of mesoderm by a viral oncogene in early *Xenopus embryos*. *Science* 244, 803–806. doi: 10.1126/science.2658054

Whitman, M., and Melton, D. A. (1992). Involvement of p21ras in *Xenopus mesoderm* induction. *Nature* 357, 252–254. doi: 10.1038/357252a0

Wylie, L. A., Hardwick, L. J., Papkovskaia, T. D., Thiele, C. J., and Philpott, A. (2015). Ascl1 phospho-status regulates neuronal differentiation in a Xenopus developmental model of neuroblastoma. *Dis. Models Mech.* 8, 429–441. doi: 10.1242/dmm.018630

Yang, S., Lockwood, A., Hollett, P., Ford, R., and Kao, K. (1998). Overexpression of a novel Xenopus Rel mRNA gene induces tumors in early embryos. *J. Biol. Chem.* 273, 13746–13752. doi: 10.1074/jbc.273.22.13746

Zhang, H., and Chen, J. (2018). Current status and future directions of cancer immunotherapy. *J. Cancer* 9, 1773–1781. doi: 10.7150/jca.24577

Conflict of Interest Statement: The authors declare that the research was conducted in the absence of any commercial or financial relationships that could be construed as a potential conflict of interest.

frontiers in Physiology

ORIGINAL RESEARCH
published: 04 December 2018
doi: 10.3389/fphys.2018.01705

Candidate Heterotaxy Gene FGFR4 Is Essential for Patterning of the Left-Right Organizer in Xenopus

Emily Sempou, Osaamah Ali Lakhani, Sarah Amalraj and Mustafa K. Khokha*

Department of Pediatrics, Yale School of Medicine, Yale University, New Haven, CT, United States

Congenital heart disease (CHD) is the most common birth defect, yet its genetic causes continue to be obscure. Fibroblast growth factor receptor 4 (*FGFR4*) recently emerged in a large patient exome sequencing study as a candidate disease gene for CHD and specifically heterotaxy. In heterotaxy, patterning of the left-right (LR) body axis is compromised, frequently leading to defects in the heart's LR architecture and severe CHD. FGF ligands like FGF8 and FGF4 have been previously implicated in LR development with roles ranging from formation of the laterality organ [LR organizer (LRO)] to the transfer of asymmetry from the embryonic midline to the lateral plate mesoderm (LPM). However, much less is known about which FGF receptors (FGFRs) play a role in laterality. Here, we show that the candidate heterotaxy gene *FGFR4* is essential for proper organ situs in *Xenopus* and that frogs depleted of fgfr4 display inverted cardiac and gut looping. *Fgfr4* knockdown causes mispatterning of the LRO even before cilia on its surface initiate symmetry-breaking fluid flow, indicating a role in the earliest stages of LR development. Specifically, *fgfr4* acts during gastrulation to pattern the paraxial mesoderm, which gives rise to the lateral pre-somitic portion of the LRO. Upon *fgfr4* knockdown, the paraxial mesoderm is mispatterned in the gastrula and LRO, and crucial genes for symmetry breakage, like *coco*, *xnr1,* and *gdf3* are subsequently absent from the lateral portions of the organizer. In summary, our data indicate that FGF signaling in mesodermal LRO progenitors defines cell fates essential for subsequent LR patterning.

Keywords: FGF signaling, left-right patterning, gastrulation, Xenopus, congenital heart disease, heterotaxy

OPEN ACCESS

Edited by:
Amanda Sferruzzi-Perri, University of Cambridge, United Kingdom

Reviewed by:
Aris N. Economides, Regeneron Pharmaceuticals, Inc., United States
Raj Ladher, National Centre for Biological Sciences, India
Timothy J. Moss, Ritchie Centre, Australia

****Correspondence:***
Emily Sempou
emily.sempou@yale.edu

Specialty section:
This article was submitted to Embryonic and Developmental Physiology, a section of the journal Frontiers in Physiology

Received: *02 July 2018*
Accepted: *12 November 2018*
Published: *04 December 2018*

Citation:
Sempou E, Lakhani OA, Amalraj S and Khokha MK (2018) Candidate Heterotaxy Gene FGFR4 Is Essential for Patterning of the Left-Right Organizer in Xenopus. Front. Physiol. 9:1705. doi: 10.3389/fphys.2018.01705

INTRODUCTION

Left-right (LR) asymmetry is a major characteristic of the vertebrate body plan. While externally symmetric, chordates display a specific internal LR arrangement of their visceral organs. In patients with heterotaxy, LR development is defective and organs are mispatterned relative to the LR axis, which often results in compromised LR architecture of the heart and clinically severe cardiac dysfunction. Although heterotaxy is a predominantly genetic disease, causal genes remain largely unidentified (Zaidi and Brueckner, 2017). Exome sequencing of congenital heart disease (CHD) patients identified three individuals with damaging mutations in fibroblast growth factor receptor 4 (*FGFR4*). The first patient, with hypoplastic left heart syndrome, had a *de novo* mutation (Asp297Asn). The second patient, with an L-transposition of the great arteries and tricuspid atresia, had an inherited stopgain at Gly705. And finally, a third patient had an inherited damaging splice mutation associated with a hypoplastic main pulmonary artery and a left superior vena cava that

emptied into the coronary sinus (Zaidi et al., 2013; Jin et al., 2017). The patients' phenotypes suggest defects in LR patterning consistent with an established role for FGF signaling in LR patterning. We sought to investigate this further by studying the role of FGFR4 in the LR patterning cascade.

FGF signaling is governed by an array of FGF ligands and their receptors (FGFRs). In mammals, 18 FGFs and four FGFRs (FGFR1-4) are employed in a broad variety of developmental processes, including LR patterning (Teven et al., 2014). LR patterning begins at the left-right organizer (LRO) which forms in the posterior mesoderm at the end of gastrulation. At the LRO, cilia beat to create leftward extracellular fluid flow that breaks bilateral symmetry (Essner et al., 2002; Schweickert et al., 2007; Babu and Roy, 2013; Yoshiba and Hamada, 2014). For LR patterning to occur properly, LRO progenitor cells must be specified in the mesoderm, and the LRO has to be physically formed and properly engage in ciliogenesis and cilia signaling. Once the flow signal is detected in the left margin of the LRO, it is transmitted via nodal signaling to the left lateral plate mesoderm (LPM), inducing asymmetric pitx2c expression, which then results in asymmetric organogenesis (Logan et al., 1998; Piedra et al., 1998; Ryan et al., 1998; Yoshioka et al., 1998; Campione et al., 1999; Kawasumi et al., 2011). FGF signaling plays a role in several steps in this process.

Zebrafish homozygous for a stopgain mutation of FGF8 have been shown to physically lack a LRO (Albertson and Yelick, 2005). On the other hand, FGF8 acts differentially in chick, mouse, and rabbit to regulate asymmetric gene expression at the LRO and LPM (Boettger et al., 1999; Meyers and Martin, 1999; Fisher et al., 2002). In contrast, FGF4, stimulates ciliogenesis in the zebrafish LRO, but is not required to physically form the organizer (Yamauchi et al., 2009). Therefore, FGF ligands may act at different steps in the LR cascade; however, the FGF receptors (FGFR) that convey these effects are less well-understood. In zebrafish, FGFR1 is required to establish proper cilia length in several ciliated organs, including the LRO, confirming a role for FGF signals in ciliogenesis (Neugebauer et al., 2009). However, whether any of the other FGFRs play a role in earlier LR patterning steps or ciliogenesis is unknown.

Here, we show in *Xenopus* that *fgfr4* is required during gastrulation to differentiate the paraxial mesoderm that gives rise to the lateral gastrocoel roof plate (GRP), which is the amphibian LRO. F0 CRISPR mediated knockdown of *fgfr4* results in failure to specify the paraxial pre-somitic LRO, resulting in a smaller, mispatterned GRP. Consistently, *fgfr4* depletion leads to inverse LR heart architecture (L-loop) as well as abnormal LR patterning of the LPM, recapitulating the patient heterotaxy phenotype. Altogether, our results indicate that the heterotaxy candidate gene *FGFR4* acts early in gastrulation to specify pre-somitic tissue that is crucial to LRO function and correct organ situs.

MATERIALS AND METHODS

Xenopus

Xenopus tropicalis were housed and cared for in our aquatics facility according to established protocols that were approved by the Yale IRB—Institutional Animal Care and Use Committee (IACUC). Embryos were produced by *in vitro* fertilization and raised to appropriate stages in 1/9X MR as per standard protocol (del Viso and Khokha, 2012).

CRISPR Injection and Validation

Injections of *Xenopus* embryos were carried out at the one-cell stage using a fine glass needle and Picospritzer system, as previously described (del Viso and Khokha, 2012). Small guide RNAs (sgRNAs) containing the following *fgfr4* target sites were designed from the v7.1 model of the *X. tropicalis* genome: CRISPR-1 (exon 3): 5′-AGGAACGTTTGCTGCCGGGAGGG-3′, CRISPR-2 (exon 6): 5′-AGTGTGGTTCCATCAGACCGTGG-3′, and CRISPR-3 (in exon 8): 5′-TGCAGGGGAATACACATGTCTGG-3′. One-cell embryos were injected with 1.5 ng Cas9 Protein (PNA-Bio) and 400 pg of targeting sgRNA and raised to desired stages as previously described in detail (Bhattacharya et al., 2015). For genotyping, F0 embryos were raised to stage 45 and lyzed in 50 mM NaOH as previously described (Bhattacharya et al., 2015). Editing by CRISPR-1 was verified by amplifying from tadpole genomic DNA an 800 bp fragment around the prospective cut site in *fgfr4*, Sanger sequencing and subsequent ICE (Inference of CRISPR Edits) analysis with Synthego software (Hsiau et al., 2018). The efficacies of CRISPR-2 and−3 were assessed by amplifying a ∼1 kb fragment around the prospective cut sites and performing the T7 Endonuclease assay (Guschin et al., 2010). For this, PCR products were denatured and re-annealed, and mismatches between re-annealed wildtype and CRISPR-edited sequences were detected by T7 Endonuclease I digest (NEB). Digests were visualized on 2% agarose gels. The following primers were used to produce PCR products containing the prospective cut sites:

sgRNA	TARGET SITE (5′-3′)	FORWARD PRIMER	REVERSE PRIMER
1	*AGGAACG* *TTTGC* TGCCG GGAGGG	*CTGTAC* *TCC*GTAGA CTAGCC	*TGCTCT* *CTCA*CCTTG GAAAAA
2	AGTGTG GTTCCATC AGACCGTGG	*ACTGT* *CAAG*TTCCG CTGTCC	*ACAGG* *CATC*TCA CAGGCATT
3	TGCAGGGGA ATACACAT GTCTGG	*TTAAGAT* *GCG*TGTGT GAGCAC	*TGGAG* *AGTT*TGCT TGCTGTG

Cardiac Looping

Stage 45 *Xenopus* tadpoles were paralyzed with benzocaine and scored under a stereomicroscope. Looping was determined by position of the outflow tract. D-loops were defined as outflow tracts directed to the right, and L-loops to the left.

In situ Hybridization

Digoxigenin-labeled antisense probes for *pitx2* (TNeu083k20), *coco* (TEgg007d24), *xnr1* (TGas124h10), *gdf3* (Tgas137g21), *gsc* (TNeu077f20), *xnr3* (Tgas011k18), *foxj1* (Tneu058M03), *vent2*

(BG885317), *myf5* (TGas127b01), *xbra* (TNeu024F07), *fgfr4* (Dharmacon, Clone ID: 7521919) were *in vitro* transcribed using T7 High Yield RNA Synthesis Kit (E2040S) from New England Biolabs. Embryos were collected at the desired stages, fixed in MEMFA for 1–2 h at room temperature (RT) and dehydrated in 100% ethanol. GRPs were dissected post fixation prior to dehydration. Briefly, whole mount *in situ* hybridization of digoxigenin-labeled antisense probes was performed overnight, the labeled embryos were then washed, incubated with anti-digoxigenin-AP Fab fragments (Roche 11093274910), and signal was detected using BM-purple (Roche 11442074001), as previously described in detail (Khokha et al., 2002).

GRP Immunofluorescence

Xenopus embryos were collected at stage 17 and fixed for 2 h at RT in 4% paraformaldehyde/PBS. All samples were washed three times in PBS + 0.1% TritonX-100 (PBST) before incubating in PBST + 3% BSA blocking solution for 2 h at RT. Samples were then placed in blocking solution + primary antibody ON at 4°C. Samples were washed three times in PBST before incubating in blocking solution + secondary antibody/Phalloidin for 2 h at RT. Samples were washed three times in PBST and one time in PBS before mounting in Pro-Long Gold (Invitrogen) and imaging on a Zeiss 710 confocal microscope. Primary antibodies and dilutions for IF: Mouse monoclonal anti-acetylated tubulin, clone 6-11B-1, SIGMA Catalog: T-6793 (1:1,000); rabbit polyclonal anti-MYOD (aa1-150), LSBio, Catalog: LS-C143580 (1:200). Alexa488 and 594 conjugated anti-mouse and rabbit secondary antibodies were obtained from Thermo Fisher Scientific and used at a 1:500 dilution. Alexa647 phalloidin (Molecular Probes, 1:50) was used to stain cell boundaries.

Quantifications

All quantifications were done using standard Student's *t*-tests and taking into account three or more replicate experiments. To measure GRP area, the GRP area was outlined based on cell morphology and measured in ImageJ. To measure the presomitic area of the GRP, the GRP was first outlined based on morphology and the myoD positive portion of this area was subsequently outlined and similarly measured. Cilia were counted by thresholding individual acetylated-tubulin immunostaining images in ImageJ and performing particle analysis. The cilia count was then additionally verified by manual counting. Embryo numbers: $N = 15–25$ for total GRP and PSM area and $N = 10$ for cilia numbers. Embryo numbers for phenotype quantification and *in situ* hybridization experiments are indicated in each figure.

RESULTS

Fgfr4 Is Required for LR Development

To investigate whether *FGFR4* plays a role in LR development, we performed F0 CRISPR editing of the gene in *X. tropicalis*. This strategy effectively introduces damaging mutations in both alleles within 2 h after microinjection, and F0 tadpoles can be scored for organ situs 3 days later by simple inspection. We have found that known gene knockdown phenotypes can be replicated using F0 CRISPR editing in 9 out of 10 cases (Bhattacharya et al., 2015). In vertebrates, the cardiac tube initially forms in the midline, but then normally loops to the right (D-loop). Looping to the left (L-loop) or remaining midline (A-loop) is abnormal and suggests LR patterning defects consistent with heterotaxy (Baker et al., 2008; de Campos-Baptista et al., 2008; Rohr et al., 2008). Similarly, the gut depends on correct LR patterning to become coiled counter-clockwise and the intestinal rotation can be inverted in heterotaxy (Campione et al., 1999). We generated three sgRNAs independently targeting three non-overlapping sites in exons 3 (CRISPR-1), 6 (CRISPR-2), and 8 (CRISPR-3) of *fgfr4,* respectively. We verified gene modification using PCR amplification of the cut site followed by either Sanger sequencing and ICE (Inference of CRISPR Edits) analysis or the T7 Endonuclease I assay (**Supplementary Figure 1**). F0 CRISPR for all three sgRNAs led to tadpoles with cardiac L-loops and inverted gut looping (**Figures 1A–C**), indicating that *fgfr4* plays a role in establishing organ laterality.

Next, we tested if *fgfr4* depletion affected global LR patterning. Heart and gut looping both depend on activation of asymmetric gene expression in the left LPM prior to heart and gut tube morphogenesis (Logan et al., 1998; Piedra et al., 1998; Ryan et al., 1998; Yoshioka et al., 1998; Campione et al., 1999). Pitx2c, a homeobox transcription factor, is normally expressed in the left LPM. In a third of *fgfr4* CRISPR animals, we found *pitx2c* transcripts to be completely absent from the LPM, while a small minority displayed abnormal right-sided or bilateral *pitx2c* expression (**Figures 1D,E**). These results confirm that global LR development is compromised prior to organogenesis in *fgfr4*-depleted animals.

Fgfr4 Is Required for GRP Patterning

One of the first molecular targets to be asymmetrically expressed in the embryo upstream of *pitx2c* is the nodal antagonist *coco*. At the frog LR organizer (LRO), known as the GRP, *coco* expression is initially bilateral and then becomes downregulated on the left in response to leftward fluid flow generated by surface cilia (Schweickert et al., 2010). This allows downstream signaling via TGFbeta factors *xnr1* (nodal) and *gdf3* to take place exclusively on the left and become further transmitted to the left LPM (Vonica and Brivanlou, 2007), a cascade that is conserved among vertebrates (Nakamura and Hamada, 2012; Blum et al., 2014). To examine whether asymmetric gene expression was affected upstream of *pitx2c* at the LRO level, we examined *coco* expression at stage 19 after fluid flow in *fgfr4*-depleted embryos. Interestingly, we found *coco* to be bilaterally reduced or completely absent in almost half of the CRISPR embryos we analyzed (**Figure 2B**). We would predict that absence of *coco* would allow for bilateral TGFbeta signaling, resulting in bilateral *pitx2c* expression later in the LPM. Contrary to this scenario, we primarily encountered entirely absent *pitx2c* expression in *fgfr4* CRISPR animals. To understand this discrepancy, we examined the expression of TGFbeta factors *xnr1* and *gdf3* at the LRO. We found both transcripts, which normally have a predominantly bilateral expression, to be dramatically reduced or absent in over 50% of post-flow CRISPR embryos (**Figures 2D,F**). The absence of *xnr1* explains the complete bilateral lack of a left-handed

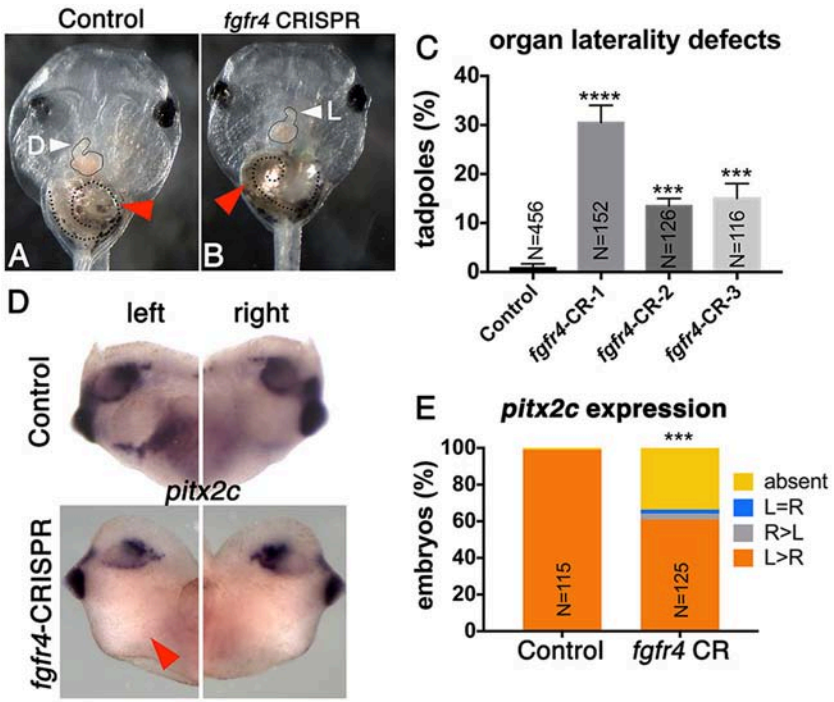

FIGURE 1 | *Fgfr4* F0 CRISPR editing disrupts LR development. **(A,B)** *fgfr4* CRISPR tadpoles display organ laterality defects. Ventral view of a stage 45 live tadpole with a cardiac L-loop (**B**; outlined) and inverse gut coiling (**B**; dashed line and red arrowhead). **(C)** Percentages of tadpoles with laterality defects (L-loops and inverse gut coiling) for three different CRISPRs; tadpoles with L-loops and inverse gut coils were scored; only tadpoles with inverse but otherwise intact gut coiling were considered; animals with completely uncoiled guts were scored as normal, as this phenotype occurs in the control population as well. Tadpoles with both cardiac and gut looping defects were only counted once in this analysis. **(D)** *Pitx2c* expression in the LPM of tailbud stage animals (stage 28); red arrowhead indicates absent expression. **(E)** Percentages of stage 28 animals with different *pitx2c* phenotypes; $^{****}p < 0.0001$, $^{***}p < 0.001$.

signal and is consistent with absence of *pitx2c* expression. The reduction/absence of *gdf3* is also consistent with absent *pitx2c*, since *gdf3* facilitates the transmission of the nodal signal to the LPM (Vonica and Brivanlou, 2007).

To further investigate the loss of these lateral nodal-related signals, we considered the possibility that the GRPs of *fgfr4*-depleted embryos were fundamentally mispatterned even prior to fluid flow. At stage 16, before cilia driven flow is established, *coco*, *xnr1,* and *gdf3* transcripts are expressed mostly bilaterally in control embryos. Notably, *all* three transcripts were strongly reduced or absent (**Figures 2A,C,E**), indicating that the GRP is not patterned correctly in *fgfr4*-depleted embryos, irrespectively of fluid flow.

Abnormal patterning of the GRP suggests that its cellular composition may be affected. To assess GRP morphology, we performed F-actin/phalloidin stain and acetylated tubulin immunostaining to visualize cell boundaries and cilia, respectively (**Figures 3A–H**). LRO cells of the GRP normally form a teardrop structure composed of small mesodermal ciliated cells. GRPs of *fgfr4* CRISPR embryos were morphologically distinct and composed of larger cells lacking cilia, resembling the neighboring endoderm (**Figures 3A–D**; phalloidin). Consistently, we measured a dramatically reduced total LRO area upon *fgfr4* knockdown (**Figure 3L**). In mildly affected GRPs, the natural teardrop shape of the LRO was preserved, albeit reduced in area (**Figures 3B,F**), whereas more severe cases displayed only one or two rows of mesodermal cells and lacked the regular teardrop structure (**Figure 3D,H**). Because pre-somitic GRP markers *coco*, *xnr1,* and *gdf3* were reduced or absent in *fgfr4* CRISPR embryos, we used an antibody against the myogenic transcription factor myoD to visualize the pre-somitic GRP (**Figures 3I–K**). The pre-somitic mesoderm (PSM) protrudes into the gastrocoel between the hypochordal central portion of the GRP and the surrounding endoderm. We found the myoD-positive portion of the GRP to be notably reduced relative to total GRP area in CRISPR embryos (**Figures 3I–K,M**), indicating a specific loss of pre-somitic GRP, which is consistent with the reduction in *coco*, *xnr1,* and *gdf3* expression. Finally, even though we counted fewer cilia per GRP in *fgfr4* CRISPR embryos (**Supplementary Figure 2B**), we quantified a similar cilia per GRP area ratio to that of control embryos (**Supplementary Figures 2A,C**), suggesting that *fgfr4* does not exert an effect on cilia differentiation *per se*, but rather affects the area of pre-somitic LRO. Altogether, this data suggests that *fgfr4* is required for pre-somitic GRP patterning.

Fgfr4 Patterns the Paraxial Mesoderm During Gastrulation

Fgfr1 is expressed in the zebrafish LRO, where it activates essential ciliogenesis genes (Neugebauer et al., 2009). We

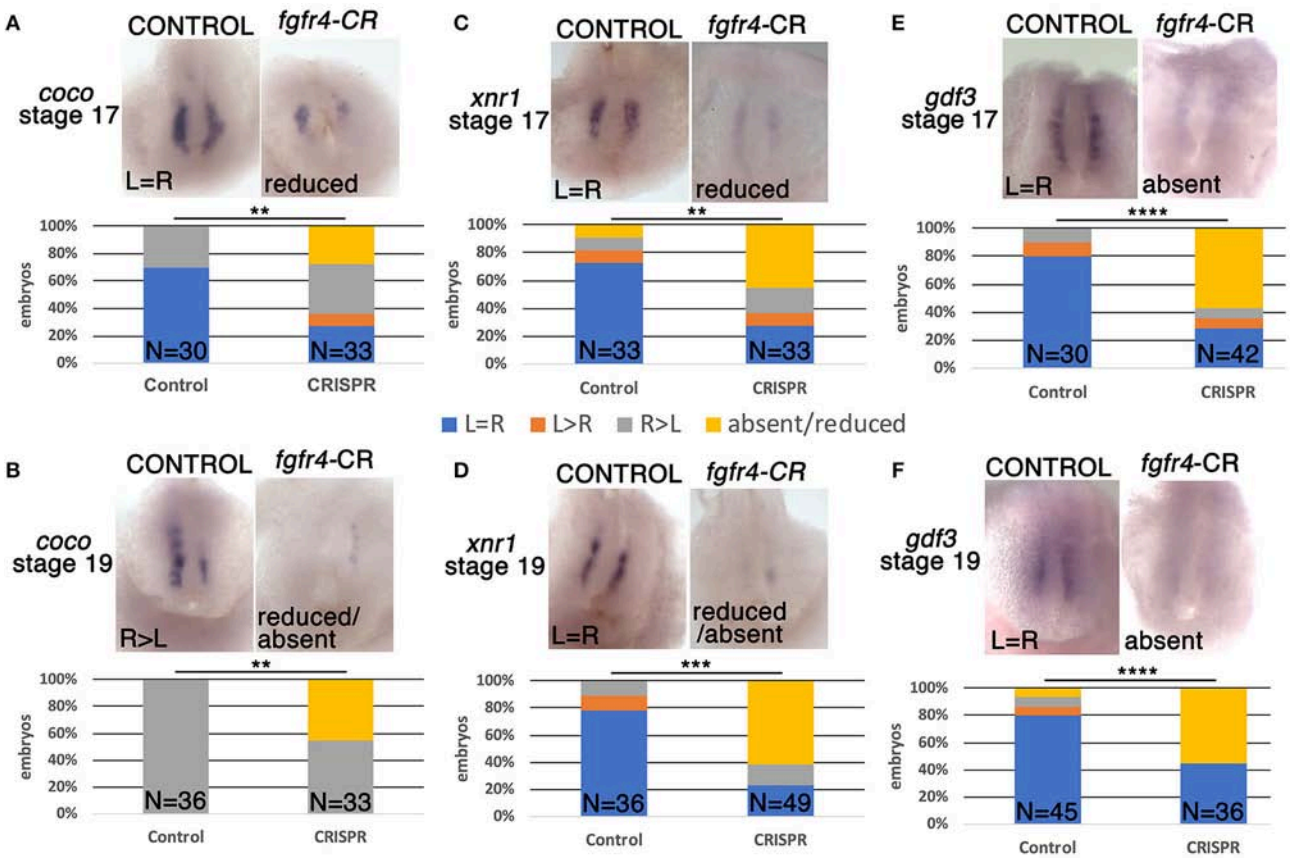

FIGURE 2 | GRP patterning is defective in *fgfr4* CRISPR mutants. Most representative expression patterns of pre-somitic GRP markers *coco*, *xnr1,* and *gdf3* in stage 17 **(A,C,E)** and stage 19 **(B,D,F)**. GRPs of control and *fgfr4* F0 CRISPR animals; ventral view of GRPs, anterior is to the top. Graphs show percentages of embryos with differential expression patterns of *coco*, *xnr1,* and *gdf3*. $^{**}p < 0.01$, $^{***}p < 0.001$, $^{****}p < 0.0001$.

considered that *fgfr4* may play a similar role in the GRP but were unable to detect *fgfr4* transcripts in the GRP (**Figures 4C,D**). Expression in the developing somites, eyes, and LPM of neurula stage embryos (**Figures 4A,B,D**) served as a positive control for transcript detection. The GRP is composed of hypochordal and PSM and both these tissues are specified during early gastrulation from dorsally located superficial (SM) and paraxial/myogenic mesoderm, respectively (Hopwood et al., 1989, 1991; Zetser et al., 2001; Shook et al., 2004; Stubbs et al., 2008; Walentek et al., 2013). Because *fgfr4* is expressed in the dorsal mesoderm during gastrulation (**Figures 4E–H**), we hypothesized that it could regulate early mesodermal patterning. In the early gastrula (stage 10), an array of markers is expressed in the mesoderm in a regionally restricted manner. We analyzed gene expression specific for the dorsal organizer (*gsc*, *xnr3*), paraxial/myogenic (*myf5*) mesoderm, superficial (*foxj1*) mesoderm, and ventral (*vent2*) mesoderm. Early gastrula (stage 10) *fgfr4*-depleted embryos showed intact patterning of the organizer, ventral, and superficial mesoderm but had absent *myf5* expression in the paraxial/myogenic mesoderm (**Figures 5A–F**). Moreover, the pan-mesodermal marker *xbra* was normally expressed throughout the mesoderm of stage 10 *fgfr4* CRISPR embryos, indicating that basic mesodermal identity was preserved even though *myf5* expression was absent (**Figures 5F,K**). Toward the end of gastrulation (stage 12), *myf5* expression was partially recovered, but markedly mispatterned (**Figure 5H**) and the upstream myogenic factor *myoD* was mispatterned in the same region (**Figure 5I**). The superficial mesoderm remained correctly patterned via *foxj1* at this stage (**Figure 5G**). Interestingly, midline bisection of late gastrula fgfr4-depleted embryos revealed an additional reduction in *xbra* expression in the involuted mesoderm (**Figures 5J,L**), confirming a previously reported relationship between FGF signaling and mesodermal *xbra* expression (Isaacs et al., 1994). These results altogether suggest that *fgfr4* is specifically required during gastrulation to pattern the paraxial/myogenic mesoderm and also maintain *xbra* expression in the involuted mesoderm. Loss of this paraxial mesoderm is then reflected in loss of lateral LRO markers *coco*, *xnr1*, and *gdf3* which results in LR patterning defects.

DISCUSSION

In this study, we propose a role for the candidate heterotaxy gene *FGFR4* in pattering the paraxial mesoderm, which

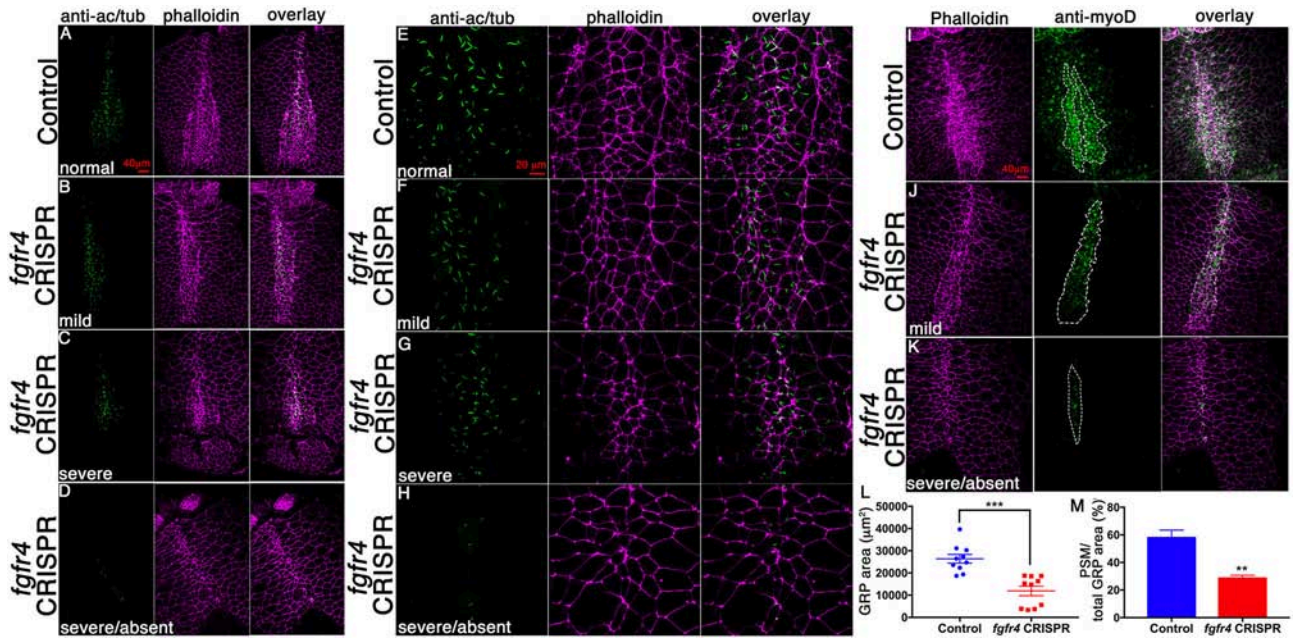

FIGURE 3 | GRP morphology and identity are altered in *fgfr4* CRISPR embryos. **(A–D)** GRPs of *fgfr4* CRISPR animals are morphologically distinct, as shown by phalloidin (actin) and anti-acetylated tubulin (cilia) stain; phenotypes ranging from mild **(B)** to severe **(C,D)**, depending on loss of small mesodermal ciliated cells. **(E–H)** Higher magnification of GRPs shows loss of ciliated GRP area in *fgfr4* CRISPR embryos **(G, H)**. **(I–K)** The pre-somitic, myoD positive portion of the GRP (outlined) is drastically reduced in *fgfr4* CRISPR embryos, even in embryos in which the overall GRP morphology is preserved **(J)**. **(L)** Quantification of total GRP area, defined morphologically by small, ciliated cells, is reduced in *fgfr4* CRISPR embryos. **(M)** The myoD positive area of the GRP, normalized to total GRP area, is specifically reduced in *fgfr4* CRISPR embryos. Scale bars in **(A–D, I–K)** = 40 μm, in **(E–H)** = 20 μm. $^{**}p < 0.01$, $^{***}p < 0.001$.

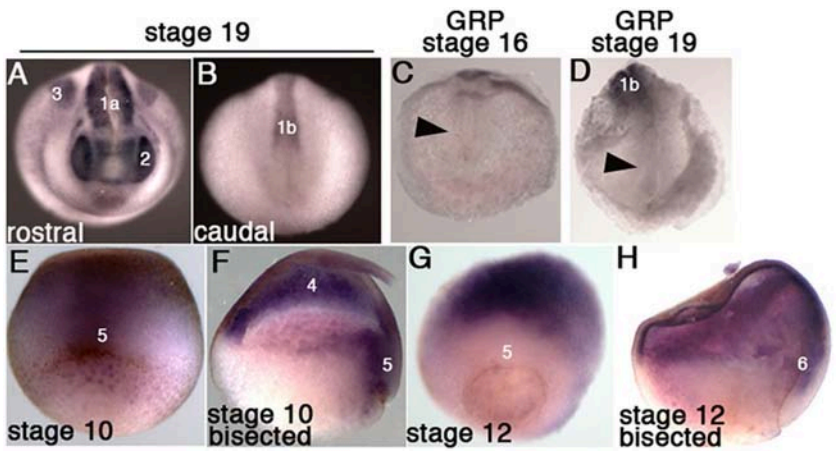

FIGURE 4 | *Fgfr4* expression during early *X. tropicalis* development, detected by *in situ* hybridization. **(A,B)** Whole stage 19 embryos; expression is detected in the head region (2: eyes), lateral plate mesoderm (3), anterior somites (1a) and posterior pre-somitic mesoderm (1b). **(C,D)** Transcripts were not detected in stage 16 and 19 GRPs (arrowheads). **(E,F)** Stage 10.5 embryos, whole (**E**, dorsal view) or bisected through the dorsal midline **(F)**; *fgfr4* is broadly expressed in the ectoderm (4) and dorsal marginal zone (5). **(G,H)** Stage 12 embryos, whole (**G**, dorso-vegetal view) or bisected **(H)**; *fgfr4* is absent from the marginal zone (5), but is expressed in the anterior migrating involuted mesoderm (6).

contributes to the formation of the lateral LRO. The PSM of the GRP of *fgfr4* knockdown embryos lacks general myogenic patterning via *myoD*, but also *coco*, *xnr1*, and *gdf3*, which are specific markers for the PSM exposed to the gastrocoel and are indispensable for the GRP's function as a LRO (Vonica and Brivanlou, 2007; Schweickert et al., 2010).

Both the hypochordal and PSM, which compose the GRP, are specified during early gastrulation from superficial (SM) and paraxial mesoderm, respectively. Multiple genes are known

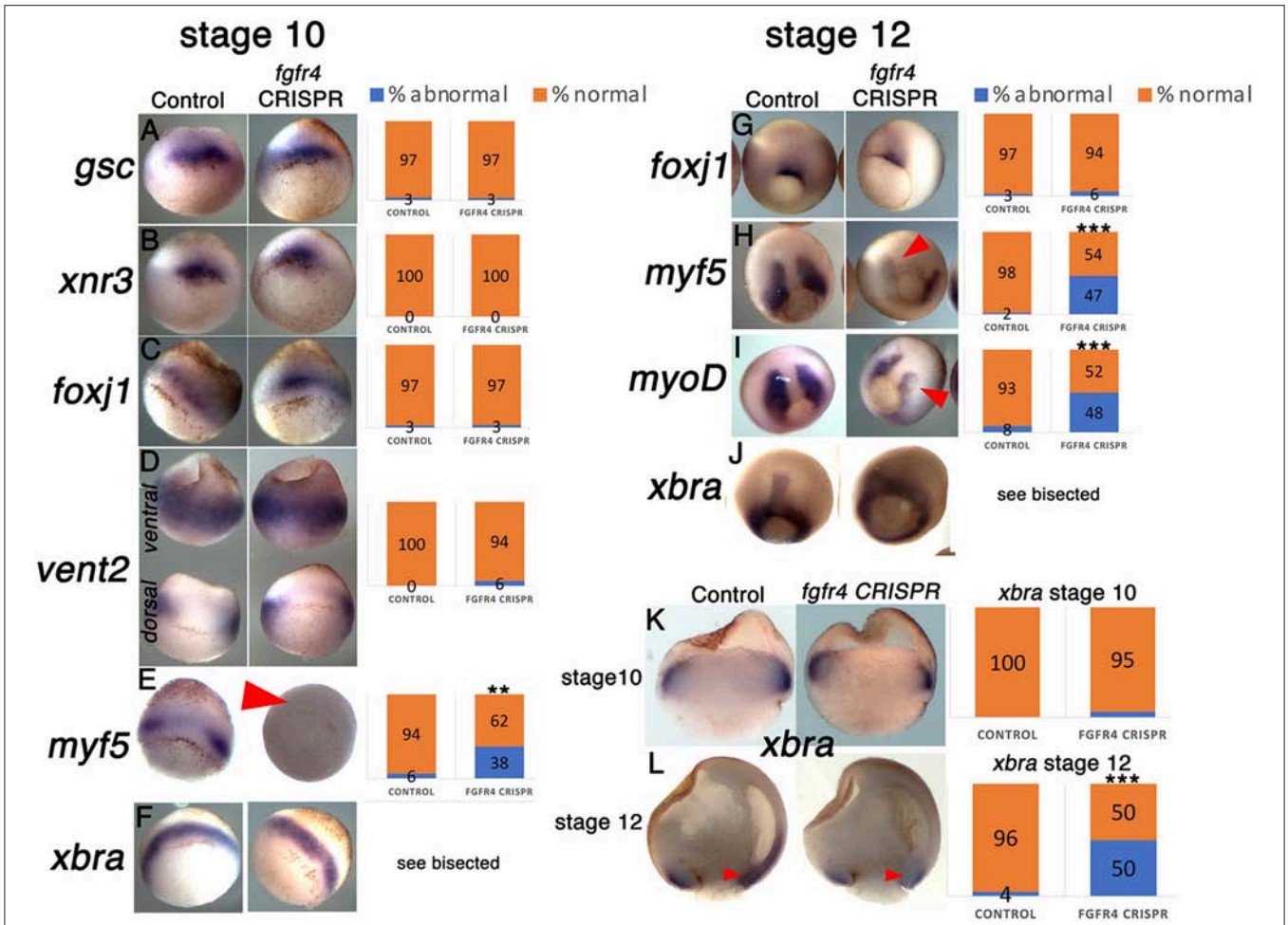

FIGURE 5 | The paraxial myogenic mesoderm is mispatterned in *fgfr4* CRISPR embryos. **(A–F, G–J)** Dorsal-vegetal views showing expression of an array of mesodermal markers in stage 10 **(A–F)** and stage 12 **(G–J)** embryos. Expression of paraxial mesoderm markers *myf5* and *myoD* is perturbed in *fgfr4* CRISPR embryos. **(K, L)** *Xbra* expression in embryos bisected through their dorsal midline at stages 10.5 and 12; red arrowheads point at xbra expression in the involuted mesoderm. Graphs show percentages of embryos with normal vs. abnormal expression of each marker; $N = 32–40$ embryos per Control or *fgfr4* CRISPR; $^{**}p < 0.001$, $^{***}p < 0.0001$.

to affect LR patterning via SM patterning, most of them via the ciliogenesis gene *foxj1* (Caron et al., 2012; Walentek et al., 2012; Griffin et al., 2018). In addition, knockdown of the global mesodermal determinant *Brachyury*/*xbra* results in LR defects both in frogs and mice (King et al., 1998; Kitaguchi et al., 2002). However, little is known about the signals that determine the fate of the PSM portion of the GRP during gastrulation, and while SM specification has been previously connected to candidate heterotaxy genes (Griffin et al., 2018), it is unclear whether PSM specification is similarly relevant. The PSM GRP is part of the greater paraxial mesoderm and thus also expresses myogenic markers during gastrulation (Shook et al., 2004; Schweickert et al., 2010). After gastrulation, the layer of PSM exposed to the gastrocoel becomes distinct from the more superficial PSM by additional patterning through factors (e.g., *coco*, *xnr1,* and *gdf3*) that facilitate its role as LRO tissue and enable the onset of asymmetric gene expression. At that stage, the PSM of the GRP still maintains the expression of myogenic factors like *myoD* (Schweickert et al., 2010). Given the key role of the PSM in the frog GRP, it is not surprising that paraxial mesoderm specification affects LR patterning. In mammals, the exact lineage of node cells and thus the contribution of paraxial mesoderm to the LRO remains to be determined. In mice, *Fgfr4* expression is detectable in paraxial myogenic mesoderm during node stages (Stark et al., 1991), and it would be interesting to examine whether its transcripts are present in the node region before LR cues become upregulated. Given that there are no reported LR phenotypes upon knockdown of the few known genes required for muscle development (Rudnicki et al., 1993; Pownall et al., 2002), it seems unlikely that the myogenic properties of paraxial mesoderm *per se* affect LRO function. It is rather likely that *fgfr4* controls an array of paraxial mesodermal genes during gastrulation, and that one or more of these genes are key to specify the GRP for LR cue expression.

FGF ligands FGF8 and FGF4 are required at several steps of LR development, which include LRO morphogenesis, ciliogenesis, and asymmetric gene expression at the LPM (Boettger et al., 1999; Meyers and Martin, 1999; Albertson and Yelick, 2005; Yamauchi et al., 2009). In addition, FGFR1 has been identified as essential for ciliogenesis once the LRO is shaped (Neugebauer et al., 2009). The role of FGFR4 appears distinctly different than that of FGFR1, since it acts to specify LRO tissue during gastrulation and is not expressed in the established LRO. We also observe fewer and sometimes shorter cilia in GRPs of *fgfr4* CRISPR embryos, but this effect is likely secondary to the patterning defect.

A long-standing connection exists between FGF signaling and gastrulation, and mesodermal patterning and morphogenesis in particular. Expression of dominant negative constructs for FGFR1 and FGFR4 effectively perturbs mesoderm induction by abolishing *xbra* expression (Amaya et al., 1991, 1993; Isaacs et al., 1994; Hardcastle et al., 2000). Moreover, depletion of ligand FGF4 (eFGF) strikingly resembles *fgfr4* knockdown by inhibiting *myoD* expression (Fisher et al., 2002) in the early mesoderm, suggesting that a fgf4/fgfr4 interaction may convey paraxial mesodermal specification during gastrulation.

Altogether our study establishes a link between FGFR4 and induction of paraxial mesoderm during gastrulation, which impinges on the specification of the pre-somitic GRP and its function as a LRO. These results help to construct the complex puzzle of FGF ligands and receptors that contribute to mesodermal and LR patterning in the early embryo.

AUTHOR CONTRIBUTIONS

ES performed GRP and gastrulation marker analyses, and manuscript writing. OL performed cardiac looping, *fgfr4* and *pitx2 in situ* hybridization analyses. SA collected embryos at various stages and contributed significantly to manuscript preparation. ES and MK conceived and planned experiments, and interpreted data.

ACKNOWLEDGMENTS

Thanks to M. Lane, S. Kubek, and M. Slocum for animal husbandry and the Center for Cellular and Molecular Imaging at Yale for confocal imaging. We also thank E. Mis for critical reading of the manuscript.

SUPPLEMENTARY MATERIAL

The Supplementary Material for this article can be found online at: https://www.frontiersin.org/articles/10.3389/fphys.2018.01705/full#supplementary-material

Supplementary Figure 1 | Injection of CRISPRs 1–3 results in edits in *fgfr4* in the genome of F0 frogs. **(A–C)** ICE (Inference of CRSIPR Edits) analysis of Sanger sequencing data from a genomic 800 bp PCR-fragment that contains the target site for CRISPR-1. **(A)** Average editing and knock-out scores for CRISPR-1 as identified by the ICE/Synthego software ($N = 8$ for control/$N = 8$ for CRISPR). All eight CRISPR F0 tadpoles displayed edits at the *fgfr4* target cut site, with overall editing efficiency within a single tadpole ranging from 75 to 95%, and knockout efficiency from 27 to 61%. In contrast, none of the Control tadpoles displayed mutations in the same genomic region. **(B)** Inferred distribution of Indels around the *fgfr4* CRISPR-1 target site within a single F0 CRISPR animal. The x-axis indicates the size of the insertion/deletion and the y-axis shows the percentage of sequences that contained it. **(C)** Relative contributions of inferred sequences present in a single CRISPR-1 F0 animal. An example for one single animal is shown. The cut site is presented with a black vertical dotted line and the wildtype sequence is marked by a "+" symbol on the far left. **(D)** T7 Endonuclease assay for *fgfr4* CRISPRs-2 (up) and−3 (down). Lanes show PCR products that contain the prospective cut sites, amplified from genomic DNA of different animals (numbered; $N = 3$–4 per CRISPR, $N = 2$ per Control), prior to digestion with T7 Endonuclease I (a) and after digestion (b). Red arrowheads point at fragments that are unique in CRISPR animals post-digestion and correspond to predicted fragment sizes: 300/550 bp for CRISPR-2 and 400/600 bp for CRISPR-3.

Supplementary Figure 2 | Cilia number in the GRP of *fgfr4* CRISPR-1 F0 embryos. **(A)** An example of how GRPs were outlined in order to count cilia and measure GRP area. **(B,C)** The total number of cilia per GRP is reduced in *fgfr4* CRISPR embryos **(B)**, however when the cilia numbers are normalized to total GRP area, no difference is visible between control and CRISPR embryos **(C)**. Scale bar = 40 μm.

REFERENCES

Albertson, R. C., and Yelick, P. C. (2005). Roles for fgf8 signaling in left-right patterning of the visceral organs and craniofacial skeleton. *Dev. Biol.* 283, 310–321. doi: 10.1016/j.ydbio.2005.04.025

Amaya, E., Musci, T. J., and Kirschner, M. W. (1991). Expression of a dominant negative mutant of the FGF receptor disrupts mesoderm formation in Xenopus embryos. *Cell* 66, 257–270. doi: 10.1016/0092–86749 0616-7

Amaya, E., Stein, P. A., Musci, T. J., and Kirschner, M. W. (1993). FGF signalling in the early specification of mesoderm in Xenopus. *Development* 118, 477–487.

Babu, D., and Roy, S. (2013). Left-right asymmetry: cilia stir up new surprises in the node. *Open Biol.* 3:130052. doi: 10.1098/rsob.130052

Baker, K., Holtzman, N. G., and Burdine, R. D. (2008). Direct and indirect roles for Nodal signaling in two axis conversions during asymmetric morphogenesis of the zebrafish heart. *Proc. Natl. Acad. Sci. U.S.A.* 105, 13924–13929. doi: 10.1073/pnas.0802159105

Bhattacharya, D., Marfo, C. A., Li, D., Lane, M., and Khokha, M. K. (2015). CRISPR/Cas9: an inexpensive, efficient loss of function tool to screen human disease genes in *Xenopus*. *Dev. Biol.* 408, 196–204. doi: 10.1016/j.ydbio.2015.11.003

Blum, M., Feistel, K., Thumberger, T., and Schweickert, A. (2014). The evolution and conservation of left-right patterning mechanisms. *Development* 141, 1603–1613. doi: 10.1242/dev.100560

Boettger, T., Wittler, L., and Kessel, M. (1999). FGF8 functions in the specification of the right body side of the chick. *Curr. Biol.* 9, 277–280. doi: 10.1016/S0960-982280119-5

Campione, M., Steinbeisser, H., Schweickert, A., Deissler, K., van Bebber, F., and Lowe, L. A. (1999). The homeobox gene Pitx2: mediator of asymmetric left-right signaling in vertebrate heart and gut looping. *Development* 126, 1225–1234.

Caron, A., Xu, X., and Lin, X. (2012). Wnt/beta-catenin signaling directly regulates Foxj1 expression and ciliogenesis in zebrafish Kupffer's vesicle. *Development* 139, 514–524. doi: 10.1242/dev.071746

de Campos-Baptista, M. I., Holtzman, N. G., Yelon, D., and Schier, A. F. (2008). Nodal signaling promotes the speed and directional movement of cardiomyocytes in zebrafish. *Dev. Dyn.* 237, 3624–3633. doi: 10.1002/dvdy.21777

del Viso, F., and Khokha, M. (2012). Generating diploid embryos from *Xenopus tropicalis*. *Methods Mol. Biol.* 917, 33–41. doi: 10.1007/978-1-61779-992-1-3

Essner, J. J., Vogan, K. J., Wagner, M. K., Tabin, C. J., Yost, H. J., and Brueckner, M. (2002). Conserved function for embryonic nodal cilia. *Nature* 418, 37–38. doi: 10.1038/418037a

Fisher, M. E., Isaacs, H. V., and Pownall, M. E. (2002). eFGF is required for activation of XmyoD expression in the myogenic cell lineage of *Xenopus laevis*. *Development* 129, 1307–1315. doi: 10.1016/j.ydbio.2012.08.027

Griffin, J. N., Del Viso, F., Duncan, A. R., Robson, A., Hwang, W., Kulkarni, S. et al. (2018). RAPGEF5 regulates nuclear translocation of β-catenin. *Dev. Cell* 44, 248–260. doi: 10.1016/j.devcel.2017.12.001

Guschin, D. Y., Waite, A. J., Katibah, G. E., Miller, J. C., Holmes, M. C., and Rebar, E. J. (2010). A rapid and general assay for monitoring endogenous gene modification. *Methods Mol. Biol.* 649, 247–256. doi: 10.1007/978-1-60761-753-2_15

Hardcastle, Z., Chalmers, A. D., and Papalopulu, N. (2000). FGF-8 stimulates neuronal differentiation through FGFR-4a and interferes with mesoderm induction in Xenopus embryos. *Curr. Biol.* 10, 1511–1514. doi: 10.1016/S0960-982200825-3

Hopwood, N. D., Pluck, A., and Gurdon, J. B. (1989). MyoD expression in the forming somites is an early response to mesoderm induction in Xenopus embryos. *EMBO J.* 8, 3409–3417. doi: 10.1002/j.1460-2075.1989.tb08505.x

Hopwood, N. D., Pluck, A., and Gurdon, J. B. (1991). Xenopus Myf-5 marks early muscle cells and can activate muscle genes ectopically in early embryos. *Development* 111, 551–560.

Hsiau, T., Maures, T., Waite, K., Yang, J., Kelso, R., Holden, K., et al. (2018). Inference of CRISPR edits from sanger trace data. *bioRxiv [preprint]*. doi: 10.1101/251082

Isaacs, H. V., Pownall, M. E., and Slack, J. M. (1994). eFGF regulates Xbra expression during Xenopus gastrulation. *EMBO J.* 13, 4469–4481. doi: 10.1002/j.1460-2075.1994.tb06769.x

Jin, S. C., Homsy, J., Zaidi, S., Lu, Q., Morton, S., DePalma, S, et al. (2017). Contribution of rare inherited and *de novo* variants in 2,871 congenital heart disease probands. *Nat. Genet.* 49, 1593–1601. doi: 10.1038/ng.3970

Kawasumi, A., Nakamura, T., Iwai, N., Yashiro, K., Saijoh, Y., Belo, J. A., et al. (2011). Left-right asymmetry in the level of active Nodal protein produced in the node is translated into left-right asymmetry in the lateral plate of mouse embryos. *Dev. Biol.* 353, 321–330. doi: 10.1016/j.ydbio.2011.03.009

Khokha, M. K., Chung, C., Bustamante, E. L., Gaw, L. W., Trott, K. A., Yeh, J., et al. (2002). Techniques and probes for the study of *Xenopus tropicalis* development. *Dev. Dyn.* 225, 499–510. doi: 10.1002/dvdy.10184

King, T., Beddington, R. S., and Brown, N. A. (1998). The role of the brachyury gene in heart development and left-right specification in the mouse. *Mech. Dev.* 79, 29–37. doi: 10.1016/S0925-477300166-X

Kitaguchi, T., Mizugishi, K., Hatayama, M., Aruga, J., and Mikoshiba, K. (2002). Xenopus Brachyury regulates mesodermal expression of Zic3, a gene controlling left-right asymmetry. *Dev. Growth Differ.* 44, 55–61. doi: 10.1046/j.1440-169x.2002.00624.x

Logan, M., Pagán-Westphal, S. M., Smith, D. M., Paganessi, L., and Tabin, C. J. (1998). The transcription factor Pitx2 mediates situs-specific morphogenesis in response to left-right asymmetric signals. *Cell* 94, 307–317. doi: 10.1016/S0092-867481474-9

Meyers, E. N., and Martin, G. R. (1999). Differences in left-right axis pathways in mouse and chick: functions of FGF8 and SHH. *Science* 285, 403–406. doi: 10.1126/science.285.5426.403

Nakamura, T., and Hamada, H. (2012). Left-right patterning: conserved and divergent mechanisms. *Development* 139, 3257–3262. doi: 10.1242/dev.061606

Neugebauer, J. M., Amack, J. D., Peterson, A. G., Bisgrove, B. W., and Yost, H. J. (2009). FGF signalling during embryo development regulates cilia length in diverse epithelia. *Nature* 458, 651–654. doi: 10.1038/nature 07753

Piedra, M. E., Icardo, J. M., Albajar, M., Rodriguez-Rey, J. C., and Ros, M. A. (1998). Pitx2 participates in the late phase of the pathway controlling left-right asymmetry. *Cell* 94, 319–324. doi: 10.1016/S0092-867481475-0

Pownall, M. E., Gustafsson, M. K., and Emerson, C. P. Jr. (2002). Myogenic regulatory factors and the specification of muscle progenitors in vertebrate embryos. *Annu. Rev. Cell Dev. Biol.* 18, 747–783. doi: 10.1146/annurev.cellbio.18.012502.105758

Rohr, S., Otten, C., and Abdelilah-Seyfried, S. (2008). Asymmetric involution of the myocardial field drives heart tube formation in zebrafish. *Circ. Res.* 102, e12–e19. doi: 10.1161/CIRCRESAHA.107.165241

Rudnicki, M. A., Schnegelsberg, P. N., Stead, R. H., Braun, T., Arnold, H. H., and Jaenisch, R. (1993). MyoD or Myf-5 is required for the formation of skeletal muscle. *Cell* 75, 1351–1359. doi: 10.1016/0092-867490621-V

Ryan, A. K., Blumberg, B., Rodriguez-Esteban, C., Yonei-Tamura, S., Tamura, K., Tsukui, T. J., et al. (1998). Pitx2 determines left-right asymmetry of internal organs in vertebrates. *Nature* 394, 545–551. doi: 10.1038/29004

Schweickert, A., Vick, P., Getwan, M., Weber, T., Schneider, I., Eberhardt, M., et al. (2010). The nodal inhibitor Coco is a critical target of leftward flow in Xenopus. *Curr. Biol.* 20, 738–743. doi: 10.1016/j.cub.2010.02.061

Schweickert, A., Weber, T., Beyer, T., Vick, P., Bogusch, S., Feistel, K., et al. (2007). Cilia-driven leftward flow determines laterality in Xenopus. *Curr. Biol.* 17, 60–66. doi: 10.1016/j.cub.2006.10.067

Shook, D. R., Majer, C., and Keller, R. (2004). Pattern and morphogenesis of presumptive superficial mesoderm in two closely related species, *Xenopus laevis* and *Xenopus tropicalis*. *Dev. Biol.* 270, 163–185. doi: 10.1016/j.ydbio.2004.02.021

Stark, K. L., McMahon, J. A., and McMahon, A. P. (1991). FGFR-4, a new member of the fibroblast growth factor receptor family, expressed in the definitive endoderm and skeletal muscle lineages of the mouse. *Development* 113, 641–651.

Stubbs, J. L., Oishi, I., Izpisúa Belmonte, J. C., and Kintner, C. (2008). The forkhead protein Foxj1 specifies node-like cilia in Xenopus and zebrafish embryos. *Nat. Genet.* 40, 1454–1460. doi: 10.1038/ng.267

Teven, C. M., Farina, E. M., Rivas, J., and Reid, R. R. (2014). Fibroblast growth factor (FGF) signaling in development and skeletal diseases. *Genes. Dis.* 1, 199–213. doi: 10.1016/j.gendis.2014.09.005

Vonica, A., and Brivanlou, A. H. (2007). The left-right axis is regulated by the interplay of Coco, Xnr1 and derriere in Xenopus embryos. *Dev. Biol.* 303, 281–294. doi: 10.1016/j.ydbio.2006.09.039

Walentek, P., Beyer, T., Thumberger, T., Schweickert, A., and Blum, M. (2012). ATP4a is required for Wnt-dependent Foxj1 expression and leftward flow in Xenopus left-right development. *Cell Rep.* 1, 516–527. doi: 10.1016/j.celrep.2012.03.005

Walentek, P., Schneider, I., Schweickert, A., and Blum, M. (2013). Wnt11b is involved in cilia-mediated symmetry breakage during Xenopus left-right development. *PLoS ONE* 8:e73646. doi: 10.1371/journal.pone.0073646

Yamauchi, H., Miyakawa, N., Miyake, A., and Itoh, N. (2009). Fgf4 is required for left-right patterning of visceral organs in zebrafish. *Dev. Biol.* 332, 177–185. doi: 10.1016/j.ydbio.2009.05.568

Yoshiba, S., and Hamada, H. (2014). Roles of cilia, fluid flow, and Ca2+ signaling in breaking of left-right symmetry. *Trends Genet.* 30, 10–17. doi: 10.1016/j.tig.2013.09.001

Yoshioka, H., Meno, C., Koshiba, K., Sugihara, M., Itoh, H., Ishimaru, Y., et al. (1998). Pitx2, a bicoid-type homeobox gene, is involved in a lefty-signaling pathway in determination of left-right asymmetry. *Cell* 94, 299–305. doi: 10.1016/S0092-867481473-7

Zaidi, S., and Brueckner, M. (2017). Genetics and genomics of congenital heart disease. *Circ. Res.* 120, 923–940. doi: 10.1161/CIRCRESAHA.116.309140

Zaidi, S., Choi, M., Wakimoto, H., Ma, L., Jiang, J., Overton, J. D., et al. (2013). *De novo* mutations in histone-modifying genes in congenital heart disease. *Nature* 498, 220–223. doi: 10.1038/nature12141

Zetser, A., Frank, D., and Bengal, E. (2001). MAP kinase converts MyoD into an instructive muscle differentiation factor in Xenopus. *Dev. Biol.* 240, 168–181. doi: 10.1006/dbio.2001.0465

Conflict of Interest Statement: The authors declare that the research was conducted in the absence of any commercial or financial relationships that could be construed as a potential conflict of interest.

frontiers in Physiology

ORIGINAL RESEARCH
published: 04 December 2018
doi: 10.3389/fphys.2018.01758

Xenopus Hybrids Provide Insight Into Cell and Organism Size Control

Romain Gibeaux[1†‡], *Kelly Miller*[1‡], *Rachael Acker*[1], *Taejoon Kwon*[2] *and Rebecca Heald*[1*]

[1] Department of Molecular and Cell Biology, University of California, Berkeley, CA, United States, [2] Department of Biomedical Engineering, Ulsan National Institute of Science and Technology, Ulsan, South Korea

Determining how size is controlled is a fundamental question in biology that is poorly understood at the organismal, cellular, and subcellular levels. The *Xenopus* species, *X. laevis* and *X. tropicalis* differ in size at all three of these levels. Despite these differences, fertilization of *X. laevis* eggs with *X. tropicalis* sperm gives rise to viable hybrid animals that are intermediate in size. We observed that although hybrid and *X. laevis* embryogenesis initiates from the same sized zygote and proceeds synchronously through development, hybrid animals were smaller by the tailbud stage, and a change in the ratio of nuclear size to cell size was observed shortly after zygotic genome activation (ZGA), suggesting that differential gene expression contributes to size differences. Transcriptome analysis at the onset of ZGA identified twelve transcription factors paternally expressed in hybrids. A screen of these *X. tropicalis* factors by expression in *X. laevis* embryos revealed that Hes7 and Ventx2 significantly reduced *X. laevis* body length size by the tailbud stage, although nuclear to cell size scaling relationships were not affected as in the hybrid. Together, these results suggest that transcriptional regulation contributes to biological size control in *Xenopus*.

Keywords: ***Xenopus laevis***, ***Xenopus tropicalis***, **hybrid, biological scaling, zygotic genome activation**

OPEN ACCESS

Edited by:
Karen Liu,
King's College London,
United Kingdom

Reviewed by:
Patrick Narbonne,
Université du Québec à Trois-Rivières, Canada
Rachel Katherine Miller,
University of Texas, United States

***Correspondence:**
Rebecca Heald
bheald@berkeley.edu

†Present Address:
Romain Gibeaux,
Univ Rennes, CNRS, IGDR (Institute of Genetics and Development of Rennes) - UMR 6290, Rennes, France

‡*These authors have contributed equally to this work*

Specialty section:
This article was submitted to Embryonic and Developmental Physiology, a section of the journal Frontiers in Physiology

Received: *12 August 2018*
Accepted: *20 November 2018*
Published: *04 December 2018*

Citation:
Gibeaux R, Miller K, Acker R, Kwon T and Heald R (2018) Xenopus Hybrids Provide Insight Into Cell and Organism Size Control. Front. Physiol. 9:1758. doi: 10.3389/fphys.2018.01758

INTRODUCTION

Biological size control and scaling are important and fundamental features of living systems. However, the molecular mechanisms that control size at the organism, cell, and subcellular levels are poorly understood. The frog *Xenopus* has emerged as a powerful system to explore nuclear and spindle size differences that occur between related species with different-sized eggs (Levy and Heald, 2010; Loughlin et al., 2011; Kitaoka et al., 2018), as well as subcellular scaling during early development, when cleavage divisions cause a rapid reduction in cell size (Good et al., 2013; Wilbur and Heald, 2013). We therefore set out to investigate whether *Xenopus* frogs could also be used to study size control at the level of the cell and the whole organism.

Cell size correlates strongly and linearly with genome size in a myriad of different organisms (Mirsky, 1951; Gregory, 2001; Cavalier-Smith, 2005), and increases in genome copy number through polyploidy have been shown to increase cell size within tissues or cell types (Lee et al., 2009; Frawley and Orr-Weaver, 2015). However, the molecular link between genome size and cell size remains an open question. Although increases in ploidy may globally affect gene expression, work in unicellular organisms such as yeast suggests that the maintenance of scaling between genome size and cell size does not simply reflect gene dosage (Galitski et al., 1999; Neumann and Nurse, 2007; Marguerat et al., 2012). Furthermore, the correlation between genome size and cell size is independent of the proportion of the genome that codes for genes (Gregory, 2001; Cavalier-Smith, 2005; Taft et al., 2007). A number of factors involved in many different processes, such as

growth, metabolism and protein synthesis, development, differentiation, and cell cycle regulation (Björklund et al., 2006) can influence cell size in a variety of organisms, from bacteria, to yeast, to *Drosophila*, to mammals (Marguerat and Bähler, 2012). Many of these genes are conserved and contribute to tissue and organ size in a variety of multicellular organisms, however, how they influence organism size, and how organism size feeds back to organ/tissue/cell size to attain homeostasis remains unclear.

Interestingly, in the related frog species *Xenopus laevis* and *Xenopus tropicalis*, the size of the genome, cells, and component subcellular structures scale with body size (Brown et al., 2007; Levy and Heald, 2010). Furthermore, the larger allotetraploid *Xenopus laevis* (6.2×10^9 base pairs, $N = 36$ chromosomes, average body length 10 cm) and smaller diploid *Xenopus tropicalis* (3.4×10^9 base pairs, $N = 20$ chromosomes, 4 cm in length) can hybridize. While fertilization of an *X. tropicalis* egg with a *X. laevis* sperm produces an inviable hybrid embryo that dies as a late blastula (Gibeaux et al., 2018), fertilization of an *X. laevis* egg with a *X. tropicalis* sperm ($l_e \times t_s$) produces a viable adult frog intermediate in genome size ($N = 28$ chromosomes) and body length between the two species (Narbonne et al., 2011). This viable hybrid thus provides a unique *in vivo* vertebrate model for investigating biological size control at the organismal, cellular, and subcellular levels.

In this study, we characterized size scaling in viable $l_e \times t_s$ hybrids and used this system to establish a novel screening method for candidate genes involved in size control to identify factors that affect the body size of the frog, as well as the scaling of its component cells and subcellular structures.

RESULTS

Reduced Size in Viable $l_e \times t_s$ Hybrids

Whereas, cross-fertilization of *X. tropicalis* eggs with *X. laevis* sperm produces hybrid embryos that die during zygotic genome activation (ZGA), the reverse cross of *X. laevis* eggs and *X. tropicalis* sperm ($l_e \times t_s$) results in viable hybrid embryos that possess genetic features of both *X. laevis* and *X. tropicalis* parents (Bürki, 1985; Lindsay et al., 2003; Narbonne et al., 2011; Elurbe et al., 2017; Gibeaux et al., 2018). Hybrid embryos progressed through tadpole, froglet, and adult stages (**Figures 1A,B**), although with significant morbidity. Using standard husbandry conditions for *X. laevis*, only four adults were obtained from hundreds of embryos in two separate attempts to generate $l_e \times t_s$ hybrid frogs. Early development in the $l_e \times t_s$ hybrid proceeded normally according to Nieuwkoop and Faber staging (Nieuwkoop and Faber, 1994) until the end of neurulation, and at a similar rate compared to wild type *X. laevis* embryos (**Figure 1C**, **Supplementary Movie S1**). However, by the tailbud stage, body length was significantly decreased in $l_e \times t_s$ hybrids (**Figure 1D**). Relative shortening of body length continued, although development remained similar to *X. laevis,* and both hybrid and control animals initiated metamorphosis with the same timing (**Figure 1E**). As soon as metamorphosis was complete, size scaling stopped and the body length of both the $l_e \times t_s$ hybrid and *X. laevis* froglets increased at the same rate, retaining the difference in size (**Figure 1F**). Strikingly, in adult hybrid frogs, both cell and nuclear size of erythrocytes was reduced (**Figure 1G**). Since the hybrid genome (28 chromosomes) is smaller than the *X. laevis* genome (36 chromosomes), these observations are consistent with genome size-dependent scaling at the organism, cellular, and subcellular levels.

Nuclear to Cell Size Scaling in $l_e \times t_s$ Hybrids Is More Similar to That of *X. laevis* Haploids, Despite a Larger Genome Size

We wondered whether the scaling observed in hybrid embryos was due to the decrease in genome size, or if the paternal *X. tropicalis* genome also influenced size scaling. To examine the effect of altering genome size alone, we utilized haploid *X. laevis* embryos produced by fertilizing wild type *X. laevis* eggs with irradiated *X. laevis* sperm (**Figure 2A**). While the sperm DNA is inactivated and does not contribute to the genome of the offspring, the sperm centrosome induces embryonic development yielding haploid embryos containing only the $N = 18$ maternal genome (Hamilton, 1957). Haploid embryos developed normally to the tailbud stage, and at a similar developmental rate to wild type *X. laevis* embryos (**Figure 2B**, **Supplementary Movie S2**). However, by the tailbud stage, body length was significantly reduced in *X. laevis* haploids (**Figure 2C**). Haploid embryos never reach metamorphosis and stop developing as stunted tadpoles (Hamilton, 1963).

We then evaluated nuclear to cell size scaling relationships before and after ZGA, comparing *X. laevis*, $l_e \times t_s$ hybrids and haploid *X. laevis* embryos (**Figures 2D–G**). Interestingly, no difference in the nuclear to cell size ratio was observed at early stages (6 and 8) among the 3 embryo types (**Figure 2E**). However, we found that, from stage 10, haploid embryos possessed reduced nuclear sizes at similar cell sizes compared to *X. laevis* (**Figure 2F**). Consistent with their intermediate genome size ($36 > 28 > 18$ chromosomes), the scaling curve of hybrids fell between that of *X. laevis* and haploids. Strikingly however, by stage 21, nuclear to cell size scaling in hybrids was more similar to that of haploids than to wild type *X. laevis* (**Figure 2G**). Therefore, we hypothesized that upon ZGA, gene expression of the *X. tropicalis* paternal genome, rather than bulk genome size alone, contributes to the reduced size of $l_e \times t_s$ hybrids.

Transcriptome Analysis Identifies 12 *X. tropicalis* Transcription Factors Expressed in Hybrids

To identify paternal *X. tropicalis* genes that could contribute to size control in hybrid embryos at ZGA, we performed RNA sequencing and transcriptome analysis of embryos at stage 9. We detected many tropicalis-derived paternally expressed genes in hybrid embryos. Differential expression analysis revealed one maternally expressed *X. laevis* gene that was significantly less abundant in the $l_e \times t_s$ hybrid (**Figure 3A**, **Supplementary Table S1**), and 41 paternally expressed *X. tropicalis* genes that were significantly more abundant in $l_e \times t_s$ hybrid, compared to *X. laevis* embryos (**Figure 3B**, **Supplementary Table S1**). Gene ontology (GO) term analysis

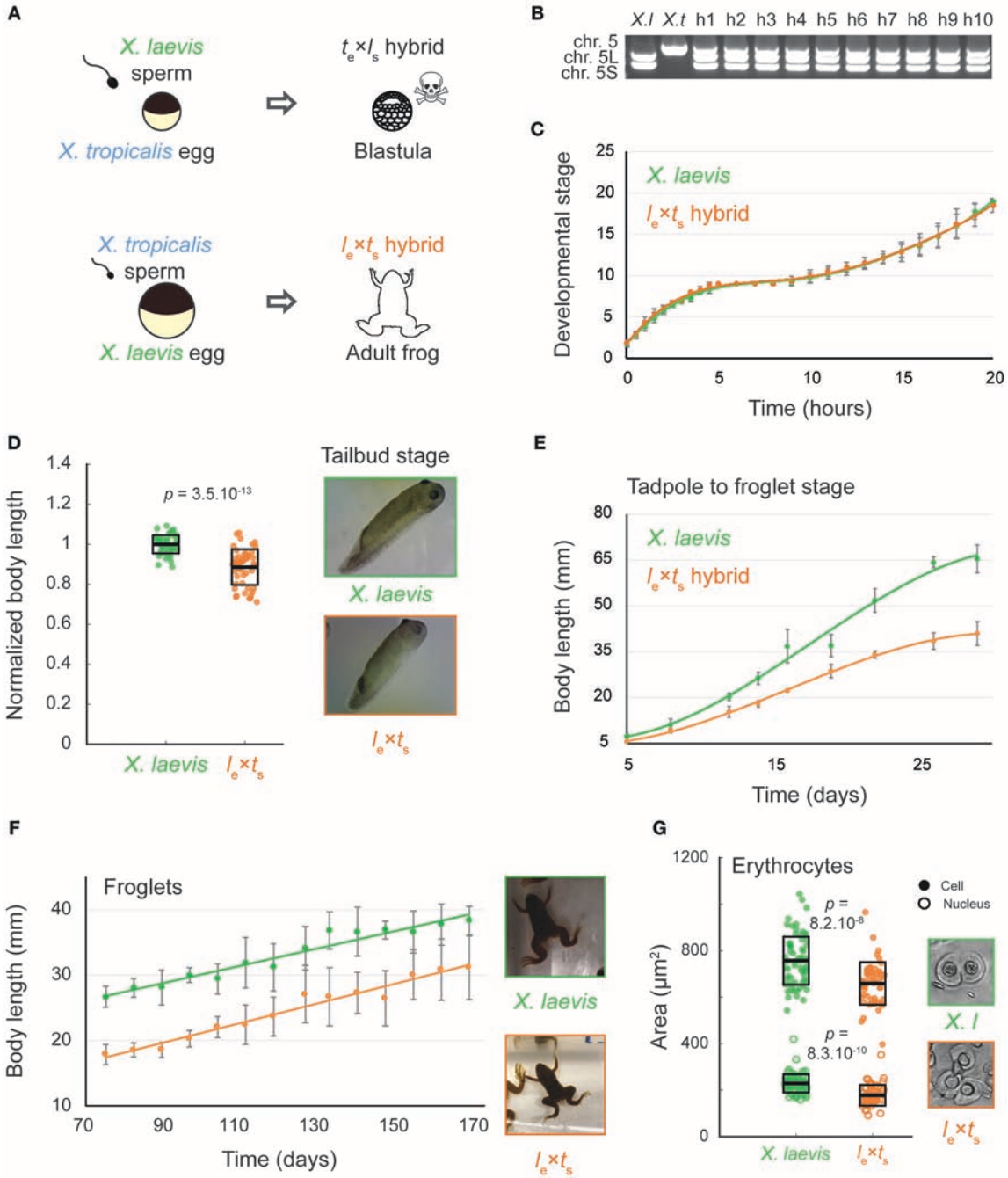

FIGURE 1 | Growth and development of *Xenopus* $l_e \times t_s$ viable hybrids. **(A)** Schematic of developmental outcomes of *Xenopus laevis* and *Xenopus tropicalis* cross-fertilization. **(B)** Agarose gel electrophoresis showing PCR amplification of 2 genomic loci in *X. laevis* (*X. l*, on chromosomes 5L and S) and one locus in *X. tropicalis* (*X. t*, chromosome 5). H1-10 indicates 10 randomly chosen hybrid tadpoles tested, confirming the consistent presence of all 3 subgenomes in hybrids. **(C)** Developmental timing in *X. laevis* and $l_e \times t_s$ hybrid embryos. Average is plotted for each time point. Error bars show standard deviation. **(D)** Body length of tailbud stage *X. laevis* and $l_e \times t_s$ hybrids. Box plots show all individual body lengths. Thick line inside box = average length, upper and lower box boundaries = ±standard deviation (SD). *P*-value was determined by two-tailed heteroscedastic *t*-test. Representative images of tailbuds at identical scale are shown on the right. **(E)** Body length of tadpoles throughout metamorphosis for *X. laevis* and $l_e \times t_s$ hybrids. Average is plotted for each time point. Error bars show standard deviation. **(F)** Body length of *X. laevis* and $l_e \times t_s$ hybrid froglets. Average is plotted for each time point. Error bars show standard deviation. Representative images of froglets at identical scale are shown on the right. **(G)** Size of erythrocyte cells and nuclei in *X. laevis* and $l_e \times t_s$ hybrid adult frogs. Box plots show all individual cell or nuclear areas. Thick line inside box = average area, upper and lower box boundaries = ± SD. *P*-values were determined by two-tailed heteroscedastic *t*-test. Representative images of erythrocytes at identical scale are shown on the right.

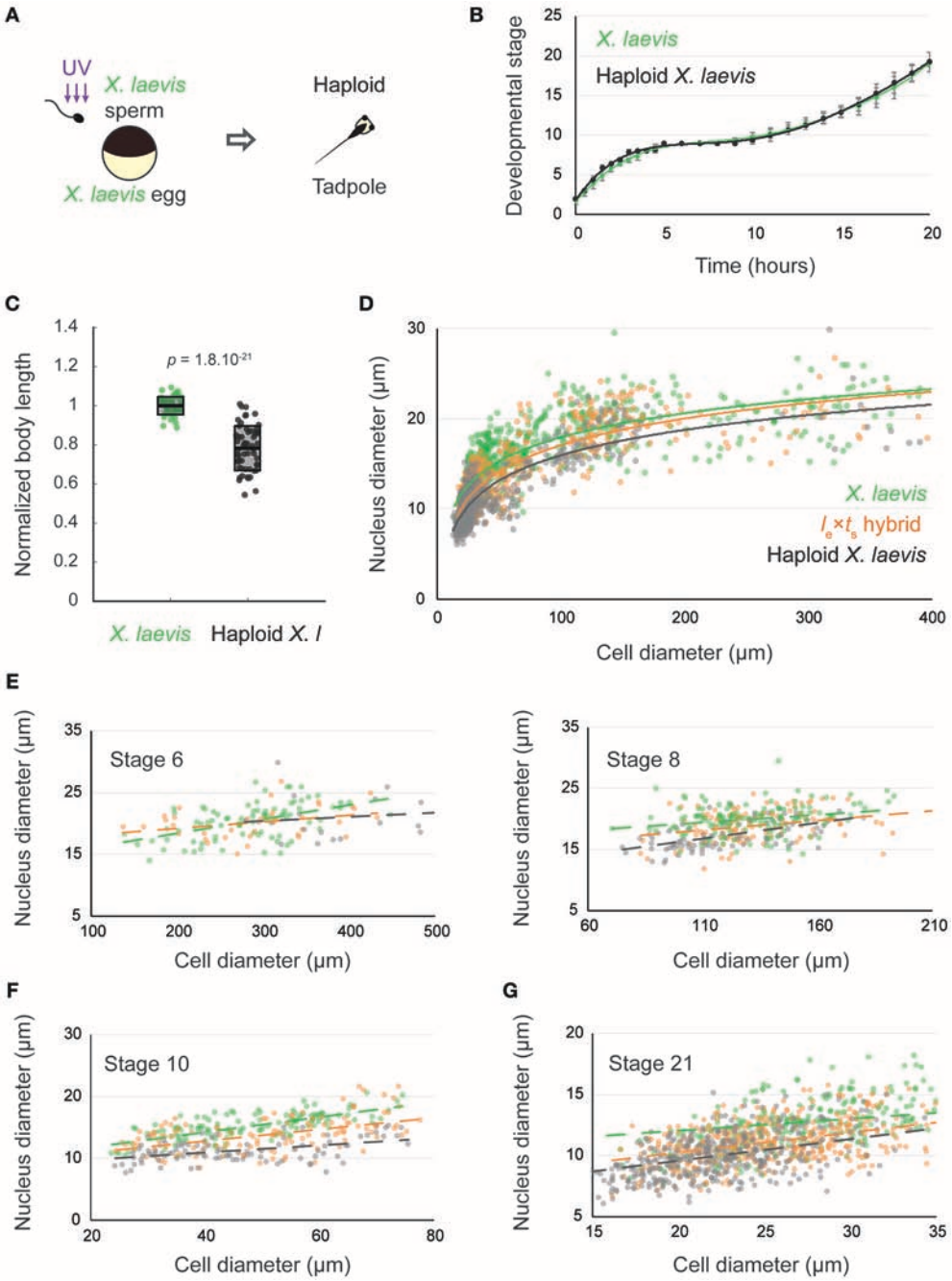

FIGURE 2 | Nuclear to cell size relationships pre- and post-zygotic genome activation in $l_e \times t_s$ hybrids compared to *X. laevis* diploids and haploids. **(A)** Schematic of generation of haploid *X. laevis* tadpoles via UV irradiation of sperm. **(B)** Developmental timing in *X. laevis* and haploid *X. laevis* embryos. Average is plotted for each time point. Error bars show standard deviation. **(C)** Body length of tailbud stage *X. laevis* and haploid *X. laevis*. Box plots show all individual body lengths. Thick line inside box = average length, upper and lower box boundaries = ± SD. *P*-value was determined by two-tailed heteroscedastic *t*-test. **(D)** Nuclear diameter vs. cell diameter in *X. laevis*, *X. laevis* haploid, and $l_e \times t_s$ hybrid embryos. **(E)** Nuclear diameter vs. cell diameter in *X. laevis*, *X. laevis* haploid, and $l_e \times t_s$ hybrid embryos at developmental stages 6 and 8. **(F)** Nuclear diameter vs. cell diameter in *X. laevis*, *X. laevis* haploid, and $l_e \times t_s$ hybrid embryos at developmental stage 10. **(G)** Nuclear diameter vs. cell diameter in *X. laevis*, *X. laevis* haploid, and $l_e \times t_s$ hybrid embryos at developmental stage 21. For **(E–G)**, we ran an analysis of covariance (ANOCOVA test) to determine whether the nuclear to cell size scaling significantly depends on the embryo types. At stage 6, $p = 0.132$, at stage 8, $p = 0.126$, at stage 10, $p = 2.558 \times 10^{-6}$, and at stage 21, $p = 1.110 \times 10^{-7}$.

of differentially expressed paternal genes revealed significant overrepresentation of the molecular function "DNA binding" (GO:0003677; 4.38-fold enrichment, with a 2.90e-3 false discovery rate), and of the biological process "transcription, DNA-templated" (GO:0006351; 4.65-fold enrichment, with a 3.93e-04 false discovery rate). Therefore, we conclude that

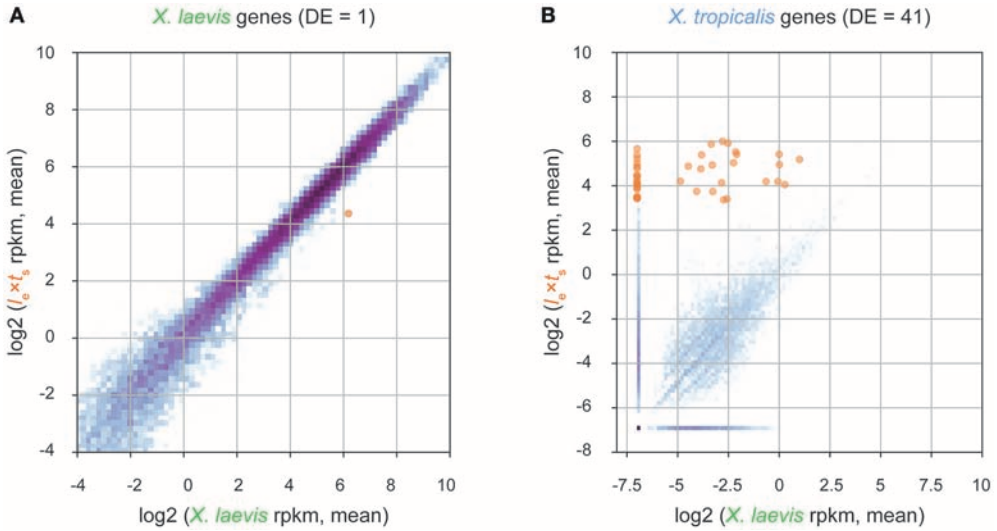

FIGURE 3 | Transcriptome analysis of $l_e \times t_s$ hybrid embryos at the onset of zygotic genome activation. **(A)** Differential expression analysis of *X. laevis* maternal genes in stage 9 $l_e \times t_s$ hybrid vs. *X. laevis* embryos. **(B)** Differential expression analysis of *X. tropicalis* paternal genes in stage 9 $l_e \times t_s$ hybrid vs. *X. laevis* embryos. For both figures, RNA-seq reads are mapped to a database of combined *X. laevis* and *X. tropicalis* transcriptomes and significantly differentially expressed genes (DE; fold-change >2 and false discovery rate <0.05) are marked in orange (see section Materials and Methods for more information).

transcriptional regulators with DNA binding functions are significantly enriched in paternally expressed genes in hybrid embryos. To finalize our list of candidates, we used Xenbase (James-Zorn et al., 2012; Karimi et al., 2018) to validate the transcription factor function of the candidate genes. From this, we set out to screen the following 12 transcription factors, Ers10, Hes7, Mix1, Ventx2, Foxi4, Sox3, Tgif2, Klf17, Sia2, Id3, Not, and Oct 25 as potential paternal scaling factors.

X. tropicalis Transcription Factors Hes7 and Ventx2 Reduce Body Length in Tailbud Stage *X. laevis* Embryos

To test whether identified candidate transcription factors were responsible for reducing the size of hybrid embryos, we mimicked overexpression of each transcription factor (as in the $l_e \times t_s$ hybrid) by microinjecting mRNA encoding each *X. tropicalis* candidate gene into fertilized one-cell *X. laevis* embryos. Cell and nuclear size were assessed in embryos fixed for immunofluorescence around the time of ZGA (10 h post-fertilization, ∼ stage 10) and several hours post ZGA (24 h post-fertilization, ∼ stage 21). Head to tail body length was measured at late tailbud stage, 48 h post-fertilization (**Figure 4A**). Two candidate transcription factors, Hes7 and Ventx2, significantly reduced overall body length (**Figures 4B,C**). Interestingly, the body length of embryos injected with Hes7 or Ventx2 was not significantly different from the body length in the $l_e \times t_s$ hybrid ($p = 0.64$ and $p = 0.48$, respectively; two-tailed heteroscedastic *t*-test). It is not clear whether this effect is due to the level of overexpression, or to sequences differences between *X. laevis* and *X. tropicalis* proteins. Sequence comparisons revealed that *X. laevis* homeologs from L and S chromosomes share approximately 90% similarity, while the *X. tropicalis* Ventx2 and Hes7 from *X. tropicalis* are ∼85% similar to the *X. laevis* proteins (**Supplementary Figures S1A,B**). The reduction in body length was however not accompanied by a change in nuclear to cell size scaling relationships as significant as that observed in the $l_e \times t_s$ hybrid (**Supplementary Figures S2A,B**). To test whether co-expression of both genes had an additive or synergistic effect, Hes7 and Ventx2 were co-injected. This caused embryo death (27.39 ± 9.25% lethality on average) with viable embryos more similar in size distribution to Ventx2 than to Hes7-injected embryos (**Supplementary Figure S2C**; $p = 0.18$ and $p = 0.04$, respectively, two-tailed heteroscedastic *t*-test). We also observed significant embryo death in Sia2-injected embryos (to 100% by 48 h post-fertilization), preventing measurement at tailbud stage. Embryo death may be due to higher levels of Sia2 expression in injected embryos compared to the hybrid. However, neither nuclear nor cell size at stage 10 or 21 was altered as observed in hybrid embryos, indicating that death was not due to size scaling defects (**Supplementary Figure S2D**). Altogether, while the screen did not reveal factors that significantly affected cell and nuclear size, overexpression of either *X. tropicalis* Hes7 and Ventx2 resulted in a decrease in embryo size that could potentially contribute to organism size scaling in $l_e \times t_s$ hybrids.

DISCUSSION

Little is known about how organisms scale in size and how size scaling is coordinated at the organismal, cellular, and subcellular levels. Uniquely, between the frogs *X. laevis* and *X. tropicalis,* linear size scaling is observed at the level of the genome, subcellular structures, cell, and organism. The specific factors that influence this phenomenon are unknown.

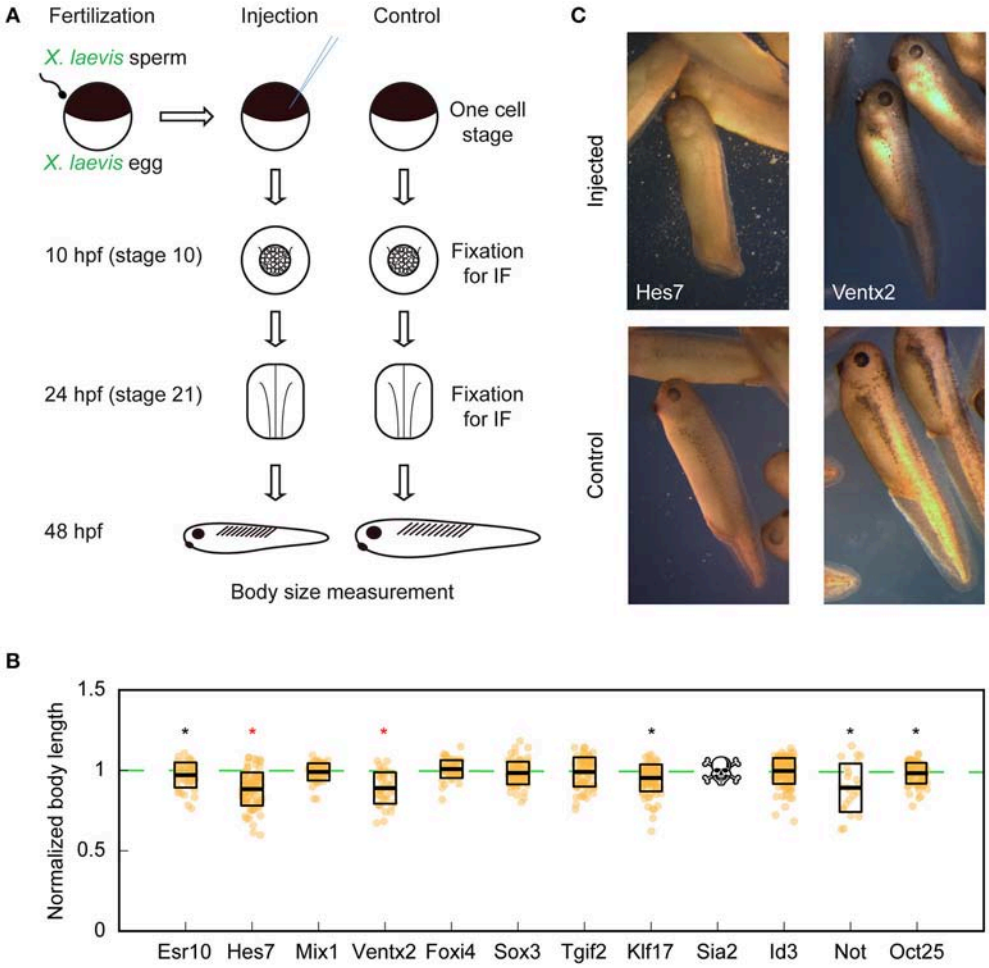

FIGURE 4 | Organismal size in *X. laevis* embryos upon overexpression of candidate *X. tropicalis* transcription factors. **(A)** Workflow of candidate scaling factor screen. **(B)** Body length of tailbud stage injected *X. laevis* embryos. Thick line inside box = average length, upper and lower box boundaries = ±SD. Stars indicate the significance of the pooled results of 3 experiments with $p < 0.05$ (two-tailed heteroscedastic *t*-test). Red coloring indicates significance of each 3 individual technical replicates with $p < 0.05$ (two-tailed heteroscedastic *t*-test). Reduced number of measured embryos in Not is due to the fact that, overall, 67.5% of injected-embryos exogastrulated, indicating a developmental defect. **(C)** Representative images of injected *X. laevis* embryos 48 h post-fertilization. Hes7- (left) and Ventx2-injected (right) are shown (top) with corresponding controls (bottom). Images are at identical scale.

Generating viable $l_e \times t_s$ hybrids intermediate in genome size, cell size, and body size between *X. laevis* and *X. tropicalis* allowed us to examine whether size scaling in *Xenopus* results from differences in genome size alone, or whether gene expression plays a role. While genome size clearly correlates with cell and organism size in $l_e \times t_s$ hybrids, other factors likely influence these parameters. Even though the genome size of the $l_e \times t_s$ hybrid is closer to that of a wild type *X. laevis* embryo, the nuclear to cell size scaling curve tracked more closely with that of haploid *X. laevis* embryos. Moreover, changes in nuclear to cell size ratios in $l_e \times t_s$ hybrids began at zygotic genome activation, rather than in the early cleaving embryo, which lacks transcription and growth phases. It is therefore likely that size scaling in hybrids is at least in part a consequence of *X. tropicalis* paternal gene expression rather than from reduced genome size alone.

Two transcription factors from our screen, Ventx2 and Hes7, caused a significant decrease in body length, but did not cause a change in nuclear to cell size scaling as observed in the hybrid. Reduced head-to-tail body length may be caused by different mechanisms. Ventx transcription factors have been observed to maintain pluriopotency and inhibit cell differentiation during *Xenopus* embryogenesis (Scerbo et al., 2012). Therefore, overexpression may cause a developmental delay that interferes with tissue growth. Moreover, these transcription factors may affect only specific regions of the embryo. For example, in Hes7 injected embryos, tail length is shortened, whereas head and body length remain similar to *X. laevis* controls. Hes7 is essential for regulating somite segmentation in vertebrates via oscillatory expression in presomitic mesoderm. Dampening Hes7 oscillations either by deleting or overexpressing Hes7 causes somite fusion (Bessho et al., 2003; Takashima et al., 2011) which

shortens tail length in mice (Hirata et al., 2004). Interestingly, mutation of Hes7 is similarly implicated in shortening tail length in cats (Xu et al., 2016) and miniaturization of dogs (Willet et al., 2015). It is also involved in human diseases such as spondylocostal dysostosis, which causes abnormal fusion of the bones of the ribs and spine, leading to a type of dwarfism characterized by a short trunk with normal-length arms and legs (Sparrow et al., 2013).

What then precisely regulates cell and subcellular scaling in $l_e \times t_s$ hybrids, and how can gene expression influence these parameters? We propose a model whereby cell size in *Xenopus* is largely dictated by genome size, but can be "fine-tuned" by differential gene expression. Such differential gene expression can also influence organism size, which may be uncoupled from cell size. Our study illustrates an example of both a unique model system and a screening approach to study biological size control and scaling. Future experiments will take advantage of the improving *Xenopus* genome assemblies to identify and screen other candidate genes, particularly those involved in other biological processes such as growth factor signaling and cell proliferation.

MATERIALS AND METHODS

Xenopus Frogs

All animal handling and procedures were performed according to the Animal Use Protocol approved by the UC Berkeley Animal Care and Use Committee. Mature *X. laevis* and *X. tropicalis* frogs were obtained from NASCO (Fort Atkinson, WI).

Generation of Viable *Xenopus* $l_e \times t_s$ Hybrid Embryos

X. laevis females were primed with 100 IU of pregnant mare serum gonadotropin (PMSG, National Hormone and Peptide Program, Torrance, CA) at least 48 h before use and boosted with 500 IU of HCG (Human Chorionic Gonadotropin CG10, Sigma) 14–16 h before experiments. *X. tropicalis* males were primed with 250 IU of HGC 24 h before dissection. To obtain testes, *X. tropicalis* males were euthanized by anesthesia through immersion in double-distilled (dd)H_2O containing 0.15% MS222 (tricaine) neutralized with 5 mM sodium bicarbonate before dissection. Testes were collected in Leibovitz L-15 media (Gibco – Thermo Fisher Scientific, Waltham, MA) supplemented with 10% Fetal Bovine Serum (FBS; Gibco), and stored at room temperature until fertilization. To prepare the sperm solution, one testis was added to 1 mL of ddH_2O in a 1.5 mL microcentrifuge tube, and homogenized using scissors and a pestle. *X. laevis* females were squeezed gently to deposit eggs onto petri dishes coated with 1.5% agarose in 1/10X MMR. Any liquid in the petri dishes was removed and the eggs were fertilized with 1 mL of sperm solution per dish. Fertilized embryos were swirled in the solution to form a monolayer on the bottom of the petri dish and incubated for 10 min with the dish slanted to ensure submersion of eggs. Dishes were then flooded with 1/10X MMR, swirled and incubated for 10 min. To remove egg jelly coats, the 1/10X MMR was completely exchanged for freshly prepared Dejellying Solution (2% L-cysteine in ddH_2O-NaOH, pH 7.8). After dejellying, eggs were washed extensively (>4X) with 1/10X MMR before incubation at 23°C. At Nieuwkoop and Faber stage 2–3, fertilized embryos were sorted and placed in fresh 1/10X MMR in new petri dishes coated with 1.5% agarose in 1/10X MMR.

Confirmation of Presence of Both *X. laevis* and *X. tropicalis* Genomes in $l_e \times t_s$ Hybrids

Genomic DNA was extracted from $l_e \times t_s$ hybrid embryos by incubating overnight in lysis buffer (50 mM Tris-HCl, 5 mM EDTA, 100 mM NaCl, 0.5% SDS) containing 250 µg/mL Proteinase K (Roche, Basel, Switzerland). DNA was isolated using Phenol-Chloroform extraction and ethanol precipitation. The genomic DNA was used as a PCR template for a single pair of primers that amplify a specific locus that differs ∼100 bp in size between all 3 (sub)genomes. In *X. tropicalis,* the locus is on chromosome 5 and PCR product size is 510 bp. In *X. laevis*, one locus is on chromosome 5L for which the PCR product size is 408 bp and another one is on chromosome 5S for which the PCR product size is 305 bp. The sequences of the primer pair are fwd GTACTCTTCCCCAGCTTGCTG and rev GCCTGTATGGCTCCTAGGTTTTC.

Generation of Wild Type *X. laevis* Embryos for Microinjection

Ovulations, euthanasias, dissections, and fertilizations were carried out as described above for $l_e \times t_s$ hybrids above, with the following modifications: *X. laevis* males were primed by injecting 500 IU of HCG 24 h before dissection. Dissected testes were collected in 1X Modified Ringer (MR) (100 mM NaCl, 1.8 mM KCl, 1 mM MgCl2, 5 mM HEPES-NaOH pH 7.6 in ddH_2O), and stored at room temp for short periods, or at 4°C for up to 5 days. To make sperm solution, 1/3–1/2 of a testis was added to 1 mL of ddH_2O in a 1.5 mL microcentrifuge tube.

Generation of Haploid *X. laevis* Embryos

Euthanasia of males and dissection/collection of testes proceeded as described for *X. laevis* males above. 1/3–1/2 of a testis was added to 1.1 mL of ddH_2O in a 1.5 mL microcentrifuge tube and homogenized with scissors and a pestle. The tube was briefly centrifuged using a benchtop microcentrifuge for several seconds to pellet large pieces of tissue. One mL of supernatant was removed, avoiding pieces of tissue, and transferred to a non-coated glass petri dish. The open dish was placed into a UV-Crosslinker (Stratalinker, Stratagene) and the sperm solution irradiated twice using 30,000 microjoules. The solution was swirled between the two irradiations. The irradiated sperm solution was then retrieved and used for fertilization by depositing at least 0.5 mL solution on top of freshly squeezed *X. laevis* eggs in a petri dish coated with 1.5% agarose in 1/10x MMR. Fertilization, dejelly, and embryo storage then proceeded as described for $l_e \times t_s$ hybrid embryos above.

Embryo Video Imaging

Imaging dishes were prepared using a homemade PDMS mold designed to print a pattern of 1 mm large wells in agarose

that allowed us to image 4 embryos simultaneously within the 3 × 4 mm camera field of view for each type of embryo. Embryos were imaged from stage 2. *X. laevis* and $l_e \times t_s$ hybrid or haploid videos were taken simultaneously using two AmScope MD200 USB cameras, (AmScope, Irvine, CA) each mounted on an AmScope SE305R stereoscope. Time lapse movies were acquired at a frequency of 1 frame every 10 s for 20 h and saved as Motion JPEG using a MATLAB (The MathWorks, Inc., Natick, MA) script. Movie post-processing (cropping, concatenation, resizing, addition of scale bar) was done using MATLAB and Fiji (Schindelin et al., 2012). All MATLAB scripts written for this study are available upon request. Two of the scripts used here were obtained through the MATLAB Central File Exchange: "videoMultiCrop" and "concatVideo2D" by Nikolay S.

Imaging and Measurement of Tailbud, Tadpole, and Frog Body Size

Tailbud stage embryos were placed in an ice-cold agarose-coated imaging chamber and imaged at 12× magnification using a Wild Heerbrugg M7A StereoZoom microscope coupled to a Leica MC170HD camera and Leica LAS X software. Tadpoles were imaged by placing in a petri dish filled with a limited amount of water to prevent depth-biased measurements. Images were taken with an iphone camera, including a ruler in the field of view. Tadpole measurements were stopped when the tail began to recede at the end of metamorphosis. Froglets were placed in a transparent-bottom container placed on a ruler and fill with a minimal amount of water, and imaged with an iphone camera. Images were analyzed and length measured head to tail for tadpoles, or head to cloaca for froglets. Length measurements were done using the line tool in Fiji.

Erythrocyte Preparation and Measurements

A small drop of blood was collected from the frog foot with a sterile needle, and the drop was smeared on a slide. The smear was then fixed with methanol and stained with Giemsa stain (Sigma GS). Cell were imaged in brightfield using micromanager software (Edelstein et al., 2014) with an Olympus BX51 microscope equipped with an ORCA-II camera (Hamamatsu Photonics, Hamamatsu city, Japan).

RNA Isolation and Sequencing

To isolate RNA, embryos at stage 9 were homogenized mechanically in TRIzol® (Thermo Fisher Scientific, Waltham, MA) using up to a 30-gauge needle and processed according to manufacturer instructions. After resuspension in nuclease-free H2O, RNAs were cleaned using a RNeasy kit (Qiagen Inc.) according to manufacturer instructions. Libraries were prepared using manufacturer's non-standard specific RNA-seq library protocol with poly-A capturing mRNA enrichment method (Illumina, CA, USA). The paired-end 2 × 100 bp reads were generated by the Genome Sequencing and Analysis Facility (GSAF) at the University of Texas at Austin using Illumina HiSeq 2000. Transcriptome data generated in this study are available from NCBI Gene Expression Omnibus (Series record GSE118382).

Gene Expression Analysis

We mapped RNA-seq reads to the database of combined *X. laevis* and *X. tropicalis* transcriptome (available at http://genome.taejoonlab.org/pub/xenopus/annotation/; WorldCup_201407 version), using Bowtie1 (version 1.0). To prevent misalignment to other species, we applied stringent criteria, allowing no mismatches (–v 0), and ignoring a read mapped more than one target (–m 1). We estimated relative transcript abundance with "transcripts per million reads (TPM)" calculated by RSEM (version 1.2.19), and differential expression analysis was conducted using edgeR (version 3.36.1), with greater than 2-fold changes and false discovery rate (FDR) less than 0.05 cutoff to determine the significance.

Gene Ontology Analysis

We conducted Gene Ontology analysis with Panther DB (version 13.1). For statistical analysis for overrepresented terms, we used Fischer's exact test and FDR adjustment, and applied FDR <0.05 as a significance cutoff. To validate our list of candidates, we searched Xenbase (http://www.xenbase.org/) using the gene name as the query.

Cloning and mRNA Synthesis of Candidate Transcription Factors

Total RNA was isolated from *X. tropicalis* embryos as described above in "RNA isolation and sequencing," and cDNA was synthesized from RNA using the SuperScript III First Strand Synthesis system (Invitrogen- Thermo Fisher Scientific, Waltham, MA) according to manufacturer instructions. Transcription factor sequences were then PCR-amplified from the cDNA using the following primer sequences (all are written 5′-3′) concatenated with ∼30 bp plasmid-homologous sequences: Esr10, fwd ATGGCTCCTTACAGCGCTAC, rev TTCTCTGGAGACCCTGGAAC; Sox3, fwd ATGTATAGCATG TTGGACAC, rev CTGTACCGCTCACTCACATA; Foxi4.2, fwd ATGAACCCAGTCCAGCAACC, rev CTTTGTACCAGG GAAGGTAC; Hes7.1, fwd ATGAAGGGAGCGAGTGAAGT, rev AGACCTGGAGACCTTGGGTA; Mix1, fwd ATGGAC TCATTCAGCCAACA, rev TCTGTGTGCTCCTCCACCTT; Tgif2, fwd ATGATGAATTCGACTTTTGA, rev TCACGA CAAGCACCCCCAAT; Ventx2.1, fwd ATGAACACAAGG ACTACTAC, rev TTGGGCAGCCTCTGGCCTAC; Klf17, fwd ATGAGTGTGGCTTTCTCAAC, rev CATGTGTCTCTTCAT GTGCAG; Not, fwd ATGTTACACAGCCCTGTCTTTC, rev CAGTTCAACATCCACATCATC; Oct25 fwd ATGTACAGC CAACAGCCCTTC, rev ACCAATATGGCCGCCCATGG; Sia2 fwd ATGACTTGTGACTCTGAGCTTG, rev GCCCCACAT ATCCGGATATTG; Id3 fwd ATGAAAGCCATCAGCCCA GTG, rev GTGGCAGACACTGGCGTCCC. These amplified sequences were then subcloned using Gibson assembly (New England Biolabs, Ipswich, MA) into a PCS2 expression vector obtained at the 2013 Advanced Imaging in *Xenopus* Workshop from the Wallingford lab (UT Austin, USA). mRNAs were synthetized from these expression constructs using mMessage

mMachine SP6 Transcription Kit (Ambion – Thermo Fisher Scientific, Waltham, MA) following the manufacturer protocol. The mRNAs were then purified using Phenol-Chloroform extraction, resuspended in ddH_2O, aliquoted and stored at −80°C.

Microinjection of Candidate Transcription Factors Into *Xenopus* Embryos

Stage 1 (one-cell) embryos about 30 min post-fertilization were transferred into a mesh-bottom dish containing 1/9X MMR 3% Ficoll for microinjection. Injections were done using a Picospritzer III microinjection system (Parker, Hollis, NH) equipped with a MM-3 micromanipulator (Narishige, Amityville, NY). To mimic overexpression of each transcription factor, each embryo was injected with 750 picograms of mRNA, a dose we determined was large enough to see phenotypes, but was not associated with embryo toxicity. Injected embryos were transferred to a new dish coated with 1.5% agarose in 1/10x MMR, and incubated at 23°C in 1/9X MMR 3% Ficoll for at least 6 h. The embryos were then transferred to fresh 1/10x MMR in a new agarose-coated dish, and incubated at 23°C with buffer changes into fresh 1/10x MMR several times daily until ready for fixation or imaging.

Embryo Whole Mount Immunofluorescence

Embryos at the desired developmental stage were fixed for 1 h using MAD fixative (2 parts methanol [Thermo Fisher Scientific, Waltham, MA], 2 parts acetone [Thermo Fisher Scientific, Waltham, MA]), 1 part DMSO [Sigma]). After fixation, embryos were dehydrated in methanol and stored at −20°C. Embryos were then processed as previously described (Lee et al., 2008) with modifications. Following gradual rehydration in 0.5× SSC (1X SSC: 150 mM NaCl, 15 mM Na citrate, pH 7.0), embryos were bleached with 1–2% H_2O_2 (Thermo Fisher Scientific, Waltham, MA) in 0.5× SSC containing 5% formamide (Sigma) for 2–3 h under light, then washed in PBT (137 mM NaCl, 2.7 mM KCl, 10 mM Na_2HPO_4, 0.1% Triton X-100 [Thermo Fisher Scientific, Waltham, MA]) and 2 mg/mL bovine serum albumin (BSA). Embryos were blocked in PBT supplemented with 10% goat serum (Gibco–Thermo Fisher Scientific, Waltham, MA) and 5% DMSO for 1–3 h and incubated overnight at 4°C in PBT supplemented with 10% goat serum and primary antibodies. The following antibodies were used to label tubulin and DNA, respectively: 1:500 mouse anti-beta tubulin (E7; Developmental Studies Hybridoma Bank, Iowa City, IA), and 1:500 rabbit anti-histone H3 (ab1791; Abcam, Cambridge, MA). Embryos were then washed 4 × 2 h in PBT and incubated overnight in PBT supplemented with 1:500 goat anti-mouse or goat anti-rabbit secondary antibodies coupled either to Alexa Fluor 488 or 568 (Invitrogen–Thermo Fisher Scientific, Waltham, MA). Embryos were then washed 4 × 2 h in PBT and gradually dehydrated in methanol. Embryos were cleared in Murray's clearing medium (2 parts of Benzyl Benzoate, 1 part of Benzyl Alcohol).

Confocal Imaging and Measurement of Embryos, Cells and Nuclei After Whole Mount Immunofluorescence

Embryos were placed in a chamber made using a flat nylon washer (Grainger, Lake Forest, IL) attached with nail polish (Sally Hansen, New York, NY) to a slide, filled with Murray's clearing medium, and covered by a coverslip (Beckman coulter, Brea, CA) for confocal microscopy. Confocal microscopy was performed on a Zeiss LSM 780 NLO AxioExaminer running the Zeiss Zen Software. Embryos were imaged using a Plan-Apochromat 20 × /1.0 water objective and laser power of 12%, on multiple 1024 × 1024 pixel plans spaced 0.68 μm apart in Z.

Nuclear area was measured in Fiji using the ellipse tool. From this, we calculated the diameter of a circle of the same area, a value that we could directly compare the cell size determined through the measurement of the cell diameter at the nucleus central plane. To test whether the nuclear to cell size scaling significantly depends on the embryo types or whether embryos were microinjected or not, we ran an analysis of covariance (ANOCOVA test) using the 'aoctool' in MATLAB with a "separate lines" model.

Protein Sequence Alignments

Multiple sequence alignments were performed using Clustal Omega (default parameters). Sequence identities and similarities were determined by pairwise alignments using EMBOSS Needle (default parameters).

AUTHOR CONTRIBUTIONS

RH and RG designed the project. RG and RA characterized and measured nuclear and cell sizes in hybrids and haploids. TK performed the transcriptome analysis. KM and RG cloned the candidates and conducted the screen. KM measured nuclear and cell sizes in injected embryos. KM wrote the manuscript with inputs from RH and RG.

FUNDING

RG was initially supported by EMBO long-term fellowship ALTF 836-2013 and for most of this project by Human Frontier Science Program long-term fellowship LT 0004252014-L. KM was supported by the National Science Foundation Graduate Research Fellowship Program and National Institutes of Health training grant 2T32GM007232-36. RA was supported in part by a National Science Foundation REU Summer Fellowship in 2014. TK was supported by the Basic Science Research Program through the National Research Foundation of Korea funded by the Ministry of Science, ICT and Future Planning (NRF-2016R1C1B2009302), and the UNIST Research Fund (grant number 1.180063.01). RH was supported by NIH MIRA grant R35 GM118183 and the Flora Lamson Hewlett Chair. The confocal microscopy performed in this work was done at the UC Berkeley CRL Molecular Imaging Center, supported by National Science Foundation DBI-1041078.

ACKNOWLEDGMENTS

We thank members of the Heald laboratory, present and past, for support and discussions, especially C. Cadart for critical reading of the manuscript. We thank E. M. Marcotte and colleagues at the Genome Sequencing and Analysis Facility (UT Austin) for RNA-seq analysis, and J. Chapman for assistance designing primers to loci on chromosome 5 for *X. laevis* and *tropicalis*. We also thank students K. Shih, M. Fitzsimmons, and S. Kawada for their dedicated assistance with experiments.

SUPPLEMENTARY MATERIAL

The Supplementary Material for this article can be found online at: https://www.frontiersin.org/articles/10.3389/fphys.2018.01758/full#supplementary-material

Supplementary Figure S1 | Protein sequence alignments of *Xenopus* Ventx2 and Hes7. **(A)** Ventx2 protein sequences of *X. tropicalis*, *X. laevis* L, and S copies aligned using Clustal Omega. **(B)** Hes7 protein sequences of *X. tropicalis*, *X. laevis* L, and S copies aligned using Clustal Omega. For **(A,B)**, identities and similarities were calculated using EMBOSS Needle.

Supplementary Figure S2 | Nuclear to cell size relationships post-zygotic genome activation in injected *X. laevis* embryos. **(A)** Nuclear diameter vs. cell diameter in Ventx2-injected *X. laevis* embryos at stage 10 and 21. Analysis of covariance at stage 10 gave a *p*-value of 0.865 and at stage 21 of 0.016. **(B)** Nuclear diameter vs. cell diameter in Hes7-injected *X. laevis* embryos at stage 10 and 21. Analysis of covariance at stage 10 gave a *p*-value of 0.820 and at stage 21 of 0.077. **(C)** Normalized body length of tailbud stage *X. laevis* embryos co-injected with Ventx2 and Hes7 (top). Percent fatality in Ventx2 and Hes7 co-injected embryos (bottom). Embryos were injected with 375 pg mRNA of each factor for a total injection of 750 pg. Thick line inside box = average length, upper, and lower box boundaries = ±SD. **(D)** Nuclear diameter vs. cell diameter in Sia2 injected *X. laevis* embryos at stages 10 and 21. Analysis of covariance at stage 10 gave a *p*-value of 0.171 and at stage 21 of 0.497.

Supplementary Table S1 | Significantly differentially expressed transcripts in $l_e \times t_s$ hybrids compared to *X. laevis* embryos.

Supplementary Movie S1 | Characterization of $l_e \times t_s$ hybrid embryo development. *X. laevis* vs. $l_e \times t_s$ *X. laevis* eggs were fertilized with *X. laevis* (left) or *X. tropicalis* sperm (right). and simultaneously imaged in separate dishes. The video plays 20 h in 12 s (rate of 120 fps) and the scale bar corresponds to 200 μm.

Supplementary Movie S2 | Characterization of haploid *X. laevis* embryo development. *X. laevis* vs. haploid *X. laevis*. *X. laevis* eggs were fertilized with *X. laevis* (left) or irradiated *X. laevis* sperm (right) and simultaneously imaged in separate dishes. The video plays 20 h in 12 s (rate of 120 fps) and the scale bar corresponds to 200 μm.

REFERENCES

Bessho, Y., Hirata, H., Masamizu, Y., and Kageyama, R. (2003). Periodic repression by the bHLH factor Hes7 is an essential mechanism for the somite segmentation clock. *Genes Dev.* 17, 1451–1456. doi: 10.1101/gad.1092303

Björklund, M., Taipale, M., Varjosalo, M., Saharinen, J., Lahdenperä, J., and Taipale, J. (2006). Identification of pathways regulating cell size and cell-cycle progression by RNAi. *Nature* 439, 1009–1013. doi: 10.1038/nature04469

Brown, K. S., Blower, M. D., Maresca, T. J., Grammer, T. C., Harland, R. M., and Heald, R. (2007). *Xenopus tropicalis* egg extracts provide insight into scaling of the mitotic spindle. *J. Cell Biol.* 176, 765–770. doi: 10.1083/jcb.200610043

Bürki, E. (1985). The expression of creatine kinase isozymes in *Xenopus tropicalis, Xenopus laevis* laevis, and their viable hybrid. *Biochem. Genet.* 23, 73–88.

Cavalier-Smith, T. (2005). Economy, speed and size matter: evolutionary forces driving nuclear genome miniaturization and expansion. *Ann Bot.* 147–175. doi: 10.1093/aob/mci010

Edelstein, A. D., Tsuchida, M., a, Amodaj, N., Pinkard, H., Vale, R. D., and Stuurman, N. (2014). Advanced methods of microscope control using μManager software. *J. Biol. Methods* 1:e10. doi: 10.14440/jbm.2014.36.

Elurbe, D. M., Paranjpe, S. S., Georgiou, G., van Kruijsbergen, I., Bogdanovic, O., Gibeaux, R., et al. (2017). Regulatory remodeling in the allo-tetraploid frog *Xenopus laevis*. *Genome Biol.* 18:198. doi: 10.1186/s13059-017-1335-7

Frawley, L. E., and Orr-Weaver, T. L. (2015). Polyploidy. *Curr. Biol.* 25, R353–R358. doi: 10.1016/j.cub.2015.03.037

Galitski, T., Saldanha, A. J., Styles, C. A., Lander, E. S., and Fink, G. R. (1999). Ploidy regulation of gene expression. *Science* 285, 251–254. doi: 10.1126/science.285.5425.251

Gibeaux, R., Acker, R., Kitaoka, M., Georgiou, G., Van Kruijsbergen, I., Ford, B., et al. (2018). Paternal chromosome loss and metabolic crisis contribute to hybrid inviability in Xenopus. *Nature* 553, 337–341. doi: 10.1038/nature25188

Good, M. C., Vahey, M. D., Skandarajah, A., Fletcher, D. A., and Heald, R. (2013). Cytoplasmic volume modulates spindle size during embryogenesis. *Science* 342, 856–860. doi: 10.1126/science.1243147

Gregory, T. R. (2001). Coincidence, coevolution, or causation? DNA content, cell size, and the C-value enigma. *Biol. Rev. Camb. Philos. Soc.* 76, 65–101. doi: 10.1111/j.1469-185X.2000.tb00059.x

Hamilton, L. (1957). Androgenic haploids of a toad, *Xenopus laevis*. *Nature* 179:159. doi: 10.1038/179159a0

Hamilton, L. (1963). An experimental analysis of the development of the haploid syndrome in embryos of *Xenopus laevis*. *J. Embryol. Exp. Morphol.* 11, 267–278.

Hirata, H., Bessho, Y., Kokubu, H., Masamizu, Y., Yamada, S., Lewis, J., et al. (2004). Instability of Hes7 protein is crucial for the somite segmentation clock. *Nat. Genet.* 36, 750–754. doi: 10.1038/ng1372

James-Zorn, C., Ponferrada, V. G., Jarabek, C. J., Burns, K. A., Segerdell, E. J., Lee, J., et al. (2012). Xenbase: expansion and updates of the Xenopus model organism database. *Nucleic Acids Res.* 41(Database issue), D865–D870. doi: 10.1093/nar/gks1025

Karimi, K., Fortriede, J. D., Lotay, V. S., Burns, K. A., Wang, D. Z., Fisher, M. E., et al. (2018). Xenbase: a genomic, epigenomic and transcriptomic model organism database. *Nucleic Acids Res.* 46, D861–D868. doi: 10.1093/nar/gkx936

Kitaoka, M., Heald, R., and Gibeaux, R. (2018). Spindle assembly in egg extracts of the Marsabit clawed frog, *Xenopus borealis*. *Cytoskeleton* 75, 244–267. doi: 10.1002/cm.21444

Lee, C., Kieserman, E., Gray, R. S., Park, T. J., and Wallingford, J. (2008). Whole-mount fluorescence immunocytochemistry on Xenopus embryos. *CSH Protoc.* 2008:pdb.prot4957. doi: 10.1101/pdb.prot4957

Lee, H. O., Davidson, J. M., and Duronio, R. J. (2009). Endoreplication: polyploidy with purpose. *Genes Dev.* 23, 2461–2477. doi: 10.1101/gad.1829209

Levy, D. L., and Heald, R. (2010). Nuclear size is regulated by importin α and Ntf2 in Xenopus. *Cell* 143, 288–298. doi: 10.1016/j.cell.2010.09.012

Lindsay, L. L., Peavy, T. R., Lejano, R. S., and Hedrick, J. L. (2003). Cross-fertilization and structural comparison of egg extracellular matrix glycoproteins from *Xenopus laevis* and *Xenopus tropicalis*. *Comp. Biochem. Physiol. Part A Mol. Integr. Physiol.* 136, 343–352. doi: 10.1016/S1095-6433(03)00169-7

Loughlin, R., Wilbur, J. D., McNally, F. J., Nedelec, F. J., and Heald, R. (2011). Katanin contributes to interspecies spindle length scaling in xenopus. *Cell* 147, 1397–1407. doi: 10.1016/j.cell.2011.11.014

Marguerat, S., and Bähler, J. (2012). Coordinating genome expression with cell size. *Trends Genet.* 28, 560–565. doi: 10.1016/j.tig.2012.07.003

Marguerat, S., Schmidt, A., Codlin, S., Chen, W., Aebersold, R., and Bähler, J. (2012). Quantitative analysis of fission yeast transcriptomes and proteomes in proliferating and quiescent cells. *Cell* 151, 671–683. doi: 10.1016/j.cell.2012.09.019

Mirsky, A. E. (1951). The desoxyribonucleic acid content of animal cells and its evolutionary significance. *J. Gen. Physiol.* 34, 451–462. doi: 10.1085/jgp.34.4.451

Narbonne, P., Simpson, D. E., and Gurdon, J. B. (2011). Deficient induction response in a Xenopus nucleocytoplasmic hybrid. *PLoS Biol.* 9: e1001197. doi: 10.1371/journal.pbio.1001197

Neumann, F. R., and Nurse, P. (2007). Nuclear size control in fission yeast. *J. Cell Biol.* 179, 593–600. doi: 10.1083/jcb.200708054

Nieuwkoop, P. D., and Faber, J. (1994). *Normal Table of Xenopus laevis (Daudin)*. New York, NY: Garland Publishing Inc.

Scerbo, P., Girardot, F., Vivien, C., Markov, G. V., Luxardi, G., Demeneix, B., et al. (2012). Ventx factors function as Nanog-like guardians of developmental potential in Xenopus. *PLoS ONE* 7:e36855. doi: 10.1371/journal.pone.0036855

Schindelin, J., Arganda-Carreras, I., Frise, E., Kaynig, V., Longair, M., Pietzsch, T., et al. (2012). Fiji: an open-source platform for biological-image analysis. *Nat. Methods* 9, 676–682. doi: 10.1038/nmeth.2019

Sparrow, D. B., Faqeih, E. A., Sallout, B., Alswaid, A., Ababneh, F., Al-Sayed, M., et al. (2013). Mutation of HES7 in a large extended family with spondylocostal dysostosis and dextrocardia with situs inversus. *Am. J. Med. Genet. Part A* 161, 2244–2249. doi: 10.1002/ajmg.a.36073

Taft, R. J., Pheasant, M., and Mattick, J. S. (2007). The relationship between non-protein-coding DNA and eukaryotic complexity. *Bioessays* 29, 288–299. doi: 10.1002/bies.20544

Takashima, Y., Ohtsuka, T., Gonzalez, A., Miyachi, H., and Kageyama, R. (2011). Intronic delay is essential for oscillatory expression in the segmentation clock. *Proc. Natl. Acad. Sci. U.S.A.* 108, 3300–3305. doi: 10.1073/pnas.1014418108

Wilbur, J. D., and Heald, R. (2013). Mitotic spindle scaling during Xenopus development by kif2a and importin α. *Elife* 2:e00290. doi: 10.7554/eLife.00290

Willet, C. E., Makara, M., Reppas, G., Tsoukalas, G., Malik, R., Haase, B., et al. (2015). Canine disorder mirrors human disease: exonic deletion in HES7 causes autosomal recessive spondylocostal dysostosis in miniature schnauzer dogs. *PLoS ONE* 10:e0117055. doi: 10.1371/journal.pone.0117055

Xu, X., Sun, X., Hu, X. S., Zhuang, Y., Liu, Y. C., Meng, H., et al. (2016). Whole genome sequencing identifies a missense mutation in HES7 associated with short tails in Asian Domestic cats. *Sci. Rep.* 6:31583. doi: 10.1038/srep31583

Conflict of Interest Statement: The authors declare that the research was conducted in the absence of any commercial or financial relationships that could be construed as a potential conflict of interest.

frontiers in Physiology

PERSPECTIVE
published: 01 February 2019
doi: 10.3389/fphys.2019.00048

Xenopus tropicalis: Joining the Armada in the Fight Against Blood Cancer

Dionysia Dimitrakopoulou[1,2], *Dieter Tulkens*[1,2], *Pieter Van Vlierberghe*[2,3] and *Kris Vleminckx*[1,2,3]*

[1] Department of Biomedical Molecular Biology, Ghent University, Ghent, Belgium, [2] Cancer Research Institute Ghent (CRIG), Ghent, Belgium, [3] Department of Biomolecular Medicine, Ghent University, Ghent, Belgium

Aquatic vertebrate organisms such as zebrafish have been used for over a decade to model different types of human cancer, including hematologic malignancies. However, the introduction of gene editing techniques such as CRISPR/Cas9 and TALEN, have now opened the road for other organisms featuring large externally developing embryos that are easily accessible. Thanks to its unique diploid genome that shows a high degree of synteny to the human, combined with its relatively short live cycle, *Xenopus tropicalis* has now emerged as an additional powerful aquatic model for studying human disease genes. Genome editing techniques are very simple and extremely efficient, permitting the fast and cheap generation of genetic models for human disease. Mosaic disruption of tumor suppressor genes allows the generation of highly penetrant and low latency cancer models. While models for solid human tumors have been recently generated, genetic models for hematologic malignancies are currently lacking for *Xenopus.* Here we describe our experimental pipeline, based on mosaic genome editing by CRISPR/Cas9, to generate innovative and high-performing leukemia models in *X. tropicalis*. These add to the existing models in zebrafish and will extend the experimental platform available in aquatic vertebrate organisms to contribute to the field of hematologic malignancies. This will extend our knowledge in the etiology of this cancer and assist the identification of molecular targets for therapeutic intervention.

Keywords: *Xenopus*, CRISPR/Cas9, leukemia, T-ALL, genome editing, thymus, tumor suppressor genes, cancer

OPEN ACCESS

Edited by:
John Noel Griffin,
Duke University, United States

Reviewed by:
Jacques Robert,
University of Rochester Medical Center, United States
Ira Daar,
National Cancer Institute (NCI), United States

***Correspondence:**
Kris Vleminckx
kris.vleminckx@ugent.be

Specialty section:
This article was submitted to Embryonic and Developmental Physiology, a section of the journal Frontiers in Physiology

Received: *16 November 2018*
Accepted: *17 January 2019*
Published: *01 February 2019*

Citation:
Dimitrakopoulou D, Tulkens D, Van Vlierberghe P and Vleminckx K (2019) Xenopus tropicalis: Joining the Armada in the Fight Against Blood Cancer. Front. Physiol. 10:48. doi: 10.3389/fphys.2019.00048

INTRODUCTION

Xenopus laevis and *Xenopus tropicalis* have been used extensively in developmental and cell biology, biochemistry, functional genomics and immunology. Embryos develop externally and tadpoles are transparent, features that facilitate experimental manipulation and post-factum analysis of animals (Robert and Ohta, 2009; Banach and Robert, 2017). Interestingly, in contrast to *X. laevis* and teleosts, *X. tropicalis* has a true diploid genome with high conservation of gene synteny with the human genome (Hellsten et al., 2010), making it an attractive biomedical genetic model organism. The immune system of *Xenopus* demonstrates striking similarities to that of mammals and a considerable number of immunological studies have already been performed (Banach and Robert, 2017). Recent advances in genome editing technologies have now made it possible to efficiently

disrupt gene function in *Xenopus*, reinforcing it as an organism for modeling human disease, including the generation of solid tumor models (Van Nieuwenhuysen et al., 2015; Naert et al., 2016). Evidently, these genome editing strategies could also be applied for detailed studies in immunology and especially in generating models for hematologic malignancies. Here, we elaborate on strategies to generate and analyze hematologic malignancy models in *X. tropicalis*. We discuss how these *Xenopus* models can be applied for identifying driver and modifier genes and cancer dependency factors with possible therapeutic potential.

THE IMMUNE SYSTEM OF *XENOPUS TROPICALIS*

The innate immune system of *Xenopus* consists of the same cell types as mammals and their primary function is to eradicate infected cells. Neutrophils, basophils, eosinophils as well as polymorphonuclear cells, macrophages dendritic cells and lymphocytes have all been detected (Hadji-Azimi et al., 1987; Robert and Ohta, 2009; Neely et al., 2018). Toll like receptor (TLR) genes are present and execute the same role as their mammalian counterparts in recognizing pathogen-associated molecular patterns (PAMPs; Roach et al., 2005). *Xenopus* has NK cells that eliminate virally infected and cancer cells by cytotoxic activity (Horton et al., 2000; Horton et al., 2003). Furthermore, innate immunity includes the three activation pathways of the complement system (classical, alternative and lectin) as well as antimicrobial peptides secreted by the epidermal layers (Zasloff, 2002).

Also the overall pattern and function of adaptive immunity is conserved with mammals. Orthologs of all major mammalian immune genes have been identified (Schwager et al., 1988, 1991; Chretien et al., 1997; Shi and Ishizuya-Oka, 1997; Flajnik, 2018). IgM is widely expressed and, similar to IgX (homolog of mammalian *IgA*), its expression is not dependent on the thymus (Tochinai, 1976). In contrast, expression of IgY (homolog of IgG and IgE) is thymus dependent and is detected in the thymus, spleen and peripheral blood (Mussmann et al., 1998). Next to those three major Ig isotypes, IgD has been reported (Ohta et al., 2006; Flajnik, 2018). Accessory molecules like the B7 family (and B7 receptor) (Hansen et al., 2009), cytokines like the TNFSF family (and TNFSF receptor) (Bernard et al., 2007), IFN gamma and the interleukins IL-2, -6, -7, -17, -21 and -23 have all been identified (Qi and Nie, 2008). B cell receptors (BCR) recognize specific epitopes on foreign antigens and T-cell receptors (TCRs) recognize short peptides presented by MHC class I and II. CD4 and CD8 T cells recognize and bind to MHC class II and MHC class I epitopes, respectively. Naive T cells demand an extra stimulatory signal (by costimulatory molecules B7 and CD40) to execute an immunological response. Activated T cells propagate and differentiate into cytotoxic T lymphocytes and CD4 T helper cells. The latter release cytokines that act either on CD8 T cells and B cells, or directly on pathogens. After immunological response, the majority of T cells die through apoptosis, except for T memory cells, which orchestrate secondary immune responses.

Despite the similarities to mammals, there are some fundamental developmental differences that confer special features to the *Xenopus* immune system. (1) The fetal liver is the main site for hematopoiesis, unlike the bone marrow (BM) in mammals (Ciau-Uitz et al., 2014). In adult *Xenopus*, the BM functions as a reservoir pool (Robert and Ohta, 2009), while no BM is present in tadpoles (Du Pasquier et al., 2000). (2) Lymph nodes are absent in *Xenopus*, and the spleen functions as a major secondary lymphoid organ, which interestingly is deprived of germinal centers (GCs; Du Pasquier and Schwager, 1991; Du Pasquier et al., 2000; Neely et al., 2018). *Xenopus* also lack follicular dendritic cells but their function in the spleen is taken over by "double-duty" antigen presenting cells (Neely et al., 2018). (3) During metamorphosis, the thymus undergoes histolysis and 50–90% of thymic lymphocytes die (Du Pasquier and Weiss, 1973; Du Pasquier et al., 1989). The thymic remnants shift toward the tympanum and tissue is regenerated simultaneously with a second wave of lymphoid stem cells colonizing the renewed thymus (Bechtold et al., 1992; Robert and Ohta, 2009). Premature B cells diminish during metamorphosis and regenerate in the liver at Nieuwkoop stage 60. In adult life, the major site of B cell differentiation shifts from the liver to the spleen (Hadji-Azimi et al., 1987). The larval type BCR repertoire is less variable compared to the adult. This could be explained by deficiency of N-nucleotide diversity during BCR rearrangement (Du Pasquier et al., 2000). However, VH diversity is similar between larvae and adults (Du Pasquier et al., 2000). Even though the *Xenopus* spleen has no GCs, somatic hypermutation occurs in adults and larvae. As in mammals, αβ T cell differentiation is thymus dependent (Robert and Ohta, 2009). Little information is available regarding the TCR repertoire. However, the TCR gene rearrangements (both larvae and adult stage) exhibit many similarities to mammals (Robert et al., 2001).

Because of its unique and conserved features, *Xenopus* provided important insights concerning regulation of MHC expression and immunotolerance. MHC class expression differs between larvae and adult and thus affects differently the tolerance toward skin grafts (Du Pasquier and Flajnik, 1990; Rollins-Smith et al., 1997). Moreover, *Xenopus* is a reliable system for immune-cancer studies. *Xenopus* can develop lymphoid tumors from which cell lines have been derived (Du Pasquier and Robert, 1992; Robert et al., 1994). These cell lines have been obtained from different strains and exhibited differential tumorigenicity, which was attributed to divergent expression of MHC Ia and MHC Ib genes (Goyos et al., 2007).

HEMATOLOGIC MALIGNANCIES

Leukemia is among the leading cancers worldwide (Bray et al., 2018). In adult patients, the most frequent types are acute myeloid leukemia (AML) and chronic myeloid leukemia (CML). Acute lymphoblastic leukemia (ALL), a malignant transformation and propagation of lymphoid progenitor cells in the BM, peripheral blood and various extramedullary sites, affects both adults and children (Van Vlierberghe and Ferrando, 2012; Terwilliger and Abdul-Hay, 2017). Most incidences of ALL are derived

from the B cell lineage (B-ALL) while 25% of adult ALL and 15% of pediatric ALLs originate in the T cell lineage (T-ALL; You et al., 2015). B-ALL involves characteristic chromosomal translocations such as *t*(12;21) [*ETV6-RUNX1*], *t*(1;19) [*TCF3-PBX1*], *t*(9;22) [*BCR-ABL1*] and rearrangements of the MLL locus (Woo et al., 2014). T-ALL most frequent mutational events include activation of the Notch pathway, deregulation of cell cycle regulators and mutations in chromatin remodeling complexes (Van Vlierberghe and Ferrando, 2012). Although prognosis for B-ALL and T-ALL in general is good, still 15–20% of patients experience disease relapse (Cooper and Brown, 2015; You et al., 2015). In addition, patients often experience severe therapy related toxicities (Van Vlierberghe and Ferrando, 2012). Thus, identification of more effective and less toxic therapies is important. More effective therapies are also required for AML, where older patients, and those who exhibit relapsed disease, demonstrate poor prognosis (Dombret and Gardin, 2016). For CML patients treated with targeted therapies, like tyrosine kinase inhibitors, prognosis is significantly improved (Jabbour and Kantarjian, 2018). Animal models have already contributed majorly to leukemia research and have expanded the molecular biomedical knowledge, allowing the design, development and testing of novel anti-leukemic drugs.

GENETIC *XENOPUS TROPICALIS* MODELS FOR ALL

The majority of mouse ALL models have been generated by transgenic strategies or by cells transduced retrovirally to express mutant proteins or genomic aberrations (chromosomal translocations, activating and inactivating mutations) associated with ALL (Gutierrez et al., 2014; Jacoby et al., 2014; Kohnken et al., 2017). In addition, xenografts models of human ALL samples engrafted in immunocompromised mice have also been generated. Xenografts models enlighten topics that were previously difficult to address concerning ALL microenvironment, leukemic stem cells, prognostic markers and new therapeutic agents (Gopalakrishnapillai et al., 2016). The last decade has also seen the emergence of leukemia models in zebrafish, mostly mediated by mosaic transgenic expression of oncogenes such as MYC in the lymphocytic lineage. However, details regarding the established murine and zebrafish ALL models go beyond the scope of this perspective.

As mentioned before, the recent progress in genome editing technologies has created a true revolution in generating models for human disease. This also applies to *X. tropicalis,* which unlike zebrafish (Taylor et al., 2001; Howe et al., 2013) favorably has a true diploid genome (Naert et al., 2017). Evidently, homology between human and mice is greater compared to *X. tropicalis*. Nevertheless, signaling pathways that are involved in TCR and BCR formation as well as immune system cell types are highly conserved (Robert and Ohta, 2009). Therefore, *X. tropicalis* is suitable for modeling hematologic diseases. Targeting of tumor suppressor genes (TSGs) by CRISPR/Cas9 (or TALENs) results in F_0 mosaic mutants, commonly mentioned as crispants. In these crispants, the cell clones that acquired bi-allelic loss of function (LOF) of the TSG may be able to form tumors.

Our lab published two genetically engineered tumor models in *X. tropicalis* (Naert et al., 2017). In both cases, solid tumors were obtained (e.g., desmoid tumors and retinoblastoma) and histological and immuno-histochemical evaluation, as well as genotyping, was straightforward and further confirmed these tumors to closely resemble their human counterparts (Naert et al., 2017). Recently, we also generated leukemia models in *Xenopus* by inducing LOF mutations in TSGs that are frequently mutated in T-ALL. While genotypic and phenotypic analysis of solid tumor models in *X. tropicalis* is straightforward, this is not the case for hematologic malignancies. In mice and humans, characterization of hematologic malignancies relies primarily on immunophenotyping with sets of antibodies recognizing specific surface markers on the transformed leukocytes. Unfortunately, such antibodies are largely lacking for *Xenopus*. Therefore, we designed and applied alternative strategies inspired by those used to analyze solid tumors. Our strategies, encompass both phenotypic and genotypic analysis of F_0 mosaic mutants that are symptomatic leukemic (**Figure 1**).

Phenotypic Analysis of F_0 Crispants

Embryos are injected in the blastomeres that contribute to the definitive blood and animals are raised until they present symptoms of leukemic disease such as abnormal swimming behavior, lethargy, pallor and hemorrhagic spots. Animals with these symptoms are sedated and whole blood is withdrawn from the heart by glass capillaries. Identification of leukocytes in the blood is complicated by the fact that amphibians, like fish, birds and reptiles, have nucleated erythrocytes (Maxham et al., 2016). Unfortunately, red blood cell lysis buffer, usually applied to lyse erythrocytes and facilitate leukocytes isolation, cannot be used. Hence, blood from tadpoles is processed either by manual cell count in a hemocytometer or by flow cytometry.

Analyzing the Blood (Figure 1)

A first indication for leukemia may be abnormal hematocrit levels. However, this analysis is not possible for tadpoles and young froglets since it requires larger amounts of blood (∼50 μl). For manual cell counting, whole blood is diluted in Natt-Herrick solution (Maxham et al., 2016). By using a common hemocytometer, single blood cells are counted and categorized as white blood cells (WBCs), red blood cells (RBCs) or platelets, to calculate the WBC/RBC ratio. Natt-Herrick staining allows discrimination between myeloid derivatives and lymphocytes. Wright-Giemsa staining of a blood smear can also be used as an alternative way to identify overrepresentation of lymphoblast-like cells. In our experience, analysis of blood smears can be complicated by partially lysed erythrocytes.

Compared to manual cell counting, flow cytometric analysis is more quantitative, especially if the blood sample can be stained for lymphocyte markers. Even though the markers available for *Xenopus* are very limited, we are still able to define whether the leukemia has a T cell or B cell origin. For now, no good myeloid markers are available. For larval stage blood (or for metamorphic stages) we suggest staining for CD8 and CD3. Both are used

A

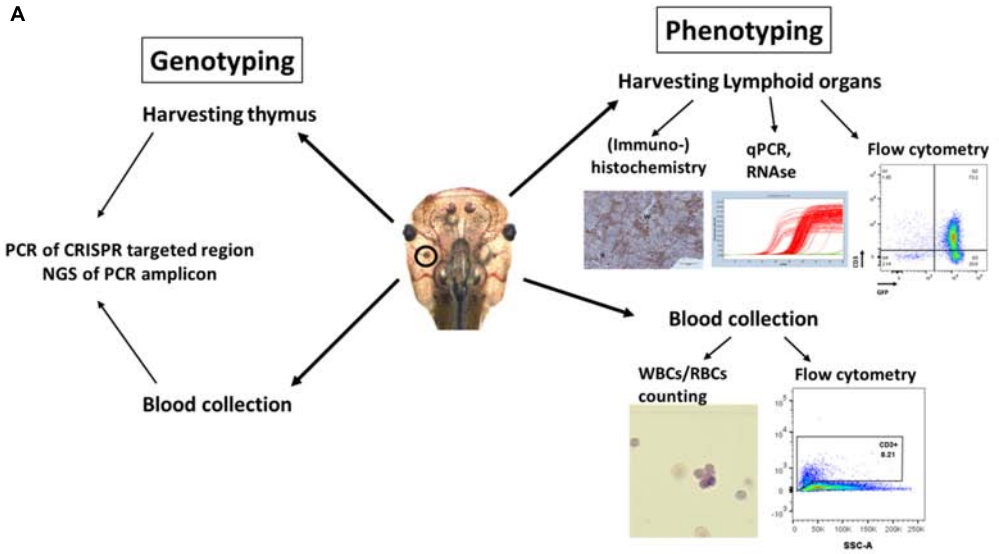

B

		Stage <55	Stage 55-63	Stage >63
Manual cell counting		--[a]	+	++
Hematocrit		--	--	++
Flow cytometry	*Thymus*	+[b]	++	+[c]
	Whole blood	--[d]	+	++
IHC lymphoid organs	*Thymus*	++	++	+[c]
	Spleen	--[e]	+	++
	Kidney	+	++	++
	Liver	++	++	++
Genotyping	*Thymus*	++	++	+[c]
	Whole blood	++	++	++
RT-qPCR (thymus)		++	++	+[c]

FIGURE 1 | (A) Overview illustrating the experimental approaches to document the development of hematologic malignancies. **(A)** Scheme documenting the different types of analysis performed to investigate the presence of hematologic malignancies. Genotyping is performed on the blood and the dissected thymus by PCR amplification of the CRISPR/Cas9 targeted regions followed by deep sequencing of the PCR fragments and analysis of the INDEL signatures (left). Phenotyping is done by manual counting of the blood cells or by flow cytometry. In addition, lymphoid organs such as the thymus, and spleen are subjected to immunohistological analysis and transcriptomic profiling. Other organs like the kidneys and the liver are evaluated for the presence of proliferating and disseminating lymphoblasts (right). **(B)** Timing of the analyses that can be performed for assessing the presence of leukemic disease and to evaluate disease progression. Legend: "++," "+" and "–" refer to straightforward, difficult and impossible to nearly impossible to perform, respectively. Analysis can be impossible to do due to (a) immature cells jeopardizing cell discrimination, (b) too low input of thymocytes for flow cytometry in early stage tadpoles, (c) shrinking of thymi in older animals, which impedes successful dissection, (d) aberrant scattering in immature cells, (e) extremely small size of the spleen in early stage tadpoles, which therefore is difficult to dissect. Drawings adopted from Xenbase (http://www.xenbase.org/anatomy/alldev.do).

as T cell specific surface markers. However, cytoplasmic CD3, detected upon cell permeabilization, is a marker of immature lymphoblast, which are clonally expanded in T-ALL (Robert and Ohta, 2009; Van Vlierberghe and Ferrando, 2012). Furthermore, larval and post-metamorphosis stage blood can be stained for MHC class II and cytoplasmic IgM, markers for B cells (Loftin et al., 1985). Next to these early lymphocyte markers, IgY staining can be included for identifying more mature B cells (Robert and Ohta, 2009). While the current lymphocyte surface and cytoplasmic markers allow us to discriminate between T- and B-ALL, they do not allow to define the different ALL subtypes. Of note, a recent report describes the use of acridine orange staining to discriminate different blood cell types by flow cytometry in *Xenopus* (Sato et al., 2018).

Analogs to zebrafish, a transgenic *rag2:EGFP* line in *X. tropicalis* can reinforce and facilitate phenotypic analysis of leukemic animals. Since *rag2* guides development and maturation of both T and B cells (Langenau et al., 2003), both cell populations will be GFP positive in these transgenic animals. Performing CRISPR/Cas9 injections in this transgenic line to generate ALL F_0 mosaic crispants, will offer unique opportunities. Firstly, due to the transparency of larval stages, circulating and infiltrating lymphoblasts can be detected. Secondly, GFP positive lymphocytes/lymphoblasts can be easily separated by flow cytometry. This obviates the need for lymphocyte markers. Thirdly, sorted lymphoblasts can be transplanted into immunocompromised animals to evaluate the tumorigenic potential of these leukemic cells/blasts. Importantly, all aforementioned applications have already been used successfully in zebrafish (Langenau et al., 2003, 2005). In our lab, we have established a r*ag2:EGFP* F_0 line and a *rag2*$^{+/-}$ lines for these experiments. These tools will strengthen the validity of our model and facilitate future applications, especially for compound screening.

Analyzing Internal Lymphoid Organs (Figure 1)

Next to the blood, also the analysis of the lymphoid organs like the thymus, spleen and liver can be informative regarding leukemia establishment and progression. Healthy spleens, contain white and red pulp, that are well delineated by a boundary layer (Manning, 1991; Lametschwandtner et al., 2016). The red pulp establishes a network of reticular cells, which accommodate blood vessels and sinuses, and a perifollicular area of lymphocytes around the white pulp (Lametschwandtner et al., 2016). The murine spleen in ALL demonstrates disturbed architecture and especially in T-ALL, white pulp overrules the red pulp and GC organization is compromised (Chen et al., 2015). Even though the *Xenopus* spleen lacks GCs, in leukemic animals tissue architecture is disorganized. CD3 immuno-histochemical staining in tissue sections of spleen is informative to determine abnormalities in the organization of the T cell and B cell zones. Interestingly in thymic sections of leukemic animals in *Xenopus*, the medulla of the thymus invades the cortex and disturbs the architecture of these tissues. This abnormality is obvious in both H&E staining as well as in CD3 stained thymi sections. Furthermore, in murine ALL models, infiltration of liver, spleen and kidneys by lymphoblasts is observed (Jacoby et al., 2014; Pan et al., 2018). Similarly, CD3 immuno-histochemical staining of *Xenopus* liver and kidney tissue sections can easily assess lymphoblasts infiltration. Alternatively, cell suspensions derived from lymphoid organs can be examined for distribution of the same lymphocyte markers that are used in whole blood flow cytometric analysis.

Genotypic Analysis of F_0 Crispants (Figure 1)

Leukemia is a disease of the hematologic system that results in clonal expansion of malignant lymphoblasts. Depending on the stage of oncogenic transformation, the clone of malignant cells can show a uniform rearrangement of their BCR (B-ALL) or TCR (T-ALL; Schultz and Farkas, 1993). This genomic BCR/TCR rearrangement can be used as a signature to identify an expanded malignant clone and can be detected by Southern Blot analysis (Schultz and Farkas, 1993) or by Rapid Amplification of cDNA Ends (RACE; Rosati et al., 2017). We apply alternative methods exploiting the specifics of the genome editing techniques. Mosaic mutant animals generated by CRISPR/Cas9, that bear frame shifting LOF mutations in TSGs have unique genomic features. When Cas9 creates double strand breaks (DSBs) in targeted DNA sequences, the majority of DSBs is repaired by Non-Homologs End Joining (NHEJ). NHEJ repairs the DSBs by incorporating or omitting random nucleotides (Zhang et al., 2014; Wang et al., 2016). As a result, variable patterns of insertions/deletions (INDELS) are generated in the cells of the F_0 crispants (Naert et al., 2017). However, the leukemic cells of a F_0 crispant will present with clear enrichment for limited INDEL patterns. Therefore, an effective way to evaluate clonal lymphoblasts expansion is to subject the PCR amplicon of the CRISPR targeted region to Next Generation Sequencing (NGS) (**Figure 1**). For T-ALL, thymi, which are the main localization site for the T cell lymphoblasts, are dissected from F_0 crispants and genomic DNA is extracted. The area of interest (i.e., the target site of the sgRNA) in the CRISPR/Cas9 targeted gene(s), is PCR amplified, bar-coded and included in a NGS run. INDEL patterns can subsequently be detected by BATCH-GE analysis (Boel et al., 2016) and evaluated for the presence of dominant clones (**Figure 2A**).

CHALLENGES FOR MODELING HEMATOLOGIC MALIGNANCES IN *X. TROPICALIS*

Some complications and challenges for modeling hematologic malignancies still remain. *X. tropicalis* has a small size compared to *X. laevis*. Cardiac puncture in tadpoles with glass capillary needles is challenging and only small amounts of blood can be collected. Larval blood cells are also very fragile compared to adult blood. The small blood volumes restrict subsequent phenotypic analysis, especially flow cytometry. Detailed immunophenotyping of the blood from a symptomatic animal is not possible. However, these complications could be partially bypassed by using transgenic lines such as *rag2:EGFP*.

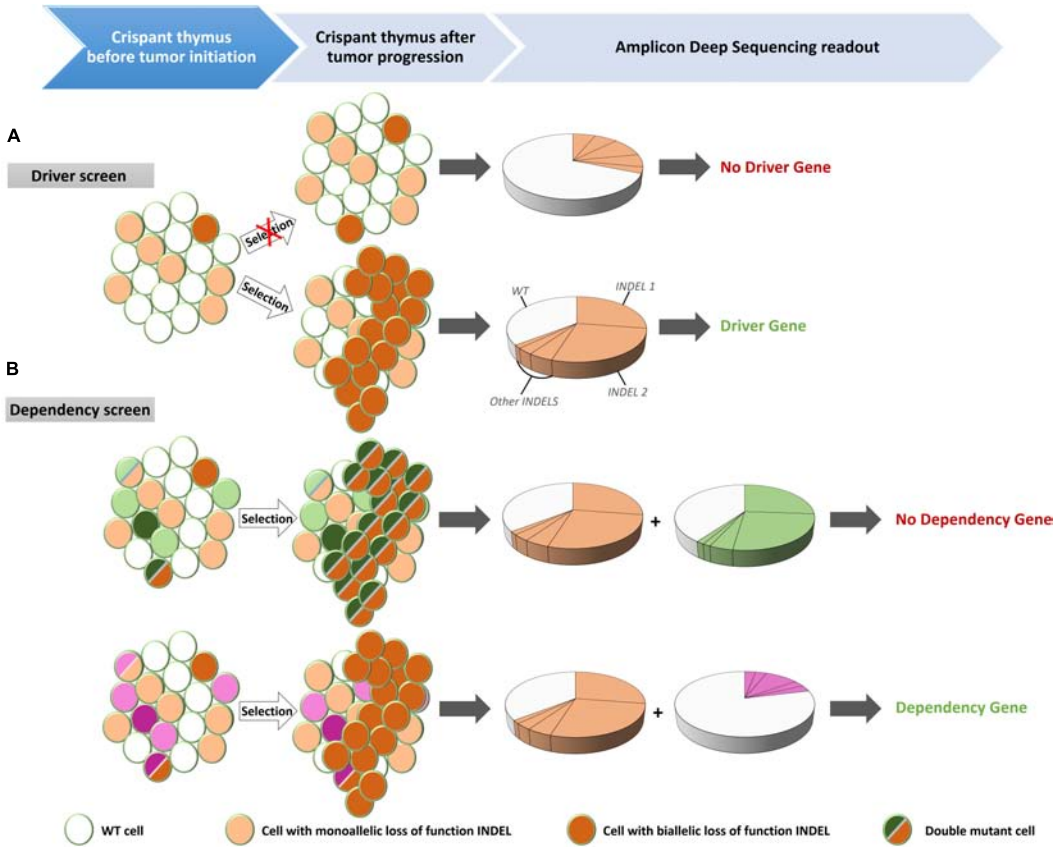

FIGURE 2 | Experimental set-up for the identification of driver mutations in tumor suppressor genes (TSG) and for dependency factors. **(A)** Injection of Cas9 recombinant proteins and guide RNAs targeting putative TSGs created mosaic mutant animals (crispants) that contain cells with mono-allelic or bi-allelic inactivation of the driver genes. Cells with bi-allelic inactivation will have a proliferative advantages over the wild type (WT) or mono-allelic mutant cells. When disease is observed, DNA is extracted from the thymus and after PCR amplification of the targeted regions, the PCR amplicon is subjected to deep sequencing. The presence of two unique frame shifting INDELs at equal proportion is indicative of a clonally expanding subpopulation, characteristic for leukemic disease. **(B)** Multiplexing of guide RNAs targeting a known driver gene together with a candidate dependency factor gene. If the candidate is not a dependency factor, clonal expanding cells will be present – identified by the INDEL signature of the driver gene (orange) – with bi-allelic inactivation of the analyzed gene (green) (top). However, in case of a genuine dependency factor gene (purple), expanding clones will never contain bi-allelic inactivation of this gene (bottom).

Indeed, the *rag2:EGFP* line in zebrafish has greatly facilitated the analysis of the leukemic models in this organisms. This transgenic line allows to gate out lymphocytes from other blood cell types and thus reduces the number of cell markers to be used. In addition, it allows for *in vivo* detection of leukemic animals, facilitates follow up of disease progression, and provides the opportunity for the development of transplantation assays for further disease characterization.

FUTURE PERSPECTIVES AND DIRECTIONS

In addition to current cancer models, *X. tropicalis* could expand the toolbox of model systems for detailed *in vivo* characterization and identification of novel therapeutic strategies. It shares with zebrafish the external development and the associated ease with which to generate mosaic or full knockout models, but has the unique property of a true diploid genome. In addition, although it still lacks some typical secondary lymphoid organs found in mammals, like lymph nodes and GCs, other features such as a clear separation of the red pulp and white pulp in the spleen and canonical class switch recombination of immunoglobulin receptors are still absent in teleosts (Neely et al., 2018). Exploiting the easy and efficient CRISPR/Cas9 mediated multiplexed genome editing and positive clonal selection of leukemic cells will allow the identification of novel driver and modifier mutations (**Figure 2A**). Alternatively, an existing crispant *Xenopus* leukemic model can be exploited for screening of genes that are essential for proliferation and/or viability of the leukemic cells, the so-called dependency factors (McDonald et al., 2017) (**Figure 2B**). This application is well established in our lab for solid tumor models (Naert et al., unpublished). This efficient pipeline could be transferred to our ALL model by disrupting the gene of interest with CRISPR/Cas9. Since dependency factor expression is under positive selection, there will be selective pressure to maintain at least one functional allele in the expanding leukemic clones. Besides identifying new target genes for

therapies, our model can also be used for compound screening. We have already successfully treated F_0 crispants exhibiting solid tumors with candidate compounds. The experimental approach was straightforward since compounds could be easily taken up by the animal via the water by several routes (gills, skin, water uptake) or alternatively by intraperitoneal injection. The administration route is determined by the (water) solubility and the price of the compound. Poorly soluble or very expensive compounds are preferentially injected intraperitoneally. Evidently, a critical point is the amount of compound to be administered to the animals. For injections, we rely on the concentrations and injection schemes described for the compound in mouse studies. For administration via the water, we base the concentrations on cell culture studies. Toxicity can first be tested on early pre-feeding tadpoles. We usually start with a five-fold concentration of the IC50 value. Ideally a biological response (e.g., modification of a protein substrate or expression of a known target gene) is used as a readout for effectiveness of the compound (e.g., in lysed liver extracts). Evidently it is important to obtain ethical approval for these treatments.

The previously mentioned use of *rag2* knockout lines for cancer cell grafting may ultimately be not straightforward. Evidently, these animals still have an innate immune system where for instance natural killer cells could still affect the transplanted cells. Also, these animals may be prone to disease. Therefore, an interesting future direction will be the use of *X. tropicalis* inbred strains. This will be a great tool for grafting of cancer cells directly from a diseased donor or from cell lines established derived from these strains. Several inbred strains are currently available from the National BioResource Project (NBRP), the Japanese *X. tropicalis* stock center[1].

[1] http://nbrp-xt.hiroshima-u.ac.jp/xenobiores_en/iweb_en/Top.html

In sum, *X. tropicalis* is an emerging organism for modeling hematologic malignancies. With some investment, this aquatic vertebrate could become a strong tool for laboratories that are active in identifying new molecular targets for therapy as well as new driver mutations in hematological malignancies.

ETHICS STATEMENT

Approval of the experiments was obtained from the Ethical Committee for Animal Experimentation, Ghent University, Faculty of Sciences.

AUTHOR CONTRIBUTIONS

DD and KV wrote the manuscript. DT and PVV provided experimental know-how and input on human leukemia.

ACKNOWLEDGMENTS

Research in the authors' laboratory is supported by the Research Foundation – Flanders (FWO-Vlaanderen) (grants G0A1515N and G029413N), by the Belgian Science Policy (Interuniversity Attraction Poles – IAP7/07) and by the Concerted Research Actions from Ghent University (BOF15/GOA/011). Further support was obtained by the Hercules Foundation, Flanders (grant AUGE/11/14). DT has a PhD fellowship from the Research Foundation – Flanders (FWO-Vlaanderen). We thank the *Xenopus laevis* Resource for Immunobiology (Rochester, NY, NIH R24 AI059830) for the kind gift of monoclonal antibodies and experimental advise. We are indebted to Tim Deceuninck for animal care.

REFERENCES

Banach, M., and Robert, J. (2017). Tumor immunology viewed from alternative animal models-the Xenopus story. *Curr. Pathobiol. Rep.* 5, 49–56. doi: 10.1007/s40139-017-0125-y

Bechtold, T. E., Smith, P. B., and Turpen, J. B. (1992). Differential stem cell contributions to thymocyte succession during development of Xenopus laevis. *J. Immunol.* 15, 2975–2982.

Bernard, D., Hansen, J. D., Du Pasquier, L., Lefranc, M. P., Benmansour, A., and Boudinot, P. (2007). Costimulatory receptors in jawed vertebrates: conserved CD28, odd CTLA4 and multiple BTLAs. *Dev. Comp. Immunol.* 31, 255–271. doi: 10.1016/j.dci.2006.06.003

Boel, A., Steyaert, W., De Rocker, N., Menten, B., Callewaert, B., De Paepe, A., et al. (2016). BATCH-GE: batch analysis of next-generation sequencing data for genome editing assessment. *Sci. Rep.* 27:30330. doi: 10.1038/srep30330

Bray, F., Ferlay, J., Soerjomataram, I., Siegel, R. L., Torre, L. A., and Jemal, A. (2018). Global cancer statistics 2018: GLOBOCAN estimates of incidence and mortality worldwide for 36 cancers in 185 countries. *CA Cancer J. Clin.* 68, 394–424. doi: 10.3322/caac.21492

Chen, S. Y., Yang, X., Feng, W. L., Liao, J. F., Wang, L. N., Feng, L., et al. (2015). Organ-specific microenvironment modifies diverse functional and phenotypic characteristics of leukemia-associated macrophages in mouse T cell acute lymphoblastic leukemia. *J. Immunol.* 15, 2919–2929. doi: 10.4049/jimmunol.1400451

Chretien, I., Marcuz, A., Fellah, J., Charlemagne, J., and Du Pasquier, L. (1997). The T cell receptor beta genes of Xenopus. *Eur. J. Immunol.* 27, 763–771. doi: 10.1002/eji.1830270327

Ciau-Uitz, A., Monteiro, R., Kirmizitas, A., and Patient, R. (2014). Developmental hematopoiesis: ontogeny, genetic programming and conservation. *Exp. Hematol.* 42, 669–683. doi: 10.1016/j.exphem.2014.06.001

Cooper, S. L., and Brown, P. A. (2015). Treatment of pediatric acute lymphoblastic leukemia. *Pediatr. Clin. North Am.* 62, 61–73. doi: 10.1016/j.pcl.2014.09.006

Dombret, H., and Gardin, C. (2016). An update of current treatments for adult acute myeloid leukemia. *Blood* 7, 53–61. doi: 10.1182/blood-2015-08-604520

Du Pasquier, L., and Flajnik, M. F. (1990). Expression of MHC class II antigens during Xenopus development. *Dev. Immunol.* 1, 85–95. doi: 10.1155/1990/67913

Du Pasquier, L., and Robert, J. (1992). In vitro growth of thymic tumor cell lines from Xenopus. *Dev. Immunol.* 2, 295–307. doi: 10.1155/1992/41823

Du Pasquier, L., Robert, J., Courtet, M., and Mussmann, R. (2000). B-cell development in the amphibian Xenopus. *Immunol. Rev.* 175, 201–213. doi: 10.1111/j.1600-065X.2000.imr017501.x

Du Pasquier, L., and Schwager, J. (1991). Immunoglobulin genes and B cell development in amphibians. *Adv. Exp. Med. Biol.* 292, 1–9. doi: 10.1007/978-1-4684-5943-2_1

Du Pasquier, L., Schwager, J., and Flajnik, M. F. (1989). The immune system of Xenopus. *Annu. Rev. Immunol.* 7, 251–275. doi: 10.1146/annurev.iy.07.040189.001343

Du Pasquier, L., and Weiss, N. (1973). The thymus during the ontogeny of the toad Xenopus laevis: growth, membrane-bound immunoglobulins and mixed lymphocyte reaction. *Eur. J. Immunol.* 3, 773–777. doi: 10.1002/eji.1830031207

Flajnik, M. F. (2018). A cold-blooded view of adaptive immunity. *Nat. Rev. Immunol.* 18, 438–453. doi: 10.1038/s41577-018-0003-9

Gopalakrishnapillai, A., Kolb, E. A., Dhanan, P., Bojja, A. S., Mason, R. W., Corao, D., et al. (2016). Generation of pediatric leukemia xenograft models in NSG-B2m mice: comparison with NOD/SCID mice. *Front. Oncol.* 6:162. doi: 10.3389/fonc.2016.00162

Goyos, A., Guselnikov, S., Chida, A. S., Sniderhan, L. F., Maggirwar, S. B., Nedelkovska, H., et al. (2007). Involvement of nonclassical MHC class Ib molecules in heat shock protein-mediated anti-tumor responses. *Eur. J. Immunol.* 37, 1494–1501. doi: 10.1002/eji.200636570

Gutierrez, A., Pan, L., Groen, R. W., Baleydier, F., Kentsis, A., Marineau, J., et al. (2014). Phenothiazines induce PP2A-mediated apoptosis in T cell acute lymphoblastic leukemia. *J. Clin. Invest.* 124, 644–655. doi: 10.1172/JCI65093

Hadji-Azimi, I., Coosemans, V., and Canicatti, C. (1987). Atlas of adult Xenopus laevis laevis hematology. *Dev. Comp. Immunol.* 11, 807–874. doi: 10.1016/0145-305X(87)90068-1

Hansen, J. D., Du Pasquier, L., Lefranc, M. P., Lopez, V., Benmansour, A., and Boudinot, P. (2009). The B7 family of immunoregulatory receptors: a comparative and evolutionary perspective. *Mol. Immunol.* 46, 457–472. doi: 10.1016/j.molimm.2008.10.007

Hellsten, U., Harland, R. M., Gilchrist, M. J., Hendrix, D., Jurka, J., Kapitonov, V., et al. (2010). The genome of the western clawed frog Xenopus tropicalis. *Science* 30, 633–636. doi: 10.1126/science.1183670

Horton, T. L., Minter, R., Stewart, R., Ritchie, P., Watson, M. D., and Horton, J. D. (2000). Xenopus NK cells identified by novel monoclonal antibodies. *Eur. J. Immunol.* 30, 604–613. doi: 10.1002/1521-4141(200002)30:2<604::AID-IMMU604>3.0.CO;2-X

Horton, T. L., Stewart, R., Cohen, N., Rau, L., Ritchie, P., Watson, M. D., et al. (2003). Ontogeny of Xenopus NK cells in the absence of MHC class I antigens. *Dev. Comp. Immunol.* 27, 715–726. doi: 10.1016/S0145-305X(03)00040-5

Howe, K., Clark, M. D., Torroja, C. F., Torrance, J., Berthelot, C., Muffato, M., et al. (2013). The zebrafish reference genome sequence and its relationship to the human genome. *Nature.* 25, 498–503. doi: 10.1038/nature12111

Jabbour, E., and Kantarjian, H. (2018). Chronic myeloid leukemia: 2018 update on diagnosis, therapy and monitoring. *Am. J. Hematol.* 93, 442–459. doi: 10.1002/ajh.25011

Jacoby, E., Chien, C. D., and Fry, T. J. (2014). Murine models of acute leukemia: important tools in current pediatric leukemia research. *Front. Oncol.* 4:95. doi: 10.3389/fonc.2014.00095

Kohnken, R., Porcu, P., and Mishra, A. (2017). Overview of the use of murine models in leukemia and lymphoma research. *Front. Oncol.* 7:22. doi: 10.3389/fonc.2017.00022

Lametschwandtner, A., Radner, C., and Minnich, B. (2016). Microvascularization of the spleen in larval and adult Xenopus laevis: histomorphology and scanning electron microscopy of vascular corrosion casts. *J. Morphol.* 277, 1559–1569. doi: 10.1002/jmor.20595

Langenau, D. M., Feng, H., Berghmans, S., Kanki, J. P., Kutok, J. L., and Look, A. T. (2005). Cre/lox-regulated transgenic zebrafish model with conditional myc-induced T cell acute lymphoblastic leukemia. *Proc. Natl. Acad. Sci. U.S.A.* 26, 6068–6073. doi: 10.1073/pnas.0408708102

Langenau, D. M., Traver, D., Ferrando, A. A., Kutok, J. L., Aster, J. C., Kanki, J. P., et al. (2003). Myc-induced T cell leukemia in transgenic zebrafish. *Science* 7, 887–890. doi: 10.1126/science.1080280

Loftin, K. C., Reuben, J. M., Hersh, E. M., and Sujansky, D. (1985). Cytoplasmic IgM in leukemic B cells by flow cytometry. *Leuk. Res.* 9, 1379–1387. doi: 10.1016/0145-2126(85)90126-2

Manning, M. J. (1991). Histological organization of the spleen: implications for immune functions in amphibians. *Res. Immunol.* 142, 355–359. doi: 10.1016/0923-2494(91)90091-V

Maxham, L. A., Forzan, M. J., Hogan, N. S., Vanderstichel, R. V., and Gilroy, C. V. (2016). Hematologic reference intervals for Xenopus tropicalis with partial use of automatic counting methods and reliability of long-term stored samples. *Vet. Clin. Pathol.* 45, 291–299. doi: 10.1111/vcp.12362

McDonald, E. R. III, de Weck, A., Schlabach, M. R., Billy, E., Mavrakis, K. J., Hoffman, G. R., et al. (2017). Project DRIVE: a compendium of cancer dependencies and synthetic lethal relationships uncovered by large-scale, deep RNAi screening. *Cell* 170:e510. doi: 10.1016/j.cell.2017.07.005

Mussmann, R., Courtet, M., and Du Pasquier, L. (1998). Development of the early B cell population in Xenopus. *Eur. J. Immunol.* 28, 2947–2959. doi: 10.1002/(SICI)1521-4141(199809)28:09<2947::AID-IMMU2947>3.0.CO;2-A

Naert, T., Colpaert, R., Van Nieuwenhuysen, T., Dimitrakopoulou, D., Leoen, J., Haustraete, J., et al. (2016). CRISPR/Cas9 mediated knockout of rb1 and rbl1 leads to rapid and penetrant retinoblastoma development in Xenopus tropicalis. *Sci. Rep.* 14:35264. doi: 10.1038/srep35264

Naert, T., Van Nieuwenhuysen, T., and Vleminckx, K. (2017). TALENs and CRISPR/Cas9 fuel genetically engineered clinically relevant Xenopus tropicalis tumor models. *Genesis* 55. doi: 10.1002/dvg.23005

Neely, H. R., Guo, J., Flowers, E. M., Criscitiello, M. F., and Flajnik, M. F. (2018). "Double-duty" conventional dendritic cells in the amphibian Xenopus as the prototype for antigen presentation to B cells. *Eur. J. Immunol.* 48, 430–440. doi: 10.1002/eji.201747260

Ohta, Y., Goetz, W., Hossain, M. Z., Nonaka, M., and Flajnik, M. F. (2006). Ancestral organization of the MHC revealed in the amphibian Xenopus. *J. Immunol.* 15, 3674–3685. doi: 10.4049/jimmunol.176.6.3674

Pan, Z., Yang, M., Huang, K., Busche, G., Glage, S., Ganser, A., et al. (2018). Flow cytometric characterization of acute leukemia reveals a distinctive "blast gate" of murine T-lymphoblastic leukemia/lymphoma. *Oncotarget* 5, 2320–2328. doi: 10.18632/oncotarget.23410

Qi, Z. T., and Nie, P. (2008). Comparative study and expression analysis of the interferon gamma gene locus cytokines in Xenopus tropicalis. *Immunogenetics* 60, 699–710. doi: 10.1007/s00251-008-0326-y

Roach, J. C., Glusman, G., Rowen, L., Kaur, A., Purcell, M. K., Smith, K. D., et al. (2005). The evolution of vertebrate Toll-like receptors. *Proc. Natl. Acad. Sci. U.S.A.* 5, 9577–9582. doi: 10.1073/pnas.0502272102

Robert, J., Guiet, C., and Du Pasquier, L. (1994). Lymphoid tumors of Xenopus laevis with different capacities for growth in larvae and adults. *Dev. Immunol.* 3, 297–307. doi: 10.1155/1994/37392

Robert, J., and Ohta, Y. (2009). Comparative and developmental study of the immune system in Xenopus. *Dev. Dyn.* 238, 1249–1270. doi: 10.1002/dvdy.21891

Robert, J., Sung, M., and Cohen, N. (2001). In vitro thymocyte differentiation in MHC class I-negative Xenopus larvae. *Dev. Comp. Immunol.* 25, 323–336. doi: 10.1016/S0145-305X(00)00066-5

Rollins-Smith, L. A., Flajnik, M. F., Blair, P. J., Davis, A. T., and Green, W. F. (1997). Involvement of thyroid hormones in the expression of MHC class I antigens during ontogeny in Xenopus. *Dev. Immunol.* 5, 133–144. doi: 10.1155/1997/38464

Rosati, E., Dowds, C. M., Liaskou, E., Henriksen, E. K. K., Karlsen, T. H., and Franke, A. (2017). Overview of methodologies for T-cell receptor repertoire analysis. *BMC Biotechnol.* 10:61. doi: 10.1186/s12896-017-0379-9

Sato, K., Uehara, A., Kinoshita, S., Nomura, I., Yagi, M., Tanizaki, Y., et al. (2018). Flow cytometric analysis of *Xenopus laevis* and *X. tropicalis* blood cells using acridine orange. *Sci. Rep.* 8:16245. doi: 10.1038/s41598-018-34631-0

Schultz, D. L., and Farkas, D. H. (1993). B- and T-cell gene rearrangement test: an overview of application and methodology. *Clin. Lab. Sci.* 6, 291–294.

Schwager, J., Burckert, N., Schwager, M., and Wilson, M. (1991). Evolution of immunoglobulin light chain genes: analysis of Xenopus IgL isotypes and their contribution to antibody diversity. *EMBO J.* 10, 505–511. doi: 10.1002/j.1460-2075.1991.tb07976.x

Schwager, J., Mikoryak, C. A., and Steiner, L. A. (1988). Amino acid sequence of heavy chain from Xenopus laevis IgM deduced from cDNA sequence: implications for evolution of immunoglobulin domains. *Proc. Natl. Acad. Sci. U.S.A.* 85, 2245–2249. doi: 10.1073/pnas.85.7.2245

Shi, Y. B., and Ishizuya-Oka, A. (1997). Autoactivation of xenopus thyroid hormone receptor beta genes correlates with larval epithelial apoptosis and adult cell proliferation. *J. Biomed. Sci.* 4, 9–18. doi: 10.1007/BF02255588

Taylor, J. S., Van de Peer, Y., Braasch, I., and Meyer, A. (2001). Comparative genomics provides evidence for an ancient genome duplication event in fish. *Philos. Trans. R. Soc. Lond. B Biol. Sci.* 29, 1661–1679. doi: 10.1098/rstb.2001.0975

Terwilliger, T., and Abdul-Hay, M. (2017). Acute lymphoblastic leukemia: a comprehensive review and 2017 update. *Blood Cancer J.* 30:e577. doi: 10.1038/bcj.2017.53

Tochinai, S. (1976). Demonstration of thymus-independent immune system in Xenopus laevis. Response to polyvinylpyrrolidone. *Immunology* 31, 125–128.

Van Nieuwenhuysen, T., Naert, T., Tran, H. T., Van Imschoot, G., Geurs, S., Sanders, E., et al. (2015). TALEN-mediated apc mutation in Xenopus tropicalis phenocopies familial adenomatous polyposis. *Oncoscience* 2, 555–566. doi: 10.18632/oncoscience.166

Van Vlierberghe, P., and Ferrando, A. (2012). The molecular basis of T cell acute lymphoblastic leukemia. *J. Clin. Invest.* 122, 3398–3406. doi: 10.1172/JCI61269

Wang, H., La Russa, M., and Qi, L. S. (2016). CRISPR/Cas9 in Genome editing and beyond. *Annu. Rev. Biochem.* 2, 227–264. doi: 10.1146/annurev-biochem-060815-014607

Woo, J. S., Alberti, M. O., and Tirado, C. A. (2014). Childhood B-acute lymphoblastic leukemia: a genetic update. *Exp. Hematol. Oncol.* 3:16. doi: 10.1186/2162-3619-3-16

You, M. J., Medeiros, L. J., and Hsi, E. D. (2015). T-lymphoblastic leukemia/lymphoma. *Am. J. Clin. Pathol.* 144, 411–422. doi: 10.1309/AJCPMF03LVSBLHPJ

Zasloff, M. (2002). Antimicrobial peptides of multicellular organisms. *Nature* 24, 389–395. doi: 10.1038/415389a

Zhang, F., Wen, Y., and Guo, X. (2014). CRISPR/Cas9 for genome editing: progress, implications and challenges. *Hum. Mol. Genet.* 15, R40–R46. doi: 10.1093/hmg/ddu125

Conflict of Interest Statement: The authors declare that the research was conducted in the absence of any commercial or financial relationships that could be construed as a potential conflict of interest.

frontiers in Physiology

CORRECTION
published: 14 March 2019
doi: 10.3389/fphys.2019.00210

Corrigendum: *Xenopus tropicalis*: Joining the Armada in the Fight Against Blood Cancer

Dionysia Dimitrakopoulou[1,2], *Dieter Tulkens*[1,2], *Pieter Van Vlierberghe*[2,3] and *Kris Vleminckx*[1,2,3]*

[1] Department of Biomedical Molecular Biology, Ghent University, Ghent, Belgium, [2] Cancer Research Institute Ghent (CRIG), Ghent, Belgium, [3] Department of Biomolecular Medicine, Ghent University, Ghent, Belgium

Keywords: ***Xenopus***, **CRISPR/Cas9, leukemia, T-ALL, genome editing, thymus, tumor suppressor genes, cancer**

OPEN ACCESS

Approved by:
Frontiers in Physiology,
Frontiers Media SA, Switzerland

***Correspondence:**
Kris Vleminckx
kris.vleminckx@ugent.be

Specialty section:
This article was submitted to Embryonic and Developmental Physiology, a section of the journal Frontiers in Physiology

Received: *15 February 2019*
Accepted: *18 February 2019*
Published: *14 March 2019*

Citation:
Dimitrakopoulou D, Tulkens D, Van Vlierberghe P and Vleminckx K (2019) Corrigendum: Xenopus tropicalis: Joining the Armada in the Fight Against Blood Cancer. Front. Physiol. 10:210. doi: 10.3389/fphys.2019.00210

A Corrigendum on

***Xenopus tropicalis*: Joining the Armada in the Fight Against Blood Cancer**
by Dimitrakopoulou, D., Tulkens, D., Van Vlierberghe, P., and Vleminckx, K. (2019). Front. Physiol. 10:48. doi: 10.3389/fphys.2019.00048

An author name was incorrectly spelled as **"Pieter Van Vlieberghe."** The correct spelling is **"Pieter Van Vlierberghe."**

The authors apologize for this error and state that this does not change the scientific conclusions of the article in any way. The original article has been updated.

frontiers in Physiology

REVIEW
published: 08 February 2019
doi: 10.3389/fphys.2019.00081

More Than Just a Bandage: Closing the Gap Between Injury and Appendage Regeneration

*Anneke D. Kakebeen and Andrea E. Wills**

Department of Biochemistry, University of Washington School of Medicine, Seattle, WA, United States

The remarkable regenerative capabilities of amphibians have captured the attention of biologists for centuries. The frogs *Xenopus laevis* and *Xenopus tropicalis* undergo temporally restricted regenerative healing of appendage amputations and spinal cord truncations, injuries that are both devastating and relatively common in human patients. Rapidly expanding technological innovations have led to a resurgence of interest in defining the factors that enable regenerative healing, and in coupling these factors to human therapeutic interventions. It is well-established that early embryonic signaling pathways are critical for growth and patterning of new tissue during regeneration. A growing body of research now indicates that early physiological injury responses are also required to initiate a regenerative program, and that these differ in regenerative and non-regenerative contexts. Here we review recent insights into the biophysical, biochemical, and epigenetic processes that underlie regenerative healing in amphibians, focusing particularly on tail and limb regeneration in *Xenopus*. We also discuss the more elusive potential mechanisms that link wounding to tissue growth and patterning.

Keywords: regeneration, *Xenopus*, limb bud, tail, reactive oxygen species, epigenetic, innate immune, proliferation

OPEN ACCESS

Edited by:
John Noel Griffin,
Duke University, United States

Reviewed by:
Catherine D. McCusker,
University of Massachusetts Boston, United States
Karen Echeverri,
Marine Biological Laboratory (MBL), United States

***Correspondence:**
Andrea E. Wills
aewills@uw.edu

Specialty section:
This article was submitted to Embryonic and Developmental Physiology, a section of the journal Frontiers in Physiology

Received: *30 November 2018*
Accepted: *24 January 2019*
Published: *08 February 2019*

Citation:
Kakebeen AD and Wills AE (2019) More Than Just a Bandage: Closing the Gap Between Injury and Appendage Regeneration. Front. Physiol. 10:81. doi: 10.3389/fphys.2019.00081

INTRODUCTION

Injuries that sever tissues such as the limb or spinal cord are met with radically different outcomes among vertebrates. In mammals, a limb amputation or spinal cord transection is followed by inflammation and fibrotic scarring that leaves the animal with a permanent disability. In urodele amphibians such as axolotls and newts, the same injury is followed by scarless regenerative healing that can fully restore both the lost tissue and its function (reviewed in Tanaka, 2016). The anuran frogs *Xenopus laevis* and *Xenopus tropicalis* represent a middle ground: injuries to the tadpole tail, limb bud, or spinal cord are readily repaired through regeneration, but this ability declines during metamorphosis (Cannata et al., 2001). As adults, *Xenopus* can no longer functionally recover from a spinal cord transection (Filoni and Bosco, 1981), while amputation of the hindlimb results in regeneration of a single digit, rather than the whole limb (DENT, 1962; Suzuki et al., 2006). This temporally restricted regenerative competence therefore makes *Xenopus* an appealing model for defining the features that enable or inhibit regenerative healing. In addition to the loss of regenerative competence undergone during metamorphosis, *Xenopus* tadpoles also experience a transient loss of regenerative competence called the refractory period at Nieuwkoop and Faber

stages 45–47, shortly after the onset of independent feeding (Beck et al., 2003). Appendage regeneration, particularly of the tadpole tail, has been widely studied before, during and after this period. As a complement to the limb or limb bud, the tail is an excellent model for appendage regeneration because it comprises multiple cell types from epidermal, neural, mesodermal, and neural crest lineages, is easily accessible experimentally, and regenerates fully in a matter of days (Beck et al., 2009; Chen et al., 2014).

The regeneration of a tissue intuitively recapitulates aspects of its embryonic development. In both processes, rapid proliferation gives rise to new tissue, cell fate has to be specified within that tissue, and distinct positional identities have to be established to generate a properly patterned structure. Molecular evidence has validated multiple aspects of this parallel. Experimental perturbations using small molecule inhibitors and heat-shock inducible inhibitory proteins have established that BMP, FGF, Wnt, Notch, Shh, and Nodal/TGF-b signaling pathways are required for proper formation of the regenerated tail, paralleling their requirements in early embryonic patterning (Beck et al., 2003; Ho and Whitman, 2008; Lin and Slack, 2008; Taniguchi et al., 2014). Elegant experiments using heat-shock inducible expression of inhibitory proteins have further refined these observations to establish epistatic relationships, in which BMP acts upstream of Wnt, which in turn acts upstream of FGF during regeneration of the limb bud and tail (Lin and Slack, 2008). As during development, the establishment of positional identity appears to rely on the action of posterior Hox transcription factors (Christen et al., 2003). Numerous genes expressed in the developing limb and tail buds are re-expressed during tail regeneration, suggesting that many factors used to form these structures during embryogenesis are recapitulated during regeneration (Love et al., 2011; Chang et al., 2017).

More recently, next-generation sequencing approaches have endeavored to comprehensively catalog the transcriptional responses undergone by regenerating tissues in *Xenopus*. Microarray and RNA-Seq studies of the whole regenerating tail (Love et al., 2011; Chang et al., 2017), proliferating blastemal cells (Tsujioka et al., 2015), and spinal cord (Lee-Liu et al., 2014), have highlighted that embryonic patterning and developmental processes are indeed highly prioritized beginning at 1 day after amputation. However, these studies show that the initial transcriptional responses triggered by injury include a distinct set of target genes that characterize regeneration independent from development, and also hold clues to how regenerative healing may be differentiated from other forms of wounding response. These include changes in cell metabolic enzymes, factors used to generate reactive oxygen species (ROS), ion channels, innate immune cell factors, and epigenetic modifiers (**Figure 1**). Functional interrogation of many of these cell physiological mechanisms has begun to confirm that they are not only upregulated but are also necessary for regeneration of the tail, limb, or spinal cord.

In this review, we examine emerging categories of intercellular and intracellular responses to complex tissue injury that are associated with the initialization of a regenerative program in *X. laevis* and *X. tropicalis*. We also explore emerging models for how the initial wounding responses might be coupled to activation of proliferation and patterning programs that allow these animals to fully restore lost structures.

RAPID CHANGES IN ROS SIGNALING AND MEMBRANE POTENTIAL FOLLOWING INJURY

Following tail amputation, the first suite of signaling events reflect both short range intracellular damage responses and long-range signals activated by wounding. Among the earliest of these is ROS signaling, which can be detected using the H_2O_2-sensitive fluorescent reporter HyPER (Belousov et al., 2006; **Figure 2A**). In *X. laevis* that transgenically express HyPER, increased ROS is detectable within 20 min after tail amputation, and is strongly detectable by 6 h post amputation (hpa) (Love et al., 2013). Recently, it has been suggested that ROS production depends on a rapid influx of molecular oxygen from the surrounding environment, and that this influx is perturbed during the refractory period (Ferreira et al., 2018). Inhibition of ROS by treatment with the NADPH oxidase (NOX) inhibitors DPI or APO prevents full tail regeneration (Love et al., 2013; Ferreira et al., 2016, 2018) and inhibition of ROS more generally using free-radical scavengers such as MCI-186 delays regeneration. Morpholino knockdown of *cyba*, a member of NOX complexes 1, 2, and 4, also prevents regeneration, supporting the role of NOX complexes in this process (Love et al., 2013). Notably, DPI treatment prevents transcriptional activation of a Wnt reporter and of the Wnt target gene *fgf20*, suggesting that ROS is critical for activation of these later embryonic signaling pathways. HyPER activity is sustained for up to 4 days after injury, long after the closure of the wound epithelium. The prolonged activation of ROS, as well as transcriptional upregulation of ROS-associated pathway members (Love et al., 2011), suggest that ongoing production and response to ROS likely occur beyond the initial infiltration of atmospheric O_2. It is not yet clear how ROS is sustained for long periods, or what cell types serve as the signaling source. Notably, while *spiB*-expressing innate immune cells such as macrophages are rapidly recruited to the injury site and are capable of producing ROS, *spiB* knockdown did not prevent ROS activation in the first few hours after injury (Love et al., 2013). However, innate immune cells may contribute to later phases of ROS signaling, as may the injured and newly regenerated tissues themselves.

Bioelectrical changes, particularly in membrane potential, are also rapidly triggered by amputation (**Figure 2B**). Shortly after tadpole tail amputation, staining with the membrane voltage dye DiBAC4(3) demonstrates depolarization of the regeneration bud (Adams et al., 2007). In the non-regenerative refractory period, this depolarization fails to occur. Depolarization is coincident with upregulation of the V-ATPase H+ pump in the regeneration bud, and when depolarization is prevented by inhibition of V-ATPase H+ pump function, regeneration fails to occur, implicating H+ ion flow as the source of membrane depolarization in this context. Activation of V-ATPase H+ pump activity improves regeneration during the refractory period (Adams et al., 2013), suggesting that this channel is both

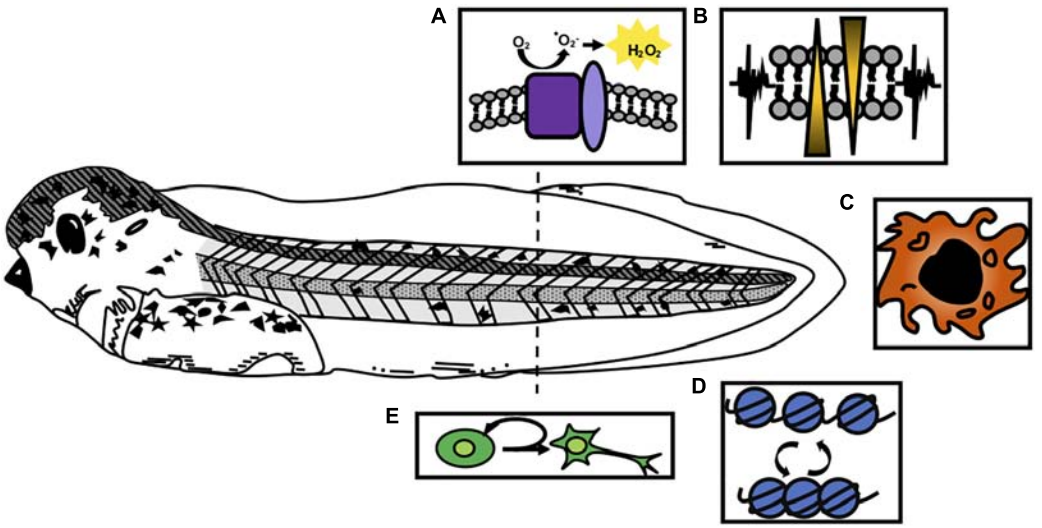

FIGURE 1 | Cellular processes activated by injury in *Xenopus* tail regeneration. A regenerative stage 41 tadpole is shown, prior to the onset of independent feeding and the refractory period. Responses to injury that are critical for regeneration include **(A)** formation of reactive oxygen species such as H_2O_2 through the action of NOX complexes (purple) and p22-phox/cyba (light purple); **(B)** bioelectrical signaling mediated by ion channel activation; **(C)** recruitment of innate immune cell types such as macrophages; **(D)** epigenetic modifications that affect chromatin accessibility and transcription, and **(E)** activation of proliferation of blastemal cells and tissue-specific progenitors.

necessary and sufficient for induction of regeneration. V-ATPase H+ pump function is also required for appendage regeneration in zebrafish (Monteiro et al., 2014), suggesting a conserved role. The initial depolarization of the regeneration bud is transient, and by 24 hpa, an influx of sodium ions mediated by NaV1.2 is triggered following membrane repolarization (Tseng et al., 2010). Pharmacological inhibition of NaV1.2 activity also impedes regeneration, preventing proliferation, or activation of BMP and Notch pathways (Tseng et al., 2010). Other perturbations of membrane potential (V_{mem}) similarly inhibit regeneration in tadpoles (Tseng and Levin, 2012) and in axolotls (Franklin et al., 2017). Numerous ion channels, including those for H^+, Na^+, K^+, Ca^{++}, and Cl^-, are transcriptionally differentially expressed over the course of regeneration with variable temporal dynamics (Chang et al., 2017), suggesting that the role of ion channel activity in regeneration may be complex and interregulated with other mechanisms.

Bioelectrical signaling is also notable for its role in nerve conductance during regeneration. The nerve dependence of regeneration has long been noted in urodeles, dating from initial observations by Todd (1823). His descriptions of salamander hindlimb regeneration (or "re-production") noted that excision or diversion of the sciatic nerve inhibited tissue growth, and also predicted that the nerve itself produced factors contributing to regenerative healing: "if the nerve be divided after reproduction has commenced, or considerably advanced, the new growth remains stationary, or it wastes, becomes shriveled and shapeless, or entirely disappears. This derangement cannot, in my opinion, be fairly attributed to the vascular derangement induced in the limb by the wound of the division, but must arise from something peculiar in the influence of the nerve (Todd, 1823)." Subsequent studies have confirmed that denervation of adult or larval limbs prevents cell proliferation and results in impaired regeneration (Singer and Craven, 1948), although this effect is abrogated in limbs where no nerve was initially present (Yntema, 1959), and can be rescued by addition of NRG1 (Farkas et al., 2016), or by activation of BMP and FGF signaling (Makanae et al., 2014). In zebrafish, nerve conductance is also critical to fin regeneration (Simões et al., 2014). In the late-stage *Xenopus* tadpole, peripheral nerves are required for limb bud regeneration (Cannata et al., 2001), while the spinal cord is required for tadpole tail regeneration (Taniguchi et al., 2008). Remarkably, there is evidence that bioelectrical signaling may also present a mechanism for long-range sensing and response to injury. After performing limb amputations, the uninjured contralateral limb also exhibits a rapid depolarization that mimics the timing and localization of the injured limb (Busse et al., 2018).

INNATE IMMUNE RESPONSES IN REGENERATION

Both regenerative and non-regenerative vertebrates respond to injury by recruiting innate immune cells to the injury site (**Figure 2C**). Transcriptomic studies of the regenerating tail and injured spinal cord implicate innate immune responses, which are highly upregulated beginning at 24 h post amputation (Lee-Liu et al., 2014; Chang et al., 2017). In *X. laevis*, transgenic fluorescent reporters in macrophage-like cells (*mpeg: mCherry*; *lurp: GFP* double positive) and neutrophil-like cells (*lurp: GFP* positive, *mpeg1: mCherry* negative) have been used to track cell behavior in these populations (Paredes et al., 2015). Fin injury is followed by rapid recruitment of both these cell types to the wound site, beginning with the migration of neutrophil-like cells

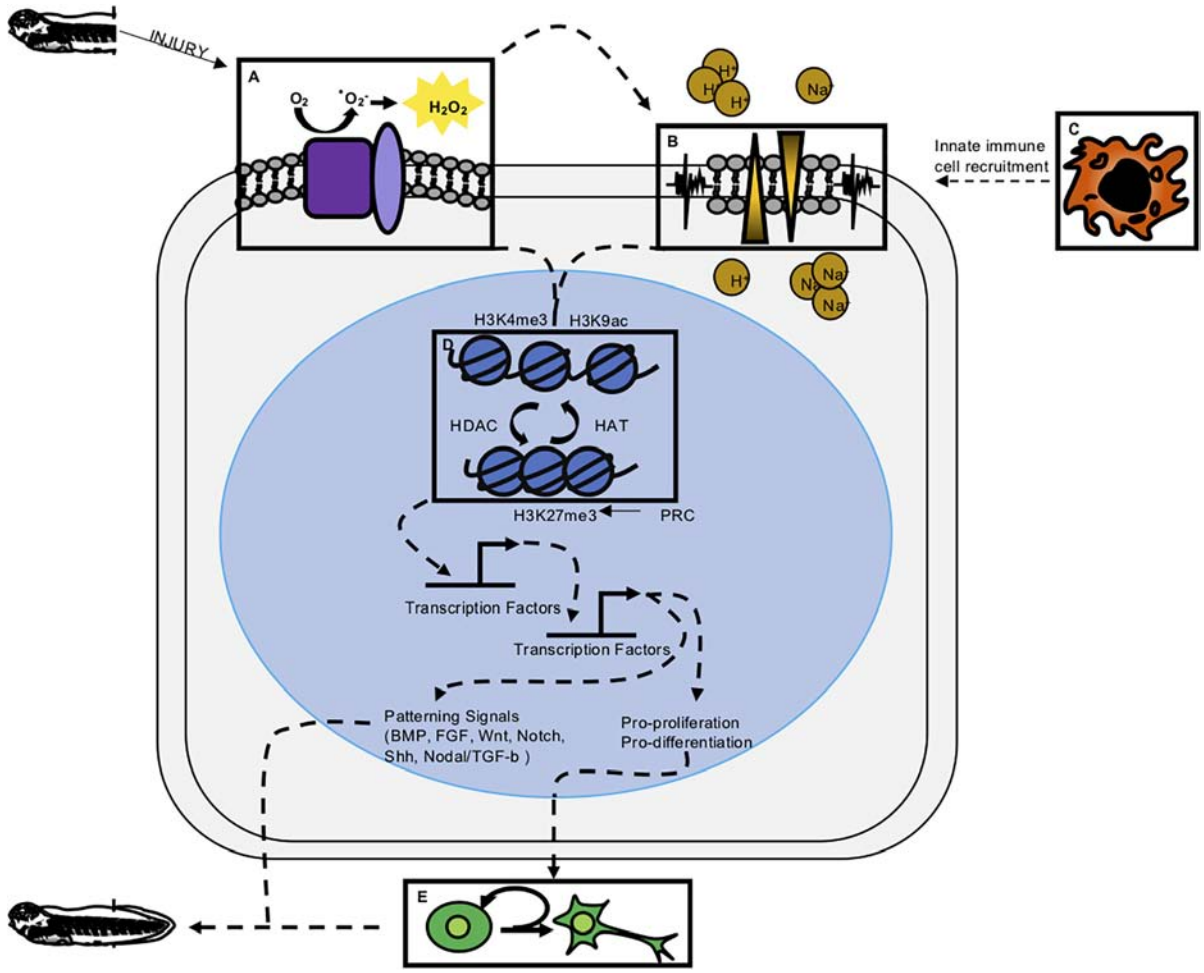

FIGURE 2 | Integrative model of regeneration. Experimental evidence reviewed here suggests the five modalities of early wound response and regeneration discussed in this paper are interconnected. Experimentally determined, indirect connections are denoted by dashed lines. **(A)** ROS has been shown to be one of the most early activated signaling modalities and is upstream of ion channel activity, proliferation, epigenetic modification, and transcription factor activation. **(B)** Membrane depolarization and ion channel activity have been shown to act upstream of proliferation and innate immune cell recruitment. **(C)** Innate immune cells are shown to act upstream of proliferation and perhaps release cytokines necessary for successful regeneration. **(D)** Epigenetic modifications have been profiled to look at repressive and active marks in regeneration. Presence of these marks along with the epigenetic enzymes that remodel chromatin have been shown to be important for regeneration. **(E)** Cell proliferation appears to be downstream of early wound responses and perhaps part of a transition from wound repair to regeneration.

to the injury site after 20 min, and followed by macrophage-like cells after an hour. This timing coincides closely with ROS activation. These cell infiltration behaviors were seen both in minor lateral fin injuries, such as a pin prick or hole punch, and in tail amputation.

Both neutrophils and macrophages act as producers of reactive oxygen signals and contribute to inflammatory responses, although neutrophils are associated with more inflammatory cytokine profiles (Kolaczkowska and Kubes, 2013). The role of neutrophils in regeneration has not yet been articulated clearly and may be variable (Rosales, 2018), but persistent infiltration of neutrophils at the wound site, as well as inflammatory signals such as nitric oxide (NO) that arise from these cells, is associated with scarring in mammals and may interfere with regenerative healing (Wilgus et al., 2013; Kryczka and Boncela, 2015). Pro-inflammatory agents such as beryllium sulfate also interfere with regeneration in *Xenopus* (Mescher et al., 2013). Macrophages serve as both a source and a responder cell type for ROS such as H_2O_2 and for numerous cytokines, several of which have now been explicitly investigated for their role in regeneration. Some of these, such as *mmp9* and *interleukin 7*, are transcriptionally activated both in regenerative and non-regenerative stages (Mescher et al., 2013). Certain macrophages are a source of pro-repair interleukins, such as IL6, which may contribute to regenerative healing. A transcriptomic study of proliferating blastemal cells in the regenerating tail identified the Il6 family member interleukin 11, and subsequent inducible gain-of-function experiments using CRISPR in *X. tropicalis* suggest that

interleukin 11 acts upstream of stem cell proliferation in tail regeneration (Tsujioka et al., 2015, 2017).

Although the role of innate immune cells has not been deeply interrogated functionally in *Xenopus* regeneration, work from other species suggest that macrophages may be critical. In axolotls, peritoneal injection of the macrophage inhibitor clodronate results in impaired limb regeneration (Godwin et al., 2013). Macrophages are also critical for regenerative healing following cardiac injury in zebrafish (Lai et al., 2017), and for regenerative healing of dermal and cartilage injuries in the regenerative African spiny mouse *Acomys* (Simkin et al., 2017). A comparison of innate immune responses in *Acomys* and the non-regenerative house mouse showed that in both species, neutrophils are rapidly recruited to the wound site, but this is followed by infiltration from pro-repair M2 type macrophages only in *Acomys*, while in the house mouse, inflammatory M1 type macrophages are recruited, leading to greater tissue damage and scarring (Simkin et al., 2017). In *Xenopus*, it is not yet clear what molecular characteristics define populations or subpopulations of macrophages, or how these cell types contribute to regenerative versus non-regenerative healing. However, with the greater versatility of functional tools as well as genomic assessment tools now available in both *Xenopus* species, these are questions that can readily be addressed in the near future.

EPIGENETIC RESPONSES THAT INTERPRET WOUNDING SIGNALS

A fundamental distinction in regenerative versus non-regenerative healing lies in the transcriptional response to injury (**Figure 2D**). Non-regenerative wound healing is followed by extensive fibrosis, characterized by dense cell matrix deposition and, in the spinal cord, by reactive gliosis. In regenerative healing fibrosis is minimized and proliferation and patterning of new tissue follows instead. How then, is the gene regulatory program associated with these latter behaviors activated? While transcriptomic analysis has shed considerable light on the plethora of genes that are both upregulated and downregulated during injury, experimental attention has also begun to turn to the epigenetic landscape that allows transcriptional activation of these targets. These experiments have included interrogating cell fate plasticity during regeneration, as well as investigations of chromatin marks and dynamics during regeneration.

In the axolotl, adult limb amputation and larval tail amputation are both followed by formation of a morphologically distinct blastema: a mass of highly proliferative mesenchymal cells with minimal morphological differentiation, protected by an apical epithelial cap that serves as a signaling source (McCusker et al., 2015). Because blastemal cells lack the clear morphological characteristics of differentiated cell types such as neurons or myocytes, it was long presumed that they represented a pluripotent cell type, analogous to embryonic stem cells. Indeed, in invertebrates that undergo morphallactic regeneration, such as planaria, blastemal cells have been clearly demonstrated to be pluripotent (Sánchez Alvarado, 2007; Aboobaker, 2011). However, lineage tracing experiments have made it clear that regenerating limb cells (in the axolotl) and tail cells (in *Xenopus*) retain a memory of their cell type of origin (Gargioli and Slack, 2004; Kragl et al., 2009). In both species, this was demonstrated by grafting specific tissues from a GFP-expressing donor into an unlabeled host, letting a full limb or tail develop, and then amputating the resulting, tissue-specifically labeled appendage. In axolotls, GFP-labeled muscle gave rise to muscle in the regenerated limb (but not skin or cartilage), labeled skin gave rise to skin (but not muscle or cartilage), and cartilage to cartilage (but not skin or muscle) (Kragl et al., 2009). It is worth noting that in axolotls, cartilage, and bone from the truncated limb do not contribute to the final regenerated skeleton, suggesting that other connective tissue cells are responsible for skeletogenesis, and therefore exhibit plasticity of fate (McCusker et al., 2016). Similar lineage tracing experiments in *Xenopus* examined animals where either the spinal cord, notochord, or muscle had been labeled with GFP, and found that only the same tissue was labeled following tail amputation and regeneration (Gargioli and Slack, 2004).

These grafting experiments suggested that cells might retain an epigenetically encoded memory of their tissue of origin. To begin to interrogate the nature of epigenetic memory, Hayashi et al. (2015a) collected limb bud tissue and analyzed the pattern of repressed and active promoter marks using ChIP-Seq for H3K27me3 and H3K4me3, respectively. They then profiled the epigenome of regenerated limb bud tissue 72 h after amputation, and found that genome-wide, most enhancers were similarly marked, including at genes associated with several signaling pathways critical for regeneration, including Shh and FGF. Notably, the Shh enhancer had previously been shown to gain methylation during metamorphosis, suggesting that methylation may contribute to loss of patterning gene expression during the loss of regenerative competence, although this hypothesis has not been queried more globally (Yakushiji et al., 2007). Hayashi and colleagues concluded that active enhancer marks were maintained at many enhancers throughout regeneration and might contribute to epigenetic memory. However, it should be noted that the temporal dynamics were not sampled at very high resolution in this study, and so it also remains possible that enhancer marks were instead re-established in the regenerating tissue. There may also be substantial variations in the epigenetic signature of specific cell types that have not yet been captured in studies like this one, which looked at the blastema in aggregate.

While lineage tracing experiments have implicated a stably maintained epigenetic memory in at least some regenerating tissues, other experiments have also demonstrated that epigenetic modifiers are required during regeneration, implicating dynamic regulation of chromatin marks and underlying transcriptional accessibility. DNA methylation and methyltransferases are dynamically regulated during limb regeneration in axolotls (Aguilar and Gardiner, 2015). In *Xenopus*, treating regenerating tails with the histone deacetylase (HDAC) inhibitors trichostatin A or valproic acid leads to minimal tissue regeneration and a loss of BMP target gene expression in the regenerate (Tseng et al., 2011; Taylor and Beck, 2012), and the HDAC inhibitor Sodium butyrate similarly inhibited regeneration (Tseng and Levin, 2012). These experiments suggest that HDACs are likely critical to tail

regeneration. Acetylation serves to neutralize the positive change on lysine residues, which are abundant in histone tails and can form electrostatic interactions with negatively charged DNA. HDACs therefore generally have a chromatin closing effect by removing acetyl groups, while acetyl group deposition, carried out by histone acetyltransferases (HATs), generally acts to reduce chromatin density and increase accessibility. HAT activity is also affected during tail regeneration. To visualize dynamics of the activating mark H3K9ac, Suzuki et al. (2016) made use of an *in vivo* fluorescent mintbody, which demonstrated a ROS-dependent accumulation of H3K9ac in the notochord at 24 h of regeneration. Deposition or maintenance of the facultative heterochromatin mark H3K27me3 is also required: inhibition of the Polycomb Repressor Complex by treatment with DZNep results in a failure of limb bud regeneration (Hayashi et al., 2015b). The principal functional enzyme in the PRC is Ezh2, a methyltransferase that deposits the facultative heterochromatin mark H3K27me3 and serves to repress chromatin. These experiments demonstrate that enzymatic activities that serve both to increase and decrease chromatin accessibility are important for successful regeneration. They provide a first foray into defining epigenetic dynamics during regeneration, opening the door for ongoing functional and epigenomic analyses to define the timing, cell-type specificity, and genomic distribution of epigenetic modifications.

INITIATING PROLIFERATION: PARALLELS TO TUMORIGENESIS AND THE ROLE OF TISSUE-SPECIFIC STEM CELLS

In *Xenopus*, amputation injuries are not immediately followed by upregulation of proliferation. Instead proliferation, marked by phospho-Histone H3 or by incorporation of nucleotide analogs, is increased strongly beginning at 1–2 days post amputation and continues through the remainder of tissue regeneration (Love et al., 2014; Tsujioka et al., 2015; **Figure 2E**). This timing is consistent with several relay steps being required between wounding and activation of proliferation, and is actually somewhat later than transcriptional activation of many patterning genes, including members of the Wnt, FGF, BMP, and Shh pathways (Love et al., 2011; Chang et al., 2017). Following tail amputation, proliferation occurs throughout the regenerating tailbud, and several studies have noted molecular similarities between the densely proliferating tail bud and tumorigenesis. Other tumorigenic signals are required for regeneration, including the Hippo pathway effector transcription factor YAP (Hayashi et al., 2014) and Shh (Taniguchi et al., 2014). Parallels to tumorigenesis have been more clearly articulated in the axolotl, where the physical resemblance of the loose mesenchymal blastema to a tumor has been described (Rojas-Muñoz et al., 2009), as have tumor activation programs (Knapp et al., 2013; Stewart et al., 2013). Activation of p53 also appears to be critical for proliferation in the axolotl, as pharmacological inhibition of p53 with nutlin or pifithrin impairs regeneration (Yun et al., 2013). The p53 amino acid sequence of axolotls has also been suggested to mimic that of activating mutations in human patients (Villiard et al., 2007).

There is reason to predict that there may be additional molecular parallels between tumorigenesis and blastema formation. In an intriguing hypothesis, Love et al. (2014) have noted that the pentose phosphate pathway, which serves to generate NADPH needed for NOX function, is also upregulated in cancer cells as part of the Warburg effect, where NADPH is required for biosynthesis of macromolecules needed for proliferation such as fatty acids and nucleotide precursors. This suggests an exciting potential metabolic link between ROS production and cell proliferation. In cancer cells, aerobic glycolysis is highly prioritized, and is enhanced by transcriptional upregulation of glycolytic enzymes induced by the hypoxia inducible factor HIF1a, which is itself stabilized in the hypoxic microenvironment of the tumor (Denko, 2008). Numerous growth factor inputs or oncogenes active in both cancer and regeneration, including PI3K/AKT, AMPK, p53, and Myc, stabilize or strengthen expression of the glycolytic and pentose phosphate pathway enzymes that perpetuate aerobic glycolysis and enable high rates of fatty acid and nucleotide biosynthesis (Vander Heiden et al., 2009). Although the metabolomics of regeneration are only beginning to be interrogated, similar transcriptional regulatory mechanisms may well be at play at least in *Xenopus* tail regeneration, where HIF1a is also critical (Ferreira et al., 2018) and ROS and NOX are activated.

In addition to widespread proliferation throughout the regenerate, there is clear evidence for tissue-specific stem cell proliferation. In *Xenopus* tail and spinal cord regeneration, Sox2/3-positive cells proliferate, contribute to new neurons and are required for regeneration of spinal cord form and function (Gaete et al., 2012; Muñoz et al., 2015). Birth dating of neurons by electroporation of Sox3:GFP into the tadpoles during regeneration provide evidence that Sox3 positive neural stem cells give rise to new neurons in regenerated tissue (Muñoz et al., 2015). Knockdown of Sox2/3 by morpholino or a dominant-negative construct impair regeneration of the spinal cord in stage 50 tadpoles (Gaete et al., 2012). The necessity for Sox2 specifically in spinal cord regeneration has also been found in axolotls by CRISPR mediated deletion of the gene, which results in impaired spinal cord regeneration but successful regeneration of other tissues (Fei et al., 2014).

While lineage tracing experiments have demonstrated that muscle cells retain cellular memory and become muscle cells in the regenerate, characterization of satellite cells has provided better resolution into the mechanism of muscle regeneration. Pax7 is a reliable marker of muscle satellite cells in *Xenopus*. Expression of *pax7* is upregulated in response to tail amputations. Experiments using a dominant-negative form of Pax7 (pax7EnR) did not significantly reduce muscle regeneration in response to an initial amputation, but secondary amputation of the regenerated tail that has been depleted of pax7 cells did show changes in muscle morphology, suggesting a role for satellite cells (Chen et al., 2006). Similarly, *pax7*-expressing cells have also been studied in axolotl muscle regeneration and have been

TABLE 1 | Summary of signaling modalities and known effects on regeneration.

Signal type	Observation	Method	Tail	Limb
ROS	ROS detected up to 4 dpi	HyPER	Belousov et al., 2006; Love et al., 2013	
	LOF	APO	Love et al., 2013	
	LOF, inhibition of fgf20 expression	DPI	Love et al., 2013; Ferreira et al., 2016, 2018	
	LOF	MCI186	Love et al., 2013; Ferreira et al., 2016	
	LOF	cybaMO	Love et al., 2013	
	Improved regeneration	Activation of ROS during refractory period	Ferreira et al., 2016, 2018	
	Perturbed influx of oxygen	Refractory period	Ferreira et al., 2018	
Bioelectrical	Depolarization of membrane detected	DiBAC4(3)	Adams et al., 2007	
	No depolarization	Refractory period	Adams et al., 2007	
	LOF	Inhibition of V-ATPase	Adams et al., 2013	
	GOF	Activation of V-ATPase in refractory period	Adams et al., 2007, 2013	
	Failure to proliferate, failure to activate BMP and Notch	Inhibition of NaV1.2	Tseng et al., 2010	
	Prevent macrophage recruitment	Inhibition of ion channel activity	Paré et al., 2017	
	LOF	Vmem perturbation	Tseng and Levin, 2012	
	LOF	Denervation	Singer and Craven, 1948	
	LOF	Peripheral nerve removal		Cannata et al., 2001
	LOF	Spinal cord removal	Taniguchi et al., 2008	
Innate immune	Impaired regeneration	Beryllium sulfate		Mescher et al., 2013
	LOF reduced cell proliferation GOF rescues LOF	IL-11 targeted CRISPR LOF IL-ll targeted CRISPR GOF	Tsujioka et al., 2017	
Epigenetic	Cells in blastema retain memory	Lineage tracing	Gargioli and Slack, 2004	
	Repressed and active promoter markers genome wide	ChIP-Seq for H3K27me3 and H3K4me3		Hayashi et al., 2015
HDAC	Impaired regeneration	TSA	Tseng et al., 2011; Taylor and Beck, 2012	Taylor and Beck, 2012
	Impaired regeneration, loss of BMP target expression	Valproic Acid	Tseng et al., 2011; Taylor and Beck, 2012	Taylor and Beck, 2012
	Impaired regeneration	Sodium butyrate	Tseng and Levin, 2012	
HAT	ROS-dependent accumulation of H3K9ac	*In vivo* fluorescent mintbody	Suzuki et al., 2016	
PRC	LOF	DZNep		Hayashi et al., 2015
Tumorigenesis/proliferation	Reduced proliferation, Impaired regeneration	Inhibition of p53: nutlin or pifithrin		Yun et al., 2013
	Impaired spinal cord regeneration, decrease in cell proliferation	Sox2MO/sox2 dominant-negative/sox2 CRISPR	Gaete et al., 2012; Muñoz et al., 2015	
	Rescues number of muscle satellite cells	pax7EnR	Chen et al., 2006	

shown to proliferate in response to damage and participate in regeneration (Morrison et al., 2006; Fei et al., 2017). The growing catalog of tools and markers to study specific cells will allow the field to increase the resolution into cell-type specific contributions to regeneration.

RELATIONSHIPS BETWEEN WOUNDING RESPONSES, AND LOOKING AHEAD TO AN INTEGRATED MECHANISM OF APPENDAGE REGENERATION

It is now clear that immediate cellular injury responses are activated during regenerative healing, and that preventing them adversely affects regenerative outcomes. Researchers have begun to address how these responses are integrated with each other and with downstream effects on proliferation and patterning, and our present understanding of these relationships is summarized in **Figure 2**. Several studies have placed ROS activation as one of the most immediate responses to regeneration, upstream of changes in membrane potential, innate immune cell recruitment, proliferation, and patterning. In two separate studies, Ferreira and colleagues found that pharmacological inhibition of ROS after tail amputation prevented membrane depolarization and opening of Na^+ channels (Ferreira et al., 2016, 2018), while activation of ROS during the refractory period was sufficient to restore V_{mem}, channel activation and improved regenerative outcomes. This places ROS upstream of bioelectrical responses executed by ion channel activity (**Figure 2A**). In turn, inhibition of ion channel activity was shown to prevent macrophage recruitment to the injury site after tail amputation (Paré et al., 2017; **Figures 2B,C**). Similarly, ion channel activity is required for innate immune cell recruitment in axolotl regeneration (Franklin et al., 2017). Both ROS and ion-channel mediated depolarization act upstream of proliferation, which is not substantially upregulated until the second day after tail amputation. Proliferation is markedly decreased in tails treated with ROS-abrogating compounds (DPI, APO, MCI-186, Trolx) or channel inhibitors [DiBAC4(3)] (Adams et al., 2007; Tseng et al., 2010; Love et al., 2013; Ferreira et al., 2016, 2018).

At present, a major gap in our understanding of early regeneration lies in defining the transcription factors that interpret immediate wounding signals and couple them to epigenetic and transcriptional effects in the genome (**Figure 2D**). Several hypotheses have been advanced, summarized in **Figure 2**. These include the possibility that bioelectrical signals, possibly interpreted through regulated transport of sodium butyrate, may serve as an epigenetic modifier (Tseng and Levin, 2012; Pai et al., 2016), or that ROS may serve to activate transcription factor mobilization (Love et al., 2014). Support for the latter hypothesis recently came via the demonstration that the hypoxia-inducible factor HIF1A is turned on downstream of ROS during tail regeneration, and is required for activation of stress response genes such as hsp90 (Ferreira et al., 2018). HIF1A can also act as a transcriptional activator of numerous genes associated with processes important to regeneration, including angiogenesis, cell proliferation, and metabolic regulation, although the range of targets activated by HIF1A in regeneration is not yet known. In other regenerative species, ROS has been shown to act upstream of JNK and JAK/STAT (Santabárbara-Ruiz et al., 2015), and while these signaling pathways are required for tail or spinal cord regeneration in *Xenopus* (Sugiura et al., 2009; Tapia et al., 2017), a direct link between ROS and their activation has not yet been demonstrated in this context. Several lines of evidence therefore place epigenetic modification, and potentially several rounds of signaling, transcription factor binding activity, and transcriptional response, upstream of a relatively late burst in proliferation (**Figure 2E**). While these connections are promising, a more mechanistic dissection of how transcription factors are activated and their direct targets are needed in order to clarify how wounding is coupled to growth and patterning.

Our vision of regeneration has gained considerable nuance over the past decade, and is now beginning to fill in. Moving forward, focused attention is needed to define the mechanisms that link each required signaling modality to the next. This includes identifying how ROS and ion channel activities are

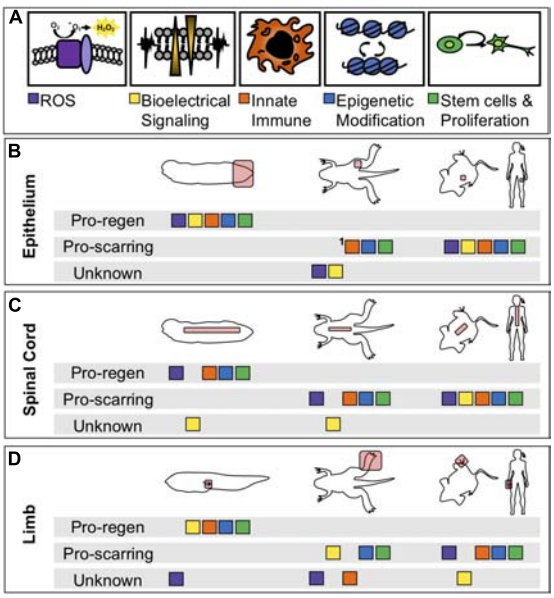

FIGURE 3 | Comparison of physiological phenomena during healing between regenerative and non-regenerative organisms. **(A)** Color coded boxes correspond to either ROS (purple), changes in membrane potential (yellow), innate immune cell recruitment (orange), epigenetic reprogramming (blue), or tissue-specific stem cell proliferation and differentiation (green). **(B-D)** Summarization of physiological phenomena either known to be associated with regenerative healing, known to be associated with scarring, or not yet studied (unknown) in regenerative and non-regenerative contexts or species. "Pro-regen" refers to epimorphic regeneration as described in this review. "Pro-scarring" refers to injuries that undergo wound healing and scarring. **(B)** Regeneration or scarring of the epithelium in tadpoles (left), late-metamorphic froglets with minimal regeneration (middle), non-regenerative mammals (right). **(C)** Regeneration or scarring of the spinal cord. **(D)** Regeneration or scarring of the amphibian limb and mammalian digit tip. [1]In adult frogs and mammals, the epidermal layer regenerates, however, the dermis is replaced by fibrous tissue.

sustained and regulated over regenerative time, and how their activation serves to recruit innate immune cells, as well as defining the subtypes of immune cells required for regeneration. We must also better define the cytokines or signals that directly mobilize transcription factors and epigenetic modifying enzymatic activities in the nucleus and define the direct targets of these factors. This latter step is critical to building an integrated picture of how upstream wounding events are coupled to the now vast amount of transcriptional data available in regeneration.

More fundamentally, while many of these processes have been identified as critical in a particular tissue or at a particular stage, few have been systematically interrogated at multiple stages of tadpole development, during limb regeneration, in specific tissues such as spinal cord regeneration, and during regenerative loss in the refractory period and metamorphosis. The current state of sampling of each experiment is summarized in **Table 1**. As demonstrated in the table, early injury responses have been well studied in tail regeneration but are understudied in spinal cord or limb regeneration. The information we have learned about ROS, bioelectrical signaling, and immune cell response in the spinal cord have been suggested from expression profiles but have not been explicitly tested (Lee-Liu et al., 2014). Moreover, it is unclear what roles these modalities play in non-regenerative contexts (**Figure 3**). In the non-regenerative frog, very few of these modalities have been directly tested leaving many open questions. Are these modalities used by wound healing and scarring? Do they serve a different role than in regeneration? In the short term, we can use well studied mammalian wound healing as a guide for the use of these modalities in wound healing. In a non-regenerative mammalian context, an epithelial wound or digit tip wound are followed by re-epithelialization, inflammation, proliferation, and fibrotic scarring (Gurtner et al., 2008; Choi et al., 2017). A spinal cord injury slightly differs as it does not undergo re-epithelialization and the scar is a product of reactive gliosis (Ahuja et al., 2017). Each of these injury types have shown the participation of ROS, bioelectrical signaling, epigenetic modification and chromatin accessibility changes, and proliferation. Although we see parallels between mammals and non-regenerative frogs we cannot draw direct comparisons, making the evaluation of regenerative and non-regenerative stage *Xenopus* difficult. By linking our current models of regeneration at the wounding and patterning level, and by leveraging the unique utility of *Xenopus* for examining regeneration in multiple tissues and ages, we eagerly anticipate a clearer and therapeutically tractable understanding of how to activate regenerative healing.

AUTHOR CONTRIBUTIONS

AK contributed to the writing and editing of the manuscript, drafting and editing of the figures, and drafting and editing of the table. AW contributed to the writing and editing of the manuscript, and editing of the figures and table.

FUNDING

This work was supported by NIH grants R01NS099124 and R03HD091716 to AW and training grant NIH T32GM007270 to AK.

ACKNOWLEDGMENTS

We thank members of the Wills Lab for helpful discussion contributing to this manuscript.

REFERENCES

Aboobaker, A. A. (2011). Planarian stem cells: a simple paradigm for regeneration. *Trends Cell. Biol.* 21, 304–311. doi: 10.1016/j.tcb.2011.01.005

Adams, D. S., Masi, A., and Levin, M. (2007). H+ pump-dependent changes in membrane voltage are an early mechanism necessary and sufficient to induce *Xenopus tail* regeneration. *Development* 134, 1323–1335. doi: 10.1242/dev.02812

Adams, D. S., Tseng, A.-S., and Levin, M. (2013). Light-activation of the Archaerhodopsin H+-pump reverses age-dependent loss of vertebrate regeneration: sparking system-level controls *in vivo*. *Biol. Open* 2, 306–313. doi: 10.1242/bio.20133665

Aguilar, C., and Gardiner, D. M. (2015). DNA methylation dynamics regulate the formation of a regenerative wound epithelium during axolotl limb regeneration. *PLoS One* 10:e0134791. doi: 10.1371/journal.pone.0134791

Ahuja, C. S., Wilson, J. R., Nori, S., Kotter, M. R. N., Druschel, C., Curt, A., et al. (2017). Traumatic spinal cord injury. *Nat. Rev. Dis. Primers* 3:17018. doi: 10.1038/nrdp.2017.18

Beck, C. W., Christen, B., and Slack, J. M. (2003). Molecular pathways needed for regeneration of spinal cord and muscle in a vertebrate. *Dev. Cell* 5, 429–439. doi: 10.1016/S1534-5807(03)00233-8

Beck, C. W., Izpisúa Belmonte, J. C., and Christen, B. (2009). Beyond early development: Xenopus as an emerging model for the study of regenerative mechanisms. *Dev. Dyn.?* 238, 1226–1248. doi: 10.1002/dvdy.21890

Belousov, V. V., Fradkov, A. F., Lukyanov, K. A., Staroverov, D. B., Shakhbazov, K. S., Terskikh, A. V., et al. (2006). Genetically encoded fluorescent indicator for intracellular hydrogen peroxide. *Nat. Methods* 3, 281–286. doi: 10.1038/nmeth866

Busse, S. M., McMillen, P. T., and Levin, M. (2018). Cross-limb communication during *Xenopus hindlimb* regenerative response: non-local bioelectric injury signals. *Development* 145:dev164210. doi: 10.1242/dev.164210

Cannata, S. M., Bagni, C., Bernardini, S., Christen, B., and Filoni, S. (2001). Nerve-independence of limb regeneration in larval *Xenopus laevis* is correlated to the level of fgf-2 mRNA expression in limb tissues. *Dev. Biol.* 231, 436–446. doi: 10.1006/dbio.2001.0161

Chang, J., Baker, J., and Wills, A. (2017). Transcriptional dynamics of tail regeneration in *Xenopus tropicalis*. *Genesis* 55:e23015. doi: 10.1002/dvg.23015

Chen, Y., Lin, G., and Slack, J. M. W. (2006). Control of muscle regeneration in the *Xenopus tadpole* tail byPax7. *Development* 133, 2303–2313. doi: 10.1242/dev.02397

Chen, Y., Love, N. R., and Amaya, E. (2014). Tadpole tail regeneration in Xenopus. *Biochem. Soc. Trans.* 42, 617–623. doi: 10.1042/BST20140061

Choi, Y., Meng, F., Cox, C. S., Lally, K. P., Huard, J., and Li, Y. (2017). Regeneration and regrowth potentials of digit tips in amphibians and mammals. *Int. J. Cell Biol.* 2017, 1–13. doi: 10.1155/2017/5312951

Christen, B., Beck, C. W., Lombardo, A., and Slack, J. M. W. (2003). Regeneration-specific expression pattern of three posterior Hox genes. *Dev. Dyn.* 226, 349–355. doi: 10.1002/dvdy.10231

Denko, N. C. (2008). Hypoxia, HIF1 and glucose metabolism in the solid tumour. *Nat. Rev. Cancer* 8, 705–713. doi: 10.1038/nrc2468

DENT, J. N. (1962). Limb regeneration in larvae and metamorphosing individuals of the South African clawed toad. *J. Morphol.* 110, 61–77. doi: 10.1002/jmor.1051100105

Farkas, J. E., Freitas, P. D., Bryant, D. M., Whited, J. L., and Monaghan, J. R. (2016). Neuregulin-1 signaling is essential for nerve-dependent axolotl limb regeneration. *Development* 143, 2724–2731. doi: 10.1242/dev.133363

Fei, J. F., Schuez, M., Knapp, D., Taniguchi, Y., Drechsel, D. N., and Tanaka, E. M. (2017). Efficient gene knockin in axolotl and its use to test the role of satellite cells in limb regeneration. *Proc. Natl. Acad. Sci. U.S.A.* 114, 12501–12506. doi: 10.1073/pnas.1706855114

Fei, J. F., Schuez, M., Tazaki, A., Taniguchi, Y., Roensch, K., and Tanaka, E. M. (2014). CRISPR-mediated genomic deletion of Sox2 in the axolotl shows a requirement in spinal cord neural stem cell amplification during tail regeneration. *Stem Cell Rep.* 3, 444–459. doi: 10.1016/j.stemcr.2014.06.018

Ferreira, F., Luxardi, G., Reid, B., and Zhao, M. (2016). Early bioelectric activities mediate redox-modulated regeneration. *Development* 143, 4582–4594. doi: 10.1242/dev.142034)

Ferreira, F., Raghunathan, V., Luxardi, G., Zhu, K., and Zhao, M. (2018). Early redox activities modulate *Xenopus tail* regeneration. *Nat. Commun.* 9:4296. doi: 10.1038/s41467-018-06614-2

Filoni, S., and Bosco, L. (1981). Comparative analysis of the regenerative capacity of caudal spinal cord in larvae of serveral Anuran amphibian species. *Acta Embryol. Morphol. Exp.* 2, 199–226.

Franklin, B. M., Voss, S. R., and Osborn, J. L. (2017). Ion channel signaling influences cellular proliferation and phagocyte activity during axolotl tail regeneration. *Mech. Dev.* 146, 42–54. doi: 10.1016/j.mod.2017.06.001

Gaete, M., Muñoz, R., Sánchez, N., Tampe, R., Moreno, M., Contreras, E. G., et al. (2012). Spinal cord regeneration in Xenopus tadpoles proceeds through activation of Sox2-positive cells. *Neural Dev.* 7:13. doi: 10.1186/1749-8104-7-13

Gargioli, C., and Slack, J. M. W. (2004). Cell lineage tracing during Xenopus tail regeneration. *Development* 131, 2669–2679. doi: 10.1242/dev.01155

Godwin, J. W., Pinto, A. R., and Rosenthal, N. A. (2013). Macrophages are required for adult salamander limb regeneration. *Proc. Natl. Acad. Sci. U.S.A.* 110, 9415–9420. doi: 10.1073/pnas.1300290110

Gurtner, G. C., Werner, S., Barrandon, Y., and Longaker, M. T. (2008). Wound repair and regeneration. *Nature* 453, 314–321. doi: 10.1038/nature07039

Hayashi, S., Kawaguchi, A., Uchiyama, I., Kawasumi-Kita, A., Kobayashi, T., Nishide, H., et al. (2015). Epigenetic modification maintains intrinsic limb-cell identity in Xenopus limb bud regeneration. *Dev. Biol.* 406, 271–282. doi: 10.1016/j.ydbio.2015.08.013

Hayashi, S., Kawaguchi, A., Uchiyama, I., Kawasumi-Kita, A., Kobayashi, T., Nishide, H., et al. (2015a). Epigenetic modification maintains intrinsic limb-cell identity in *Xenopus* limb bud regeneration. *Dev. Biol.* 406, 271–282. doi: 10.1016/j.ydbio.2015.08.013

Hayashi, S., Ochi, H., Ogino, H., Kawasumi, A., Kamei, Y., Tamura, K., et al. (2014). Transcriptional regulators in the Hippo signaling pathway control organ growth in *Xenopus* tadpole tail regeneration. *Dev. Biol.* 396, 31–41. doi: 10.1016/j.ydbio.2014.09.018

Ho, D. M., and Whitman, M. (2008). TGF-beta signaling is required for multiple processes during *Xenopus* tail regeneration. *Dev. Biol.* 315, 203–216. doi: 10.1016/j.ydbio.2007.12.031

Knapp, D., Schulz, H., Rascon, C. A., Volkmer, M., Scholz, J., Nacu, E., et al. (2013). Comparative transcriptional profiling of the axolotl limb identifies a tripartite regeneration-specific gene program. *PLoS One* 8:e61352. doi: 10.1371/journal.pone.0061352

Kolaczkowska, E., and Kubes, P. (2013). Neutrophil recruitment and function in health and inflammation. *Nat. Rev. Immunol.* 13, 159–175. doi: 10.1038/nri3399

Kragl, M., Knapp, D., Nacu, E., Khattak, S., Maden, M., Epperlein, H. H., et al. (2009). Cells keep a memory of their tissue origin during axolotl limb regeneration. *Nature* 460, 60–65. doi: 10.1038/nature08152

Kryczka, J., and Boncela, J. (2015). Leukocytes: the double-edged sword in fibrosis. *Mediators Inflamm.* 2015:652035. doi: 10.1155/2015/652035

Lai, S. L., Marín-Juez, R., Moura, P. L., Kuenne, C., Lai, J. K. H., Tsedeke, A. T., et al. (2017). Reciprocal analyses in zebrafish and medaka reveal that harnessing the immune response promotes cardiac regeneration. *eLife* 6:e25605. doi: 10.7554/eLife.25605

Lee-Liu, D., Moreno, M., Almonacid, L. I., Tapia, V. S., Muñoz, R., von, Marées J, et al. (2014). Genome-wide expression profile of the response to spinal cord injury in *Xenopus laevis* reveals extensive differences between regenerative and non-regenerative stages. *Neural Dev.* 9:12. doi: 10.1186/1749-8104-9-12

Lin, G., and Slack, J. M. W. (2008). Requirement for Wnt and FGF signaling in *Xenopus tadpole* tail regeneration. *Dev. Biol.* 316, 323–335. doi: 10.1016/j.ydbio.2008.01.032

Love, N. R., Chen, Y., Bonev, B., Gilchrist, M. J., Fairclough, L., Lea, R., et al. (2011). Genome-wide analysis of gene expression during Xenopus tropicalis tadpole tail regeneration. *BMC Dev. Biol.* 11:70. doi: 10.1186/1471-213X-11-70

Love, N. R., Chen, Y., Ishibashi, S., Kritsiligkou, P., Lea, R., Koh, Y., et al. (2013). Amputation-induced reactive oxygen species are required for successful *Xenopus tadpole* tail regeneration. *Nat. Cell. Biol.* 15, 222–228. doi: 10.1038/ncb2659

Love, N. R., Ziegler, M., Chen, Y., and Amaya, E. (2014). Carbohydrate metabolism during vertebrate appendage regeneration: What is its role? How is it regulated? *Bioessays* 36, 27–33. doi: 10.1002/bies.201300110

Makanae, A., Mitogawa, K., and Satoh, A. (2014). Co-operative Bmp- and Fgf-signaling inputs convert skin wound healing to limb formation in urodele amphibians. *Dev. Biol.* 396, 57–66. doi: 10.1016/j.ydbio.2014.09.021

McCusker, C., Bryant, S. V., and Gardiner, D. M. (2015). The axolotl limb blastema: cellular and molecular mechanisms driving blastema formation and limb regeneration in tetrapods. *Regeneration* 2, 54–71. doi: 10.1002/reg2.32

McCusker, C. D., Diaz-Castillo, C., Sosnik, J., Phan, A. Q., et al. (2016). Cartilage and bone cells do not participate in skeletal regeneration in *Ambystoma mexicanum* limbs. *Dev. Biol.* 416, 26–33. doi: 10.1016/j.ydbio.2016.05.032

Mescher, A. L., Neff, A. W., and King, M. W. (2013). Changes in the inflammatory response to injury and its resolution during the loss of regenerative capacity in developing *Xenopus* Limbs. *PLoS One* 8:e80477. doi: 10.1371/journal.pone.0080477

Monteiro, J., Aires, R., Becker, J. D., Jacinto, A., Certal, A. C., and Rodríguez-León, J. (2014). V-ATPase proton pumping activity is required for adult zebrafish appendage regeneration. *PLoS One* 9:e92594. doi: 10.1371/journal.pone.0092594

Morrison, J. I., Lööf, S., He, P., and Simon, A. (2006). Salamander limb regeneration involves the activation of a multipotent skeletal muscle satellite cell population. *J. Cell Biol.* 172, 433–440. doi: 10.1083/jcb.200509011

Muñoz, R., Edwards-Faret, G., Moreno, M., Zuñiga, N., Cline, H., and Larraín, J. (2015). Regeneration of *Xenopus laevis* spinal cord requires Sox2/3 expressing cells. *Dev. Biol.* 408, 229–243. doi: 10.1016/j.ydbio.2015.03.009

Pai, V. P., Martyniuk, C. J., Echeverri, K., Sundelacruz, S., Kaplan, D. L., and Levin, M. (2016). Genome-wide analysis reveals conserved transcriptional responses downstream of resting potential change in *Xenopus* embryos, axolotl regeneration, and human mesenchymal cell differentiation. *Regeneration* 3, 3–25. doi: 10.1002/reg2.48

Paré, J.-F., Martyniuk, C. J., and Levin, M. (2017). Bioelectric regulation of innate immune system function in regenerating and intact *Xenopus laevis*. *NPJ Regen. Med.* 2:15. doi: 10.1038/s41536-017-0019-y

Paredes, R., Ishibashi, S., Borrill, R., Robert, J., and Amaya, E. (2015). Xenopus: an *in vivo* model for imaging the inflammatory response following injury and bacterial infection. *Dev. Biol.* 408, 213–228. doi: 10.1016/j.ydbio.2015.03.008

Rojas-Muñoz, A., Rajadhyksha, S., Gilmour, D., van, Bebber F, Antos, C., Rodríguez, Esteban C, et al. (2009). ErbB2 and ErbB3 regulate amputation-induced proliferation and migration during vertebrate regeneration. *Dev. Biol.* 327, 177–190. doi: 10.1016/j.ydbio.2008.12.012

Rosales, C. (2018). Neutrophil: a cell with many roles in inflammation or several cell types? *Front. Physiol.* 9:113. doi: 10.3389/fphys.2018.00113

Sánchez Alvarado, A. (2007). Stem cells and the planarian *Schmidtea mediterranea*. *C. R. Biol.* 330, 498–503. doi: 10.1016/j.crvi.2007.05.005

Santabárbara-Ruiz, P., López-Santillán, M., Martínez-Rodríguez, I., Binagui-Casas, A., Pérez, L., Milán, M., et al. (2015). ROS-induced JNK and p38 signaling is required for unpaired cytokine activation during drosophila regeneration. *PLoS Genet.* 11:e1005595. doi: 10.1371/journal.pgen.1005595

Simkin, J., Gawriluk, T. R., Gensel, J. C., and Seifert, A. W. (2017). Macrophages are necessary for epimorphic regeneration in African spiny mice. *eLife* 6:e24623. doi: 10.7554/eLife.24623

Simões, M. G., Bensimon-Brito, A., Fonseca, M., Farinho, A., Valério, F., Sousa, S., et al. (2014). Denervation impairs regeneration of amputated zebrafish fins. *BMC Dev. Biol.* 14:49. doi: 10.1186/s12861-014-0049-2

Singer, M., and Craven, L. (1948). The growth and morphogenesis of the regenerating forelimb of adult Triturus following denervation at various stages of development. *J. Exp. Zool.* 108, 279–308. doi: 10.1002/jez.1401080207

Stewart, R., Rascón, C. A., Tian, S., Nie, J., Barry, C., Chu, L. F., et al. (2013). Comparative RNA-seq analysis in the unsequenced axolotl: the oncogene burst highlights early gene expression in the blastema. *PLoS Comput. Biol.* 9:e1002936. doi: 10.1371/journal.pcbi.1002936

Sugiura, T., Tazaki, A., Ueno, N., Watanabe, K., and Mochii, M. (2009). Xenopus Wnt-5a induces an ectopic larval tail at injured site, suggesting a crucial role for noncanonical Wnt signal in tail regeneration. *Mech. Dev.* 126, 56–67. doi: 10.1016/j.mod.2008.10.002

Suzuki, M., Takagi, C., Miura, S., Sakane, Y., Suzuki, M., Sakuma, T., et al. (2016). In vivo tracking of histone H3 lysine 9 acetylation in Xenopus laevis during tail regeneration. *Genes Cells* 21, 358–369. doi: 10.1111/gtc.12349

Suzuki, M., Yakushiji, N., Nakada, Y., Satoh, A., Ide, H., and Tamura, K. (2006). Limb regeneration in xenopus laevis froglet. *Sci. World J.* 6, 26–37. doi: 10.1100/tsw.2006.325

Tanaka, E. M. (2016). The molecular and cellular choreography of appendage regeneration. *Cell* 165, 1598–1608. doi: 10.1016/j.cell.2016.05.038

Taniguchi, Y., Sugiura, T., Tazaki, A., Watanabe, K., and Mochii, M. (2008). Spinal cord is required for proper regeneration of the tail in Xenopus tadpoles. *Dev. Growth Differ.* 50, 109–120. doi: 10.1111/j.1440-169X.2007.00981.x

Taniguchi, Y., Watanabe, K., and Mochii, M. (2014). Notochord-derived hedgehog is essential for tail regeneration in Xenopus tadpole. *BMC Dev. Biol.* 14:27. doi: 10.1186/1471-213X-14-27

Tapia, V. S., Herrera-Rojas, M., and Larrain, J. (2017). JAK-STAT pathway activation in response to spinal cord injury in regenerative and non-regenerative stages of *Xenopus laevis*. *Regeneration* 4, 21–35. doi: 10.1002/reg2.74

Taylor, A. J., and Beck, C. (2012). WHistone deacetylases are required for amphibian tail and limb regeneration but not development. *Mech. Dev.* 129, 208–218. doi: 10.1016/j.mod.2012.08.001

Todd, J. T. (1823). On the process of reproduction of the members of the aquatic salamander. *Quart. J. Sci. Lit. Arts* 16, 84–96.

Tseng, A. S., Beane, W. S., Lemire, J. M., Masi, A., and Levin, M. (2010). Induction of vertebrate regeneration by a transient sodium current. *J. Neurosci.* 30, 13192–13200. doi: 10.1523/JNEUROSCI.3315-10.2010

Tseng, A.-S., Carneiro, K., Lemire, J. M., and Levin, M. (2011). HDAC activity is required during Xenopus tail regeneration. *PLoS One* 6:e26382. doi: 10.1371/journal.pone.0026382

Tseng, A.-S., and Levin, M. (2012). Transducing bioelectric signals into epigenetic pathways during tadpole tail regeneration. *Anat. Rec.* 295, 1541–1551. doi: 10.1002/ar.22495

Tsujioka, H., Kunieda, T., Katou, Y., Shirahige, K., Fukazawa, T., and Kubo, T. (2017). Interleukin-11 induces and maintains progenitors of different cell lineages during Xenopus tadpole tail regeneration. *Nat. Commun.* 8:495. doi: 10.1038/s41467-017-00594-5

Tsujioka, H., Kunieda, T., Katou, Y., Shirahige, K., and Kubo, T. (2015). Unique gene expression profile of the proliferating *Xenopus* Tadpole tail blastema cells deciphered by RNA-sequencing analysis. *PLoS One* 10:e0111655. doi: 10.1371/journal.pone.0111655

Vander Heiden, M. G., Cantley, L. C., and Thompson, C. B. (2009). Understanding the warburg effect: the metabolic requirements of cell proliferation. *Science* 324, 1029–1033. doi: 10.1126/science.1160809

Villiard, E., Brinkmann, H., Moiseeva, O., Mallette, F. A., Ferbeyre, G., and Roy, S. (2007). Urodele p53 tolerates amino acid changes found in p53 variants linked to human cancer. *BMC Evol. Biol.* 7:180. doi: 10.1186/1471-2148-7-180

Wilgus, T. A., Roy, S., and McDaniel, J. C. (2013). Neutrophils and wound repair: positive actions and negative reactions. *Adv. Wound Care* 2, 379–388. doi: 10.1089/wound.2012.0383

Yakushiji, N., Suzuki, M., Satoh, A., Sagai, T., Shiroishi, T., Kobayashi, H., et al. (2007). Correlation between Shh expression and DNA methylation status of the limb-specific Shh enhancer region during limb regeneration in amphibians. *Dev. Biol.* 312, 171–182. doi: 10.1016/j.ydbio.2007.09.022

Yntema, C. (1959). Regeneration in sparsely innervated and aneurogenic orelimbs of *Ambystoma larvae*. *J. Exp. Zool.* 140, 101–123. doi: 10.1002/jez.1401400106

Yun, M. H., Gates, P. B., and Brockes, J. P. (2013). Regulation of p53 is critical for vertebrate limb regeneration. *Proc. Natl. Acad. Sci. U.S.A.* 110, 17392–17397. doi: 10.1073/pnas.1310519110

Conflict of Interest Statement: The authors declare that the research was conducted in the absence of any commercial or financial relationships that could be construed as a potential conflict of interest.

frontiers in Physiology

ORIGINAL RESEARCH
published: 25 February 2019
doi: 10.3389/fphys.2019.00134

The Frog *Xenopus* as a Model to Study Joubert Syndrome: The Case of a Human Patient With Compound Heterozygous Variants in *PIBF1*

Tim Ott[1], Lilian Kaufmann[2], Martin Granzow[2], Katrin Hinderhofer[2], Claus R. Bartram[2], Susanne Theiß[2], Angelika Seitz[3], Nagarajan Paramasivam[4,5], Angela Schulz[6], Ute Moog[2], Martin Blum[1†] and Christina M. Evers[2†]*

[1] Institute of Zoology, University of Hohenheim, Stuttgart, Germany, [2] Institute of Human Genetics, Heidelberg University, Heidelberg, Germany, [3] Department of Neuroradiology, University Hospital Heidelberg, Heidelberg, Germany, [4] Medical Faculty Heidelberg, Heidelberg University, Heidelberg, Germany, [5] Division of Theoretical Bioinformatics, German Cancer Research Center (DKFZ), Heidelberg, Germany, [6] Genomics & Proteomics Core Facility, German Cancer Research Center (DKFZ), Heidelberg, Germany

OPEN ACCESS

Edited by:
Emily Sempou,
Yale University, United States

Reviewed by:
Mustafa Khokha,
Yale University, United States
Sally Ann Moody,
George Washington University,
United States

***Correspondence:**
Christina M. Evers
christina.evers@med.uni-heidelberg.de

[†] These authors have contributed equally to this work

Specialty section:
This article was submitted to Embryonic and Developmental Physiology, a section of the journal Frontiers in Physiology

Received: 14 September 2018
Accepted: 04 February 2019
Published: 25 February 2019

Citation:
Ott T, Kaufmann L, Granzow M, Hinderhofer K, Bartram CR, Theiß S, Seitz A, Paramasivam N, Schulz A, Moog U, Blum M and Evers CM (2019) The Frog Xenopus as a Model to Study Joubert Syndrome: The Case of a Human Patient With Compound Heterozygous Variants in PIBF1. Front. Physiol. 10:134. doi: 10.3389/fphys.2019.00134

Joubert syndrome (JS) is a congenital autosomal-recessive or—in rare cases–X-linked inherited disease. The diagnostic hallmark of the so-called molar tooth sign describes the morphological manifestation of the mid- and hind-brain in axial brain scans. Affected individuals show delayed development, intellectual disability, ataxia, hyperpnea, sleep apnea, abnormal eye, and tongue movements as well as hypotonia. At the cellular level, JS is associated with the compromised biogenesis of sensory cilia, which identifies JS as a member of the large group of ciliopathies. Here we report on the identification of novel compound heterozygous variants (p.Y503C and p.Q485*) in the centrosomal gene *PIBF1* in a patient with JS via trio whole exome sequencing. We have studied the underlying disease mechanism in the frog *Xenopus*, which offers fast assessment of cilia functions in a number of embryological contexts. Morpholino oligomer (MO) mediated knockdown of the orthologous *Xenopus pibf1* gene resulted in defective mucociliary clearance in the larval epidermis, due to reduced cilia numbers and motility on multiciliated cells. To functionally assess patient alleles, mutations were analyzed in the larval skin: the p.Q485* nonsense mutation resulted in a disturbed localization of PIBF1 to the ciliary base. This mutant failed to rescue the ciliation phenotype following knockdown of endogenous *pibf1*. In contrast, the missense variant p.Y503C resulted in attenuated rescue capacity compared to the wild type allele. Based on these results, we conclude that in the case of this patient, JS is the result of a pathogenic combination of an amorphic and a hypomorphic *PIBF1* allele. Our study underscores the versatility of the *Xenopus* model to study ciliopathies such as JS in a rapid and cost-effective manner, which should render this animal model attractive for future studies of human ciliopathies.

Keywords: PIBF1, Joubert syndrome, *Xenopus*, molar tooth sign, cilia, ciliopathy

INTRODUCTION

Joubert syndrome (JS, OMIM # 213300) comprises a group of autosomal recessive or X-linked inherited disorders with a distinct cerebellar and brainstem malformation recognizable on brain imaging, the "molar tooth sign." The typical brain malformation of JS patients gives their midbrain an appearance reminiscent of a molar or wisdom tooth on axial MRI (**Figures 1E–H**). The "molar tooth" appearance results from three anatomical abnormalities of brainstem and cerebellum: (a) an abnormally deep "interpeduncular fossa," (b) prominent, thickened, and elongated "superior cerebellar peduncles," and (c) absence or hypoplasia of the midline portion of the cerebellum, the "cerebellar vermis" (see **Figures 1E–H** for the "molar tooth sign" and **Figures 1I–L** showing the corresponding MRI of a healthy control individual) (Maria et al., 1997, 1999). Typical clinical symptoms of JS are hypotonia, global developmental delay, intellectual disability, abnormal breathing pattern, abnormal eye movements, and cerebellar ataxia. Additional features include retinal dystrophy, cystic kidney disease, liver fibrosis, polydactyly, cleft palate, and facial dysmorphism in some patients (for review see (Parisi and Glass, 1993)). The estimated birth prevalence of JS is 1:80,000–1:100,000 (Parisi and Glass, 1993), but this may represent an underestimate due to many undiagnosed cases. A higher prevalence is found in the French–Canadian population, with several founder variants noted (Badhwar et al., 2000; Srour et al., 2012a,b, 2015). Founder variants in different genes have also been identified in the Canadian Hutterite, the Ashkenazi Jewish, and the Dutch population (Edvardson et al., 2010; Valente et al., 2010; Huang et al., 2011; Shaheen et al., 2014; Kroes et al., 2016). To date, pathogenic variants in more than 30 genes are known to cause JS (for review see Parisi and Glass, 1993). The encoded proteins of all these genes localize either to the primary cilium, basal body and/or centrosome and play a role in the formation, morphology, and/or function of these organelles, rendering JS a member of the rapidly expanding family of ciliopathies (Parisi and Glass, 1993; Romani et al., 2013). Common features of many ciliopathies include brain malformation, renal disease, retinal dystrophy, and polydactyly. Pathogenic variants in genes that cause Joubert syndrome have also been identified in ciliopathies with clinical findings that overlap with JS, e.g., Meckel-Gruber syndrome (MKS), Jeune asphyxiating thoracic dystrophy (JATD), Bardet-Biedl syndrome (BBS), oral-facial-digital syndrome (OFD), and juvenile nephronophthisis. The severe end of the clinical spectrum is represented by the lethal disorder MKS (Barker et al., 2014). Most of the genes causative of MKS are also associated with JS, namely *CEP290, TMEM67, RPGRIP1L, CC2D2A, CEP41, MKS1, B9D1, B9D2, TMEM138, TMEM231, TCTN2, TCTN3, TMEM237, CPLANE1, CSPP1, CEP120, TMEM107,* and *TMEM216* (Parisi and Glass, 1993; Valente et al., 2010; Thomas et al., 2012; Romani et al., 2014; Bachmann-Gagescu et al., 2015; Knopp et al., 2015; Shaheen et al., 2015; Roosing et al., 2016; Slaats et al., 2016). In addition, several families with occurrence of JS and MKS in siblings have been reported (Brancati et al., 2009; Valente et al., 2010). Features of the skeletal ciliopathy JATD have been reported in several children with JS caused by mutations in *CSPP1* and *KIAA0586* (Tuz et al., 2014; Malicdan et al., 2015). Pathogenic variants in the three BBS genes *CEP290*, *MKS1*, and *NPHP1* have been shown to cause both BBS and JS (Leitch et al., 2008; Zaghloul and Katsanis, 2009; Knopp et al., 2015). Patients with oral-facial-digital syndrome (OFD) show features that overlap considerably with JS, as do several genes causative for OFD (Franco and Thauvin-Robinet, 2016). Patients with juvenile nephrophthisis can also show clinical overlap with JS: about 10% of individuals have extrarenal findings, including the molar tooth sign in some cases (Saunier et al., 2005). Conversely, nephronophthisis, can also be a renal manifestation in JS (Parisi and Glass, 1993). These examples illustrate the complex clinical and genetic background of JS and related ciliopathies. Preliminary genotype-phenotype correlation for some genes indicate that biallelic null alleles lead to MKS while at least one hypomorphic (e.g., missense) variant is associated with JS (Delous et al., 2007; Mougou-Zerelli et al., 2009; Tallila et al., 2009; Iannicelli et al., 2010; Romani et al., 2014). However, the molecular and cellular mechanisms that lead to a specific phenotype in patients with ciliopathies are not fully understood. Altered sonic hedgehog (SHH) signaling via defective cilia has been proposed to be the causative pathomechanism for the characteristic molar tooth sign in JS, but does not fully explain the mid-hindbrain phenotype (Spassky et al., 2008; Doherty, 2009).

Recently, mutations in *PIBF1* have been identified as a cause of JS, using a combination of a siRNA-based functional genomics screen and exome sequencing data (Wheway et al., 2015). A second publication reported a girl with a biallelic 36-bp insertion in *PIBF1* and clinical signs of JS (Hebbar et al., 2018). The patients presented with ataxia and developmental delay, ranging from mild to moderate. Imaging ranged from the classic molar tooth sign to moderate vermis hypoplasia with mildly thick superior cerebellar peduncles and characteristic superior cerebellar dysplasia (Wheway et al., 2015). In addition, thinning of corpus callosum, facial dysmorphism, hypotonia and enlarged cystic kidneys were observed in one patient (Hebbar et al., 2018). Polymicrogyria has not been described in association with *PIBF1* variants so far.

PIBF1, also known as *PIBF, CEP90, JBTS33,* and *C13orf24,* consists of 22 coding exons and is widely expressed in different human tissues, including the brain, kidney, and liver, with the highest expression in testis and thyroid (Fagerberg et al., 2014). *PIBF1* encodes the progesterone immunomodulatory binding factor 1 that is induced by the steroid hormone progesterone and overexpressed in highly proliferating cells (Lachmann et al., 2004; Cohen et al., 2016). The parent compound measures 90 kDa and is associated with the centrosome (Lachmann et al., 2004). A splice variant that is found in cytoplasm measures 34–36 kDa (Polgar et al., 2003; Lachmann et al., 2004). The protein regulates the immune system to maintain a normal pregnancy, may play a role in preterm labor and promotes the proliferation, migration, and invasion of astrozytoma/glioblastoma cells (Gonzalez-Arenas et al., 2014; Hudic et al., 2015, 2016; Gutierrez-Rodriguez et al., 2017). *PIBF1* encodes a centrosomal protein that may play an important role in ciliogenesis (Wheway et al., 2015). However, the precise molecular and cellular mechanisms that cause the

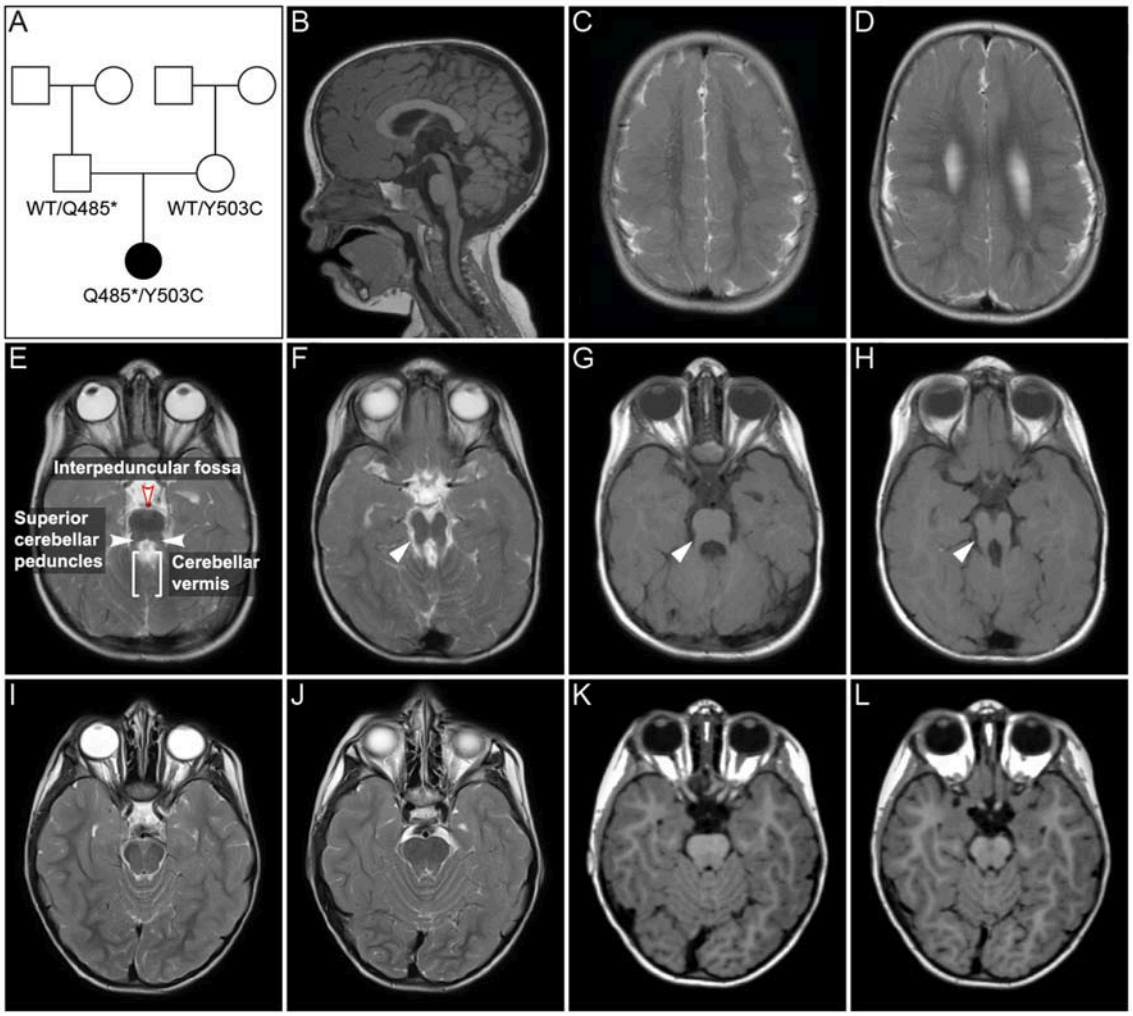

FIGURE 1 | Pedigree and MRI scans. **(A)** Pedigree of patient family. Black symbol, affected individual; White symbols, unaffected individuals. **(B–H)** MR imaging of the patient at age 2 years and 6 months. Sagittal **(B)** and axial **(C–H)** images showed polymicrogyria in the parietal and temporal region **(C,D)** and hypoplasia of vermis cerebellum **(B,E–H)**. Axial MR images of cerebellum and brainstem **(E–H)** showed a mild "molar tooth sign" (marked with white arrows in **F–H**) due to a deep interpeduncular fossa, prominent and elongated superior cerebellar peduncles and a hypoplastic cerebellar vermis. **(I–L)** Corresponding MR images of a healthy control individual.

complex JS phenotype in individuals with *PIBF1* mutations have not yet been elucidated.

Here, we report on novel *PIBF1* variants in a girl with JS. The variants were identified by whole-exome sequencing (WES) and functionally assessed in the *Xenopus* model. Our analyses demonstrate that both *PIBF1* alleles reflected loss of function variants. In general terms, the *Xenopus* model proves to be an excellent model to study the functional impact of rare genetic variants identified by diagnostic exome sequencing in patients with human ciliopathies.

MATERIALS AND METHODS

Participants

The patient and her parents were recruited and clinically phenotyped by the Outpatient Clinic of the Institute of Human Genetics, University Hospital Heidelberg, as part of the "Genome-wide genetic analysis of rare hereditary disorders" study. Written informed consent for participation in the study and publication of study results was obtained from both parents. The study was approved by the Ethics Committee of the Faculty of Medicine at the University of Heidelberg and adhered to the tenets of the Declaration of Helsinki. A summary of the study results and its clinical implications have been published elsewhere (Evers et al., 2017). Written informed consent for the publication of this case report and parental results was obtained from the patient's parents.

Case Report

The girl was the first child of non-consanguineous healthy parents from Germany. Her pedigree is shown in **Figure 1A**. She was born after 40 weeks of gestation with a birth weight

of 2,620 g (1st centile), length of 48 cm (3rd centile), and head circumference (OFC) of 34 cm (20th centile). Soon after birth, spastic tetraparesis, truncal hypotonia, and feeding difficulties were noted. At age 6 months, she developed abnormal eye movements. An electroencephalogram (EEG) was normal. The girl showed a severe failure to thrive and developmental delays. Routine pediatric investigations, including basic laboratory testing and metabolic screening, resulted in normal values with the exception of mildly elevated liver enzymes (GOT: 134U/l, GTP: 164 U/l, GGT: 493 U/l), which persisted during childhood. Regular abdominal ultrasound examinations were normal with no signs of hepatic fibrosis. Ophthalmological examination including fundoscopy at age 3 years showed no abnormalities. At her first visit to the Genetic Outpatient Department at age 4 years 2 month, she presented with global developmental delay, no speech, spastic tetraplegia and a submucosal cleft palate. Her height was 85 cm (<1st centile, −4.99 SDS), her weight 11.47 kg (<1st centile, −3.08 SDS) and her OFC 49.5 cm (8th centile, −1.43 SDS). At follow up examination at age 6 years 9 months, she had a height of 98.0 cm (<1st centile, −5.49 SDS), a weight of 13.6 kg (<1st centile, −4.30 SDS) and an OFC of 50 cm (2nd centile, −2.09 SDS). cMRI at age 6 months revealed bilateral polymicrogyria in the parietal and temporal areas. Follow up MRIs at age 23 months and 2 years and 6 months showed polymicrogyria, hypoplasia of vermis cerebelli, and a mild molar tooth sign (**Figures 1E–H**). Chromosomal analysis and molecular karyotyping (array analysis) gave normal results. Gene panel diagnostics for Joubert syndrome by next generation sequencing of 129 known and potentially ciliopathy genes showed no pathogenic mutation. The gene panel did not include *PIBF1*, which was not known to cause JS at the time of analysis. A single gene test by Sanger sequencing of *GPR5*, a gene associated with polymicrogyria, gave normal results.

Exome Sequencing

Genomic DNA was isolated from leukocytes of the patient and both parents by standard procedures (Miller et al., 1988). Whole exome sequencing (WES) and analysis of the sequence data of the patient and her parents was performed at the German Cancer Research Center (DKFZ) in Heidelberg, Germany, as described previously (Paramasivam et al., 2018). Variants with a minor allele frequency (MAF) >1% in the 1000 genome phase III and Exome Aggregation Consortium (ExAC) database (Lek et al., 2016) were considered common alleles and discarded, as were variants detected in 328 WES and 177 whole genome sequencing (WGS) local control samples with a frequency above 2%. Gene-based annotations from Gencode V19 were added using ANNOVAR (Wang et al., 2010). All single nucleotide variants (SNVs) and indels affecting protein sequences and variants within ±2 bases around the intron-exon junction were considered as functional. Variants were further assessed by the seven different variant effect prediction tools SIFT, PolyPhen2, LRT, MutationTaster, MutationAssessor, FATHMM, and PROVEAN from dbNSFP (Ng and Henikoff, 2003; Chun and Fay, 2009; Adzhubei et al., 2010; Schwarz et al., 2010; Reva et al., 2011; Choi et al., 2012; Liu et al., 2013; Shihab et al., 2013) and CADD scores (Kircher et al., 2014). Variants were classified according to standards and guidelines of the American College of Medical Genetics and Genomics (ACMG) (Richards et al., 2015). To confirm WES data by Sanger sequencing, exons 11 and 12 and adjacent intron boundaries of *PIBF1* (RefSeq NM_006346.2, ensemble transcript ENST00000326291.6) were sequenced using Big Dye Terminator V1.1 cycle sequencing kit and ABI 3130xl genetic analyzer. Primer sequences and PCR conditions are available upon request.

RT PCR, qPCR, and Sequencing

Total RNA from patients, parents, and control blood was extracted using the MasterPure RNA Purification Kit (Epicentre Biotechnologies). cDNA was synthesized using random hexamer primers and reverse transcriptase RT Maxima (Fermentas). qPCR was carried out using SybrGreen mix (Thermo Scientific). Expression levels using primer pairs for the three regions of *PIBF1* (exon 2–4, exon 10–12, exon 15–17) were normalized to *ADP-ribosylation factor 1 (ARF1)*. PCR products of patient, parents and control were sequenced by Sanger sequencing (GATC).

Western Blot Analysis of Overexpressed Protein

To analyze the expression of overexpressed PIBF1 variants, Hek293T cells were transfected in 6-well plates with 1 μg of the corresponding plasmids using Turbofect transfection reagent (Thermo Scientific. Cells were lysed 24 h post transfection and proteins were separated by 10% SDS-PAGE. For Western blot analysis, a rabbit anti-GFP antibody (1:1,000, Adgene) and a mouse anti-PIBF1 antibody (1:500, Biozol) were used.

Protein Structure Analysis

For analyzing putative protein domains, the following algorithms were used: NCBI conserved domain search (https://www.ncbi.nlm.nih.gov/Structure/cdd/wrpsb.cgi), InterProScan (https://www.ebi.ac.uk/interpro/search/sequence-search), WoLF PSORT (https://wolfpsort.hgc.jp), and epestfind (http://emboss.bioinformatics.nl/cgi-bin/emboss/epestfind).

Xenopus Injection Experiments

Adult *Xenopus laevis* frogs were obtained from Nasco (U.S.A.; https://www.enasco.com/c/Education-Supplies/Xenopus-Frogs). *Xenopus laevis* embryos were injected at the 4-cell stage into the ventral marginal zone to target the epidermal cell lineage (Moody, 2000). Translation blocking morpholino oligomere (TBMO; 5′-CCGGGACATCTTTACACTTTACATA-3′) was injected at 4 pmol per embryo. mRNAs of *EGFP* or *PIBF1* fusion constructs were injected at a dose of 0.4 pmol per embryo. Lineage tracer Fluorescein Dextran (FD, 10,000 MW, anionic, lysine fixable) was used at 50 ng per injection. Embryos were cultured until stage 30 and subsequently processed for analyses.

RNA *in situ* Hybridization and Immunofluorescence Staining

Xenopus embryos were fixed using 4% paraformaldehyde solution (for *in situ* hybridization and acetylated Tuba4a staining) or Dent's (for Pibf1 and Tjp1 staining). RNA *in*

situ hybridization was performed as described previously (Belo et al., 1997) using a full length digoxigenin labeled *pibf1* probe. The following reagents were used for immunofluorescence staining: anti-acetylated Tuba4a (T6793, Sigma; 1:800), anti-Pibf1 (SAB1401526, Sigma; 1:200), and anti-Tjp1 (21773-1-AP, Proteintech Europe; 1:400).

High-Speed Video-Microscopy

Capturing of ciliary beating required flat mounting of the specimens in a chamber constructed on a slide with tape and a cover slip. Only the most ventral cells allowed differential interference contrast microscopy of the ciliary tufts, which were recorded at 600 fps using a Hamamatsu X high speed video camera. Kymographs were generated using ImageJ (https://imagej.net/Generate_and_exploit_Kymographs).

RESULTS

The phenotypic features of the patient (cf. section Case Report), including developmental delay, hypotonia, polymicrogyria, vermian hypoplasia, and mild molar tooth sign (**Figure 1**), led to the clinical diagnosis of JS. The observed liver involvement with elevated GOT/GRP is also a typical finding of this ciliopathy. A cleft palate reported here is a rare finding in JS and demonstrates its clinical overlap with oral-facial-digital syndrome. The microcephaly of the patient is not part of the classical JS spectrum, but has been reported in a patient with a *PIBF1* missense mutation (Kodani et al., 2015).

Exome Sequencing

Exome sequencing variants were filtered as described above and only heterozygous *de novo* variants and variants being consistent with an autosomal recessive disease model were considered. Applying these filter criteria, 10 variants remained (**Table 1**). These were further assessed by *in silico* predicted effects on protein function, as described above (**Table 1**). Subsequently, a literature search was performed to gain further information about gene function and to determine if the gene had been previously associated with intellectual disability, neurological or developmental disorders in humans. This narrowed the candidate list to *PIBF1* variants c.1453C>T; p.(Q485*) and c.1508A>G; p.(Y503C). The variant c.1453C>T; p.(Q485*) was classified as pathogenic [class 5, according to ACMG criteria; (Richards et al., 2015)]. The variant c.1508A>G; p.(Y503C) was classified as variant of unknown significance [class 3, according to (Richards et al., 2015)].

Expression Analysis of *PIBF1* Variants in the Patient

cDNA fragments of three different regions of *PIBF1* (exons 2–4, 10–12, and 15–17) were amplified from the patient and both parents, showing a higher expression in the patient compared to mother, father, adult, and infant control (**Figure S1A**). Interestingly, the cDNA of exons 15–17, which are localized 3′ of the predicted premature stop codon of the variant p.(Q485*), showed a higher expression in the patient as well. However, whether both variants are transcribed in the patient was still unclear. Sequencing of the PCR product of the patient showed that both *PIBF1* variants could be detected in the patient (**Figure 2A**). The parents' cDNAs carried either the missense or the nonsense variant in heterozygous state (data not shown). This indicated that mRNA harboring the predicted pathogenic variant was not degraded by nonsense-mediated mRNA decay (NMD) and that both variants resulted in stable mRNAs. The enhanced transcription of both *PIBF1* variants in the patient could be a compensatory response to decreased PIBF1 protein levels due to protein instability of the mutants. The *PIBF1* nonsense variant p.(Q485*) was expected to result in the synthesis of a truncated protein lacking the C-terminal 273 amino acids. Expression

TABLE 1 | *De novo* and compound heterozygous variants and prediction of their functional effects.

Affected genes	RefSeq transcript and variant information*	Variant status	*in silico* parameters **: MT/MA/SIFT/PPH2(HDIV: HVAR)//FATMM/PROVEAN/LRT
ATXN1	ENST00000436367.1:exon7:c.G630T:p.Q210H	Heterozygous *de novo*	N/N/D/-:-/T/N/-
DSPP	ENST00000399271.1:exon5:c.2001_2003del:p.667_668del	Heterozygous *de novo*	Poly/-/-/-:-/-/-/-
EPS8L2	ENST00000318562.8:exon8:c.G616T:p.A206S	Heterozygous	DC/M/T/B:B/T/N/Del
EPS8L2	ENST00000318562.8:exon13:c.1071_1072insCTG:p.T357delinsTL	Heterozygous	Poly /-/-/-:-/-/-/-
OBSCN	ENST00000366707.4:exon52:c.A5292T:p.Q1764H	Heterozygous	N/N/T/D:P/T/N/N
OBSCN	ENST00000422127.1:exon94:c.20514_20515del:p.6838_6839del	Heterozygous	DC/-/-/-:-/-/-/-
PIBF1	ENST00000326291.6:exon11:c.C1453T:p.Q485X	Heterozygous	DC/-/-/-:-/-/-/-
PIBF1	ENST00000326291.6:exon12:c.A1508G:p.Y503C	Heterozygous	DC/M/D/D:D/T/D/Del
ZFHX3	ENST00000397992.5:exon9:c.C7543T:p.R2515C	Heterozygous	DC/N/T/D:B/D/N/Del
ZFHX3	ENST00000397992.5:exon8:c.G5535T:p.Q1845H	Heterozygous	DC/L/T/D:D/T//Del

**According to Ensembl database (http://www.ensembl.org).*

***Obtained by prediction tools MutationTaster (MT) (Schwarz et al., 2010), MutationAssessor (MA) (Reva et al., 2011), SIFT (Ng and Henikoff, 2003), PolyPhen2 (PPH2) HDIV and PPH2 HVAR (Adzhubei et al., 2010), FATHMM (Shihab et al., 2013), PROVEAN (Choi et al., 2012) and LRT (Chun and Fay, 2009).*

B, benign; D, damaging; DC, disease causing; Del, deleterious; L, predicted functional effect is low; M, predicted functional effect is medium, N, neutral; Poly, Polymorphism; ProbD, probably damaging; T, tolerated; PosD, possibly damaging.

analysis of wildtype (WT) and mutated EGFP-PIBF1 constructs using an anti GFP antibody showed expression of WT and both mutated proteins, the one with the missense and the one with the truncating variant at expected size (**Figure S1B**). This result indicated that both, missense and the nonsense variant, resulted in the synthesis of stable proteins with the nonsense variant being smaller than the WT and the missense, as expected. Analyses using an antibody against the full length PIBF1 protein could detect the WT and the missense variant, but not the truncated nonsense variant. However, the sensitivity of the antibody was far lower than that of the GFP antibody and it has not been tested on truncated PIBF1 proteins so far. Whether its epitope is in the lacking C-terminus has to be determined.

Protein Structure and Evolutionary Conservation of *Pibf1*

A comparison of PIBF1 protein sequences from various vertebrate species revealed a high degree of conservation (**Figure 2B**). The *Xenopus* sequence showed 69.5% identity (84.2% similarity) to human PIBF1, very close to the mouse (**Figure 2B**). Functional studies at the protein level have not been reported for PIBF1 so far. Applying the NCBI conserved domain search algorithm highlighted three possible SMC-related domains (structural maintenance of chromosomes; **Figure 2C**). Additional searches identified a putative PEST domain, two ER membrane retention signals including one R-4 motiv, two nuclear localization sequences (NLS), a peroxisomal targeting signal (PTS), and two leucine zipper sequences as well as 11 coiled-coil domains along the 757 amino acids (**Figure 2C**). The three known JS mutations as well as the two novel alleles reported here localize to the C-terminal half of the protein and within coil-coiled domain, while a 6th mutation, which caused microcephaly, was found at the N-terminus, again in a coiled-coil domain (**Figure 2C**).

The above *in silico* analyses thus showed that the two novel mutations are located in important regions of a highly conserved JS candidate gene. In order to prove that these alleles indeed were causative for JS in the patient, they needed to be functionally tested in a relevant vertebrate model organism, particularly because the variant p.(Y503C) did not fulfill the ACMG-criteria to be classified as pathogenic or likely pathogenic (Richards et al., 2015). We chose to apply the *Xenopus* model, because of its suitability for studying ciliopathies: speed, high-throughput, and low cost of analyses (Johnston et al., 2017; Blum and Ott, 2018).

Expression of *pibf1* in Ciliated Tissues During *Xenopus* Embryonic Development

As a prerequisite to functionally analyzing the putative JS alleles, we analyzed whether the endogenous *pibf1* mRNA was expressed in tissues related to cilia. Transcription of *pibf1* in embryos of defined developmental stages was analyzed using whole-mount *in situ* hybridization. Maternally deposited *pibf1* mRNA was present in the cytoplasm of the animal hemisphere in cleavage stage embryos (**Figure 3A**). At the onset of gastrulation, signals were found in future mesodermal tissues (**Figure 3B**; involuting marginal zone). From neurulation onwards, expression was found in the axial (notochord) and paraxial (somites) mesoderm (**Figures 3C,D**). Additionally, a dotted epidermal pattern was obvious which resembled the distribution of multiciliated cells (MCCs) in the larval skin and was maintained until the end of neurulation (**Figures 3C,D**). In the 2-day larva (stage 25, **Figure 3E**), mRNA transcripts were seen in the ciliated otic vesicle (**Figure 3E′**) as well as in the forming ciliated nephrostomes of the embryonic kidney. The latter staining intensified and was prominently visible in sections of stage 30 tadpoles (**Figures 3F,F′**). A persistent staining in the head region became more pronounced from stage 30 onwards (**Figures 3F–H**). Enrichment of *pibf1* transcripts in the head region as well as in the spinal cord was in agreement with the expected function of Pibf1 during neural development (**Figures 3E–G**). At these stages, the *pibf1* signal became less discrete, appeared more diffuse and was present at low levels in most tissues (**Figures 3E–G**). Histological sectioning revealed enrichment in the retina and inner nuclear cell layer (**Figure 3H′**). In summary, *pibf1* was expressed in many tissues harboring cilia, namely otic vesicle, nephrostomes, brain, retina, and possibly MCCs.

Pibf1 Protein Localization in Larval Skin MCCs

JS is associated with dysfunctional primary, i.e., immotile and sensory cilia. The unexpected mRNA expression in the larval skin hinted at localization in MCCs, which harbor hundreds of motile cilia. In order to investigate the possible expression of Pibf1 in MCCs, immunofluorescence staining using a monoclonal mouse PIBF1 antibody raised against the human protein was applied. This antibody detected hundreds of spots on individual cells dotted on the larval skin (**Figures 4A,A′**). Co-staining with the basal body marker (Cetn1; Park et al., 2008) unequivocally demonstrated that Pibf1 indeed localized to the base of individual cilia on MCCs, specifically to basal bodies, as Pibf1 and Cetn1 partially overlapped (**Figures 4A–C**). Therefore, Pibf1 seemed to be a *bona fide* component of all basal bodies in ciliated cells in *Xenopus*.

In order to ascertain whether or not the missense or nonsense mutations have impact on the localization of PIBF1 to basal bodies, we cloned fusion constructs in which the N-terminus of the human WT or mutant ORFs of *PIBF1* were linked to *EGFP*. Injection of the WT PIBF1 construct into the *Xenopus* epidermis recapitulated the endogenous distribution at the basal bodies of MCCs (**Figures 4D–F**), demonstrating that ectopic expression of a fusion protein did not interfere with correct localization of the protein. In many cases, aggregates of fusion protein were additionally found in targeted cells (**Figures 4D,G**). The missense construct fully phenocopied this localization (**Figures 4G–I**). In contrast, the signal of the nonsense variant was much attenuated at basal bodies and was additionally found in a non-localized manner throughout the cell (**Figures 4J–L**). Taken together, these analyses showed that (1) Pibf1 was unexpectedly expressed in motile cilia of the larval skin; (2) Pibf1 localized to basal bodies, in agreement with its centrosomal expression in other contexts (Kim and Rhee, 2011; Kim et al., 2012); (3) the nonsense allele

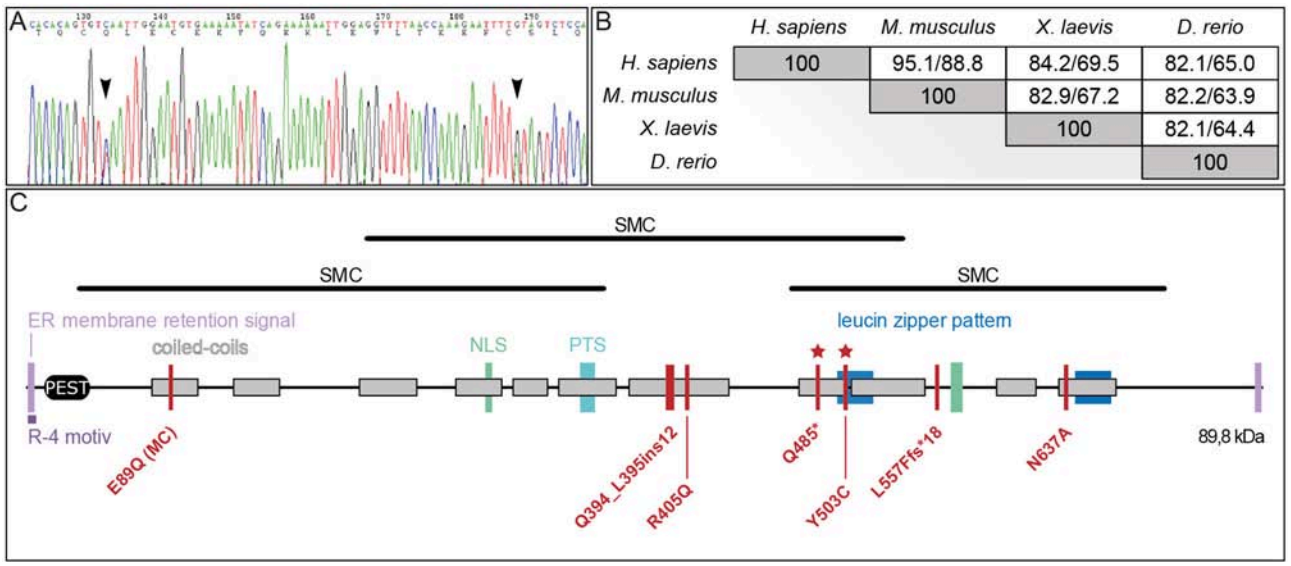

FIGURE 2 | PIBF1 protein conservation and domain structure. **(A)** Sanger sequencing of *PIBF1* from RT-PCR product of the patient mRNA extracted from blood. Black arrow heads indicate position of mutations. **(B)** Conservation of amino acid sequences between human, mouse, *Xenopus,* and zebrafish PIBF1. **(C)** Putative domain structure. JS and microcephaly (MC) mutations are indicated as red bars. For details see text. *Novel mutations identified in this study.

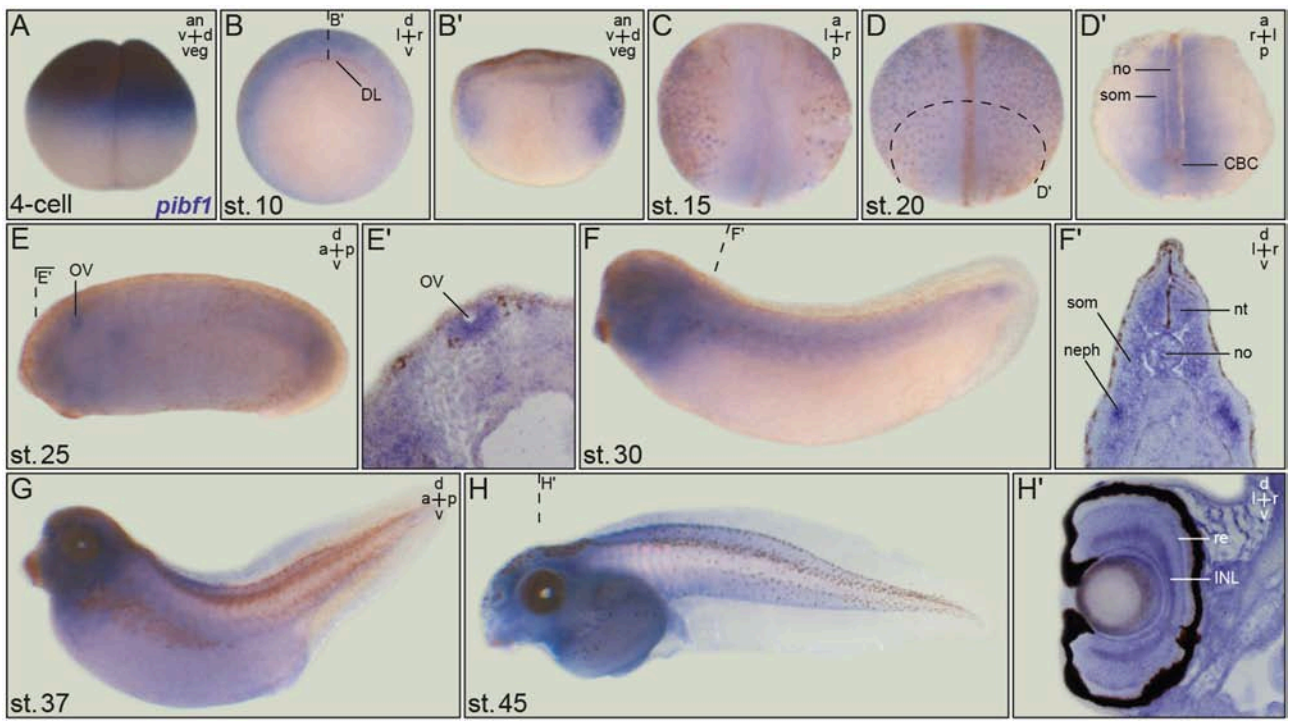

FIGURE 3 | Embryonic *pibf1* expression correlates with ciliated tissues. Embryos of defined stages were analyzed for *pibf1* mRNA by whole-mount *in situ* hybridization using a digoxigenin-labeled antisense probe. **(A)** Maternal transcripts in the animal hemisphere of the 4-cell embryo. **(B)** Expression in the involuting marginal zone tissue of the early gastrula embryo. **(C)** Staining of *pibf1* in the axial and paraxial mesoderm at early neurula stages. **(D)** *Pibf1* signals in skin MCCs and axial/paraxial mesoderm. **(E)** Expression in the otic vesicle at stage 25. **(F–H)** Expression pattern in tadpoles, including the head region, somites, and nephrostomes. Histological section of the eye **(H′)** revealed signals in the retina as well as the inner nuclear cell layer. Planes of histological sections in **(B′,D′,E′,F′,H′)** are indicated in the respective panels. an, animal; a, anterior; d, dorsal; DL, dorsal lip; INL, inner nuclear layer; l, left; neph, nephrostomes; no, notochord; nt, neural tube; ov, otic vesicle; p, posterior; r, right; re, retina; som, somite; v, ventral; veg, vegetal.

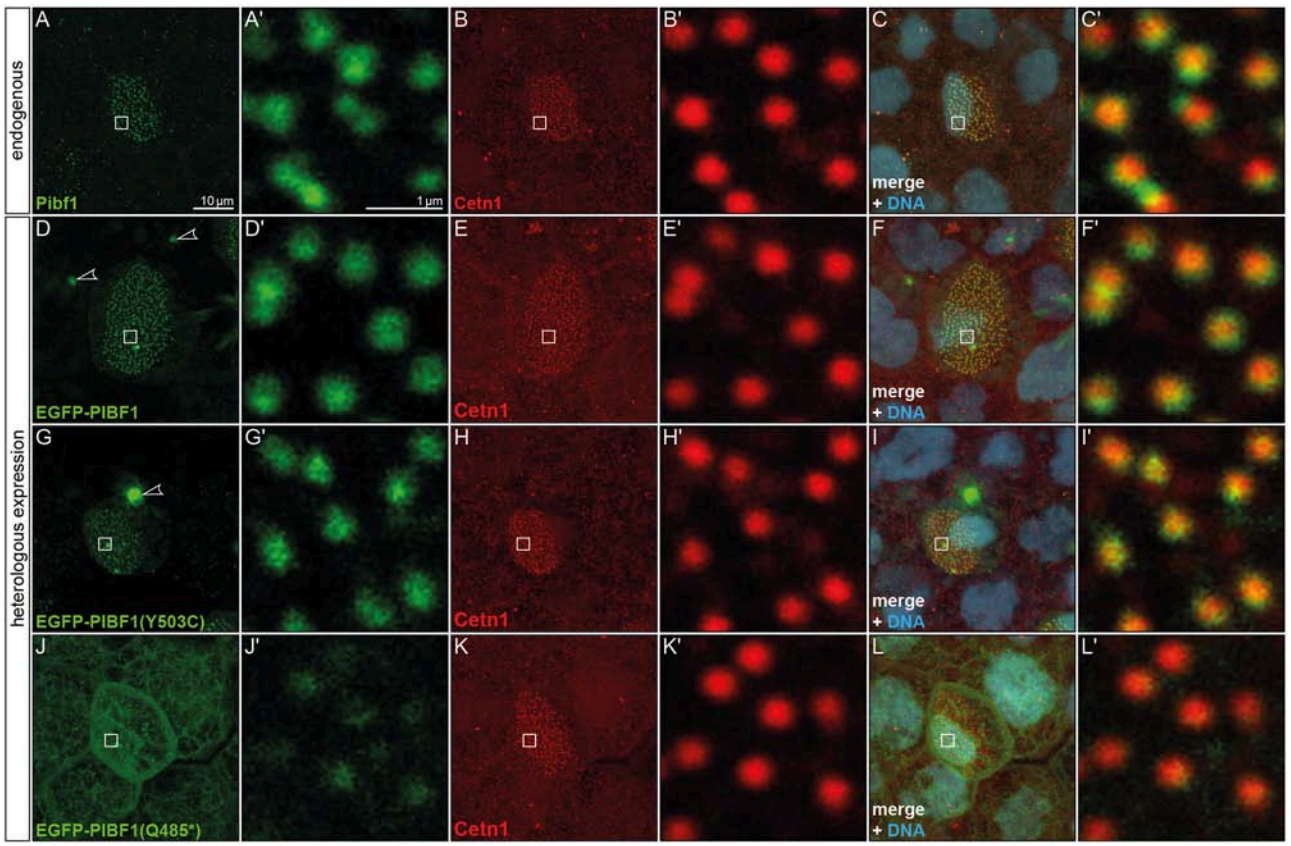

FIGURE 4 | Pibf1 localization to MCC basal bodies is attenuated in nonsense JS variant. **(A–C)** Localization of the endogenous Pibf1 protein, using an anti-PIBF1 antibody **(A)** and co-staining with Centrin 1 **(B)** and Hoechst 33342 to highlight the nucleus **(C)**. **(D–F)** An EGFP-PIBF1 fusion protein recapitulates the staining of the endogenous protein. **(G–I)** Unaltered expression of the missense allele Y503C. **(J–L)** Attenuated basal body localization of the truncated Q485* variant of PIBF1. Arrowheads mark protein aggregates observed upon overexpression of EGFP fusion proteins.

was much reduced in its localization to ciliary basal bodies, indicative of a ciliary function; (4) the missense allele appeared unaffected in its ciliary localization, raising questions as to the underlying mechanism of JS in the patient.

Functional Analysis of Wildtype and Mutant *PIBF1* Alleles in the *Xenopus* Larval Skin

Although JS is not related to motile cilia, the expression and localization of Pibf1 in basal bodies of MCCs afforded the opportunity of testing whether this protein played a role in motile cilia as well and whether the mutant alleles were affected in this function. Skin MCCs of *Xenopus* larvae function in much the same way as human airway epithelia, namely in mucociliary clearance as a first line of defense against pathogens (Dubaissi and Papalopulu, 2011; Walentek et al., 2014; Blum and Ott, 2018). MCC cilia beat in a coordinated manner to move mucus, produced by goblet cells, from anterior to posterior (head to tail), and to thereby remove environmental particles and pathogens caught by the mucus layer (Brooks and Wallingford, 2014). In order to assess a possible role of *pibf1* in this process, an antisense morpholino oligomer (MO) targeting the translational start site of the mRNA (translation blocking MO, TBMO) was designed. In retinal epithelial cells (RPE-1) and inner medullary collecting duct cells (IMCD3), loss of Pibf1 resulted in fewer or absent cilia (Kim et al., 2012; Wheway et al., 2015). We therefore analyzed the presence of MCC cilia in morphant larvae that were injected with TBMO into the skin lineage at the 4-cell stage. Successful gene knockdown was proven by immunofluorescence staining for Pibf1, which demonstrated the efficient depletion of the protein from MCCs of morphant specimens (**Figure 5**). Immunofluorescence staining of cilia in morphant specimens was performed by staining the ciliary axoneme with an antibody against acetylated tubulin (Tuba4a). This analysis clearly demonstrated markedly reduced numbers of cilia on morphant MCCs (**Figures 6A–E**). Functional consequences of reduced cilia numbers were assessed by high-speed video microscopy of larval skin at stage 30. **Movie S1** shows that coordinated ciliary beating was lost in morphants as compared to WT specimens. The loss of cilia was also apparent in kympgraphs from high-speed movies (**Figure 6L,M**). Ciliary tufts on WT and morphant MCCs were grouped into three classes, representing normal, mild, or strong reduction of cilia numbers. No unaffected ciliary tufts were retained in morphant MCCs, as displayed in **Figure 6M**.

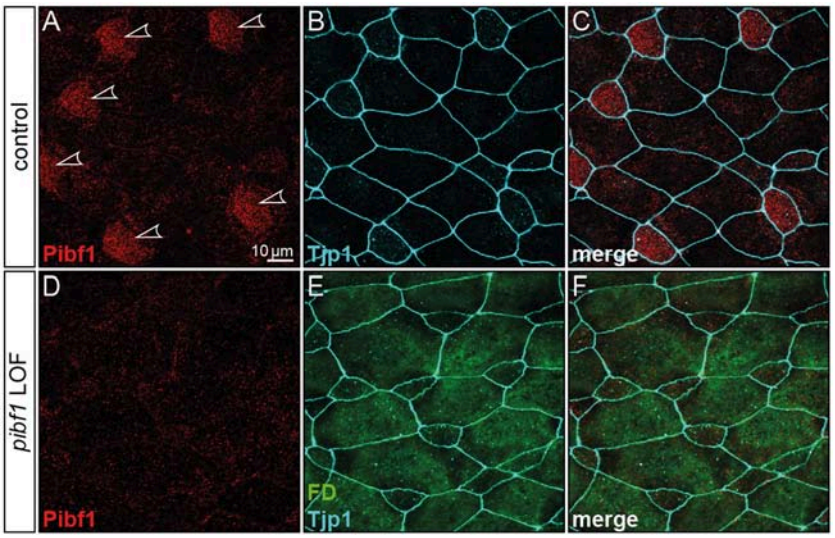

FIGURE 5 | Loss of Pibf1 protein in *pibf1* morphant *Xenopus* skin MCCs. Basal body staining of Pibf1 **(A–C)** was lost in TBMO injected specimen **(D–F)**. Tjp1 immunofluorescence was used to mark cell boundaries **(B,C,E,F)**. Fluorescent dextrane (green) was co-injected as lineage tracer to control targeting of injections **(E,F)**. Arrowheads highlight MCC cilia in WT embryo.

Next, we asked whether heterologous expression of a WT human *PIBF1* construct was able to rescue cilia numbers in morphants. To that end, TBMO and WT PIBF1 were co-injected into 4-cell embryos and targeted to the larval skin. As shown in **Figures 6E–G**, the WT human gene rescued cilia numbers in a highly significant manner. In a last set of experiments, we analyzed the rescue capacity of equimolar amounts of the two novel *Pibf1* alleles identified in our JS patient. While the nonsense mutant was unable to rescue the gene knockdown (**Figures 6E,H,I**), a residual and attenuated rescue capability was observed when the missense mutant allele was co-injected (**Figures 6E,J,K**). In summary, our functional analysis of mutant *Pibf1* alleles demonstrated a role of Pibf1 in motile cilia of larval skin MCCs in *Xenopus*, and identified both nonsense and missense allele as non-functional, in agreement with the manifested JS in the patient girl.

DISCUSSION

Mutant gene alleles identified in patient DNAs represent a valuable resource for studying protein function and are a prerequisite for the elucidation of pathomechanisms at the molecular level. A given mutation may not, however, reveal its pathogenicity at first glance. In the case of the compound heterozygous JS patient analyzed here, one of the mutations, the truncation variant p.Q485*, was highlighted as pathogenic according to ACMG criteria (Richards et al., 2015). Our analysis in ciliated *Xenopus* cells confirmed its predicted pathogenicity. The disturbed localization of this variant at basal bodies in combination with the inability to rescue the ciliation phenotype of Pibf1 deficient frog MCCs identifies it as an amorphic allele. Clinically even more important, our studies of the missense-variant p.Y503C indicated a pathogenic effect of this variant, too. A careful cell by cell analysis of mutant MCCs revealed that this mutant showed an about 50% rescue capacity, significantly below the >80% achieved with the WT allele (**Figure 6**). It should be noted, that this analysis was performed in a tissue that is not relevant in JS patients and on motile cilia, while JS is caused by defects of primary, immotile cilia. Therefore, in the context of a *bona fide* JS target tissues, the combination of these mutations may give rise to even more pronounced defects at high frequency. Recapitulating the patient gene setup in any animal model would be experimentally more challenging, require more time and be more expensive. The attenuated rescue ability, however, unequivocally demonstrates that the missense variant is hypomorphic in nature, leading to a re-classification of the allele from "unkown significant" to "likely pathogenic," according to ACMG criteria (Richards et al., 2015). The finding of a hypomorphic allele due to a missense mutation in combination with a null allele due to a truncating mutation is a typical finding in patients with JS and has been reported for a number of other causative genes (such as *RPGRIP1L*, *TMEM67*, *CCD2D2A*, and *TCTN3*), whereas biallelic null alleles in these genes are associated with a more severe phenotype (Delous et al., 2007; Mougou-Zerelli et al., 2009; Tallila et al., 2009; Iannicelli et al., 2010; Romani et al., 2014).

The precise role of PIBF1 in the context of ciliary biogenesis is not well-understood. All JS-associated mutations in *PIBF1* identified so far cluster in the C-terminal region of the protein [**Figure 2**; (Wheway et al., 2015; Hebbar et al., 2018)]. In contrast, a homozygous missense mutation that is linked to microcephaly is present within the N-terminus [**Figure 2**; (Kodani et al., 2015)]. The large structural maintenance of chromosomes (SMC) domains constitute almost 90% of the protein, suggesting that PIBF serves as a scaffolding factor which may dimerize with ciliary SMC proteins such as SMC1A or SMC3 (Khanna

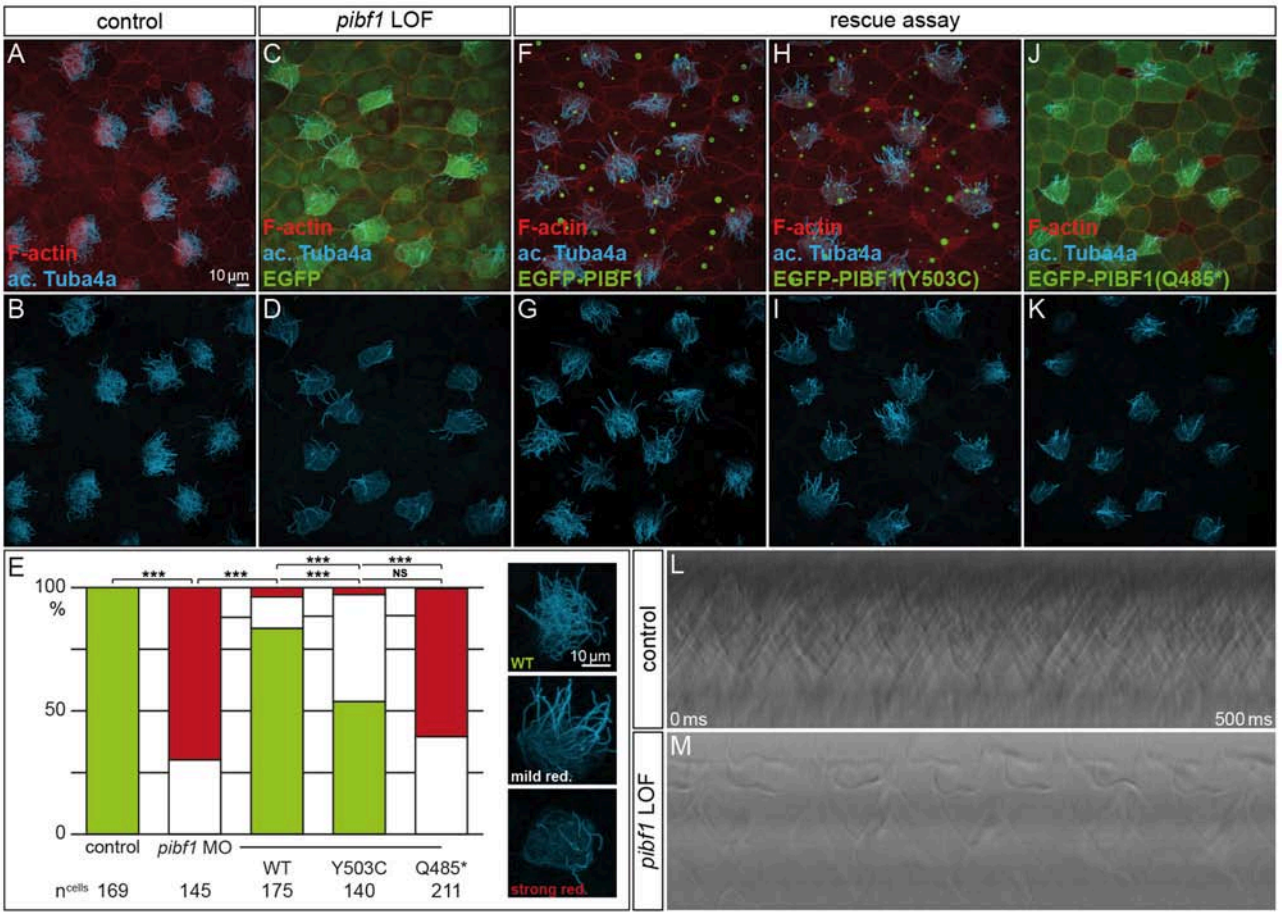

FIGURE 6 | Rescue of morphant MCC ciliation is lost with mutant *PIBF1* alleles. **(A–E)** MCC ciliation in WT embryos was lost in *pibf1* TBMO-injected specimens. **(E–G)** Rescue of ciliation upon co-injection of TBMO and *EGFP-PIBF1*. **(E,H,I)** Attenuated rescue in embryos co-injected with missense *PIBF1* allele. **(E,J,K)** Defective rescue upon co-injection of the nonsense *PIBF1* allele. **(E)** Quantification of results. **(L,M)** Kymographs representing ciliary beating in WT and TBMO-injected stage 30 larval skin MCCs. ***Very highly significant, $p < 0.01$.

et al., 2005). A search of the protein interaction database IntAct (https://www.ebi.ac.uk/intact/) revealed a number of SMC proteins that were shown to interact with PIBF1, for example CEP63 and PCM1 (Kim et al., 2012; Gupta et al., 2015; Yachie et al., 2016). As PCM1 is not relevant for cilia formation in multiciliated mouse tracheal epithelial cells, it is not a promising candidate to explain the loss of cilia in PIBF1 depleted MCCs (Vladar and Stearns, 2007). CEP63, in contrast, is required during the centriolar duplication cycle, acts in parallel with its paralog deup1 in basal body formation in MCCs and harbors an SMC related domain (Zhao et al., 2013). The reduced number of cilia on morphant MCCs may result from such a mechanism. *Xenopus* MCC offer themselves for in-depth analyses of potential interaction partners, which are beyond the scope of the present study.

The advent of high-throughput sequencing technology, in particular whole exome sequencing (WES), has led to a revolution of genetic diagnostics of rare diseases, e.g., developmental disorders. Before the era of WES many patients had undergone a long and frustrating "diagnostic odyssey" to obtain an accurate diagnosis. This has been widely overcome with the introduction of WES, which has emerged as an effective diagnostic tool leading to diagnostic rates of around 40% in patients with previously undiagnosed neurodevelopmental or pediatric neurologic disorders [for review see (Wright et al., 2018)]. A diagnosis is essential for an optimal clinical management of the particular patient, e.g., initiation of a specific therapy or surveillance program, and appropriate access to education, social care and patient support groups (Boycott et al., 2017). A molecular diagnosis is also important for the patients' parents and other family members, in particular for informed decision-making with regard to family planning, and possibly prenatal diagnosis (PD) or preimplantation genetic diagnosis (PGD). In the case reported here, a molecular diagnosis could not have been established without the *Xenopus* analysis of the *PIBF1* missense variant and the resulting re-classification as likely pathogenic. Important consequence for the parents, who previously had decided against further children for fear of another disabled child, was that they now opt for a further pregnancy with PD.

Furthermore, identifying the molecular genetic cause of a disease is essential for a better understanding of its pathogenesis and the development of novel treatment strategies. However, interpretation of high-throughput sequencing data can be difficult. WES also uncovers many rare variants of which the functional impact is not known. Thus, a molecular diagnosis may be missed. Furthermore, recent studies in the field of cancer genetics and prenatal diagnosis indicate that unambiguous genetic results such as the finding of unclassified variants can lead to false treatment decisions and dissatisfaction with genomic testing (Kurian et al., 2017; Desai et al., 2018). Therefore, animal models are needed to verify or discard candidate disease alleles. Because of its genetic closeness, the mouse has been the model of choice to assess human genetic diseases. However, analyses in mice are costly and slow; in addition, the mouse is not suited for high-throughput analysis and cannot possibly keep up with the pace at which candidate variants keep being identified by WES. Therefore, additional and complementing animal models need to be promoted. Among the non-mammalian models, the zebrafish is widely used, while *Xenopus* is less well-known among clinical scientists. The frog, however, offers unique advantages particularly when investigating ciliopathies (Blum and Ott, 2018). The developing embryo presents its ciliated skin for a total of 3 days and allows easy and straightforward observation (including video microscopy) and functional analyses. Manipulations can be performed in a unilateral fashion, such that the non-manipulated side serves as an internal control. Given the inter-individual variability of phenotypes, this represents a unique advantage of the *Xenopus* model. The present analysis demonstrates that a syndrome like JS, which is caused by defects of primary, immotile cilia, can be successfully dissected in the context of motile cilia, as the expression analysis revealed a pan-ciliary presence of *pibf1* mRNA. This is likely true for most ciliopathies of primary cilia. Other organs that are easily addressed in the *Xenopus* model include the kidney (Getwan and Lienkamp, 2017) and heart (Duncan and Khokha, 2016). It seems, therefore, warranted to promote *Xenopus* among clinical scientist as a complementing model to mouse and zebrafish, in order to allow for the most efficient assessment of disease alleles.

AUTHOR'S NOTE

The authors dedicate this paper to the memory of the late Herbert Steinbeißer, who has been an inspiration to all of us and who has brought this group of people together.

AUTHOR CONTRIBUTIONS

TO conceived *Xenopus* experiments together with MB, performed and evaluated all *Xenopus* experiments, and wrote the manuscript together with MB and CE. MB conceived and evaluated experiments and wrote the paper. LK and ST performed mRNA/cDNA analysis of the patient and parents and westernblots. LK wrote sections of the manuscript. WES study coordination was done by CB and UM. NP and ASc performed WES analysis. Bioinformatic WES data analysis was done by NP, ASc, and MG, further evaluation of WES data was done by CE and UM. KH performed confirmation of WES variants by Sanger-Sequencing. ASe performed MRI images and their interpretation. Genotype–Phenotype correlation was done by CE, MG, KH, LK, and UM. All authors contributed to manuscript revision, read and approved the submitted version.

SUPPLEMENTARY MATERIAL

The Supplementary Material for this article can be found online at: https://www.frontiersin.org/articles/10.3389/fphys.2019.00134/full#supplementary-material

Movie S1 | Uncoordinated beating of MCC cilia upon *pibf1* gene knockdown. Coordinated ciliary beating of MCC (left) was lost in *pibf1* morphant specimen (right). Note the reduced number of cilia on morphant cell. Time lapse movie was recorded at 600 fps and plays at 30 fps (0.05 × real time).

Figure S1 | Expression anlayses of PIBF1 variants. **(A)** Relative expression levels of *PIBF1* exons analyzed by qPCR from patient, parents' and control blood. Shown are the mean ± SD of three independent RT-PCRs and subsequent qPCRs. *ARF1* expression was used for normalization. **(B)** Western blot analyses of overexpressed EGFP-PIBF1 constructs in HEK293 cells, using anti-GFP and anti-PIBF1 antibodies, respectively.

REFERENCES

Adzhubei, I. A., Schmidt, S., Peshkin, L., Ramensky, V. E., Gerasimova, A., Bork, P., et al. (2010). A method and server for predicting damaging missense mutations. *Nat. Methods* 7, 248–249. doi: 10.1038/nmeth0410-248

Bachmann-Gagescu, R., Dempsey, J. C., Phelps, I. G., O'Roak, B. J., Knutzen, D. M., Rue, T. C., et al. (2015). Joubert syndrome: a model for untangling recessive disorders with extreme genetic heterogeneity. *J. Med. Genet.* 52, 514–522. doi: 10.1136/jmedgenet-2015-103087

Badhwar, A., Andermann, F., Valerio, R. M., and Andermann, E. (2000). Founder effect in Joubert Syndrome. *Ann. Neurol.* 48, 435–436.

Barker, A. R., Thomas, R., and Dawe, H. R. (2014). Meckel-Gruber syndrome and the role of primary cilia in kidney, skeleton, and central nervous system development. *Organogenesis* 10, 96–107. doi: 10.4161/org.27375

Belo, J. A., Bouwmeester, T., Leyns, L., Kertesz, N., Gallo, M., Follettie, M., et al. (1997). Cerberus-like is a secreted factor with neutralizing activity expressed in the anterior primitive endoderm of the mouse gastrula. *Mech. Dev.* 68, 45–57. doi: 10.1016/S0925-4773(97)00125-1

Blum, M., and Ott, T. (2018). Xenopus: an undervalued model organism to study and model human genetic disease. *Cells Tissues Organs*. doi: 10.1159/000490898. [Epub ahead of print].

Boycott, K. M., Rath, A., Chong, J. X., Hartley, T., Alkuraya, F. S., Baynam, G., et al. (2017). International cooperation to enable the diagnosis of all rare genetic diseases. *Am. J. Hum. Genet.* 100, 695–705. doi: 10.1016/j.ajhg.2017.04.003

Brancati, F., Iannicelli, M., Travaglini, L., Mazzotta, A., Bertini, E., Boltshauser, E., et al. (2009). MKS3/TMEM67 mutations are a major cause of COACH Syndrome, a Joubert Syndrome related disorder with liver involvement. *Hum. Mutat.* 30, E432–E442. doi: 10.1002/humu.20924

Brooks, E. R., and Wallingford, J. B. (2014). Multiciliated cells. *Curr. Biol.* 24, R973–R982. doi: 10.1016/j.cub.2014.08.047

Choi, Y., Sims, G. E., Murphy, S., Miller, J. R., and Chan, A. P. (2012). Predicting the functional effect of amino acid substitutions and indels. *PLoS ONE* 7:e46688. doi: 10.1371/journal.pone.0046688

Chun, S., and Fay, J. C. (2009). Identification of deleterious mutations within three human genomes. *Genome Res.* 19, 1553–1561. doi: 10.1101/gr.092619.109

Cohen, R. A., Check, J. H., and Dougherty, M. P. (2016). Evidence that exposure to progesterone alone is a sufficient stimulus to cause a precipitous rise in the immunomodulatory protein the progesterone induced blocking factor (PIBF). *J. Assist. Reprod. Genet.* 33, 221–229. doi: 10.1007/s10815-015-0619-7

Delous, M., Baala, L., Salomon, R., Laclef, C., Vierkotten, J., Tory, K., et al. (2007). The ciliary gene RPGRIP1L is mutated in cerebello-oculo-renal syndrome (Joubert syndrome type B) and Meckel syndrome. *Nat. Genet.* 39, 875–881. doi: 10.1038/ng2039

Desai, P., Haber, H., Bulafka, J., Russell, A., Clifton, R., Zachary, J., et al. (2018). Impacts of variants of uncertain significance on parental perceptions of children after prenatal chromosome microarray testing. *Prenat. Diagn.* 38, 740–747. doi: 10.1002/pd.5323

Doherty, D. (2009). Joubert syndrome: insights into brain development, cilium biology, and complex disease. *Semin. Pediatr. Neurol.* 16, 143–154. doi: 10.1016/j.spen.2009.06.002

Dubaissi, E., and Papalopulu, N. (2011). Embryonic frog epidermis: a model for the study of cell-cell interactions in the development of mucociliary disease. *Dis. Model. Mech.* 4, 179–192. doi: 10.1242/dmm.006494

Duncan, A. R., and Khokha, M. K. (2016). Xenopus as a model organism for birth defects-Congenital heart disease and heterotaxy. *Semin. Cell Dev. Biol.* 51, 73–79. doi: 10.1016/j.semcdb.2016.02.022

Edvardson, S., Shaag, A., Zenvirt, S., Erlich, Y., Hannon, G. J., Shanske, A. L., et al. (2010). Joubert syndrome 2 (JBTS2) in Ashkenazi Jews is associated with a TMEM216 mutation. *Am. J. Hum. Genet.* 86, 93–97. doi: 10.1016/j.ajhg.2009.12.007

Evers, C., Staufner, C., Granzow, M., Paramasivam, N., Hinderhofer, K., Kaufmann, L., et al. (2017). Impact of clinical exomes in neurodevelopmental and neurometabolic disorders. *Mol. Genet. Metab.* 121, 297–307. doi: 10.1016/j.ymgme.2017.06.014

Fagerberg, L., Hallstrom, B. M., Oksvold, P., Kampf, C., Djureinovic, D., Odeberg, J., et al. (2014). Analysis of the human tissue-specific expression by genome-wide integration of transcriptomics and antibody-based proteomics. *Mol. Cell. Proteomics* 13, 397–406. doi: 10.1074/mcp.M113.035600

Franco, B., and Thauvin-Robinet, C. (2016). Update on oral-facial-digital syndromes (OFDS). *Cilia* 5:12. doi: 10.1186/s13630-016-0034-4

Getwan, M., and Lienkamp, S. S. (2017). Toolbox in a tadpole: Xenopus for kidney research. *Cell Tissue Res.* 369, 143–157. doi: 10.1007/s00441-017-2611-2

Gonzalez-Arenas, A., Valadez-Cosmes, P., Jimenez-Arellano, C., Lopez-Sanchez, M., and Camacho-Arroyo, I. (2014). Progesterone-induced blocking factor is hormonally regulated in human astrocytoma cells, and increases their growth through the IL-4R/JAK1/STAT6 pathway. *J. Steroid Biochem. Mol. Biol.* 144(Pt B), 463–46470. doi: 10.1016/j.jsbmb.2014.09.007

Gupta, G. D., Coyaud, E., Goncalves, J., Mojarad, B. A., Liu, Y., Wu, Q., et al. (2015). A Dynamic protein interaction landscape of the human centrosome-cilium interface. *Cell* 163, 1484–1499. doi: 10.1016/j.cell.2015.10.065

Gutierrez-Rodriguez, A., Hansberg-Pastor, V., and Camacho-Arroyo, I. (2017). Proliferative and invasive effects of progesterone-induced blocking factor in human glioblastoma cells. *Biomed. Res. Int.* 2017:1295087. doi: 10.1155/2017/1295087

Hebbar, M., Kanthi, A., Shukla, A., Bielas, S., and Girisha, K. M. (2018). A biallelic 36-bp insertion in PIBF1 is associated with Joubert syndrome. *J. Hum. Genet.* 63, 935–939. doi: 10.1038/s10038-018-0462-7

Huang, L., Szymanska, K., Jensen, V. L., Janecke, A. R., Innes, A. M., Davis, E. E., et al. (2011). TMEM237 is mutated in individuals with a Joubert syndrome related disorder and expands the role of the TMEM family at the ciliary transition zone. *Am. J. Hum. Genet.* 89, 713–730. doi: 10.1016/j.ajhg.2011.11.005

Hudic, I., Stray-Pedersen, B., Szekeres-Bartho, J., Fatusic, Z., Dizdarevic-Hudic, L., Tomic, V., et al. (2015). Maternal serum progesterone-induced blocking factor (PIBF) in the prediction of preterm birth. *J. Reprod. Immunol.* 109, 36–40. doi: 10.1016/j.jri.2015.02.006

Hudic, I., Szekeres-Bartho, J., Stray-Pedersen, B., Fatusic, Z., Polgar, B., and Ecim-Zlojutro, V. (2016). Lower urinary and serum progesterone-induced blocking factor in women with preterm birth. *J. Reprod. Immunol.* 117, 66–69. doi: 10.1016/j.jri.2016.07.003

Iannicelli, M., Brancati, F., Mougou-Zerelli, S., Mazzotta, A., Thomas, S., Elkhartoufi, N., et al. (2010). Novel TMEM67 mutations and genotype-phenotype correlates in meckelin-related ciliopathies. *Hum. Mutat.* 31, E1319–E1331. doi: 10.1002/humu.21239

Johnston, J. J., Lee, C., Wentzensen, I. M., Parisi, M. A., Crenshaw, M. M., Sapp, J. C., et al. (2017). Compound heterozygous alterations in intraflagellar transport protein CLUAP1 in a child with a novel Joubert and oral-facial-digital overlap syndrome. *Cold Spring Harb. Mol. Case Stud.* 3:a001321. doi: 10.1101/mcs.a001321

Khanna, H., Hurd, T. W., Lillo, C., Shu, X., Parapuram, S. K., He, S., et al. (2005). RPGR-ORF15, which is mutated in retinitis pigmentosa, associates with SMC1, SMC3, and microtubule transport proteins. *J. Biol. Chem.* 280, 33580–33587. doi: 10.1074/jbc.M505827200

Kim, K., Lee, K., and Rhee, K. (2012). CEP90 is required for the assembly and centrosomal accumulation of centriolar satellites, which is essential for primary cilia formation. *PLoS ONE* 7:e48196. doi: 10.1371/journal.pone.0048196

Kim, K., and Rhee, K. (2011). The pericentriolar satellite protein CEP90 is crucial for integrity of the mitotic spindle pole. *J. Cell Sci.* 124(Pt 3), 338–347. doi: 10.1242/jcs.078329

Kircher, M., Witten, D. M., Jain, P., O'Roak, B. J., Cooper, G. M., and Shendure, J. (2014). A general framework for estimating the relative pathogenicity of human genetic variants. *Nat. Genet.* 46, 310–315. doi: 10.1038/ng.2892

Knopp, C., Rudnik-Schoneborn, S., Eggermann, T., Bergmann, C., Begemann, M., Schoner, K., et al. (2015). Syndromic ciliopathies: from single gene to multi gene analysis by SNP arrays and next generation sequencing. *Mol. Cell. Probes* 29, 299–307. doi: 10.1016/j.mcp.2015.05.008

Kodani, A., Yu, T. W., Johnson, J. R., Jayaraman, D., Johnson, T. L., Al-Gazali, L., et al. (2015). Centriolar satellites assemble centrosomal microcephaly proteins to recruit CDK2 and promote centriole duplication. *eLife* 4:7519. doi: 10.7554/eLife.07519

Kroes, H. Y., Monroe, G. R., van der Zwaag, B., Duran, K. J., de Kovel, C. G., van Roosmalen, M. J., et al. (2016). Joubert syndrome: genotyping a Northern European patient cohort. *Eur. J. Hum. Genet.* 24, 214–220. doi: 10.1038/ejhg.2015.84

Kurian, A. W., Li, Y., Hamilton, A. S., Ward, K. C., Hawley, S. T., Morrow, M., et al. (2017). Gaps in incorporating germline genetic testing into treatment decision-making for early-stage breast cancer. *J. Clin. Oncol.* 35, 2232–2239. doi: 10.1200/JCO.2016.71.6480

Lachmann, M., Gelbmann, D., Kalman, E., Polgar, B., Buschle, M., Von Gabain, A., et al. (2004). PIBF (progesterone induced blocking factor) is overexpressed in highly proliferating cells and associated with the centrosome. *Int. J. Cancer* 112, 51–60. doi: 10.1002/ijc.20326

Leitch, C. C., Zaghloul, N. A., Davis, E. E., Stoetzel, C., Diaz-Font, A., Rix, S., et al. (2008). Hypomorphic mutations in syndromic encephalocele genes are associated with Bardet-Biedl syndrome. *Nat. Genet.* 40, 443–448. doi: 10.1038/ng.97

Lek, M., Karczewski, K. J., Minikel, E. V., Samocha, K. E., Banks, E., Fennell, T., et al. (2016). Analysis of protein-coding genetic variation in 60,706 humans. *Nature* 536, 285–291. doi: 10.1038/nature19057

Liu, X., Jian, X., and Boerwinkle, E. (2013). dbNSFP v2.0: a database of human non-synonymous SNVs and their functional predictions and annotations. *Hum. Mutat.* 34, E2393–E2402. doi: 10.1002/humu.22376

Malicdan, M. C., Vilboux, T., Stephen, J., Maglic, D., Mian, L., Konzman, D., et al. (2015). Mutations in human homologue of chicken talpid3 gene (KIAA0586) cause a hybrid ciliopathy with overlapping features of Jeune and Joubert syndromes. *J. Med. Genet.* 52, 830–839. doi: 10.1136/jmedgenet-2015-103316

Maria, B. L., Hoang, K. B., Tusa, R. J., Mancuso, A. A., Hamed, L. M., Quisling, R. G., et al. (1997). "Joubert syndrome" revisited: key ocular motor signs with magnetic resonance imaging correlation. *J. Child Neurol.* 12, 423–430. doi: 10.1177/088307389701200703

Maria, B. L., Quisling, R. G., Rosainz, L. C., Yachnis, A. T., Gitten, J., Dede, D., et al. (1999). Molar tooth sign in Joubert syndrome: clinical, radiologic, and pathologic significance. *J. Child Neurol.* 14, 368–376. doi: 10.1177/088307389901400605

Miller, S. A., Dykes, D. D., and Polesky, H. F. (1988). A simple salting out procedure for extracting DNA from human nucleated cells. *Nucleic Acids Res.* 16:1215. doi: 10.1093/nar/16.3.1215

Moody, S. A. (2000). Cell lineage analysis in Xenopus embryos. *Methods Mol. Biol.* 135, 331–347. doi: 10.1385/1-59259-685-1:331

Mougou-Zerelli, S., Thomas, S., Szenker, E., Audollent, S., Elkhartoufi, N., Babarit, C., et al. (2009). CC2D2A mutations in Meckel and Joubert syndromes indicate a genotype-phenotype correlation. *Hum. Mutat.* 30, 1574–1582. doi: 10.1002/humu.21116

Ng, P. C., and Henikoff, S. (2003). SIFT: predicting amino acid changes that affect protein function. *Nucleic Acids Res.* 31, 3812–3814. doi: 10.1093/nar/gkg509

Paramasivam, N., Granzow, M., Evers, C., Hinderhofer, K., Wiemann, S., Bartram, C. R., et al. (2018). Identification and prioritization of causal variants of human genetic disorders from exome or whole genome sequencing data. *OBM Genet.* doi: 10.1101/209882. [Epub ahead of print].

Parisi, M., and Glass, I. (1993). "Joubert syndrome," in *GeneReviews®*, eds M. P. Adam, H. H. Ardinger, R. A. Pagon, S. E. Wallace, L. J. H. Bean, K. Stephens, and A. Amemiya (Seattle, WA).

Park, T. J., Mitchell, B. J., Abitua, P. B., Kintner, C., and Wallingford, J. B. (2008). Dishevelled controls apical docking and planar polarization of basal bodies in ciliated epithelial cells. *Nat. Genet.* 40, 871–879. doi: 10.1038/ng.104

Polgar, B., Kispal, G., Lachmann, M., Paar, C., Nagy, E., Csere, P., et al. (2003). Molecular cloning and immunologic characterization of a novel cDNA coding for progesterone-induced blocking factor. *J. Immunol.* 171, 5956–5963. doi: 10.4049/jimmunol.171.11.5956

Reva, B., Antipin, Y., and Sander, C. (2011). Predicting the functional impact of protein mutations: application to cancer genomics. *Nucleic Acids Res.* 39:e118. doi: 10.1093/nar/gkr407

Richards, S., Aziz, N., Bale, S., Bick, D., Das, S., Gastier-Foster, J., et al. (2015). Standards and guidelines for the interpretation of sequence variants: a joint consensus recommendation of the American College of Medical Genetics and Genomics and the Association for Molecular Pathology. *Genet. Med.* 17, 405–424. doi: 10.1038/gim.2015.30

Romani, M., Micalizzi, A., Kraoua, I., Dotti, M. T., Cavallin, M., Sztriha, L., et al. (2014). Mutations in B9D1 and MKS1 cause mild Joubert syndrome: expanding the genetic overlap with the lethal ciliopathy Meckel syndrome. *Orphanet J. Rare Dis.* 9:72. doi: 10.1186/1750-1172-9-72

Romani, M., Micalizzi, A., and Valente, E. M. (2013). Joubert syndrome: congenital cerebellar ataxia with the molar tooth. *Lancet Neurol.* 12, 894–905. doi: 10.1016/S1474-4422(13)70136-4

Roosing, S., Romani, M., Isrie, M., Rosti, R. O., Micalizzi, A., Musaev, D., et al. (2016). Mutations in CEP120 cause Joubert syndrome as well as complex ciliopathy phenotypes. *J. Med. Genet.* 53, 608–615. doi: 10.1136/jmedgenet-2016-103832

Saunier, S., Salomon, R., and Antignac, C. (2005). Nephronophthisis. *Curr. Opin. Genet. Dev.* 15, 324–331. doi: 10.1016/j.gde.2005.04.012

Schwarz, J. M., Rodelsperger, C., Schuelke, M., and Seelow, D. (2010). MutationTaster evaluates disease-causing potential of sequence alterations. *Nat. Methods* 7, 575–576. doi: 10.1038/nmeth0810-575

Shaheen, R., Almoisheer, A., Faqeih, E., Babay, Z., Monies, D., Tassan, N., et al. (2015). Identification of a novel MKS locus defined by TMEM107 mutation. *Hum. Mol. Genet.* 24, 5211–5218. doi: 10.1093/hmg/ddv242

Shaheen, R., Shamseldin, H. E., Loucks, C. M., Seidahmed, M. Z., Ansari, S., Ibrahim Khalil, M., et al. (2014). Mutations in CSPP1, encoding a core centrosomal protein, cause a range of ciliopathy phenotypes in humans. *Am. J. Hum. Genet.* 94, 73–79. doi: 10.1016/j.ajhg.2013.11.010

Shihab, H. A., Gough, J., Cooper, D. N., Stenson, P. D., Barker, G. L., Edwards, K. J., et al. (2013). Predicting the functional, molecular, and phenotypic consequences of amino acid substitutions using hidden Markov models. *Hum. Mutat.* 34, 57–65. doi: 10.1002/humu.22225

Slaats, G. G., Isabella, C. R., Kroes, H. Y., Dempsey, J. C., Gremmels, H., Monroe, G. R., et al. (2016). MKS1 regulates ciliary INPP5E levels in Joubert syndrome. *J. Med. Genet.* 53, 62–72. doi: 10.1136/jmedgenet-2015-103250

Spassky, N., Han, Y. G., Aguilar, A., Strehl, L., Besse, L., Laclef, C., et al. (2008). Primary cilia are required for cerebellar development and Shh-dependent expansion of progenitor pool. *Dev. Biol.* 317, 246–259. doi: 10.1016/j.ydbio.2008.02.026

Srour, M., Hamdan, F. F., McKnight, D., Davis, E., Mandel, H., Schwartzentruber, J., et al. (2015). Joubert syndrome in French Canadians and identification of mutations in CEP104. *Am. J. Hum. Genet.* 97, 744–753. doi: 10.1016/j.ajhg.2015.09.009

Srour, M., Hamdan, F. F., Schwartzentruber, J. A., Patry, L., Ospina, L. H., Shevell, M. I., et al. (2012a). Mutations in TMEM231 cause Joubert syndrome in French Canadians. *J. Med. Genet.* 49, 636–641. doi: 10.1136/jmedgenet-2012-101132

Srour, M., Schwartzentruber, J., Hamdan, F. F., Ospina, L. H., Patry, L., Labuda, D., et al. (2012b). Mutations in C5ORF42 cause Joubert syndrome in the French Canadian population. *Am. J. Hum. Genet.* 90, 693–700. doi: 10.1016/j.ajhg.2012.02.011

Tallila, J., Salonen, R., Kohlschmidt, N., Peltonen, L., and Kestila, M. (2009). Mutation spectrum of Meckel syndrome genes: one group of syndromes or several distinct groups? *Hum. Mutat.* 30, E813–E830. doi: 10.1002/humu.21057

Thomas, S., Legendre, M., Saunier, S., Bessieres, B., Alby, C., Bonniere, M., et al. (2012). TCTN3 mutations cause Mohr-Majewski syndrome. *Am. J. Hum. Genet.* 91, 372–378. doi: 10.1016/j.ajhg.2012.06.017

Tuz, K., Bachmann-Gagescu, R., O'Day, D. R., Hua, K., Isabella, C. R., Phelps, I. G., et al. (2014). Mutations in CSPP1 cause primary cilia abnormalities and Joubert syndrome with or without Jeune asphyxiating thoracic dystrophy. *Am. J. Hum. Genet.* 94, 62–72. doi: 10.1016/j.ajhg.2013.11.019

Valente, E. M., Logan, C. V., Mougou-Zerelli, S., Lee, J. H., Silhavy, J. L., Brancati, F., et al. (2010). Mutations in TMEM216 perturb ciliogenesis and cause Joubert, Meckel and related syndromes. *Nat. Genet.* 42, 619–625. doi: 10.1038/ng.594

Vladar, E. K., and Stearns, T. (2007). Molecular characterization of centriole assembly in ciliated epithelial cells. *J. Cell Biol.* 178, 31–42. doi: 10.1083/jcb.200703064

Walentek, P., Bogusch, S., Thumberger, T., Vick, P., Dubaissi, E., Beyer, T., et al. (2014). A novel serotonin-secreting cell type regulates ciliary motility in the mucociliary epidermis of Xenopus tadpoles. *Development* 141, 1526–1533. doi: 10.1242/dev.102343

Wang, K., Li, M., and Hakonarson, H. (2010). ANNOVAR: functional annotation of genetic variants from high-throughput sequencing data. *Nucleic Acids Res.* 38:e164. doi: 10.1093/nar/gkq603

Wheway, G., Schmidts, M., Mans, D. A., Szymanska, K., Nguyen, T. T., Racher, H., et al. (2015). An siRNA-based functional genomics screen for the identification of regulators of ciliogenesis and ciliopathy genes. *Nat. Cell Biol.* 17, 1074–1087. doi: 10.1038/ncb3201

Wright, C. F., McRae, J. F., Clayton, S., Gallone, G., Aitken, S., FitzGerald, T. W., et al. (2018). Making new genetic diagnoses with old data: iterative reanalysis and reporting from genome-wide data in 1,133 families with developmental disorders. *Genet. Med.* 20, 1216–1223. doi: 10.1038/gim.2017.246

Yachie, N., Petsalaki, E., Mellor, J. C., Weile, J., Jacob, Y., Verby, M., et al. (2016). Pooled-matrix protein interaction screens using Barcode Fusion Genetics. *Mol. Syst. Biol.* 12:863. doi: 10.15252/msb.20156660

Zaghloul, N. A., and Katsanis, N. (2009). Mechanistic insights into Bardet-Biedl syndrome, a model ciliopathy. *J. Clin. Invest.* 119, 428–437. doi: 10.1172/JCI37041

Zhao, H., Zhu, L., Zhu, Y., Cao, J., Li, S., Huang, Q., et al. (2013). The Cep63 paralogue Deup1 enables massive *de novo* centriole biogenesis for vertebrate multiciliogenesis. *Nat. Cell Biol.* 15, 1434–1444. doi: 10.1038/ncb2880

Conflict of Interest Statement: The authors declare that the research was conducted in the absence of any commercial or financial relationships that could be construed as a potential conflict of interest.

frontiers in Physiology

ORIGINAL RESEARCH
published: 26 February 2019
doi: 10.3389/fphys.2019.00143

Dynamin Binding Protein Is Required for *Xenopus laevis* Kidney Development

*Bridget D. DeLay[1], Tanya A. Baldwin[2,3] and Rachel K. Miller[1,3,4,5]**

[1] Department of Pediatrics, McGovern Medical School, Pediatric Research Center, University of Texas Health Science Center, Houston, TX, United States, [2] Department of Integrative Biology and Pharmacology, McGovern Medical School, University of Texas Health Science Center, Houston, TX, United States, [3] Program in Biochemistry and Cell Biology, Graduate School of Biomedical Sciences, University of Texas MD Anderson Cancer Center, University of Texas Health Science Center, Houston, TX, United States, [4] Program in Genetics and Epigenetics, Graduate School of Biomedical Sciences, University of Texas MD Anderson Cancer Center, University of Texas Health Science Center, Houston, TX, United States, [5] Department of Genetics, University of Texas MD Anderson Cancer Center, Houston, TX, United States

The adult human kidney contains over one million nephrons, with each nephron consisting of a tube containing segments that have specialized functions in nutrient and water absorption and waste excretion. The embryonic kidney of *Xenopus laevis* consists of a single functional nephron composed of regions that are analogous to those found in the human nephron, making it a simple model for the study of nephrogenesis. The exocyst complex, which traffics proteins to the cell membrane in vesicles via CDC42, is essential for normal kidney development. Here, we show that the CDC42-GEF, dynamin binding protein (Dnmbp/Tuba), is essential for nephrogenesis in *Xenopus*. *dnmbp* is expressed in *Xenopus* embryo kidneys during development, and knockdown of Dnmbp using two separate morpholino antisense oligonucleotides results in reduced expression of late pronephric markers, whereas the expression of early markers of nephrogenesis remains unchanged. A greater reduction in expression of markers of differentiated distal and connecting tubules was seen in comparison to proximal tubule markers, indicating that Dnmbp reduction may have a greater impact on distal and connecting tubule differentiation. Additionally, Dnmbp reduction results in glomus and ciliary defects. *dnmbp* knockout using CRISPR results in a similar reduction of late markers of pronephric tubulogenesis and also results in edema formation in later stage embryos. Overexpression of *dnmbp* in the kidney also resulted in disrupted pronephric tubules, suggesting that *dnmbp* levels in the developing kidney are tightly regulated, with either increased or decreased levels leading to developmental defects. Together, these data suggest that Dnmbp is required for nephrogenesis.

Keywords: Dnmbp, Tuba, *Xenopus*, nephrogenesis, pronephros, CRISPR

OPEN ACCESS

Edited by:
Karen Liu,
King's College London,
United Kingdom

Reviewed by:
Oliver Wessely,
Cleveland Clinic, Lerner Research Institute, United States
Mustafa Khokha,
Yale University, United States

***Correspondence:**
Rachel K. Miller
Rachel.K.Miller@uth.tmc.edu

Specialty section:
This article was submitted to Embryonic and Developmental Physiology, a section of the journal Frontiers in Physiology

Received: *14 September 2018*
Accepted: *07 February 2019*
Published: *26 February 2019*

Citation:
DeLay BD, Baldwin TA and Miller RK (2019) Dynamin Binding Protein Is Required for Xenopus laevis Kidney Development. Front. Physiol. 10:143. doi: 10.3389/fphys.2019.00143

INTRODUCTION

Kidney development is conserved in amphibians and mammals, making *Xenopus* embryos a good model for studying nephrogenesis. Mammalian kidney development proceeds through three stages: the pronephros, mesonephros, and metanephros (Vize et al., 1997). Similarly, amphibian embryos have a pronephros, and adults have a metanephros (Vize et al., 1995, 1997). The basic unit of filtration for all kidney forms is the nephron, with the same signaling cascades and

inductive events leading to nephrogenesis in mammals and amphibians (Brandli, 1999; Hensey et al., 2002). The *Xenopus* pronephros consists of a single, large, functional nephron (Brennan et al., 1998; Carroll et al., 1999), making it a simple model for studying vertebrate nephron development. Additionally, the *Xenopus* tadpole epidermis is transparent and the kidney is located just under the epidermis, allowing visualization of the pronephros without dissection (Carroll et al., 1999). It is also possible to easily modulate gene expression in *Xenopus* embryos through overexpression, knockdown and knockout experiments via microinjection of RNA constructs, antisense morpholino oligonucleotides (MOs) and CRISPR constructs (Miller et al., 2011; Corkins et al., 2018; DeLay et al., 2018b). The established cell fate maps of the early *Xenopus* embryo facilitate tissue-targeted modulation of gene expression by microinjection into the appropriate blastomere (Moody, 1987a,b; DeLay et al., 2016, 2018b). Taken together, *Xenopus* is a powerful model for studying essential nephrogenesis genes.

One gene that plays an essential role in kidney development is *cdc42*. Cdc42 is a Rho family small GTPase that was first discovered in *Saccharomyces cerevisiae* (Johnson and Pringle, 1990). It plays a role in cell migration, polarity, differentiation and proliferation, as well as branching of blood vessels and regulation of actin dynamics (Melendez et al., 2013; Schulz et al., 2015; Mizukawa et al., 2017; Nguyen et al., 2017; Lavina et al., 2018). Cdc42 is a molecular switch that cycles between active (GTP-bound) and inactive (GDP-bound) states through its interaction with guanine exchange factors (GEFs) and GTPase activating proteins (GAPs) (Bishop and Hall, 2000; Schmidt and Hall, 2002). While GAPs increase the intrinsic GTPase activity of CDC42, GEFs exchange GDP bound to Cdc42 for GTP and assemble complexes between Cdc42, scaffold proteins and kinases (Cerione, 2004).

Loss of Cdc42 in the mouse ureteric bud leads to abnormal nephron tubulogenesis due to branching, polarity and cytoskeletal defects, while loss of Cdc42 in the mouse metanephric mesenchyme results in failure of the renal vesicle and S-shaped body to develop (Elias et al., 2015). Similarly, loss of Cdc42 in the distal tubules of mouse kidney leads to death within a few weeks of birth due to kidney failure, cyst development and a decrease in ciliogenesis within the kidney cysts (Choi et al., 2013). Knockdown of Cdc42 via MO in zebrafish leads to dilated kidney tubules, glomerulus defects and disorganized cilia within kidney tubules (Choi et al., 2013).

Although Cdc42 localizes on the apical surface of the kidney tubule epithelium, it needs to be activated by a GEF in order to regulate tubulogenesis and ciliogenesis (Martin-Belmonte et al., 2007; Zuo et al., 2011). Dynamin binding protein (Dnmbp, Tuba) is a Cdc42-specific GEF that is known to be concentrated on the apical surface of kidney epithelial cells (Otani et al., 2006; Qin et al., 2010). Knockdown of Dnmbp in MDCK cells leads to a decrease in cilia, polarity defects and inhibition of tubulogenesis, similar to that seen when Cdc42 is knocked down (Zuo et al., 2011; Baek et al., 2016). Here, we demonstrate that knockdown, CRISPR knockout and overexpression of *dnmbp* lead to tubulogenesis and cilia defects in *Xenopus* pronephric kidneys, indicating that this protein is required for nephrogenesis.

MATERIALS AND METHODS

Embryos

Adult pigmented *X. laevis* were purchased from Nasco (LM00531MX). Eggs were obtained from female frogs, fertilized *in vitro* and the embryos reared as described previously (Sive et al., 2000). The Center for Laboratory Animal Medicine Animal Welfare Committee at the University of Texas Health Science Center at Houston, which serves as the Institutional Animal Care and Use Committee, approved this protocol (protocol #AWC-16-0111).

Western Blots

Embryos were collected at various stages (Nieuwkoop and Faber, 1994) for lysate creation. Protein lysates from 20 pooled embryos of the same stage were created as described previously (Kim et al., 2002), and one embryo equivalent was added per lane of an 8% SDS-PAGE polyacrylamide gel. Following transblotting of the protein onto a 0.45 μm PVDF membrane (Thermo Scientific), the blot was blocked for 3 h in KPL block (SeraCare) at room temperature. After blocking, the membrane was incubated overnight at 4°C in 1:500 mouse anti-Dnmbp antibody (Abcam 88534) or 1:1000 rabbit anti-GAPDH antibody (Santa Cruz FL-335). Blots were rinsed with TBST and incubated in 1:5000 goat anti-mouse or goat anti-rabbit IgG horseradish peroxidase secondary antibody (BioRad, Hercules, CA) for 2 h at room temperature. Blots were rinsed again in TBST and imaged using enhanced chemiluminescence (Pierce Supersignal West Pico) on a BioRad ChemiDoc XRS+.

In situ Hybridization

A DIG RNA labeling kit (Roche) was used to generate digoxigenin-labeled RNA probes for *in situ* hybridization. Constructs were linearized prior to generating probes using the listed enzyme and polymerase: *atp1a1*-antisense *Sma*I/T7 (Eid and Brandli, 2001), *lhx1*-antisense *Xho*I/T7 (Taira et al., 1992; Carroll and Vize, 1999), *hnf1*β-antisense *Sma*I/T7 (Demartis et al., 1994), *nphs1*-antisense *Sma*I/T7 (Gerth et al., 2005), *clcnkb*-antisense *Eco*RI/T7 (Vize, 2003), *slc5a1*-antisense *Sma*I/T7 (Zhou and Vize, 2004), and *pax2*-antisense *Eco*RI/T7 (Carroll and Vize, 1999).

Digoxigenin-labeled *dnmbp* RNA probes were generated by first extracting DNA from stage 40 embryos as previously described (Bhattacharya et al., 2015). Regions of *dnmbp.L* and *dnmbp.S* were amplified from embryo DNA by PCR using the following primers: *dnmbp.L*-sense-Sp6 (5′-CTAGCATTTAGGTGACACTATAGGTCAAAGGACACTCGAAACAC-3′), *dnmbp.L*-antisense-T7 (5′-CTAGCTAATACGACTCACTATAGAGAAACATTCGTCTCGCGAGG-3′), *dnmbp.S*-sense-Sp6 (5′-CTAGCATTTAGGTGACACTATAGGTTAAAGGACACTCGAAACAC-3′) and *dnmbp.S*-antisense-T7 (5′-CTAGCTAATACGACTCACTATAGAGAAACGTTCGTGGAGGGT

AC-3′). PCR products were transcribed to create digoxigenin-labeled RNA probes using a DIG RNA labeling kit (Roche) and the appropriate polymerase (T7 or Sp6).

MOs and RNA Constructs

Two translation-blocking MOs were designed to target the 5′ untranslated region of *dnmbp*: Dnmbp MO 1, 5′-TCGAACCACCGATCCCACCTCCATC-3′; Dnmbp MO 2, 5′-ACCACCGACCCCACCTCCATCCTAA-3′. A Standard control MO (5′-CCTCTTACCTCAGTTACAATTTATA-3′) was used as a control for all MO experiments. MOs were ordered from Genetools. Single cell embryos were injected with 40 ng MO for Western blot analysis and 8-cell embryos were injected with 20 ng MO for phenotypic analysis.

Human *DNMBP* RNA was created by linearizing pcDNA3-HA-Tuba (Addgene plasmid 22214) DNA with *Xba*I (Salazar et al., 2003). Capped RNA for rescue and overexpression experiments was transcribed and purified from the linearized DNA using a T7 mMachine mMessage kit (Ambion). A pCS2-β-*galactosidase* construct was obtained from the McCrea laboratory for use as a control for rescue and overexpression experiments (Lyons et al., 2009; Miller et al., 2011). β-*galactosidase* RNA was transcribed from plasmid DNA linearized with *Not*I using a Sp6 mMachine mMessage kit (Ambion).

sgRNA Design and Creation

One sgRNA that was complimentary against both homeologs of *dnmbp* (5′-CTAGCTAATACGACTCACTATAG GGAGCGCTCCTGGTTCATGGGGTTTTAGAGCTAGAAATA GCAAG-3′) was designed as previously reported (DeLay et al., 2018b). A sgRNA against *slc45a2* was generated for use as a control (DeLay et al., 2018b). DNA templates for sgRNAs were produced by PCR, and T7 polymerase was used to transcribe sgRNA from the DNA templates as previously described (Bhattacharya et al., 2015; DeLay et al., 2018b). For long-term storage, sgRNA was diluted to 1000 ng/μL and kept at −80°C. For working stocks, sgRNA was diluted to 500 ng/μL and stored in 5 μL aliquots of at −20°C. Working stock aliquots were limited to five freeze-thaw cycles prior to disposal. Single cell and 8-cell embryos were injected with 1 ng Cas9 protein and 500 pg sgRNA.

CRISPR Genomic Analysis

Embryos injected at the 1-cell stage with 1 ng Cas9 protein and 500 pg sgRNA were reared to stage 40. DNA was extracted from individual embryos as previously described (Bhattacharya et al., 2015), and the region surrounding the sgRNA binding site was amplified by PCR as previously described (DeLay et al., 2018b). *dnmbp.L* DNA was amplified using nested PCR. The outer set of primers used were *dnmbp.L*-outer-forward (5′-AGCTGACCCCATCTTAAAACAA-3′) and *dnmbp.L*-reverse (5′-GTTTTTAGCTGCTTGGCTCAGT-3′). Following the outer PCR reaction, the resulting PCR product was used to amplify *dnmbp.L* using primers *dnmbp.L*-reverse and *dnmbp.L*-inner-forward (5′-TTCATGGCCTCTCCTACTCATT-3′). *dnmbp.L* was sequenced using primer *dnmbp.L*-outer-forward. *dnmbp.*S DNA was amplified with primers *dnmbp.S*-forward (5′-GACCCCATAATTGAGCCATAAG-3′) and *dnmbp.S*-reverse (5′-CAGTGGTTTTGACGATTGTAGC-3′) and sequenced using *dnmbp.S*-forward. TIDE was used to determine insertion and deletion frequencies in the amplified gene region (Brinkman et al., 2014).

Microinjection

Individual blastomeres were microinjected with 10 nL of injection mix as described previously (DeLay et al., 2016). Blastomere V2 of 8-cell embryos was injected to target the kidney (Moody, 1987a). Cas9 protein (CP01; PNA Bio) and sgRNA were incubated together at room temperature for at least 5 min prior to microinjection (DeLay et al., 2018b). MOs, RNA constructs and Cas9/sgRNAs were co-injected with either membrane-RFP RNA, Alexa Fluor 488 fluorescent dextran or rhodamine dextran as a tracer (Davidson et al., 2006; DeLay et al., 2016, 2018b). For edema experiments, embryos were injected into both ventral blastomeres at the 4-cell stage.

Immunostaining

Staged embryos (Nieuwkoop and Faber, 1994) were fixed (DeLay et al., 2016) prior to immunostaining as described previously (Lyons et al., 2009). The lumens of the proximal kidney tubules were labeled using 3G8 antibody (1:30) and the distal and connecting kidney tubules were labeled using 4A6 antibody (1:5) (Vize et al., 1995). Additionally, proximal tubules were detected using fluorescein-labeled *Erythrina cristagalli* lectin (50 μg/mL; Vector Labs). Somites were labeled using antibody 12/101 (1:100) (Kintner and Brockes, 1984) and membrane-RFP tracer was labeled with anti-RFP antibody (1:250; MBL International PM005). Kidney, somite and membrane-RFP tracer staining were visualized using goat anti-mouse IgG Alexa 488 (1:2000; Invitrogen) and goat anti-rabbit IgG Alexa 488 and Alexa 555 (1:2000; Invitrogen).

Imaging

Embryo phenotypes were scored and *in situ* images were taken using an Olympus SZX16 fluorescent stereomicroscope with an Olympus DP71 camera or a Leica S8 A80 stereomicroscope with a Leica MC120 HD camera. Confocal images were taken with a Zeiss LSM800 microscope. Adobe Photoshop and Illustrator CS6 were used to process images and create figures.

RESULTS

Dnmbp Is Expressed in the Developing *Xenopus* Pronephros

To assess whether Dnmbp protein is expressed during kidney development, protein lysates were collected from embryos at different developmental stages. Using a commercial antibody against Dnmbp, we found that Dnmbp protein (170 kD) is present in *Xenopus* embryos from single cell through tadpole stages by Western blot (**Figure 1A**). Importantly, Dnmbp protein was

present from gastrula (stage 12) through tadpole (stage 38) stages when pronephric kidney specification and development occur.

To determine if *dnmbp* is present in the *Xenopus* kidney throughout pronephric development, embryos ranging from stage 26 to 38 were subjected to *in situ* hybridization (**Figure 1B** and **Supplementary Figure S1**). Antisense probes were created against each homeolog of *dnmbp*, and sense probes against each homeolog were used to verify that staining was specific for *dnmbp*. Starting at stage 26, both antisense probes against *dnmbp* stained the kidney tubules, with the strongest staining in the proximal tubules (**Figure 1B**). In addition to the kidney, the antisense *dnmbp* probes stained head structures and somites (**Supplementary Figure S1**). In comparison, the sense control *dnmbp* probes did not label any embryonic structures when processed in parallel to the antisense probes, indicating that the antisense *dnmbp* probe staining was specific

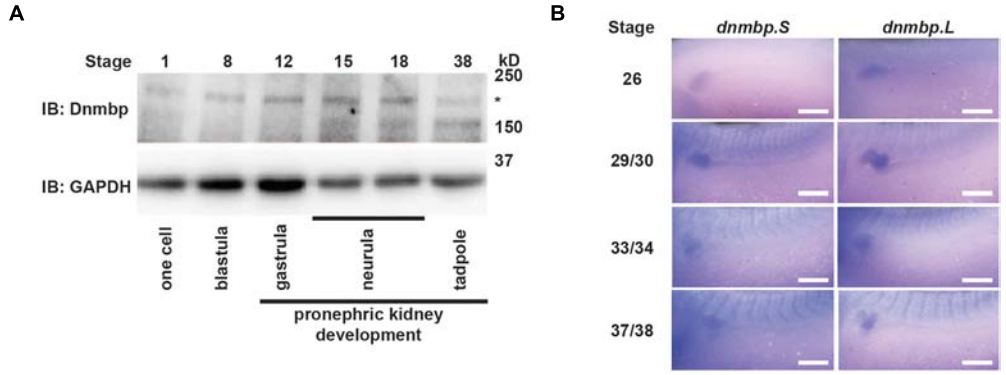

FIGURE 1 | Dnmbp is present throughout *Xenopus* pronephric development. **(A)** Western blot showing that Dnmbp is present in embryos ranging from stage one to stage 38. * indicates Dnmbp. **(B)** *In situ* hybridization using probes against *dnmbp.S* and *dnmbp.L* showing *dnmbp* expression in the developing pronephros from stage 26 through stage 37/38. White bar is 500 μm.

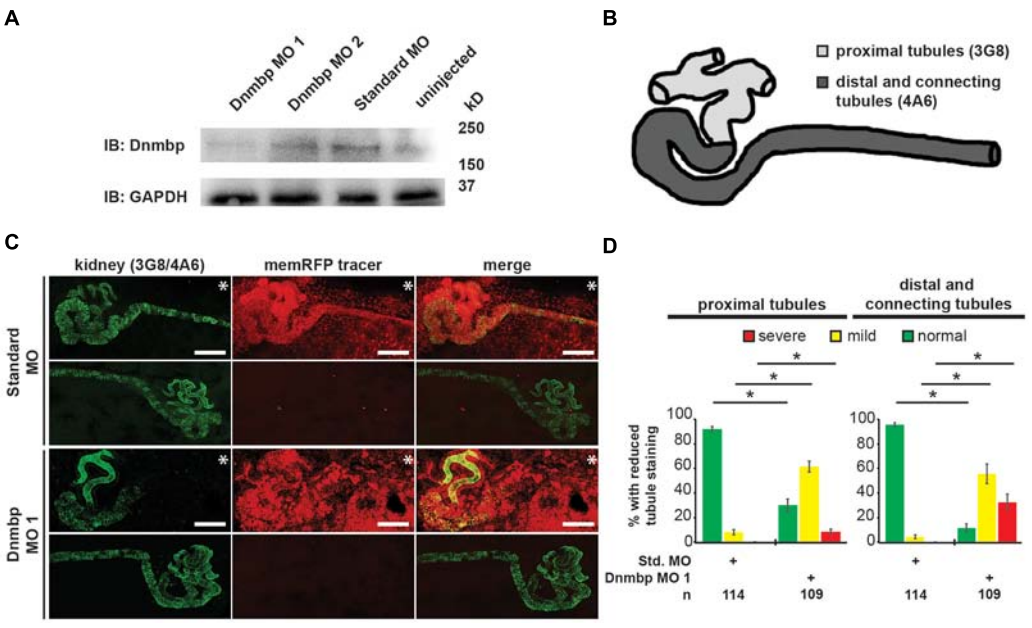

FIGURE 2 | Knockdown of Dnmbp results in reduced kidney tubulogenesis. **(A)** Western blot showing the efficiency of two different MOs targeting Dnmbp. Single cell embryos were injected with 40ng of Dnmbp MO 1, Dnmbp MO 2 or Standard MO. One embryo equivalent per lane was loaded on to the SDS-PAGE gel. **(B)** Schematic of the *Xenopus* pronephros showing the proximal, distal and connecting tubule regions. **(C)** Unilateral injection of 20ng Dnmbp MO 1 into blastomere V2 at the 8-cell stage leads to defects in kidney tubulogenesis in comparison to embryos injected with Standard MO. Antibody 3G8 used to label the lumen of the proximal tubule, antibody 4A6 used to label the distal and connecting tubules. memRFP used as an injection tracer. White bar indicates 200 μm.* indicates injected side of embryo. **(D)** Knockdown of Dnmbp leads to reduced expression of differentiated kidney tubule markers in comparison to embryos injected with Standard MO. *n* = number of embryos across 3 replications. Error bars represent Standard error. *Significantly different from control, $p < 0.05$.

for *dnmbp* (**Supplementary Figure S1**). Taken together, this indicates that *dnmbp* transcripts are present in the kidney during nephrogenesis.

Knockdown of Dnmbp Leads to Altered Pronephric Development in *Xenopus*

To determine whether Dnmbp is necessary for the development of the *Xenopus* pronephros, we examined the expression pattern of markers of differentiated kidney tubules upon depletion of Dnmbp. Dnmbp was knocked down using two different translation-blocking MOs: Dnmbp MO 1 and Dnmbp MO 2. Both MOs were designed to target the 5′ untranslated region of *dnmbp*. Knockdown in single cell embryos was confirmed by Western blot (**Figure 2A**) of stage 10–12 embryos in comparison to embryos injected with a Standard MO control. Dnmbp MO 1 showed a marked decrease in Dnmbp protein levels in comparison to both Standard MO and uninjected controls. Dnmbp MO 2 showed a decrease in Dnmbp in comparison to Standard MO controls, but did not show a clear reduction in comparison to uninjected controls. For this reason, phenotypic analysis was carried out for Dnmbp MO 1 knockdown embryos.

Pronephric tubule development was assessed upon Dnmbp knockdown using 3G8 and 4A6 antibodies (Vize et al., 1995), which label the differentiated proximal tubules versus the distal and connecting tubules, respectively (**Figure 2B**). Knockdown phenotypes of embryos injected in the left V2 blastomere at the 8-cell stage were assessed using a previously described scoring system by comparing the tubules on the MO-injected side of the embryo to the tubules on the uninjected side (DeLay et al., 2018b). Phenotypes were scored as "normal" if there was no difference between the injected and uninjected side, "mild" if there was a reduction in tubule development and/or antibody staining on the injected side in comparison to the injected side or "severe" if there was little to no tubule and/or antibody staining on the injected side of the embryo.

Knockdown of Dnmbp resulted in disrupted proximal tubule development in stage 40–41 embryos that had been injected with either Dnmbp MO in comparison to Standard MO-injected controls (**Figures 2C,D** and **Supplementary Figure S2**). The proximal tubules in Dnmbp knockdown embryos had shorter branches and were less convoluted than Standard MO-injected control embryos. Similarly, distal and connecting tubule development was disrupted upon Dnmbp knockdown, resulting in decreased convolution of the distal and connecting tubules of Dnmbp knockdown embryos in comparison with those of Standard MO-injected controls (**Figures 2C,D** and **Supplementary Figure S2**). Interestingly, there was a decrease in 4A6 staining of the distal and connecting tubules even though these tubules could be visualized using the co-injected memRFP

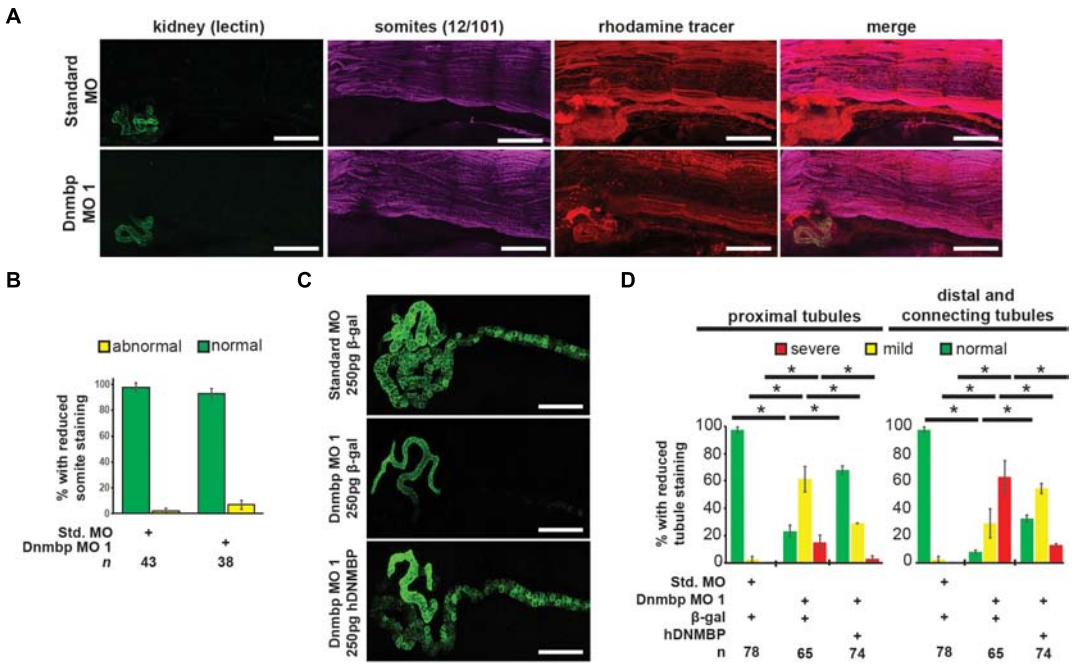

FIGURE 3 | Dnmbp knockdown is specific and does not cause somite development defects. **(A)** Unilateral injection of 20 ng Dnmbp MO 1 into blastomere V2 at the 8-cell stage does not cause somite defects in comparison to embryos injected with Standard MO. 12/101 antibody labels somites, lectin labels the proximal tubule lumen, rhodamine used as a tracer. Images are stitched from 6 tiles. White bar is 200 μm. **(B)** Knockdown of Dnmbp does not lead to reduced somite development compared to embryos injected with Standard MO. **(C)** Representative embryos showing that co-injection of β-*galactosidase* RNA with Dnmbp MO 1 does leads to kidney defects in comparison to control embryos injected with Standard MO and β-*galactosidase* RNA. Co-injection of human *DNMBP* mRNA with Dnmbp MO 1 rescues the knockdown phenotype. Stage 40 embryos stained with antibody 3G8 to label the proximal tubule and antibody 4A6 to label the distal and connecting tubules. White bar is 200 μm. **(D)** Quantitation of the rescue phenotype. *n* = number of embryos across 3 replications. Error bars represent Standard error. *Significantly different, $p < 0.05$.

tracer (**Figure 2C** and **Supplementary Figure S2**) indicating that the distal and connecting tubules are either absent or they are less differentiated than the tubules in the Standard MO-injected control embryos.

To assess whether the pronephric defects observed in Dnmbp knockdown embryos are secondary defects caused by defects in somite development, immunostaining was performed. Somites of stage 40–41 embryos were stained with 12/101 antibodies, and the lumen of the proximal tubules was stained with lectin. Embryos were injected with either Standard MO or Dnmbp MO 1 at the 8-cell stage (left V2 blastomere) with rhodamine used as a tracer, and somite staining on the injected side of the embryo was compared to staining on the uninjected side of the embryo. There was no difference between somite staining of Standard MO- and Dnmbp MO-injected embryos (**Figures 3A,B**), although lectin staining indicated that there were proximal tubule defects in the Dnmbp knockdown embryos (**Figure 3A**). Note that the rhodamine tracer is present in the somites as well as in the kidney, indicating that both the somites and the kidney received MO. Additionally, it is possible to visualize distal and connecting tubule defects in the Dnmbp knockdown embryos by observing the rhodamine tracer localization in the kidney. The lack of somite defects in the Dnmbp knockdown embryos indicates that the observed tubule defects are not likely to be due to somite development defects.

To assess the specificity of the Dnmbp knockdown, Dnmbp MO 1 was co-injected with human *DNMBP* RNA in an attempt to rescue the knockdown phenotype. β-*galactosidase* (β-*gal*) was used as a negative RNA control. Embryos were assessed at stages 40–41. Co-injection of Dnmbp MO 1 and β-*gal* RNA led to the expected decrease in proximal, distal and connecting tubule development (**Figures 3C,D**). Similarly, co-injection of Standard MO and β-*gal* RNA did not lead to defects in tubulogenesis (**Figures 3C,D**). Co-injection of Dnmbp MO 1 and human *DNMBP* RNA resulted in fewer tubulogenesis defects than in Dnmbp MO 1 and β-*gal* RNA control embryos, indicating that human *DNMBP* RNA is able to rescue the kidney phenotypic defects caused by the Dnmbp MO 1. This result indicates that the kidney phenotype observed is due to Dnmbp knockdown specifically.

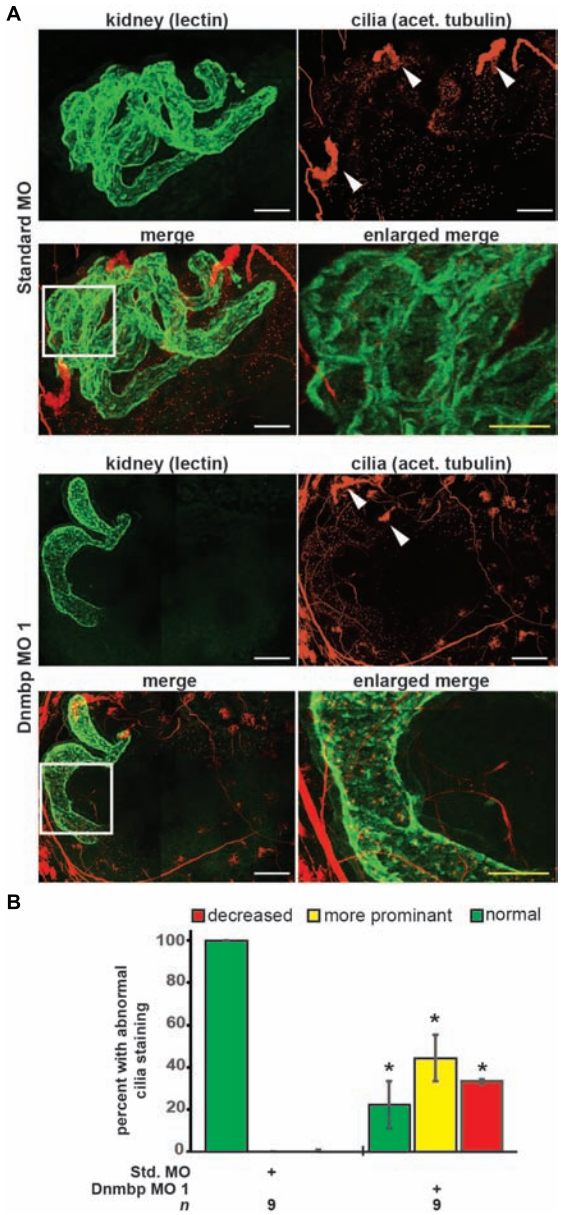

FIGURE 4 | Dnmbp knockdown alters ciliogenesis. **(A)** Unilateral injection of 20ng Dnmbp MO 1 into blastomere V2 at the 8-cell stage causes altered primary ciliogenesis in comparison to embryos injected with Standard MO. Longer primary cilia are visible in the proximal tubules of the Dnmbp knockdown embryos ("more prominent cilia" phenotype). Acetylated tubulin antibody used to label cilia and nerves and lectin used to label the proximal tubule lumen. Images are stitched from 6 tiles. White bar is 50 μm, yellow bar is 25 μm. White arrowhead indicates nephrostome. White box indicates region represented in the enlarged merge panel. **(B)** Knockdown of Dnmbp leads to altered primary cilia development compared to embryos injected with Standard MO. *n* = number of embryos across 3 replications. Error bars represent Standard error. *Significantly different from control, $p < 0.05$.

Knockdown of Dnmbp Leads to Disruption of Nephric Cilia Organization in *Xenopus*

As defects in cilia development have been reported in zebrafish in which Dnmbp has been knocked down (Baek et al., 2016), cilia development in the pronephros was assessed. Embryos were injected with Standard MO or Dnmbp MO 1 in the left V2 blastomere at the 8-cell stage, reared to stage 40–41 and stained with lectin to label the proximal tubules and an acetylated tubulin antibody to label cilia and nerves. Control embryos showed very short cilia in the proximal tubules and longer-appearing cilia in the distal and connecting tubules (**Figure 4A**). 78% (7/9) of Dnmbp knockdown embryos displayed primary cilia defects in the kidney tubules (**Figure 4B**). Of these, the abnormal primary cilia phenotypes were broken down into two distinct groups: "more prominent cilia" and "reduced cilia." 44% (4/9) of Dnmbp knockdown embryos displayed more prominent cilia within the proximal tubules in comparison to

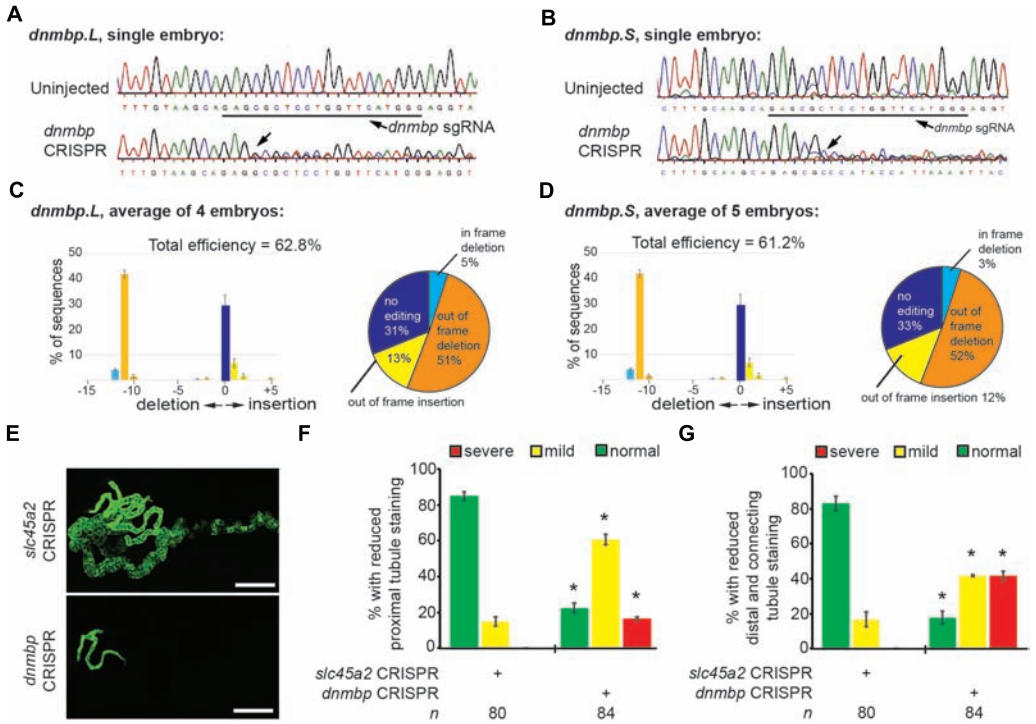

FIGURE 5 | sgRNA targeting *dnmbp* efficiently edits *Xenopus* embryo DNA. Stage 40 embryos injected with *dnmbp* sgRNA and Cas9 protein at the 1-cell stage. **(A)** Chromatogram showing CRISPR editing of *dnmbp.L* in a single embryo. The underlined sequence corresponds to the *dnmbp* sgRNA binding sequence, and the arrow indicates sequence degradation due to CRISPR. **(B)** Chromatogram showing CRISPR editing of *dnmbp.S* in a single embryo. The underlined sequence corresponds to the *dnmbp* sgRNA binding sequence, and the arrow indicates sequence degradation due to CRISPR. **(C)** TIDE analysis of *dnmbp.L* sequence trace degradation after the expected Cas9 cut site. $*p < 0.001$. Percentage of *dnmbp.L* DNA sequence containing insertions and deletions. Bars indicate the mean of the percent of insertion/deletion sequences from four embryos, with the error bars representing the Standard error of the mean. Results are the mean of sequencing data from four embryos. **(D)** TIDE analysis of *dnmbp.S* sequence trace degradation after the expected Cas9 cut site. $*p < 0.001$. Percentage of *dnmbp.S* DNA sequence containing insertions and deletions. Bars indicate the mean of the percent of insertion/deletion sequences from four embryos, with the error bars representing the Standard error of the mean. Results are the mean of sequencing data from four embryos. **(E)** Representative stage 40 embryos showing that 8-cell targeted knockout of *dnmbp* leads to disrupted kidney tubulogenesis in comparison to *slc45a2* knockout controls. Antibody 3G8 labels the proximal tubule lumen and antibody 4A6 labels cell membranes of the distal and connecting tubules. White bar is 200 μm. **(F)** Knockout of *dnmbp* reduces proximal tubule development. **(G)** Knockout of *dnmbp* reduces distal and intermediate tubule development. **(F,G)** *n* = number of embryos across 3 replications. Error bars represent Standard error. *Significantly different from control, $p < 0.05$.

the controls, while the cilia in the distal and connecting tubules appeared to be normal (**Figure 4A**, compare panels labeled enlarged merge). 33% (3/9) of Dnmbp knockdown embryos displayed reduced cilia in the proximal, distal and intermediate tubules in comparison to controls and 22% (2/9) of Dnmbp knockdown embryos showed no obvious primary cilia defect. Cilia were present on the nephrostomes of all control and Dnmbp knockdown embryos (**Figure 4A**, white arrowheads) and multiciliated cells on the epidermis of all of the Dnmbp knockdown embryos appeared to be normal (data not shown). These data suggest that there is a primary cilia defect in the kidneys of Dnmbp knockdown embryos, while motile cilia appear to be grossly unaffected.

CRISPR *dnmbp* Knockout Phenocopies Dnmbp Knockdown

To further confirm that loss of *dnmbp* leads to kidney tubulogenesis defects, we designed a single sgRNA with complete complementarity to both homeologs of *dnmbp*. Embryos were injected with 500 pg *dnmbp* sgRNA and 1 ng Cas9 protein, and a region surrounding the sgRNA binding site was amplified by PCR. Different sets of sequencing primers, each specific for one of the two *dnmbp* homeologs, were used to distinguish between *dnmbp.L* and *dnmbp.S* DNA sequences (**Supplementary Figure S3**). Sequences were analyzed using TIDE, a web-based tool that allows the user to easily compare DNA sequence trace decomposition around the predicted Cas9 cut site to an unedited control sequence while providing output on indel composition and percent of DNA edited (Brinkman et al., 2014; DeLay et al., 2018b). TIDE analysis indicated that the *dnmbp* sgRNA efficiently knocked out both homeologs in F0 embryos (**Figure 5**). Individual embryo sequence traces showed an increase in sequence trace decomposition around the expected sgRNA binding site, indicating CRISPR editing (**Figures 5A,B**). Overall, CRISPR knockout of *dnmbp* resulted in 62.8% editing efficiency of the *dnmbp.L* homeolog and 61.2% editing efficiency of the

dnmbp.S homeolog (**Figures 5C,D**). The most common mutation for both homeologs was an 11 base pair out of frame deletion (**Figures 5C,D**).

Embryos were injected at the 8-cell stage (left V2 blastomere) with 1 ng Cas9 protein and either 500 pg *dnmbp* sgRNA or control *slc45a2* sgRNA and reared to stage 40 to assess kidney development (DeLay et al., 2018b). *slc45a2* was knocked out as a control because loss of this gene leads to decreased pigmentation of the eyes and melanocytes, but does not alter kidney development (DeLay et al., 2018b). Therefore, knockout of *slc45a2* was used as a negative control with which to compare *dnmbp* knockout embryo phenotype.

Proximal tubule staining of *dnmbp* knockout embryos using 3G8 antibodies indicated a reduction in proximal tubule branching and convolution in comparison to *slc45a2* knockout controls (**Figures 5E,F**). Distal and connecting tubule development was also disrupted in *dnmbp* knockout embryos in comparison to *slc45a2* knockout controls, with a decrease in 4A6 staining indicating less differentiated distal and connecting tubules (**Figures 5E,G**). The phenotype observed in *dnmbp* knockout embryos was similar to that seen in MO knockdown embryos.

dnmbp knockout specificity was tested by attempting to rescue the knockout phenotype through co-injection of *dnmbp* sgRNA and Cas9 protein with human *DNMBP* RNA. Control embryos injected with *slc45a2* sgRNA, Cas9 protein and β-*galactosidase* RNA exhibited normal kidney development at stage 40–41 (**Figures 6A,B**), while embryos injected with *dnmbp* sgRNA, Cas9 protein and β-*galactosidase* RNA had decreased proximal, distal and connecting tubule development. In contrast, the *dnmbp* rescue embryos injected with *dnmbp* sgRNA, Cas9 protein and human *DNMBP* RNA had an intermediate phenotype, with a significant reduction in the proximal, distal and connecting tubule defects (**Figures 6A,B**). This result indicates that human *DNMBP* RNA is able to rescue the kidney defects seen in *dnmbp* CRISPR knockout embryos and suggests that the observed kidney phenotype is specific to *dnmbp* knockout.

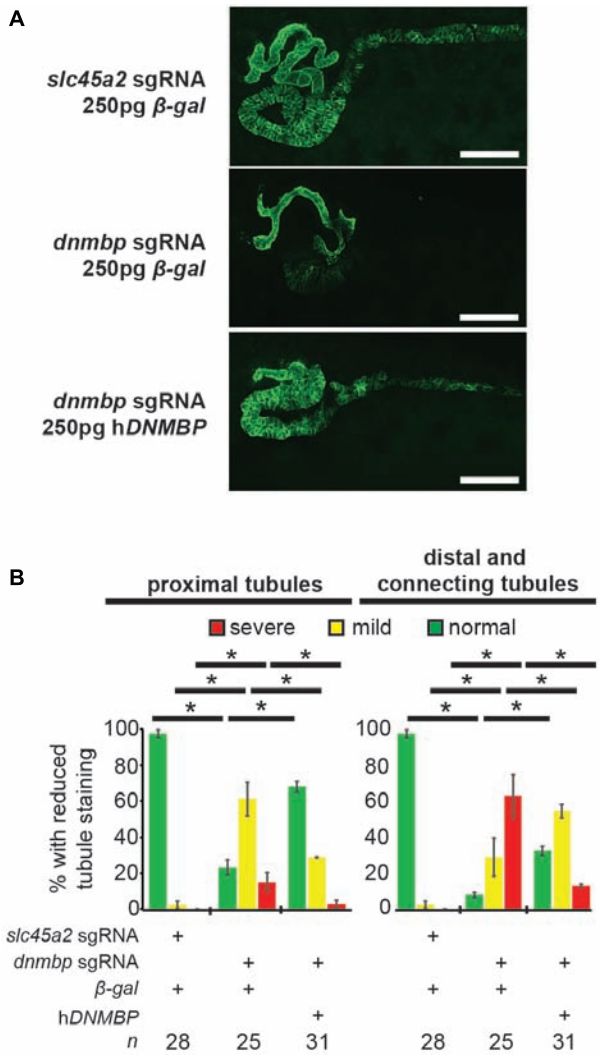

FIGURE 6 | Human *DNMBP* mRNA rescues kidney defects caused by CRISPR *dnmbp* knockout in *Xenopus* embryos. **(A)** Representative embryos showing that co-injection of β-*galactosidase* RNA with a sgRNA against *dnmbp* does leads to kidney defects in comparison to control embryos injected with a sgRNA against *slc45a2* and β-*galactosidase* RNA. Co-injection of human *DNMBP* mRNA with a sgRNA against *dnmbp* rescues the knockdown phenotype. Stage 40 embryos stained with antibody 3G8 to label the proximal tubule and antibody 4A6 to label the distal and connecting tubules. White bar is 200 μm. **(B)** Quantitation of the rescue phenotype. *n* = number of embryos across 2 replications. Error bars represent Standard error. *Significantly different, $p < 0.05$.

DNMBP Overexpression Results in Altered Pronephric Tubulogenesis

Knockdown and knockout of Dnmbp leads to disrupted pronephric development, so studies were carried out to determine whether *DNMBP* overexpression also leads to tubulogenesis defects. Human *DNMBP* RNA was injected into single-cell embryos, which were then collected for protein lysate preparation at stage 10–12. DNMBP was detected by Western blot using an antibody against full-length human DNMBP protein that also recognizes *Xenopus* Dnmbp (**Figure 7A**). Note that the human DNMBP protein, which has an HA tag, runs at a slightly higher kD than the *Xenopus* Dnmbp protein. Therefore, both the human DNMBP band and the *Xenopus* Dnmbp band together represent the overall amount of Dnmbp in the embryo lysate of embryos overexpressing Dnmbp. Overexpression of human *DNMBP* RNA led to a decrease in endogenous embryo Dnmbp, with higher levels of human *DNMBP* overexpression leading to a greater decrease in endogenous Dnmbp protein. Overall, injection of human *DNMBP* RNA led to greater levels of Dnmbp protein in the resulting embryo lysates.

Similar to disruption of Dnmbp expression by knockdown or knockout, overexpression of Dnmbp led to kidney tubulogenesis defects (**Figures 7B,C**). Embryos were injected with either β-*gal* RNA as a negative control or human *DNMBP* RNA at the 8-cell stage (left V2 blastomere). Proximal tubule development was assessed using antibody 3G8, and distal and connecting

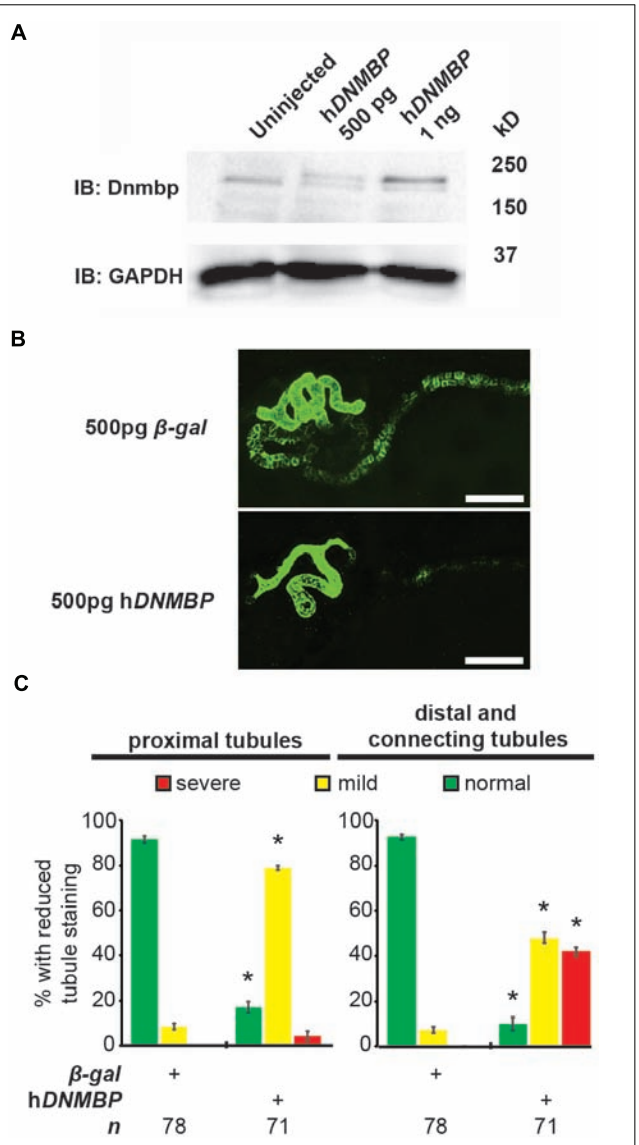

FIGURE 7 | Overexpression of human *DNMBP* results in kidney tubule defects. **(A)** Western blot showing expression of both endogenous (*Xenopus*) Dnmbp (lower band) and exogenous (human) HA::DNMBP (upper band). Embryos injected at the one-cell stage and assayed at stage 10–12. One embryo equivalent loaded per lane. **(B)** Representative stage 40 embryos injected with either β-*galactosidase* control mRNA or human *DNMBP* mRNA. Overexpression of h*DNMBP* leads to disrupted kidney tubulogenesis in comparison to controls. Embryos injected at the 8-cell stage (blastomere V2) to target the kidney and stained with 3G8 antibodies to label the proximal tubule and 4A6 antibodies to label the distal and connecting tubules. White bar indicates 200 μm. **(C)** Quantitation of phenotypes showing that overexpression of h*DNMBP* leads to a reduction in proximal, distal and connecting tubule staining. *n* = number of embryos across 3 replications. Error bars represent Standard error. *Significantly different from control, $p < 0.05$.

tubule development were assessed using antibody 4A6 in stage 40–41 embryos. Dnmbp overexpression led to less convoluted proximal tubules with shorter branches in comparison to β-*gal* RNA control embryos. Likewise, Dnmbp overexpression led to less convoluted distal and connecting tubules, as well as decreased 4A6 staining indicating that the distal and connecting tubules were less differentiated than in β-*gal* RNA controls.

Disruption of *dnmbp* Expression Does Not Alter Expression of Early Markers of Nephrogenesis

To further understand the role that Dnmbp plays in *Xenopus* kidney development, early markers of nephrogenesis were assessed by *in situ* hybridization. Embryos were injected with either Dnmbp MO 1 or Standard MO at the 8-cell stage (left V2 blastomere) and allowed to develop to stage 29–30 (*lhx1*), 32–33 (*hnf1*β), or 33–34 (*pax2*). Marker expression on the injected side was compared to the uninjected side of the embryo. Knockdown of these early markers of pronephric development (*lhx1*, *hnf1*β, and *pax2*) did not result in reduction of marker expression (**Figure 8**). This indicates that loss of *dnmbp* does not alter early kidney specification and development.

To assess if the observed lack of early kidney defects in Dnmbp knockdown embryos also held true for *dnmbp* CRISPR knockout embryos, embryos were injected with a sgRNA against either *dnmbp* or *slc45a2* and Cas9 protein at the 8-cell stage. Embryos were assessed for *lhx1* staining by *in situ* hybridization at stage 29–30. Similar to Dnmbp knockdown embryos, there was no difference in *lhx1* staining between the *dnmbp* knockout embryos and the *slc45a2* knockout control embryos, suggesting that knockout of *dnmbp* gives a similar early kidney development phenotype to Dnmbp knockdown (**Figure 9**).

Disruption of *dnmbp* Expression Perturbs Expression of Late Markers of Nephrogenesis

Next, late markers of nephrogenesis were assessed by *in situ* hybridization after injection of either Dnmbp MO 1 or Standard MO at the 8-cell stage (left V2 blastomere). The proximal tubule development of stage 40–41 embryos was assessed using an *in situ* probe against *slc5a1*. Although early stage embryos did not show nephrogenesis defects by *in situ* hybridization, Dnmbp knockdown embryos displayed a significant decrease in *slc5a1* staining on the injected side in comparison to the Standard MO control embryos at stage 40–41 (**Figure 10**). This phenotype corresponds to the phenotype seen by immunostaining stage 40–41 embryos with antibody 3G8, which also labels the proximal tubules (**Figure 2C**).

Distal and connecting tubule development in stage 40–41 embryos was assessed using a probe against *clcnkb*. Knockdown of Dnmbp resulted in decreased *clcnkb* staining of the distal and connecting tubules (**Figure 10**) in comparison to control embryos injected with Standard MO. The kidney tubules of these later stage Dnmbp knockdown embryos were less convoluted than the Standard MO control embryos, but did not exhibit a loss of staining as was observed using the 4A6 antibody (**Figure 2C**). This further indicates that the distal and connecting tubules are present in embryos depleted of Dnmbp, but that these tubules regions are less differentiated than they are in control embryos.

Glomus development was assessed using a probe against *nphs1*. Stage 36–37 Dnmbp knockdown embryos displayed a

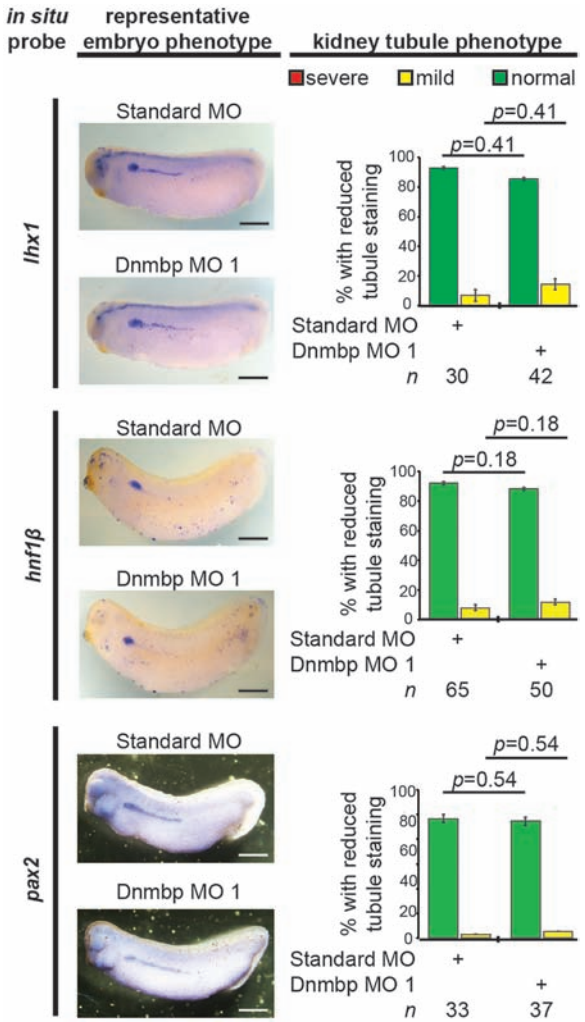

FIGURE 8 | Dnmbp knockdown does not alter expression of early markers of kidney development, as assessed by *in situ* analysis. Embryos injected unilaterally at the 8-cell stage (blastomere V2) to target the kidney and reared to stage 29–30 for *lhx1* expression assessment, stage 32–33 for *hnf1*β expression assessment and stage 33–34 for *pax2* expression assessment. Representative embryo phenotypes shown. Scale bar indicates 500 μm. *n* = number of embryos across 2 (*pax2*) or 3 replications (*lhx1*, *hnf1*β). Error bars represent Standard error. *Significantly different from control, $p < 0.05$.

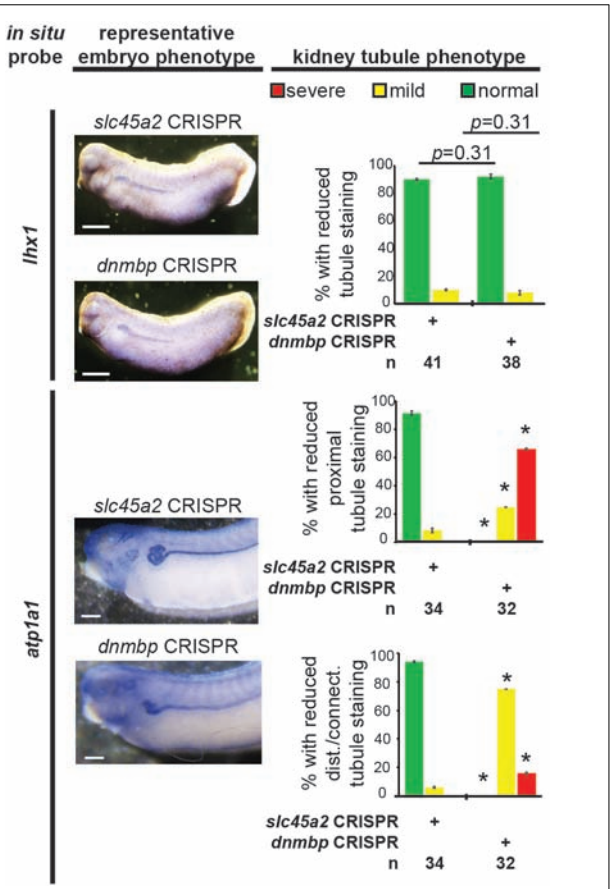

FIGURE 9 | *dnmbp* CRISPR knockout does not alter expression of early markers of kidney development, however late marker expression is altered by *in situ* analysis. Embryos injected unilaterally at the 8-cell stage (blastomere V2) to target the kidney and reared to stage 29–30 for *lhx1* expression assessment and stage 40–41 for *atp1a1* expression assessment. Representative embryo phenotypes shown. Scale bar indicates 500 μm. *n* = number of embryos across 2 replications. Error bars represent Standard error. *Significantly different from control, $p < 0.05$.

significant reduction in glomus development on the injected side of the embryo in comparison to control embryos injected with Standard MO (**Figure 10**). This indicates that Dnmbp is necessary for normal glomus development in addition to kidney tubulogenesis.

Finally, embryos were stained at stage 40–41 with *atp1a1*, which lightly stains the proximal tubules and strongly stains the distal and connecting tubules. Dnmbp knockdown embryos showed a marked decrease in proximal tubule expression of *atp1a1* (**Figure 10**). Similar to staining with *clcnkb*, the distal and intermediate tubules of Dnmbp knockdown embryos were less convoluted than Standard MO control embryo tubules and there was no distinct loss of distal and connecting tubule staining as was observed using the 4A6 antibody (**Figure 2C**). This result provides further evidence that the distal and connecting tubules of Dnmbp knockdown embryos are present but are less differentiated than control embryos.

Similarly, *atp1a1* staining was used to assess CRISPR knockout of *dnmbp* in stage 40–41 embryos. *dnmbp* knockout led to a decrease in proximal, distal and connecting tubule staining in comparison to *slc45a2* knockout controls (**Figure 9**). Like Dnmbp knockdown embryos, *dnmbp* knockout embryos displayed a reduction in the convolution of the distal and intermediate tubules.

dnmbp Knockout Leads to Edema Formation

To determine if loss of Dnmbp leads to defects in kidney function, either *dnmbp* or *slc45a2* sgRNA and Cas9 protein were injected into both ventral blastomeres of 4-cell embryos. Embryos were allowed to develop to stage 45–46 and edema formation was

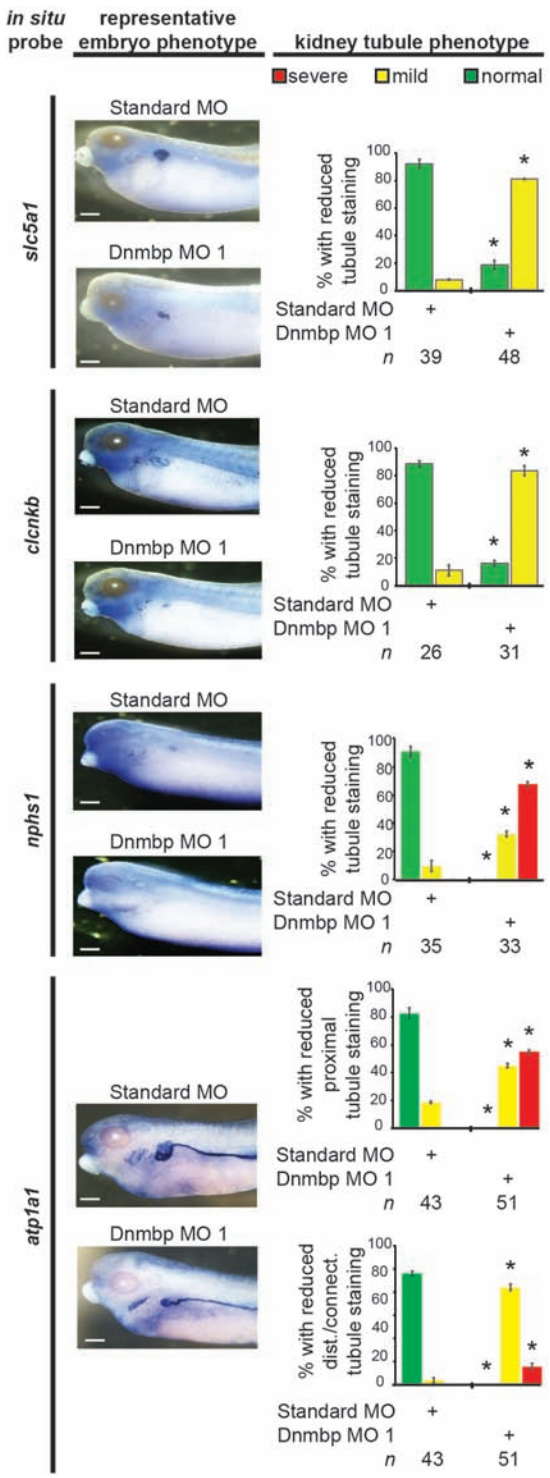

FIGURE 10 | Dnmbp knockdown alters expression of late markers of kidney development, as assessed by *in situ* analysis. Embryos injected unilaterally at the 8-cell stage (blastomere V2) to target the kidney and reared to stage 40–41 for *slc5a1*, *clcnkb,* and *atp1a1* expression assessment or stage 36–37 for *nphs1* expression assessment. Representative embryo phenotypes shown. Scale bar indicates 500 μm. *n* = number of embryos across 2 (*slc5a1*, *clcnkb*, *nphs1*) or 3 replications (*atp1a1*). Error bars represent Standard error. *Significantly different from control, $p < 0.05$.

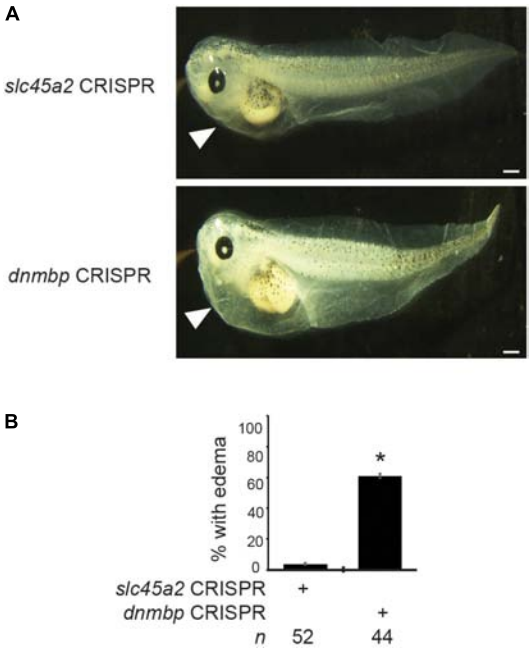

FIGURE 11 | *dnmbp* CRISPR knockout results in edema formation. **(A)** Bilateral injection of *dnmbp* sgRNA and Cas9 protein into both ventral blastomeres at the 4-cell stage leads to edema formation in comparison to embryos injected with *slc45a2* sgRNA and Cas9 protein. Representative stage 45–46 embryos shown. White arrowhead indicates area of fluid accumulation. Scale bar indicates 500 μm. **(B)** Percent of embryos exhibiting edema formation. *n* = number of embryos across 3 replications. Error bars represent Standard error. *Significantly different from control, $p < 0.05$.

assessed. Embryos were scored as positive for edema if fluid accumulation was present in the head and thorax (Corkins et al., 2018; DeLay et al., 2018b). A majority of *dnmbp* knockout embryos exhibited significant fluid accumulation in the thorax in comparison to control *slc45a2* knockout embryos (**Figure 11**).

DISCUSSION

Dnmbp was first discovered in a yeast two-hybrid screen designed to identify ligands that interact with EVL, a member of the Ena/VASP family of proteins (Salazar et al., 2003). Subsequent work determined that *DNMBP* transcripts were highly expressed in human kidney tissue, in addition to other organs such as the heart, brain, lungs and liver (Salazar et al., 2003). DNMBP directly interacts with actin regulatory proteins such as N-WASP and ENA/VASP and specifically activates CDC42, thereby playing a role in the assembly of actin (Salazar et al., 2003). In the kidney, Dnmbp depletion is associated with defects in ciliogenesis and tubulogenesis (Zuo et al., 2011; Baek et al., 2016).

Here, we describe the role that Dnmbp plays in *Xenopus* pronephric development. Dnmbp protein is present in whole embryo lysates starting in single cell embryos and continuing throughout kidney development. *In situ* hybridization showed that *dnmbp* transcripts are present in the developing kidney, as well as in head structures and somites. This finding is consistent

with previous work showing that *DNMBP* transcripts are present in human kidney tissue and in the zebrafish pronephros, brain and eye (Salazar et al., 2003; Baek et al., 2016). The presence of Dnmbp during *Xenopus* embryonic development, and specifically in the kidney, suggests that it plays a role in kidney development.

Knockdown of Dnmbp with MOs shows that Dnmbp depletion leads to defects in *Xenopus* pronephric development. Proximal tubule branching was decreased upon *dnmbp* knockdown and the distal and connecting tubules were less convoluted than in control embryos. 3G8 and 4A6 antibodies were used to assess kidney development. Both of these antibodies label differentiated regions of the pronephric tubules, with antibody 3G8 staining the proximal tubules starting at stage 34 and 4A6 beginning to stain the distal and connecting tubules at stage 38, with complete staining by stage 41 (Vize et al., 1995). 4A6 antibody staining of the distal and connecting tubules was decreased in dnmbp knockdown embryos suggesting that these tubules were less differentiated than those of control embryos. These results are consistent with cell culture work that suggests that Dnmbp is necessary for tubulogenesis (Baek et al., 2016). Interestingly, previous work in zebrafish found no disruption of tubulogenesis upon *Dnmbp* MO knockdown (Baek et al., 2016). One possible explanation for this discrepancy is that the zebrafish pronephros has a less convoluted structure than the *Xenopus* pronephros (Drummond et al., 1998). Therefore, the decrease in tubule looping seen in *Xenopus* upon *dnmbp* depletion may not be apparent in the simpler zebrafish pronephros at the stages the authors examined. Dnmbp knockdown also resulted in glomus defects, similar to previous work that showed altered glomerulus development in zebrafish upon Dnmbp MO knockdown (Baek et al., 2016).

In addition to tubulogenesis and glomus defects, Dnmbp knockdown in *Xenopus* embryos results in altered primary cilia development within the kidney tubules. This result is similar to a previous report that MO knockdown of Dnmbp in zebrafish results not in loss of cilia, but in altered and disorganized primary cilia development within the pronephric tubules (Baek et al., 2016). Although primary cilia within the kidney tubule are altered by Dnmbp knockdown, there was no obvious defect in nephrostome development or in the multiciliated cells on the embryo epidermis (data not shown). Together, these data indicate that loss of Dnmbp does not result in the loss of cilia, but instead results in changes in primary cilia development within the developing kidney tubules.

Dnmbp loss also leads to functional defects of the kidney. To assess kidney function, edema development was assessed upon *dnmbp* knockout. The majority of the *dnmbp* knockout embryos displayed fluid accumulation in the thorax, indicative of kidney function defects. As edema formation may result from heart defects in addition to kidney defects, *dnmbp* knockout was targeted to the two ventral cells of 4-cell embryos. These cells will eventually give rise to the kidney, but do not contribute to heart formation (Moody, 1987a,b), thereby ruling out heart defects as a likely cause for edema formation. There are several possible explanations for the edema development observed due to *dnmbp* knockout. One possibility is that kidney tubule defects prevent normal fluid flow through the kidney tubules, resulting in edema. Another possibility is that although the kidney tubules are present, they may not be functional because they have not properly differentiated and epithelialized. Although cilia were present on the nephrostomes, it is possible that they have motility defects that prevent normal fluid flow through the kidney tubules. Finally, the glomus defects observed upon *dnmbp* knockout may also prevent proper fluid flow through the kidney, resulting in edema formation.

The specificity of the Dnmbp MOs was confirmed by rescue experiments, where human *DNMBP* RNA was able to rescue the knockdown phenotype. Additionally, CRISPR knockout of both *dnmbp* homeologs resulted in a similar phenotype to knockdown embryos and this phenotype could be rescued by co-injection with human *DNMBP* RNA. Together, these results suggest that disruption of Dnmbp expression leads to a decrease in pronephric tubulogenesis. Previous work suggests that defects in pronephric development can be secondary to defects in somite development (Mauch et al., 2000). To rule out the possibility that the kidney defects seen in knockdown embryos were the result of secondary defects due to somitogenesis defects, the somites of Dnmbp knockdown embryos were examined. There was no difference in somite development between Dnmbp knockdown and control embryos even though a co-injected tracer indicated that the somites were indeed subjected to Dnmbp knockdown, indicating that the kidney defects were not likely due to larger developmental defects. This point is especially important because *dnmbp* is expressed in the somites of developing *Xenopus* embryos.

Knockdown, knockout and overexpression of *dnmbp* led to similar defects in kidney development. All three of these manipulations led to a disruption in proximal tubule development, decreased looping of the distal and connecting tubules and less differentiation of the distal and connecting tubules. These results suggest that perturbations in the level of Dnmbp protein present during *Xenopus* embryonic developments result in pronephric defects.

Although Dnmbp knockdown results in pronephric tubule defects in stage 40 embryos, Dnmbp depletion did not result in a reduction of early markers of pronephric determination and patterning. This result indicates that the pronephros of Dnmbp knockdown embryos undergoes normal specification, and the pronephric defects seen in later embryos are due to changes in pronephric differentiation, ciliogenesis and/or function. The idea that the observed tubule defects are due to a lack of distal and connecting tubule differentiation is supported by our *in situ* hybridization results in stage 40 embryos, where probes for *clcnkb* and *atp1a1* completely stained the distal and connecting tubules of Dnmbp knockdown embryos, indicating that the distal and connecting tubules are indeed present. However, a loss of 4A6 staining of the distal and connecting tubules of stage 40 Dnmbp knockdown embryos indicates that the distal and connecting tubules are not completely differentiated. Therefore, in addition to the observed changes in primary cilia development within the pronephric tubules and decrease in kidney function as evidenced by edema formation, loss of Dnmbp results in a lack of pronephric tubule differentiation. In conclusion, we demonstrate for the first time that Dnmbp is essential for normal vertebrate

tetrapod kidney development and function. Our findings suggest that depletion of Dnmbp does not affect pronephric specification, but instead alters differentiation, ciliogenesis and function of the developing kidney tubules.

AUTHOR CONTRIBUTIONS

BD performed microinjections, *in situ* hybridization, Western blots, designed *dnmbp* sgRNA and *in situ* probes, conducted sequencing and TIDE analysis, and wrote the manuscript. TB performed initial overexpression Western blot and phenotypic experiments. RM conceived of the project, designed Dnmbp MOs and oversaw the experiments, and manuscript preparation. All authors edited the article and approved of the final version.

FUNDING

This work was supported by a National Institutes of Health grants (K01DK092320 and R03DK118771 to RM), startup funding from the Department of Pediatrics, Pediatric Research Center at the University of Texas McGovern Medical School (to RM), and Just-Missed Grant funding from the McGovern Medical School Research Committee.

ACKNOWLEDGMENTS

We would like to thank M.E. Corkins for performing microinjections for *in situ* experiments and critical reading of the manuscript. We are grateful for the advice and suggestions provided by members of the laboratories of RM and P.D. McCrea, as well as M. Kloc and R.R. Behringer. We thank the University of Texas Health Science Center Office of the Executive Vice President and Chief Academic Officer and the Department of Pediatrics Microscopy Core for funding and maintaining the Zeiss LSM800 confocal microscope that was used for these studies. Additionally, we are grateful for the support of the animal care technicians and veterinarians, in particular J.C. Whitney and T.H. Gomez, who maintain our *Xenopus* colony. A preprint of this manuscript was deposited in Biorxiv prior to submission to this journal (DeLay et al., 2018a).

SUPPLEMENTARY MATERIAL

The Supplementary Material for this article can be found online at: https://www.frontiersin.org/articles/10.3389/fphys.2019.00143/full#supplementary-material

FIGURE S1 | *In situ* hybridization of both homeologs of *dnmbp*. Antisense probes (AS) labeling *dnmbp* expression in the pronephros, head structures and somites. Sense (S) probes shown as a control for non-specific probe binding were processed in parallel with the AS probes. Scale bar indicates 500 μm.

FIGURE S2 | Knockdown of Dnmbp results in reduced kidney tubulogenesis. **(A)** Unilateral injection of 20 ng Dnmbp MO 2 into blastomere V2 at the 8-cell stage leads to defects in kidney tubulogenesis in comparison to embryos injected with Standard MO. Antibody 3G8 used to label the lumen of the proximal tubule, antibody 4A6 used to label the distal and connecting tubules. memRFP used as an injection tracer. White bar indicates 200 μm. *Indicates injected side of embryo. **(B)** Knockdown of Dnmbp leads to reduced expression of differentiated kidney tubule markers in comparison to embryos injected with Standard MO. n = number of embryos across 3 replications. Error bars represent Standard error. *Significantly different from control, $p < 0.05$.

FIGURE S3 | Primers used to amplify regions of *dnmbp* for TIDE analysis. **(A)** DNA sequence of the region surrounding exon 3 of *dnmbp.L* indicating sgRNA and sequencing primer binding sites. **(B)** DNA sequence of the region surrounding exon 3 of *dnmbp.S* indicating sgRNA and sequencing primer binding sites.

REFERENCES

Baek, J. I., Kwon, S. H., Zuo, X., Choi, S. Y., Kim, S. H., and Lipschutz, J. H. (2016). Dynamin binding protein (tuba) deficiency inhibits ciliogenesis and nephrogenesis in vitro and in vivo. *J. Biol. Chem.* 291, 8632–8643. doi: 10.1074/jbc.M115.688663

Bhattacharya, D., Marfo, C. A., Li, D., Lane, M., and Khokha, M. K. (2015). CRISPR/Cas9: an inexpensive, efficient loss of function tool to screen human disease genes in *Xenopus*. *Dev. Biol.* 408, 196–204. doi: 10.1016/j.ydbio.2015.11.003

Bishop, A. L., and Hall, A. (2000). Rho GTPases and their effector proteins. *Biochem. J.* 348, 241–255. doi: 10.1042/bj3480241

Brandli, A. W. (1999). Towards a molecular anatomy of the *Xenopus* pronephric kidney. *Int. J. Dev. Biol.* 43, 381–395.

Brennan, H. C., Nijjar, S., and Jones, E. A. (1998). The specification of the pronephric tubules and duct in *Xenopus laevis*. *Mech. Dev.* 75, 127–137. doi: 10.1016/S0925-4773(98)00094-X

Brinkman, E. K., Chen, T., Amendola, M., and van Steensel, B. (2014). Easy quantitative assessment of genome editing by sequence trace decomposition. *Nucleic Acids Res.* 42:e168. doi: 10.1093/nar/gku936

Carroll, T., and Vize, P. D. (1999). Synergism between Pax-8 and lim-1 in embryonic kidney development. *Dev. Biol.* 214, 46–59. doi: 10.1006/dbio.1999.9414

Carroll, T. J., Wallingford, J. B., and Vize, P. D. (1999). Dynamic patterns of gene expression in the developing pronephros of *Xenopus laevis*. *Dev. Genet.* 24, 199–207. doi: 10.1002/(SICI)1520-6408(1999)24:3/4<199::AID-DVG3>3.0.CO;2-D

Cerione, R. A. (2004). Cdc42: new roads to travel. *Trends Cell Biol.* 14, 127–132. doi: 10.1016/j.tcb.2004.01.008

Choi, S. Y., Chacon-Heszele, M. F., Huang, L., McKenna, S., Wilson, F. P., Zuo, X., et al. (2013). Cdc42 deficiency causes ciliary abnormalities and cystic kidneys. *J. Am. Soc. Nephrol.* 24, 1435–1450. doi: 10.1681/ASN.2012121236

Corkins, M. E., Hanania, H. L., Krneta-Stankic, V., DeLay, B. D., Pearl, E. J., Lee, M., et al. (2018). Transgenic *Xenopus laevis* line for in vivo labeling of nephrons within the kidney. *Genes* 9:E197. doi: 10.3390/genes9040197

Davidson, L. A., Marsden, M., Keller, R., and Desimone, D. W. (2006). Integrin alpha5beta1 and fibronectin regulate polarized cell protrusions required for *Xenopus* convergence and extension. *Curr. Biol.* 16, 833–844. doi: 10.1016/j.cub.2006.03.038

DeLay, B. D., Baldwin, T. A., and Miller, R. K. (2018a). Dynamin binding protein is required for *Xenopus laevis* kidney development. *bioRxiv* [Preprint]. doi: 10.1101/414458

DeLay, B. D., Corkins, M. E., Hanania, H. L., Salanga, M., Deng, J. M., Sudou, N., et al. (2018b). Tissue-specific gene inactivation in *Xenopus laevis*: knockout of lhx1 in the kidney with CRISPR/Cas9. *Genetics* 208, 673–686. doi: 10.1534/genetics.117.300468

DeLay, B. D., Krneta-Stankic, V., and Miller, R. K. (2016). Technique to target microinjection to the developing *Xenopus* kidney. *J. Vis. Exp.* 111:53799. doi: 10.3791/53799

Demartis, A., Maffei, M., Vignali, R., and Barsacchi, G. (1994). Cloning and developmental expression of LFB3/HNFIβ transcription factor in *Xenopus laevis*. *Mech. Dev.* 47, 19–28. doi: 10.1016/0925-4773(94)90092-2

Drummond, I. A., Majumdar, A., Hentschel, H., Elger, M., Solnica-Krezel, L., Schier, A. F., et al. (1998). Early development of the zebrafish pronephros and analysis of mutations affecting pronephric function. *Development* 125, 4655–4667.

Eid, S. R., and Brandli, A. W. (2001). *Xenopus* Na,K-ATPase: primary sequence of the beta2 subunit and in situ localization of alpha1, beta1, and gamma expression during pronephric kidney development. *Differentiation* 68, 115–125. doi: 10.1046/j.1432-0436.2001.680205.x

Elias, B. C., Das, A., Parekh, D. V., Mernaugh, G., Adams, R., Yang, Z., et al. (2015). Cdc42 regulates epithelial cell polarity and cytoskeletal function during kidney tubule development. *J. Cell Sci.* 128, 4293–4305. doi: 10.1242/jcs.164509

Gerth, V. E., Zhou, X., and Vize, P. D. (2005). Nephrin expression and three-dimensional morphogenesis of the *Xenopus* pronephric glomus. *Dev. Dyn.* 233, 1131–1139. doi: 10.1002/dvdy.20415

Hensey, C., Dolan, V., and Brady, H. R. (2002). The *Xenopus* pronephros as a model system for the study of kidney development and pathophysiology. *Nephrol. Dial. Transplant.* 17, 73–74. doi: 10.1093/ndt/17.suppl_9.73

Johnson, D. I., and Pringle, J. R. (1990). Molecular characterization of CDC42, a *Saccharomyces cerevisiae* gene involved in the development of cell polarity. *J. Cell Biol.* 111, 143–152. doi: 10.1083/jcb.111.1.143

Kim, S. W., Fang, X., Ji, H., Paulson, A. F., Daniel, J. M., Ciesiolka, M., et al. (2002). Isolation and characterization of XKaiso, a transcriptional repressor that associates with the catenin Xp120(ctn) in *Xenopus laevis*. *J. Biol. Chem.* 277, 8202–8208. doi: 10.1074/jbc.M109508200

Kintner, C. R., and Brockes, J. P. (1984). Monoclonal antibodies identify blastemal cells derived from dedifferentiating limb regeneration. *Nature* 308, 67–69. doi: 10.1038/308067a0

Lavina, B., Castro, M., Niaudet, C., Cruys, B., Alvarez-Aznar, A., Carmeliet, P., et al. (2018). Defective endothelial cell migration in the absence of Cdc42 leads to capillary-venous malformations. *Development* 145:dev161182. doi: 10.1242/dev.161182

Lyons, J. P., Miller, R. K., Zhou, X., Weidinger, G., Deroo, T., Park, J. I., et al. (2009). Requirement of Wnt/β-catenin signaling in pronephric kidney development. *Mech. Dev.* 126, 142–159. doi: 10.1016/j.mod.2008.11.007

Martin-Belmonte, F., Gassama, A., Datta, A., Yu, W., Rescher, U., Gerke, V., et al. (2007). PTEN-mediated apical segregation of phosphoinositides controls epithelial morphogenesis through Cdc42. *Cell* 128, 383–397. doi: 10.1016/j.cell.2006.11.051

Mauch, T. J., Yang, G., Wright, M., Smith, D., and Schoenwolf, G. C. (2000). Signals from trunk paraxial mesoderm induce pronephros formation in chick intermediate mesoderm. *Dev. Biol.* 220, 62–75. doi: 10.1006/dbio.2000.9623

Melendez, J., Liu, M., Sampson, L., Akunuru, S., Han, X., Vallance, J., et al. (2013). Cdc42 coordinates proliferation, polarity, migration, and differentiation of small intestinal epithelial cells in mice. *Gastroenterology* 145, 808–819.break doi: 10.1053/j.gastro.2013.06.021

Miller, R. K., Canny, S. G., Jang, C. W., Cho, K., Wagner, D. S., Jones, E. A., et al. (2011). Pronephric tubulogenesis requires Daam1-mediated planar cell polarity signaling. *J. Am. Soc. Nephrol.* 22, 1654–1664. doi: 10.1681/ASN.2010101086

Mizukawa, B., O'Brien, E., Moreira, D. C., Wunderlich, M., Hochstetler, C. L., Duan, X., et al. (2017). The cell polarity determinant CDC42 controls division symmetry to block leukemia cell differentiation. *Blood* 130, 1336–1346. doi: 10.1182/blood-2016-12-758458

Moody, S. A. (1987a). Fates of the blastomeres of the 16-cell stage *Xenopus* embryo. *Dev. Biol.* 119, 560–578. doi: 10.1016/0012-1606(87)90059-5

Moody, S. A. (1987b). Fates of the blastomeres of the 32-cell-stage *Xenopus* embryo. *Dev. Biol.* 122, 300–319.

Nguyen, D. T., Gao, L., Wong, A., and Chen, C. S. (2017). Cdc42 regulates branching in angiogenic sprouting in vitro. *Microcirculation* 24:e12372. doi: 10.1111/micc.12372

Nieuwkoop, P. D., and Faber, J. (1994). *Normal Table Of Xenopus Laevis (Daudin): A Systematical & Chronological Survey of the Development From the Fertilized Egg Till the End of Metamorphosis*. New York, NY: Garland Publishing, Inc.

Otani, T., Ichii, T., Aono, S., and Takeichi, M. (2006). Cdc42 GEF Tuba regulates the junctional configuration of simple epithelial cells. *J. Cell Biol.* 175, 135–146. doi: 10.1083/jcb.200605012

Qin, Y., Meisen, W. H., Hao, Y., and Macara, I. G. (2010). Tuba, a Cdc42 GEF, is required for polarized spindle orientation during epithelial cyst formation. *J. Cell Biol.* 189, 661–669. doi: 10.1083/jcb.201002097

Salazar, M. A., Kwiatkowski, A. V., Pellegrini, L., Cestra, G., Butler, M. H., Rossman, K. L., et al. (2003). Tuba, a novel protein containing bin/amphiphysin/Rvs and Dbl homology domains, links dynamin to regulation of the actin cytoskeleton. *J. Biol. Chem.* 278, 49031–49043. doi: 10.1074/jbc.M308104200

Schmidt, A., and Hall, A. (2002). Guanine nucleotide exchange factors for Rho GTPases: turning on the switch. *Genes Dev.* 16, 1587–1609. doi: 10.1101/gad.1003302

Schulz, A. M., Stutte, S., Hogl, S., Luckashenak, N., Dudziak, D., Leroy, C., et al. (2015). Cdc42-dependent actin dynamics controls maturation and secretory activity of dendritic cells. *J. Cell Biol.* 211, 553–567. doi: 10.1083/jcb.201503128

Sive, H. L., Grainger, R. M., and Harland, R. M. (2000). *Early development of Xenopus laevis: A laboratory manual*. New York, NY: Cold Spring Harbor Laboratory Press.

Taira, M., Jamrich, M., Good, P. J., and Dawid, I. B. (1992). The LIM domain-containing homeo box gene Xlim-1 is expressed specifically in the organizer region of *Xenopus* gastrula embryos. *Genes Dev.* 6, 356–366. doi: 10.1101/gad.6.3.356

Vize, P. D. (2003). The chloride conductance channel Clc-K is a specific marker for the *Xenopus* pronephric distal tubule and duct. *Gene Express. Patt.* 3, 347–350. doi: 10.1016/S1567-133X(03)00032-2

Vize, P. D., Jones, E. A., and Pfister, R. (1995). Development of the *Xenopus* pronephric system. *Dev. Biol.* 171, 531–540. doi: 10.1006/dbio.1995.1302

Vize, P. D., Seufert, D. W., Carroll, T. J., and Wallingford, J. B. (1997). Model systems for the study of kidney development: use of the pronephros in the analysis of organ induction and patterning. *Dev. Biol.* 188, 189–204. doi: 10.1006/dbio.1997.8629

Zhou, X., and Vize, P. D. (2004). Proximo-distal specialization of epithelial transport processes within the *Xenopus* pronephric tubules. *Dev. Biol.* 271, 322–338. doi: 10.1016/j.ydbio.2004.03.036

Zuo, X., Fogelgren, B., and Lipschutz, J. (2011). The small GTPase Cdc42 is necessary for primary ciliogenesis in renal tubular epithelial cells. *J. Biol. Chem.* 286, 22469–22477. doi: 10.1074/jbc.M111.238469

Conflict of Interest Statement: The authors declare that the research was conducted in the absence of any commercial or financial relationships that could be construed as a potential conflict of interest.

frontiers in Physiology

REVIEW
published: 26 February 2019
doi: 10.3389/fphys.2019.00154

Xenbase: Facilitating the Use of *Xenopus* to Model Human Disease

Mardi J. Nenni[1], Malcolm E. Fisher[1]*, Christina James-Zorn[1], Troy J. Pells[2], Virgilio Ponferrada[1], Stanley Chu[2], Joshua D. Fortriede[1], Kevin A. Burns[1], Ying Wang[2], Vaneet S. Lotay[2], Dong Zhou Wang[2], Erik Segerdell[3], Praneet Chaturvedi[1], Kamran Karimi[2], Peter D. Vize[2] and Aaron M. Zorn[1]**

[1] Division of Developmental Biology, Cincinnati Children's Hospital, Cincinnati, OH, United States, [2] Department of Biological Sciences, University of Calgary, Calgary, AB, Canada, [3] Institute of Ecology and Evolution, University of Oregon, Eugene, OR, United States

OPEN ACCESS

Edited by:
John Noel Griffin,
Duke University, United States

Reviewed by:
Emily K. Mis,
Yale University, United States
Radek Sindelka,
Institute of Biotechnology (ASCR), Czechia
Jose G. Abreu,
Universidade Federal do Rio de Janeiro, Brazil
Anne H. Monsoro-Burq,
Université Paris-Sud, France

***Correspondence:**
Mardi J. Nenni
mardi.nenni@cchmc.org
Malcolm E. Fisher
malcolm.fisher@cchmc.org
Aaron M. Zorn
aaron.zorn@cchmc.org

Specialty section:
This article was submitted to Embryonic and Developmental Physiology, a section of the journal Frontiers in Physiology

Received: 06 November 2018
Accepted: 08 February 2019
Published: 26 February 2019

Citation:
Nenni MJ, Fisher ME, James-Zorn C, Pells TJ, Ponferrada V, Chu S, Fortriede JD, Burns KA, Wang Y, Lotay VS, Wang DZ, Segerdell E, Chaturvedi P, Karimi K, Vize PD and Zorn AM (2019) Xenbase: Facilitating the Use of Xenopus to Model Human Disease. Front. Physiol. 10:154. doi: 10.3389/fphys.2019.00154

At a fundamental level most genes, signaling pathways, biological functions and organ systems are highly conserved between man and all vertebrate species. Leveraging this conservation, researchers are increasingly using the experimental advantages of the amphibian *Xenopus* to model human disease. The online *Xenopus* resource, Xenbase, enables human disease modeling by curating the *Xenopus* literature published in PubMed and integrating these *Xenopus* data with orthologous human genes, anatomy, and more recently with links to the Online Mendelian Inheritance in Man resource (OMIM) and the Human Disease Ontology (DO). Here we review how Xenbase supports disease modeling and report on a meta-analysis of the published *Xenopus* research providing an overview of the different types of diseases being modeled in *Xenopus* and the variety of experimental approaches being used. Text mining of over 50,000 *Xenopus* research articles imported into Xenbase from PubMed identified approximately 1,000 putative disease- modeling articles. These articles were manually assessed and annotated with disease ontologies, which were then used to classify papers based on disease type. We found that *Xenopus* is being used to study a diverse array of disease with three main experimental approaches: cell-free egg extracts to study fundamental aspects of cellular and molecular biology, oocytes to study ion transport and channel physiology and embryo experiments focused on congenital diseases. We integrated these data into Xenbase Disease Pages to allow easy navigation to disease information on external databases. Results of this analysis will equip *Xenopus* researchers with a suite of experimental approaches available to model or dissect a pathological process. Ideally clinicians and basic researchers will use this information to foster collaborations necessary to interrogate the development and treatment of human diseases.

Keywords: *Xenopus*, Xenbase, model organism database, human disease, ontologies, oocyte, cell-free egg extract

XENOPUS AS A MODEL FOR HUMAN DISEASE

Xenopus is used in biomedical research to study fundamental biological and pathological processes. The research community utilizes *Xenopus* to gain a deeper understanding of human disease through molecular analysis of disease-gene function and in-depth disease modeling. The advantages of the *Xenopus* model, including ease of housing, large oocyte and embryo size, high fecundity,

rapid external development, and ease of genomic manipulation, make them invaluable tools to study the molecular basis of human development and disease. Compared to other aquatic models, this tetrapod is conservatively closer to humans with lungs, a three-chambered heart, and a close evolutionary relationship with mammals. *Xenopus* has been estimated to share 79% of the identified human disease genes (Hellsten et al., 2010; Khokha, 2012; Tandon et al., 2017). Compared to mammalian models, *Xenopus* is a rapid, cost-effective model with the ease of morpholino knock-down, the generation of efficient transgenics and targeted gene mutations using TALENs (transcription activator-like effector nucleases) or CRISPR/Cas (clustered regularly interspaced short palindromic repeats-CRISPR associated nucleases). Notably, many studies report the ease and efficiency of CRISPR/Cas modifications allowing phenotype analysis in the F0 generations of both *Xenopus laevis* and *Xenopus tropicalis* (Blitz et al., 2013; Bhattacharya et al., 2015; Wang et al., 2015). Similarly, CRISPR/Cas technology can be used to introduce small DNA fragments containing patient-specific variants for disease modeling in *Xenopus* (Aslan et al., 2017). In addition to in-depth disease modeling, these tools allow for efficient functional screening of genes identified in human genomic studies (Bhattacharya et al., 2015; Sater and Moody, 2017).

XENBASE SUPPORT FOR HUMAN DISEASE MODELING

Xenbase[1] (RRID:SCR_003280), the *Xenopus* model organism database, is an NICHD-funded data repository with a major goal to help accelerate basic research and disease modeling (James-Zorn et al., 2018; Karimi et al., 2018). Xenbase collates all the *Xenopus* research data, and enhances the value of these data through high-quality curation. In this way Xenbase makes information, that would otherwise get buried in the scientific literature, computer searchable and highly integrated with an ever-growing knowledgebase. Xenbase links *Xenopus* genomic, epigenetic, mRNA and protein sequence with gene expression and gene function as well as physical reagents such as morpholinos and antibodies together with transgenic and mutant lines from the published literature. A second major goal of Xenbase is to enable the effective translation between *Xenopus* and human data by linking orthologous genes. In addition, Xenbase Gene Pages provide a link to the human ortholog gene-disease association via the Online Mendelian Inheritance in Man resource (OMIM[2]; RRID:SCR_006437), the comprehensive online catalog of genetically determined phenotypes. Additional links are made to inter-relate gene ontology (GO) (Ashburner et al., 2000; The Gene Ontology Consortium, 2017) and anatomy ontology terms.

In an ongoing effort to increase support for human disease modeling, Xenbase recently incorporated links to the Human Disease Ontology (DO[3]; RRID:SCR_000476), a standardized ontology for human disease terms and phenotype characteristics, with a long-term goal of merging disease annotations across species (Bello et al., 2018). DO integration facilitates annotation to a much broader scope of human diseases than OMIM alone, including non-Mendelian and environmentally induced diseases. Similarly, the hierarchical structure of the DO allows less specific high-level terms such as "cancer" in addition to more specific descendent terms such as "prostate cancer," which can facilitate linking specific genes with classes of diseases.

The integration of the DO into Xenbase provides new support to combine human disease information and *Xenopus* experimental data. The three main areas of integration are the Gene Page, Disease Page, and Article Page. *Xenopus* orthologs to human disease genes are given DO annotations on Gene Pages via DO-OMIM cross references and manual curation. For example, the *zic3* Gene Page contains the DO annotation for visceral heterotaxy (**Figure 1**). The "visceral heterotaxy" link leads to a new Xenbase feature, the Disease Page (**Figure 2**), where a user will find information including definitions, synonyms, and human disease resource links. Additional links to Xenbase genes and equivalent disease pages for other model organisms are provided. A compilation of DO annotation data from rat, mouse, zebrafish, fly, worm, and yeast is provided via the Alliance of Genome Resources (AGR) link[4] (RRID:SCR_015850) (Howe et al., 2018). The Literature tab on the Disease Page provides a list of all disease-specific *Xenopus* literature. Similarly, Article Pages on Xenbase (**Figure 3**) contain links to any associated Disease Page. In addition to Disease Page links on Gene and Article Pages, diseases can be searched using the "Search Diseases" link on the Anatomy and Development tile of the homepage or via the search bar in the top right corner of the homepage. Type ahead will match terms or the ID number for a disease. A user can go directly to a specific Disease Page by highlighting the term or display all matches by searching a partial term.

TEXT MINING AND ANNOTATION OF *XENOPUS*-HUMAN DISEASE LITERATURE

We used these newly implemented features on Xenbase to explore the landscape of human disease research that has used the *Xenopus* model system. Below we present a meta-analysis of approximately 1,000 human disease articles, from the corpus of 50,000+ articles in Xenbase, of which 554 were annotated with DO and/or OMIM terms, as well as gene, GO and anatomy assertions linking the *Xenopus* and human data. A meta-analysis of the resulting annotations was used to obtain an overview of the past and present use of *Xenopus* to study human disease. Finally, we discuss how these new features and the future integration

[1]http://www.xenbase.org
[2]https://omim.org
[3]http://www.disease-ontology.org
[4]https://www.alliancegenome.org

FIGURE 1 | Xenbase Gene Page for *zic3*. Gene-disease annotations are located below Interactants on the Summary tab of the Xenbase Gene Page. Disease Ontology (DO) annotations (red arrowhead) are made via DO-OMIM cross reference or manual curation. OMIM annotations (blue arrowhead) are imported from the National Center for Biotechnology Information (NCBI). DO and OMIM terms link to Xenbase Disease Pages.

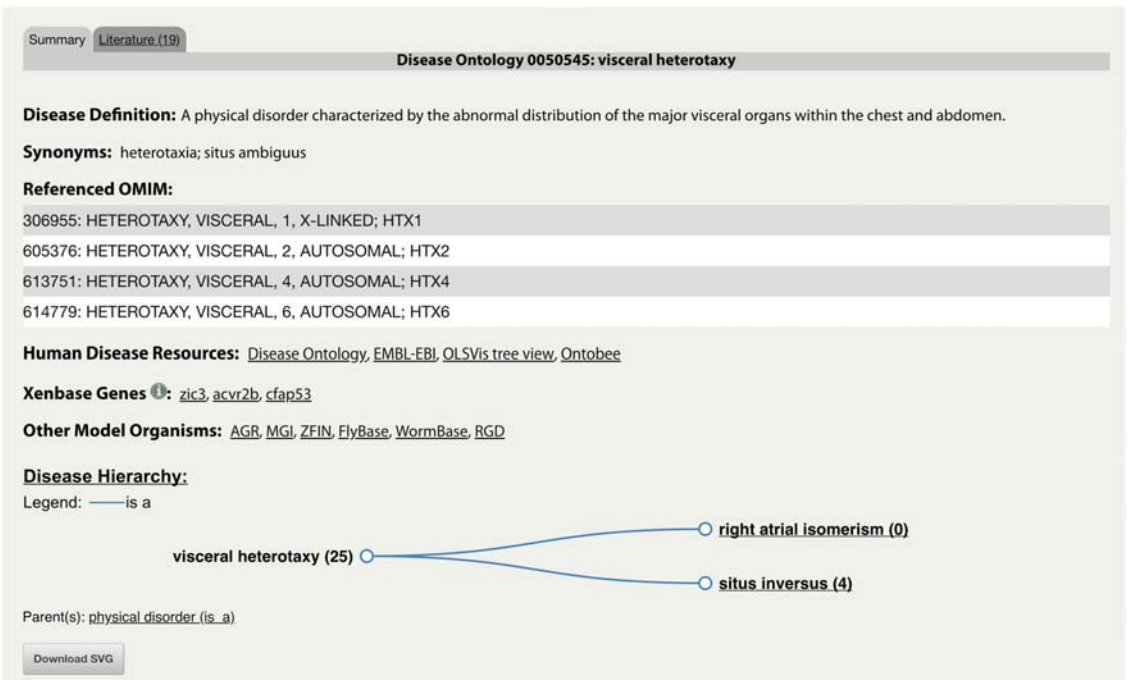

FIGURE 2 | Xenbase Disease Page for "DOID:0050545: visceral heterotaxy." An example of a new Disease Page with disease-specific supporting information including associated human and model organism resource links. The representative disease and its descendants are displayed in a Disease Hierarchy with the number of associated Xenbase articles in parentheses. The Literature tab provides a list of all associated Xenbase articles.

of phenotypes will enhance support for researchers studying human disease.

A candidate human disease article list was established by three methods: (1) a PubMed search (n = 226), (2) by searching the full-text of articles imported into Xenbase (n = 466) using the text mining tool Textpresso v2.5[5] (RRID:SCR_008737) (Muller et al., 2004) and (3) by selecting papers that had been identified from recent manual curation (n = 270). Details

[5]http://textpresso.org

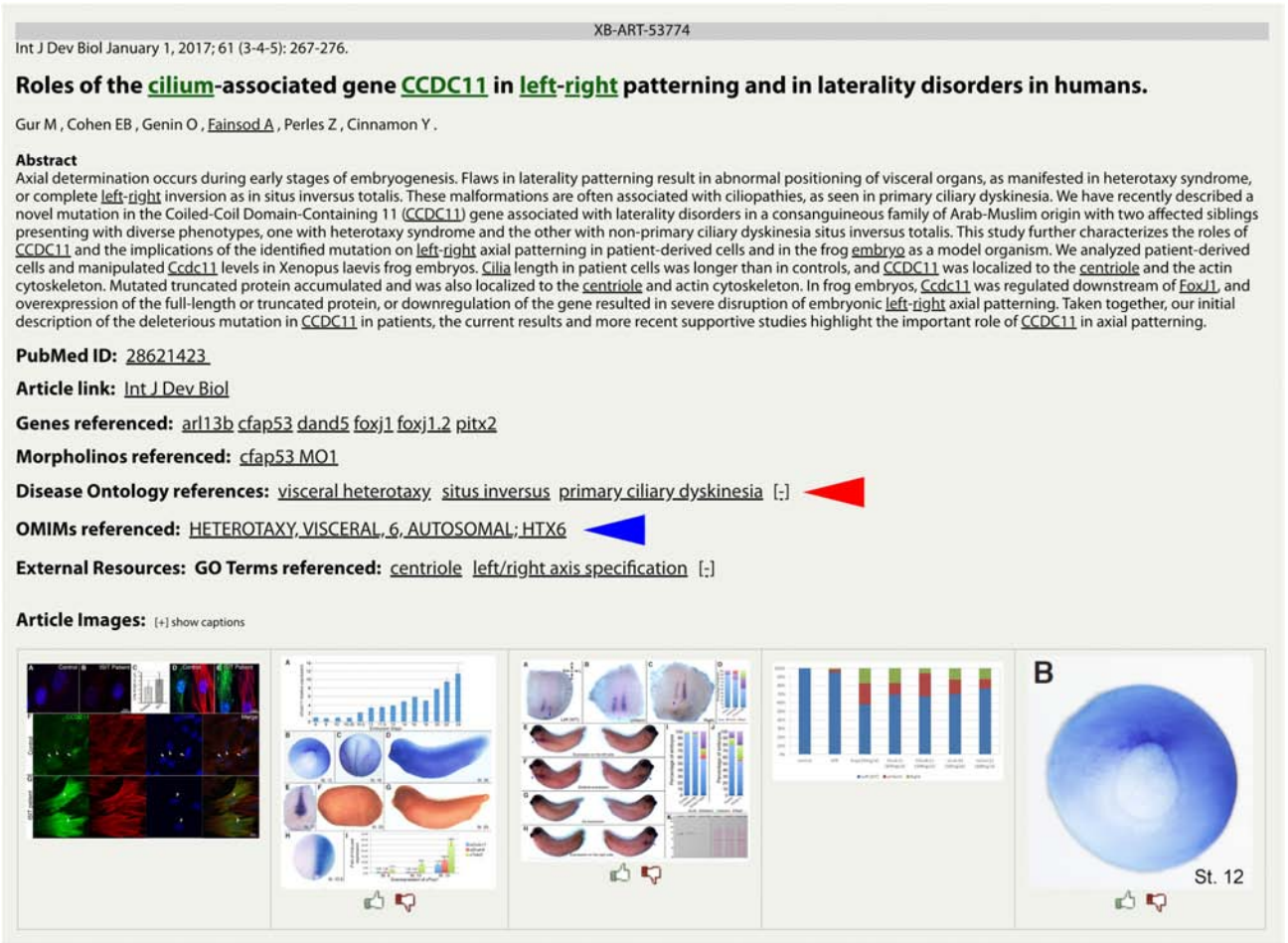
XB-ART-53774
Int J Dev Biol January 1, 2017; 61 (3-4-5): 267-276.

Roles of the cilium-associated gene CCDC11 in left-right patterning and in laterality disorders in humans.

Gur M , Cohen EB , Genin O , Fainsod A , Perles Z , Cinnamon Y .

Abstract

Axial determination occurs during early stages of embryogenesis. Flaws in laterality patterning result in abnormal positioning of visceral organs, as manifested in heterotaxy syndrome, or complete left-right inversion as in situs inversus totalis. These malformations are often associated with ciliopathies, as seen in primary ciliary dyskinesia. We have recently described a novel mutation in the Coiled-Coil Domain-Containing 11 (CCDC11) gene associated with laterality disorders in a consanguineous family of Arab-Muslim origin with two affected siblings presenting with diverse phenotypes, one with heterotaxy syndrome and the other with non-primary ciliary dyskinesia situs inversus totalis. This study further characterizes the roles of CCDC11 and the implications of the identified mutation on left-right axial patterning in patient-derived cells and in the frog embryo as a model organism. We analyzed patient-derived cells and manipulated Ccdc11 levels in Xenopus laevis frog embryos. Cilia length in patient cells was longer than in controls, and CCDC11 was localized to the centriole and the actin cytoskeleton. Mutated truncated protein accumulated and was also localized to the centriole and actin cytoskeleton. In frog embryos, Ccdc11 was regulated downstream of FoxJ1, and overexpression of the full-length or truncated protein, or downregulation of the gene resulted in severe disruption of embryonic left-right axial patterning. Taken together, our initial description of the deleterious mutation in CCDC11 in patients, the current results and more recent supportive studies highlight the important role of CCDC11 in axial patterning.

PubMed ID: 28621423

Article link: Int J Dev Biol

Genes referenced: arl13b cfap53 dand5 foxj1 foxj1.2 pitx2

Morpholinos referenced: cfap53 MO1

Disease Ontology references: visceral heterotaxy situs inversus primary ciliary dyskinesia [-]

OMIMs referenced: HETEROTAXY, VISCERAL, 6, AUTOSOMAL; HTX6

External Resources: GO Terms referenced: centriole left/right axis specification [-]

Article Images: [+] show captions

FIGURE 3 | DO and OMIM references on a Xenbase Article Page. Disease terms link directly to the collated data on a Disease Page for DO (red arrowhead) annotations and OMIM (blue arrowhead) annotations. Multiple disease annotations can be seen by clicking the [+/–] toggle to show more or fewer results. Article Pages also list GO terms as keywords to cover the major topics of an article.

on the search parameters and keywords are provided in the **Supplementary Material**. The combined search identified 983 articles which were filtered for duplicates and then manually curated to a final set of 554 disease modeling papers based on one or more of the following conditions: (1) modeled human disease via gene knockdown, mutations or chemical manipulation in *Xenopus*; (2) examined the function of human disease-causing protein variants in *Xenopus*; (3) modeled a pathological process; (4) dissected the function of a gene or gene family implicated in human disease; (5) or pharmacological screen of compounds that cause or treat human disease.

THE LANDSCAPE OF HUMAN DISEASE RESEARCH IN *XENOPUS*

Each of the 554 papers were curated with OMIM and DO terms and analyzed to obtain an overview of the major areas of human disease that were investigated using *Xenopus*. In total we annotated 887 DO terms from the 554 papers and then we assigned each of these DO annotations to one of 18 major disease groups using the hierarchical structure of the DO and selected the higher level DO terms (**Table 1**). A complete list of the DO terms with associated PubMed IDs is provided in **Supplementary Table S1**. We then clustered the DO terms using the Markov clustering (MCL) algorithm of clusterMaker2 (v1.2.1) and visualized the results with the network tool Cytoscape (Cytoscape; RRID:SCR_003032) (Shannon et al., 2003; Morris et al., 2011) (**Figure 4** and **Supplementary Material**).

Experimental Approaches for Disease Modeling in *Xenopus*

Our examination of the DO annotated literature revealed that *Xenopus* researchers tend to use three broad experimental approaches to study human disease: (1) the cell-free egg extract, (2) expression of proteins in oocytes, and (3) manipulations of developing *Xenopus* embryos and larva.

Cell-free egg extracts have long been used as a unique biochemical system to study fundamental components of the

TABLE 1 | High-level, less-specific, DO terms with summary numbers of total attributions, which includes direct annotations and indirect annotations from descendent, less-specific, terms and number of articles annotated.

DOID	DO term	Total Attributions	Articles
DOID:863	Nervous system disease	231	177
DOID:630	Genetic disease	125	101
DOID:0050155	Sensory system disease	80	63
DOID:17	Musculoskeletal system disease	74	61
DOID:1287	Cardiovascular system disease	70	62
DOID:162	Cancer	67	59
DOID:18	Urinary system disease	63	49
DOID:0014667	Disease of metabolism	44	36
DOID:150	Disease of mental health	41	36
DOID:0080015	Physical disorder	37	33
DOID:74	Hematopoietic system disease	28	14
DOID:77	Gastrointestinal system disease	24	19
DOID:28	Endocrine system disease	22	20
DOID:2914	Immune system disease	19	12
DOID:0050117	Disease by infectious agent	18	13
DOID:15	Reproductive system disease	13	10
DOID:16	Integumentary system disease	10	10
DOID:1579	Respiratory system disease	10	7

cell cycle including DNA check point, function of oncogenes, and tumor suppressor proteins (Cross and Powers, 2009; Willis et al., 2012; Hoogenboom et al., 2017). For example, researchers have used extracts to investigate biochemical mechanisms of genetic instability associated with variants in genes encoding DNA-damage checkpoint and repair proteins such as in Fanconi anemia (Sobeck et al., 2006; Stone et al., 2007; Landais et al., 2009; Sareen et al., 2012).

Xenopus oocytes, unfertilized eggs removed from the adult female, are used extensively to study a wide range of human diseases involved in ion transport and channel physiology, sometimes referred to as "channelopathies," ranging from Alzheimer's (Miledi et al., 2004; Ullah et al., 2015) to various forms of heart, kidney, and musculoskeletal disease (Felix, 2000; Vindas-Smith et al., 2016). Human proteins containing patient variants can be easily expressed in oocytes by micro-injection of recombinant mRNAs, and the large size (>1 mm) of the oocytes make them amenable to single-cell physiological analysis to determine how the variants affect protein function (Lehmann-Horn and Jurkat-Rott, 1999; Miledi et al., 2004; Sigel and Minier, 2005).

Finally, researchers use *Xenopus* embryos and tadpoles to model a broad range of human diseases from cardiovascular to mental health disorders. Experimental advantages include the large abundant externally developing embryos and transparent skin of later tadpoles, allowing one to examine organ development and disease, such as those occurring in the foregut, kidney, heart and brain (Salanga and Horb, 2015; Lienkamp, 2016; Dubey and Saint-Jeannet, 2017; Garfinkel and Khokha, 2017; Sater and Moody, 2017; Blum and Ott, 2018). Candidate human disease-causing genes are commonly studied by overexpression or knockdown of the orthologous *Xenopus* gene and analyzing the resulting phenotype, which if it resembles the human condition, can be used to study the details of pathogenesis or even provide a platform for therapeutics. Easy microinjection of *Xenopus* embryos enables gene knockdown by antisense morpholino oligos or more recently by CRISPR gene mutations (Bhattacharya et al., 2015; Shi et al., 2015; Wang et al., 2015), whereas wild type and mutant proteins can be overexpressed by mRNAs or tissue specific transgenics. Furthermore, the well-defined fate map (Moody, 1987a,b) allows researchers to perform targeted injection of specific tissues such as the nervous system or just the right side of the body. Many studies take advantage of unilateral injection, unique to *Xenopus*, to manipulate embryos and examine the phenotypic effects while the contralateral side functions as an internal control.

In addition to genetic mutations, the effects of environmental toxins are also studied in the embryo using established protocols such as the frog embryo teratogenesis assay in *Xenopus* (FETAX) (Dawson et al., 1989; Fort et al., 1989; Bantle et al., 1990; Morgan et al., 1996). In addition to the molecular and morphological analysis that the embryo and tadpole provide, behavioral studies are also employed to assess mental health function associated with human disease-causing toxins (Pratt and Khakhalin, 2013). A description of the predominant diseases studied and the associated *Xenopus* experimental approaches utilized are summarized below. A list of DO terms with associated *Xenopus* experimental approaches is provided in **Supplementary Table S2**.

Nervous System Disease

The DO term "nervous system disease" had the greatest number of total attributions (n = 231). The specific nervous system diseases with the most DO annotations were epilepsy and Alzheimer's disease. In general, two broad experimental approaches are used to study nervous system disease: (1) oocytes to study the function of mutant receptors and ion channels and (2) embryo manipulation to study neurodevelopmental disorders. For example, Simons et al. (2015) utilized the oocyte to characterize mutant or wildtype human KCNH1, a potassium channel implicated in Temple-Baraitser syndrome and epilepsy, and analyze the electrophysiological function by single-cell voltage-clamp. These experiments demonstrated that the variants lead to deleterious gain in function, which decreases the threshold of activation and delayed deactivation. Similarly, Miledi et al. (2004) demonstrated that cell membranes from post-mortem brains of Alzheimer's patients can integrate into the *Xenopus* oocyte plasma membrane and maintain their neurotransmitter and voltage-gated channels, allowing researchers to investigate the cause and possible treatments for Alzheimer's disease. Using embryo manipulations, Bell et al. (2011) utilized a developmental seizure model by treating embryos and tadpoles with the known convulsant, pentylenetetrazole (PTZ) to discover a novel neuroprotective role of polyamines in the developing brain.

Genetic Disease

Genetic diseases, defined by the DO as a disease that has material basis in genetic variation in the human genome, had the second highest number of attributions (n = 125). Cystic fibrosis,

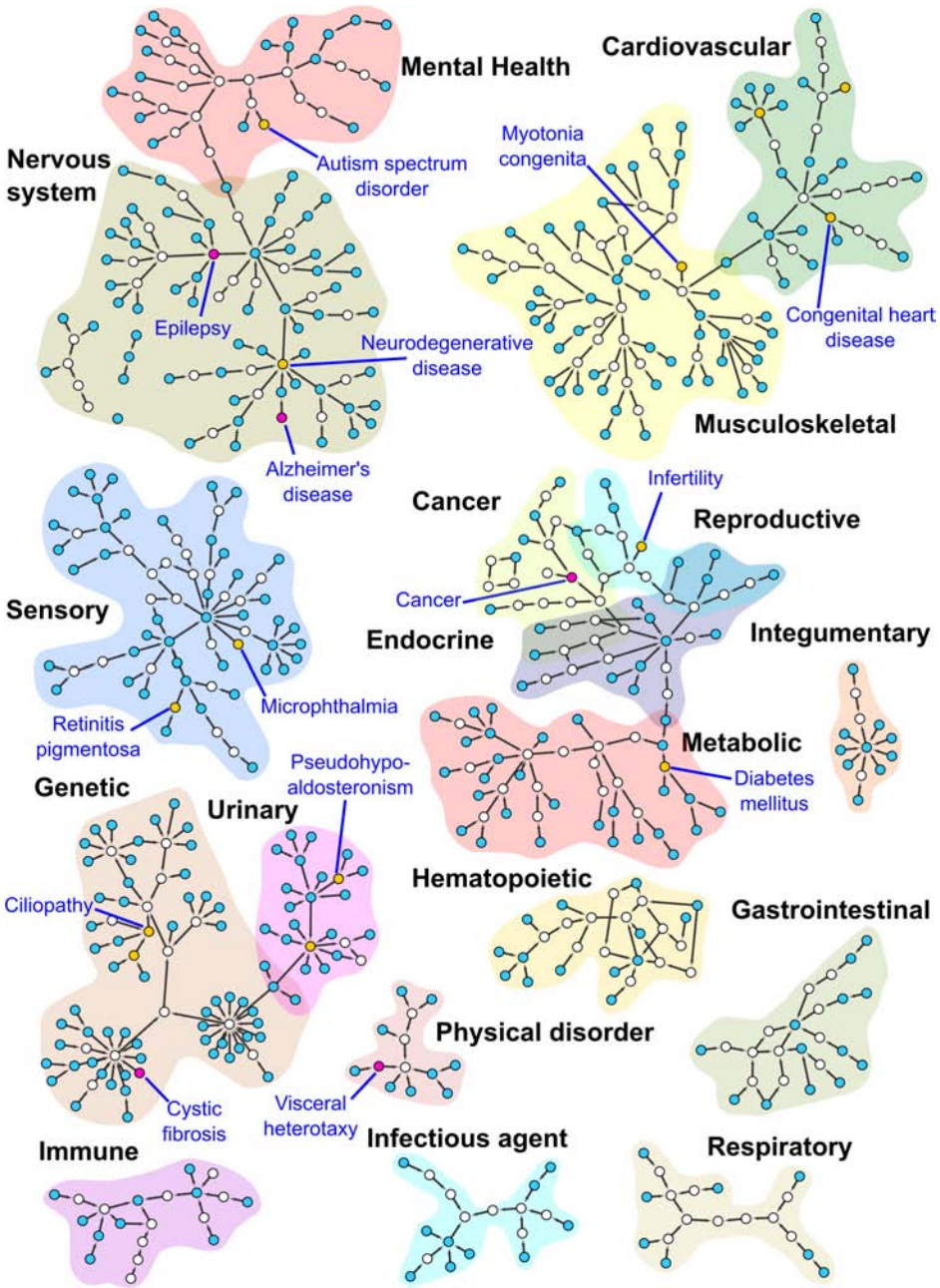

FIGURE 4 | Subnetworks from the DO. This figure shows MCL clustered subnetworks from a subset of the DO, consisting of terms annotated during our curation of the Xenbase human disease corpus detailed in the **Supplementary Material**. Nodes in the network are colored according to the number of direct annotations to the term they represent. Empty nodes have no direct annotations, blue nodes 1–5, yellow nodes 6–14 and purple nodes 15 and higher. Purple nodes and the yellow node(s) with the highest number of annotations for each cluster have been labeled. Cluster regions corresponding to high level DO terms have been highlighted for contrast and labeled. Some small subnetworks and singleton nodes have been moved to proximity with the high level DO term to which they are associated.

an autosomal recessive disease, dominated the annotations in the genetic disease group with the majority of studies using the oocyte to examine ion transport and channel function. Cystic fibrosis is caused by variants in the *CFTR* gene, a chloride channel that regulates fluid flow across membranes that line vital organs such as lungs, intestine, and pancreas. Chen et al. (2012) used the oocyte to perform functional analyses of human single nucleotide polymorphisms (SNPs) in a potential CF modifier gene, *SLC26A9A*, encoding an anion transporter involved in chloride and bicarbonate exchange. These experiments shed light on the contribution of allelic variation in the pathophysiology of diseases affected by variants in *SLC26* family members, such as Pendred syndrome, an autosomal recessive disease characterized by hearing loss and euthyroid

goiter. On the other hand, manipulation via knockdown and gain of function with morpholino and mRNA injections, respectively, were common techniques used to analyze genetic diseases such as branchiootorenal syndrome (BOS), an autosomal dominant disorder characterized by sensorineural, ear, branchial and renal defects. Knockdown of *pa2g4*, the *Xenopus* ortholog of a candidate human gene implicated in BOS, resulted in altered gene expression in neural crest and cranial placode providing insight into the molecular disease pathogenesis (Neilson et al., 2017). Similarly, Hoff et al. (2013) identified *ANKS6* variants in six families with nephronophthisis, an autosomal recessive cystic kidney disease that leads to adolescent renal failure, making this gene a strong disease-causing candidate. This was confirmed when targeted morpholino injections to knockdown *Xenopus anks6* in the intermediate mesoderm of one side of the embryos resulted in renal defects similar to patients. In general, screening for congenital disease-causing genes is a common use of *Xenopus* for many organ systems.

Sensory System Disease

Sensory system diseases had the third highest number of DO attributions (n = 80), with the most common type being eye diseases. *Xenopus* embryos have long been used to study fundamental aspects of early eye development and are used to model diseases such as microphthalmia, retinitis pigmentosa, exudative vitreoretinopathy, and aniridia. Feehan et al. (2017) utilized CRISPR/Cas9-mediated mutations in *Xenopus* genes encoding rhodopsin to model both dominant and recessive forms of retinitis pigmentosa, a disease caused by retinal degeneration that leads to gradual loss of sight. Assays on retinal extracts and confocal microscopy were used to characterize the genotype-phenotype relationships. To a lesser extent, oocytes have also been used to study ion transport in eye diseases such as cataract. Staubli et al. (2017) utilized oocytes to assess the function of mutant versions of the human creatine transporter MCT12 by screening cDNAs from patients with age-related cataracts. A portion of the variants revealed decreased uptake of creatine, suggesting that non-invasive pharmacological interventions might be able to treat creatine deficiency in age related cataract.

Musculoskeletal System Disease

The predominant diseases in the musculoskeletal category (n = 74) were myotonia congenita, a disease of chloride channels and congenital myasthenic syndrome, a neuromuscular junction disease, both of which used oocyte assays. Vindas-Smith et al. (2016) functionally characterized variants in the human gene, *CLCN1,* encoding a skeletal muscle chloride channel, found in non-syndromic myotonia congenita patients. Biophysical characterizations such as fast or slow gating, single channel conductance, current density and surface expression between wildtype and mutant channels expressed in *Xenopus* oocytes provided invaluable information on the complex genotype-phenotype relationship and provided molecular insight into potential therapeutics. Embryos have also been used to examine musculoskeletal diseases, such as Nager acrofacial dysostosis (Devotta et al., 2016) and idiopathic scoliosis (Lambert et al., 2009, 2013). Devotta et al. (2016) utilized antisense morpholinos to knockdown Sf3b4 function in *Xenopus* to generate an animal model of Nager acrofacial dysostosis (NAD), a disease characterized by underdeveloped cheek bones, very small lower jaw, cleft palate, defects in the middle ear, absent eyelashes, and a notch in the lower eyelid called a coloboma. The Sf3b4-depleted *Xenopus* embryos demonstrated reduced neural crest gene expression in the early embryo and resulted in hypoplastic neural crest-derived cartilages and craniofacial skeletal defects, similar to NAD patients. This has allowed researchers to dissect the pathogenesis of NAD and investigate targets of Sf3b4, one of the major genetic culprits of the disease.

Cardiovascular System Disease

Congenital heart defect studies using embryos were the most frequently annotated DO term in the cardiovascular system disease category (n = 70). The transparent nature of *Xenopus* tadpole skin facilitates easy examination of heart development just 3 days post-fertilization (Duncan and Khokha, 2016). Mandel et al. (2010) utilized a cardiac-specific transgenic EGFP reporter to define the DNA cis-regulatory enhancers controlling expression of *tbx20*, the *Xenopus* ortholog of the human gene which has been linked to congenital heart disease. This allowed researchers to determine that the BMP/SMAD signaling pathway regulated *tbx20* expression in the heart and that disrupted BMP activity may also underlie other congenital heart defects. Importantly, the element was not specific to *Xenopus* and showed conservation in other species. The identification of this element provides researchers and clinicians with a non-coding region of *TBX20* in humans with the potential to contribute to congenital heart defects. Other cardiovascular diseases studied in *Xenopus* include long QT syndrome (LQTS), hypertension, and atrial fibrillation predominantly using oocytes to investigate the function of cardiac channel proteins. For example, Steffensen et al. (2015) functionally characterized human variants of unknown significance in two genes encoding potassium channels, *KCNQ1* and *KCNQ2*, from patients diagnosed with LQTS, an electrophysiological disorder of the heart that can lead to cardiac arrest or death. Single cell voltage clamping and confocal imaging of oocytes expressing these human proteins revealed loss-of-function phenotypes that resulted in abnormal electrophysiology as well as defects in cellular trafficking. These experiments highlighted the increased incidence of channel dysfunction in patients with LQTS.

Cancer

All three *Xenopus* experimental approaches have been used to study cancer (n = 67). Each experimental approach offers unique advantages to study key cellular processes involved in tumorigenesis and metastasis such as division, differentiation, signaling and metabolism. The *Xenopus* embryo is a versatile model to characterize oncogenes and examine similarities between development and tumorigenesis (Hardwick and Philpott, 2015) with additional papers utilizing the cell-free egg extract (Cross and Powers, 2009) and oocyte (Nutt, 2012). A good example is Haynes-Gilmore et al. (2014) who used *Xenopus* embryos to study the tumor microenvironment

by transplanting thymic lymphoid tumor cells under the dorsal skin of the tadpole. This xenograft model phenocopies many aspects of mammalian tumorigenesis and allows real time visualization of the tumor microenvironment including neovascularization, immune response, tissue rearrangements, and cellular migration. On the other hand, Joukov et al. (2006) utilized cell-free extracts to observe mitotic spindle assembly and reveal a previously unknown role for the heterodimeric tumor-suppressor BRCA1/BARD1 in this process, which is important for chromosome stability and tumor suppression. In general, hundreds of *Xenopus* studies have examined cell cycle and DNA-check point offering valuable information on general cancer mechanisms but did not pass our screening for specific human disease articles and are not represented here.

Urinary System Disease

The *Xenopus* pronephric kidney offers a simplified model of the more complex mammalian kidney to study development, repair, and disease (Vize et al., 1997; Lienkamp, 2016). Top DO annotations in this category include kidney disease, nephrolithiasis, nephrogenic diabetes insipidus, pseudohypoaldosteronism, Liddle syndrome and Dent disease. The oocyte was the major experimental approach used to study urinary system diseases (n = 63) with a focus on defects in channel and ion transport that impact fluid homeostasis, blood filtration and urine production. For example, Ludwig et al. (2005) utilized the oocyte in structure-function studies of the human voltage-gated chloride channel, CIC-5, that when mutated, causes Dent disease, a renal tubular transport disease that leads to chronic kidney failure. Electrophysiology and imaging of oocytes expressing these channels provided insight into the importance of different amino acid sequences necessary for proper trafficking and recruitment throughout the trans-Golgi network.

Diseases of Metabolism

Diabetes mellitus was the predominant condition annotated for diseases of metabolism (n = 44) with experiments utilizing either the embryos or oocytes. Pancreas development is highly conserved between *Xenopus* and mammals, making it an ideal model to study and screen genetic candidates involved in congenital pancreas defects (Kofent and Spagnoli, 2016) such as those occurring in type 1 diabetes mellitus. Simaite et al. (2014) took advantage of this high conservation with a combination of whole-genome sequencing with linkage analysis in a consanguineous family with early onset antibody-negative diabetes and morpholino knockdown of candidate orthologous genes in *Xenopus* to identify a variant in the patient gene *PCBD1* as the likely cause of pancreatic insufficiency and type 1 diabetes in these families. Oocytes have also been used to functionally characterize variants found in diabetes patients. For example, Proks et al. (2006) identified a variant in the *SUR1* gene, in a patient with DEND syndrome, which has a range of symptoms including neonatal diabetes. SUR1 is a regulatory subunit of a K(ATP) channel in pancreatic beta cells, and functional assays in oocytes revealed that the variants resulted in reduced channel sensitivity suggesting a novel genetic cause for neonatal diabetes. Other metabolic diseases studied in *Xenopus* oocytes included hemochromatosis, hypophosphatemia, and hypokalemic periodic paralysis.

Disease of Mental Health

Xenopus embryos have long been used to study the effects of alcohol on development (Fainsod and Kot-Leibovich, 2018) and the resulting diseases of the mental health category (n = 41) including fetal alcohol spectrum disorder (FASD) or fetal alcohol syndrome (FAS). For example, Yelin et al. (2005) exposed embryos to various concentrations of alcohol at different time points to determine that the greatest period of sensitivity was early during gastrulation. At the molecular and morphological level, alcohol disrupted axial patterning and initial induction of the central nervous system. Further studies demonstrated the antagonistic effect of retinol (vitamin A) that resulted in phenotypic characteristics similar to those observed in humans with FAS including shortened rostro-caudal axis, microcephaly and microphthalmia.

Xenopus is also an ideal model to study mental health disorders resulting from defective nervous system development (Pratt and Khakhalin, 2013). Our analysis found six articles annotated as models for autism spectrum disorder (ASD). James et al. (2015) used a novel neurodegenerative model caused by valproic acid exposure during critical timepoints of neural circuit formation, which can lead to defective cognitive development, similar to those observed in ASD. Researchers took advantage of *Xenopus* behavioral assays known to be sensitive to abnormal circuit development, such as collision avoidance and schooling behavior, and found that valproic acid treatment resulted in tadpole behavioral abnormalities that were correlated with defects in brain morphology, dendritic structure and synaptic connectivity. These findings strengthened the hypothesis that changes in early neural circuitry can result in later behavioral deficits. Other studies have used oocytes to examine the impact of neurotransmitter function in ASD. Limon et al. (2008) examined the activity of GABA and glutamate neurotransmitter receptors from autistic brain tissue samples transplanted into *Xenopus* oocytes offering a novel approach to the study of autism, other neurological disorders, and drug discovery. Additional mental health disorders studied with *Xenopus* oocytes included schizophrenia, pain disorder, and intellectual disability.

Physical Disorders

Many diseases in the physical disorder category (n = 37) involving defects in left-right patterning, neural tube closure or craniofacial birth defects have been studied in the frog embryo. Studies of left-right patterning disorders such as visceral heterotaxy and *situs inversus* predominated the physical disorder category. *Xenopus* studies have been instrumental in elucidating the molecular and cellular mechanisms of left-right patterning in the vertebrate embryo and have shown that this starts shortly after gastrulation with a group of mono-ciliated cells known as the left-right organizer (LRO) associated with the node or gastrocoel roof plate. Studies in *Xenopus* have defined the function of a candidate disease gene, *GALNT1*, identified in a patient with visceral heterotaxy (Boskovski et al., 2013). The quantitative live

imaging of the LRO in *galnt1* knockdown embryos revealed disrupted cilia and defects in left-right asymmetry, suggesting a novel etiology for human heterotaxy. Similar to left-right patterning defects, *Xenopus* embryos have been used to study other physical disorders including craniofacial and neural tube defects, such as holoprosencephaly, microcephaly, and orofacial clefts because these structures can be easily observed in embryos several days after fertilization (Dickinson, 2016; Dubey and Saint-Jeannet, 2017).

Hematopoietic System Disease

Xenopus was one of the early models for understanding developmental hematopoiesis (Dzierzak and Bigas, 2018) and our meta-analysis identified 28 total attributions to hematopoietic disease. Fanconi anemia had the greatest number of annotations, including four articles using cell-free egg extracts to study how the mechanisms of DNA-repair during replication and transcription are compromised in Fanconi anemia patients (Sobeck et al., 2006; Stone et al., 2007; Landais et al., 2009; Sareen et al., 2012). Similarly, Dominguez-Sola et al. (2007) took advantage of the nuclear-free egg extract system to define a non-transcriptional role of MYC in DNA replication which informed our mechanistic understanding of Burkitt lymphoma that is caused by chromosomal translocations involving MYC. Two other articles studied Diamond-Blackfan anemia with embryo experiments (Robson et al., 2016; Calo et al., 2018).

Gastrointestinal System Disease

The predominant diseases of the gastrointestinal (GI) system studied in *Xenopus* (n = 24) were gastritis, cholestasis, and congenital secretory chloride diarrhea 1, all of which utilized the oocyte. Additional articles studying colorectal cancer, colon cancer and inflammatory bowel disease utilized either the oocyte or embryo studies. Notably, TALEN-mediated mutation of a *Xenopus* ortholog gene, *apc*, implicated in human colorectal cancer, was used to generate a *Xenopus* cancer model, enabling in-depth mechanistic analysis and therapeutic screenings which are not possible in other commonly used animal such as mice (Van Nieuwenhuysen et al., 2015).

Endocrine System Disease

Xenopus has long been a model to study the role of endocrine hormones in metamorphosis, which are analogous to many of the hormonal changes occurring in the perinatal period of human birth (Yaoita et al., 1990; Buchholz, 2017). Endocrine hormones affect early embryonic organogenesis, brain development, metabolism and the reproductive system (Cossette and Drysdale, 2004; Bronchain et al., 2017). Moreover, endocrine disruption by chemical pollutants has been shown to lead to diseases of the reproductive system, thus a common focus for environmental toxicology studies using FETAX and other assays with *Xenopus* embryos (Mouche et al., 2017; Mughal et al., 2018). There were 22 DO attributions of endocrine system disease examining conditions such as Kallman syndrome, a disorder of sexual maturation, and hermaphroditism which encompasses disorders of sex chromosomes and sex determination, as well as the less specific term "endocrine system disease."

Diseases by Infectious Agent

The top DO terms annotated to diseases by infectious agent (n = 18) were related to malaria and HIV. These studies predominantly used *Xenopus* oocytes to study the effects of drugs. For example, Hertel et al. (2004) examined the mechanism of glucose transporter inhibition in oocytes, following HIV protease inhibitor treatment, a frequent side effect of these drugs that increases a patient's risk for diabetes and cardiovascular disease.

Immune, Integumentary, Respiratory, Reproductive System Diseases

Our meta-analysis of the *Xenopus* literature identified a diversity of other diseases that did not fall into major categories such as immune (n = 19), integumentary (n = 10), respiratory (n = 10),

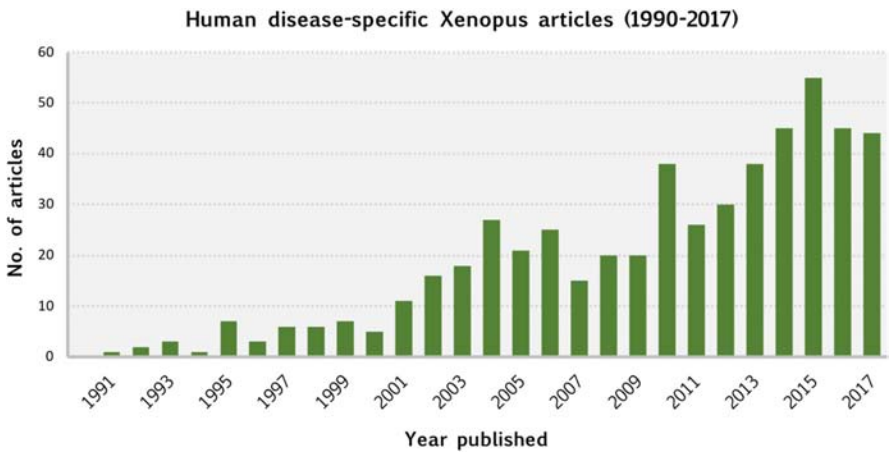

FIGURE 5 | Human disease-specific *Xenopus* articles (1990–2017). This chart shows the number of articles published, by year, between 1990 and 2017 that our curation identified as utilizing *Xenopus* as a model system for studying human disease. Publication dates were obtained from NCBI's PubMed database.

or reproductive (n = 13) systems. Notable examples include integumentary system diseases where Sangrithi et al. (2005) utilized cell-free egg extracts to link defective DNA replication with Rothmund-Thompson syndrome, a chromosome fragility disorder that is associated with skin disease. In the respiratory system disease category, Walentek et al. (2015) used morpholino to knockdown *atp4a*, a gastric ATPase that in humans is targeted by proton pump inhibitor (PPI) drugs to treat ulcers and other gastrointestinal diseases. The *Xenopus* studies helped explain why patients taking PPI have an increased risk of pneumonia. Knockdown of *Xenopus atp4a* resulted in multiciliated cell (MCC) defects of the *Xenopus* embryonic epidermis- a common model for mucociliary cells in the human airway epithelia (Walentek and Quigley, 2017), which are critical for ciliary-driven clearance of the lungs. These results suggest a possible causative linkage between PPIs and pneumonia due to defective function of the mucociliary epithelium of patient's airways resulting in chronic congestion.

FUTURE HUMAN DISEASE SUPPORT ON XENBASE

Our meta-analysis of the *Xenopus* literature was made possible by the curation and data integration of Xenbase. This comprehensive analysis revealed the breadth and depth of human disease modeling using *Xenopus* which continues to show an increasing trend (**Figure 5**). It is clear that *Xenopus* is an extremely versatile model system, and offers human disease researchers a broad suite of experimental approaches.

Modeling human disease is a major focus of the *Xenopus* research community and the recent incorporation of DO annotations into Xenbase facilitates this goal. Ongoing development in Xenbase includes the curation of *Xenopus* phenotypes using a new *Xenopus* Phenotype Ontology (XPO), which will enable us to directly link the results from *Xenopus* experiments to similar phenotypes in mice and men through cross references to the Mammalian Phenotype Ontology (MP) (Smith and Eppig, 2015) and the Human Phenotype Ontology (HPO) (Kohler et al., 2017), respectively. The XPO uses easy to understand anatomy-based (e.g., abnormal eye morphology) and GO term-based phrases (e.g., abnormal eye development) as well as clinical terms (e.g., microphthalmia). The planned strategy for future phenotype curation will align with other MODs with extensive manual curation of phenotypes such as the Mouse Genome Informatics (MGI) consortium[6] (RRID:SCR_006460).

Xenopus high throughput datasets such as RNA-Seq and ChIP-Seq are increasing at a rapid pace. Xenbase is expanding support for these experimental approaches by processing all such public datasets from the Gene Expression Omnibus (GEO[7]; RRID:SCR_007303). Xenbase plans to integrate gene expression phenotypes with anatomical phenotypes. This gene expression as a phenotype (EaP) (Howe et al., 2017) approach will be used to describe experiments in which an experimental manipulation affects the expression of a gene in a tissue or embryo (e.g., *pax6* increased amount [in the] retina) as assayed by *in situ* hybridization or RNA-Seq assays. These new tools will enable researchers to use a systems biological approach to interrogate the gene regulatory networks underlying disease and therapeutic mechanisms, an area where the experimental advantages of the *Xenopus* system are well suited.

[6] http://www.informatics.jax.org

[7] https://www.ncbi.nlm.nih.gov/geo/

AUTHOR CONTRIBUTIONS

MN, MF, and CJ-Z conceptualized and designed the scope of the review, identified and curated the research articles, and analyzed and interpreted the results. MN drafted and wrote the manuscript. VP and MF generated the figures. MF, TP, and CJ-Z generated the data tables. MF, CJ-Z, KB, JF, AZ, and PV reviewed and revised the manuscript. AZ and PV, CO-PIs on the Xenbase grant, coordinated curation and development of the support for disease modeling, and assessed methodological quality. DW, TP, SC, VL, YW, and KK developed code and database support for disease pages and disease integration. All authors developed the support for disease modeling and approved the final manuscript as submitted.

FUNDING

Major funding for Xenbase was provided by the Eunice Kennedy Shriver National Institute of Child Health and Human Development, Grant P41 HD064556.

ACKNOWLEDGMENTS

The authors would like to thank Sally A. Moody, Daniel R. Buchholz, and the reviewers for critical evaluation and comments on this manuscript.

SUPPLEMENTARY MATERIAL

The Supplementary Material for this article can be found online at: https://www.frontiersin.org/articles/10.3389/fphys.2019.00154/full#supplementary-material

REFERENCES

Ashburner, M., Ball, C. A., Blake, J. A., Botstein, D., Butler, H., Cherry, J. M., et al. (2000). Gene ontology: tool for the unification of biology. The Gene Ontology Consortium. *Nat. Genet.* 25, 25–29. doi: 10.1038/75556

Aslan, Y., Tadjuidje, E., Zorn, A. M., and Cha, S. W. (2017). High-efficiency non-mosaic CRISPR-mediated knock-in and indel mutation in F0 *Xenopus*. *Development* 144, 2852–2858. doi: 10.1242/dev.152967

Bantle, J. A., Fort, D. J., Rayburn, J. R., DeYoung, D. J., and Bush, S. J. (1990). Further validation of FETAX: evaluation of the developmental

toxicity of five known mammalian teratogens and non-teratogens. *Drug Chem. Toxicol.* 13, 267–282. doi: 10.3109/01480549009032286

Bell, M. R., Belarde, J. A., Johnson, H. F., and Aizenman, C. D. (2011). A neuroprotective role for polyamines in a *Xenopus* tadpole model of epilepsy. *Nat. Neurosci.* 14, 505–512. doi: 10.1038/nn.2777

Bello, S. M., Shimoyama, M., Mitraka, E., Laulederkind, S. J. F., Smith, C. L., Eppig, J. T., et al. (2018). Disease Ontology: improving and unifying disease annotations across species. *Dis. Model. Mech.* 11:dmm032839. doi: 10.1242/dmm.032839

Bhattacharya, D., Marfo, C. A., Li, D., Lane, M., and Khokha, M. K. (2015). CRISPR/Cas9: an inexpensive, efficient loss of function tool to screen human disease genes in *Xenopus*. *Dev. Biol.* 408, 196–204. doi: 10.1016/j.ydbio.2015.11.003

Blitz, I. L., Biesinger, J., Xie, X., and Cho, K. W. (2013). Biallelic genome modification in F(0) *Xenopus tropicalis* embryos using the CRISPR/Cas system. *Genesis* 51, 827–834. doi: 10.1002/dvg.22719

Blum, M., and Ott, T. (2018). *Xenopus*: an undervalued model organism to study and model human genetic disease. *Cells Tissues Organs* doi: 10.1159/000490898 [Epub ahead of print].

Boskovski, M. T., Yuan, S., Pedersen, N. B., Goth, C. K., Makova, S., Clausen, H., et al. (2013). The heterotaxy gene GALNT11 glycosylates Notch to orchestrate cilia type and laterality. *Nature* 504, 456–459. doi: 10.1038/nature12723

Bronchain, O. J., Chesneau, A., Monsoro-Burq, A. H., Jolivet, P., Paillard, E., Scanlan, T. S., et al. (2017). Implication of thyroid hormone signaling in neural crest cells migration: evidence from thyroid hormone receptor beta knockdown and NH3 antagonist studies. *Mol. Cell. Endocrinol.* 439, 233–246. doi: 10.1016/j.mce.2016.09.007

Buchholz, D. R. (2017). *Xenopus* metamorphosis as a model to study thyroid hormone receptor function during vertebrate developmental transitions. *Mol. Cell. Endocrinol.* 459, 64–70. doi: 10.1016/j.mce.2017.03.020

Calo, E., Gu, B., Bowen, M. E., Aryan, F., Zalc, A., Liang, J., et al. (2018). Tissue-selective effects of nucleolar stress and rDNA damage in developmental disorders. *Nature* 554, 112–117. doi: 10.1038/nature25449

Chen, A. P., Chang, M. H., and Romero, M. F. (2012). Functional analysis of nonsynonymous single nucleotide polymorphisms in human SLC26A9. *Hum. Mutat.* 33, 1275–1284. doi: 10.1002/humu.22107

Cossette, S. M., and Drysdale, T. A. (2004). Early expression of thyroid hormone receptor beta and retinoid X receptor gamma in the *Xenopus* embryo. *Differentiation* 72, 239–249. doi: 10.1111/j.1432-0436.2004.07205006.x

Cross, M. K., and Powers, M. A. (2009). Learning about cancer from frogs: analysis of mitotic spindles in *Xenopus* egg extracts. *Dis. Model. Mech.* 2, 541–547. doi: 10.1242/dmm.002022

Dawson, D. A., Fort, D. J., Newell, D. L., and Bantle, J. A. (1989). Developmental toxicity testing with FETAX: evaluation of five compounds. *Drug Chem. Toxicol.* 12, 67–75. doi: 10.3109/01480548908999144

Devotta, A., Juraver-Geslin, H., Gonzalez, J. A., Hong, C. S., and Saint-Jeannet, J. P. (2016). Sf3b4-depleted *Xenopus* embryos: a model to study the pathogenesis of craniofacial defects in Nager syndrome. *Dev. Biol.* 415, 371–382. doi: 10.1016/j.ydbio.2016.02.010

Dickinson, A. J. (2016). Using frogs faces to dissect the mechanisms underlying human orofacial defects. *Semin. Cell Dev. Biol.* 51, 54–63. doi: 10.1016/j.semcdb.2016.01.016

Dominguez-Sola, D., Ying, C. Y., Grandori, C., Ruggiero, L., Chen, B., Li, M., et al. (2007). Non-transcriptional control of DNA replication by c-Myc. *Nature* 448, 445–451. doi: 10.1038/nature05953

Dubey, A., and Saint-Jeannet, J. P. (2017). Modeling human craniofacial disorders in *Xenopus*. *Curr. Pathobiol. Rep.* 5, 79–92. doi: 10.1007/s40139-017-0128-8

Duncan, A. R., and Khokha, M. K. (2016). *Xenopus* as a model organism for birth defects-Congenital heart disease and heterotaxy. *Semin. Cell Dev. Biol.* 51, 73–79. doi: 10.1016/j.semcdb.2016.02.022

Dzierzak, E., and Bigas, A. (2018). Blood development: hematopoietic stem cell dependence and independence. *Cell Stem Cell* 22, 639–651. doi: 10.1016/j.stem.2018.04.015

Fainsod, A., and Kot-Leibovich, H. (2018). *Xenopus* embryos to study fetal alcohol syndrome, a model for environmental teratogenesis. *Biochem. Cell Biol.* 96, 77–87. doi: 10.1139/bcb-2017-0219

Feehan, J. M., Chiu, C. N., Stanar, P., Tam, B. M., Ahmed, S. N., and Moritz, O. L. (2017). Modeling dominant and recessive forms of retinitis pigmentosa by editing three *Rhodopsin*-encoding genes in *Xenopus laevis* using crispr/Cas9. *Sci. Rep.* 7:6920. doi: 10.1038/s41598-017-07153-4

Felix, R. (2000). Channelopathies: ion channel defects linked to heritable clinical disorders. *J. Med. Genet.* 37, 729–740. doi: 10.1136/jmg.37.10.729

Fort, D. J., James, B. L., and Bantle, J. A. (1989). Evaluation of the developmental toxicity of five compounds with the frog embryo teratogenesis assay: *Xenopus* (FETAX) and a metabolic activation system. *J. Appl. Toxicol.* 9, 377–388. doi: 10.1002/jat.2550090603

Garfinkel, A. M., and Khokha, M. K. (2017). An interspecies heart-to-heart: using *Xenopus* to uncover the genetic basis of congenital heart disease. *Curr. Pathobiol. Rep.* 5, 187–196. doi: 10.1007/s40139-017-0142-x

Hardwick, L. J., and Philpott, A. (2015). An oncologists friend: how *Xenopus* contributes to cancer research. *Dev. Biol.* 408, 180–187. doi: 10.1016/j.ydbio.2015.02.003

Haynes-Gilmore, N., Banach, M., Edholm, E. S., Lord, E., and Robert, J. (2014). A critical role of non-classical MHC in tumor immune evasion in the amphibian *Xenopus* model. *Carcinogenesis* 35, 1807–1813. doi: 10.1093/carcin/bgu100

Hellsten, U., Harland, R. M., Gilchrist, M. J., Hendrix, D., Jurka, J., Kapitonov, V., et al. (2010). The genome of the Western clawed frog *Xenopus tropicalis*. *Science* 328, 633–636. doi: 10.1126/science.1183670

Hertel, J., Struthers, H., Horj, C. B., and Hruz, P. W. (2004). A structural basis for the acute effects of HIV protease inhibitors on GLUT4 intrinsic activity. *J. Biol. Chem.* 279, 55147–55152. doi: 10.1074/jbc.M410826200

Hoff, S., Halbritter, J., Epting, D., Frank, V., Nguyen, T. M., van Reeuwijk, J., et al. (2013). ANKS6 is a central component of a nephronophthisis module linking NEK8 to INVS and NPHP3. *Nat. Genet.* 45, 951–956. doi: 10.1038/ng.2681

Hoogenboom, W. S., Klein Douwel, D., and Knipscheer, P. (2017). *Xenopus* egg extract: a powerful tool to study genome maintenance mechanisms. *Dev. Biol.* 428, 300–309. doi: 10.1016/j.ydbio.2017.03.033

Howe, D. G., Blake, J. A., Bradford, Y. M., Bult, C. J., Calvi, B. R., Engel, S. R., et al. (2018). Model organism data evolving in support of translational medicine. *Lab. Anim.* 47, 277–289. doi: 10.1038/s41684-018-0150-4

Howe, D. G., Bradford, Y. M., Eagle, A., Fashena, D., Frazer, K., Kalita, P., et al. (2017). The Zebrafish Model Organism Database: new support for human disease models, mutation details, gene expression phenotypes and searching. *Nucleic Acids Res.* 45, D758–D768. doi: 10.1093/nar/gkw1116

James, E. J., Gu, J., Ramirez-Vizcarrondo, C. M., Hasan, M., Truszkowski, T. L., Tan, Y., et al. (2015). Valproate-induced neurodevelopmental deficits in *Xenopus laevis* tadpoles. *J. Neurosci.* 35, 3218–3229. doi: 10.1523/jneurosci.4050-14.2015

James-Zorn, C., Ponferrada, V., Fisher, M. E., Burns, K., Fortriede, J., Segerdell, E., et al. (2018). Navigating xenbase: an integrated *Xenopus* genomics and gene expression database. *Methods Mol. Biol.* 1757, 251–305. doi: 10.1007/978-1-4939-7737-6_10

Joukov, V., Groen, A. C., Prokhorova, T., Gerson, R., White, E., Rodriguez, A., et al. (2006). The BRCA1/BARD1 heterodimer modulates ran-dependent mitotic spindle assembly. *Cell* 127, 539–552. doi: 10.1016/j.cell.2006.08.053

Karimi, K., Fortriede, J. D., Lotay, V. S., Burns, K. A., Wang, D. Z., Fisher, M. E., et al. (2018). Xenbase: a genomic, epigenomic and transcriptomic model organism database. *Nucleic Acids Res.* 46, D861–D868. doi: 10.1093/nar/gkx936

Khokha, M. K. (2012). *Xenopus* white papers and resources: folding functional genomics and genetics into the frog. *Genesis* 50, 133–142. doi: 10.1002/dvg.22015

Kofent, J., and Spagnoli, F. M. (2016). *Xenopus* as a model system for studying pancreatic development and diabetes. *Semin. Cell Dev. Biol.* 51, 106–116. doi: 10.1016/j.semcdb.2016.01.005

Kohler, S., Vasilevsky, N. A., Engelstad, M., Foster, E., McMurry, J., Ayme, S., et al. (2017). The human phenotype ontology in 2017. *Nucleic Acids Res.* 45, D865–D876. doi: 10.1093/nar/gkw1039

Lambert, F. M., Malinvaud, D., Glaunes, J., Bergot, C., Straka, H., and Vidal, P. P. (2009). Vestibular asymmetry as the cause of idiopathic scoliosis: a possible answer from *Xenopus*. *J. Neurosci.* 29, 12477–12483. doi: 10.1523/jneurosci.2583-09.2009

Lambert, F. M., Malinvaud, D., Gratacap, M., Straka, H., and Vidal, P. P. (2013). Restricted neural plasticity in vestibulospinal pathways after unilateral

labyrinthectomy as the origin for scoliotic deformations. *J. Neurosci.* 33, 6845–6856. doi: 10.1523/jneurosci.4842-12.2013

Landais, I., Hiddingh, S., McCarroll, M., Yang, C., Sun, A., Turker, M. S., et al. (2009). Monoketone analogs of curcumin, a new class of Fanconi anemia pathway inhibitors. *Mol. Cancer* 8:133. doi: 10.1186/1476-4598-8-133

Lehmann-Horn, F., and Jurkat-Rott, K. (1999). Voltage-gated ion channels and hereditary disease. *Physiol. Rev.* 79, 1317–1372. doi: 10.1152/physrev.1999.79.4.1317

Lienkamp, S. S. (2016). Using *Xenopus* to study genetic kidney diseases. *Semin. Cell Dev. Biol.* 51, 117–124. doi: 10.1016/j.semcdb.2016.02.002

Limon, A., Reyes-Ruiz, J. M., and Miledi, R. (2008). Microtransplantation of neurotransmitter receptors from postmortem autistic brains to *Xenopus* oocytes. *Proc. Natl. Acad. Sci. U.S.A.* 105, 10973–10977. doi: 10.1073/pnas.0804386105

Ludwig, M., Doroszewicz, J., Seyberth, H. W., Bokenkamp, A., Balluch, B., Nuutinen, M., et al. (2005). Functional evaluation of Dent's disease-causing mutations: implications for ClC-5 channel trafficking and internalization. *Hum. Genet.* 117, 228–237. doi: 10.1007/s00439-005-1303-2

Mandel, E. M., Kaltenbrun, E., Callis, T. E., Zeng, X. X., Marques, S. R., Yelon, D., et al. (2010). The BMP pathway acts to directly regulate Tbx20 in the developing heart. *Development* 137, 1919–1929. doi: 10.1242/dev.043588

Miledi, R., Duenas, Z., Martinez-Torres, A., Kawas, C. H., and Eusebi, F. (2004). Microtransplantation of functional receptors and channels from the Alzheimer's brain to frog oocytes. *Proc. Natl. Acad. Sci. U.S.A.* 101, 1760–1763. doi: 10.1073/pnas.0308224100

Moody, S. A. (1987a). Fates of the blastomeres of the 16-cell stage *Xenopus* embryo. *Dev. Biol.* 119, 560–578. doi: 10.1016/0012-1606(87)90059-5

Moody, S. A. (1987b). Fates of the blastomeres of the 32-cell-stage *Xenopus* embryo. *Dev. Biol.* 122, 300–319.

Morgan, M. K., Scheuerman, P. R., Bishop, C. S., and Pyles, R. A. (1996). Teratogenic potential of atrazine and 2,4-D using FETAX. *J. Toxicol. Environ. Health* 48, 151–168. doi: 10.1080/009841096161401

Morris, J. H., Apeltsin, L., Newman, A. M., Baumbach, J., Wittkop, T., Su, G., et al. (2011). *clusterMaker*: a multi-algorithm clustering plugin for Cytoscape. *BMC Bioinformatics* 12:436. doi: 10.1186/1471-2105-12-436

Mouche, I., Malesic, L., and Gillardeaux, O. (2017). FETAX assay for evaluation of developmental toxicity. *Methods Mol. Biol.* 1641, 311–324. doi: 10.1007/978-1-4939-7172-5_17

Mughal, B. B., Demeneix, B. A., and Fini, J. B. (2018). Evaluating thyroid disrupting chemicals in vivo using *Xenopus laevis*. *Methods Mol. Biol.* 1801, 183–192. doi: 10.1007/978-1-4939-7902-8_15

Muller, H. M., Kenny, E. E., and Sternberg, P. W. (2004). Textpresso: an ontology-based information retrieval and extraction system for biological literature. *PLoS Biol.* 2:e309. doi: 10.1371/journal.pbio.0020309

Neilson, K. M., Abbruzzesse, G., Kenyon, K., Bartolo, V., Krohn, P., Alfandari, D., et al. (2017). Pa2G4 is a novel Six1 co-factor that is required for neural crest and otic development. *Dev. Biol.* 421, 171–182. doi: 10.1016/j.ydbio.2016.11.021

Nutt, L. K. (2012). The *Xenopus* oocyte: a model for studying the metabolic regulation of cancer cell death. *Semin. Cell Dev. Biol.* 23, 412–418. doi: 10.1016/j.semcdb.2012.03.015

Pratt, K. G., and Khakhalin, A. S. (2013). Modeling human neurodevelopmental disorders in the *Xenopus* tadpole: from mechanisms to therapeutic targets. *Dis. Model. Mech.* 6, 1057–1065. doi: 10.1242/dmm.012138

Proks, P., Arnold, A. L., Bruining, J., Girard, C., Flanagan, S. E., Larkin, B., et al. (2006). A heterozygous activating mutation in the sulphonylurea receptor SUR1 (ABCC8) causes neonatal diabetes. *Hum. Mol. Genet.* 15, 1793–1800. doi: 10.1093/hmg/ddl101

Robson, A., Owens, N. D., Baserga, S. J., Khokha, M. K., and Griffin, J. N. (2016). Expression of ribosomopathy genes during *Xenopus tropicalis* embryogenesis. *BMC Dev. Biol.* 16:38. doi: 10.1186/s12861-016-0138-5

Salanga, M. C., and Horb, M. E. (2015). *Xenopus* as a model for GI/pancreas disease. *Curr. Pathobiol. Rep.* 3, 137–145. doi: 10.1007/s40139-015-0076-0

Sangrithi, M. N., Bernal, J. A., Madine, M., Philpott, A., Lee, J., Dunphy, W. G., et al. (2005). Initiation of DNA replication requires the RECQL4 protein mutated in Rothmund-Thomson syndrome. *Cell* 121, 887–898. doi: 10.1016/j.cell.2005.05.015

Sareen, A., Chaudhury, I., Adams, N., and Sobeck, A. (2012). Fanconi anemia proteins FANCD2 and FANCI exhibit different DNA damage responses during S-phase. *Nucleic Acids Res.* 40, 8425–8439. doi: 10.1093/nar/gks638

Sater, A. K., and Moody, S. A. (2017). Using *Xenopus* to understand human disease and developmental disorders. *Genesis* 55:e22997. doi: 10.1002/dvg.22997

Shannon, P., Markiel, A., Ozier, O., Baliga, N. S., Wang, J. T., Ramage, D., et al. (2003). Cytoscape: a software environment for integrated models of biomolecular interaction networks. *Genome Res.* 13, 2498–2504. doi: 10.1101/gr.1239303

Shi, Z., Wang, F., Cui, Y., Liu, Z., Guo, X., Zhang, Y., et al. (2015). Heritable CRISPR/Cas9-mediated targeted integration in *Xenopus tropicalis*. *FASEB J.* 29, 4914–4923. doi: 10.1096/fj.15-273425

Sigel, E., and Minier, F. (2005). The *Xenopus* oocyte: system for the study of functional expression and modulation of proteins. *Mol. Nutr. Food. Res.* 49, 228–234. doi: 10.1002/mnfr.200400104

Simaite, D., Kofent, J., Gong, M., Ruschendorf, F., Jia, S., Arn, P., et al. (2014). Recessive mutations in PCBD1 cause a new type of early-onset diabetes. *Diabetes* 63, 3557–3564. doi: 10.2337/db13-1784

Simons, C., Rash, L. D., Crawford, J., Ma, L., Cristofori-Armstrong, B., Miller, D., et al. (2015). Mutations in the voltage-gated potassium channel gene KCNH1 cause Temple-Baraitser syndrome and epilepsy. *Nat. Genet.* 47, 73–77. doi: 10.1038/ng.3153

Smith, C. L., and Eppig, J. T. (2015). Expanding the mammalian phenotype ontology to support automated exchange of high throughput mouse phenotyping data generated by large-scale mouse knockout screens. *J. Biomed. Semantics* 6:11. doi: 10.1186/s13326-015-0009-1

Sobeck, A., Stone, S., Costanzo, V., de Graaf, B., Reuter, T., de Winter, J., et al. (2006). Fanconi anemia proteins are required to prevent accumulation of replication-associated DNA double-strand breaks. *Mol. Cell Biol.* 26, 425–437. doi: 10.1128/MCB.26.2.425-437.2006

Staubli, A., Capatina, N., Fuhrer, Y., Munier, F. L., Labs, S., Schorderet, D. F., et al. (2017). Abnormal creatine transport of mutations in monocarboxylate transporter 12 (MCT12) found in patients with age-related cataract can be partially rescued by exogenous chaperone CD147. *Hum. Mol. Genet.* 26, 4203–4214. doi: 10.1093/hmg/ddx310

Steffensen, A. B., Refaat, M. M., David, J. P., Mujezinovic, A., Calloe, K., Wojciak, J., et al. (2015). High incidence of functional ion-channel abnormalities in a consecutive Long QT cohort with novel missense genetic variants of unknown significance. *Sci. Rep.* 5:10009. doi: 10.1038/srep10009

Stone, S., Sobeck, A., van Kogelenberg, M., de Graaf, B., Joenje, H., Christian, J., et al. (2007). Identification, developmental expression and regulation of the *Xenopus* ortholog of human FANCG/XRCC9. *Genes Cells* 12, 841–851. doi: 10.1111/j.1365-2443.2007.01096.x

Tandon, P., Conlon, F., Furlow, J. D., and Horb, M. E. (2017). Expanding the genetic toolkit in *Xenopus*: approaches and opportunities for human disease modeling. *Dev. Biol.* 426, 325–335. doi: 10.1016/j.ydbio.2016.04.009

The Gene Ontology Consortium (2017). Expansion of the Gene Ontology knowledgebase and resources. *Nucleic Acids Res.* 45, D331–D338. doi: 10.1093/nar/gkw1108

Ullah, G., Demuro, A., Parker, I., and Pearson, J. E. (2015). Analyzing and modeling the kinetics of amyloid beta pores associated with Alzheimer's disease pathology. *PLoS One* 10:e0137357. doi: 10.1371/journal.pone.0137357

Van Nieuwenhuysen, T., Naert, T., Tran, H. T., Van Imschoot, G., Geurs, S., Sanders, E., et al. (2015). TALEN-mediated apc mutation in *Xenopus tropicalis* phenocopies familial adenomatous polyposis. *Oncoscience* 2, 555–566. doi: 10.18632/oncoscience.166

Vindas-Smith, R., Fiore, M., Vasquez, M., Cuenca, P., Del Valle, G., Lagostena, L., et al. (2016). Identification and functional characterization of CLCN1 mutations found in nondystrophic myotonia patients. *Hum. Mutat.* 37, 74–83. doi: 10.1002/humu.22916

Vize, P. D., Seufert, D. W., Carroll, T. J., and Wallingford, J. B. (1997). Model systems for the study of kidney development: use of the pronephros in the analysis of organ induction and patterning. *Dev. Biol.* 188, 189–204. doi: 10.1006/dbio.1997.8629

Walentek, P., Beyer, T., Hagenlocher, C., Muller, C., Feistel, K., Schweickert, A., et al. (2015). ATP4a is required for development and function of the

Xenopus mucociliary epidermis - a potential model to study proton pump inhibitor-associated pneumonia. *Dev. Biol.* 408, 292–304. doi: 10.1016/j.ydbio.2015.03.013

Walentek, P., and Quigley, I. K. (2017). What we can learn from a tadpole about ciliopathies and airway diseases: using systems biology in *Xenopus* to study cilia and mucociliary epithelia. *Genesis* 55:e23001. doi: 10.1002/dvg.23001

Wang, F., Shi, Z., Cui, Y., Guo, X., Shi, Y. B., and Chen, Y. (2015). Targeted gene disruption in *Xenopus laevis* using CRISPR/Cas9. *Cell Biosci.* 5:15. doi: 10.1186/s13578-015-0006-1

Willis, J., DeStephanis, D., Patel, Y., Gowda, V., and Yan, S. (2012). Study of the DNA damage checkpoint using *Xenopus* egg extracts. *J. Vis. Exp.* 69:e4449. doi: 10.3791/4449

Yaoita, Y., Shi, Y. B., and Brown, D. D. (1990). *Xenopus laevis* alpha and beta thyroid hormone receptors. *Proc. Natl. Acad. Sci. U.S.A.* 87, 7090–7094. doi: 10.1073/pnas.87.18.7090

Yelin, R., Schyr, R. B., Kot, H., Zins, S., Frumkin, A., Pillemer, G., et al. (2005). Ethanol exposure affects gene expression in the embryonic organizer and reduces retinoic acid levels. *Dev. Biol.* 279, 193–204. doi: 10.1016/j.ydbio.2004.12.014

Conflict of Interest Statement: The authors declare that the research was conducted in the absence of any commercial or financial relationships that could be construed as a potential conflict of interest.

frontiers in Physiology

ORIGINAL RESEARCH
published: 05 March 2019
doi: 10.3389/fphys.2019.00155

Liver Specification in the Absence of Cardiac Differentiation Revealed by Differential Sensitivity to Wnt/β Catenin Pathway Activation

*Kim Haworth†, Lee Samuel†, Sarah Black, Pavel Kirilenko and Branko Latinkic**

School of Biosciences, Cardiff University, Cardiff, United Kingdom

OPEN ACCESS

Edited by:
John Noel Griffin, Duke University, United States

Reviewed by:
Adam John Watkins, University of Nottingham, United Kingdom
Florencia Del Viso, Stowers Institute for Medical Research, United States

***Correspondence:**
Branko Latinkic
latinkicb@cardiff.ac.uk

† These authors have contributed equally to this work

Specialty section:
This article was submitted to Embryonic and Developmental Physiology, a section of the journal Frontiers in Physiology

Received: *19 October 2018*
Accepted: *08 February 2019*
Published: *05 March 2019*

Citation:
Haworth K, Samuel L, Black S, Kirilenko P and Latinkic B (2019) Liver Specification in the Absence of Cardiac Differentiation Revealed by Differential Sensitivity to Wnt/β Catenin Pathway Activation. Front. Physiol. 10:155. doi: 10.3389/fphys.2019.00155

Embryonic precursors of liver and heart, whilst not sharing cellular origin, develop in close proximity through a dynamic series of inductive signaling events. During gastrulation anterior endoderm (AE) provides cardiogenic signals that act on adjacent mesoderm, resulting in induction of cardiac precursors. Subsequently cardiogenic mesoderm generates a FGF signal that acts on adjacent AE to induce foregut organ specification. Additional signals such as BMP and Wnt provide further information required for liver specification. Most findings on liver specification were derived from mouse explant studies as well as experiments with *Xenopus* and zebrafish embryos. To address some of the limitations of these models, here we used two complementary *ex vivo* models based on *Xenopus* embryos: pluripotent animal cap explants expressing Gata4 transcription factor and conjugates of gastrula-stage AE with animal caps (AC). We show that in these models liver specification is not sensitive to Wnt signaling manipulation, in contrast to the requirement for Wnt antagonism shown *in vivo*. FGF pathway is not necessary for Gata4-induced liver specification in animal cap explants but is required for prolonged period in sandwiches of AE and AC. In contrast, BMP signaling is shown to be essential for Gata4-induced liver specification. Our findings may have implications for research on liver differentiation from embryonic stem cells.

Keywords: Gata4, *Xenopus*, liver, heart, Wnt, FGF, BMP

INTRODUCTION

During embryonic development liver is induced in foregut endoderm by diverse and dynamic signaling from surrounding mesodermal tissue. Classical embryological experiments in the avian model have identified cardiac mesoderm as a source of an essential signal that specifies liver primordium induction and outgrowth from the adjacent gut tube (Zaret, 2008, 2016; Zorn and Wells, 2009). These findings were confirmed in the mouse explant system, which reconstitutes interactions between cardiogenic mesoderm and ventral endoderm (Gualdi et al., 1996). The mouse explant assay has been used to identify FGF signaling as a cardiac mesoderm-derived factor that induces liver-specific gene expression (Jung et al., 1999). Furthermore, BMP derived from the adjacent septum transversum mesenchyme was shown to be required together with FGF for liver

specification (Rossi et al., 2001). In addition to FGF and BMP signaling, the Wnt pathway has been implicated in liver specification (McLin et al., 2007; Gordillo et al., 2015; Zaret, 2016). The actions of these signaling pathways in early liver development are highly dynamic and dose-dependent.

The close relationship between embryonic liver and heart likely begins early in development, during gastrulation. Experimental evidence from chick and frog models have suggested that during gastrulation dorso-anterior endoderm, a tissue that will contribute to the liver formation, is required to induce cardiac tissue in adjacent mesoderm (Lough and Sugi, 2000). Later on, after hepatic specification, signals arising from developing liver bud appear to induce the formation of the proepicardium in the mesothelium in later cardiac development (Ishii et al., 2007). Therefore, the fates of developing heart and liver may be tied by several rounds of reciprocal signaling.

Liver-inducing signals regulate the transcriptional program in foregut endoderm via pioneer transcription factors FoxA and Gata4 which have the ability to associate with target genes in compacted heterochromatin (Zaret, 2016). Gata4 and Gata6 zinc-finger transcription factors have conserved roles in liver development in the mouse, zebrafish, and frog (Gordillo et al., 2015). In addition, Gata5 has been shown to regulate liver development in *Xenopus* (Haworth et al., 2008). The Gata4/5/6 family of transcription factors have well-documented roles in other tissues, notably the heart (Charron and Nemer, 1999).

Of relevance for the current study, Gata4, a hepatic pioneer transcription factor, has cardiogenic activity: gain of function of Gata4 alone, or together with other cardiac factors, can induce cardiogenesis in *Xenopus* and mouse embryos, respectively (Latinkic et al., 2003; Takeuchi and Bruneau, 2009). In pluripotent animal pole cells from *Xenopus* blastula embryos Gata4 induces not just cardiac cell fate, but also liver cell fate (Latinkic et al., 2003). This finding provides an experimentally amenable model of co-induction of cardiac and liver fates to study the mechanisms involved.

We have complemented the Gata4-based induction model with another *Xenopus* model developed for investigating the inductive capacity of anterior endoderm (AE) (Samuel and Latinkic, 2009). In this model, early gastrula anterior endoderm explants are conjugated with pluripotent responding tissue, blastula stage animal caps (AC). AC/AE conjugates were shown to recapitulate cardiogenic signaling between the source, AE, and the responder, AC (Samuel and Latinkic, 2009). Here we show that AC/AE closely mimic cellular and molecular interactions as they occur during liver induction as well. AE explants in isolation retain endodermal characteristics but fail to adopt liver fate, which can be induced if AE is conjugated with AC tissue. An AE-derived signal first induces cardiac precursors in AC, which appear to generate a signal that acts on AE to induce liver cell fate.

Using both the Gata4 and AC/AE models, we show that active Wnt signaling is compatible with hepatic specification despite the well-known inhibitory effect on cardiac differentiation. In addition, we show that Gata4 induces liver cell fate independently of FGF signaling but requires BMP signaling.

MATERIALS AND METHODS

Embryos and Explants

All work with *Xenopus laevis* (obtained from Nasco or raised in our facility) was approved by Cardiff University's Ethical Review Committee and was undertaken under a license from the United Kingdom Home Office. *Xenopus laevis* embryos were obtained by mating of frogs primed with human chorionic gonadotrophin (Sigma; 700 units per female and ∼150 units per male) or by *in vitro* fertilization (Sive et al., 2000). Jelly membrane was removed with 2% cysteine-HCl, ph7.8 (Sive et al., 2000). Embryos were grown in 10% Normal Amphibian Media (NAM) and staged as described (Sive et al., 2000). AC and AE explants were carried out in 75% NAM as described (Samuel and Latinkic, 2009). Typical samples had 12–20 AC/AE explants and 25–30 ACs. AC/AE experiments and gel RT-PCR analysis of AC experiments were repeated at least twice. Whole embryos (WE) or explants were cultured until age match control siblings had reached desired stage. Microinjections were carried using an IM 300 Micro-injector (Narishige Scientific), in 75% NAM containing 3% Ficoll (Sigma). Morpholino Oligonucleotides (MOs) were supplied from Gene Tools[1] and injected at 10 nl/embryo. *Cerberus* antisense morpholino oligomer (CerMO) (Kuroda et al., 2004), *hhex*MO (Smithers and Jones, 2002), and Control MO (Haworth et al., 2008) were injected as described (Haworth et al., 2008). 20 ng/embryo of Control MO was injected (**Supplementary Figure S5**). mMESSAGE mMACHINE kit (Ambion) was used for capped mRNA synthesis. Templates used have been previously described: Gata4 (Gallagher et al., 2012), Cerberus (Bouwmeester et al., 1996), *dkk-1* (Glinka et al., 1998), dominant-negative FGFR1 (XFD; Amaya et al., 1991), dominant-negative BMPR (tBR; Graff et al., 1994), LEF-β-GR (Domingos et al., 2001), *sox17* (Hudson et al., 1997), *hhex*-VP2 (Brickman et al., 2000), and CSKA-Wnt8 DNA (Smith and Harland, 1991) and were injected at 100 pg/embryo. Injection solutions included lineage tracers biotin- and rhodamine-dextran (Invitrogen; Latinkic et al., 2003). LEF-β-GR was induced by adding dexamethasone [DEX (Sigma); stored as 2 mM stock in ethanol] into embryonic media to a final concentration of 2 μM.

Drug Treatment

SU5402 (Calbiochem; Mohammadi et al., 1998) and Dorsomorphin (Sigma; Yu et al., 2008) were dissolved in DMSO and used at indicated concentrations.

Gene Expression Analyses

Total RNA was isolated from samples using TRIzol reagent (Invitrogen) or the acid guanidinium thiocyanate-phenol-chloroform method (Chomczynski and Sacchi, 1987). cDNA was synthesized using MMLTV or RevertAid (Thermo Fisher Scientific) according to manufacturer's instructions, using random hexamers. Approximately 1 μg of total RNA was used per sample. PCR was carried out using GoTaq polymerase (Promega, United Kingdom) according to manufacturer instruction. Primers were described (Samuel and Latinkic, 2009)

[1] http://www.gene-tools.com/

except for: *nkx2-1*F 5′-tctcaggccagtatgcaaca; *nkx2-1* R 5′-cacttgag cctgggagaga (34 cycles); *insulin* F 5′-tgggtctcacctggtagaagc; *insulin* R 5′-tgggcaacattgctccacaatcc (36 cycles); *amy2a* F: 5′-cgtg gcaagattgccgaatac; *amy2a* R 5′-ccattccatttgcggatgactc (36 cycles); *pdx1* F 5′-tgccattcccagatgacaacg; *pdx1* R 5′-ccttctctagttccagctg (35 cycles); *pdia2* F 5′-atttcaacaaggccctagagacc; *pdia2* R 5′-atcga tgtggcctgtttc (34 cycles); *fabp1* F 5′-accgagattgaacagaatgg; *fabp1* R 5′-cctccatgtttaccacggac (32 cycles) (AF068301); *fabp2* F 5′-tacccttgcacaaccctttg; *fabp2* R 5′-aatagatggcccgtcaggtc (32 cycles) (NM_001085877); *nr1h5* F 5′-agtgggaagatctggagca; *nr1h5* R 5′-tgcactgaacttcagtgagc (35 cycles). Quantitative PCR (Q-PCR) was performed on a Bio-Rad Mini Opticon MJ mini cycler using SYBR green fluorescent reagent. Samples were amplified in duplicate or triplicate and amplification of the endogenous reference gene *odc1* was performed in wells alongside target genes of interest. Primer pairs were described (Samuel and Latinkic, 2009) or were newly designed: *nr1h5* qF 5′-gagtatgcattactttcagcag; *nr1h5* qR 5′-tgttagacgtccaatcagtcga; *foxA2* qF 5′-gacacgaagctacagattggagc; *foxA2* qR 5′-ctcatgccc gtgttcacatagg; *sox17* qF 5′-gcagagcagatcacatccaa; *sox17* qR 5′-ttgtctgcagtaggcaccac. Ct values were determined and fold change relative to odc1 as described by Livak and Schmittgen (2001). Q-PCR data is shown in graphs with standard deviations and number of independent experiments (*n*) indicated. Repeated RT-PCR experiments showed that the data is semi-quantitative, providing good overall agreement with qPCR data (Samuel and Latinkic, 2009).

Double Whole Mount *in situ* Hybridization was performed as described (Sive et al., 2000; Haworth et al., 2008). Probes used were described: *myl7* (Chambers et al., 1994) and *nr1h5* (Seo et al., 2002).

Western blotting to detect exogenous (injected) Gata4 protein using HA tag was as described (Gallagher et al., 2012).

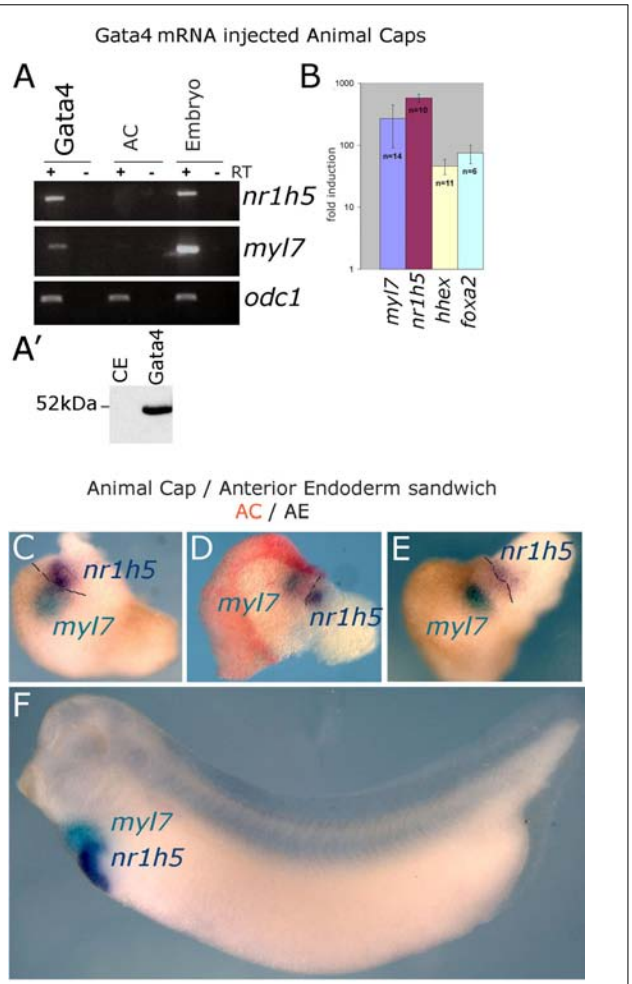

FIGURE 1 | Induction of hepatogenesis in Gata4-expressing AC explants and AC/AE conjugates. **(A,B)** Marker gene analysis in Gata4-expressing animal caps. **(A)** RT-PCR showing expression of cardiac fate marker *myl7*, liver fate marker *nr1h5* and control marker *odc1* in Gata4 mRNA-injected ACs, control ACs and stage 33 sibling control embryo. Representative of four independent experiments. **(A′)** Western blotting shows efficient translation of exogenous Gata4 protein. An equivalent of ½ embryo at st. 9 from a sample of five embryos has been loaded on the gel. **(B)** qPCR showing fold difference in expression between Gata4 treated animal caps and control animal caps grown to st. 33, induction of expression of *myl7*, *nr1h5*, *hhex* and marker of endoderm *foxa2* is shown. Number of independent experiments (*n*) and standard error of the mean are shown. **(C–E)** Cardiac and liver domains are adjacent in AC/AE conjugates and **(F)** age matched sibling controls. AC/AE conjugates (sandwiches) were cultured until sibling control embryos reached st. 34 and were processed for *myl7* expression (turquoise) and *nr1h5* (purple) by WMISH. AC-derived tissue is shown in pink/red. Three AC/AE examples are shown demonstrating adjacent expression domains of *myl7* in the AC-derived tissue and nr1h5 in the AE-derived component of the explant (12/12 specimens showed the same pattern). Dashed line highlights the border between AC and AE.

RESULTS

Induction of Hepatogenesis in Gata4-Expressing Animal Cap Explants and Animal Cap/Anterior Endoderm Conjugates

Expression of transcription factor Gata4 in animal cap explants from blastula stage embryos has been shown to lead to cardiac differentiation (Latinkic et al., 2003). In this model Gata4 does not act with exclusive cardiac specificity but also induces early endoderm markers as well as a liver marker *fabp1* (formerly known as *lfabp*). High level of liver-specific expression of *fabp1* appears in late tadpole stages, beyond the practical limit of culturing AC explants. We have re-examined liver induction in Gata4 mRNA-injected AC explants by using expression of a liver-specific early tadpole marker *nr1h5* (formerly known as *for1*), as well as liver-enriched markers *hhex* and *foxa2*. Our analyses demonstrate that Gata4 induces liver cell fate in AC explants, in addition to cardiac cell fate (**Figures 1A,B**).

Gata4 induces cardiac and liver cell fates in uniformly injected AC explants (Latinkic et al., 2003), suggesting that under conditions of gain of function of Gata4 in pluripotent AC explants, liver cell fate is induced cell-autonomously and that fate acquisition is stochastic. This activity of Gata4 is consistent with its well-known roles in liver specification *in vivo* (Gordillo et al., 2015; Zaret, 2016). We further explored the

question of cell autonomy of liver specification by endoderm specifiers and to that end we used Sox17, which in early vertebrate embryos is an exclusive endoderm determinant. Sox17 induces endoderm in AC explants, both when uniformly expressed and when expressed in half of each explant (Gallagher et al., 2014). Cardiac tissue is induced in hemi-injected explants only (**Supplementary Figure S1**; Gallagher et al., 2014). Similarly, liver marker *nr1h5* expression is induced only in hemi-injected *sox17* AC explants, strongly suggesting that liver cell fate is induced non-cell autonomously by a determinant of early endoderm (**Supplementary Figure S1**).

In addition to Gata4-triggered cardiogenesis in AC explants, we have developed a model that uses endogenous cardiogenic signal produced by the gastrula stage AE to induce cardiac cell fate in juxtaposed (conjugated) AC tissue (Samuel and Latinkic, 2009). AE explants express endodermal markers *a2m* and *sox17* as well as AE marker *hhex* (**Supplementary Figure S2**). During culturing period, AE explants retain endodermal characteristics (*a2m* and *sox17*) as well as *hhex* expression. Given that AE express *hhex*, which at tadpole stages marks both liver and endothelial cells, and that AC/AE conjugates contain endothelial cells (Samuel and Latinkic, 2009), the expression of *hhex* cannot be used to monitor liver specification in this model.

At tadpole stage (st. 34) AC/AE conjugates showed *nr1h5* expression in AE, adjacent to the domain of cardiomyocytes marked by *myl7*, in a manner resembling the close spatial relationship of the developing heart and liver in the embryo (**Figures 1C–F**). Upon prolonged culture until st. 43, the conjugates showed evidence of endodermal fate diversification, by expressing liver (*fabp1*), intestine (*fabp2*), pancreas (*pdia2* and *pdx1*), and lung/thyroid (*nkx2-1*) markers (**Figure 2**). Despite expressing *pdia2* and *pdx1*, AC/AE conjugates did not express *insulin* or *amy2a*, suggesting incomplete pancreatic reprogramming. As previously shown (Samuel and Latinkic, 2009), AC/AE expressed cardiac ventricular marker *myl3* as well.

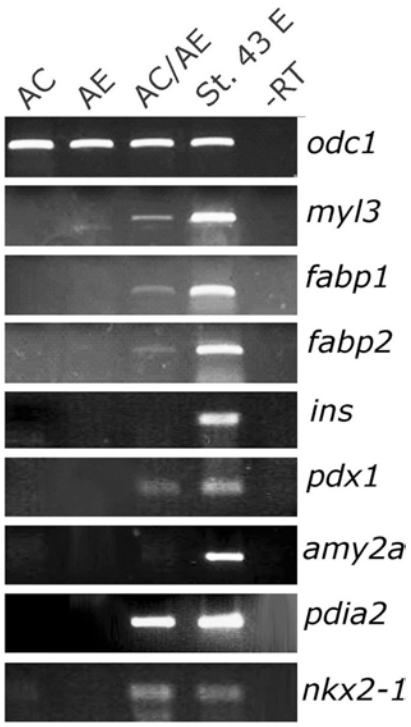

FIGURE 2 | Endoderm diversification in AC/AE conjugates. Examination of gene expression in st. 43 AC/AE explants by RT-PCR reveals expression of liver (*fabp1*), intestine (*fabp2*), pancreas (*pdia2* and *pdx1*, but not *ins* and *amy2a*), thyroid/lung (*nkx2-1*) as well as ventricular cardiomyocyte (*myl3*) markers. St. 43 E-sibling control embryo at st. 43.

Cerberus and *hhex* Are Required in Anterior Endoderm for Liver and Cardiac Specification

Cerberus (*cer1*) and *hhex* have both been shown to be required for normal development of the anterior end of the embryonic axis and for cardiac and AE specification (Brickman et al., 2000; Martinez Barbera et al., 2000; Foley and Mercola, 2005; Foley et al., 2007). We took advantage of the AC/AE model to specifically downregulate *hhex* or *cer1* in AC (**Figure 3A**) or AE (**Figure 3B**) using previously described MOs against *cer1* (Kuroda et al., 2004) and *hhex* (Smithers and Jones, 2002). We have confirmed effectiveness of *cer1*MO and *hhex*MO by showing that they affect heart development (**Supplementary Figure S5**). Our results demonstrate that both *hhex* and *cer1* are specifically required in AE for cardiac and liver specification, in agreement with previous work (Foley and Mercola, 2005; Foley et al., 2007). Interference with Hhex function in AE by using dominant-negative construct HhexVP2 (Brickman et al., 2000) produced the same result as *hhex*MO (**Figure 3B**). Additional experiments have shown that *cer1* deficiency in the AE can be rescued by expression of *cer1* mRNA in AC, in a strict dose-dependent manner (**Figure 3C**).

Differential Effect of Wnt/β Catenin Signaling Activation on Cardiac and Liver Specification

Wnt pathway activation has a well-documented attenuating effect on cardiac differentiation *in vivo*, in embryonic stem (ES) cell differentiation model and in Gata4-expressing AC from *Xenopus* embryos (Marvin et al., 2001; Schneider and Mercola, 2001; Tzahor and Lassar, 2001; Latinkic et al., 2003; Naito et al., 2006; Liu et al., 2007; Ueno et al., 2007). We have activated Wnt signaling in control animal cap explants or in those expressing Gata4 by zygotic co-expression of Wnt8. Wnt8 had no effect on its own on cardiac or liver markers but it attenuated cardiogenesis induced by Gata4 (**Figures 4A,B**; Latinkic et al., 2003). At the same time, the expression of the liver marker *nr1h5* was unaffected (**Figures 4A,B**).

We have previously shown that activation of Wnt signaling opposes cardiac differentiation but not specification in AC/AE conjugates (Samuel and Latinkic, 2009). Using the same experimental approach, we have activated Wnt/β-catenin

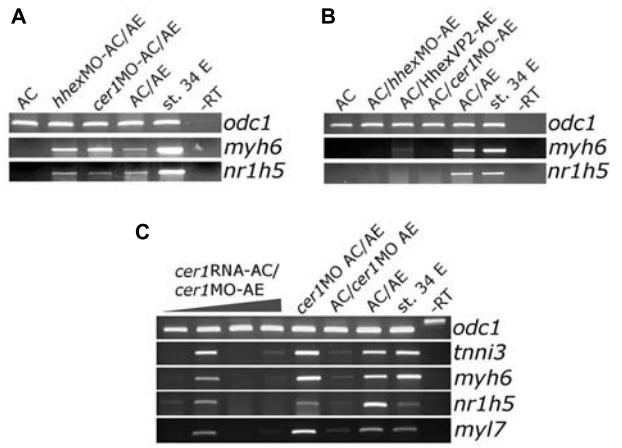

FIGURE 3 | Cerberus and *hhex* are required in anterior endoderm for liver and cardiac specification. **(A)** Injection of *cer1* or *hhex* MOs (10 or 20 ng/embryo, respectively) in AC have no effect on heart and liver marker expression in AC/AE conjugates. This is in contrast to **(B)**, where injection of *cer1* or *hhex* MOs in AE leads to downregulation of both cardiac and liver marker gene mRNA levels in conjugates. Injection of mRNA (500 pg/embryo) coding for dominant negative Hhex-VP2 construct had the same effect as *hhex* MO. **(C)** Cardiac and liver specification deficiency in AC/*cer1* MO-AE conjugates can be rescued by Cerberus. *cer1* mRNA was injected in AC at increasing concentrations, from left to right; 100, 200, 500, and 1000 pg per embryo. All samples were cultured until stage control had reached stage 34 where PCR was carried out for indicated markers.

signaling in AC/AE at different time points, either uniformly by LiCl (**Figure 4C**) or specifically in AC or AE by activation of an inducible chimaeric construct Lef-β-catenin-GR (LEF-β-GR, **Figures 4D,E**). Brief LiCl treatment causes a strong but transient activation of Wnt target genes *siamois* (*sia*) and *nodal3.1*, whose expression is undetectable 6 h after treatment, whereas activation of Lef-β-catenin-GR leads to a milder but sustained response (Samuel and Latinkic, 2009). Our results show that treatment with LiCl at an early time point, near the time of cardiac specification (st. 9) has no effect on either cardiac or liver specification, whereas treatment at the late neurula stage (st. 21) abolishes cardiac but not liver marker expression. Similarly, activation of Wnt signaling using Lef-β-catenin-GR in AC but not in AE affects cardiac but not liver markers.

Antagonism of Wnt signaling is required for cardiac differentiation and has been shown to promote specification of AE-derived liver. In Gata4-expressing AC explants, antagonism of Wnt by secreted antagonist Dkk-1 has been shown to enhance cardiogenesis (Latinkic et al., 2003). At the same time, *nr1h5* expression is unaffected (**Figures 5A,B**). In AC/AE explants Dkk-1 does not affect cardio- and hepatogenesis (**Figure 5C**). Wnt was suggested to be required for liver bud outgrowth, suggesting that the AC/AE model does not capture those later stages of liver development.

BMP Signaling Inhibition Attenuates Liver Cell Fate Specification

BMP signaling has been shown to be required for liver specification in a wide range of models (Gordillo et al., 2015). In agreement with this we show that cell autonomous inhibition of BMP signaling using truncated BMP receptor (BMPRI) targeted to foregut interferes with liver development in tadpoles (**Figures 6A–F**). We next wished to test the dependence of liver

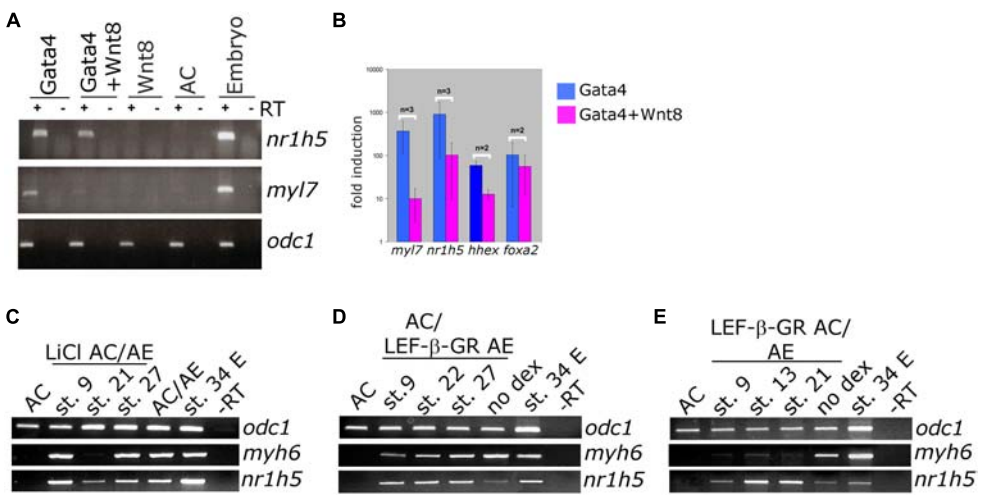

FIGURE 4 | Differential effect of Wnt/beta catenin signaling activation on cardiac and liver cell fate. **(A)** Animal caps co-injected with Gata4 mRNA and Wnt8-expressing DNA show marked reduction of *myl7* RNA levels and negligible effect on *nr1h5* expression. **(B)** qPCR analysis confirms the findings of gel RT-PCR for *myl7* and *nr1h5* and in addition shows the reduction of *hhex* expression in Gata4 + Wnt8 samples. **(C)** AC/AE conjugates were treated with LiCl at indicated stages. Treatment at st. 21 blocked cardiac differentiation but had a lesser effect on liver specification. **(D)** Cell autonomous activation of Wnt/β-catenin signaling in LEF-β-GR mRNA-injected AE was achieved by adding dexamethasone (dex) to AC/AE conjugates at indicated stages. No effect on either heart or liver marker expression was observed. **(E)** In contrast, activation of LEF-β-GR in the AC part of the conjugates greatly reduced *myh6* expression without affecting *nr1h5*. Explants were collected for RT-PCR analysis when sibling embryo controls reached st. 34.

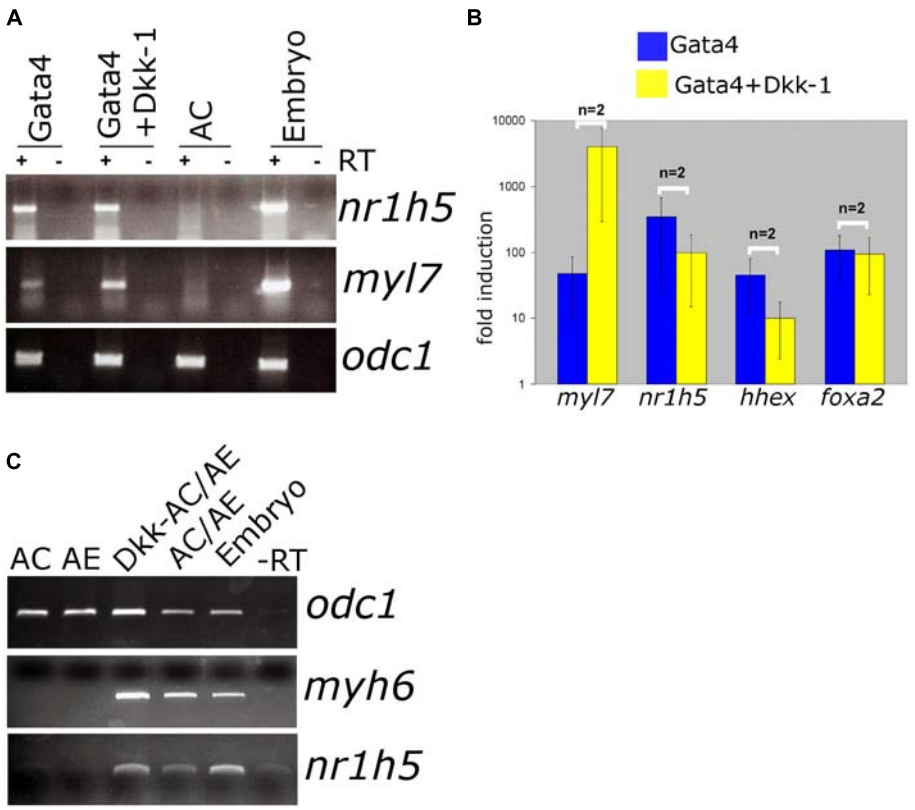

FIGURE 5 | Wnt/β-catenin signaling is not required for liver specification in Gata4-AC and AC/AE. **(A)** Gata4 and *dkk-1* mRNA co-injection in animal pole explants causes a well-described increase in cardiac marker levels but has no effect on *nr1h5*. **(B)** qPCR analysis confirms these findings and extends them by showing no significant effect on *hhex* and *foxa2*. **(C)** *dkk-1* expression in AC/AE (injected in AC) likewise has no effect on *nr1h5*. RT-PCR analyses were performed on st. 34 explants and sibling embryo controls.

specification on BMP signaling in Gata4-induced hepatogenesis. Cardiogenesis induced by Gata4 in AC explants does not require BMP signaling (Latinkic et al., 2003; **Figure 6G**), however, inhibition of BMP signaling using truncated BMP receptor or a small molecule inhibitor Dorsomorphin lead to a decrease in expression of *nr1h5* at st. 34 and *hhex* at st. 10 (**Figures 6G,H**). These results suggest that BMP signaling is required for hepatic, but not cardiac, induction by Gata4 in pluripotent AC explants.

FGF Signaling Is Not Required for Gata4-Mediated Liver Specification

FGF signaling has a well-documented role in liver specification (Zaret, 2016). We have next examined the involvement of FGF signaling in liver specification in Gata4-expressing AC explants. Downregulation of the FGF pathway using dominant-negative FGFR1 (XFD; **Figures 7A,B**) or small drug SU5402 (**Supplementary Figure S3**) has no effect on both liver and cardiac specification, suggesting that the FGF pathway is not required in Gata4-induced liver cell fate specification in AC explants. Effectiveness of SU5402 and XFD was shown by their ability to inhibit expression of early mesodermal marker and FGF target *tbxt* (formerly *xbra*; **Figure 7D**) and by induction of characteristic gastrulation defect phenotype (**Supplementary Figure S4**). In AC/AE explants, the FGF pathway is required for cardiogenesis immediately following formation of conjugates (Samuel and Latinkic, 2009; **Figure 7C**). Not surprisingly, under these conditions liver specification is also affected. In contrast, inhibition of the FGF pathway from st. 13 until the end of culturing period at st. 34 had no effect on cardiac differentiation but attenuated *nr1h5* expression (**Figure 7C**). Shorter treatment time windows (st. 16–23, 23–28, 28–34) had no major effect on cardiac and liver cell fate specification (**Figure 7C**).

DISCUSSION

In this report we have used two experimental models based on *Xenopus* embryos that permit induction of liver and cardiac fates, to investigate their specific signaling requirements.

The simpler of the models is based on Gata4-mediated induction of liver specification in pluripotent animal cap explants. In this model, when Gata4 mRNA is expressed throughout the explant, both cardiac and liver cell fates are induced, suggesting that fate acquisition is stochastic under conditions when Gata4 is most likely acting cell-autonomously. In comparison, a bona fide endoderm determinant Sox17 induces

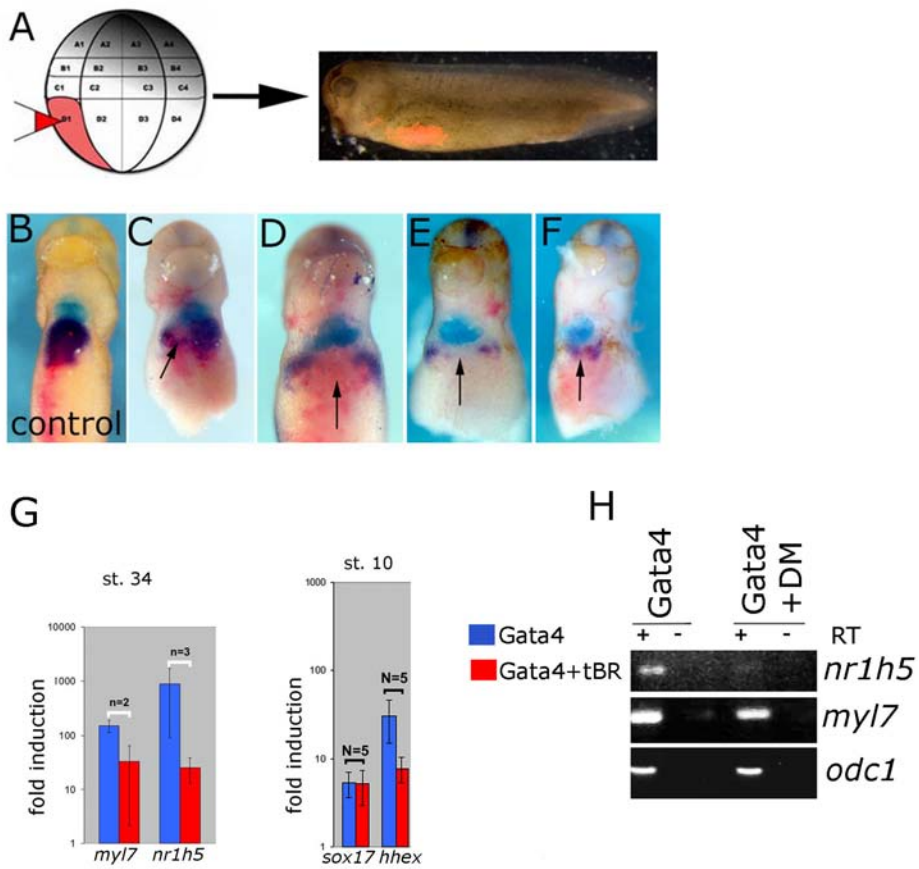

FIGURE 6 | BMP signaling is required for liver development. **(A)** Design of the experiment. Lineage tracer was injected **(B)** alone or **(C–F)** with ∼30 pg/blastomere of truncated BMP Receptor (tBR) mRNA in dorso-vegetal blastomere D1 at the 32-cell stage. Heart and liver were revealed by double WMISH of *myl7* (turquoise) and *nr1h5* (purple). **(C–F)** four examples showing attenuation of liver fate specification *in vivo* following localized BMP inhibition by tBR (red-pink; pointed by arrows). $N = 11$, all showing effect on *nr1h5* expression. Ventral views are shown, anterior is up. BMP signaling inhibition attenuates liver cell fate specification in Gata4 injected AC. **(G)** qPCR analyses of st. 34 explants show downregulation of *nr1h5* as a consequence of BMP inhibition via tBR. At st. 10, tBR has no effect on the ability of Gata4 to induce *sox17* but reduces *hhex* induction. **(H)** Treatment of Gata4-expressing AC explants with 30 μM dorsomorphin (DM) leads to downregulation of *nr1h5*.

liver gene expression in animal pole explants only non-cell autonomously. It would be of interest to further explore cell autonomous mode of Gata4 action in liver specification in animal cap explants.

The second model used in the current study is based on heterochronic conjugates of gastrula-stage AE and blastula-stage animal cap explants. In these AC/AE conjugates AE induces cardiac specification in the overlaying animal cap ectoderm (Samuel and Latinkic, 2009), and in this study we have shown that AC/AE conjugates also express a range of endoderm markers. The liver tissue in conjugates is induced in the endoderm, adjacent to the cardiac domain which has been induced in the animal cap explant (**Figure 1**). This configuration closely resembles the spatial relationship of the heart and the liver in the early embryo and suggests that AC/AE conjugates recapitulate many aspects of cellular and molecular interactions that govern cardiac and liver specification in the embryo. In addition to the liver markers, AC/AE conjugates expressed a marker of lung and thyroid, *nkx2-1*, as well as subset of pancreatic markers-*pdia2* and *pdx1*, but not *ins*, suggesting that partial reprogramming toward endocrine pancreas has been achieved by st. 43.

We have used the AC/AE model to examine the roles of *hhex* and *cer1* in AC or AE. As expected (Foley and Mercola, 2005), *hhex* was found to be required in the AE for cardiac as well as for liver specification (**Figure 3**). Similarly, *cer1* is required in the AE (**Figure 3**), in agreement with the findings by Foley et al. (2007). The deficiency of *cer1* in AE can be rescued by injection of cer1 mRNA in the AC, but only in a narrow concentration range, suggesting that the pathways regulated by the Cerberus protein, BMP, Wnt, and Nodal (Piccolo et al., 1999), operate at a finely tuned level. In future it would be of interest to use AC/AE conjugates to dissect the requirement of each of these pathways, for example by asking whether and when Cerberus function could be replaced by small molecule inhibitors of Wnt, BMP and Nodal pathways, as well as to examine epistatic relationship between *hhex* and *cer1*.

Wnt pathway activation interferes with cardiogenesis both in Gata4-expressing animal cap explants and in AC/AE conjugates

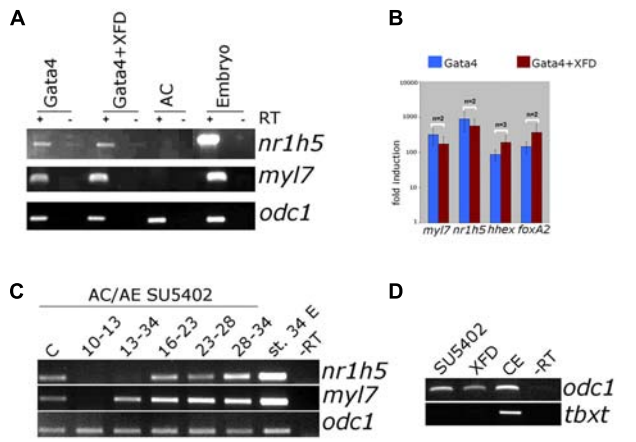

FIGURE 7 | FGF signaling is not required for liver specification by Gata4 but is essential in AC/AE explants. **(A)** Gata4 and XFD (dominant-negative FGFR1) mRNA co-expression in animal pole explants has no effect on *nr1h5* and *myl7* expression. **(B)** qPCR analysis confirms these findings and extends them by showing no significant effect on *hhex* and *foxa2*. **(C)** Treatment of AC/AE with FGFR inhibitor SU5402 (50 μM) has stage-specific effect. Immediately upon AC/AE conjugate formation, SU5402 inhibits cardiac and liver gene expression. Treatment from st. 13 until the end of incubation at st. 34 has no effect on cardiogenesis but inhibits liver specification. Shorter time windows of treatment are largely without effect. Staging is according to the stage of AE (st. 10 at the time of conjugation). C-Control explants treated with 50 μM DMSO. **(D)** SU5402 and XFD are effective inhibitors of early mesodermal marker and FGF target gene *tbxt*. CE-control (untreated) sibling embryos. RT-PCR analyses were performed on st. 34 explants and sibling embryo controls.

(Latinkic et al., 2003; Samuel and Latinkic, 2009), but it does not significantly affect liver specification in both models (**Figure 4**). In Gata4-expressing AC explants liver specification is apparently independent of the presence of differentiated cardiomyocytes. One possibility is that inductive signaling between cardiac mesoderm and endoderm in this model occurs prior to cardiac differentiation and the second one is that liver cell fate is induced cell autonomously by Gata4.

We have previously shown that expression of cardiac precursor markers *nkx2-5* and *tbx5* is not affected by Wnt activation in AC/AE conjugates, suggesting that cardiac precursors transiently produce a liver-inducing signal. Under the conditions of Wnt pathway activation cardiac precursor are prevented to undergo differentiation into cardiomyocytes, showing that the production of the liver-inducing signal does not require cardiomyocytes and that the liver-inducing signals are likely transiently produced by cardiac progenitors.

Several studies have shown that Wnt antagonism is required for liver specification (Zorn and Wells, 2009; Zaret, 2016). Most relevant for the current study is the work by McLin et al. (2007) who have shown that Wnt antagonizes foregut development in *Xenopus* embryos. The apparent discrepancy between the two studies is likely due to the differences between the models that were used, *in vivo* by McLin et al. and explants in the current study. In animal cap explants Gata4 might be acting in parallel to or downstream of *hhex* in specifying liver, as *hhex* has been shown to be downstream of Wnt antagonism (Foley and Mercola, 2005).

Our results have suggested that BMP signaling is required for liver specification downstream of Gata4. It will be of interest to examine in more detail how and when BMP antagonism interferes with Gata4-induced hepatogenesis. In addition we have found that BMP signaling is required for liver specification *in vivo*, as previously reported (Zorn and Wells, 2009; Zaret, 2016).

Unlike BMP inhibition, interference with FGF signaling was found to have no effect on Gata4-driven liver cell fate specification in animal cap explants (**Figure 7** and **Supplementary Figure S3**). In contrast, liver specification in AC/AE explants shows requirement for prolonged FGF signaling (st. 13–34), but shorter treatment windows during neurula and tailbud stages show no effect (**Figure 7**). This finding suggests that FGF signaling is required for liver specification over a prolonged period rather than within a discrete, well-defined time window. Early FGF inhibition immediately after conjugation of AC/AE explants inhibits cardiogenesis and this likely leads to an inhibition of liver specification as well.

Our results with AC/AE explant conjugates are in good overall agreement with those of Shifley et al. (2012) who reported that prolonged FGF signaling is required for liver specification in *Xenopus* embryos. Taken together with the results with manipulation of Wnt signaling, our findings suggest that cardiac precursors produce a liver specifying signal, most likely an FGF, which is required over a prolonged period to specify liver fate.

The principles of liver specification and differentiation that were established in various vertebrate embryos have been and are the key to the development and refinement of protocols for liver cell differentiation from pluripotent stem cells. This is an area of intense research due to potential medical applications and our findings may inform future attempts at refinement of differentiation protocols.

AUTHOR CONTRIBUTIONS

KH performed most of the animal cap experiments. LS performed most of the AC/AE conjugate experiments. SB and PK contributed to analysis of several experiments. BL contributed to experimental manipulation of embryos, planned the study, and wrote the manuscript.

FUNDING

This work was supported in part by project grants from Biotechnology and Biological Sciences Research Council grant BB/C517368 and British Heart Foundation (BHF) and Ph.D. studentships from BHF and Medical Research Council.

SUPPLEMENTARY MATERIAL

The Supplementary Material for this article can be found online at: https://www.frontiersin.org/articles/10.3389/fphys.2019.00155/full#supplementary-material

REFERENCES

Amaya, E., Musci, T. J., and Kirschner, M. W. (1991). Expression of a dominant negative mutant of the FGF receptor disrupts mesoderm formation in *Xenopus* embryos. *Cell* 66, 257–270. doi: 10.1016/0092-8674(91)90616-7

Bouwmeester, T., Kim, S., Sasai, Y., Lu, B., and De Robertis, E. M. (1996). Cerberus is a head-inducing secreted factor expressed in the anterior endoderm of Spemann's organizer. *Nature* 382, 595–601. doi: 10.1038/382595a0

Brickman, J. M., Jones, C. M., Clements, M., Smith, J. C., and Beddington, R. S. (2000). Hex is a transcriptional repressor that contributes to anterior identity and suppresses Spemann organiser function. *Development* 127, 2303–2315.

Chambers, A. E., Logan, M., Kotecha, S., Towers, N., Sparrow, D., and Mohun, T. J. (1994). The RSRF/MEF2 protein SL1 regulates cardiac muscle-specific transcription of a myosin light-chain gene in *Xenopus* embryos. *Genes Dev.* 8, 1324–1334. doi: 10.1101/gad.8.11.1324

Charron, F., and Nemer, M. (1999). GATA transcription factors and cardiac development. *Semin. Cell Dev. Biol.* 10, 85–91. doi: 10.1006/scdb.1998.0281

Chomczynski, P., and Sacchi, N. (1987). Single-step method of RNA isolation by acid guanidinium thiocyanate-phenol-chloroform extraction. *Anal. Biochem.* 162, 156–159. doi: 10.1016/0003-2697(87)90021-2

Domingos, P. M., Itasaki, N., Jones, C. M., Mercurio, S., Sargent, M. G., Smith, J. C., et al. (2001). The Wnt/beta-catenin pathway posteriorizes neural tissue in Xenopus by an indirect mechanism requiring FGF signalling. *Dev. Biol.* 239, 148–160. doi: 10.1006/dbio.2001.0431

Foley, A. C., Korol, O., Timmer, A. M., and Mercola, M. (2007). Multiple functions of Cerberus cooperate to induce heart downstream of Nodal. *Dev. Biol.* 303, 57–65. doi: 10.1016/j.ydbio.2006.10.033

Foley, A. C., and Mercola, M. (2005). Heart induction by Wnt antagonists depends on the homeodomain transcription factor Hex. *Genes Dev.* 19, 387–396. doi: 10.1101/gad.1279405

Gallagher, J. M., Komati, H., Roy, E., Nemer, M., and Latinkic, B. V. (2012). Dissociation of cardiogenic and postnatal myocardial activities of GATA4. *Mol. Cell. Biol.* 32, 2214–2223. doi: 10.1128/MCB.00218-12

Gallagher, J. M., Yamak, A., Kirilenko, P., Black, S., Bochtler, M., Lefebvre, C., et al. (2014). Carboxy terminus of GATA4 transcription factor is required for its cardiogenic activity and interaction with CDK4. *Mech. Dev.* 134, 31–41. doi: 10.1016/j.mod.2014.09.001

Glinka, A., Wu, W., Delius, H., Monaghan, A. P., Blumenstock, C., and Niehrs, C. (1998). Dickkopf-1 is a member of a new family of secreted proteins and functions in head induction. *Nature* 391, 357–362. doi: 10.1038/34848

Gordillo, M., Evans, T., and Gouon-Evans, V. (2015). Orchestrating liver development. *Development* 142, 2094–2108. doi: 10.1242/dev.114215

Graff, J. M., Thies, R. S., Song, J. J., Celeste, A. J., and Melton, D. A. (1994). Studies with a *Xenopus* BMP receptor suggest that ventral mesoderm-inducing signals override dorsal signals in vivo. *Cell* 79, 169–179. doi: 10.1016/0092-8674(94)90409-X

Gualdi, R., Bossard, P., Zheng, M., Hamada, Y., Coleman, J. R., and Zaret, K. S. (1996). Hepatic specification of the gut endoderm in vitro: cell signaling and transcriptional control. *Genes Dev.* 10, 1670–1682. doi: 10.1101/gad.10.13.1670

Haworth, K. E., Kotecha, S., Mohun, T. J., and Latinkic, B. V. (2008). GATA4 and GATA5 are essential for heart and liver development in Xenopus embryos. *BMC Dev. Biol.* 8:74. doi: 10.1186/1471-213X-8-74

Hudson, C., Clements, D., Friday, R. V., Stott, D., and Woodland, H. R. (1997). Xsox17alpha and -beta mediate endoderm formation in *Xenopus*. *Cell* 91, 397–405. doi: 10.1016/S0092-8674(00)80423-7

Ishii, Y., Langberg, J. D., Hurtado, R., Lee, S., and Mikawa, T. (2007). Induction of proepicardial marker gene expression by the liver bud. *Development* 134, 3627–3637. doi: 10.1242/dev.005280

Jung, J., Zheng, M., Goldfarb, M., and Zaret, K. S. (1999). Initiation of mammalian liver development from endoderm by fibroblast growth factors. *Science* 284, 1998–2003. doi: 10.1126/science.284.5422.1998

Kuroda, H., Wessely, O., and De Robertis, E. M. (2004). Neural induction in *Xenopus*: requirement for ectodermal and endomesodermal signals via Chordin, Noggin, beta-Catenin, and Cerberus. *PLoS Biol.* 2:E92. doi: 10.1371/journal.pbio.0020092

Latinkic, B. V., Kotecha, S., and Mohun, T. J. (2003). Induction of cardiomyocytes by GATA4 in Xenopus ectodermal explants. *Development* 130, 3865–3876. doi: 10.1242/dev.00599

Liu, Y., Asakura, M., Inoue, H., Nakamura, T., Sano, M., Niu, Z., et al. (2007). Sox17 is essential for the specification of cardiac mesoderm in embryonic stem cells. *Proc. Natl. Acad. Sci. U.S.A.* 104, 3859–3864. doi: 10.1073/pnas.0609100104

Livak, K. J., and Schmittgen, T. D. (2001). Analysis of relative gene expression data using real-time quantitative PCR and the 2(-Delta Delta C(T)) Method. *Methods* 25, 402–408. doi: 10.1006/meth.2001.1262

Lough, J., and Sugi, Y. (2000). Endoderm and heart development. *Dev. Dyn.* 217, 327–342. doi: 10.1002/(SICI)1097-0177(200004)217:4<327::AID-DVDY1>3.0.CO;2-K

Martinez Barbera, J. P., Clements, M., Thomas, P., Rodriguez, T., Meloy, D., Kioussis, D., et al. (2000). The homeobox gene Hex is required in definitive endodermal tissues for normal forebrain, liver and thyroid formation. *Development* 127, 2433–2445.

Marvin, M. J., Di Rocco, G., Gardiner, A., Bush, S. M., and Lassar, A. B. (2001). Inhibition of Wnt activity induces heart formation from posterior mesoderm. *Genes Dev.* 15, 316–327. doi: 10.1101/gad.855501

McLin, V. A., Rankin, S. A., and Zorn, A. M. (2007). Repression of Wnt/beta-catenin signaling in the anterior endoderm is essential for liver and pancreas development. *Development* 134, 2207–2217. doi: 10.1242/dev.001230

Mohammadi, M., Froum, S., Hamby, J. M., Schroeder, M. C., Panek, R. L., Lu, G. H., et al. (1998). Crystal structure of an angiogenesis inhibitor bound to the FGF receptor tyrosine kinase domain. *EMBO J.* 17, 5896–5904. doi: 10.1093/emboj/17.20.5896

Naito, A. T., Shiojima, I., Akazawa, H., Hidaka, K., Morisaki, T., Kikuchi, A., et al. (2006). Developmental stage-specific biphasic roles of Wnt/beta-catenin signaling in cardiomyogenesis and hematopoiesis. *Proc. Natl. Acad. Sci. U.S.A.* 103, 19812–19817. doi: 10.1073/pnas.0605768103

Piccolo, S., Agius, E., Leyns, L., Bhattacharyya, S., Grunz, H., Bouwmeester, T., et al. (1999). The head inducer Cerberus is a multifunctional antagonist of Nodal, BMP and Wnt signals. *Nature* 397, 707–710. doi: 10.1038/17820

Rossi, J. M., Dunn, N. R., Hogan, B. L., and Zaret, K. S. (2001). Distinct mesodermal signals, including BMPs from the septum transversum mesenchyme, are required in combination for hepatogenesis from the endoderm. *Genes Dev.* 15, 1998–2009. doi: 10.1101/gad.904601

Samuel, L. J., and Latinkic, B. V. (2009). Early activation of FGF and nodal pathways mediates cardiac specification independently of Wnt/beta-catenin signaling. *PLoS One* 4:e7650. doi: 10.1371/journal.pone.0007650

Schneider, V. A., and Mercola, M. (2001). Wnt antagonism initiates cardiogenesis in *Xenopus laevis*. *Genes Dev.* 15, 304–315. doi: 10.1101/gad.855601

Seo, Y. W., Sanyal, S., Kim, H. J., Won, D. H., An, J. Y., Amano, T., et al. (2002). FOR, a novel orphan nuclear receptor related to farnesoid X receptor. *J. Biol. Chem.* 277, 17836–17844. doi: 10.1074/jbc.M111795200

Shifley, E. T., Kenny, A. P., Rankin, S. A., and Zorn, A. M. (2012). Prolonged FGF signaling is necessary for lung and liver induction in Xenopus. *BMC Dev. Biol.* 12:27. doi: 10.1186/1471-213X-12-27

Sive, H. L., Grainger, R. M., and Harland, R. M. (eds) (2000). *Early Development of Xenopus laevis: A Laboratory Manual*. New York, NY: Cold Spring Harbor Laboratory Press.

Smith, W. C., and Harland, R. M. (1991). Injected Xwnt-8 RNA acts early in *Xenopus* embryos to promote formation of a vegetal dorsalizing center. *Cell* 67, 753–765. doi: 10.1016/0092-8674(91)90070-F

Smithers, L. E., and Jones, C. M. (2002). Xhex-expressing endodermal tissues are essential for anterior patterning in *Xenopus*. *Mech. Dev.* 119, 191–200. doi: 10.1016/S0925-4773(02)00361-1

Takeuchi, J. K., and Bruneau, B. G. (2009). Directed transdifferentiation of mouse mesoderm to heart tissue by defined factors. *Nature* 459, 708–711. doi: 10.1038/nature08039

Tzahor, E., and Lassar, A. B. (2001). Wnt signals from the neural tube block ectopic cardiogenesis. *Genes Dev.* 15, 255–260. doi: 10.1101/gad.871501

Ueno, S., Weidinger, G., Osugi, T., Kohn, A. D., Golob, J. L., Pabon, L., et al. (2007). Biphasic role for Wnt/beta-catenin signaling in cardiac specification in zebrafish and embryonic stem cells. *Proc. Natl. Acad. Sci. U.S.A.* 104, 9685–9690. doi: 10.1073/pnas.0702859104

Yu, P. B., Hong, C. C., Sachidanandan, C., Babitt, J. L., Deng, D. Y., Hoyng, S. A., et al. (2008). Dorsomorphin inhibits BMP signals required for embryogenesis and iron metabolism. *Nat. Chem. Biol.* 4, 33–41. doi: 10.1038/nchembio.2007.54

Zaret, K. S. (2008). Genetic programming of liver and pancreas progenitors: lessons for stem-cell differentiation. *Nat. Rev. Genet.* 9, 329–340. doi: 10.1038/nrg2318

Zaret, K. S. (2016). From endoderm to liver bud: paradigms of cell type specification and tissue morphogenesis. *Curr. Top. Dev. Biol.* 117, 647–669. doi: 10.1016/bs.ctdb.2015.12.015

Zorn, A. M., and Wells, J. M. (2009). Vertebrate endoderm development and organ formation. *Annu. Rev. Cell Dev. Biol.* 25, 221–251. doi: 10.1146/annurev.cellbio.042308.113344

Conflict of Interest Statement: The authors declare that the research was conducted in the absence of any commercial or financial relationships that could be construed as a potential conflict of interest.

frontiers in Physiology

ORIGINAL RESEARCH
published: 08 April 2019
doi: 10.3389/fphys.2019.00388

A YWHAZ Variant Associated With Cardiofaciocutaneous Syndrome Activates the RAF-ERK Pathway

Ivan K. Popov[1], Susan M. Hiatt[2], Sandra Whalen[3], Boris Keren[3], Claudia Ruivenkamp[4], Arie van Haeringen[4], Mei-Jan Chen[5], Gregory M. Cooper[2], Bruce R. Korf[5] and Chenbei Chang[1]**

[1] Department of Cell, Developmental and Integrative Biology, The University of Alabama at Birmingham, Birmingham, AL, United States, [2] HudsonAlpha Institute for Biotechnology, Huntsville, AL, United States, [3] UF de Génétique Clinique, Hôpital Armand Trousseau, Assistance Publique Hôpitaux de Paris, Centre de Référence Maladies Rares des Anomalies du Développement et Syndromes Malformatifs, Paris, France, [4] Department of Clinical Genetics, Leiden University Medical Center, Leiden, Netherlands, [5] Department of Genetics, The University of Alabama at Birmingham, Birmingham, AL, United States

OPEN ACCESS

Edited by:
Emily Sempou,
Yale University, United States

Reviewed by:
Dominique Alfandari,
University of Massachusetts Amherst, United States
Shuyi Nie,
Georgia Institute of Technology, United States

***Correspondence:**
Susan M. Hiatt
shiatt@hudsonalpha.org
Chenbei Chang
cchang@uab.edu

Specialty section:
This article was submitted to Embryonic and Developmental Physiology, a section of the journal Frontiers in Physiology

Received: *15 January 2019*
Accepted: *21 March 2019*
Published: *08 April 2019*

Citation:
Popov IK, Hiatt SM, Whalen S, Keren B, Ruivenkamp C, van Haeringen A, Chen M-J, Cooper GM, Korf BR and Chang C (2019) A YWHAZ Variant Associated With Cardiofaciocutaneous Syndrome Activates the RAF-ERK Pathway. Front. Physiol. 10:388. doi: 10.3389/fphys.2019.00388

Cardiofaciocutaneous (CFC) syndrome is a genetic disorder characterized by distinctive facial features, congenital heart defects, and skin abnormalities. Several germline gain-of-function mutations in the RAS/RAF/MEK/ERK pathway are associated with the disease, including *KRAS*, *BRAF*, *MEK1,* and *MEK2*. CFC syndrome thus belongs to a group of disorders known as RASopathies, which are all caused by pathogenic mutations in various genes encoding components of the RAS pathway. We recently identified novel variants in *YWHAZ*, a 14-3-3 family member, in individuals with a phenotype consistent with CFC that may potentially be deleterious and disease-causing. In the current study, we take advantage of the vertebrate model *Xenopus laevis* to analyze the functional consequence of a particular *YWHAZ* variant, S230W, and investigate the molecular mechanisms underlying its activity. We show that compared with wild type *YWHAZ*, the S230W variant induces severe embryonic defects when ectopically expressed in early *Xenopus* embryos. The S230W variant also rescues the defects induced by a dominant negative FGF receptor more efficiently and enhances Raf-stimulated Erk phosphorylation to a higher level than wild type *YWHAZ*. Although neither *YWHAZ* nor the variant promotes membrane recruitment of Raf proteins, the variant binds to more Raf and escapes phosphorylation by casein kinase 1a. Our data provide strong support to the hypothesis that the S230W variant of *YWHAZ* is a gain-of-function mutation in the RAS-ERK pathway and may underlie a CFC phenotype.

Keywords: YWHAZ, CFC, RASopathy, Raf, Erk activation, *Xenopus*

INTRODUCTION

Cardiofaciocutaneous (CFC) syndrome is an autosomal dominant genetic disorder characterized by distinctive facial features, heart malformation, and skin abnormalities (Roberts et al., 2006). Affected individuals typically have a prominent forehead with bitemporal constriction, hypoplastic supraorbital ridges, orbital hypertelorism, down-slanting palpebral fissures, and a depressed

nasal bridge. Heart defects include pulmonic stenosis, atrial septal defect, and hypertrophic cardiomyopathy. Most patients have dry, hyperkeratotic, scaly skin and sparse and curly hair. Many of these clinical manifestations overlap with those of Noonan syndrome or Costello syndrome. These phenotypically overlapping syndromes are collectively referred to as RASopathies, owing to the fact that they all share germline gain-of-function mutations in genes encoding components of the RAS-RAF-MEK-ERK pathway (Aoki et al., 2008; Simanshu et al., 2017; Bustelo et al., 2018; Dard et al., 2018).

RAS signaling transmits external cues, such as growth factors, cytokines, and extracellular matrix factors, to intracellular machineries to govern cell proliferation, differentiation, and survival (Simanshu et al., 2017). At the core of the RAS signaling pathway are the RAS family of small GTPases and the kinase cascade comprising RAF, MEK and ERK kinases and the KSR scaffolding protein (Lavoie and Therrien, 2015; Simanshu et al., 2017). Pathway activation is achieved through binding of membrane receptors to their ligands, which stimulates RAS guanosine nucleotide exchange factors (GEFs), such as SOS, that promote the GTP-bound, active form of RAS. Membrane-associated RAS-GTP then recruits RAF family kinases to the plasma membrane, facilitating their dimerization and activation (Weber et al., 2001; Light et al., 2002). Active RAF interacts with KSR scaffold proteins to recruit and activate MEK, leading to ERK phosphorylation (Therrien et al., 1996; Muller et al., 2001; Roy et al., 2002; Brennan et al., 2011; Lavoie et al., 2018). This in turn allows ERK to phosphorylate various effector proteins to influence cell cycle, apoptosis, and differentiation (Khokhlatchev et al., 1998; Casar et al., 2008). Germline mutations in genes encoding different components or regulators of the RAS pathway have been shown to be responsible for the congenital anomalies displayed in individuals with RASopathies. For example, about 75% of CFC patients have gain-of-function (GOF) variants in the *B-RAF* gene, and GOF variants in *K-RAS*, *MEK1* and *MEK2* are also found in some affected individuals (Aoki et al., 2008; Bustelo et al., 2018; Dard et al., 2018). Noonan syndrome is associated with variants in the gene encoding tyrosine phosphatase SHP2 (*PTPN11*, 50% of patients), an activator of the RAS signaling, as well as in genes of *SOS1*, *C-RAF*, and other pathway components (Bustelo et al., 2018; Dard et al., 2018). Costello syndrome seems to arise mainly from mutations in *H-RAS*, with more than 90% of affected individuals having pathogenic variants in the gene and a minority harboring mutations in other genes, such as *K-RAS*, *B-RAF*, and *MEK1* (Bustelo et al., 2018; Dard et al., 2018). Variants at different sites in the same gene can be found with distinct frequencies in affected individuals, and both kinase-activating and kinase-impairing variants, especially in CFC-associated *B-RAF*, can lead to ERK phosphorylation and pathway activation (Garnett et al., 2005; Aoki et al., 2008; Anastasaki et al., 2009; Heidorn et al., 2010; Freeman et al., 2013). This highlights disease heterogeneity and the complexity of RASopathies, and implies that other regulators of RAS signaling may modulate disease phenotypes.

A key intermediary in the RAS pathway that has not been associated with the RASopathies previously is the 14-3-3 family of proteins (Aitken, 2006; Morrison, 2008; Sluchanko, 2018). The 14-3-3 family contains seven members in mammals, which are 14-3-3β, γ, ε, σ, ζ, τ and η, also known as *YWHAB*, *YWHAG*, *YWHAE*, *SFN*, *YWHAZ*, *YWHAQ* and *YWHAH* in humans. 14-3-3 proteins form homo- or heterodimers amongst themselves and are conserved regulators of myriad signals via their binding to hundreds of partner proteins, most of which contain consensus motifs surrounding phosphorylated serine or threonine residues. Binding of 14-3-3 proteins can lead to conformational changes of their partners, masking of sequence or structural features in the partners, and/or facilitation of protein interaction and complex formation of the partners (Aitken, 2006; Morrison, 2008; Obsil and Obsilova, 2011). One of the earliest identified and best characterized interaction partners of 14-3-3 are RAF family members (Fantl et al., 1994). 14-3-3 proteins bind to two conserved phosphoserine residues in RAF: one in the N-terminal regulatory region and the other near the C-terminal end of the RAF kinase domain (Muslin et al., 1996; Rommel et al., 1996; MacNicol et al., 2000; Hekman et al., 2004; Fischer et al., 2009). 14-3-3 dimers can either bind phosphoserine residues on the same molecule to hold RAF proteins in an inactive conformation or bridge two molecules by binding the *C*-terminal phosphoserine on each, thereby stabilizing active RAF dimers (Tzivion et al., 1998). Activation of RAF by RAS results in release of 14-3-3 binding from the N-terminal phosphoserine residue, but does not affect 14-3-3 association with the C-terminal residue (Rommel et al., 1996). These observations lead to the current model that in the absence of stimulating signals, 14-3-3 binds to cytosolic RAF at both the *N*- and the *C*-terminal sites to lock the protein in a closed conformation to prevent basal signaling. Upon RAS activation, RAF is recruited to the plasma membrane via its *N*-terminal domain and dissociates from 14-3-3 at its *N*-terminal site. However, 14-3-3 still binds to RAF at the *C*-terminal site, and this binding is required for RAF activation, possibly by facilitating RAF dimerization and/or formation of a protein complex with other factors, such as KSR (Aitken, 2006; Freeman et al., 2013). Hence, depending on the presence or absence of activating signals, 14-3-3 can switch from an inhibitor to an activator of the RAS/RAF pathway.

We have identified several *YWHAZ* variants in individuals with neurodevelopmental phenotypes, two of which had a clinical diagnosis of a RASopathy. However, the consequence of these variants on 14-3-3 function has not been described, and thus their pathogenicity is unclear. In this study, we employed the *Xenopus* model system to characterize the functional effect of *YWHAZ* variation, seeking to dissect molecular mechanisms underlying the activity of the S230W variant. We report that the S230W variant induced more severe embryonic defects than wild type *YWHAZ* when expressed in early *Xenopus* embryos. Though the variant did not enhance membrane recruitment of Raf, it bound to more Raf and activated Erk phosphorylation to a higher level than the wild type protein. Our data indicate that the S230W variant promotes Raf/Erk signal transduction and likely causes gain-of-function in RAS signaling in humans, supporting the hypothesis that the *YWHAZ* variant is a new RASopathy-associated allele.

RESULTS

Identification of YWHAZ Variants in Human Patients

Through a genome sequencing research study, we identified a heterozygous genetic variant in *YWHAZ* (c.689C > G, p.S230W) in a male with a clinical diagnosis of CFC syndrome (proband 1, **Figure 1A**, **Supplementary Text 1**). He has short stature, global developmental delay, bilateral proptosis and ptosis, high forehead, pulmonic stenosis, hyperkeratosis, and seizures. Previous clinical testing included a negative RASopathy panel, but trio genome sequencing revealed a *de novo* serine to tryptophan change in *YWHAZ* at amino acid (aa) position 230, a location close to the *C*-terminal end and two residues away from a known casein kinase phosphorylation site at T232 (**Supplementary Table 1**). This missense variant is extremely rare and is absent from the gnomAD population database (Lek et al., 2016). The alteration is predicted to have a deleterious effect by multiple lines of computational evidence (SIFT score of 0; GERP score of 4.60; CADDv1.4 score of 33), though its specific functional consequences have not been examined. Through the data-sharing platform GeneMatcher (Sobreira et al., 2015), another *YWHAZ* variant was found in a child who also had a clinical diagnosis of RASopathy (proband 2, **Figure 1B**, **Supplementary Text 1**). The female individual has short stature, low body weight, and facial features similar to other patients with RASopathies, including a triangular face and a mild ptosis (**Figure 1B**, **Supplementary Text 1**). Trio exome sequencing identified a heterozygous *de novo YWHAZ* variant (c.157G > A, p.G53R) that results in an amino acid change from glycine to arginine at residue 53 (**Supplementary Table 1**). This missense variant is also absent from the gnomAD population database (Lek et al., 2016) and has multiple lines of computational evidence predicting a deleterious effect (SIFT score of 0; GERP score of 5.64; CADDv1.4 score of 32). Like S230W, the specific functional impact of this sequence variant has not been examined. Three additional *YWHAZ* variants were also identified in three individuals with distinct phenotypes (Probands 3–5, **Figures 1C–E**, **Supplementary Table 1**, **Supplementary Text 1**). While one of these probands harbors a missense variant (S145L, proband 3, **Figure 1C**), two others have premature termination (E14X, proband 4, **Figure 1D**) and frameshift (S230Yfs*44, proband 5, **Figure 1E**) variants, respectively. Each of these probands shows developmental delay or intellectual disability, but none has cardiac or skin abnormalities (**Supplementary Table 1**, **Supplementary Text 1**). The distinct clinical features of individuals with different *YWHAZ* variants suggest that the altered gene products may affect the protein function differently. While premature termination of *YWHAZ* most likely represents a loss-of-function allele, the change in activities of the other variants is less clear. The presence of other gene variants in several of the probands (**Supplementary Text 1**) also makes it difficult to confidently relate clinical phenotypes to *YWHAZ* variation. Because of this, the variants can only be classified as variants of uncertain significance (VUS) according to the ACMG classification guideline (Richards et al., 2015). To explore possible pathogenicity of the *YWHAZ* variants, direct functional characterization is required. In the following, we used the *Xenopus* embryonic system to investigate the functional consequence of the amino acid changes, with a focus specifically on the S230W variant.

The YWHAZ(S230W) Variant Induces More Severe Embryonic Defects Than Wild Type YWHAZ

To examine whether the *YWHAZ*(S230W) variant has altered activity from its wild type counterpart, we injected the RNAs encoding the wild type or the variant form of *YWHAZ* into the animal (ectodermal) or the marginal zone (mesodermal) regions of early *Xenopus* embryos. At the gastrula stages, many embryos injected with high doses of the S230W variant (2–4 ng) displayed dark pigmentation in the animal region, and the clusters of darkly pigmented cells persisted to the neurula stages (**Figures 2A,B**). This phenotype normally reflects changes in cell morphology in a process called apical constriction, which results in concentration of pigment granules near the apical cell surface of epithelial cells, hence the dark color of the cells on the surface (Sawyer et al., 2010). Although S230W might induce cell shape changes, it did not seem to induce definitive apical constriction as the epithelial cell sheet

FIGURE 1 | Facial features of probands with variations in *YWHAZ*. **(A)** Proband 1. **(B)** Proband 2. **(C)** Proband 3 (photo taken at the age of 13 and a half years old). **(D)** Proband 4 (photo taken at the age of 4 years and 8 months old). **(E)** Proband 5 (photo taken at the age of 7 years and 5 months old). Written informed consent to publish pictures was obtained from all families.

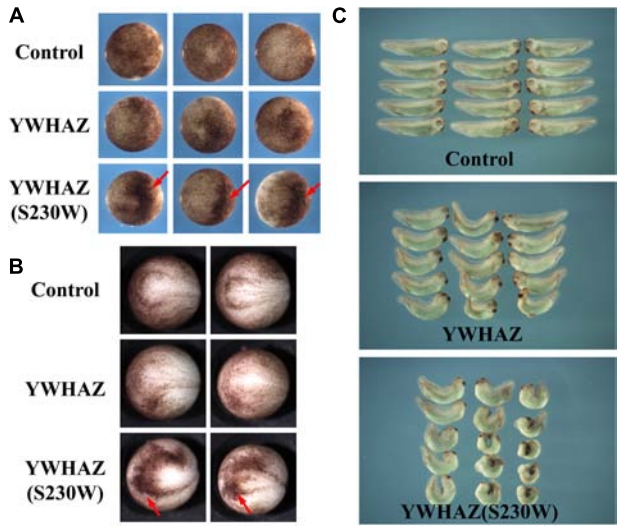

FIGURE 2 | *YWHAZ*(S230W) induces more severe embryonic defects than wild type *YWHAZ*. **(A)** Ectopic expression of *YWHAZ*(S230W) in the animal region induces darkly pigmented cells at the gastrula stages. Arrows point to the darkly pigmented cell clusters. **(B)** Clusters of darkly pigmented cells induced by ectodermal expression of *YWHAZ*(S230W) persist to the neurula stages. Arrows point to the darkly pigmented cell clusters. **(C)** Overexpression of wild type *YWHAZ* leads to defects in the head structure and bent body axis in the resulting tadpoles. Expression of the *YWHAZ*(S230W) variant induces more severe defects than *YWHAZ*, with the tadpoles displaying a significantly shortened and severely bent body axis in addition to stronger defects in the head structure. The experiment has been repeated four times, with 10 to 18 treated embryos in each experiment. In all the experiments, the length of the embryos was significantly shorter in the *YWHAZ*(S230W)-expressing group. RNA doses are 2–4 ng.

did not bend toward the pigmented cell clusters (data not shown). Embryos injected with wild type *YWHAZ* RNA only showed minor pigmentation changes (**Figures 2A,B**). At the tadpole stages, embryos injected with the *YWHAZ*(S230W) RNA in the marginal zone showed severe defects in the head structures and a shortened and bent body axis. In contrast, embryos expressing *YWHAZ* displayed much milder defects, with a lesser degree of head malformation and bending of the body axis (**Figure 2C**). The differential phenotypes induced by the same doses of RNAs of the wild type or the variant *YWHAZ* indicate that the variant has different activity from its wild type allele.

YWHAZ(S230W) Rescues the Defects Induced by a Dominant Negative (DN) FGF Receptor More Efficiently Than YWHAZ

Genetic variation identified in CFC individuals often shows gain-of-function activity, resulting in activation of the RAS-RAF-MEK-ERK pathway. If the S230W variant is responsible for the CFC phenotype in our proband, it is likely to promote Erk activation as well. To test this hypothesis, we examined the ability of *YWHAZ* or *YWHAZ*(S230W) to rescue the defects induced by blocking the FGF signal using dominant negative FGF receptor 1 (DN-FGFR1). In *Xenopus*, the FGF signal (e.g., bFGF/FGF2; Kimelman et al., 1988) activates the Raf-MEK-Erk pathway to regulate mesoderm formation (Amaya et al., 1991, 1993; MacNicol et al., 1993; LaBonne and Whitman, 1994; LaBonne et al., 1995; Umbhauer et al., 1995). Blocking the signal with DN-FGFR1 impairs mesoderm development, leading to gastrulation defects (Amaya et al., 1991, 1993). When we expressed the RNA encoding DN-FGFR1 in the dorsal marginal zone of early *Xenopus* embryos, we observed that the injected embryos frequently displayed a reduced and bent body axis, and some showed failure in blastopore closure ("open back" phenotype; **Figure 3A**). Co-expression of DN-FGFR1 with either *YWHAZ* or *YWHAZ*(S230W) led to rescue of embryo morphology, but the S230W variant was more efficient in its ability to restore axial structures (**Figure 3A**). *In situ* hybridization analysis of expression of the pan-mesodermal marker brachyury (Smith et al., 1991) showed that DN-FGFR1 interfered with expression of this marker, and *YWHAZ*(S230W) rescued marker expression to a greater extent than *YWHAZ* (**Figure 3B**). To investigate whether overexpression of *YWHAZ* or *YWHAZ*(S230W) was sufficient to induce the mesodermal marker in early embryos by itself, we co-injected RNAs encoding wild type *YWHAZ* or the S230W variant with the lineage tracer encoding nuclear beta-galactosidase into the marginal zone of early embryos. Detection of brachyury expression at mid-gastrula stages revealed that while neither gene product induced brachyury expression in the ectodermal region by itself, both could expand the expression domain of brachyury in the marginal zone. *YWHAZ* weakly enhanced the expression of the marker in the area labeled by the tracer (red color, **Figure 3C**), whereas *YWHAZ*(S230W) strongly expanded the width of the brachyury expression domain outside its normal territory (**Figure 3C**). Taken together, our data suggest that overexpression of either *YWHAZ* or *YWHAZ*(S230W) activates the mesodermal induction pathway downstream of the FGF signal in proper tissue contexts, and the S230W variant has higher activity than wild type *YWHAZ*. It is important to note that the activities of *YWHAZ*(S230W) were similar to that of the active mutant of MEK1, MEK1(SESE) (Gotoh et al., 1995). When expressed at high doses, MEK1(SESE) induced defects in body axis, even though it positively regulated mesodermal induction (**Supplementary Figure 1A**; Gotoh et al., 1995). The defect was likely due to the requirement of the proper levels of Erk signaling in gastrulation movements subsequent to mesodermal formation (Nie and Chang, 2007). When expressed at a lower dose, MEK1(SESE) rescued the defects induced by DN-FGFR1 in a similar way as *YWHAZ*(S230W) (**Supplementary Figure 1B**). The results imply that *YWHAZ*(S230W) activates Erk signaling in its rescue of the DN-FGFR1 phenotype.

YWHAZ(S230W) Stimulates Raf-Dependent Erk Phosphorylation More Efficiently Than YWHAZ

The above phenotypic and marker expression analyses imply that the S230W variant is more active than its wild type counterpart.

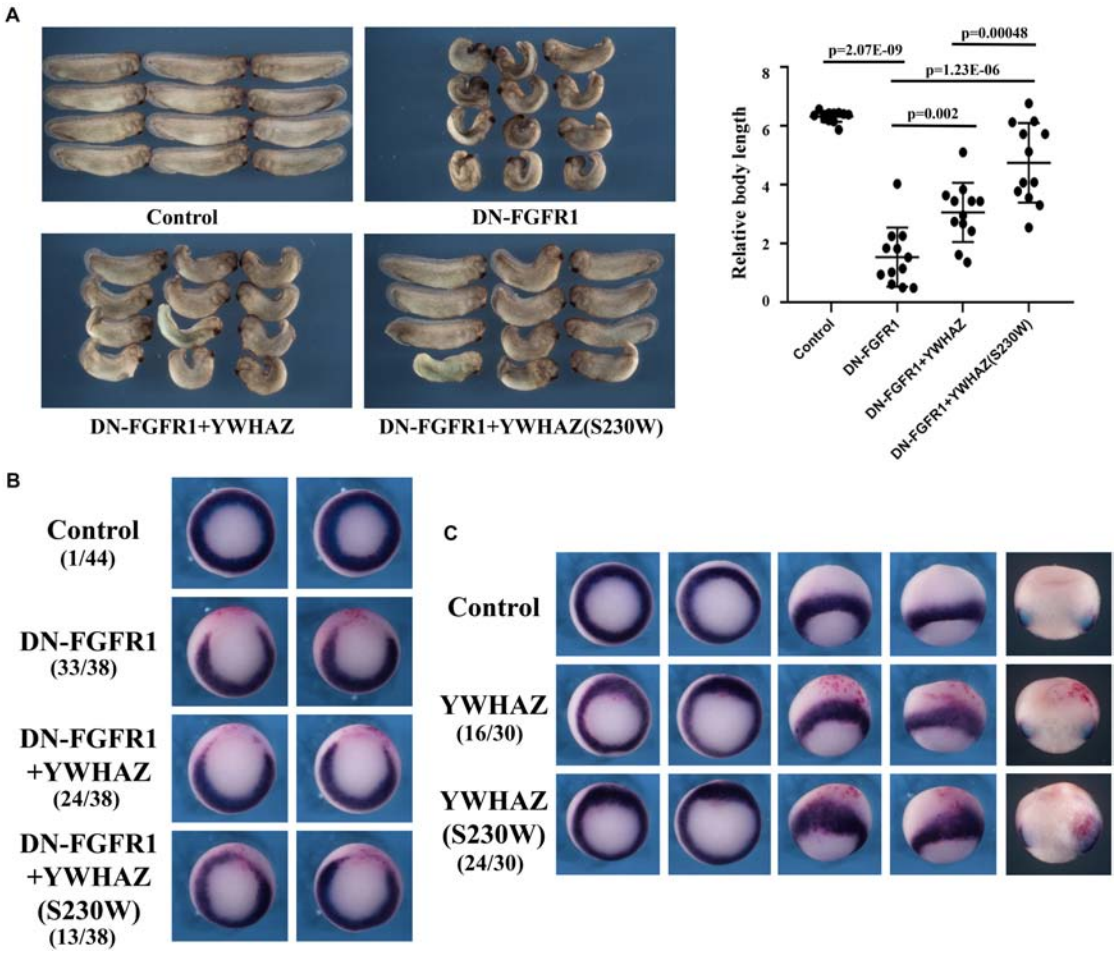

FIGURE 3 | *YWHAZ*(S230W) rescues embryonic defects induced by DN-FGFR1 more efficiently than *YWHAZ*. **(A)** Expression of DN-FGFR1 (25 pg or 50 pg) in the dorsal marginal zone of early embryos results in gastrulation defects, characterized by reduced body length and exposed mesendoderm ("open back"). Co-expression of either *YWHAZ* or *YWHAZ*(S230W) (250 pg) with DN-FGFR1 leads to phenotypic rescue, but the S230W variant is more efficient in restoring body length and embryo morphology. The scatter plot of the body length of the embryos showed that the S230W variant rescued the defects more efficiently than YWHAZ. Student's *t*-tests were performed in a pairwise fashion and the results revealed significant differences in the samples we compared. This experiment has been repeated four times, with 12 to 18 treated embryos in each experiment. Since the embryos were collected at slightly different stages and the body length was thus different, scatter plot was made for the embryos for each experiment separately. In all the experiments, there was a significant difference between *YWHAZ* and *YWHAZ*(S230W) in phenotype rescue. **(B)** DN-FGFR1 interferes with the expression of the pan-mesodermal marker brachyury, and *YWHAZ*(S230W) rescues marker expression to a greater extent compared to wild type *YWHAZ*. The experiment was repeated 3 times. For control embryos, 1/44 embryos showed a gap in the brachyury ring, and 33/38 embryos injected with *DN-FGFR1* RNA had a big gap in the brachyury domain. Expression of *YWHAZ* and *YWHAZ*(S230W) led to partial rescue of brachyury expression, resulting in similar brachyury gap in 24/38 and 13/38 embryos, respectively. These numbers are indicated in the panel. **(C)** Ectopic expression of *YWHAZ* weakly expands, whereas ectopic expression of *YWHAZ*(S230W) strongly expands, the domain of *brachyury* in gastrulating *Xenopus* embryos. The experiment has been repeated 3 times. The expansion of *brachyury* domain was observed in 16/30 embryos expressing *YWHAZ* and 24/30 embryos expressing *YWHAZ*(S230W). The doses of RNAs used in this panel are 1 to 2 ng. The red color in panels B and C are staining of beta-galactosidase-expressing cells with the chemical red-Gal to mark the injected cells.

To assess whether the functional difference between the two forms is based on their differential ability to activate the Erk pathway, we analyzed their effect on Erk phosphorylation. As *Xenopus* embryos have high endogenous Erk signals, especially in the mesodermal region (LaBonne and Whitman, 1997; Schohl and Fagotto, 2002), which can mask the effects of ectopically expressed *craf* and *YWHAZ*/S230W, we co-expressed these genes with GFP-Erk2 in the ectodermal region and assayed for phosphorylation of this chimeric protein. Ectodermal cells have low endogenous Erk signals, thus the level of GFP-Erk2 phosphorylation can reflect the activity of locally injected activator products. As shown in **Figure 4A**, *YWHAZ*(S230W), but not *YWHAZ*, strongly enhanced GFP-Erk2 phosphorylation when co-expressed with *craf*. Quantification of the ratio of phosphorylated over total GFP-Erk2 levels revealed that *YWHAZ*(S230W) stimulated Erk phosphorylation by 4 to 5 fold over that when *craf* was expressed alone, whereas wild type *YWHAZ* did not significantly change the ratio. This result was

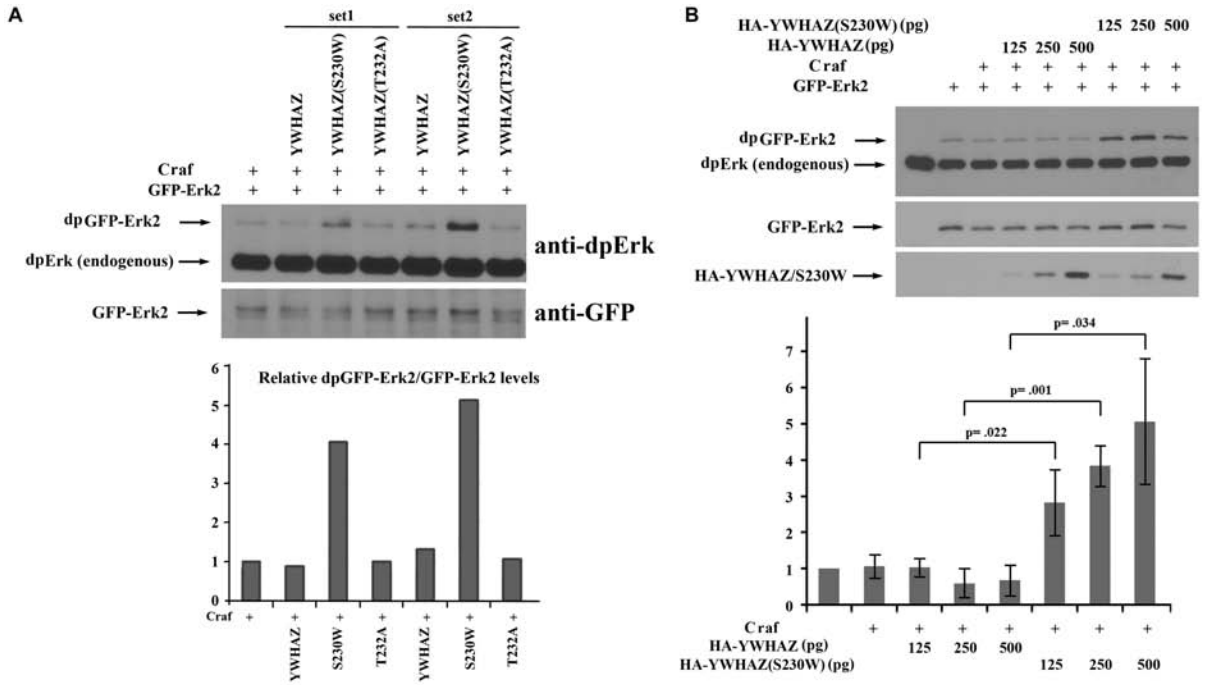

FIGURE 4 | *YWHAZ*(S230W) strongly stimulates Raf-dependent Erk phosphorylation when compared with wild type *YWHAZ*. **(A)** Co-expression of Craf (250 pg) and GFP-Erk2 (250 pg) with wild type *YWHAZ*, the S230W variant, or the T232A mutant (250 pg) shows that only the S230W variant strongly enhances Craf-stimulated Erk phosphorylation. Quantification of the Western blot was performed using NIH ImageJ software and the relative ratio of phosphorylated GFP-Erk2 (dpGFP-Erks) over total GFP-Erk2 is shown in the bar graph. **(B)** Co-expression of Craf (125 pg), GFP-Erk2 (125 pg) and an increasing amount of HA-*YWHAZ* or HA-*YWHAZ*(S230W) (125, 250, and 500 pg) shows that the S230W variant stimulates Erk phosphorylation significantly more than *YWHAZ* at all doses used. The bottom bar graph displays the results of three independent experiments, with the average of relative Erk phosphorylation level (dpGFP-Erk2/total GFP-Erk2) and the standard deviation plotted on the graph. The *p*-values from Student's *t*-test for each dose of *YWHAZ*/S230W are shown in the graph.

further confirmed by co-injection of a low dose of *craf* RNA with an increasing amount of RNAs of *YWHAZ* or *YWHAZ*(S230W), which demonstrated that the S230W variant had a statistically significant higher activity over that of *YWHAZ* in stimulating Erk phosphorylation (**Figure 4B**). To examine whether *YWHAZ* or *YWHAZ*(S230W) alone could induce Erk phosphorylation, we expressed these genes in the ectodermal region with GFP-Erk2 in the absence of *craf*. At higher doses (1 ng), *YWHAZ* and *YWHAZ*(S230W) weakly stimulated Erk phosphorylation, but the level of activation was lower compared to that when co-expressed with *craf* (compare data in **Supplementary Figure 2** and **Figure 4**). The S230W variant again displayed higher activity than *YWHAZ* in this context (**Supplementary Figure 2**). These data indicate that like other CFC-associated variants, *YWHAZ*(S230W) functions as an activating mutant which facilitates Raf-Erk signaling.

YWHAZ and YWHAZ(S230W) Do Not Promote Membrane Recruitment of Craf Protein

Several distinct mechanisms may underlie the elevated activity of YWHAZ(S230W). YWHAZ normally binds to Raf proteins and holds them in a closed conformation in the cytosol. Upon stimulating signals to activate Ras, YWHAZ releases its binding at the N-terminal site of Raf proteins to allow their recruitment to the plasma membrane (Rommel et al., 1996; Tzivion et al., 1998; Light et al., 2002). It is possible that the S230W variant has reduced affinity for the N-terminal binding site of Raf to permit more efficient association of Raf with RAS and consequently better recruitment to the plasma membrane. To test this hypothesis, we made a Craf-GFP construct and examined its membrane localization in the presence of either YWHAZ or YWHAZ(S230W) by confocal microscopy. The RNA encoding a membrane-associated mCherry fluorescent protein was used to mark the plasma membrane in this experiment. Expression of Craf-GFP alone in the ectodermal cells resulted in both membrane and cytosolic localization of the protein (**Figure 5A**). The membrane association of Craf was likely due to the presence of endogenous FGF signal in these cells (Schohl and Fagotto, 2002). When Craf-GFP was co-expressed with either YWHAZ or YWHAZ(S230W), the Craf protein was seen from the surface view to spread underneath the cell membrane and at the cell-cell junctions. The widespread distribution under the plasma membrane did not seem to indicate a membrane recruitment of the protein, as the side view of the cells revealed a lack of membrane enrichment of the protein (**Figure 5A**). This pattern was distinct from that when Craf-GFP was co-expressed with FGFR1, in which case the Craf protein was detected to localize more intensely to the plasma

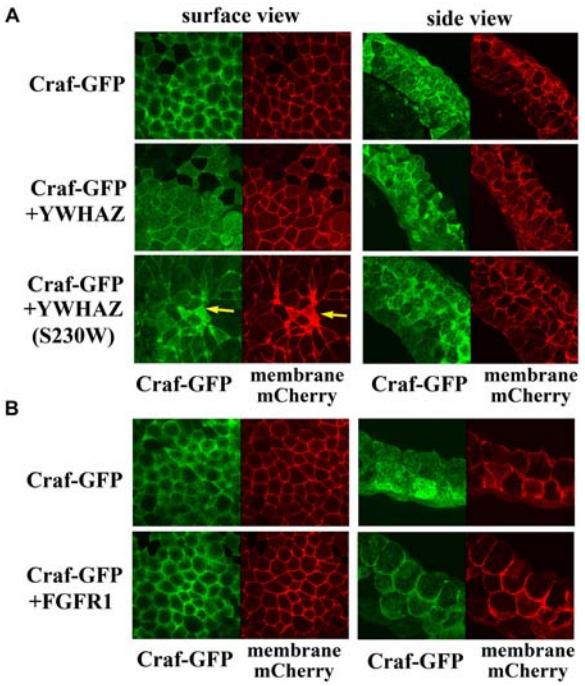

FIGURE 5 | YWHAZ and YWHAZ(S230W) do not promote membrane recruitment of Raf. **(A)** Craf-GFP is localized both at the plasma membrane and in the cytosol in Xenopus ectodermal cells. Co-expression with YWHAZ or YWHAZ(S230W) does not significantly change the membrane fraction of the protein. The surface view reveals a population of Craf at the cell-cell junction in the presence of YWHAZ or the S230W variant in addition to the widespread Craf underneath the cell surface. Cell morphological changes are observed only in cells expressing the S230W variant and manifested as clusters of smaller cells displaying apical constriction-like morphology from the surface view (arrows). The side view shows intense Craf clusters at the juxtamembrane locations in cells expressing YWHAZ or YWHAZ(S230W). **(B)** Unlike wild type YWHAZ or its variant, FGFR1 recruits Craf to the plasma membrane in ectodermal cells. The doses of the RNAs used are: *Craf-GFP*, 250 pg, *YWHAZ*/*YWHAZ*(S230W), 2 ng, FGFR1, 1 ng.

membrane (**Figure 5B**). Although the effect of YWHAZ and YWHAZ(S230W) on Craf distribution seemed to be similar, we observed that YWHAZ(S230W)-expressing samples displayed some small cells with strong mCherry signal (yellow arrows, **Figure 5A**). This is consistent with our phenotypic studies at the gastrula stages when we observed darkly pigmented cells in the animal region (**Figure 2A**) and indicates that YWHAZ(S230W) could induce apical constriction-like cell shape changes. Taken together, our results show that YWHAZ and YWHAZ(S230W) do not promote membrane recruitment of Raf proteins, but YWHAZ(S230W) can induce cell morphological changes that are not obvious in YWHAZ-expressing samples.

YWHAZ(S230W) Displays Increased Binding to Raf Proteins Compared With YWHAZ

Binding of YWHAZ to the Raf C-terminal phosphorylation site (S728 in BRAF and S621 in CRAF) is critical for Raf activation (Tzivion et al., 1998; MacNicol et al., 2000; Light et al., 2002; Garnett et al., 2005). The enhanced function of YWHAZ(S230W) in Raf-Erk activation may thus rely on differential ability of YWHAZ and YWHAZ(S230W) to interact with Raf. To explore this possibility, we performed co-immunoprecipitation (co-IP) studies to analyze the interaction of YWHAZ and the S230W variant with the Raf proteins. We co-injected RNAs encoding HA-tagged *YWHAZ*/S230W and *Craf-GFP* into the ectodermal region of early *Xenopus* embryos. Protein lysate was obtained at the gastrula stages and subjected to IP with anti-HA antibody. Western blot using anti-GFP antibody was then performed to examine the Craf-GFP protein that was pulled down by the anti-HA antibody. As shown in **Figure 6A**, the amount of Craf-GFP co-precipitated with HA-YWHAZ(S230W) was substantially higher than that pulled down by HA-YWHAZ, demonstrating that the S230W variant binds more Craf than wild type YWHAZ. Similarly, we performed co-IP with HA-YWHAZ/S230W and Braf-Flag and demonstrated that HA-YWHAZ(S230W) has an increased interaction with Braf-Flag than HA-YWHAZ (**Figure 6B**). These data thus reveal that the S230W variant differs from YWHAZ in its ability to bind to Craf and Braf.

YWHAZ(S230W) Cannot Be Phosphorylated by Casein Kinase 1a

It has been shown that binding of YWHAZ to Raf is affected by the phosphorylation state of YWHAZ itself. Casein kinase 1a (CK1a) can phosphorylate YWHAZ at threonine 232 (T232) to inhibit its association with CRAF (Rommel et al., 1996; Dubois et al., 1997; Obsilova et al., 2004). Since our variant alters the protein sequence at serine 230, which is positioned two residues away from T232, it is possible that the S230W variation will interfere with YWHAZ phosphorylation at T232, hence enhancing its interaction with Raf proteins. To investigate this hypothesis, we co-expressed RNAs of *HA-YWHAZ/HA-YWHAZ*(S230W) with that of *CK1a* and assessed phosphorylation of the protein by Western blot. In this experiment, we also used the YWHAZ(T232A) mutant that cannot be phosphorylated by CK1a as a control. As shown in **Figure 7**, CK1a phosphorylated YWHAZ efficiently, but was incapable of modifying either the T232A or the S230W mutant proteins.

To further investigate whether the loss of CK1a phosphorylation could account for the augmented activity of the S230W variant, we compared the functions of the S230W and the T232A proteins. Unlike the S230W variant, overexpression of the T232A mutant did not lead to elevated activation of Erk phosphorylation (**Figure 4**), did not enhance the binding to Raf over wild type YWHAZ (**Figure 6**), and did not rescue the embryonic defects induced by DN-FGFR1 (data not shown). These results imply that while loss of CK1a phosphorylation at Thr232 may impact binding of YWHAZ to Raf to some degree, it is not sufficient to activate Raf-Erk signaling. Additional factor(s) may influence the activity of the S230W variant.

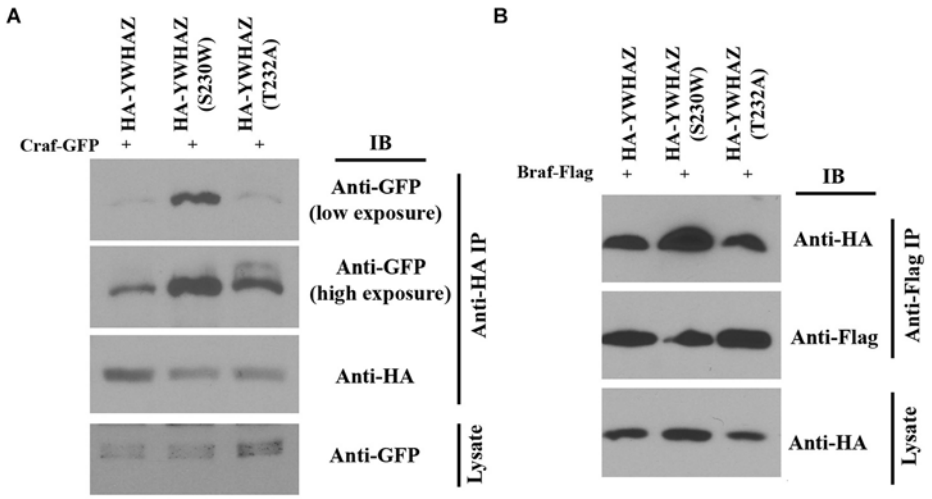

FIGURE 6 | YWHAZ(S230W) binds to more Raf proteins than YWHAZ. Binding of HA-tagged YWHAZ(S230W) to either Craf (panel **A**) or Braf (panel **B**) is increased compared to that of HA-tagged YWHAZ. The doses of the RNAs used are: *Craf-GFP*, 250 pg, *Braf-Flag*, 125 pg, *HA-YWHAZ/HA-YWHAZ(S230W)/HA-YWHAZ(T232A)*, 250 pg.

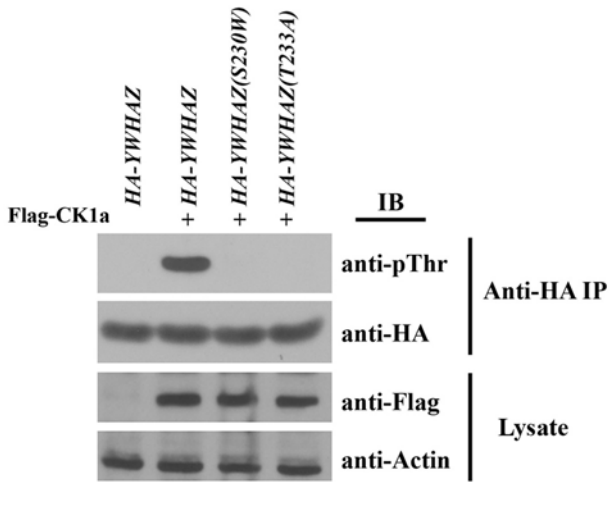

FIGURE 7 | YWHAZ(S230W) cannot be phosphorylated by casein kinase 1a (CK1a). The S230W variant, like the phospho-null T232A mutant of YWHAZ, cannot be phosphorylated by CK1a. The doses of RNAs used are: *HA-YWHAZ/HA-YWHAZ(S230W)/HA-YWHAZ(T232A)*, 1 ng; *Flag-CK1a*, 500 pg.

DISCUSSION

With improved depth, precision, and reduced cost, genome or exome sequencing has been increasingly used to identify the molecular etiology of congenital diseases. As a result, a growing list of genomic variants have been uncovered which associate with specific pathological phenotypes. The pathogenicity of many of these variants, however, remains uncertain in the absence of supportive functional data. The bottleneck in assigning functional significance to variants is often the lack of assays to examine the activities of the variant gene products. Animal models, such as *Xenopus*, can be used to investigate gene function in an unbiased fashion. *Xenopus* embryos develop quickly, contain tissue types and organs equivalent to those in humans, undergo cell differentiation and morphogenesis both *in vivo* and in tissue explants, have conserved signaling and gene regulatory pathways, and are available for genetic, embryological, molecular, and biochemical studies. In this work, we have employed the *Xenopus* model to interrogate the function of a human gene variant that appeared to be associated with CFC syndrome.

Cardiofaciocutaneous syndrome is a rare autosomal dominant genetic disorder that affects 1 in 800,000 newborns (Roberts et al., 2006; Aoki et al., 2008; Dard et al., 2018). Currently, all known mutations linked to CFC syndrome act in the RAS-RAF-MEK pathway to enhance ERK signaling (Aoki et al., 2008; Simanshu et al., 2017; Bustelo et al., 2018; Dard et al., 2018). Although 14-3-3 proteins are thought to modulate RAF-ERK signaling both positively and negatively in mammalian cells, partially depending on the presence or absence of signals (Aitken, 2006; Morrison, 2008), no pathogenic variants in 14-3-3 family members have been identified in CFC patients. Genome sequencing of a CFC individual revealed a *de novo* heterozygous variant allele of the human 14-3-3ζ protein. If the variant is responsible for the CFC phenotype, it may act either as a haploinsufficient loss-of-function product which may impair Raf inhibition in cells or as a dominantly activating protein that promotes Erk signaling. Using the *Xenopus* overexpression system, we show here that the *YWHAZ*(S230W) variant induces more severe embryonic defects when ectopically expressed at high doses (2–4 ng) and rescues DN-FGFR1-induced defects more efficiently at low doses (0.25 ng) when compared with wild type *YWHAZ*. Analysis of mesodermal marker expression and Erk phosphorylation confirms that the variant enhances Erk signaling over that of *YWHAZ*.

YWHAZ(S230W) expands the domain of the mesodermal gene brachyury more widely than its wild type counterpart; and the variant enhances the activation of Erk to higher levels than wild type *YWHAZ*. While definitive proof will require additional patients with variants in *YWHAZ*, our data, combined with the evidence that variations in other genes associated with CFC syndrome cause disease by stimulating Erk signaling, provide evidence that *YWHAZ* variation is causally related to CFC and developmental delay.

The mechanisms underlying the potential disease effects of the S230W variant is specifically investigated in this study. Unlike upstream growth factor signaling that activates Ras, such as the FGF pathway, neither YWHAZ nor its variant promotes membrane recruitment of the Craf protein (**Figure 5**). Instead, the S230W variant shows increased binding to both Braf and Craf when compared with wild type YWHAZ. Although phosphorylation of YWHAZ by casein kinase 1a is shown to inhibit the binding of YWHAZ to Raf in an *in vitro* assay using a Raf peptide substrate (Rommel et al., 1996; Dubois et al., 1997; Obsilova et al., 2004), and the S230W variant protein displays impaired phosphorylation by CK1a, loss of CK1a phosphorylation *per se* does not seem to contribute to the enhanced activity of the variant. The phospho-null mutant YWHAZ, YWHAZ(T232A), does not activate Erk signaling or rescue DN-FGFR1-induced defects any more than the wild type protein. Hence, the S230W variant seems to employ an alternative mechanism to bind Raf and activate Erk more efficiently. Inspection of the nature of the amino acid substitution in the context of the structural features of 14-3-3 proteins yields a clue to potential mechanisms. 14-3-3 proteins form dimeric, rigid cup shaped structures that contain a deep central channel with two amphipathic grooves that bind their substrates (Liu et al., 1995; Yaffe et al., 1997; Obsil and Obsilova, 2011). The *C*-terminal segment of 14-3-3 is located outside the cup-shaped structure and is more flexible. Nonetheless, this region can interact with both 14-3-3 itself and the partner proteins to regulate 14-3-3 conformation (Obsilova et al., 2004). The amino acid change in our YWHAZ variant occurs at position 230 to alter the serine residue into tryptophan. This residue is situated between the end of the helix that forms part of the ligand-binding groove of 14-3-3 and the beginning of the *C*-terminal stretch. Alteration of the amino acid sequence is thus expected to modify the conformation of the 14-3-3 dimer and influence its binding to partner proteins (Obsilova et al., 2004). We therefore speculate that structural changes in YWHAZ S230W variant can facilitate formation of a functional signaling complex by bringing downstream signaling components together more efficiently via the 14-3-3 dimer. This may involve promoting dimerization of BRAF and CRAF, stimulating formation of protein complexes between Raf and other signaling molecules, such as MEK or KSR, or shifting binding preference at the negative (e.g., S259 in CRAF) and the positive (e.g., S621 in CRAF) sites. Future biochemical studies combining Raf mutagenesis, for example *N*- and/or *C*-terminal serine to alanine (phospho-null) or aspartic acid (phosphomimetic), and protein interaction assays will help to shed further light on the mechanism of S230W action.

The structure of 14-3-3 proteins also provides some clues to the possible functional changes of the other YWHAZ variants we have identified. The amino acid alteration for G53R occurs in the helix 3, which is involved in both protein dimerization and ligand binding (Liu et al., 1995; Yaffe et al., 1997; Obsil and Obsilova, 2011). As glycine 53 normally induces a bend in this helix (Liu et al., 1995), the change would straighten the helix. Furthermore, the variant introduces a basic residue in the helix and may potentially strengthen the interaction with the phosphate group in the substrate (Yaffe et al., 1997). Hence the G53R variant may bind partners more strongly than the wild type protein. The S145L variant is in the helix 6, which is located outside the dimerization interface and the ligand binding groove. It is possible that the variant does not directly affect interactions with other proteins via its ligand binding channels, but may still alter the function of the protein by modification of auxiliary protein interactions at the outer surface. The S230Y-frameshift variant is interesting in that the first 229 amino acids, which form the rigid cup structure with the amphipathic ligand binding groove, are exactly the same as in the S230W variant, yet the two individuals with these variants show distinct phenotypes. This may be caused by the nature of the C-terminal amino acid sequence. In 14-3-3 proteins, the C-terminal region is flexible and can fold back to interact with the ligand binding groove in the absence of other partners (Liu et al., 1995). Removal of this region has been shown to enhance ligand binding by 14-3-3 proteins (Truong et al., 2002). The frameshift variation in S230Yfs*44 alters the C-terminal sequence, which may either block ligand access more efficiently or enhance ligand binding. Alternatively, it is also possible that the frameshift leads to nonsense mediated decay of the messenger RNA of S230Yfs*44 so that no protein will be made from the variant locus. Future functional, biochemical (protein stability, modification, and interaction) and structural analyses are required to determine the activities and the mechanisms of these other variants.

In *Xenopus*, as in other vertebrates, multiple 14-3-3 proteins play redundant roles in regulating early embryonic development (Wu and Muslin, 2002; Bunney et al., 2003; Muslin and Lau, 2005; Lau et al., 2006). Knockdown of individual 14-3-3 members results in either no defects, eye malformation, or impaired mesodermal induction and axial patterning defects (Lau et al., 2006). The results indicate that 14-3-3 proteins have overlapping and distinct functions in different tissue contexts. As 14-3-3 members can form both homo- and heterodimers, knockdown phenotypes likely do not capture the full range of 14-3-3 function during embryogenesis due to compensation. Tissue-specific overexpression or activation of 14-3-3 proteins have not been carried out, hence it is unclear whether the spectrum of morphological changes seen in CFC syndrome can be faithfully recapitulated if 14-3-3ζ is activated from its endogenous locus or replaced with a S230W equivalent allele in *Xenopus*. Nevertheless, our studies demonstrate that the *Xenopus* model can be used effectively to determine functional consequences of human genetic variants. This type of study may help to pave the way to use *Xenopus* embryos to screen for drugs that can modulate the activities of gene variants in the future.

MATERIALS AND METHODS

Identification of YWHAZ Variants Using Genomic Medicine Approaches

For proband 1, trio whole genome sequencing and variant calling were performed as previously described (Bowling et al., 2017). For proband 2, trio whole exome sequencing was performed on a NextSeq 500 Sequencing System (Illumina, San Diego, CA, United States), with a 2 × 150 bp high output sequencing kit after a 12-plex enrichment with SeqCap EZ MedExomekit (Roche, Basel, Switzerland), according to manufacturer's specifications. Sequence quality was assessed with FastQC 0.11.5, then the reads were mapped using BWA-MEM (version 0.7.13), sorted and indexed in a bam file (samtools 1.4.1), duplicates were flagged (sambamba 0.6.6), coverage was calculated (picard-tools 2.10.10). Variant calling was done with GATK 3.7 Haplotype Caller. Variants were then annotated with SnpEff 4.3, dbNSFP 2.9.3, gnomAD, ClinVar, HGMD, Variome Great Middle East and an internal database. Coverage for these samples was 93% at a 20x depth threshold. For probands 3, 4 and 5, exome sequencing was outsourced to GenomeScan (Leiden, The Netherlands). In brief, exomes were captured using the Agilent SureSelectXT Human all Exon v5 library kit (Agilent, Santa Clara, United States) accompanied by Illumina paired end sequencing on the Hiseq2500 platform (Illumina, San Diego, United States), generating 2 × 150 bp paired end reads with at least 80 × median coverage. Data analysis was performed at the LDGA using the in-house sequence analysis pipeline "Modular GATK-Based Variant Calling Pipeline" (MAGPIE) (LUMC Sequencing Analysis Support Core, LUMC) based on read alignment using Burrows-Wheeler Alignment (BWA-MEM) and variant calling using the Genome Analysis Toolkit (GATK). LOVDplus (Leiden Genome Technology Center, LUMC, Leiden) was used for interpretation of variants. Variants were classified according to the American College of Medical Genetics and Genomics (ACMG) guidelines. Written informed consent to publish pictures was obtained from all families.

Obtaining Embryos and Microinjection

Xenopus laevis frogs were used in this study according to the institutional IACUC protocol 09658. Female frogs were primed with 800 units/frog of human chorionic gonadotropin hormone (Sigma) the night before usage. Embryos were obtained by *in vitro* fertilization, dejellied with 2% cysteine solution, and micro-injected with the RNAs indicated in the text. The injection was done in the animal regions of both blastomeres of 2–cell stage embryos or the marginal zone regions of the two dorsal cells of 4-cell stage embryos. The doses of the RNAs used in each experiment were indicated in the figure legends.

Plasmid Constructs and RNA Synthesis

The construct containing the human YWHAZ sequence, pMCSG19-YWHAZ, was purchased from the Plasmid Repository at Arizona State University[1] and was cloned into the pCS105 vector. The Craf, Braf and CK1a sequences were isolated by PCR amplification from *Xenopus* cDNA using the sequence reference from Xenbase[2] (RRID:SCR_003280; James-Zorn et al., 2015; Karimi et al., 2018) and cloned into pCS105. The protein tags were added and the mutagenesis of YWHAZ was performed using the PCR-based method. All constructs were sequenced to confirm their identity. The plasmids were linearized with the AscI enzyme and transcribed using the SP6 mMessage mMachine RNA synthesis kit (Ambion) to make RNAs for injection.

In situ Hybridization (ISH)

In situ Hybridization was performed as described by Harland (1991).

Imaging and Embryo Quantification

For stereo imaging of embryonic phenotypes and *in situ* hybridization, Nikon AZ100 microscope was used. The body length of the embryos was measured as a straight line from the head to the tip of the tail, which would reflect the effects of both the length and the curvature. NIH ImageJ software was used in body length measurement, and the scatter plot was made using GraphPad Prism 8 software. Student's *t*-test was used to determine statistical significance of the changes in body length of different samples in pairwise comparisons. For confocal imaging of Craf-GFP localization, Olympus Fluoview 2000 upright confocal microscope was used. Most of the images were taken using a 20× (NA0.95) lens. Maximum intensity projections of Z-stack images were used for the figures.

Western Blot

Western blot was performed as described previously (Tien et al., 2015). Briefly, RNAs encoding tagged proteins were injected into 2- to 4-cell stage embryos. Embryonic lysate was obtained at gastrula stages by lysing embryos with cold buffer containing 50 mM Tris–HCl, pH 7.5, 150 mM NaCl, 1mM EDTA, 10% glycerol and 0.5% Triton X-100. The lysate was either loaded on the SDS–PAGE directly (for the dpErk assay) with the 2× SDS gel-loading buffer (100 mM Tris.Cl, pH6.8, 200mM DTT, 4% SDS, 0.2% bromophenol blue, 20% glycerol) or subjected to the co-IP assay. Western blot was performed using rabbit anti-Flag (1:3000, Sigma), rabbit anti-HA (1:3000, Cell Signaling Technology), rabbit anti-dpErk (1:4000, Cell Signaling Technology), rabbit anti-GFP (1:3000, Cell Signaling Technology), or mouse anti-p-threonine (1:2000, Cell Signaling Technology) antibodies. Quantification was performed using NIH ImageJ software. The Student's *t*-test was used to assess the statistical significance in differences between YWHAZ and YWHAZ(S230W) in dose-response experiments shown in **Figure 4**.

[1] https://dnasu.org/DNASU/

[2] http://www.xenbase.org/

ETHICS STATEMENT

This study was carried out in accordance with the recommendations of "the UAB Institutional Review Board for Human Use (IRB)" with written informed consent from all subjects. The protocol was approved by the "The UAB Institutional Review Board for Human Use (IRB)." This study was carried out in accordance with the recommendations of "UAB IACUC committee." The protocol was approved by the "UAB IACUC." All subjects gave written informed consent in accordance with the Declaration of Helsinki.

AUTHOR CONTRIBUTIONS

SW, AvH, and BRK were involved in patient recruitment, examination, and clinical diagnosis. SH, BK, CR, GC, and M-JC performed genomic analyses. IP and CC carried out Xenopus studies to characterize the wild type and the variant gene products.

FUNDING

This study makes use of data generated by the DECIPHER Consortium (Probands 3, 4 and 5; Firth et al., 2009). A full list of centers who contributed to the generation of the data is available from https://decipher.sanger.ac.uk/ and via email from decipher@sanger.ac.uk. Funding for the project was provided by the Wellcome Trust. Those who carried out the original analysis and collection of the Data bear no responsibility for the further analysis or interpretation of it by the Recipient or its Registered Users. Proband 1 was sequenced as part of a grant from the State of Alabama (Alabama Genomic Health Initiative, AGHI). Genomic analysis of proband 1 was supported by a grant from The National Human Genome Research Institute (NHGRI, UM1HG007301) to SH and GC. The Xenopus work was supported by the NIH grant R01GM098566 and the NSF grant ISO-1558067 to CC.

ACKNOWLEDGMENTS

We thank Dr. Jianbo Wang for allowing us to use his Olympus Fluoview confocal microscope, and we also thank National Xenopus Resource (PRID:SCR_013731; Pearl et al., 2012) for the imaging workshop.

SUPPLEMENTARY MATERIAL

The Supplementary Material for this article can be found online at: https://www.frontiersin.org/articles/10.3389/fphys.2019.00388/full#supplementary-material

FIGURE S1 | Activated MEK1 induces gastrulation defects when expressed at high doses and rescues defects induced by DN-FGFR1 when expressed at low doses. **(A)** Injection of 0.5 ng RNA of MEK1(SESE), an activated MEK1 mutant, induces gastrulation defects. **(B)** When expressed at a lower dose (0.1 ng), MEK1(SESE) rescues defects induced by DN-FGFR1 to a similar degree to that when *YWHAZ*(S230W) was used, and both were more efficient than *YWHAZ*. This experiment has been repeated twice and the results from both experiments are similar.

FIGURE S2 | High doses of *YWHAZ* and *YWHAZ*(S230W) weakly stimulate Erk phosphorylation. When injected at the 1 ng doses into the ectodermal cells, *YWHAZ* and *YWHAZ*(S230W) activate Erk signaling weakly. The level of activation is much lower than that when these genes were co-expressed with Raf, as seen in **Figure 4**.

TABLE S1 | Genotypes and phenotypes of individuals with variation in YWHAZ.

REFERENCES

Aitken, A. (2006). 14-3-3 proteins: a historic overview. *Sem. Cancer Biol.* 16, 162–172. doi: 10.1016/j.semcancer.2006.03.005

Amaya, E., Musci, T. J., and Kirschner, M. W. (1991). Expression of a dominant negative mutant of the FGF receptor disrupts mesoderm formation in *Xenopus* embryos. *Cell* 66, 257–270. doi: 10.1016/0092-867428912990616-7

Amaya, E., Stein, P. A., Musci, T. J., and Kirschner, M. W. (1993). FGF signalling in the early specification of mesoderm in *Xenopus*. *Development* 118, 477–487.

Anastasaki, C., Estep, A. L., Marais, R., Rauen, K. A., and Patton, E. E. (2009). Kinase-activating and kinase-impaired cardio-facio-cutaneous syndrome alleles have activity during zebrafish development and are sensitive to small molecule inhibitors. *Hum. Mol. Genet.* 18, 2543–2554. doi: 10.1093/hmg/ddp186

Aoki, Y., Niihori, T., Narumi, Y., Kure, S., and Matsubara, Y. (2008). The RAS/MAPK syndromes: novel roles of the RAS pathway in human genetic disorders. *Hum. Mutat.* 29, 992–1006. doi: 10.1002/humu.20748

Bowling, K. M., Thompson, M. L., Amaral, M. D., Finnila, C. R., Hiatt, S. M., Engel, K. L., et al. (2017). Genomic diagnosis for children with intellectual disability and/or developmental delay. *Genome Med.* 9:43. doi: 10.1186/s13073-017-0433-1

Brennan, D. F., Dar, A. C., Hertz, N. T., Chao, W. C. H., Burlingame, A. L., Shokat, K. M., et al. (2011). A Raf-induced allosteric transition of KSR stimulates phosphorylation of MEK. *Nature* 472, 366–369. doi: 10.1038/nature09860

Bunney, T. D., De Boer, A. H., and Levin, M. (2003). Fusicoccin signaling reveals 14-3-3 protein function as a novel step in left-right patterning during amphibian embryogenesis. *Development* 130, 4847–4848.

Bustelo, X. R., Crespo, P., Fernandez-Pisonero, I., and Rodriguez-Fdez, S. (2018). RAS GTPase-dependent pathways in developmental diseases: old guys, new lads, and current challenges. *Curr. Opin. Cell Biol.* 55, 42–51. doi: 10.1016/j.ceb.2018.06.007

Casar, B., Pinto, A., and Crespo, P. (2008). Essential role of ERK dimers in the activation of cytoplasmic but not nuclear substrates by ERK-scaffold complexes. *Mol. Cell* 31, 708–721. doi: 10.1016/j.molcel.2008.07.024

Dard, L., Bellance, N., Lacombe, D., and Rossignol, R. (2018). RAS signalling in energy metabolism and rare human diseases. *Biochim. Biophys. Acta Bioenerg.* 1859, 845–867. doi: 10.1016/j.bbabio.2018.05.003

Dubois, T., Rommel, C., Howell, S., Steinhussen, U., Soneji, Y., Morrice, N., et al. (1997). 14-3-3 is phosphorylated by casein kinase I on residue 233: phosphorylation at this site in vivo regulates Raf/14-3-3 interaction. *J. Biol. Chem.* 272, 28882–28888. doi: 10.1074/jbc.272.46.28882

Fantl, W. J., Muslin, A. J., Kikuchi, A., Martin, J. A., MacNicol, A. M., Gross, R. W., et al. (1994). Activation of Raf-1 by 14-3-3 proteins. *Nature* 371, 612–614.

Firth, H. V., Richards, S. M., Bevan, A. P., Clayton, S., Corpas, M., Rajan, D., et al. (2009). DECIPHER: database of chromosomal inbalance and phenotype in humans using Ensembl resources. *Am. J. Hum. Genet.* 84, 524–533. doi: 10.1016/j.ajhg.2009.03.010

Fischer, A., Baljuls, A., Reinders, J., Nekhoroshkova, E., Sibilski, C., Metz, R., et al. (2009). Regulation of RAF activity by 14-3-3 proteins: RAF kinases associate

functionally with both homo- and heterodimeric forms of 14-3-3 proteins. *J. Biol. Chem.* 284, 3183–3194. doi: 10.1074/jbc.M804795200

Freeman, A. K., Ritt, D. A., and Morrison, D. K. (2013). Effects of Raf dimerization and its inhibition on normal and disease-associated Raf signaling. *Mol. Cell* 49, 751–758. doi: 10.1016/j.molcel.2012.12.018

Garnett, M. J., Rana, S., Paterson, H., Barford, D., and Marais, R. (2005). Wild-type and mutant B-RAF activate C-RAF through distinct mechanisms involving heterodimerization. *Mol. Cell* 20, 963–969. doi: 10.1016/j.molcel.2005.10.022

Gotoh, Y., Masuyama, N., Suzuki, A., Ueno, N., and Nishida, E. (1995). Involvement of the MAP kinase cascade in *Xenopus* mesoderm induction. *EMBO J.* 14, 2491–2498. doi: 10.1002/j.1460-2075.1995.tb07246.x

Harland, R. M. (1991). In situ hybridization: an improved whole-mount method for *Xenopus* embryos. *Meth. Cell Biol.* 36, 685–695. doi: 10.1016/s0091-679x28082960307-6

Heidorn, S. J., Milagre, C., Whittaker, S., Nourry, A., Niculescu-Duvas, I., Dhomen, N., et al. (2010). Kinase-dead BRAF and oncogenic RAS cooperate to drive tumor progression through CRAF. *Cell* 140, 209–221. doi: 10.1016/j.cell.2009.12.040

Hekman, M., Wises, S., Metz, R., Albert, S., Troppmair, J., Nickel, J., et al. (2004). Dynamic changes in C-Raf phosphorylation and 14-3-3 protein binding in response to growth factor stimulation. *J. Biol. Chem.* 279, 14074–14086. doi: 10.1074/jbc.m309620200

James-Zorn, C., Ponferrada, V. G., Burns, K. A., Fortriede, J. D., Lotay, V. S., Liu, Y., et al. (2015). Xenbase: core features, data acquisition, and data processing. *Genesis* 53, 486–497. doi: 10.1002/dvg.22873

Karimi, K., Fortriede, J. D., Lotay, V. S., Burns, K. A., Wang, D. Z., Fisher, M. E., et al. (2018). Xenbase: a genomic, epigenomic and transcriptomic model organism database. *Nucleic Acids Res.* 46, D861–D868. doi: 10.1093/nar/gkx936

Khokhlatchev, A. V., Canagarajah, B., Wilsbacher, J., Robinson, M., Atkinson, M., Goldsmith, E., et al. (1998). Phosphorylation of the MAP kinase ERK2 promotes its homodimerization and nuclear translocation. *Cell* 93, 605–615. doi: 10.1016/s0092-867428002981189-7

Kimelman, D., Abraham, J. A., Haaparanta, T., Palisi, T. M., and Kirschner, M. W. (1988). The presence of fibroblast growth factor in the frog egg: its role as a natural mesoderm inducer. *Science* 242:105301056.

LaBonne, C., Burke, B., and Whitman, M. (1995). Role of MAP kinase in mesoderm induction and axial patterning during *Xenopus* development. *Development* 121, 1475–1486.

LaBonne, C., and Whitman, M. (1994). Mesoderm induction by activin requires FGF-mediated intracellular signals. *Development* 120, 463–472.

LaBonne, C., and Whitman, M. (1997). Localization of MAP kinase activity in early *Xenopus* embryos: implications for endogenous FGF signaling. *Dev. Biol.* 183, 9–20. doi: 10.1006/dbio.1996.8497

Lau, J. M. C., Wu, C., and Muslin, A. J. (2006). Differential role of 14-3-3 family members in *Xenopus* development. *Dev. Dyn.* 235, 1761–1776. doi: 10.1002/dvdy.20816

Lavoie, H., Sahmi, M., Maisonneuve, P., Marullo, S. A., Thevakumaran, N., Jin, T., et al. (2018). MEK drives BRAF activation through allosteric control of KSR proteins. *Nature* 554, 549–553. doi: 10.1038/nature25478

Lavoie, H., and Therrien, M. (2015). Regulation of RAF protein kinases in ERK signaling. *Nat. Rev. Mol. Cell. Biol.* 16, 281–298. doi: 10.1038/nrm3979

Lek, M., Karczewski, K. J., Minikel, E. V., Samocha, K. E., Banks, E., Fennell, T., et al. (2016). Analysis of protein-coding genetic variation in 60,706 humans. *Nature* 536, 285–291. doi: 10.1038/nature19057

Light, Y., Paterson, H., and Marais, R. (2002). 14-3-3 antagonizes Ras-mediated Raf-1 recruitment to the plasma membrane to maintain signaling fidelity. *Mol. Cell Biol.* 22, 4984–4996. doi: 10.1128/mcb.22.14.4984-4996.2002

Liu, D., Bienkowska, J., Potosa, C., Collier, R. J., Fu, H., and Liddington, R. (1995). Crustal structure of the zeta isoform of the 14-3-3 protein. *Nature* 376, 191–194. doi: 10.1038/376191a0

MacNicol, A. M., Muslin, A. J., and Williams, L. T. (1993). Raf-1 kinase is essential for early *Xenopus* development mediates the induction of mesoderm by FGF. *Cell* 73, 571–583. doi: 10.1016/0092-867428932990143-e

MacNicol, M. C., Muslin, A. J., and MacNicol, A. M. (2000). Disruption of the 14-3-3 binding site within the B-Raf kinase domain uncouples catalytic activity from PC12 cell differentiation. *J. Biol. Chem.* 275, 3803–3809. doi: 10.1074/jbc.275.6.3803

Morrison, D. K. (2008). The 14-3-3 proteins: integrators of diverse signaling cues that impact cell fate and cancer development. *Trends Cell Biol.* 19, 16–23. doi: 10.1016/j.tcb.2008.10.003

Muller, J., Ory, S., Copeland, T., Piwnica-Worms, H., and Morrison, D. (2001). C-TAK1 regulates Ras signaling by phosphorylating the MAPK scaffold, KSR1. *Mol. Cell* 8, 983–993. doi: 10.1016/s1097-276528012900383-5

Muslin, A. J., and Lau, J. M. C. (2005). Differential functions of 14-3-3 isoforms in vertebrate development. *Curr. Topics Dev. Biol.* 65, 211–228. doi: 10.1016/s0070-215328042965008-3

Muslin, A. J., Tanner, J. W., Allen, P. M., and Shaw, A. S. (1996). Interaction of 14-3-3 with signaling proteins is mediated by the recognition of phosphoserine. *Cell* 84, 889–897. doi: 10.1016/s0092-867428002981067-3

Nie, S., and Chang, C. (2007). PI3K and Erk MAPK mediate ErbB signaling in *Xenopus* gastrulation. *Mech. Dev.* 124, 657–667. doi: 10.1016/j.mod.2007.07.005

Obsil, T., and Obsilova, V. (2011). Structural basis of 14-3-3 protein functions. *Sem. Cell Dev. Biol.* 22, 663–672. doi: 10.1016/j.semcdb.2011.09.001

Obsilova, V., Herman, P., Vecer, J., Sulc, M., Teisinger, J., and Obsil, T. (2004). 14-3-3z C-terminal stretch changes its conformation upon ligand binding and phosphorylation at Thr232. *J. Biol. chem.* 279, 4531–4540. doi: 10.1074/jbc.m306939200

Pearl, E. J., Grainger, R. M., Guille, M., and Horb, M. E. (2012). Development of *Xenopus* resource centers: the national *Xenopus* resource and the European *Xenopus* resource center. *Genesis* 50, 155–163. doi: 10.1002/dvg.22013

Richards, S., Aziz, N., Bale, S., Bick, D., Das, S., Gastier-Foster, J., et al. (2015). Standards and guidelines for the interpretation of sequence variants: a joint consensus recommendation of the American college of medical genetics and genomics and the association for molecular pathology. *Genet. Med.* 17, 405–424.

Roberts, A., Allanson, J., Jadico, S. K., Kavamura, M. I., Noonan, J., Opitz, J. M., et al. (2006). The cardiofaciocutaneous syndrome. *J. Med. Genet.* 43, 833–842.

Rommel, C., Radziwill, G., Lovric, J., Noeldeke, J., Heinicke, T., Jones, D., et al. (1996). Activated Ras displaces 14-3-3 protein from the amino terminus of c-Raf-1. *Oncogene* 12, 609–619.

Roy, F., Laberge, G., Douziech, M., Ferland-McCollough, D., and Therrien, M. (2002). KSR is a scaffold required for activation of the ERK/MAPK module. *Genes Dev.* 16, 427–438. doi: 10.1101/gad.962902

Sawyer, J. M., Harrell, J. R., Shemer, G., Sullivan-Brown, J., Rho-Johnson, M., and Goldstein, B. (2010). Apical constriction: a cell shape change that can drive morphogenesis. *Dev. Biol.* 341, 5–19. doi: 10.1016/j.ydbio.2009.09.009

Schohl, A., and Fagotto, F. (2002). β-catenin, MAPK and Smad signaling during early *Xenopus* development. *Development* 129, 37–52.

Simanshu, D. K., Nissley, D. V., and McCormick, F. (2017). RAS proteins and their regulators in human disease. *Cell* 170, 17–33. doi: 10.1016/j.cell.2017.06.009

Sluchanko, N. N. (2018). Association of multiple phosphorylated proteins with the 14-3-3 regulatory hubs: problems and perspectives. *J. Mol. Biol.* 430, 20–26. doi: 10.1016/j.jmb.2017.11.010

Smith, J. C., Price, B. M., Green, J. B., Weigel, D., and Herrmann, B. G. (1991). Expression of a *Xenopus* homolog of Brachyury (T) is an immediate-early response to mesoderm induction. *Cell* 67, 79–87. doi: 10.1016/0092-867428912990573-h

Sobreira, N., Schiettecatte, F., Valle, D., and Hamosh, A. (2015). GeneMatcher: a matching tool for connecting investigators with an interest in the same gene. *Hum. Mutat.* 36, 928–930. doi: 10.1002/humu.22844

Therrien, M., Michaud, N. R., Rubin, G. M., and Morrison, D. K. (1996). KSR modulates signal propagation within the MAPK cascade. *Genes Dev.* 10, 2684–2695. doi: 10.1101/gad.10.21.2684

Tien, C.-L., Jones, A., Wang, H., Gerigk, M., Nozell, S., and Chang, C. (2015). Snail2/Slug cooperates with Polycomb Repressive Complex 2 (PRC2) to regulate neural crest development. *Development* 142, 722–731. doi: 10.1242/dev.111997

Truong, A. B., Masters, S. C., Yang, H., and Fu, H. (2002). Role of the 14-3-3 C-terminal loop in ligand interaction. *Proteins* 49, 321–325. doi: 10.1002/prot.10210

Tzivion, G., Luo, Z., and Avruch, J. (1998). A dimeric 14-3-3 protein is an essential cofactor for Raf kinase activity. *Nature* 394, 88–92. doi: 10.1038/27938

Umbhauer, M., Marshall, C. J., Mason, C. S., Old, R. W., and Smith, J. C. (1995). Mesoderm induction in *Xenopus* caused by activation of MAP kinase. *Nature* 376, 58–62. doi: 10.1038/376058a0

Weber, C. K., Slupsky, J. R., Kalmes, H. A., and Rapp, U. R. (2001). Active Ras induces heterodimerization of cRaf and BRaf. *Cancer Res.* 61, 3595–3598.

Wu, C., and Muslin, A. J. (2002). Role of 14-3-3 proteins in early *Xenopus* development. *Mech. Dev.* 119, 45–54. doi: 10.1016/s0925-477328022900287-3

Yaffe, M. B., Rittinger, K., Volinia, S., Caron, P. R., Aitken, A., Leffers, H., et al. (1997). The structural basis for 14-3-3:phsphopeptide binding specificity. *Cell* 91, 961–971.

Conflict of Interest Statement: The authors declare that the research was conducted in the absence of any commercial or financial relationships that could be construed as a potential conflict of interest.

frontiers in Physiology

ORIGINAL RESEARCH
published: 12 April 2019
doi: 10.3389/fphys.2019.00431

Wolf-Hirschhorn Syndrome-Associated Genes Are Enriched in Motile Neural Crest Cells and Affect Craniofacial Development in *Xenopus laevis*

*Alexandra Mills†, Elizabeth Bearce†, Rachael Cella, Seung Woo Kim, Megan Selig, Sangmook Lee and Laura Anne Lowery**

Biology Department, Boston College, Chestnut Hill, MA, United States

OPEN ACCESS

Edited by:
John Noel Griffin,
Duke University, United States

Reviewed by:
Nanette Nascone-Yoder,
North Carolina State University, United States
Andrew Robson,
University of Oxford, United Kingdom

***Correspondence:**
Laura Anne Lowery
laura.lowery@bc.edu

† These authors have contributed equally to this work

Specialty section:
This article was submitted to Embryonic and Developmental Physiology, a section of the journal Frontiers in Physiology

Received: *28 November 2018*
Accepted: *28 March 2019*
Published: *12 April 2019*

Citation:
Mills A, Bearce E, Cella R, Kim SW, Selig M, Lee S and Lowery LA (2019) Wolf-Hirschhorn Syndrome-Associated Genes Are Enriched in Motile Neural Crest Cells and Affect Craniofacial Development in Xenopus laevis. Front. Physiol. 10:431. doi: 10.3389/fphys.2019.00431

Wolf-Hirschhorn Syndrome (WHS) is a human developmental disorder arising from a hemizygous perturbation, typically a microdeletion, on the short arm of chromosome four. In addition to pronounced intellectual disability, seizures, and delayed growth, WHS presents with a characteristic facial dysmorphism and varying prevalence of microcephaly, micrognathia, cartilage malformation in the ear and nose, and facial asymmetries. These affected craniofacial tissues all derive from a shared embryonic precursor, the cranial neural crest (CNC), inviting the hypothesis that one or more WHS-affected genes may be critical regulators of neural crest development or migration. To explore this, we characterized expression of multiple genes within or immediately proximal to defined WHS critical regions, across the span of craniofacial development in the vertebrate model system *Xenopus laevis*. This subset of genes, *whsc1*, *whsc2*, *letm1*, and *tacc3*, are diverse in their currently-elucidated cellular functions; yet we find that their expression demonstrates shared tissue-specific enrichment within the anterior neural tube, migratory neural crest, and later craniofacial structures. We examine the ramifications of this by characterizing craniofacial development and neural crest migration following individual gene depletion. We observe that several WHS-associated genes significantly impact facial patterning, cartilage formation, neural crest motility *in vivo* and *in vitro*, and can separately contribute to forebrain scaling. Thus, we have determined that numerous genes within and surrounding the defined WHS critical regions potently impact craniofacial patterning, suggesting their role in WHS presentation may stem from essential functions during neural crest-derived tissue formation.

Keywords: craniofacial development, developmental disorders, Wolf-Hirschhorn Syndrome, WHSC1, WHSC2, LETM1, TACC3, neural crest

INTRODUCTION

Wolf-Hirschhorn Syndrome (WHS) is a developmental disorder characterized by intellectual disability, delayed pre- and post-natal growth, heart and skeletal defects, and seizures (Hirschhorn et al., 1965; Wolf et al., 1965; Zollino et al., 2000; Battaglia et al., 2015). A common clinical marker of WHS is the "Greek Warrior Helmet" appearance; a facial pattern with a characteristic wide and flattened nasal bridge, a high forehead, prominent eyebrow arches and pronounced brow bones, hypertelorism (widely spaced eyes), a short philtrum (space between nose and lip), and micrognathia (undersized jaw). The majority of children with the disorder are microcephalic, and have abnormally positioned ears with underdeveloped cartilage. Comorbid midline deficits can occur, including cleft palate and facial asymmetries (Battaglia et al., 2015).

Craniofacial malformations are one of the most prevalent forms of congenital defects (Gorlin et al., 2001; Trainor, 2010), and can significantly complicate palliative care and quality of life (Merrow, 2016). Given the commanding role of cranial neural crest (CNC) cells in virtually all facets of craniofacial patterning, craniofacial abnormalities are typically attributable to aberrant CNC development (Walker and Trainor, 2006; Trainor, 2010). A striking commonality in the tissues that are impacted by WHS is that a significant number derive from the CNC. Despite this, little is known about how the vast diversity of genetic disruptions that underlie WHS pathology can contribute to craniofacial malformation, and no study has sought to characterize impacts of these genotypes explicitly on CNC behavior.

WHS is typically caused by small, heterozygous deletions on the short-arm of chromosome 4 (4p16.3) (**Figure 1**), which can vary widely in position and length. Initially, deletion of a very small critical region, only partial segments of two genes, was thought to be sufficient for full syndromic presentation (Gandelman et al., 1992; Wright et al., 1997; Stec et al., 1998; Bergemann et al., 2005). These first putative associated genes were appropriately denoted as Wolf-Hirschhorn Syndrome Candidates 1 and 2 (*WHSC1, WHSC2*) (Wright et al., 1997; Stec et al., 1998; Rauch et al., 2001; Simon and Bergemann, 2008; Nimura et al., 2009; Ahmed et al., 2015). However, children with WHS largely demonstrate 4p disruptions that impact not only this intergenic region between *WHSC1* and *WHSC2*, but instead affect multiple genes both telomeric and centromeric from this locus (Zollino et al., 2003). Focus was drawn to these broader impacted regions when cases were identified that neglected this first critical region entirely but still showed either full or partial WHS presentation, prompting the expansion of the originally defined critical region to include a more telomeric segment of *WHSC1*, and a new candidate, LETM1 (Zollino et al., 2000; South et al., 2008). These discrepancies are increasingly rectified by mounting evidence that true cases of the syndrome are multigenic (Zollino et al., 2008; Andersen et al., 2014; Battaglia et al., 2015); the disorder can arise from numerous and varied microdeletions, but no singular gene depletion appears sufficient to drive its full presentation.

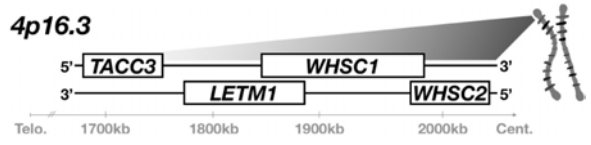

FIGURE 1 | WHS is typically caused by heterozygous microdeletion of numerous genes within 4p16.3. A segment of this region is illustrated here. A microdeletion that spans at least *WHSC1, WHSC2,* and *LETM1* is currently assumed to be necessary for full WHS diagnostic presentation; children affected by the disorder often possess larger deletions that extend further telomeric and impact additional genes, such as *TACC3*.

This multigenic nature gains new layers of complexity in the context of the functional diversity of WHS's affected genes. The first described gene in WHS, *WHSC1*, encodes for a global histone methyltransferase (Nimura et al., 2009). *WHSC2* encodes the protein Negative Elongation Factor A (NELF-A), which has multiple DNA binding motifs, and has been shown to interact with pre-mRNAs and to inhibit RNA polymerase II activity (Mariotti et al., 2000; Kerzendorfer et al., 2012; Battaglia et al., 2015). Leucine zipper and EF-hand containing transmembrane protein (LETM1*)* plays a role as a mitochondrial ion transporter (Schlickum et al., 2004). Transforming acidic coiled-coil protein 3 (TACC3) is a cytoskeletal regulator which facilitates microtubule growth in multiple embryonic cells (Nwagbara et al., 2014), in addition to critical functions in microtubule elongation at the mitotic spindle (Gergely et al., 2000; Peset and Vernos, 2008; Cheeseman et al., 2011; Ha et al., 2013a,b). Few concrete links can be made between these gene products to speculate how or why their collective depletion is required to produce full WHS pathology.

Our emerging understanding of WHS as a multigenic developmental disorder necessitates its study as such – with a renewed focus on how the depletion of these genes combinatorially contribute to a collaborative phenotype. However, a central problem arises that entirely precludes this effort: we largely lack a fundamental understanding of how singular WHS-affected genes function in basic developmental processes. Furthermore, animal models of WHS-associated gene depletion have occurred across numerous species and strains, with no unifying model to offer a comparative platform. Given the disorder's consistent and extensive craniofacial malformations, it seems especially prudent to establish whether these genes serve critical functions explicitly during processes governing craniofacial morphogenesis.

To better understand the role of these four genes in WHS pathogenesis, we examined the contributions of *whsc1*, *whsc2*, *letm1*, and *tacc3* to early craniofacial patterning in *Xenopus laevis*. We first examined expression profiles of these transcripts across early embryonic development, and notably, observed enrichment of all four transcripts in motile CNCs of the pharyngeal arches, which invites the hypothesis that they may impact neural crest development and migration. Knockdown (KD) strategies were then utilized to examine WHS-associated gene contributions to facial morphogenesis and cartilage development. We find that all KDs could variably affect facial morphology. Perhaps most notably, Whsc1 depletion increased facial width along the

axis of the tragion (across the eyes or temples), recapitulating one feature of WHS craniofacial malformation. We performed both *in vivo* and *in vitro* CNC migration assays that illustrate that Whsc1 and Tacc3 can directly affect pharyngeal arch morphology and CNC motility rates. Separately, as most of the examined transcripts also demonstrated enrichment in the anterior neural tube, we examined their impacts on embryonic forebrain scaling. We found that depletion of three of the four genes could additionally impact forebrain size. Together, our results support a hypothesis that WHS produces consistent craniofacial phenotypes (despite a vast diversity in genetic perturbations), in part due to numerous genes within the affected 4p locus performing critical and potentially combinatorial roles in neural crest migration, craniofacial patterning, cartilaginous tissue formation, and brain development. Furthermore, this work is the first to perform depletion of multiple WHS-affected genes on a shared, directly-comparable background, laying an essential foundation for future efforts to model, integrate, or predict interactions of diverse genetic disruptions within the context of a multigenic syndrome.

RESULTS

Numerous WHS-Affected Genes Demonstrate Enriched Expression in the Pharyngeal Arches, Early Nervous System, and Embryonic Craniofacial Structures

Pronounced and characteristic craniofacial dysmorphism is one of the most recognizable features of WHS-affiliated 4p16.3 microdeletions. Children with the disorder demonstrate a low-profile nasal bridge and prevalent lower forehead, with wide-set eyes and a short philtrum (together commonly referred to as the Greek Warrior's Helmet presentation). Microcephaly and micrognathia are present with varying severity, and comorbidities commonly include facial asymmetries and cleft palate (Paradowska-Stolarz, 2014). Given the commanding role of CNC cell proliferation, migration, and differentiation in properly coordinated facial patterning of nearly all of these affected tissues, we hypothesized that certain WHS-affected genes could play critical roles in neural crest maintenance, motility, or specification, and that their depletion would thus disproportionately impact tissues derived from the neural crest.

We first performed coordinated examinations of spatiotemporal expression of commonly affected genes in the 4p16.3 locus across craniofacial development. To this end, we performed *in situ* hybridization with DIG-labeled antisense RNA probes against four genes within and proximal to the last defined WHS critical region (*whsc1*, *whsc2*, *letm1*, and *tacc3*) (**Figure 1** and **Supplementary Figure S1**; for *in situ* hybrization controls against mRNA sense strands, see **Supplementary Figure S1Y**). During early craniofacial morphogenesis at stage 25, we note enriched expression of *whsc1*, *whsc2*, and *tacc3* in the migratory CNCs that populate the pharyngeal arches (**Figures 2B,C,E**). Their enrichment closely resembles the expression pattern of the CNC-enriched transcription factor *twist* (**Figures 2A,F**). Comparatively, *letm1* (**Figure 2D**) demonstrates ubiquitous expression. Interestingly, with the exception of *tacc3,* these transcripts are not significantly enriched in specified, premigratory neural crest (st. 16) (**Supplementary Figure S1**). By stage 35, all four transcripts are enriched in pharyngeal arches (**Figures 2G–J**); *letm1* expression appears to reduce in neighboring tissues, while remaining selectively enriched in CNCs during later stages of migration within the pharyngeal arches (**Figure 2I**). There is also significant transcription of all four genes within the anterior neural tube. Later in tailbud stages, some transcripts maintain enriched expression in the forebrain, most notably *whsc2*; meanwhile, *whsc1*, *whsc2*, and *letm1* are enriched in tissues within the head and face (**Supplementary Figures S1E,F,K,L,Q,R,W,X**). Additionally, *whsc1*, *letm1*, and

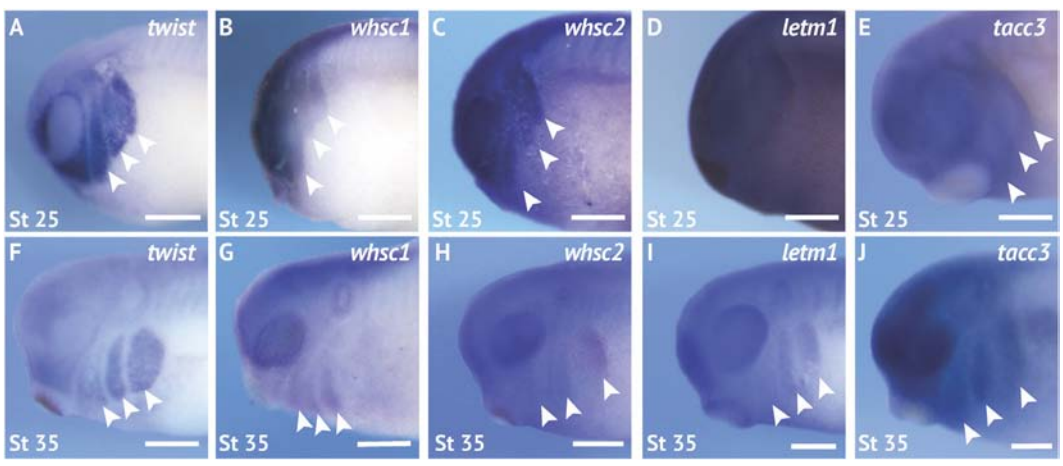

FIGURE 2 | WHS related genes are expressed in the migrating neural crest cells during embryonic development. **(A,F)** Lateral views of whole mount *in situ* hybridizations for *twist*, a CNC-enriched transcription factor. Arrows indicate the pharyngeal arches (PA). **(B–E,G–J)** *In situ* hybridizations for *whsc1*, *whsc2*, *letm1*, and *tacc3* demonstrate enrichment in CNCs that occupy the PAs (n = 20 per probe, per timepoint). Scalebar is 250 μm.

tacc3 expression show potential overlap with cardiac tissue (**Supplementary Figures S1E,Q,W**).

WHS-Affected Genes Are Critical for Normal Craniofacial Morphology

Given that all four genes showed enrichment in migratory neural crest by stage 35, and most demonstrated enduring transcription in later craniofacial tissues, we hypothesized that their protein products may function in craniofacial morphogenesis. To this end, we performed partial genetic depletions of WHS-associated genes in *X. laevis* embryos (**Supplementary Figure S2**), followed by morphometric analyses of craniofacial landmarks between WHS-associated gene KD and control conditions from the same clutch (**Figure 3**). Measurements to quantify facial width, height, midface area, and midface angle were performed as previously described (Kennedy and Dickinson, 2014) at stage 40 (**Supplementary Figure S3**).

Individual depletion of the examined WHS-affected genes demonstrated pronounced impacts on facial patterning (**Figures 3A–E**). Whsc1 depletion significantly increased facial width (**Figure 3F**), and this increase accompanied a significant increase in facial area (**Figure 3H**). Whsc2, Letm1, and Tacc3 depletion conversely narrowed facial width at this axis (**Figure 3F**), and additionally decreased facial area (**Figure 3H**). None of these changes were proportional to facial height, which was unaffected by gene depletion. In nearly all cases, the distribution of facial features was normal. Only Tacc3 depletion modestly affected the mid-face angle, a parameter describing the relationship between the eyes and mouth (**Figure 3I**). Importantly, all facial phenotypes could be rescued by co-injection with full-length mRNA transcripts of their targets (**Supplementary Figure S4**), indicating that phenotypes were specific to WHS-associated gene depletion. Taken together, these results are consistent with a possibility that Whsc1 depletion may be sufficient to drive frontonasal dysmorphism, while Whsc2, Letm1, and Tacc*3* depletions may contribute to complex or epistatic interactions, or mediate additional characteristic facial features of the disorder.

WHS-Affected Genes Maintain Craniofacial Cartilage Size and Scaling

A majority of WHS cases demonstrate defects in cartilage and skeletal formation. Notable examples include underdeveloped ears with reduced or missing cartilage, micrognathia, tooth malformation, short stature, and delayed growth of the head and body (Zollino et al., 2008; Battaglia et al., 2015), as well as jaw and throat malformations that significantly impair speech, feeding, and swallowing (Battaglia et al., 2015). The etiology of these co-morbidities is virtually unknown. As craniofacial cartilage and bone are largely derived from the CNC (Trainor and Andrews, 2013), we hypothesized that one or more of these genes may play a critical role in craniofacial cartilage formation. To test this, we performed depletion of Whsc1, Whsc2, Letm1, and Tacc3 as described above, in order to survey their impact on scaling and morphology of craniofacial cartilage in *X. laevis* larvae (**Figures 4A–I**).

Depletion of either Whsc2 or Tacc3 was sufficient to reduce the combined area of the ceratohyal and branchial arch cartilages (CH and BR, respectively, **Figure 4A**), in 6 days (stage 47) embryos (**Figure 4I**). These effects were also explicitly shown in the ceratohyal area alone (**Figure 4F**). Ceratohyal cartilage width was also reduced upon Tacc3 depletion (**Figure 4G**). Somewhat surprisingly, given the impact of Whsc1 depletion on facial width, its depletion did not increase ceratohyal width or area. Similarly, Letm1 depletion did not reduce cartilage area, despite reduction in overall facial width. These

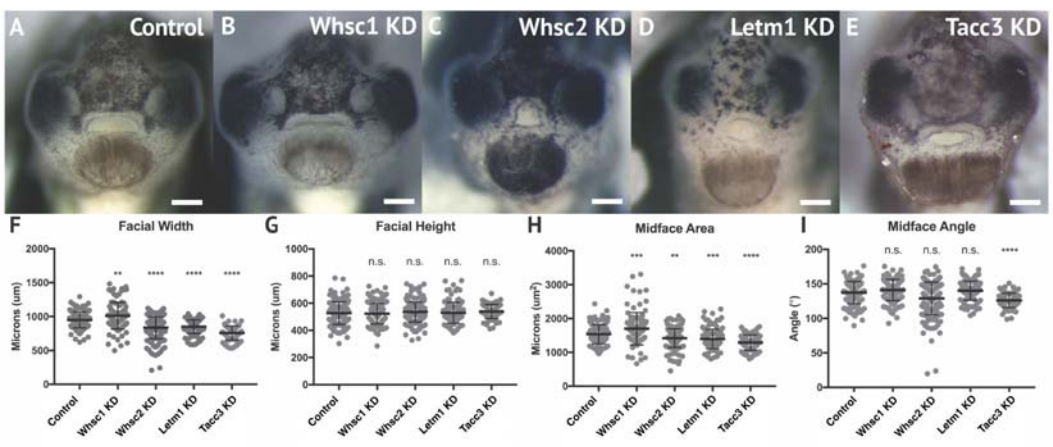

FIGURE 3 | WHS related gene depletion affects craniofacial morphology. **(A–E)** Frontal views of 3dpf embryos (st. 40) following WHS gene single KD. **(F–I)** Measurements for facial width, height, midface area, and midface angle. A significant 6.54% increase in facial width and 11.43% increase in midface area were observed for Whsc1 KD. Whsc2 KD caused a 12.01% reduction in facial width and a 6.79% reduction in midface area. Letm1 KD caused a 10.33% decrease in facial width and a 8.49% decrease in midface area. Tacc3 KD caused a 21.27% decrease in facial width and a 16.33% decrease in midface area, and an 8.27% decrease in midface angle. Significance determined using a student's unpaired *t*-test. (Embryos quantified: Control = 137, Whsc1 KD = 100, Whsc2 KD = 185, Letm1 KD = 115, Tacc3 KD = 79.) $^{****}P < 0.0001$, $^{***}P < 0.001$, $^{**}P < 0.01$, n.s., not significant. Scalebar = 250 μm.

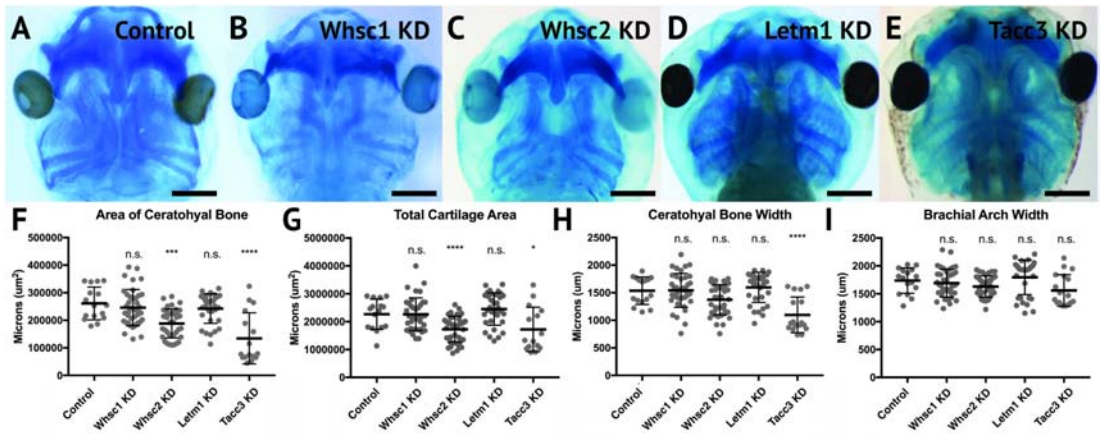

FIGURE 4 | Knockdown of Whsc2 and Tacc3 impact cartilage morphology. **(A–E)** Ventral view of 6dpf embryos following single WHS-assoc. gene KD, stained with Alcian Blue to label cartilage elements. **(F–I)** Measurements of the average area and width of the ceratohyal cartilage, total cartilage area, and width of the brachial arches. Neither Whsc1 nor Letm1 KD caused a significant change in any measured parameter. Whsc2 KD caused a 27.94% decrease in average area of the ceratohyal cartilage, and a 23.87% decrease in area of all craniofacial cartilage. Tacc3 KD caused a 48.5% decrease in the average area of the ceratohyal cartilage, a 24.03% decrease in total cartilage area, and a 28.58% decrease in ceratohyal cartilage width. Significance was determined using a student's unpaired *t*-test. (Embryos quantified: Control = 17, Whsc1 KD = 41, Whsc2 KD = 39, Letm1 KD = 34, Tacc3 KD = 11.) ****P < 0.0001, ***$P < 0.001$, *$P < 0.05$, n.s., not significant. Scalebar is 250μm.

results indicate that *whsc2* and *tacc3*, genes both within and immediately proximal to the critically-affected locus of WHS, are critical for early cartilaginous tissue formation, illustrating a potential avenue through which larger human 4p deletions may exacerbate phenotypic severity. Importantly, these effects are demonstrable at 6d post-fertilization, suggesting that early partial depletion of these transcripts produces lingering impacts on craniofacial patterning (first measured at 3 days post-fertilization, **Figure 3**) that are not ameliorated later in development. We hypothesized that these persistent patterning defects following early depletion of WHS-associated genes may then arise indirectly, from impacts on their embryonic progenitors.

Whsc1 and *tacc3* Are Critical for Normal Pharyngeal Arch Morphology and Cranial Neural Crest Cell Motility

Given the enrichment of WHS-affected gene transcripts in CNCs during stages that correspond with their migration (st. 25–35), we hypothesized that their depletion may directly compromise CNC motility. To examine this, we used single-hemisphere injection strategies to generate left-right chimeric embryos (for work flow, see **Supplementary Figure S5**), and internally compared patterns of *twist* expression to track the progress of migrating CNC along control or depleted sides.

Following single-sided Whsc1, Whsc2, Letm1, or Tacc3 depletion, embryos were staged to 25–30, fixed, and *in situ* hybridization was performed against *twist*. Measurements of length and area of *twist* expression were taken, to quantify CNC migration away from the anterior neural tube, and these were compared to their internal, contralateral controls. Whsc1 and Tacc3 depletion reduced total area of CNC streams (**Figures 5C,H**). Further, when Whsc1 levels were reduced, the CNC streams were shorter in length (**Figure 5D**), and their ventral migration distance was reduced compared to paired controls (**Figure 5E**). Whsc2 and Letm1 reduction, in contrast, did not result in any significant changes to CNC migration. This suggests a role specifically for *whsc1* and *tacc3* in maintaining normal CNC motility into the PAs.

Smaller areas of *twist* expression, as shown with either Whsc1 or Tacc3 depletion, could result from reduced migration rates, as cells accumulate into denser, slower packs; but it is also possible that CNCs may occupy smaller regions if a genetic perturbation affects their proliferation rates (resulting in fewer cells overall). To determine whether Whsc1 depletion could specifically impact neural crest migration speed, *in vitro* migration assays were performed as described previously (Alfandari et al., 2001; Milet and Monsoro-Burq, 2014). Whole embryos were injected with either control or Whsc1 KD strategies, and their CNCs were dissected prior to delamination from the neural tube (st. 17). These tissue explants were cultured on fibronectin-coated coverslips, and trajectories of individual cells that escaped the explant were mapped using automated particle tracking (Schindelin et al., 2012; Tinevez et al., 2017). Whsc1 depletion resulted in slower individual cell speeds compared to controls (**Figures 6B–D** and **Supplementary Video S1**). Tacc3 KD was also sufficient to reduce individual CNC speeds (not shown). We then compared these results to those obtained following Whsc2 depletion. As Whsc2 KD was not sufficient to alter CNC streaming areas *in vivo* (**Figures 5K–O**), we hypothesized that cell motility speed *in vitro* would not be affected by this depletion. Instead, Whsc2 KD resulted in a significant increase in speed of CNCs migrating in culture (**Figure 6D**). As CNC migration is heavily restricted *in vivo* due to repellent and non-permissive substrate boundaries within the Pas (Szabó et al.,

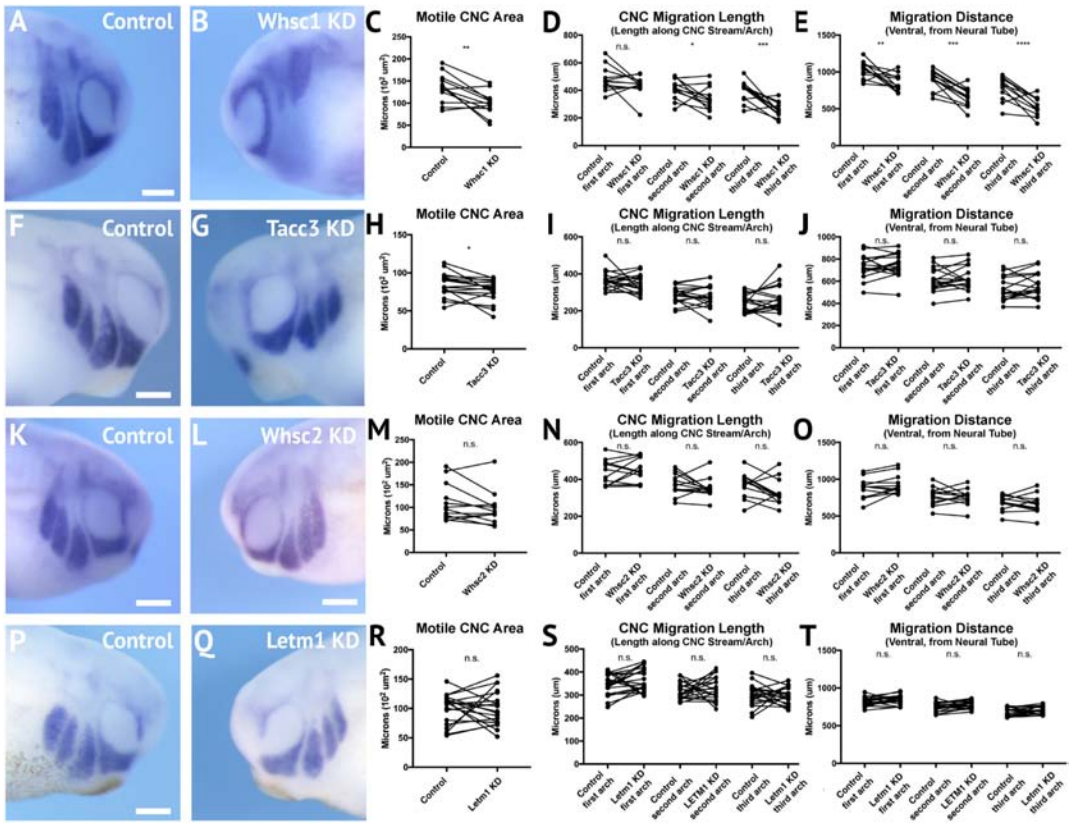

FIGURE 5 | Knockdown of Whsc1 and Tacc3 decrease CNC migration *in vivo*. **(A,B,F,G,K,L,P,Q)** Anterior lateral views of tailbud stage embryos (depicted at st. 27), following whole mount *in situ* hybridization against *twist*. Each column of panels **(A,B,F,G,K,L,Q)** are lateral views of two sides of the same embryo. **(C–E,H–J,M–O,R–T)** Measurements were taken for the total area of the three PA (Arch 1-3 extend anterior to posterior), the length of each individual arch, and the migration distance, as measured from the dorsal most tip of each arch to the neural tube. Embryos were stained and quantified at stages 25–30. **(K–T)** Letm1 or Whsc2 KD did not significantly affect any of the measured parameters. **(F–J)** Tacc3 KD expression caused an 8.33% decrease in the total PA area, but did not affect length or arch migration. **(A–E)** Whsc1 KD caused a 23.57% decrease in PA area. Additionally, the length of the second and third pharyngeal arches decreased by 14.72 and 31.70%, respectively. The migration distance of the first, second and third pharyngeal arches decreased by 15.75, 24.04, and 29.29%, respectively. Significance determined using a student's paired *t*-test. (Embryos quantified: Whsc1 KD = 13, Tacc3 KD = 18, Whsc2 KD = 12, Letm1 KD = 19.) $^{****}P < 0.0001$, $^{***}P < 0.001$, $^{*}P < 0.05$, n.s., not significant. Scalebar is 250 μm.

2016), in addition to the coordinated relationships between CNC and placodal cell migration (Theveneau et al., 2013), it is not surprising that a moderate increase in individual cell motility speeds *in vitro* may not correspond to a notable increases in CNC streaming within the PAs. In contrast, a deficit in individual cell migration rate, as shown with Whsc1 and Tacc3 depletion, may lack compensatory strategies and more directly delay CNC streaming. Thus, we show that Whsc1 depletion alters CNC infiltration into the PAs, and that this effect could be directly driven by a reduction in individual CNC migration rates.

WHS-Related Genes Impact Forebrain Morphology

In addition to craniofacial dysmorphism, children with 4p16.3 microdeletions demonstrate mild to profound intellectual disability, with a large majority displaying significant psychomotor and language delays that entirely preclude effective communication (Zollino et al., 2008; Battaglia et al., 2015; Bernardini et al., 2018). Larger microdeletions have generally been correlated to more severe intellectual disability and microcephaly, implying that numerous WHS-affected genes may function combinatorially or synergistically to facilitate central nervous system development and cognitive function (Zollino et al., 2008). Alternatively, this may suggest that genes that are further telomeric within the affected loci could be more impactful contributors to cognitive deficits.

We have largely focused our current efforts to examine the developmental contributions of WHS-affected genes to neural crest migration and craniofacial development, and development of the central nervous system should largely be considered to function distinctly and be examined in future works. However, given the significant craniofacial malformations demonstrated with WHS-associated gene depletion, and the intimate ties between central nervous system and craniofacial development (Demyer et al., 1964; Aoto and Trainor, 2015), we also performed

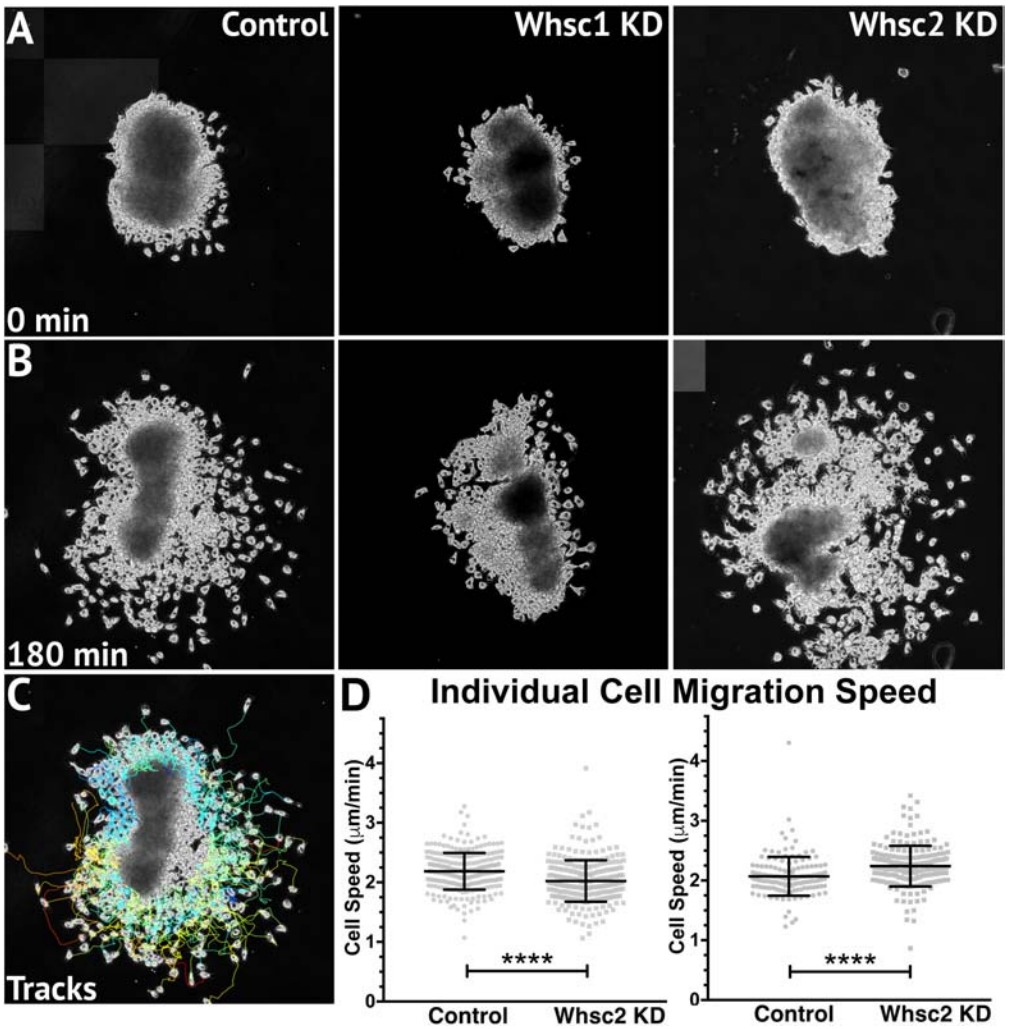

FIGURE 6 | Whsc1 manipulation alters CNC migration speeds *in vitro*. Dissected CNC explants from control, Whsc1 KD, or Whsc2 KD embryos were plated on fibronectin-coated coverslips, allowed to adhere and begin migration, and imaged for 3 h using 20× phase microscopy. **(A)** Representative explants at initial timepoint (0 min). **(B)** Explants after 3 h migration time. **(C)** Representative tracks generated by FiJi Trackmate plug-in. **(D)** Mean track speeds of Whsc1 or Whsc2 KD explants compared to their controls. (Explants quantified: 3–4 explants from control and KD embryos were plated for each experiment, explants with neural or epithelial contaminant were excluded from analysis. Three separate experiments were performed for each depletion. Whsc1 controls: 272 cells, 9 explants. Whsc1 KD: 282 cells, 9 explants. Whsc2 controls: 151 cells, 12 explants. Whsc2 KD: 195 cells, 8 explants.) $^{****}P < 0.0001$, n.s., not significant. Scalebar is 250μm.

initial characterization of how these WHS-affected genes may singularly contribute to one aspect of neurodevelopment; embryonic forebrain scaling.

To address the impact of Whsc1, Whsc2, Letm1, and Tacc3 on forebrain size, we performed half-embryo depletions as above, and examined the outcomes on embryonic brain size. Embryos were injected with single-hemisphere depletion strategies at the 2-cell stage, and then allowed to mature to 6 days (st. 47) prior to fixation. Immunolabeling for alpha-tubulin was carried out to highlight neuronal morphology (**Figure 7**; for experimental workflow, see **Supplementary Figure S5**), and brain areas were compared using paired *t*-tests between KD and control hemispheres. Forebrain size was significantly reduced with Whsc1, Whsc2, or Tacc3 KD (**Figures 7B,C,E,F,K,L**). Control injections did not affect brain size, relative to internal non-injected controls (**Supplementary Figure S5**). Whsc2 depletion caused an additional decrease to midbrain area (**Figure 7F**). Letm1 depletion did not impact forebrain sizing (**Figures 7G–I**), however, *LETM1* deletion is suspected to be the major contributor to seizure development in children with the disorder (Jiang et al., 2009; Andersen et al., 2014). This only highlights the importance of future characterizations of the cell biological functions of WHS-impacted genes, as it could be suggested that LETM1 depletion may instead disrupt normal neuronal excitation, connectivity, or survival (Huang et al., 2017). These initial investigations suggest that *whsc1*, *whsc2*, and *tacc3* facilitate normal forebrain development, and perhaps that their depletion is relevant to WHS-associated microcephaly.

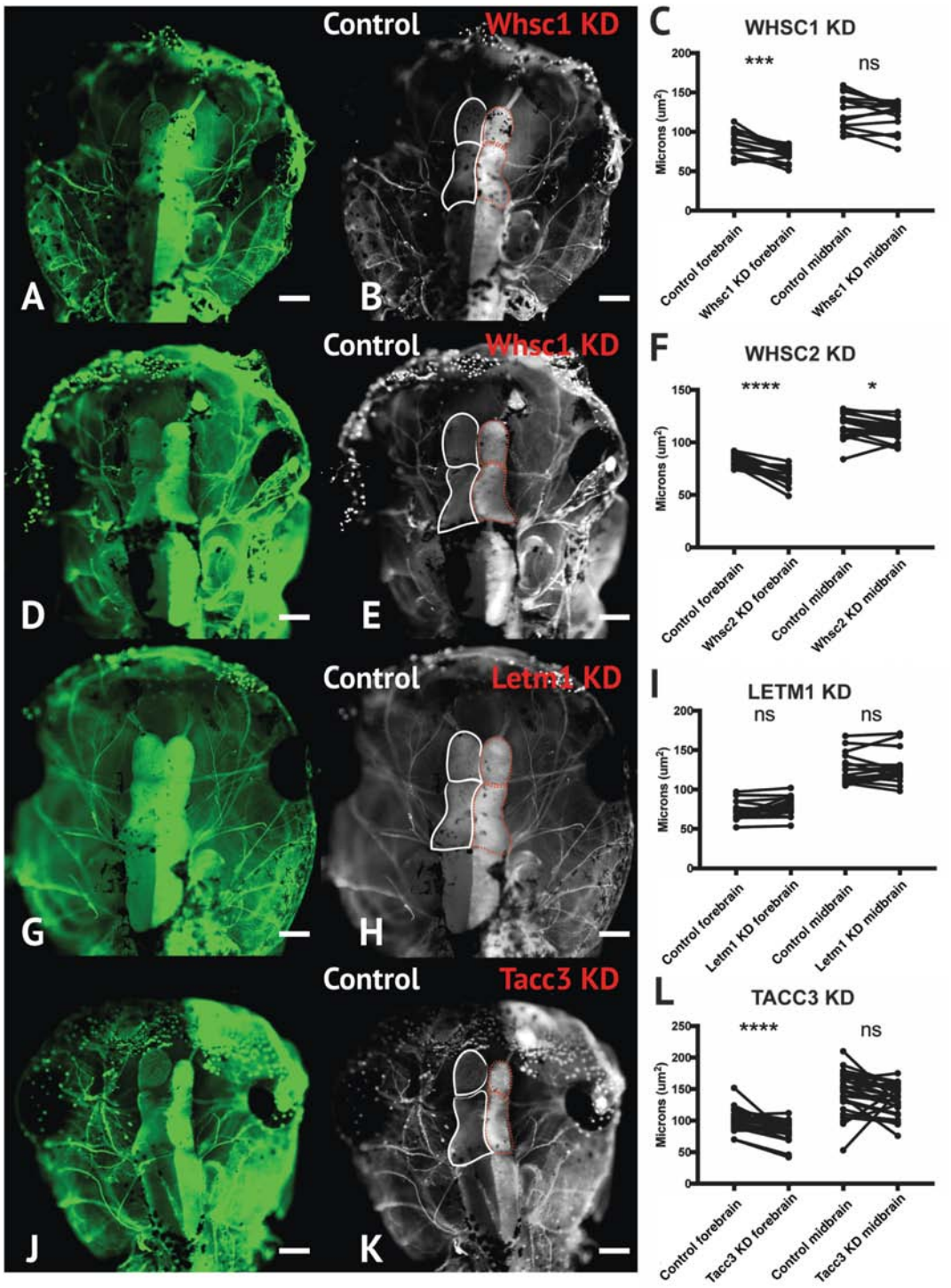

FIGURE 7 | Whsc1, whsc2, and tacc3 facilitate normal forebrain development. **(A,B,D,E,G,H,J,K)** Dorsal view of *X. laevis* half-embryo gene depletions (6 days post-fertilization), following alpha-tubulin immunolabeling to highlight nervous system. **(B,E,H,K)** Dorsal view of embryos with superimposed outlines of forebrain and midbrain structures. Internal control is on left (white), depleted side is on right (dashed red). (Alpha-tubulin staining is bilateral; exogenous eGFP on KD side persisted in embryos shown, causing a unilaterally enriched green signal.) **(C,F,I,L)** Area of forebrain and midbrain. Whsc1 KD reduced forebrain area by 17.65%. Whsc2 KD reduced forebrain area by 17.33% and midbrain area by 4.14%. Letm1 KD caused no significant change in brain size. Tacc3 KD caused a 16.05% decrease in forebrain area. Significance determined using a student's paired *t*-test. (Embryos quantified: Whsc1 KD = 14, Whsc2 KD = 18, Letm1 KD = 12, Tacc3 KD = 26.) $^{****}P < 0.0001$, $^{***}P < 0.001$, $^{*}P < 0.05$, n.s., not significant. Scalebar is 250 μm.

DISCUSSION

We have shown that four genes frequently affected in WHS, a human genetic disorder stemming from a heterozygous microdeletion on the short arm of chromosome four, can contribute to normal craniofacial morphogenesis in *Xenopus laevis* (**Figure 8**). We also provide evidence that neural crest migration deficits may significantly contribute to the signature craniofacial dysmorphism of WHS. Specifically, we demonstrate, for the first time, that WHS-associated genes are enriched in motile neural crest and contribute to normal craniofacial patterning and cartilage formation (*whsc1*, *whsc2*, *letm1*, and *tacc3*). Two of these genes directly impact individual CNC cell migration (*whsc1* and *tacc3*), revealing new basic roles for these genes in embryonic development.

It is increasingly appreciated that full WHS presentation is multigenic (Zollino et al., 2008); case studies of children with singular gene depletions even in critical regions have historically demonstrated milder syndromic presentations that lack the full range of expected symptoms (intellectual disability, craniofacial abnormalities, seizures, and heart, skeletal, and urogenital defects) (Rauch et al., 2001). While we have narrowed our examinations to focus on how WHS-affected genes contribute to facial patterning, our findings align well with the idea that WHS presentation is a cumulative product of the impacted locus. While Whsc1 and Tacc3 depletions impacted all or nearly all examined aspects of craniofacial development at these stages, Whsc1 KD did not produce significant cartilage malformations in isolation, and Tacc3 KD narrowed and condensed facial features in a way that appears less analogous to the human "Greek Warrior Helmet" phenotypic presentation.

Of important note, then, only Whsc1 depletion appeared to cause hypertelorism, or facial widening at the level of the eyes and nasal bridge (**Figures 3**, **8**). As the eyes correspond to the peripheral extrema of the tadpole face, this contributed to a wider face along the axis of the tragion, which may correlate with 3D morphological mapping data that demonstrates an overall facial widening in children with WHS along the same axis (Hammond et al., 2012). It is interesting to predict that normal WHSC1 levels could facilitate normal neural crest migration, and in a separate role more explicit to this tissue region, also limit inappropriate proliferation and expansion. In potential support of this, one of WHSC1's more established roles is that of an H3K36 methyltransferase, an epigenetic regulator that has been billed as oncogenic, given high levels of dysregulation in some cancer tissues (Huang et al., 2013; Kuo et al., 2013), and its potential to orchestrate transcriptional programs that drive unchecked proliferation (Park et al., 2018). Other studies report its function to be that of a tumor suppressor, given its high mutation rate in lymphomas (Beà et al., 2013; Zhang et al., 2014); additionally, *whsc1* knockout or depletion in zebrafish demonstrated enlarged hearts, brains, and predisposition to swim bladder tumors (Yamada-Okabe et al., 2010; Yu et al., 2017), suggesting unchecked expansion of developmental progenitors. As this duality likely partially reflects differential regulation of WHSC1 behavior during development and in the context of oncogenesis, an explicit examination of how WHSC1 functions to regulate tissue expansion and development in the extreme anterior domain may be warranted (Jacox et al., 2016). Additionally, given that the other three WHS-affected genes instead narrowed facial width and area, this invites further investigation into how these depletions function combinatorially to generate the full signature of WHS craniofacial dysmorphism.

Within that effort, however, it is worthwhile to note that WHS-associated gene depletion in *X. laevis* almost certainly diverges from perfect recapitulation of WHS pathology. *Xenopus* has proven to be an invaluable model for the study of human craniofacial development and disorders (Kennedy and Dickinson, 2014; Tabler et al., 2014; Devotta et al., 2016; Dickinson, 2016; Liu, 2016; Deniz et al., 2017;

4p16.3 Gene	Expression		Morphology		Cartilage		PA Morph.		Motility		Brain size	
whsc2	✓	Enriched in PA (st. 25, 35)	✓	Reduced width -12.0% area -6.8%	✓	Reduced ceratohyal area -27.9%				Increased mean CNC speed +8.2%	✓	Reduced forebrain -17.3% midbrain -4.1%
whsc1	✓	Enriched in PA (st. 25, 35)	✓	Increased width +6.5% area +11.4%			✓	Reduced PA area -23.6% migration (Fig. 5)	✓	Reduced mean CNC speed -7.5%	✓	Reduced forebrain -17.7%
letm1	✓	Enriched in PA (st. 35)	✓	Reduced width -10.3% area -8.5%								
tacc3	✓	Enriched in PA (st. 16*, 25, 35)	✓	Reduced width -21.3% area -16.3% angle -8.3%	✓	Reduced ceratohyal area -48.5% width -28.6%	✓	Reduced PA area -8.3%	✓		✓	Reduced forebrain -16.1%

FIGURE 8 | Partial depletion of WHS-affected genes demonstrates numerous impacts on craniofacial development and neural crest migration. Tissues are denoted as affected (checked box) if phenotypes were significantly different from control ($p \leq 0.05$); see individual figures for data distribution and statistics. (Abbreviations: PA, Pharyngeal Arch) *Denotes pre-migratory CNC (st. 16).

Dubey and Saint-Jeannet, 2017; Griffin et al., 2018), given the highly conserved developmental pathways that drive neural crest migration, differentiation, and craniofacial morphogenesis between systems. Nonetheless, there are gross morphological differences that prevent some direct correlations. It is noteworthy that the CNC that give rise to the ceratohyal cartilage in *Xenopus* will later give rise to far anterior portions of the face, and combine with contributions from the Meckel's cartilage to form some regions of the jaw (Gross and Hanken, 2008; Kerney et al., 2012), but equivalent human craniofacial structures undergo distinct development (Frisdal and Trainor, 2014). Loosely, the ceratohyal cartilage in *X. laevis* is formed from CNC of the second PA (Gross and Hanken, 2008; Dubey and Saint-Jeannet, 2017); which in human development will give rise to tissues of the hyoid (Frisdal and Trainor, 2014). Morphological impacts resulting from aberrant development of these tissues, as was shown with either Tacc3 or Whsc2 depletion (**Figure 4**), may then have more direct correlates to human WHS pathology in the context of aberrant pharyngeal development, rather than explicitly in jaw formation or WHS-associated micrognathia.

Our work has demonstrated consistent enrichment of WHS-associated genes in CNCs, and their necessity for normal formation of their derivatives, however, this largely neglects why any of these transcripts may be exceptionally critical in these tissues. This question must be left to some speculation; the precise cell biological roles of all WHS-affected genes warrant much more comprehensive study in the context of embryonic development and cell motility. We have previously summarized some of the known roles of these genes and how they may influence CNC development (Rutherford and Lowery, 2016), but a brief summary incorporating recent work is outlined here.

WHSC2 encodes the gene product NELFA, which functions within the NELF complex to decelerate or pause RNA polymerase II activity (Luo et al., 2013). This pausing mechanism is thought to function as a means of synchronizing rapid or constitutive expression of specific transcripts (Gilchrist et al., 2010; Adelman and Lis, 2012; Pan et al., 2014). NELF complex components are required during early embryogenesis (Amleh et al., 2009), but their relevance in craniofacial morphogenesis and neural crest migration is entirely unknown. Recent work suggests the NELF complex facilitates cancer cell proliferation and motility, downstream of its regulation of cell-cycle control transcripts (El Zeneini et al., 2017). Given that motility and proliferation inherently compete for cytoskeletal machinery (Matus et al., 2015), the CNC's somewhat unique need to undergo both rapid expansion and directed motility (Monsoro-Burq, 2015) within the same developmental stages may benefit from these additional levels of coordination, but this remains entirely speculative.

LETM1 localizes to the inner mitochondrial membrane (Schlickum et al., 2004), where it acts as a Ca2(+/H(+ anti-porter to regulate Ca2(+ signaling and homeostasis (Jiang et al., 2013)[72], which can directly affect activity of mitochondrial metabolic enzymes. LETM1 was shown to actively regulate pyruvate dehydrogenase activity, tying its roles directly to glucose oxidation (Durigon et al., 2018)[73]. Its ubiquitous enrichment across early development (Fig.**Figure 2D**), and enduring expression within motile CNC (Fig.**Figure 2I**) might suggest distinct and spatiotemporal metabolic needs during neurulation and craniofacial patterning. Interestingly, NELF complex (containing WHSC2/NELF-A), has been shown to stabilize transcription of fatty acid oxidation-related genes (Pan et al., 2014)[66], which would suggest dual-depletion of these in areas where they are typically enriched (Fig.**Figure 2**) may greatly impact metabolic homeostasis. This could be especially damaging in the context of the multipotent CNCs, as metabolism is increasingly demonstrated to perform a commanding role in determination of cell fate (Shyh-Chang et al., 2013; Sperber et al., 2015; Mathieu and Ruohola-Baker, 2017; Perestrelo et al., 2018).

TACC3 is predominantly known as a microtubule regulator. Originally characterized as an essential centrosome adapter during cell division (Gergely et al., 2000; Piekorz et al., 2002), its manipulation was more recently shown to impact microtubule plus-end growth in interphase cells and specifically CNCs (Nwagbara et al., 2014). It has also demonstrated effects on cytoskeletal mechanics during one form of embryonic cell motility, axon outgrowth and guidance signal response (Nwagbara et al., 2014; Erdogan et al., 2017). Its significant dysregulation in metastatic cancers (Ha et al., 2013a,b; Li et al., 2017), and roles in mitotic spindle organization (Albee and Wiese, 2008; Cheeseman et al., 2011; Nixon et al., 2015; Burgess et al., 2018) may allude to additional functions in cytoskeletal coordination of either CNC proliferation or motility, but this remains unexplored. Altogether, it is clear that our current knowledge of how these genes ultimately contribute to embryonic development is lacking, and a basic cell biological examination of WHS-associated gene function within a developmental context is necessary for a better mechanistic understanding of WHS etiology.

Finally, it will also be essential to explore how these genes ultimately synergistically or epistatically regulate WHS pathology. To this aim, our model provides the unique advantage of titratable, rapid, and inexpensive combinatorial depletion of numerous genes, and an intuitive next step will be to perform depletions in tandem that would mirror the genetic perturbations identified from both typical and atypical case studies of WHS. Altogether, our current and ongoing work suggests significant roles for numerous 4p16.3 genes as potent effectors of neural crest-derived tissues and craniofacial morphogenesis.

MATERIALS AND METHODS

Xenopus Husbandry

Eggs obtained from female *Xenopus laevis* were fertilized *in vitro*, dejellied and cultured at 13–22°C in 0.1X Marc's modified Ringer's (MMR) using standard methods (Sive et al., 2010). Embryos received injections of exogenous mRNAs or antisense oligonucleotide strategies at the two- or four- cell stage, using four total injections (1 injection per blastomere in 4-cell, 2 injections per blastomere in 2-cell) performed in 0.1X MMR media containing 5% Ficoll. Embryos were staged according to Nieuwkoop and Faber (1994). All experiments were approved by the Boston College Institutional Animal Care and Use Committee and were performed according to national regulatory standards.

Immunostaining

Whole-mount immunostaining was carried out using mouse anti-acetylated tubulin (Sigma, St. Louis, MO, United States T7451, 1:500), with goat anti-mouse Alexa Fluor 488 (Invitrogen, 1:1000) as a secondary antibody. 5 dpf embryos were fixed in 4% paraformaldehyde in PBS for 1 h, rinsed in PBS and gutted to reduce autofluorescence. Embryos were processed for immunoreactivity by incubating in 3% bovine serum albumin, 1% Triton-X 100 in PBS for 2 h, then incubated in antibodies (4°C, overnight). Embryos were cleared in 1% Tween-20 in PBS and imaged in PBS after removal of the skin dorsal to the brain. Images were taken using a Zeiss AxioCam MRc attached to a Zeiss SteREO Discovery.V8 light microscope. Images were processed in Photoshop (Adobe, San Jose, CA, United States). Area of the forebrain and midbrain were determined from raw images using the polygon area function in ImageJ (Schneider et al., 2012). Statistical significance was determined using a student's paired *t*-test.

Whole Mount *in situ* Hybridization

Embryos were fixed overnight at 4°C in a solution of 4% paraformaldehyde in phosphate-buffered saline (PBS), gradually dehydrated in ascending concentrations of methanol in PBS, and stored in methanol at −20°C for a minimum of 2 h, before *in situ* hybridization, which was performed on fixed embryos as previously described (Saint-Jeannet, 2017). After brief proteinase K treatment, embryos were bleached under white light in 1.8× saline-sodium citrate, 1.5% H_2O_2, and 5% (vol/vol) formamide for 20 min to 1 h before prehybridization. During hybridization, probe concentration was 0.5 μg/mL. The *tacc3* construct used for a hybridization probe was subcloned into the pGEM T-easy vector (Promega, Madison, WI, United States). The *Xenopus Twist* hybridization probe was a kind gift from Dr. Dominique Alfandari (University of Massachusetts at Amherst, MA, United States), which was subcloned into the pCR 2.1TOPO vector (AddGene, Cambridge, MA, United States). The template for making an antisense probe for *letm1* was PCR amplified from the reverse transcribed cDNA library, using primer set (5′- CATGGCTTCCGACTCTTGTG, CTAGCTAATACGACTCACTATAGGGCTACAGATGGTACAG AGG-3′), then subcloned into the pCS2 vector (AddGene, Cambridge, MA, United States). Templates for *whsc1* and *whsc2* antisense probes were PCR amplified from ORFeomes (European Xenopus Resource Center, United Kingdom) with the following primer sets: *Whsc1* forward 5′-CTCATATCCTCGGAAGTCCAGC-3′, *whsc1* backward 5′-CTAGCTAATACGACTCACTATAGGACCATACAACATCTCC AACAG-3′, *whsc2* forward 5′-CCTCCGTCATAGACAAC GTG-3′, and *whsc2* backward 5′-CTAGCTAATACGACTCA CTATAGGAGAGGAGTTGTTGTGTCCAG-3′; these products were cloned into the pDONR223 vector (AddGene, Cambridge, MA, United States). The antisense digoxigenin-labeled hybridization probes were transcribed in vitro using the T7 MAXIscript kit. Embryos were imaged using a Zeiss AxioCam MRc attached to a Zeiss SteREO Discovery.V8 light microscope. Images were processed in Photoshop (Adobe, San Jose, CA, United States).

Depletion

Morpholino antisense oligonucleotides (MO) were used to target WHS related genes. *Whsc2* and *tacc3* MOs targeted the translation start site of *Xenopus laevis whsc2* (5-TGTCACTATCCCTCATAGACGCCAT-3) and *tacc3* (5-AGTTGTAGGCTCATTCTAAACAGGA3), respectively. *Whsc1* MO targeted the intron exon boundary of intron 5 of *Xenopus laevis whsc1* (5-TGCGTTTTCATGTTTACCAGAGTCT-3) and *letm1* MO targeted the intron exon boundary of intron 1 of *Xenopus laevis letm1*(5-ATGACACACAAGTGCTACTTACCCT-3). These WHS gene specific MOs, or standard control MO (5-CCTCTTACCTCAGTTACAATTTATA-3) (purchased from Gene Tools, LLC, Philomath, OR, United States), were injected into two-to-four cell stage embryos (10–30 ng/embryo).

Knockdown of Whsc2 and Tacc3 were assessed by Western blot (**Supplementary Figure S4**). Embryos at stage 35 were lysed in buffer (50 mM Tris pH 7.5, 5% glycerol, 0.2% IGEPAL, 1.5 mM MgCl2, 125 mM NaCl, 25 mM NaF, 1 mM Na3VO4, 1 mM DTT, supplemented with Complete Protease Inhibitor Cocktail with EDTA, Roche). Blotting for Whsc2 was carried out using mouse monoclonal antibody to Whsc2 (Abcam, ab75359, dilution 1:3,000). *Tacc3* start site MO was validated as previously described (Monsoro-Burq, 2015). Detection was by chemiluminescence using Amersham ECL Western blot reagent (GE Healthcare BioSciences, Pittsburg PA, United States). The bands were quantified by densitometry using ImageJ (Schneider et al., 2012).

Whsc1 and *letm1* splice site MOs were validated through a reverse transcriptase polymerase chain reaction (rt PCR). Total RNA was extracted by homogenizing embryos 48hrs post fertilization in Trizol. RNA purification was performed according to the Qiagen RNA purification protocol. A phenol:chloroform extraction was performed followed by ethanol precipitation. cDNA was synthesized using SuperScript II Reverse Transcriptase. PCR was performed in a Mastercycler using HotStarTaq following the Qiagen PCR protocol. Primers for *letm1* were as follows; forward 5′-GTACGAGGCTGTGTGCTGAG-3′ and backward 5′-CGGTTTCCACTTCGCTGACG -3′. Primers for *whsc1* were as follows; forward 5′-GTCGTACAAGAGAAGACGAGTG-3(' and backward 5('- GTCAGTGAAGCAGGAGAAGAAC- 3('. Band intensity was measured using densitometry in ImageJ (Burgess et al., 2018; **Supplementary Figure S4**).

Rescue experiments were performed with exogenous mRNAs co-injected with their corresponding MO strategies. *Xenopus* ORFs for *whsc1* and *whsc2* were purchased from EXRC and gateway-cloned into pCSF107mT-GATEWAY-3′-LAP tag (Addgene plasmid #67618, a generous gift from Todd Stunkenberg). A complete coding sequence of *X. tropicalis letm1* was purchased from Dharmacon (Lafayette, CO, United States) then subcloned into pCS2+ EGFP vector. Plasmid for TACC3 cloned into pET30a was a kind gift from the Richter lab (University of Massachusetts Medical School, Worcester,

MA, United States), which was subcloned into pCS2. As a start-site MO was utilized to block *tacc3* translation, a MO-resistant exogenous mRNA was generated by creating conserved mutations in the first 7 codons. Rescue concentrations are described in **Supplementary Figure S3**.

Cartilage Staining

At 6 dpf, *Xenopus* embryos were anesthetized with benzocaine and fixed in cold 4% paraformaldehyde in PBS and were left at 4°C overnight. Alcian Blue staining of embryos was performed based on the Harland Lab protocol. Before ethanol dehydration, embryos were bleached under white light in 1.8x saline-sodium citrate, 1.5% H2O2, and 5% (vol/vol) formamide for 30 min. Embryos were imaged in PBS, using a Zeiss AxioCam MRc attached to a Zeiss SteREO Discovery.V8 light microscope. Images were processed in Photoshop (Adobe, San Jose, CA). Analysis of cartilage structures was performed in ImageJ utilizing the polygon, area, and line functions (Schindelin et al., 2012). Measurements included (1) Total cartilage area measured as the area of the cartilage from the base of the branchial arches, along either side of cartilage structure, and around the infracostal cartilage. (2) Average ceratohyal cartilage area (see outlined cartilage in **Figure 4**). (3) Branchial arch width was determined by measuring the width of the branchial arch region at the widest point. (4) Ceratohyal cartilage width was determined using the line function at the widest point on the ceratohyal cartilage. Differences were analyzed by student unpaired *t*-test.

Quantifying Craniofacial Shape and Size

Stage 40 embryos (66 hpf) were fixed in 4% paraformaldehyde in PBS overnight at 4°C. A razor blade was used to make a cut bisecting the gut to isolate the head. Isolated heads were mounted in small holes in a clay-lined dish containing PBS. The faces were imaged using a Zeiss AxioCam MRc attached to a Zeiss SteREO Discovery. V8 light microscope. ImageJ (Schindelin et al., 2012) software was used to perform craniofacial measurements. These measurements included the: (1) intercanthal distance, or the distance between the eyes, (2) face height, or the distance between the top of the eyes and the top of the cement gland at the midline, (3) midface angle, the angle created by drawing lines from the center of one eye, to the dorsal midline of the mouth, to the center of the other eye, and (4) midface area, the area measured from the top of the eyes to the cement gland encircling the edges of both eyes (see **Supplementary Figure S3**). For all facial measurements, Student's unpaired *t*-tests were performed between KD embryos and control MO injected embryos to determine statistical relationships. Protocol was lightly adapted from Kennedy and Dickinson (2014).

Half Embryo Injections

Half knockdowns were performed at the two-cell stage; *X. laevis* embryos were unilaterally injected two times with both WHS gene-specific MO and a GFP mRNA construct. Half the quantity of morpholino was injected per embryo as compared to full bilateral knockdowns. The other blastomere was injected with a control MO at the same dose. Embryos were raised in 0.1X MMR through neurulation, at which point they were sorted based on left/right fluorescence. In order to complete pharyngeal arch visualization, embryos were fixed between stage 25–30 and whole-mount *in situ* hybridization for *twist* was performed according to the previously described procedure. For brain morphology analysis, embryos were fixed 6 dpf and prepared for alpha-tubulin immunostaining.

Analysis of pharyngeal arches from *in situ* experiments was performed on lateral images in ImageJ (Schneider et al., 2012). Measurements were taken to acquire: (1) Arch area: the area of individual *twist* labeled streams within the PA, determined using the polygon tool. (2) Arch length: The length of the distance between the top and bottom of each *twist* labeled CNC stream. (3) Arch migration was determined using the line function, as measured from the ventral most part of the *twist* signal to the neural tube. Statistical significance was determined using a student's paired *t*-test in Graphpad (Prism).

Neural Crest Explants, Imaging, and Analysis

A very helpful and thorough guide to neural crest isolation has been described previously (Alfandari et al., 2001; Milet and Monsoro-Burq, 2014).

We offer only minor modifications here. Stage 18 embryos were placed in modified DFA solution (53 mM NaCl, 11.7 mM Na2CO3, 4.25 mM K Gluc, 2 mM MgSO4, 1 mM CaCl2, 17.5 mM Bicine, with 50 μg/mL Gentamycin Sulfate, pH 8.3), before being stripped of vitelline membranes and imbedded in clay with the anterior dorsal regions exposed. Skin was removed above the neural crest using an eyelash knife, and neural crest explants were dissected out. Explants were rinsed, and plated on fibronectin-coated coverslips in imaging chambers filled with fresh DFA. Tissues were allowed to adhere 45 min before being moved to the microscope for time lapse imaging of CNC motility.

Microscopy was performed on a Zeiss Axio Observer inverted motorized microscope with a Zeiss 20x N-Achroplan 0.45 NA phase contrast lens, using a Zeiss AxioCam camera controlled with Zen software. Images were collected using large tiled acquisitions to capture the entire migratory field. Eight to ten explants, from both control and experimental conditions were imaged at a 6 min interval, for 3 h. Data was imported to Fiji (Schindelin et al., 2012), background subtracted, and cropped to a uniform field size. Migration tracks of individual cells were collected using automated tracking with the Trackmate plug-in (Tinevez et al., 2017). Mean speeds were imported to Prism (Graphpad), and compared between conditions using unpaired *t*-tests. Three independent experiments were performed for each experimental condition.

AUTHOR'S NOTE

Wolf-Hirschhorn Syndrome (WHS), a developmental disorder caused by small deletions on chromosome four, manifests with pronounced and characteristic facial malformation. While

genetic profiling and case studies provide insights into how broader regions of the genome affect the syndrome's severity, we lack a key component of understanding its pathology; a basic knowledge of how individual WHS-affected genes function during development. Importantly, many tissues affected by WHS derive from shared embryonic origin, the cranial neural crest. This led us to hypothesize that genes deleted in WHS may hold especially critical roles in this tissue. To this end, we investigated the roles of four WHS-associated genes during neural crest cell migration and facial patterning. We show that during normal development, expression of these genes is enriched in migratory neural crest and craniofacial structures. Subsequently, we examine their functional roles during facial patterning, cartilage formation, and forebrain development, and find that their depletion recapitulates features of WHS craniofacial malformation. Additionally, two of these genes directly affect neural crest cell migration rate. We report that depletion of WHS-associated genes is a potent effector of neural crest-derived tissues, and suggest that this explains why WHS clinical presentation shares so many characteristics with classic neurochristopathies.

ETHICS STATEMENT

All experiments were approved by the Boston College Institutional Animal Care and Use Committee and were performed according to national regulatory standards.

AUTHOR CONTRIBUTIONS

LL, AM, and EB contributed conception and design of the study. EB, AM, RC, SK, MS, and SL performed the experiments and analyzed the data. EB wrote the first draft of the manuscript. All authors contributed to manuscript revision, read and approved the submitted version.

FUNDING

This work was supported by the NIH National Institute of Dental and Craniofacial Research (R03 DE025824), the NIH National Institute of Mental Health (MH109651), the March of Dimes (1-FY16-220), and the American Cancer Society (RSG-16–144-01-CSM). EB was funded by a National Science Foundation Graduate Research Fellowship.

ACKNOWLEDGMENTS

We thank members of the LL Lab for helpful discussions, suggestions, and editing. We also thank Eric Snow, Mitchell Lavoie, Katya Van Anderlecht, Katherine Montas, Lucas Ashley, and Molly Connors for technical assistance. We thank Nancy McGilloway and Todd Gaines for excellent Xenopus husbandry. We also thank the National Xenopus Resource (**RRID:SCR-013731**) and Xenbase (**RRID:SCR-003280**) for their support.

SUPPLEMENTARY MATERIAL

The Supplementary Material for this article can be found online at: https://www.frontiersin.org/articles/10.3389/fphys.2019.00431/full#supplementary-material

FIGURE S1 | Expression patterns for WHS related genes across early development. *In situ* hybridization utilized **(A–F)** antisense mRNA probe to *whsc1*, **(G–L)** full-length antisense mRNA probe to *whsc2*, **(M–R)** full-length antisense mRNA probe to *letm1*, and (S-X) 1 kb partial-length antisense mRNA probe to *tacc3*. Embryos shown at blastula stage **(A,G,M,S)**, in dorsal view at stage 16–20 **(B,H,N,T)**, in lateral view at stage 20–25 **(C,I,O,U)**, detail of lateral anterior region at stage 35 **(D,J,P,V)**, and in both lateral and dorsal views from stages 39–42 (**E,K,Q,W** and **F,L,R,X**). **(Y)** *In situ* hybridization probes generated against sense strands of WHS gene mRNAs, shown at stage 25. Brown coloration **(S,T)** is unbleached pigment, unrelated to *in situ* hybridization staining. Scalebar is 250 μm.bryos were anesthetized with benzocaine.

FIGURE S2 | Validation of WHS related MOs. **(A,B)** Gel of polymerase chain reaction (PCR) that shows injection of 10 ng MO targeted to *whsc1* mRNA causes a greater than 80% reduction at 2 dpf. **(C,D)** Injection of 20 ng of a MO targeted against *letm1* causes an 55% decrease in *letm1* mRNA 2 dpf. **(E,F)** Western blot showing 10 ng injection of a MO targeted against *whsc2* results in a greater than 50% reduction in Whsc2 protein by 2 dpf. **(G,H)** Western blot showing 40 ng of a MO targeted against *tacc3* results in 22% reduction. Bar graphs **(B,D,F,H)** depict densitometry of gels **(A,C)** or blot **(E,G)** shown, but is consistent across triplicate results.

FIGURE S3 | Demonstration of measurement schemes for craniofacial morphology. Measurements for **Figure 3** and **Supplementary Figure S4** were performed as indicated. **(A)** Facial width was measured from the center of each eye. **(B)** Facial height was determined at the midline, from the top of the cement gland to the top of the eyes. **(C)** Midface angle was measured from the top of the cement gland to the center of each eye. **(D)** Facial area was measured as the space encapsulated within the perimeter of each eye. Adapted from Kennedy and Dickinson (2014).

FIGURE S4 | Craniofacial defects caused by WHS-associated gene KD are rescued by co-injection of exogenous mRNA co-expression. Facial widths from control, depletion, or rescue strategies were measured in tadpoles (st. 40). Row 1: Embryos injected with **(A)** control MO (n = 17), **(B)** 10 ng *whsc1* MO (n = 14), or **(C)** 10 ng of *whsc1* MO and 250 pg of *whsc1* exogenous mRNA. **(D)** Comparisons of facial width showed an 8.76% increase in facial width with Whsc1 KD, which was rescued by *whsc1* mRNA co-injection. Row 2: Embryos injected with **(E)** control MO (n = 21), **(F)** 10 ng *whsc2* MO (n = 17), or **(G)** both 10ng of *whsc2* MO and 250 pg of *whsc2* mRNA (n = 19). **(H)** Whsc2 knockdown caused an 8.37% reduction in facial width, which was rescued by exogenous *whsc2* mRNA co-injection. Row 3: Embryos injected with **(I)** control MO (n = 10), **(J)** 20 ng of *letm1* MO, or **(K)** 20 ng *letm1* MO and 1500 pg of *letm1* mRNA (n = 11). **(L)** KD of Letm1 caused a 14.95% decrease in facial width, and was rescued by co-injection of exogenous *letm1* mRNA. Row 4: Embryos injected with **(M)** control MO (n = 9), **(N)** 20 ng of *tacc3* MO (n = 18), or O) 20 ng of *tacc3* morpholino and 1000 pg of *tacc3* mRNA (n = 16). **(P)** Tacc3 KD resulted in a 9.01% decrease in facial width, and was rescued by *tacc3* mRNA co-injection. Significance determined using a student's unpaired t-test. $^{**}P < 0.01$, $^{*}P < 0.05$, n.s., not significant. Scalebar is 250μm.

FIGURE S5 | Half embryo knockdown can be utilized for analysis of brain morphology and neural crest cell migration *in vivo*. **(A)** At the 2-cell stage, a single blastomere is injected with WHS-associated gene MOs and exogenous eGFP mRNA. After neurulation (approx. stage 21), embryos are sorted based on left or right eGFP fluorescence, to determine side of depletion. To examine neural crest cell size, migration and morphology embryos were fixed between stage 25–30, and *in situ* hybridization was performed using *twist* anti-sense probe. To characterize brain morphology, embryos were raised to st. 47, and fixed and labeled with alpha-tubulin antibody, a neuronal marker, and Alexa-488 secondary. **(B–D)** Control MO does not significantly impact brain size, compared to non-injected hemispheres (a paired internal control).

REFERENCES

Adelman, K., and Lis, J. T. (2012). Promoter-proximal pausing of RNA polymerase II: emerging roles in metazoans. *Nat. Rev. Genet.* 13, 720–731. doi: 10.1038/nrg3293

Ahmed, M., Ura, K., and Streit, A. (2015). Auditory hair cell defects as potential cause for sensorineural deafness in Wolf-Hirschhorn syndrome. *Dis. Model. Mech.* 8, 1027–1035. doi: 10.1242/dmm.019547

Albee, A. J., and Wiese, C. (2008). Xenopus TACC3/maskin is not required for microtubule stability but is required for anchoring microtubules at the centrosome. *Mol. Biol. Cell.* 19, 3347–3356. doi: 10.1091/mbc.e07-11-1204

Alfandari, D., Cousin, H., Gaultier, A., Smith, K., White, J. M., Darribère, T., et al. (2001). Xenopus ADAM 13 is a metalloprotease required for cranial neural crest-cell migration. *Curr. Biol.* 11, 918–930. doi: 10.1016/S0960-9822(01)00263-9

Amleh, A., Nair, S. J., Sun, J., Sutherland, A., Hasty, P., and Li, R. (2009). Mouse cofactor of BRCA1 (Cobra1) is required for early embryogenesis. *PLoS One* 4:e5034. doi: 10.1371/journal.pone.0005034

Andersen, E. F., Carey, J. C., Earl, D. L., Corzo, D., Suttie, M., Hammond, P., et al. (2014). Deletions involving genes WHSC1 and LETM1 may be necessary, but are not sufficient to cause Wolf-Hirschhorn Syndrome. *Eur. J. Hum. Genet.* 22, 464–470. doi: 10.1038/ejhg.2013.192

Aoto, K., and Trainor, P. A. (2015). Co-ordinated brain and craniofacial development depend upon Patched1/XIAP regulation of cell survival. *Hum. Mol. Genet.* 24, 698–713. doi: 10.1093/hmg/ddu489

Battaglia, A., Carey, J. C., and South, S. T. (2015). Wolf-Hirschhorn syndrome: a review and update. *Am. J. Med. Genet. C Semin. Med. Genet.* 169, 216–223. doi: 10.1002/ajmg.c.31449

Beà, S., Valdés-Mas, R., Navarro, A., Salaverria, I., Martín-Garcia, D., Jares, P., et al. (2013). Landscape of somatic mutations and clonal evolution in mantle cell lymphoma. *Proc. Natl. Acad. Sci. U.S.A.* 110, 18250–18255. doi: 10.1073/pnas.1314608110

Bergemann, A. D., Cole, F., and Hirschhorn, K. (2005). The etiology of Wolf-Hirschhorn syndrome. *Trends Genet.* 21, 188–195. doi: 10.1016/j.tig.2005.01.008

Bernardini, L., Radio, F. C., Acquaviva, F., Gorgone, C., Postorivo, D., Torres, B., et al. (2018). Small 4p16.3 deletions: three additional patients and review of the literature. *Am. J. Med. Genet. A* 176, 2501–2508. doi: 10.1002/ajmg.a.40512

Burgess, S. G., Mukherjee, M., Sabir, S., Joseph, N., Gutiérrez-Caballero, C., Richards, M. W., et al. (2018). Mitotic spindle association of TACC3 requires Aurora-a-dependent stabilization of a cryptic α-helix. *EMBO J.* 37:e97902. doi: 10.15252/embj.201797902

Cheeseman, L. P., Booth, D. G., Hood, F. E., Prior, I. A., and Royle, S. J. (2011). Aurora A kinase activity is required for localization of TACC3/ch-TOG/clathrin inter-microtubule bridges. *Commun. Integr. Biol.* 4, 409–412. doi: 10.4161/cib.4.4.15250

Demyer, W., Zeman, W., and Palmer, C. G. (1964). THE face predicts the brain: diagnostic significance of median facial anomalies for holoprosencephaly (arhinencephaly). *Pediatrics* 34, 256–263.

Deniz, E., Jonas, S., Hooper, M. N., Griffin, J., Choma, M. A., and Khokha, M. K. (2017). Analysis of craniocardiac malformations in xenopus using optical coherence tomography. *Sci. Rep.* 7:42506. doi: 10.1038/srep42506

Devotta, A., Juraver-Geslin, H., Gonzalez, J. A., Hong, C.-S., and Saint-Jeannet, J.-P. (2016). Sf3b4-depleted Xenopus embryos: a model to study the pathogenesis of craniofacial defects in Nager syndrome. *Dev. Biol.* 415, 371–382. doi: 10.1016/j.ydbio.2016.02.010

Dickinson, A. J. G. (2016). Using frogs faces to dissect the mechanisms underlying human orofacial defects. *Semin. Cell Dev. Biol.* 51, 54–63. doi: 10.1016/j.semcdb.2016.01.016

Dubey, A., and Saint-Jeannet, J. P. (2017). Modeling human craniofacial disorders in Xenopus. *Curr. Pathobiol. Rep.* 5, 79–92. doi: 10.1007/s40139-017-0128-8

Durigon, R., Mitchell, A. L., Jones, A. W., Manole, A., Mennuni, M., Hirst, E. M., et al. (2018). LETM1 couples mitochondrial DNA metabolism and nutrient preference. *EMBO Mol. Med.* 10:e8550. doi: 10.15252/emmm.201708550

El Zeneini, E., Kamel, S., El-Meteini, M., and Amleh, A. (2017). Knockdown of COBRA1 decreases the proliferation and migration of hepatocellular carcinoma cells. *Oncol. Rep.* 37, 1896–1906. doi: 10.3892/or.2017.5390

Erdogan, B., Cammarata, G. M., Lee, E. J., Pratt, B. C., Francl, A. F., Rutherford, E. L., et al. (2017). The microtubule plus-end-tracking protein TACC3 promotes persistent axon outgrowth and mediates responses to axon guidance signals during development. *Neural Dev.* 12:3. doi: 10.1186/s13064-017-0080-7

Frisdal, A., and Trainor, P. A. (2014). Development and evolution of the pharyngeal apparatus. *Wiley Interdiscip. Rev. Dev. Biol.* 3, 403–418. doi: 10.1002/wdev.147

Gandelman, K. Y., Gibson, L., Meyn, M. S., and Yang-Feng, T. L. (1992). Molecular definition of the smallest region of deletion overlap in the Wolf-Hirschhorn syndrome. *Am. J. Hum. Genet.* 51, 571–578.

Gergely, F., Karlsson, C., Still, I., Cowell, J., Kilmartin, J., and Raff, J. W. (2000). The TACC domain identifies a family of centrosomal proteins that can interact with microtubules. *Proc. Natl. Acad. Sci. U.S.A.* 97, 14352–14357. doi: 10.1073/pnas.97.26.14352

Gilchrist, D. A., Dos Santos, G., Fargo, D. C., Xie, B., Gao, Y., Li, L., et al. (2010). Pausing of RNA polymerase II disrupts DNA-specified nucleosome organization to enable precise gene regulation. *Cell* 143, 540–551. doi: 10.1016/j.cell.2010.10.004

Gorlin, R. J., Cohen, M. M., and Hennekam, R. C. M. (2001). *Syndromes of the Head and Neck*. New York, NY: Oxford University Press.

Griffin, J. N., Del Viso, F., Duncan, A. R., Robson, A., Hwang, W., Kulkarni, S., et al. (2018). RAPGEF5 regulates nuclear translocation of β-Catenin. *Dev. Cell* 44, 248.e4–260.e4. doi: 10.1016/j.devcel.2017.12.001

Gross, J. B., and Hanken, J. (2008). Segmentation of the vertebrate skull: neural-crest derivation of adult cartilages in the clawed frog, *Xenopus laevis*. *Integr. Comp. Biol.* 48, 681–696. doi: 10.1093/icb/icn077

Ha, G. H., Kim, J. L., and Breuer, E. K. (2013a). Transforming acidic coiled-coil proteins (TACCs) in human cancer. *Cancer Lett.* 336, 24–33. doi: 10.1016/j.canlet.2013.04.022

Ha, G. H., Park, J. S., and Breuer, E. K. (2013b). TACC3 promotes epithelial-mesenchymal transition (EMT) through the activation of PI3K/Akt and ERK signaling pathways. *Cancer Lett.* 332, 63–73. doi: 10.1016/j.canlet.2013.01.013

Hammond, P., Hannes, F., Suttie, M., Devriendt, K., Vermeesch, J. R., Faravelli, F., et al. (2012). Fine-grained facial phenotype-genotype analysis in Wolf-Hirschhorn syndrome. *Eur. J. Hum. Genet.* 20, 33–40. doi: 10.1038/ejhg.2011.135

Hirschhorn, K., Cooper, H. L., and Firschein, I. L. (1965). Deletion of short arms of chromosome 4-5 in a child with defects of midline fusion. *Humangenetik* 1, 479–482.

Huang, E., Qu, D., Huang, T., Rizzi, N., Boonying, W., Krolak, D., et al. (2017). PINK1-mediated phosphorylation of LETM1 regulates mitochondrial calcium transport and protects neurons against mitochondrial stress. *Nat. Commun.* 8:1399. doi: 10.1038/s41467-017-01435-1

Huang, Z., Wu, H., Chuai, S., Xu, F., Yan, F., Englund, N., et al. (2013). NSD2 is recruited through its PHD domain to oncogenic gene loci to drive multiple myeloma. *Cancer Res.* 73, 6277–6288. doi: 10.1158/0008-5472.CAN-13-1000

Jacox, L., Chen, J., Rothman, A., Lathrop-Marshall, H., and Sive, H. (2016). Formation of a "pre-mouth array" from the extreme anterior domain is directed by neural crest and Wnt/PCP signaling. *Cell Rep.* 16, 1445–1455. doi: 10.1016/j.celrep.2016.06.073

Jiang, D., Zhao, L., and Clapham, D. E. (2009). Genome-wide RNAi screen identifies Letm1 as a mitochondrial Ca2+/H+ antiporter. *Science* 326, 144–147. doi: 10.1126/science.1175145

Jiang, D., Zhao, L., Clish, C. B., and Clapham, D. E. (2013). Letm1, the mitochondrial Ca2+/H+ antiporter, is essential for normal glucose metabolism and alters brain function in Wolf-Hirschhorn syndrome. *Proc. Natl. Acad. Sci. U.S.A.* 110, E2249–E2254. doi: 10.1073/pnas.1308558110

Kennedy, A. E., and Dickinson, A. J. (2014). Quantitative analysis of orofacial development and median clefts in *Xenopus laevis*. *Anat. Rec.* 297, 834–855. doi: 10.1002/ar.22864

Kerney, R. R., Brittain, A. L., Hall, B. K., and Buchholz, D. R. (2012). Cartilage on the move: cartilage lineage tracing during tadpole metamorphosis. *Dev. Growth Differ.* 54, 739–752. doi: 10.1111/dgd.12002

Kerzendorfer, C., Hannes, F., Colnaghi, R., Abramowicz, I., Carpenter, G., Vermeesch, J. R., et al. (2012). Characterizing the functional consequences of haploinsufficiency of NELF-A (WHSC2) and SLBP identifies novel cellular phenotypes in Wolf-Hirschhorn syndrome. *Hum. Mol. Genet.* 21, 2181–2193. doi: 10.1093/hmg/dds033

Kuo, C. H., Chen, K. F., Chou, S. H., Huang, Y. F., Wu, C. Y., Cheng, D. E., et al. (2013). Lung tumor-associated dendritic cell-derived resistin promoted cancer progression by increasing Wolf-Hirschhorn syndrome candidate 1/Twist pathway. *Carcinogenesis* 34, 2600–2609. doi: 10.1093/carcin/bgt281

Li, Q., Ye, L., Guo, W., Wang, M., Huang, S., and Peng, X. (2017). Overexpression of TACC3 is correlated with tumor aggressiveness and poor prognosis in prostate cancer. *Biochem. Biophys. Res. Commun.* 486, 872–878. doi: 10.1016/j.bbrc.2017.03.090

Liu, K. J. (2016). Animal models of craniofacial anomalies. *Dev. Biol.* 415, 169–170. doi: 10.1016/j.ydbio.2016.06.008

Luo, M., Lu, X., Zhu, R., Zhang, Z., Chow, C. C., Li, R., et al. (2013). A conserved protein motif is required for full modulatory activity of negative elongation factor subunits NELF-A and NELF-B in modifying glucocorticoid receptor-regulated gene induction properties. *J. Biol. Chem.* 288, 34055–34072. doi: 10.1074/jbc.M113.512426

Mariotti, M., Manganini, M., and Maier, J. A. (2000). Modulation of WHSC2 expression in human endothelial cells. *FEBS Lett.* 487, 166–170. doi: 10.1016/S0014-5793(00)02335-8

Mathieu, J., and Ruohola-Baker, H. (2017). Metabolic remodeling during the loss and acquisition of pluripotency. *Development* 144, 541–551. doi: 10.1242/dev.128389

Matus, D. Q., Lohmer, L. L., Kelley, L. C., Schindler, A. J., Kohrman, A. Q., Barkoulas, M., et al. (2015). Invasive cell fate requires G1 cell-cycle arrest and histone deacetylase-mediated changes in gene expression. *Dev. Cell* 35, 162–174. doi: 10.1016/j.devcel.2015.10.002

Merrow, J. M. (2016). Feeding management in infants with craniofacial anomalies. *Facial Plast. Surg. Clin. North Am.* 24, 437–444. doi: 10.1016/j.fsc.2016.06.004

Milet, C., and Monsoro-Burq, A. H. (2014). Dissection of *Xenopus laevis* neural crest for in vitro explant culture or in vivo transplantation. *J. Vis. Exp.* 85:51118. doi: 10.3791/51118

Monsoro-Burq, A. H. (2015). PAX transcription factors in neural crest development. *Semin. Cell Dev. Biol.* 44, 87–96. doi: 10.1016/j.semcdb.2015.09.015

Nieuwkoop, P. D., and Faber, J. (eds) (1994). *Normal Table of Xenopus Laevis (Daudin): a Systematical and Chronological Survey of the Development From the Fertilized Egg Till the End of Metamorphosis*. New York, NY: Garland Pub.

Nimura, K., Ura, K., Shiratori, H., Ikawa, M., Okabe, M., Schwartz, R. J., et al. (2009). A histone H3 lysine 36 trimethyltransferase links Nkx2-5 to Wolf-Hirschhorn syndrome. *Nature* 460, 287–291. doi: 10.1038/nature08086

Nixon, F. M., Gutiérrez-Caballero, C., Hood, F. E., Booth, D. G., Prior, I. A., and Royle, S. J. (2015). The mesh is a network of microtubule connectors that stabilizes individual kinetochore fibers of the mitotic spindle. *eLife* 4:e07635. doi: 10.7554/eLife.07635

Nwagbara, B. U., Faris, A. E., Bearce, E. A., Erdogan, B., Ebbert, P. T., Evans, M. F., et al. (2014). TACC3 is a microtubule plus end-tracking protein that promotes axon elongation and also regulates microtubule plus end dynamics in multiple embryonic cell types. *Mol. Biol. Cell* 25, 3350–3362. doi: 10.1091/mbc.E14-06-1121

Pan, H., Qin, K., Guo, Z., Ma, Y., April, C., Gao, X., et al. (2014). Negative elongation factor controls energy homeostasis in cardiomyocytes. *Cell Rep.* 7, 79–85. doi: 10.1016/j.celrep.2014.02.028

Paradowska-Stolarz, A. M. (2014). Wolf-Hirschhorn syndrome (WHS) - literature review on the features of the syndrome. *Adv. Clin. Exp. Med.* 23, 485–489. doi: 10.17219/acem/24111

Park, J. W., Chae, Y. C., Kim, J. Y., Oh, H., and Seo, S. B. (2018). Methylation of aurora kinase A by MMSET reduces p53 stability and regulates cell proliferation and apoptosis. *Oncogene* 37, 6212–6224. doi: 10.1038/s41388-018-0393-y

Perestrelo, T., Correia, M., Ramalho-Santos, J., and Wirtz, D. (2018). Metabolic and mechanical cues regulating pluripotent stem cell fate. *Trends Cell Biol.* 28, 1014–1029. doi: 10.1016/j.tcb.2018.09.005

Peset, I., and Vernos, I. (2008). The TACC proteins: TACC-ling microtubule dynamics and centrosome function. *Trends Cell Biol.* 18, 379–388. doi: 10.1016/j.tcb.2008.06.005

Piekorz, R. P., Hoffmeyer, A., Duntsch, C. D., McKay, C., Nakajima, H., Sexl, V., et al. (2002). The centrosomal protein TACC3 is essential for hematopoietic stem cell function and genetically interfaces with p53-regulated apoptosis. *EMBO J.* 21, 653–664. doi: 10.1093/emboj/21.4.653

Rauch, A., Schellmoser, S., Kraus, C., Dörr, H. G., Trautmann, U., Altherr, M. R., et al. (2001). First known microdeletion within the Wolf-Hirschhorn syndrome critical region refines genotype-phenotype correlation. *Am. J. Med. Genet.* 99, 338–342. doi: 10.1002/ajmg.1203

Rutherford, E. L., and Lowery, L. A. (2016). Exploring the developmental mechanisms underlying Wolf-Hirschhorn syndrome: evidence for defects in neural crest cell migration. *Dev. Biol.* 420, 1–10. doi: 10.1016/j.ydbio.2016.10.012

Saint-Jeannet, J. P. (2017). Whole-mount in situ hybridization of *Xenopus* embryos. *Cold Spring Harb. Protoc.* 2017:db.rot097287. doi: 10.1101/pdb.prot097287

Schindelin, J., Arganda-Carreras, I., Frise, E., Kaynig, V., Longair, M., Pietzsch, T., et al. (2012). Fiji: an open-source platform for biological-image analysis. *Nat. Methods* 9, 676–682. doi: 10.1038/nmeth.2019

Schlickum, S., Moghekar, A., Simpson, J. C., Steglich, C., O'Brien, R. J., Winterpacht, A., et al. (2004). LETM1, a gene deleted in Wolf-Hirschhorn syndrome, encodes an evolutionarily conserved mitochondrial protein. *Genomics* 83, 254–261. doi: 10.1016/j.ygeno.2003.08.013

Schneider, C. A., Rasband, W. S., and Eliceiri, K. W. (2012). NIH Image to ImageJ: 25 years of image analysis. *Nat. Methods* 9, 671–675. doi: 10.1038/nmeth.2089

Shyh-Chang, N., Locasale, J. W., Lyssiotis, C. A., Zheng, Y., Teo, R. Y., Ratanasirintrawoot, S., et al. (2013). Influence of threonine metabolism on S-adenosylmethionine and histone methylation. *Science* 339, 222–226. doi: 10.1126/science.1226603

Simon, R., and Bergemann, A. D. (2008). Mouse models of Wolf-Hirschhorn syndrome. *Am. J. Med. Genet. C Semin. Med. Genet.* 148C, 275–280. doi: 10.1002/ajmg.c.30184

Sive, H. L., Grainger, R. M., and Harland, R. M. (2010). Microinjection of xenopus embryos. *Cold Spring Harb. Protoc.* 2010:pdb.i81. doi: 10.1101/pdb.ip81

South, S. T., Hannes, F., Fisch, G. S., Vermeesch, J. R., and Zollino, M. (2008). Pathogenic significance of deletions distal to the currently described Wolf-Hirschhorn syndrome critical regions on 4p16.3. *Am. J. Med. Genet. C Semin. Med. Genet.* 148C, 270–274. doi: 10.1002/ajmg.c.30188

Sperber, H., Mathieu, J., Wang, Y., Ferreccio, A., Hesson, J., Xu, Z., et al. (2015). The metabolome regulates the epigenetic landscape during naive-to-primed human embryonic stem cell transition. *Nat. Cell Biol.* 17, 1523–1535. doi: 10.1038/ncb3264

Stec, I., Wright, T. J., van Ommen, G. J., de Boer, P. A., van Haeringen, A., Moorman, A. F., et al. (1998). WHSC1, a 90 kb SET domain-containing gene, expressed in early development and homologous to a Drosophila dysmorphy gene maps in the Wolf-Hirschhorn syndrome critical region and is fused to IgH in t(4;14) multiple myeloma. *Hum. Mol. Genet.* 7, 1071–1082. doi: 10.1093/hmg/7.7.1071

Szabó, A., Melchionda, M., Nastasi, G., Woods, M. L., Campo, S., Perris, R., et al. (2016). In vivo confinement promotes collective migration of neural crest cells. *J. Cell Biol.* 213, 543–555. doi: 10.1083/jcb.201602083

Tabler, J. M., Bolger, T. G., Wallingford, J., and Liu, K. J. (2014). Hedgehog activity controls opening of the primary mouth. *Dev. Biol.* 396, 1–7. doi: 10.1016/j.ydbio.2014.09.029

Theveneau, E., Steventon, B., Scarpa, E., Garcia, S., Trepat, X., Streit, A., et al. (2013). Chase-and-run between adjacent cell populations promotes directional collective migration. *Nat. Cell Biol.* 15, 763–772. doi: 10.1038/ncb2772

Tinevez, J.-Y., Perry, N., Schindelin, J., Hoopes, G. M., Reynolds, G. D., Laplantine, E., et al. (2017). TrackMate: an open and extensible platform for single-particle tracking. *Methods* 115, 80–90. doi: 10.1016/j.ymeth.2016.09.016

Trainor, P. A. (2010). Craniofacial birth defects: The role of neural crest cells in the etiology and pathogenesis of treacher collins syndrome and the potential for prevention. *Am. J. Med. Genet. A* 152A, 2984–2994. doi: 10.1002/ajmg.a.33454

Trainor, P. A., and Andrews, B. T. (2013). Facial dysostoses: Etiology, pathogenesis and management. *Am. J. Med. Genet. Part C* 163, 283–294. doi: 10.1002/ajmg.c.31375

Walker, M. B., and Trainor, P. A. (2006). Craniofacial malformations: intrinsic vs extrinsic neural crest cell defects in treacher collins and 22q11 deletion syndromes. *Clin. Genet.* 69, 471–479. doi: 10.1111/j.0009-9163.2006.00615.x

Wolf, U., Reinwein, H., Porsch, R., Schröter, R., and Baitsch, H. (1965). [Deficiency on the short arms of a chromosome No. 4]. *Humangenetik* 1, 397–413. doi: 10.1007/BF00395654

Wright, T. J., Ricke, D. O., Denison, K., Abmayr, S., Cotter, P. D., Hirschhorn, K., et al. (1997). A transcript map of the newly defined 165 kb Wolf-Hirschhorn syndrome critical region. *Hum. Mol. Genet.* 6, 317–324. doi: 10.1093/hmg/6.2.317

Yamada-Okabe, T., Imamura, K., Kawaguchi, N., Sakai, H., Yamashita, M., and Matsumoto, N. (2010). Functional characterization of the zebrafish WHSC1-related gene, a homolog of human NSD2. *Biochem. Biophys. Res. Commun.* 402, 335–339. doi: 10.1016/j.bbrc.2010.10.027

Yu, C., Yao, X., Zhao, L., Wang, P., Zhang, Q., Zhao, C., et al. (2017). Wolf-hirschhorn syndrome candidate 1 (whsc1) functions as a tumor suppressor by governing cell differentiation. *Neoplasia* 19, 606–616. doi: 10.1016/j.neo.2017.05.001

Zhang, J., Jima, D., Moffitt, A. B., Liu, Q., Czader, M., Hsi, E. D., et al. (2014). The genomic landscape of mantle cell lymphoma is related to the epigenetically determined chromatin state of normal B cells. *Blood* 123, 2988–2996. doi: 10.1182/blood-2013-07-517177

Zollino, M., Di Stefano, C., Zampino, G., Mastroiacovo, P., Wright, T. J., Sorge, G., et al. (2000). Genotype-phenotype correlations and clinical diagnostic criteria in Wolf-Hirschhorn syndrome. *Am. J. Med. Genet.* 94, 254–261. doi: 10.1002/1096-8628(20000918)94:3<254::AID-AJMG13>3.0.CO;2-7

Zollino, M., Lecce, R., Fischetto, R., Murdolo, M., Faravelli, F., Selicorni, A., et al. (2003). Mapping the Wolf-Hirschhorn syndrome phenotype outside the currently accepted WHS critical region and defining a new critical region, WHSCR-2. *Am. J. Hum. Genet.* 72, 590–597. doi: 10.1086/367925

Zollino, M., Murdolo, M., Marangi, G., Pecile, V., Galasso, C., Mazzanti, L., et al. (2008). On the nosology and pathogenesis of Wolf-Hirschhorn syndrome: genotype-phenotype correlation analysis of 80 patients and literature review. *Am. J. Med. Genet. C Semin. Med. Genet.* 148C, 257–269. doi: 10.1002/ajmg.c.30190

Conflict of Interest Statement: The authors declare that the research was conducted in the absence of any commercial or financial relationships that could be construed as a potential conflict of interest.

frontiers in Physiology

REVIEW
published: 25 April 2019
doi: 10.3389/fphys.2019.00387

Xenopus Resources: Transgenic, Inbred and Mutant Animals, Training Opportunities, and Web-Based Support

*Marko Horb[1], Marcin Wlizla[1], Anita Abu-Daya[2], Sean McNamara[1], Dominika Gajdasik[3], Takeshi Igawa[4†], Atsushi Suzuki[4†], Hajime Ogino[4†], Anna Noble[2], Centre de Ressource Biologique Xenope Team in France[5], Jacques Robert[6], Christina James-Zorn[7] and Matthew Guille[2,3]**

[1] National Xenopus Resource, Marine Biological Laboratory, Woods Hole, MA, United States, [2] European Xenopus Resource Centre, Portsmouth, United Kingdom, [3] School of Biological Sciences, King Henry Building, Portsmouth, United Kingdom, [4] Amphibian Research Center, Hiroshima University, Higashihiroshima, Japan, [5] Centre de Ressources Biologiques Xenopes, CNRS, Inserm, BIOSIT – UMS 3480, Université de Rennes 1, Rennes, France, [6] Department of Microbiology and Immunology, University of Rochester Medical Center, Rochester, NY, United States, [7] Xenbase, Division of Developmental Biology, Cincinnati Children's Research Foundation, Cincinnati, OH, United States

OPEN ACCESS

Edited by:
Emily Sempou,
Yale University, United States

Reviewed by:
Caroline Beck,
University of Otago, New Zealand
Anna Philpott,
University of Cambridge,
United Kingdom

***Correspondence:**
Matthew Guille
matthew.guille@port.ac.uk

†On behalf of Team Xenopus tropicalis NBRP in Japan

Specialty section:
This article was submitted to Embryonic and Developmental Physiology, a section of the journal Frontiers in Physiology

Received: 31 January 2019
Accepted: 21 March 2019
Published: 25 April 2019

Citation:
Horb M, Wlizla M, Abu-Daya A, McNamara S, Gajdasik D, Igawa T, Suzuki A, Ogino H, Noble A, Centre de Ressource Biologique Xenope Team in France, Robert J, James-Zorn C and Guille M (2019) Xenopus Resources: Transgenic, Inbred and Mutant Animals, Training Opportunities, and Web-Based Support. Front. Physiol. 10:387. doi: 10.3389/fphys.2019.00387

Two species of the clawed frog family, *Xenopus laevis* and *X. tropicalis*, are widely used as tools to investigate both normal and disease-state biochemistry, genetics, cell biology, and developmental biology. To support both frog specialist and non-specialist scientists needing access to these models for their research, a number of centralized resources exist around the world. These include centers that hold live and frozen stocks of transgenic, inbred and mutant animals and centers that hold molecular resources. This infrastructure is supported by a model organism database. Here, we describe much of this infrastructure and encourage the community to make the best use of it and to guide the resource centers in developing new lines and libraries.

Keywords: *Xenopus laevis*, *Xenopus tropicalis*, transgenesis, gene editing, inbred strains, ORFeome, model organism database, resource centers

INTRODUCTION

Xenopus laevis was first described in 1802 in Daudin's "Histoire naturelle des rainettes, des grenouilles, et des crapauds" as *Bufo laevis*. For the next century it was used for comparative anatomical studies [reviewed in Gurdon and Hopwood (2000)] but then became widely distributed as a bioassay for human pregnancy (Hogben, 1939). The availability of *Xenopus* underpinned their adoption for the study of biochemical mechanisms driving development and cell physiology (Gurdon and Hopwood, 2000). *Xenopus* has an extraordinary track record as a model organism, playing key roles in discoveries as disparate as isolation of the first eukaryotic gene and transcription factor, the first demonstration of nuclear reprogramming and the discovery of the mesoderm inducing and Spemann organizer molecules, as reviewed in Harland and Grainger (2011) and Tandon et al. (2017). More recently, the size and number of its synchronous embryos, its blastomere size, its well-defined fate map (Shindo et al., 1987) and accurate genome sequences (Hellsten et al., 2010; Session et al., 2016) have enabled the allotetraploid *X. laevis* and *X. tropicalis*,

its diploid relative, to be used very successfully for transcriptome (e.g., Briggs et al., 2018), proteome (e.g., Baxi et al., 2018), and metabolome studies. Together with the genetic resources described below, and the high efficiency of gene editing in these species, which allows very rapid studies of human genetic disease variants, these techniques continue to demonstrate the value of *Xenopus* as key model organisms. Here, we review the various resources that are in place to underpin and support research using the *Xenopus* models.

TRANSGENIC RESOURCES

Transgenesis, or the ability to transfer DNA from one genome to another, is a powerful tool which can be used in established model systems for the study of regulatory and coding DNA in normal and disease-associated processes as well as changes in gene function and control that occur during evolution. The origins of transgenesis can be traced back to the discovery of bacterial restriction enzymes and their use to generate recombinant DNA plasmids in the early 1970s (Cohen et al., 1973). In *Xenopus*, a number of reports in the 1980s demonstrated that simply microinjecting exogenous plasmid DNA into fertilized eggs can result in its successful integration into the frog genome (Rusconi and Schaffner, 1981; Etkin and Roberts, 1983; Andres et al., 1984; Bendig and Williams, 1984; Etkin et al., 1984), although showing mosaic distribution in the adult tissues. Etkin and Pearman (1987) demonstrated that exogenous, linearized plasmid DNA can be successfully transmitted through the germline of the transformed male parent to following generations; however, this approach proved to be highly inefficient since only ∼1% of the injected individuals demonstrated mosaic integration of the DNA into their germline (Yergeau et al., 2010). It took another decade for the idea of using *Xenopus* in transgenic studies to become a practicable endeavor with the development of much more efficient methods of transgenesis, initially via restriction enzyme mediated integration (REMI) (Kroll and Amaya, 1996) and then through the use of phiC31 integrase (Allen and Weeks, 2005), I-SceI meganuclease (Ogino et al., 2006; Pan et al., 2006), and various transposable element-based approaches (Yergeau et al., 2007). The use of I-SceI meganuclease has been shown to be especially effective with the reported ratios of non-mosaic integration in the F0 generation and germline transmission as high as 30% in *X. tropicalis* and 20% in *X. laevis* (Ogino et al., 2006). These transgenesis methods result in random integration of the exogenous DNA and, although approaches for targeted, precise integration using gene editing have recently been described (Aslan et al., 2017), their use in the *Xenopus* community is at an early stage (see below).

Several practical aspects make *Xenopus* an enticing model to use in transgenic studies. These include the ability of a single female to produce as many as 4000 eggs per spawning (Wlizla et al., 2017), thus providing a large batch of sibling embryos that are synchronous and develop externally. Furthermore, embryonic development is relatively rapid, with most major organs formed within 5 days following fertilization, and is easily observable since the tissues surrounding major viscera are transparent during the same time frame (Nieuwkoop and Faber, 1994; Khokha et al., 2002). However, the model is somewhat limited by the generation time with the two most commonly used species, *X. laevis* and *X. tropicalis* taking approximately 6–12 and 5–8 months, respectively, to reach sexual maturity, with males maturing slightly faster than females. Due to this limitation, most individual labs tend not to spend their time and resources to generate true breeding transgenic animal lines and instead focus on experiments that take advantage of the rapid early development. The disadvantage of a long generation time is to some extent balanced by the long period of fertility in the animals with *X. laevis* as old as 15 years producing viable offspring (Tinsley and Kobel, 1996); careful breeding strategies can thus be used to avoid significant genetic drift in this species.

The *Xenopus* resource centers including the National BioResource Project (NBRP) in Japan, the European *Xenopus* Resource Centre (EXRC) in Europe, and the National *Xenopus* Resource (NXR) in the United States of America were established, in part, to serve as centralized repositories with sufficient infrastructure to allow for maintenance of the extant *Xenopus* transgenic lines at capacities allowing for their distribution to individual labs on an as needed basis (Pearl et al., 2012). The stock centers also have expertise in generating new lines which can then be grown and made available to the research community. This has effectively eliminated the need for labs to contribute crucial resources into generation of novel transgenic lines since these are readily available for distribution as adults, tadpoles, embryos, isolated testes, or cryopreserved sperm (Pearl et al., 2017). Currently, the stock centers hold over 130 different transgenic lines, a number that is continuously increasing, and which can be grouped into four different categories: (1) reporter expression lines, (2) inducible lines for disruption and regulation of signaling pathway activity, (3) GAL4 and Cre driver lines, and (4) single landing site lines (**Supplementary Table S1**).

Reporter expression lines form by far the largest category of transgenic *Xenopus* lines available and can be further subdivided into several groups. First are the tissue/region specific lines which typically contain a fluorescent protein driven by a specific promoter to mark a particular tissue, region, or organ in the developing embryo (**Supplementary Table S1A**). Besides being useful for observation of normal development, these lines are highly amenable to investigations of abnormal development following disruption of gene activity, as demonstrated by a recent study from the Miller lab using a line marking the developing kidney, *Xla.Tg (Dre.cdh17:eGFP)*^{NXR} (**RRID:NXR_0102**), to investigate the disruption in kidney development following morpholino induced knockdown of the Planar Cell Polarity pathway component, Daam1 (Corkins et al., 2018). Studies using a similar design can easily be performed in lines marking other parts of the developing embryo taking advantage of the other tissue/region specific lines available. Certain experimental conditions, in particular ones relying on the use of formalin-fixed, paraffin-embedded tissues, result in a considerable loss of true fluorescent protein signal, and an increase in tissue autofluorescence (Jiang et al., 2005; Swenson et al., 2007). In cases where such histological preparations are necessary, transgenic lines that mark tissues/regions through colorimetric methods

can be used in place of fluorescent reporters. An example of such a line is *Xtr.Tg (tubb2b:Has.ALPP;cryga:dsRed)*^{Amaya} (**RRID:EXRC_3003**, **NXR_1099**), which allows for rapid detection of axonal projections *in situ* by a simple alkaline phosphatase reaction at any stage of development in whole embryos, which can then be further processed for histology (Huang et al., 2007). This reporter group also includes lines driven by ubiquitous promoters like CMV and human ubiquitin C. These are particularly useful for cut-and-paste, transplantation-based experiments to label and fate map regions of host embryos.

The second group of reporter expression lines includes transgenics marking subcellular organelles (**Supplementary Table S1B**). These are highly useful for the study of molecular processes involved in cell function and are especially effective when utilized in the context of *Xenopus* egg extracts, the only cell-free system that permits full investigation of all DNA transactions related to cell cycle progression and DNA damage repair (Cross and Powers, 2009; Hoogenboom et al., 2017). Many of these lines have been generated by the Ueno lab and mark a diverse range of organelles including plasma membrane, *Xla.Tg (CMV:RFP-CAAX)*^{Ueno} (**RRID:EXRC_0075**, **NXR_0115**), golgi bodies, *Xla.Tg (CMV:Has.B4GALT1-eGFP)*^{Ueno} (**RRID:EXRC_0077**, **NXR_0110**), and microtubule plus ends, *Xla.Tg (CMV:Has.MAPRE3-eGFP)*^{Ueno} (**RRID:EXRC_0078**, **NXR_0109**) (Takagi et al., 2013). Lines generated by other labs, as well as by the stock centers themselves, that label other organelles are also available.

The third group of reporter lines are those that serve as indicators of signaling activity (**Supplementary Table S1C**). These include Wnt signaling reporter lines generated by the Vleminckx lab in both *X. laevis* and *X. tropicalis* (Tran et al., 2010), an apoptosis sensor (Kominami et al., 2006), a histone H3 lysine 9 acetylation sensor for *in vivo* epigenetic analysis (Sato et al., 2013; Suzuki et al., 2016), a neural tissue specific calcium signaling sensor (Chen et al., 2013), and two distinct lines for detection of oxidative stress response (Love et al., 2013).

The fourth group of reporter lines are transposable element enhancer trap lines, all generated by the Mead lab (**Supplementary Table S1D**; Yergeau and Mead, 2009; Yergeau et al., 2010). Although the integration sites for some of these lines have been identified, this is not the case for all of them. These lines are of use in studies where the particular promoter driving expression is not important and it is the labeled region of the embryo that matters. They can also be used for further study of transposable element activity and additional discovery of regulatory regions via enhancer trap approaches and include lines which result in remobilization of the transposons in the offspring produced.

The fifth group currently contains a single line generated in the Buchholz lab allowing for temporal regulation of fluorescent marker expression via treatment with doxycycline (**Supplementary Table S1E**; Rankin et al., 2009). Other lines where temporal transgene expression can be regulated through use of simple small molecule treatments or heat shock will likely be added to this group in the future.

The final group includes reporter lines that are especially suitable in fate mapping studies via temporal or regional switch in fluorescence (**Supplementary Table S1F**). These lines work best when used in crosses with transgenic driver lines designed to regulate the switch in expression pattern (**Supplementary Tables S1, S3**). Among these reporters are two Brainbow lines generated at the NXR as well as a number of lines made in the Ryffel lab (Waldner et al., 2006; Livet et al., 2007). The initial fluorescence is ubiquitous; however, these lines contain loxP or FRT sites, and the initial fluorescence can be altered through crosses with driver lines that express Cre or FLP recombinase, respectively. The change in fluorescence can be spatially or temporally regulated through use of region specific, or inducible promoters or can alternatively be induced by targeted microinjection of *Cre* or *FLP* mRNA. This group of reporters also includes two types of lines which rely on a binary effector-transactivator design to function, the GAL4-UAS system and the tet-on system (Gossen and Bujard, 1992; Chae et al., 2002; Hartley et al., 2002).

In the GAL4-UAS system, the reporter gene is regulated by a UAS effector and will only be expressed when crossed to a driver line expressing GAL4. This allows for spatial or temporal control of reporter expression dependent on the promoter used to control expression of GAL4. Similarly, in the tet-on, the reporter is regulated by a TRE effector and will only be expressed if crossed to a driver line containing an rtTA transactivator. However, besides the promoter used to control the rtTA expression, an additional level of temporal control is provided since rtTA only works in the presence of doxycycline.

The remaining three main categories are somewhat less varied than the reporter lines but have important functional applications and include: inducible lines for disruption and regulation of signaling pathway activity (**Supplementary Tables S1, S2**), GAL4 and Cre driver lines (**Supplementary Tables S1, S3**), and single landing site lines (**Supplementary Tables S1, S4**). Disrupting signaling pathways can be achieved by microinjection of constitutively active or dominant negative pathway components into early embryos, however, many of the transgenic lines available are designed to allow for precise temporal control thus permitting the study of signaling pathway roles at much later stages of development than microinjection allows.

There are two ways these transgenes are regulated. First is through use of a heat shock promoter as in the *Xla.Tg (hsp70:nog;cryga:GFP)*^{Jmws} (**RRID:EXRC_0018 NXR_0020**), which was used to study temporal requirement for BMP signaling in haematopoiesis (Kirmizitas et al., 2017), or the *Xla.Tg (hsp70:Xtr.dkk1;cryga:GFP)*^{Jmws} (**RRID:NXR_0021**), which could be used in a similar manner to interfere with Wnt signaling. The second way the expression of these transgenes can be regulated is through use of binary control systems like CRE-Lox, FLP-FRT, GAL4-UAS, and tet-on. These lines may require the use of driver transgenic lines to regulate their activity, but not always, as in the case of *Xla.Tg (Mmu.col1a2:rtTA;TRE:DNthra-GFP)*^{Brown} (**RRID:EXRC_0026**) which has both components of the tet-on system and allows, in the presence of for expression of a GFP tagged dominant negative form of the thyroid hormone receptor (DNthra) specifically in cartilage, and which was used in the study of thyroid hormone function in limb development (Brown et al., 2005).

The currently available driver lines allow for use of CRE or GAL4 in a manner described above in order to control changes in fluorescence patterns of reporter lines or activities of signaling. In *X. laevis* the CRE drivers are mainly designed to allow for temporal control through the use of a heat shock promoter or doxycycline treatments as part of a tet-on system, although a transgenic line from the Ryffel lab that allows for CRE expression specifically in muscle cells is also available (Waldner et al., 2006; Roose et al., 2009; Kerney et al., 2012). In *X. tropicalis* there is a GAL4 driver line which allows for both temporal and spatial control, *Xtr.Tg (tubb2b:PR-Gal4;cryga:CFP)*^{Zimml} (**RRID:EXRC_3033**, **NXR_1109**). The *tubb2b* promoter, used here, drives expression specifically in neural cells, however, the GAL4 DNA binding domain is fused to the ligand binding domain of the progesterone receptor and thus, to function, requires the progesterone antagonist RU-482. This allows for full temporal regulation (Waldner et al., 2006). When used together with some of the available UAS effector lines temporal disruption of Wnt or Hedgehog signaling can be induced specifically in the nervous system. Additional driver lines that allow expression in other tissues and the use of FLP-FRT or the tet-on systems will very likely become available in the future.

Finally, there is the landing site category which currently contains a single line, *Xla.Tg (CFP-ATTP)*^{Ryff} (**RRID:EXRC_0058**). This line contains an *attP* docking site within a functional blue fluorescent protein coding sequence. Using phiC31 mediated integration, exogenous proteins can be introduced into this line, and loss of blue fluorescence can be used to screen for effective integration. Transgenic animals generated this way are likely to show very similar levels of the exogenous proteins expressed, due to local transcriptional control elements and chromatin environment being the same.

The transgenic lines available from the stock centers can be used in versatile ways to investigate many questions that are essentially low hanging fruit, ready to be plucked. The whole list may be a bit overwhelming at first glance, but the staff at the centers is there to provide advice and guidance regarding the best lines available for use in the study of particular questions. Individual investigators are encouraged to take advantage of this expertise and the lines available to move their research forward. Furthermore, in particular the EXRC and the NXR have expertise in generating novel transgenic lines and growing them to adulthood. If a line of interest is not available, we encourage investigators to take the initiative and request it to be made or provide guidance to aid the stock centers in determining which lines should be generated as a priority.

GENE EDITING RESOURCES

Xenopus have proven to be excellent organisms in which to perform gene editing experiments due to their external fertilization and efficiency of RNA and protein microinjection into synchronous embryos to deliver ZFNs (Nakajima et al., 2012; Young and Harland, 2012), TALENS (Lei et al., 2013; Miyamoto et al., 2015), or CRISPR/Cas9 (Blitz et al., 2013; Nakayama et al., 2013). Numerous labs have shown that production of simple insertions and deletions (indels) is very straightforward, fast, and efficient (McQueen and Pownall, 2017; Tandon et al., 2017). Studies using CRISPR/Cas9 also allow loss of function experiments to take place much later than those previously possible in *Xenopus*, which relied on injection of mRNAs expressing dominant negative proteins (Amaya et al., 1991) or antisense morpholino oligonucleotides that have recently been shown to be able to cause off-target, generic, phenotypic effects (Gentsch et al., 2018). The main drawback to gene editing in *Xenopus* is that, in F0 animals, it produces mosaicism (Ratzan et al., 2017); this is mainly due to the rapid cell divisions that occur every 30 min and the low temperature at which *Xenopus* are raised. Frogs made this way have nonetheless been used to address various biomedical topics, including cancer, immunology, neurobiology, cell biology, and other developmental biology questions (Naert et al., 2016; Banach et al., 2017; Hassnain Waqas et al., 2017; Delay et al., 2018) as well as to provide embryos that can be used as tools to understand human genetic diseases (Feehan et al., 2017; Deniz et al., 2018; Naert and Vleminckx, 2018a; Sega et al., 2018). Although mosaic, mutations in F0 animals are useful due to the high level of penetrance, often exceeding 90% in *X. tropicalis* when measured using TIDE (Brinkman et al., 2018; Naert and Vleminckx, 2018b).

In addition to indel-based knockout F0 animals, the resource centers are also producing knockout lines both for the community and to order. Staff in the centers work closely with individual researchers to create mutants in specific target genes and then breed the animals to determine germline transmission. In addition, a large program targeting 200 developmentally important genes prioritized by the research community is being undertaken at the NXR, although it is funded separately from the resource center itself. The first of these lines are now being inbred to produce F2 homozygous mutant animals and knockout phenotypes are being assayed; phenotypic analysis is then done in collaboration with individual researchers. These mutants are being made available and cataloged on Xenbase as soon as they are initially characterized. Making locus-specific gene knock-ins in embryos has, in all vertebrates, proven a significant challenge. Although this is possible in *Xenopus* by using injection of fertilized eggs and screening large numbers of animals (for example in the *runx1* locus shown in **Figure 1**), it is inefficient and there are no reports of precise DNA construct integration in the germline by egg injection. Recent work shows, however, that being able to access the *Xenopus* oocyte to apply gene editing techniques for insertion largely overcomes this challenge (Aslan et al., 2017), most likely because the levels of the homology directed repair (HDR) machinery are much higher in oocytes than eggs (Hagmann et al., 1996). To prevent mosaicism, oocytes can be cultured long enough (3 days) for injected sgRNA and Cas9 to decay before fertilization and treatment with SCR-7, a DNA ligase IV inhibitor, and increases the likelihood that the genetic lesion is repaired via HDR mechanisms instead of the double-strand break repair pathway (DSBR) (Aslan et al., 2017). There are other approaches being taken in several organisms to improve HDR-mediated integration using CRISPR/Cas9 and it should become clear

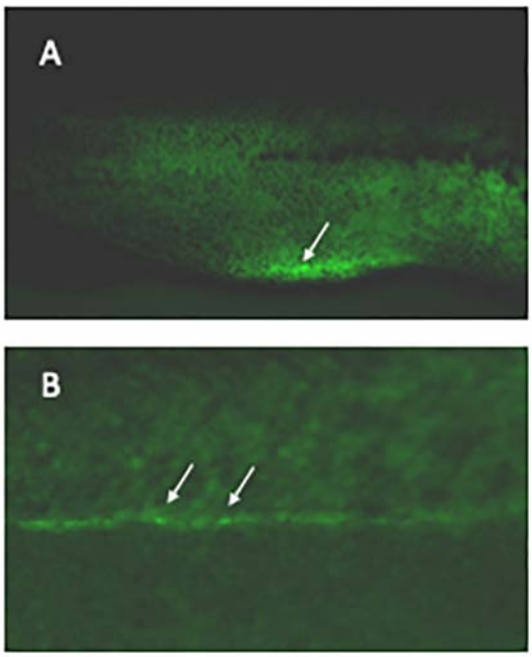

FIGURE 1 | Labeling haematopoietic stem cells in live embryos. *Xenopus laevis* eggs were microinjected with CRISPR/Cas9 targeting the 3′UTR of *runx1* together with a DNA construct containing 400 bp homology arms from either side of the cut site flanking an IRES controlling eGFP expression. Founder embryos were screened for mosaic expression of GFP in the correct regions and 24 grown to adulthood. Their offspring were then screened for germline transmission; two sets of offspring showed strong expression in the vbi (**A**, arrowed) and vasculature (**B**, examples arrowed) as expected for *runx1* at this stage. The transmission rate was 46 and 52% in the 2 sets. An F2 embryo is shown.

in the near future which becomes the dominant technology in *Xenopus*.

ROBUST INBRED STRAINS OF *X. tropicalis*

There are two major wild type strains of *X. tropicalis*: "Ivory Coast" and "Nigerian" that were originally collected from different localities (Tymowska and Fischberg, 1973; Grainger, 2012). After their introduction to the community in 1990 they were bred in several different labs, resulting in a number of strains that can be distinguished by mitochondrial haplotype and genotypic data on SSLP markers. The Ivory Coast and Nigerian strains are evolutionally diverged, and some Ivory Coast strains have diverged from one another while Nigerian strains share a unique mitochondrial haplotype (Kashiwagi et al., 2010; Igawa et al., 2015). Some of these strains are particularly suited to genetic studies, for example those with a short generation times such as Golden and Superman.

When using reverse genetic tools such as CRISPR/Cas9, that rely on a lack of polymorphisms in target regions for cutting, sequence insertion and analysis, inbred strains greatly increase the efficiency of experiments. Four strains in the NBRP *X. tropicalis* have been successfully maintained to achieve inbred status (Igawa et al., 2015). Heterozygosity value (H_E) of SSLP markers decreased following a theoretical reduction curve due to brother-sister mating in every generation (**Figure 2**). The offspring are vigorous in viability, comparable to other non-inbred strains, and thus these strains have stabilized past the stage of inbreeding depression. The inbred strains have been tested successfully for transgenesis and gene editing (Sakane et al., 2018) and should begin to become available to the community late in 2019.

TRAINING RESOURCES

As described above, new genetic and biochemical techniques are being developed for *Xenopus* research, and the application and usability of *Xenopus* in basic and biomedical sciences are expanding into a wide range of research areas such as human disease modeling in CRISPR/Cas9 induced mutants. To meet this increasing demand, the resource centers are not only distributing materials but also providing a variety of advanced training courses and research opportunities for users who are not familiar with basic or advanced methods. Each resource center organizes a unique combination of educational opportunities and updates the content of courses annually based on requests from users.

In 2013, the NBRP *X. tropicalis* started running annual technical courses in Hiroshima, to teach several basic techniques such as artificial fertilization of eggs, microinjection of synthetic mRNAs/oligonucleotides, and husbandry of tadpoles and frogs. Trainees include faculty members, post-doctoral researchers, and graduate and undergraduate students from across Japan. The training course has been continually updated, and now includes transgenesis, genome editing and bioinformatics. Moreover, a user survey resulted in further development of the course in 2018. To allow more time for genome editing techniques, the NBRP technical courses are now held in both summer and winter annually. The technical courses represent a good opportunity not only for providing training, but also for distributing and testing genetic tools – more than 200 plasmid samples from the *X. tropicalis* cDNA plasmid collection and transgenesis plasmids have been distributed during the past six courses. In addition to its technical courses, the NBRP *X. tropicalis* has been organizing a joint technical course with the NBRP Medaka in Okazaki, Japan. This joint course is designed for overseas trainees from around the world and aims to facilitate the beneficial use of two different aquatic model organisms. *Xenopus* has become a popular animal for education in schools, members of the NBRP *X. tropicalis* have been providing opportunities to introduce *Xenopus* research to medical university and high-school students across Japan and to students from other Asian countries. To reach a wider range of researchers, the NBRP *X. tropicalis* is also running XenoBiores[1], which facilitates the exchange of questions and troubleshooting among users

[1]https://home.hiroshima-u.ac.jp/amphibia/xenobiores/forum/

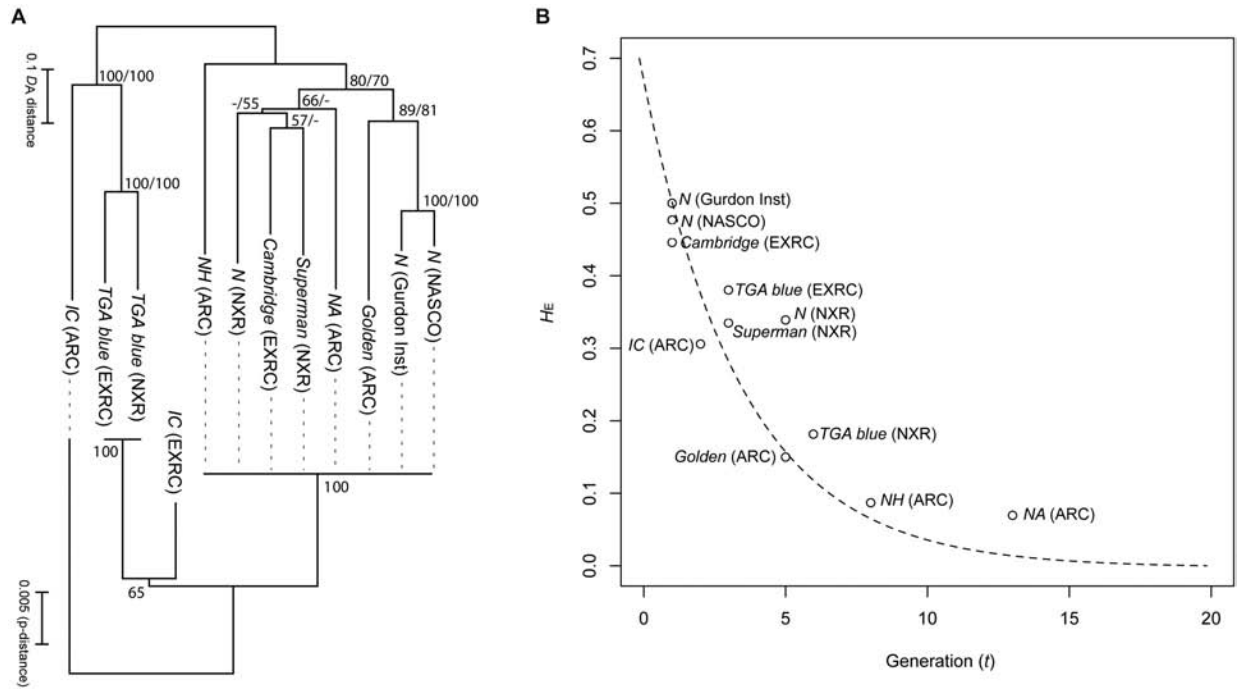

FIGURE 2 | Genetic relationships and heterozygosity reduction curve in the strains of *X. tropicalis*. **(A)** Neighbor joining trees of the strains based on genetic distances (D_A) of 60 Simple Sequence Length Polymorphism (SSLP) markers (upper) and p-distance of mitochondrial haplotypes (2,328 bp; lower). Numbers on branches indicate percent bootstrap probability (only indicated > 50%). **(B)** Plot of expected heterozygosity (H_E) against generation number (t). The curved dotted strain indicates theoretical reduction of heterozygosity via single brother-sister matings for every generation, calculated from the following equation: $H_E = H_0\left(1 - \frac{1}{2N_e}\right)^t$.

and provides the latest information on a variety of topics including conferences reports, technical courses and genetic/live-animal resources.

The NXR at the Marine Biological Laboratory (MBL) in Woods Hole, has a range of advanced training courses, which are run annually and are aimed at advanced and beginner *Xenopus* researchers. These courses bring experts in the fields of bioinformatics, specialized imaging, and gene editing to teach cutting edge techniques to the participants. The Bioinformatics Workshop is designed for wet lab biologists who want to extend their understanding of computational tools and methods and may also want to acquire grounded computational skills to enable them to work independently. The imaging workshop provides hands on training in imaging *Xenopus* embryos, including live imaging of embryos and explants and image processing, analysis and quantitation. The genome editing workshop focuses on providing theoretical and practical aspects of genome editing in *Xenopus*, allowing participants to generate mutants during the workshop. Husbandry training is also offered at the NXR to promote harmonization among *Xenopus* researchers and improve yields of healthy and productive frogs throughout the community. Furthermore, the NXR offers a research facility service, which allows visiting scientists to integrate themselves in the NXR facility and MBL. This allows full access to all available *Xenopus* lines, equipment, reagents, and expertise in gene editing. Uniquely, the NXR allows for a rich collaborative environment established by the diverse group of scientists from different disciplines who come every year to do their research at the MBL.

The EXRC at Portsmouth does not run specific training courses, but within its remit is a "research hotel" service that is becoming heavily used. Researchers, who may be very familiar with *Xenopus* or used to other models, come to the center and work alongside staff to learn new techniques and carry out their own experiments, using all of the resources at cost. Often, they make new lines to be grown up in the center then return to analyze them.

SPECIALIZED *Xenopus* RESOURCES

Also situated in Europe and regularly providing training is the French *Xenopus* Biological Resource Center (CRB[2]), which has been located in Rennes since 2008. Training is provided by members of the CRB in the fields of *Xenopus* breeding techniques, embryo manipulation and, like at the EXRC, how to care for *Xenopus* as required by EU laws. Research-wise, the CRB has special expertise in projects centered on the screening of biologically active compounds in *Xenopus* oocytes with electrophysiological assays; the center is equipped to

[2]https://xenopus.univ-rennes1.fr

perform this type of analysis at high throughput using robotic approaches. The CRB can also offer transgenesis, CRISPR/Cas9 for targeted knockouts and screening of the mutations. Many of the wild-type *X. laevis* and *X. tropicalis* used in Europe are provided by the CRB and it is closely involved with projects to improve the health of aquatic laboratory animals. Shortly the CRB will relocate to the biomedical campus in Rennes. Excitingly, this relocation should involve the development of a state-of-the-art facility for the development and housing of transgenic animals.

The *X. laevis* research resource for immunobiology (XLRRI[3]) at the University of Rochester Medical Center, is a comprehensive research resource specializing in the use of *X. laevis* as a multi-faceted experimental platform for immunological research. The XLRRI maintains and provides to the research community MHC-defined inbred strains and clones of frogs, as well as tools such as lymphoid tumor cell lines, MHC-defined fibroblast cell lines, monoclonal antibodies, MHC tetramers and batteries of validated PCR primers for immune-relevant genes. An important effort of the XLRRI is the development of *X. laevis* transgenic lines with fluorescent, traceable immune cells and specific immune deficiency, including the establishment of a reliable CRISPR/Cas9-mediated genome editing platform focused on immunity.

The XLRRI plays also plays a key role in understanding infectious diseases that plague amphibians worldwide and contribute to their decline. Notably, the XLRRI includes satellite facilities devoted to studying pathogenesis and immunity to ranaviruses and mycobacteria. Importantly, the XLRRI provides protocols, technical assistance and training to new as well as established investigators and students from a wide area of scientific disciplines from comparative, developmental and evolutionary immunology to field and conservation biology. Training and assistance cover general *Xenopus* breeding and husbandry, transgenesis and reverse genetics as well as *Xenopus*-specific *in vivo* and *in vitro* immunological methodologies.

INTEGRATION AND SUPPORT ON XENBASE

Xenopus research around the world is supported by Xenbase[4] the *Xenopus* model organism database. Xenbase maintains, curates, and freely disseminates all of the diverse genomic, genetic, expression, and functional data for *Xenopus* and interrelates these data to human and other model organisms (Karimi et al., 2018). In addition, Xenbase allows researchers to identify *Xenopus* resources and reagents, including the transgenic and mutant lines (as detailed in this paper), as well as clones (ORFeome, plasmid, fosmid, and BAC) which are supplied by the EXRC.

Xenbase links to all the major *Xenopus* stock center websites (EXRC, NXR, XLRRI, NBRP, and CRB) from the Xenbase home page and from resource pages where appropriate. A fully searchable "Lines and Strains" module includes all of the mutant and transgenic lines and wild-type strains that are, or have been, available from NXR, EXRC and NBRP. Each *Xenopus* line has a dedicated page which summarizes targeted gene (s) or transgenic construct details, phenotype, genetic background and provenance, and provides direct links to the relevant stock centre (s) from which the line may be ordered. In the database, wild-type strains are also given "XB-LINE" identifiers so that they can be assigned as background to transgenic and mutant lines. Stable research identifiers (RRIDs) are recorded for all *Xenopus* stocks, a measure taken to promote reproducibility, rigor and transparency. Lines and strains shared between stock centers have been given unique RRIDs, as these colonies are now genetically isolated, and may be affected by genetic drift.

Importantly, Xenbase staff developed the transgenic nomenclature guidelines in consultation with the *Xenopus* stock centers and following best practice used by all other model organism databases. Using standard nomenclature is essential to ensure *Xenopus* research is accessible to the broadest possible scientific community, and improves rigor and reproducibility while also establishing provenance. These naming guidelines are posted on Xenbase[5]. Help naming maintained lines is always available via emailing the Xenbase help desk (xenbase@ucalgary.ca) or by contacting stock center staff.

The *Xenopus* ORFeome project, funded by NICHD (R01 HD069352), was developed as a molecular toolkit to probe the cellular and genetic mechanisms underlying many human diseases using *Xenopus*. It is another resource that is fully integrated, cataloged and searchable on Xenbase[6]. The ORFeome project produced two sets of full-length, validated, open reading frame clones, one for *X. laevis* (representing ∼10,250 genes, ∼7,700 with human orthologs; Grant et al., 2015), and one for *X. tropicalis* (representing ∼3,970 genes, ∼3,800 with human orthologs). Each ORFeome clone has a dedicated Xenbase page with details including gene symbol and name, full sequence, translation, availability, and links to the gene page and BLAST tool, and to the EXRC which supplies small numbers of ORFeome clones (James-Zorn et al., 2018). Similarly, all IMAGE Consortium *Xenopus* Gene Collection (XGC) clones (Morin et al., 2006) have dedicated pages with supporting sequence and other data, and these clones can be searched, filtering for only those supplied by the EXRC.

Xenbase enables efficient access to the physical resources for scientists wanting to use the *Xenopus* models; these resources are already extensive and growing rapidly as can be seen from the review above. As we write, there is still capacity in the resource centers to hold and develop new transgenic and knockout lines and we encourage all *Xenopus* users to take the opportunity to enhance their research programs by using these community facilities and taking advantage of the knowledge of their staff.

[3]https://www.urmc.rochester.edu/microbiology-immunology/xenopus-laevis.aspx

[4]www.xenbase.org

[5]www.xenbase.org/gene/static/tgNomenclature.jsp

[6]www.xenbase.org/reagents/orf.do

MEMBERS OF THE CENTRE DE RESSOURCE BIOLOGIQUE XENOPE TEAM IN FRANCE AND TEAM *Xenopus tropicalis* NBRP IN JAPAN

The Centre de Ressource Biologique Xenope (CRBX) team in France is Morgane Nicolas, Thomas Lafond, Daniel Boujard, Yann Audic, and Brigitte Guillet. Team Xenopus tropicalis NBRP in Japan is Hajime Ogino, Akihiko Kashiwagi, Takeshi Igawa, Keiko Kashiwagi, Nanoka Suzuki, Atsushi Suzuki, Ichiro Tazawa, Haruki Ochi, Nobuaki Furuno, Minoru Takase, Keisuke Nakajima, Hideki Hanada, Ikuo Miura, Atsushi Kurabayashi, Takashi Kato, Kei Sato, Kimiko Takebayashi-Suzuki, and Hitoshi Yoshida.

AUTHOR CONTRIBUTIONS

All of the authors except DG wrote and reviewed the text. DG and TI produced the data shown. MW, AA-D, SM, and CJ-Z produced the table of transgenic animals.

FUNDING

The European *Xenopus* Resource Centre was funded by the Wellcome Trust (212942/Z/18/Z) and BBSRC (BB/R014841/1). The National *Xenopus* Resource was funded by the NIH (ORIP/NICHD) (Grant P40 OD010997). Major funding for Xenbase was provided by the Eunice Kennedy Shriver National Institute of Child Health and Human Development (Grant P41 HD064556). XLRRI was funded by the NIH/NIAID (R24-AI-059830 and R21AI139718). CRBX was funded by GIS-IBISA 2014 and Fondation Maladies Rares 2016. The National BioResource Project (NBRP) for *Xenopus tropicalis* was funded by Japan Agency for Medical Research and Development (AMED).

ACKNOWLEDGMENTS

The staff of all of the research centers are very grateful to those scientists who have donated lines, plasmids, and other reagents for the benefit of the community. The CRBX would like to acknowledge Christophe Heligon for his past involvement in the CRBX.

SUPPLEMENTARY MATERIAL

The Supplementary Material for this article can be found online at: https://www.frontiersin.org/articles/10.3389/fphys.2019.00387/full#supplementary-material

REFERENCES

Allen, B. G., and Weeks, D. L. (2005). Transgenic *Xenopus laevis* embryos can be generated using phiC31 integrase. *Nat. Methods* 2, 975–979. doi: 10.1038/nmeth814

Amaya, E., Musci, T. J., and Kirschner, M. W. (1991). Expression of a dominant negative mutant of the FGF receptor disrupts mesoderm formation in xenopus embryos. *Cell* 66, 257–270. doi: 10.1016/0092-8674(91)90616-7

Andres, A. C., Muellener, D. B., and Ryffel, G. U. (1984). Persistence, methylation and expression of vitellogenin gene derivatives after injection into fertilized eggs of *Xenopus laevis*. *Nucleic Acids Res.* 12, 2283–2302. doi: 10.1093/nar/12.5.2283

Aslan, Y., Tadjuidje, E., Zorn, A. M., and Cha, S.-W. (2017). High-efficiency non-mosaic CRISPR-mediated knock-in and indel mutation in F0 Xenopus. *Development* 144, 2852–2858. doi: 10.1242/dev.152967

Banach, M., Edholm, E. S., and Robert, J. (2017). Exploring the functions of nonclassical MHC class Ib genes in *Xenopus laevis* by the CRISPR/Cas9 system. *Dev. Biol.* 426, 261–269. doi: 10.1016/j.ydbio.2016.05.023

Baxi, A. B., Lombard-Banek, C., Moody, S. A., and Nemes, P. (2018). Proteomic characterization of the neural ectoderm fated cell clones in the *Xenopus laevis* embryo by high-resolution mass spectrometry. *ACS Chem. Neurosci.* 9, 2064–2073. doi: 10.1021/acschemneuro.7b00525

Bendig, M. M., and Williams, J. G. (1984). Differential expression of the *Xenopus laevis* tadpole and adult beta-globin genes when injected into fertilized *Xenopus laevis* eggs. *Mol. Cell. Biol.* 4,567–570. doi: 10.1128/MCB.4.3.567

Blitz, I. L., Biesinger, J., Xie, X., and Cho, K. W. Y. (2013). Biallelic genome modification in F0 *Xenopus tropicalis* embryos using the CRISPR/Cas system. *Genesis* 51, 827–834. doi: 10.1002/dvg.22719

Briggs, J. A., Weinreb, C., Wagner, D. E., Megason, S., Peshkin, L., Kirschner, M. W., et al. (2018). The dynamics of gene expression in vertebrate embryogenesis at single-cell resolution. *Science* 360:eaar5780. doi: 10.1126/science.aar5780

Brinkman, E. K., Kousholt, A. N., Harmsen, T., Leemans, C., Chen, T., Jonkers, J., et al. (2018). Easy quantification of template-directed CRISPR/Cas9 editing. *Nucleic Acids Res.* 46:e58. doi: 10.1093/nar/gky164

Brown, D. D., Cai, L., Das, B., Marsh-Armstrong, N., Schreiber, A. M., and Juste, R. (2005). Thyroid hormone controls multiple independent programs required for limb development in *Xenopus laevis* metamorphosis. *Proc. Natl. Acad. Sci.* 102, 12455–12458. doi: 10.1073/pnas.0505989102

Chae, J., Zimmerman, L. B., and Grainger, R. M. (2002). Inducible control of tissue-specific transgene expression in *Xenopus tropicalis* transgenic lines. *Mech. Dev.* 117, 235–241. doi: 10.1016/S0925-4773(02)00219-8

Chen, T.-W., Wardill, T. J., Sun, Y., Pulver, S. R., Renninger, S. L., Baohan, A., et al. (2013). Ultrasensitive fluorescent proteins for imaging neuronal activity. *Nature* 499, 295–300. doi: 10.1038/nature12354

Cohen, S. N., Chang, A. C. Y., Boyer, H. W., and Helling, R. B. (1973). Construction of biologically functional bacterial plasmids in vitro (R factor/restriction enzyme/transformation/endonuclease/antibiotic resistance). *PNAS* 70, 3240–3244. doi: 10.1073/PNAS.70.11.3240

Corkins, M. E., Hanania, H. L., Krneta-Stankic, V., DeLay, B. D., Pearl, E. J., Lee, M., et al. (2018). Transgenic *Xenopus laevis* line for in vivo labeling of nephrons within the kidney. *Genes* 9:197. doi: 10.3390/genes9040197

Cross, M. K., and Powers, M. A. (2009). Learning about cancer from frogs: analysis of mitotic spindles in *Xenopus* egg extracts. *Dis. Model. Mech.* 2, 541–547. doi: 10.1242/dmm.002022

Delay, B. D., Corkins, M. E., Hanania, H. L., Salanga, M., Deng, J. M., Sudou, N., et al. (2018). Tissue-specific gene inactivation in *Xenopus laevis*: knockout of lhx1 in the kidney with CRISPR/Cas9. *Genetics* 208, 673–686. doi: 10.1534/genetics.117.300468

Deniz, E., Mis, E. K., Lane, M., and Khokha, M. K. (2018). CRISPR/Cas9 F0 screening of congenital heart disease genes in *Xenopus tropicalis*. *Methods Mol. Biol.* 1865, 163–174. doi: 10.1007/978-1-4939-8784-9_12

Etkin, L. D., and Pearman, B. (1987). Distribution, expression and germ line transmission of exogenous DNA sequences following microinjection into *Xenopus laevis* eggs. *Development* 99, 15–23.

Etkin, L. D., Pearman, B., Roberts, M., and Bektesh, S. L. (1984). Replication, integration and expression of exogenous DNA injected into fertilized eggs

of *Xenopus laevis*. *Differentiation* 26, 194–202. doi: 10.1111/j.1432-0436.1984.tb01395.x

Etkin, L. D., and Roberts, M. (1983). Transmission of integrated sea urchin histone genes by nuclear transplantation in *Xenopus laevis*. *Science* 221, 67–69. doi: 10.1126/SCIENCE.6857265

Feehan, J. M., Chiu, C. N., Stanar, P., Tam, B. M., Ahmed, S. N., and Moritz, O. L. (2017). Modeling dominant and recessive forms of retinitis pigmentosa by editing three rhodopsin-encoding genes in *Xenopus laevis* using crispr/Cas9. *Sci. Rep.* 7:6920. doi: 10.1038/s41598-017-07153-4

Gentsch, G. E., Spruce, T., Monteiro, R. S., Owens, N. D. L., Martin, S. R., and Smith, J. C. (2018). Innate immune response and off-target mis-splicing are common morpholino-induced side effects in *Xenopus*. *Dev. Cell* 44, 597.e10–610.e10. doi: 10.1016/j.devcel.2018.01.022

Gossen, M., and Bujard, H. (1992). Tight control of gene expression in mammalian cells by tetracycline-responsive promoters. *Proc. Natl. Acad. Sci. U.S.A.* 89, 5547–5551. doi: 10.1073/pnas.89.12.5547

Grainger, R. M. (2012). *Xenopus tropicalis* as a model organism for genetics and genomics: past, present, and future. *Methods Mol. Biol.* 917, 3–15. doi: 10.1007/978-1-61779-992-1_1

Grant, I. M., Balcha, D., Hao, T., Shen, Y., Trivedi, P., Patrushev, I., et al. (2015). The *Xenopus* ORFeome: a resource that enables functional genomics. *Dev. Biol.* 408, 345–357. doi: 10.1016/j.ydbio.2015.09.004

Gurdon, J. B., and Hopwood, N. (2000). The introduction of *Xenopus laevis* into developmental biology: of empire, pregnancy testing and ribosomal genes. *Int. J. Dev. Biol.* 44, 43–50. doi: 10.1387/ijdb.10761846

Hagmann, M., Adlkofer, K., Pfeiffer, P., Bruggmann, R., Georgiev, O., Rungger, D., et al. (1996). Dramatic changes in the ratio of homologous recombination to nonhomologous DNA-end joining in oocytes and early embryos of *Xenopus laevis*. *Biol. Chem. Hoppe Seyler* 377, 239–250. doi: 10.1515/bchm3.1996.377.4.239

Harland, R. M., and Grainger, R. M. (2011). *Xenopus* research: metamorphosed by genetics and genomics. *Trends Genet.* 27, 507–515. doi: 10.1016/j.tig.2011.08.003

Hartley, K. O., Nutt, S. L., and Amaya, E. (2002). Targeted gene expression in transgenic *Xenopus* using the binary Gal4-UAS system. *Proc. Natl. Acad. Sci.* 99, 1377–1382. doi: 10.1073/pnas.022646899

Hassnain Waqas, S. F., Noble, A., Hoang, A. C., Ampem, G., Popp, M., Strauß, S., et al. (2017). Adipose tissue macrophages develop from bone marrow–independent progenitors in *Xenopus laevis* and mouse. *J. Leukoc. Biol.* 102, 845–855. doi: 10.1189/jlb.1A0317-082RR

Hellsten, U., Harland, R. M., Gilchrist, M. J., Hendrix, D., Jurka, J., Kapitonov, V., et al. (2010). The genome of the western clawed frog *Xenopus tropicalis*. *Science* 328, 633–636. doi: 10.1126/science.1183670

Hogben, L. (1939). *Xenopus* test for pregnancy. *Br. Med. J.* 2, 38–39. doi: 10.1136/bmj.2.4095.38-b

Hoogenboom, W. S., Klein Douwel, D., and Knipscheer, P. (2017). *Xenopus* egg extract: a powerful tool to study genome maintenance mechanisms. *Dev. Biol.* 428, 300–309. doi: 10.1016/j.ydbio.2017.03.033

Huang, J. K., Dorey, K., Ishibashi, S., and Amaya, E. (2007). BDNF promotes target innervation of *Xenopus* mandibular trigeminal axons in vivo. *BMC Dev. Biol.* 7:59. doi: 10.1186/1471-213X-7-59

Igawa, T., Watanabe, A., Suzuki, A., Kashiwagi, A., Kashiwagi, K., Noble, A., et al. (2015). Inbreeding ratio and genetic relationships among strains of the western clawed frog, *Xenopus tropicalis*. *PLoS One* 10:e0133963. doi: 10.1371/journal.pone.0133963

James-Zorn, C., Ponferrada, V., Fisher, M. E., Burns, K., Fortriede, J., Segerdell, E., et al. (2018). Navigating xenbase: an integrated *Xenopus* genomics and gene expression database. *Methods Mol. Biol.* 1757, 251–305. doi: 10.1007/978-1-4939-7737-6_10

Jiang, X., Kalajzic, Z., Maye, P., Braut, A., Bellizzi, J., Mina, M., et al. (2005). Histological analysis of GFP expression in murine bone. *J. Histochem. Cytochem.* 53, 593–602. doi: 10.1369/jhc.4A6401.2005

Karimi, K., Fortriede, J. D., Lotay, V. S., Burns, K. A., Wang, D. Z., Fisher, M. E., et al. (2018). Xenbase: a genomic, epigenomic and transcriptomic model organism database. *Nucleic Acids Res.* 46, D861–D868. doi: 10.1093/nar/gkx936

Kashiwagi, K., Kashiwagi, A., Kurabayashi, A., Hanada, H., Nakajima, K., Okada, M., et al. (2010). *Xenopus tropicalis*: an ideal experimental animal in amphibia. *Exp. Anim.* 59, 395–405. doi: 10.1538/expanim.59.395

Kerney, R. R., Brittain, A. L., Hall, B. K., and Buchholz, D. R. (2012). Cartilage on the move: cartilage lineage tracing during tadpole metamorphosis. *Dev. Growth Differ.* 54, 739–752. doi: 10.1111/dgd.12002

Khokha, M. K., Chung, C., Bustamante, E. L., Gaw, L. W. K., Trott, K. A., Yeh, J., et al. (2002). Techniques and probes for the study of *Xenopus tropicalis* development. *Dev. Dyn.* 225, 499–510. doi: 10.1002/dvdy.10184

Kirmizitas, A., Meiklejohn, S., Ciau-Uitz, A., Stephenson, R., and Patient, R. (2017). Dissecting BMP signaling input into the gene regulatory networks driving specification of the blood stem cell lineage. *Proc. Natl. Acad. Sci. U.S.A.* 114, 5814–5821. doi: 10.1073/pnas.1610615114

Kominami, K., Takagi, C., Kurata, T., Kitayama, A., Nozaki, M., Sawasaki, T., et al. (2006). The initiator caspase, caspase-10β, and the BH-3-only molecule, Bid, demonstrate evolutionary conservation in *Xenopus* of their pro-apoptotic activities in the extrinsic and intrinsic pathways. *Genes Cells* 11, 701–717. doi: 10.1111/j.1365-2443.2006.00983.x

Kroll, K. L., and Amaya, E. (1996). Transgenic *Xenopus* embryos from sperm nuclear transplantations reveal FGF signaling requirements during gastrulation. *Development* 122, 3173–3183.

Lei, Y., Guo, X., Deng, Y., Chen, Y., and Zhao, H. (2013). Generation of gene disruptions by transcription activator-like effector nucleases (TALENs) in *Xenopus tropicalis* embryos. *Cell Biosci.* 3:21. doi: 10.1186/2045-3701-3-21

Livet, J., Weissman, T. A., Kang, H., Draft, R. W., Lu, J., Bennis, R. A., et al. (2007). Transgenic strategies for combinatorial expression of fluorescent proteins in the nervous system. *Nature* 450, 56–62. doi: 10.1038/nature06293

Love, N. R., Chen, Y., Ishibashi, S., Kritsiligkou, P., Lea, R., Koh, Y., et al. (2013). Amputation-induced reactive oxygen species are required for successful *Xenopus* tadpole tail regeneration. *Nat. Cell Biol.* 15, 222–228. doi: 10.1038/ncb2659

McQueen, C., and Pownall, M. E. (2017). An analysis of MyoD-dependent transcription using CRISPR/Cas9 gene targeting in *Xenopus tropicalis* embryos. *Mech. Dev.* 146, 1–9. doi: 10.1016/j.mod.2017.05.002

Miyamoto, K., Suzuki, K. T., Suzuki, M., Sakane, Y., Sakuma, T., Herberg, S., et al. (2015). The expression of TALEN before fertilization provides a rapid knock-out phenotype in *Xenopus laevis* founder embryos. *PLoS One* 10:e0142946. doi: 10.1371/journal.pone.0142946

Morin, R. D., Chang, E., Petrescu, A., Liao, N., Griffith, M., Chow, W., et al. (2006). Sequencing and analysis of 10,967 full-length cDNA clones from *Xenopus laevis* and *Xenopus tropicalis* reveals post-tetraploidization transcriptome remodeling. *Genome Res.* 16, 796–803. doi: 10.1101/gr.4871006

Naert, T., Colpaert, R., Van Nieuwenhuysen, T., Dimitrakopoulou, D., Leoen, J., Haustraete, J., et al. (2016). CRISPR/Cas9 mediated knockout of rb1 and rbl1 leads to rapid and penetrant retinoblastoma development in *Xenopus tropicalis*. *Sci. Rep.* 6:35264. doi: 10.1038/srep35264

Naert, T., and Vleminckx, K. (2018a). CRISPR/Cas9 disease models in zebrafish and *Xenopus*: the genetic renaissance of fish and frogs. *Drug Discov. Today Technol.* 28, 41–52. doi: 10.1016/j.ddtec.2018.07.001

Naert, T., and Vleminckx, K. (2018b). Genotyping of CRISPR/Cas9 genome edited *Xenopus tropicalis*. *Methods Mol. Biol.* 1865, 67–82. doi: 10.1007/978-1-4939-8784-9_5

Nakajima, K., Nakajima, T., Takase, M., and Yaoita, Y. (2012). Generation of albino *Xenopus tropicalis* using zinc-finger nucleases. *Dev. Growth Differ.* 54, 777–784. doi: 10.1111/dgd.12006

Nakayama, T., Fish, M. B., Fisher, M., Oomen-Hajagos, J., Thomsen, G. H., and Grainger, R. M. (2013). Simple and efficient CRISPR/Cas9-mediated targeted mutagenesis in *Xenopus tropicalis*. *Genesis* 51, 835–843. doi: 10.1002/dvg.22720

Nieuwkoop, P. D., and Faber, J. (1994). *Normal Table of Xenopus laevis (Daudin): A Systematical and Chronological Survey of the Development From the Fertilized Egg Till the End of Metamorphosis*. Spokane, WA: Garland Pub & Grill.

Ogino, H., McConnell, W. B., and Grainger, R. M. (2006). High-throughput transgenesis in *Xenopus* using I-SceI meganuclease. *Nat. Protoc.* 1, 1703–1710. doi: 10.1038/nprot.2006.208

Pan, F. C., Chen, Y., Loeber, J., Henningfeld, K., and Pieler, T. (2006). I-SceI meganuclease-mediated transgenesis in *Xenopus*. *Dev. Dyn.* 235, 247–252. doi: 10.1002/dvdy.20608

Pearl, E., Morrow, S., Noble, A., Lerebours, A., Horb, M., and Guille, M. (2017). An optimized method for cryogenic storage of *Xenopus* sperm to maximise the effectiveness of research using genetically altered frogs. *Theriogenology* 92, 149–155. doi: 10.1016/j.theriogenology.2017.01.007

Pearl, E. J., Grainger, R. M., Guille, M., and Horb, M. E. (2012). Development of *Xenopus* resource centers: the national *Xenopus* resource and the European *Xenopus* resource center. *Genesis* 50, 155–163. doi: 10.1002/dvg.22013

Rankin, S. A., Hasebe, T., Zorn, A. M., and Buchholz, D. R. (2009). Improved Cre reporter transgenic *Xenopus*. *Dev. Dyn.* 238, 2401–2408. doi: 10.1002/dvdy.22043

Ratzan, W., Falco, R., Salanga, C., Salanga, M., and Horb, M. E. (2017). Generation of a *Xenopus laevis* F1 albino J strain by genome editing and oocyte host-transfer. *Dev. Biol.* 426, 188–193. doi: 10.1016/j.ydbio.2016.03.006

Roose, M., Sauert, K., Turan, G., Solomentsew, N., Werdien, D., Pramanik, K., et al. (2009). Heat-shock inducible cre strains to study organogenesis in transgenic *Xenopus laevis*. *Transgenic Res.* 18, 595–605. doi: 10.1007/s11248-009-9253-4

Rusconi, S., and Schaffner, W. (1981). Transformation of frog embryos with a rabbit beta-globin gene. *Proc. Natl. Acad. Sci. U.S.A.* 78, 5051–5055. doi: 10.1073/pnas.78.8.5051

Sakane, Y., Iida, M., Hasebe, T., Fujii, S., Buchholz, D. R., Ishizuya-Oka, A., et al. (2018). Functional analysis of thyroid hormone receptor beta in *Xenopus tropicalis* founders using CRISPR-Cas. *Biol. Open* 7:bio030338. doi: 10.1242/bio.030338

Sato, Y., Mukai, M., Ueda, J., Muraki, M., Stasevich, T. J., Horikoshi, N., et al. (2013). Genetically encoded system to track histone modification in vivo. *Sci. Rep.* 3:2436. doi: 10.1038/srep02436

Sega, A. G., Mis, E. K., Lindstrom, K., Mercimek-Andrews, S., Ji, W., Cho, M. T., et al. (2018). De novo pathogenic variants in neuronal differentiation factor 2 (NEUROD2) cause a form of early infantile epileptic encephalopathy. *J. Med. Genet.* 56, 113–122. doi: 10.1136/jmedgenet-2018-105322

Session, A. M., Uno, Y., Kwon, T., Chapman, J. A., Toyoda, A., Takahashi, S., et al. (2016). Genome evolution in the allotetraploid frog *Xenopus laevis*. *Nature* 538, 336–343. doi: 10.1038/nature19840

Shindo, A., Wallingford, J. B., Dale, L., and Slack, J. M. (1987). Fate map for the 32-cell stage of *Xenopus laevis*. *Development* 99, 527–551.

Suzuki, M., Takagi, C., Miura, S., Sakane, Y., Suzuki, M., Sakuma, T., et al. (2016). *In vivo* tracking of histone H3 lysine 9 acetylation in *Xenopus laevis* during tail regeneration. *Genes Cells* 21, 358–369. doi: 10.1111/gtc.12349

Swenson, E. S., Price, J. G., Brazelton, T., and Krause, D. S. (2007). Limitations of green fluorescent protein as a cell lineage marker. *Stem Cells* 25, 2593–2600. doi: 10.1634/stemcells.2007-0241

Takagi, C., Sakamaki, K., Morita, H., Hara, Y., Suzuki, M., Kinoshita, N., et al. (2013). Transgenic *Xenopus laevis* for live imaging in cell and developmental biology. *Dev. Growth Differ.* 55, 422–433. doi: 10.1111/dgd.12042

Tandon, P., Conlon, F., Furlow, J. D., and Horb, M. E. (2017). Expanding the genetic toolkit in *Xenopus*: approaches and opportunities for human disease modeling. *Dev. Biol.* 426, 325–335. doi: 10.1016/j.ydbio.2016.04.009

Tinsley, R. C., and Kobel, H. R. (1996). *The Biology of Xenopus*. London: Zoological Society of London.

Tran, H. T., Sekkali, B., Van Imschoot, G., Janssens, S., and Vleminckx, K. (2010). Wnt/β-catenin signaling is involved in the induction and maintenance of primitive hematopoiesis in the vertebrate embryo. *Proc. Natl. Acad. Sci.* 107, 16160–16165. doi: 10.1073/pnas.1007725107

Tymowska, J., and Fischberg, M. (1973). Chromosome complements of the genus *Xenopus*. *Chromosoma* 44, 335–342. doi: 10.1007/BF00291027

Waldner, C., Sakamaki, K., Ueno, N., Turan, G., and Ryffel, G. U. (2006). Transgenic *Xenopus laevis* strain expressing Cre recombinase in muscle cells. *Dev. Dyn.* 235, 2220–2228. doi: 10.1002/dvdy.20880

Wlizla, M., Falco, R., Peshkin, L., Parlow, A. F., and Horb, M. E. (2017). Luteinizing Hormone is an effective replacement for hCG to induce ovulation in *Xenopus*. *Dev. Biol.* 426, 442–448. doi: 10.1016/j.ydbio.2016.05.028

Yergeau, D. A., Kelley, C. M., Zhu, H., Kuliyev, E., and Mead, P. E. (2010). Transposon transgenesis in *Xenopus*. *Methods* 51, 92–100. doi: 10.1016/j.ymeth.2010.03.001

Yergeau, D. A., Kuliyev, E., and Mead, P. E. (2007). Injection-mediated transposon transgenesis in *Xenopus tropicalis* and the identification of integration sites by modified extension primer tag selection (Epts) linker-mediated pcr. *Nat. Protoc.* 2, 2975–2986. doi: 10.1038/nprot.2007.428

Yergeau, D. A., and Mead, P. E. (2009). Transposon-mediated transgenesis in the frog: new tools for biomedical and developmental studies. *Front. Biosci.* 14, 225–236. doi: 10.2741/3242

Young, J. J., and Harland, R. M. (2012). Targeted gene disruption with engineered zinc-finger nucleases (ZFNs). *Methods Mol. Biol.* 917, 129–141. doi: 10.1007/978-1-61779-992-1-7

Conflict of Interest Statement: The authors declare that the research was conducted in the absence of any commercial or financial relationships that could be construed as a potential conflict of interest.

frontiers in Physiology

ORIGINAL RESEARCH
published: 07 May 2019
doi: 10.3389/fphys.2019.00542

Cdc42 Effector Protein 3 Interacts With Cdc42 in Regulating Xenopus Somite Segmentation

Mary Kho[1], *Hongyu Shi*[1†] *and Shuyi Nie*[1,2,3*]

[1] School of Biological Sciences, Georgia Institute of Technology, Atlanta, GA, United States, [2] Petit Institute for Bioengineering and Bioscience, Georgia Institute of Technology, Atlanta, GA, United States, [3] Integrated Cancer Research Center, Georgia Institute of Technology, Atlanta, GA, United States

Somitogenesis is a critical process during vertebrate development that establishes the segmented body plan and gives rise to the vertebra, skeletal muscles, and dermis. While segmentation clock and wave front mechanisms have been elucidated to control the size and time of somite formation, regulation of the segmentation process that physically separates somites is not understood in detail. Here, we identified a cytoskeletal player, Cdc42 effector protein 3 (Cdc42ep3, CEP3) that is required for somite segmentation in *Xenopus* embryos. *CEP3* is specifically expressed in somite tissue during somite segmentation. Loss-of-function experiments showed that CEP3 is not required for the specification of paraxial mesoderm, nor the differentiation of muscle cells, but is required for the segmentation process. Live imaging analysis further revealed that CEP3 is required for cell shape changes and alignment during somitogenesis. When CEP3 was knocked down, somitic cells did not elongate efficiently along the mediolateral axis and failed to undertake the 90° rotation. As a result, cells remained in a continuous sheet without an apparent segmentation cleft. CEP3 likely interacts with Cdc42 during this process, and both increased and decreased Cdc42 activity led to defective somite segmentation. Segmentation defects caused by Cdc42 knockdown can be partially rescued by the overexpression of CEP3. Conversely, loss of CEP3 resulted in the maintenance of high levels of Cdc42 activity at the cell membrane, which is normally reduced during and after somite segmentation. These results suggest that there is a feedback regulation between Cdc42 and CEP3 during somite segmentation and the activity of Cdc42 needs to be fine-tuned to control the coordinated cell shape changes and movement required for somite segmentation.

Keywords: Cdc42, Cdc42ep3, somitogenesis, somite segmentation, epithelialization, *Xenopus*

OPEN ACCESS

Edited by:
John Noel Griffin,
Duke University, United States

Reviewed by:
Sara Serafina Sanchez,
Universidad Nacional de Tucumán, Argentina
Michela Ori,
University of Pisa, Italy

***Correspondence:**
Shuyi Nie
shuyi.nie@biology.gatech.edu

***Present Address:**
Hongyu Shi,
Gerstner Sloan-Kettering Graduate School of Biomedical Sciences,
New York, NY, United States

Specialty section:
This article was submitted to Embryonic and Developmental Physiology, a section of the journal Frontiers in Physiology

Received: *12 October 2018*
Accepted: *17 April 2019*
Published: *07 May 2019*

Citation:
Kho M, Shi H and Nie S (2019) Cdc42 Effector Protein 3 Interacts With Cdc42 in Regulating Xenopus Somite Segmentation. Front. Physiol. 10:542. doi: 10.3389/fphys.2019.00542

INTRODUCTION

Somitogenesis is an essential step during vertebrate development. During somitogenesis, the paraxial mesoderm is partitioned into bilaterally symmetric blocks called somites, which later give rise to the dermis, skeletal muscles, and axial bones including vertebrae and ribs (Christ and Ordahl, 1995; Pourquie, 2001; Saga and Takeda, 2001). Somitogenesis is critical for the establishment of the segmented body plan of all vertebrates. This step is important not only for the segmented structure of axial bones and muscle, but also

for correct patterning of the peripheral nervous system and the blood vessels. As a result, defective somite segmentation leads to severe defects in the formation and alignment of vertebrae and ribs, as well as defective vasculature, such as occurs in spondylocostal dysostosis and Alagille syndrome (Shifley and Cole, 2007; Turnpenny, 2008).

Somite segmentation takes place periodically and regularly in an anterior to posterior sequence, which is orchestrated by several coordinated signaling events. Notch pathway genes are expressed in pre-somitic mesoderm (PSM) in a cyclic manner, which determines the speed of segmentation (Sato et al., 2002). At the same time, the intersection (or wave front) of the posterior-anterior gradient of fibroblast growth factor (FGF) and Wnt and the anterior-posterior gradient of retinoic acid (RA) capacitates cells to respond to the Notch-mediated segmentation clock, thus determining where segmentation takes place (Pourquie, 2003; Dubrulle and Pourquie, 2004; Moreno and Kintner, 2004). While the segmentation clock and wave front mechanism has been established to control the timing and space of somite segmentation, the cellular events that mediate the separation of somites are less understood. A study in chick embryos demonstrated that Rho GTPases Cdc42 and Rac1 are involved in the mesenchymal-to-epithelial transition (MET) during somitogenesis (Nakaya et al., 2004). Somitomeres in birds and mammals have an outer epithelial layer and a mesenchymal interior. Nakaya et al. showed that Cdc42 activity needs to be suppressed in boundary cells for them to become epithelial, which is critical for the formation of distinct morphological boundaries between somitomeres. When cells were forced to express high levels of Cdc42, they moved to the center of the somite, where mesenchymal cells reside (Nakaya et al., 2004). In contrast, a moderate level of Rac1 activity needs to be maintained for MET to take place, and it interacts with the transcription factor Paraxis during this process (Nakaya et al., 2004). In the frog *Xenopus laevis*, somite formation is slightly different in that the somites do not become epithelialized (Youn and Malacinski, 1981a,b; Keller, 2000; Afonin et al., 2006). Instead, cells elongate mediolaterally and align with the same orientation. Then, a thin but discrete fissure appears between the developing somitomeres. This intersomitic boundary becomes more evident as cells within each somite block undergo a rearrangement and rotation event to adopt an anterior-posterior orientation. At the same time, matrix deposition and assembly occurs around each somite block, physically separating the somites and supporting the alignment of the myotome. A recent report showed that although there is no MET process during *Xenopus* somitogenesis, Paraxis is still required for regulating cell-cell adhesion during this process (Sanchez and Sanchez, 2015). Whether Cdc42 also plays a conserved role in *Xenopus* somitogenesis and which signal mediates its activity during somitogenesis is still unclear.

In this study, we identified an effector protein for Cdc42, Cdc42 effector protein 3 (Cdc42ep3 or CEP3), which is specifically expressed in the developing somite. CEP3 belongs to a small family of Cdc42 effector proteins, also named binders of Rho GTPases (Borgs) (Joberty et al., 1999; Farrugia and Calvo, 2016). There are 5 CEPs in vertebrates, and their function in development is not well-understood. In mice, CEP1 (Borg5) enhances trophectoderm differentiation by promoting the sorting of trophectodermal cells to the outer layer of the blastocyst (Vong et al., 2010). Later in microvascular angiogenesis, CEP1 regulates directional migration of endothelial cells (Liu et al., 2014). We have recently reported that CEP1 interacts with Cdc42 to regulate actin organization during neural crest cell migration in frog embryos (Cohen et al., 2018). CEP2 (Borg1) has also been studied in *Xenopus* embryos and it promotes the cell-cell adhesion of non-neural ectoderm and the involution of mesoderm during gastrulation (Nelson and Nelson, 2004). CEP3 (Borg2) has not been studied in animal development and is best studied in cancer-associated fibroblasts (CAFs). CEP3 stabilizes actin stress fibers and septin networks in CAFs and is critical for CAFs to generate and sense forces. In addition, CEP3 is required for CAFs to remodel extracellular matrix, promote angiogenesis, and to promote cancer cell growth and invasion (Calvo et al., 2015; Farrugia and Calvo, 2017). While there is little knowledge of CEP3 in development or disease, human genome-wide association studies suggest that CEP3 is associated with adult height, muscular hypotonia, and joint laxity (Lango Allen et al., 2010).

Here, we investigated the role of CEP3 during *Xenopus* somitogenesis. Our results show that CEP3 is required for somitogenesis in *Xenopus* embryos. Loss of CEP3 in paraxial mesoderm led to defective somite segmentation, without affecting paraxial mesoderm specification or myogenesis. Using Wilson explants to visualize somite segmentation in live tissue, we further showed that CEP3 is not only required for somite segmentation, but also for somitic cells to elongate mediolaterally. Cdc42 activity needs to be tightly controlled during somitogenesis, and CEP3 not only acts downstream of Cdc42 to regulate this process, but also provides feedback regulation to Cdc42 activity. During somite segmentation, active Cdc42 is normally reduced at the cell membrane. However, when CEP3 was knocked down, active Cdc42 was maintained at the cell membrane. These results demonstrate that in *Xenopus* embryos where somitic cells do not become epithelialized, Cdc42 and its effector protein CEP3 still play an essential role in the segmentation process.

MATERIALS AND METHODS

Embryo Manipulations, Morpholino Oligomers, and RNA Preparation

Xenopus laevis embryos, both pigmented and albino, were obtained and staged as described by Nieuwkoop and Faber's Normal Table of *X. laevis*. The embryos were microinjected with capped RNAs or morpholino oligomers (MO) during early cleavage stages. standard control MO (Gene Tools, Philomath, OR) and Cdc42 effector protein 3(CEP3)-MO (5′-GGAATGAAATACGCAGATGTCAGAT−3′) that hybridizes to −32 to −8 position relative to the translational start site of *Xenopus CEP3* (GenBank Accession No. NM_1095138) were used in the study. GFP-wGBD was a gift from William Bement (Addgene plasmid # 26734). pcDNA3-EGFP-Cdc42-T17N and pcDNA3-EGFP-Cdc42-Q61L were gifts from Gary Bokoch

(Addgene plasmid #12976/ #12986). RNAs of nuclear beta-galactosidase (nβGal), membrane-tethered EGFP, GFP-wGBD, Cdc42(T1N), Cdc42(Q61L), and CEP3 were synthesized with linearized templates using SP6 polymerase (Ambion mMessage mMachine Kit). To target the paraxial mesoderm, mRNA or MO was injected into the lateral marginal zone at the 2-cell stage. Five to ten nanograms of MO or 0.05–0.3 ng of RNA was injected into one side of the embryo as indicated in each experiment. All experimental procedures were performed according to the USDA Animal Welfare Act Regulations and had been approved by the Institutional Animal Care and Use Committee, in compliance of the Public Health Service Policy.

Red-Gal Staining, *in situ* Hybridization, and Immunohistochemistry

For lineage tracing, embryos co-injected with nβGal were fixed at the desired stage for half an hour in the fixative MEMFA and stained with the Red-Gal substrate (Research Organics) until they turned red. The embryos were refixed for 2 h in MEMFA, and stored in methanol before *in situ* hybridization was performed. Whole-mount *in situ* hybridization was performed as previously described (Cohen et al., 2018). Antisense probes for *cdc42ep3*, *tbxt* (*Xbra,* NM_001091696), *mef2d* (NM_001096493), *myf5* (NM_001101779), *myf6* (NM_001088008), *myod1* (NM_001087823), and *myog* (NM_001085857) were synthesized with T7 RNA polymerase with linearized plasmids. Immunohistochemistry was performed as previously described (Cohen et al., 2018) against muscle antibody 12/101 (DSHB).

Somite (Wilson) Explant Culture and Microscopy

Wilson explants were isolated from embryos at stage 13–14 as previously described (Wilson et al., 1989). Briefly, embryos were cut open along the lateral walls of the archenteron, and the endoderm of the archenteron roof was carefully peeled away, exposing the notochord and paraxial mesoderm. The explants were then gently pressed down onto fibronectin (FN, 20 μg/ml in PBS)-coated dishes by coverslips supported by silicon grease in Danilchik media (Wilson et al., 1989). Static images or time-lapse movies were acquired using the PerkinElmer Spinning Disc confocal microscope with 10x and 20x objectives. To analyze cell shape changes, the ImageJ circularity Plugin was used. To analyze the distribution of active Cdc42, intensity plots of wGBD-GFP across the medial-lateral axes of cells were analyzed in ImageJ. Both the length of the cell and the signal intensity (relative to average intensity across the same cell) was normalized for plotting.

RESULTS

CEP3 Is Specifically Expressed in the Developing Somite

Cdc42 is involved in various cell and tissue morphogenesis events, and consistently, it is broadly expressed during embryonic development (Choi and Han, 2002). CEPs, unlike many other effector proteins for Cdc42 (e.g., N-WASP and PAK1), are only evolved in vertebrates. Therefore, it is likely that they play a role in the development of vertebrate-specific structures, such as somites. To determine whether CEP3 mediates Cdc42 activity in somitogenesis, we first examined the expression of *CEP3* by *in situ* hybridization analysis. As shown in **Figure 1**, at neurula stages around the onset of somitogenesis, *CEP3* is weakly expressed throughout the paraxial mesoderm. Later at tailbud stages, *CEP3* is specifically expressed in the developing somites, but not in the pre-somitic mesoderm (PSM) posterior to the forming somite. The expression pattern of *CEP3* suggests that it may play a role in somitogenesis.

CEP3 Is Required for Somite Segmentation

Since *CEP3* is specifically expressed in developing somites, we next determined whether CEP3 is required for somite development and in which step CEP3 is required. Loss-of-function experiments were performed with a translation-blocking morpholino oligomer (MO) against *CEP3*. Ten nanograms of CEP3-MO together with a lineage tracer nuclear beta-galactosidase (nβGal) was injected into one side of 2-cell stage embryos, leaving the contralateral side as an internal control. Embryos were fixed at gastrula stage (stage 13), early tailbud stage (stage 22–23), and late tailbud stage (stage 28–30), and subject to *in situ* hybridization against different mesodermal and myogenic genes. During gastrulation, the paraxial mesoderm is specified by gradients of morphogens such as bone morphogenetic proteins (BMPs), FGFs, Wnt, and Noggin. At this stage, CEP3-MO did not affect the expression of a pan-mesodermal gene *tbxt* (*Xbra*) (**Figure 2A**; $n = 9/9$). The somite in *Xenopus* embryos primarily gives rise to myotome tissue, and some myogenic genes are already expressed in paraxial mesoderm at gastrula stages. When CEP3 was knocked down by CEP3-MO, the expression of myogenic genes *myf5* and *myod1* was not affected (**Figure 2A**; $n = 16/16$ total). These results indicate that CEP3 is not required for the specification of paraxial mesoderm.

At early tailbud stages when somite segmentation is underway, the first wave of myogenesis has occurred to generate differentiated myotome (Della Gaspera et al., 2012). *Mef2d* and *myod1* are expressed in a segmented pattern in the developing somite and uniformly in the PSM. When CEP3 was knocked down by CEP3-MO, the segmented expression pattern of *mef2d* and *myod1* was lost (arrows in **Figure 2B**; $n = 17/22$, 28/31, respectively). The expression levels of both genes were relatively unchanged, but they were expressed in a diffused and continuous manner. This result indicates that CEP3 is required for somite segmentation. Later in development, the somite is further differentiated, and more muscle-specific transcription factors are expressed. *Myog* is expressed continuously in the central domain of each somite, and in a segmented manner in the dorsal and ventral aspect of the somite. When CEP3 was knocked down, the expression level of *myog* was unaffected, but the segmented pattern was lost (**Figure 2C**; $n = 12/17$). Similarly, the segmented expression of *myf6* and muscle marker 12/101 were disrupted by CEP3-MO ($n = 9/12$, 5/6, respectively). Unlike the chevron shaped

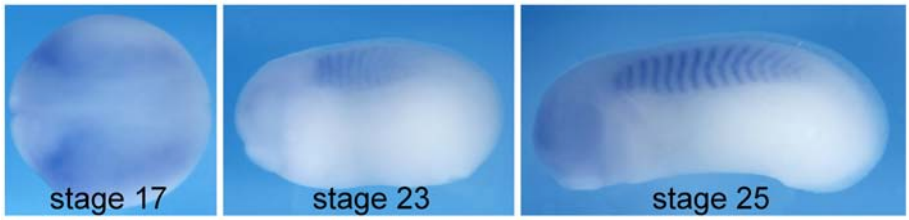

FIGURE 1 | Expression of *cdc42ep3* during *Xenopus* embryogenesis. *In situ* hybridization analysis shows that *cdc42ep3 (CEP3)* is specifically expressed in paraxial mesoderm and the developing somite. At stage 17, *CEP3* is broadly expressed in the paraxial mesoderm before somite segmentation takes place. During somite segmentation, *CEP3* is specifically expressed in segmented somites.

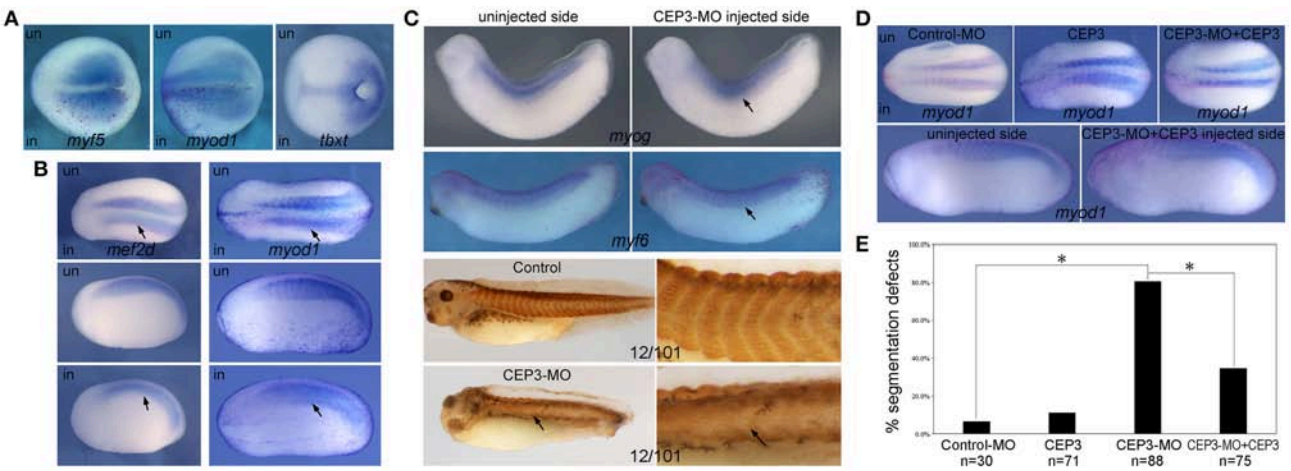

FIGURE 2 | Cdc42ep3-MO affected the expression of somitic genes. **(A–C)** Embyros were injected with 10 ng of CEP3-MO on one side, and the expression of somitic genes were compared between injected and uninjected sides. At the late gastrula stage (stage 15), CEP3-MO did not affect the expression of mesodermal genes *myf5* or *myod1* or pan-mesodermal gene *tbxt (Xbra)*. At the early neurula stage (stage 22), the expression of *mef2d* and *myod1* shows a segmented pattern in the uninjected side, but not in the CEP3-MO-injected side (arrows). At late tailbud stages, the segmented expression pattern, but not the overall expression level of myogenic genes *myog* and *myf6* was affected by CEP3-MO. Similar segmentation defect was observed in embryos stained with 12/101 antibody. **(D)** While 0.3ng CEP3 alone did not induce obvious segmentation defect, coinjection of CEP3 with CEP3-MO partially rescued the segmentation defects. Dorsal view (**A**, top panels in **B**, and top panels in **D**) or lateral view (bottom panels in **B,C**, and bottom panels in **D**, showing both sides of the same embryo) of the embryos was shown, with anterior to the left. **(E)** The percentage of defective embryos were summarized in the bar graph. χ^2 test was performed and both CEP3-MO mediated knockdown and CEP3 rescue led to significant difference in the phenotype. $^*P < 0.01$.

somites seen in control embryos, somitic tissue appeared in a disorganized and continuous form. These results confirmed that somite segmentation, but not myogenesis was inhibited by the loss of CEP3. The expression pattern of myogenic genes at late developmental stages also indicated that CEP3-MO did not cause a delay in somite segmentation, but rather inhibited segmentation. When CEP3 RNA without 5′UTR (therefore cannot be blocked by CEP3-MO) was coinjected with CEP3-MO, the segmentation defect was partially rescued (**Figure 2D**; $n = 8/27$, 18/48 with segmentation defect for *mef2d* and *myod1*, respectively), suggesting that the segmentation defect is specific to the loss of CEP3. Results obtained from the above *in situ* hybridization experiments were pooled together and summarized in **Figure 2E**. CEP3 knockdown increased the percentage of defective embryos significantly, which in turn was rescued by the addition of CEP3 significantly.

CEP3 Regulates Cell Morphology and Rotation During Somite Segmentation

Since somite segmentation is a dynamic process, we next used live imaging to document the segmentation process and to determine how CEP3-MO affected somite segmentation. Wilson explants were prepared to expose the ventral surface of the notochord and paraxial mesoderm, yet preserve tissue morphogenesis for many hours (Wilson et al., 1989). One side of the embryo was injected with membrane-tethered EGFP to reveal the shape of cells, and the other side of the embryo was injected with membrane-tethered EGFP together with 5 ng of CEP3-MO. This reduced dose of MO is used to generate a milder segmentation defect to allow for the analysis of various aspects of cell morphology and movements. The Wilson explant was imaged at 10-min intervals for around 10 h, from roughly embryonic stage 17 to stage 22 (**Supplementary Movie 1**). Time

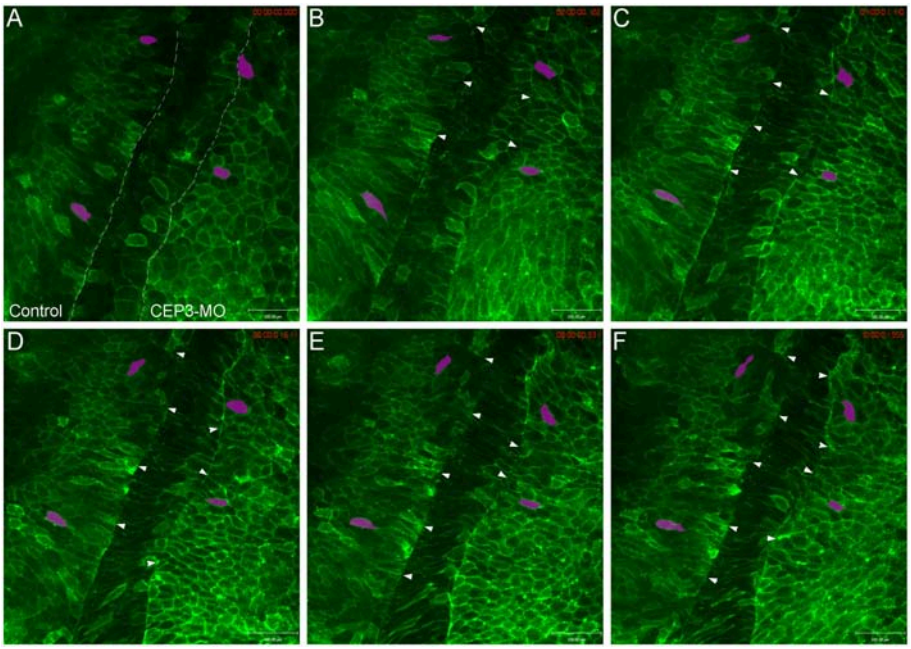

FIGURE 3 | Loss of Cdc42ep3 disrupted somite segmentation and cell shape changes. Wilson explants were dissected from embryos receiving membrane-tethered EGFP (EGFP-CAAX) on one side, and CEP3-MO plus EGFP-CAAX on the other side, and the segmentation process was followed by time-lapse microscopy. **(A–F)** Time frames at 2-h intervals. The dashed lines in **(A)** marks the boundaries between pre-somitic mesoderm and the notochord. Arrowheads marked segmentation furrows. Two cells on each side of the explant were followed by magenta shade. CEP3-MO not only impaired somite segmentation, but also affected the mediolateral elongation of cells. Scale bar = 100 μm.

frames from one representative movie are shown in **Figure 3**. In contrast to the distinct segmentation fissures on the control side (marked by arrowheads), there were fewer segmentation fissures that were obvious on CEP3-MO-injected side. A segmentation fissure was sometimes observed earlier, but disappeared at a later time points (arrowheads). We did not observe the regular 50-min pace of somite formation in our movies, which was likely caused by two reasons. First, the dissected explant cannot completely resemble the intact embryo, especially as somitogenesis involves large-scale tissue rearrangements. Second, at the same axial level, somitogenesis progresses in a dorsal to ventral sequence (Afonin et al., 2006). Therefore, somitogenesis at the ventral surface (observed in Wilson explants) may display some delay comparing to that at the dorsal surface (revealed by whole-mount immunohistochemistry). Nevertheless, our observations confirmed that CEP3 is required for somite segmentation.

Besides a failure to organize into distinct somitomeres, cells deprived of CEP3 also appeared different in shape compared to control cells. On the control side, cells elongated mediolaterally before segmentation took place. After segmentation, cells maintained their elongated shape and gradually rotated 90° to adopt an anterior-posterior orientation (see magenta-shaded cells in **Figure 3**). In contrast, cells on CEP3-MO-injected side were much rounder in shape and occasionally even elongated along the anterior-posterior axis. While they do elongate mediolaterally over time, the cells never adopt the same elongated shape as control cells. The shapes of cells were quantified by the ImageJ circularity plugin (circularity = 4pi (area/perimeter^2), with circularity = 1 for a perfect circle and circularity = 0 for a straight line). Over 100 cells were analyzed from 3 explants, with a similar number of cells picked on control and experimental sides at each axial level (before and after segementation, but not undergo rotation). While control cells have an average circularity of 0.454 ± 0.10, CEP3-MO cells have an average circularity of 0.698 ± 0.09. This difference was statistically significant (p = 2.5E-15; student t-test).

After the initial segmentation, cells start to rotate from a mediolateral orientation to an anteroposterior orientation. Possibly due to the isolation of the Wilson explant from the intact embryo, we only observed the rotation events in the first 2–3 somites on the control side. When CEP3 was knocked down, this rotation process was also hindered. While this could result from impaired segmentation in the first place, inadequate somite rotation may also exacerbate the segmentation defect. Taken together, CEP3 may regulate cell shape changes and rotation to control somite segmentation.

CEP3 Interacts With Cdc42 in Somite Segmentation

The activities of CEP3 in regulating cell shape changes and tissue arrangements likely result from its interaction with Cdc42. Cell culture studies have demonstrated that CEPs can mediate the activity of Cdc42 in the formation of membrane protrusions (Joberty et al., 1999, 2001; Hirsch et al., 2001; Calvo et al., 2015).

In chick embryos, Cdc42 has been reported to control somite segmentation through regulating the MET process (Nakaya et al., 2004). In that case, boundary cells need to turn down Cdc42 to become epithelial so that individual somitomeres can form. To determine if CEP3 interacts with Cdc42 during *Xenopus* somite segmentation, we first examined the function of Cdc42 in this process. To avoid interrupting GTPase-independent activity of Cdc42, we expressed dominant negative (DN-) and constitutively active (CA-) Cdc42 to alter the activation level of Cdc42 (Nalbant et al., 2004). DN-Cdc42 carries a point mutation (T17N) that prevents it from binding to GTP, so that it is always in the inactive, GDP-bound, state. Moreover, it sequesters guanine nucleotide exchange factors, thus also preventing the activation of endogenous Cdc42. Conversely, CA-Cdc42 [Cdc42(Q61L)] prevents GTPase activating protein-mediated GTP hydrolysis, therefore remaining active. Fifty picograms of DN-Cdc42 or CA-Cdc42 was expressed in paraxial mesodermal cells, and their effect on somite segmentation was examined by *in situ* hybridization against myogenic genes *mef2d* and *myod1* (numbers were summarized together). Both DN-Cdc42 and CA-Cdc42 disrupted the segmentation expression pattern of myogenic genes (**Figure 4A**; $n = 43/61$, 7/23, respectively), suggesting that tightly controlled Cdc42 activity is required for proper segmentation process. A rescue experiment was performed next to determine whether CEP3 mediates Cdc42 during somite segmentation. While co-expression of CA-Cdc42 with CEP3-MO could not rescue segmentation defects caused by CEP3-MO, co-expression of CEP3 RNA with DN-Cdc42 partially rescued segmentation defects caused by DN-Cdc42 (**Figure 4B**). These results suggest that CEP3 acts downstream of Cdc42 in somitogenesis.

In neural crest cells, we previously showed that CEP3 paralog CEP1 provides feedback regulation of Cdc42 by regulating the subcellular localization of active Cdc42 (Cohen et al., 2018). Here, we examined whether CEP3 also controls the localization of active Cdc42 during somitogenesis. We used GFP-wGBD [GFP fusion with the Cdc42-binding domain of N-WASP; (Benink and Bement, 2005)], which specifically binds to active Cdc42, to examine the localization of active Cdc42 in somitic cells. One side of the embryo was injected with 0.1 ng of GFP-wGBD alone, and the other side was injected with 0.1 ng of GFP-wGBD together with 5 ng of CEP3-MO. Wilson explants were prepared, and the localization of active Cdc42 was analyzed at early tailbud stage (stage 20) and compared between cells on both sides of the explant. On the control side, there were low levels of active Cdc42 at the cell membrane. Instead, the active-Cdc42 reporter was often observed inside the cell in a punctate manner, possibly reflecting reporters that failed to bind to Cdc42. In contrast, CEP3-MO-injected cells maintained a higher level of active Cdc42 on their surface (**Figure 5A**, explants from two embryos that received similar level of GFP-wGBD were shown). Although each cell may receive a different amount of the reporter, the ratio of reporter proteins on cell membrane should correlate with the level of active Cdc42. Therefore, to quantitate the levels of active Cdc42, intensity plots across the long axis of cells were generated and analyzed (**Figure 5B**). Over 170 cells from 20 Wilson explants were analyzed. Since the cells were of different sizes and have received a slightly different amount of GFP-wGBD due to injection, both the length of the cells and the pixel intensity of GFP-wGBD was normalized. To assess the ratio of wGBD reporter on the cell membrane, we normalized the signal intensity by comparing the actual pixel intensity at each location in a cell to the average pixel intensity across the same cell. Our result showed that GFP-wGBD distributed evenly across the mediolateral axis of control cells, possibly reflecting a low level of Cdc42 activity. The loss of CEP3, however, lead to high levels of GFP-wGBD at the cell periphery, suggesting a higher level of Cdc42 activity. This change in GFP-wGBD distribution was significant (white areas in **Figure 5B** are places where $p < 0.01$). This result suggests that Cdc42 activity needs to be decreased during somite segmentation and this partly explains why CA-Cdc42 also affected somite segmentation. Moreover, CEP3 may provide a negative feedback to Cdc42 to fine-tune Cdc42 activity in regulating somite segmentation.

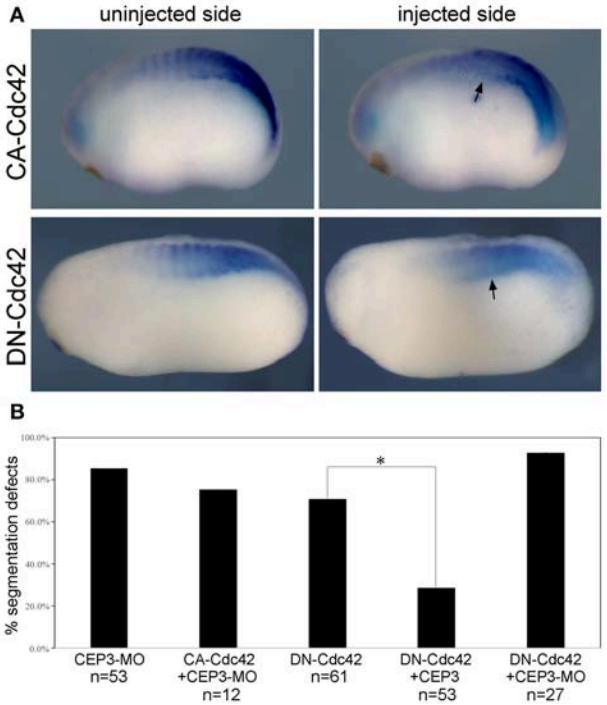

FIGURE 4 | Cdc42 needs to be tightly controlled during somite segmentation. **(A)** 0.05 ng of constitutively active (CA) or dominant negative (DN) Cdc42 was injected into one side of the embryo, and their effect on somite segmentation was examined by the expression of m*yod1*. Comparing to the uninjected control side, the segmented expression pattern of *myod1* was lost on the injected side (arrows), suggesting that both increased and decreased activity of Cdc42 will affect somite segmentation. **(B)** CA-Cdc42 was co-injected with CEP3-MO, and CEP3 or CEP3-MO was co-injected with DN-Cdc42 to determine whether they can rescue segmentation defects caused by CEP3 or Cdc42 knockdown. The percentage of embryos with segmentation defect was summarized in the bar graph. χ^2 test indicates that CA-Cdc42 failed to rescue segmentation defects caused by CEP3-MO ($p = 0.52$), but CEP3 significantly rescued segmentation defects caused by DN-Cdc42 (*$p < 0.01$). Coinjection of CEP3-MO with DN-Cdc42, on the other hand, further inhibited somite segmentation ($p = 0.02$ when comparing with DN-Cdc42 alone).

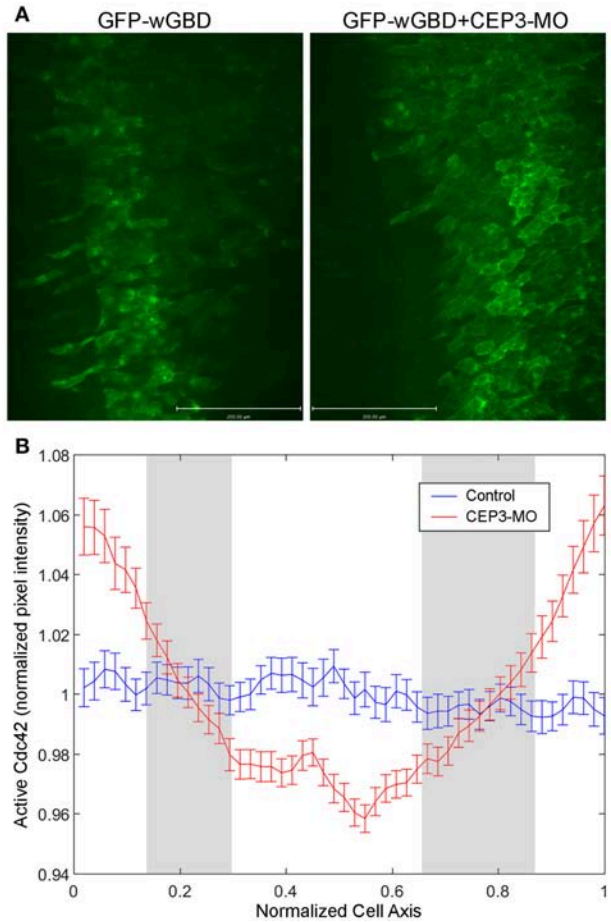

FIGURE 5 | CEP3-MO regulates Cdc42 activity in the developing somite. GFP-wGBD that binds to active Cdc42 was expressed in the paraxial mesoderm alone or together with CEP3-MO. **(A)** While GFP-wGBD was largely internalized and distributed in a diffused manner in control somitic cells, it was localized to the cell membrane in CEP3-MO-injected cells, reflecting a higher level of Cdc42 activity. **(B)** An intensity plot of GFP-wGBD across the mediolateral axis of cells was generated. There was a significantly higher level of GFP-wGBD at the cell periphery in CEP3-MO-injected cells and a significantly lower level of GFP-wGBD in the center of CEP3-MO-injected cells. Error bars: standard error of the mean. Student *t*-test was performed, and the gray area marks places where $p > 0.01$.

DISCUSSION

CEP3 in Somite Segmentation

In this study, we showed that CEP3 is required for somite segmentation in *Xenopus* embryogenesis. We think that CEP3 is involved in processes after the establishment of the segmentation clock since the expression pattern of *EphA4*/*EphrinB2* downstream of the segmentation clock was not affected (data not shown) (Watanabe et al., 2009). Our live imaging analysis of Wilson explants suggests three possible mechanisms of how CEP3 regulates somite segmentation. First, CEP3 may control segmentation by regulating cell shape changes. PSM cells usually elongate mediolaterally before segmentation takes place, and this was inhibited by CEP3-MO (**Figure 3**). Whether such elongation is required for somite segmentation is unclear, but it may enable cell-matrix interactions that promote cell alignment. Around the time of somite segmentation, PSM cells reach a long columnar shape across the entire paraxial mesoderm, contacting the extracellular matrix between the paraxial mesoderm and the notochord. This matrix interaction may also help maintain the elongated cell shape. The mediolateral elongation is not restricted to the somitic cells. It mediates a general convergent extension movement undertaken by the entire axial and paraxial mesoderm. Whether CEP3 plays a role in convergent extension, or whether it interacts with signals such as the planar cell polarity pathway that controls convergent extension remains to be tested.

The second possible way through which CEP3 regulates somite segmentation is the regulation of matrix deposition. Both fibronectin and laminin matrix are deposited and assembled at the intersomitic boundaries, as well as boundaries between notochord and the PSM. This extracellular matrix not only protects the integrity of each somitomere but also plays essential roles in somitic cell elongation, alignment, and rotation (Kragtorp and Miller, 2007; Hidalgo et al., 2009). Given that the expression of *CEP3* in somitic cells increases after somite segmentation and that intersomitic fissures can form but are not maintained at the loss of CEP3, it is possible that CEP3 also influences matrix deposition and assembly around the somitomeres. In endothelial cells, Rac1 and Cdc42 levels influence fibronectin matrix assembly during vascular morphogenesis (Fernandez-Sauze et al., 2009). Whether CEP3 regulates matrix assembly during somite segmentation through its interaction with Cdc42 remains to be elucidated.

Lastly, to maintain somite segmentation, CEP3 could also regulate cell rotation and alignment. The rotation of somitomeres has also been observed in zebrafish (Hollway et al., 2007), possibly correlating to an adapted program in swimming embryos with somites mostly comprised of myotome fibers. After rotation, cells align anteroposteriorly, contacting both intersomitic boundaries, and therefore also contribute to the stability of the somite. Afonin et al. showed that the rotation event associates with increased filopodia protrusions (Afonin et al., 2006). Since Cdc42 is critical in filopodia formation, it is possible that CEP3 interacts with Cdc42 to promote the protrusive activity of rotating cells, thus regulating the rotation event. In cell cultures, CEPs have been reported to be involved in cell protrusions. CEP1 induces membrane ruffling in Cos-7 cells and induces long actin-based protrusions in NIH 3T3 fibroblasts (Burbelo et al., 1999). In our study, CEP3 altered the activity of Cdc42, which is important for actin polymerization at the cell periphery for membrane protrusions. Whether CEP3 mediates Cdc42 in filopodia formation in somite cells remains to be examined.

Interactions Between CEP3 and Cdc42

CEP3 is an effector protein for Cdc42; therefore, its role in somite segmentation likely involves its interaction with Cdc42. Our results suggest that there is cross-regulation between

CEP3 and Cdc42. CEP3 acts downstream of Cdc42 such that segmentation defects caused by DN-Cdc42 can be partially rescued by CEP3 RNA, but segmentation defects caused by CEP3-MO cannot be rescued by CA-Cdc42 or DN-Cdc42. Conversely, CEP3 also modulates the activity of Cdc42. When CEP3 is knocked down by CEP3-MO, active Cdc42 on the plasma membrane is maintained, suggesting a feedback regulation between CEP3 and Cdc42. This is similar to our recent report that in neural crest cells, CEP3 paralog CEP1 provides feedback regulation of Cdc42 by regulating the subcellular localization of active Cdc42 (Cohen et al., 2018). We currently do not know through which mechanism CEP3 regulates Cdc42 activity. Whether CEP3 regulates the activation of Cdc42 through interacting with a GEF or GAP, or regulates the subcellular localization of Cdc42 through their physical interaction remains to be investigated.

ETHICS STATEMENT

This study was carried out in accordance with the recommendations of USDA Animal Welfare Act Regulations and Public Health Service Policy. The protocol was approved by the Institutional Animal Care and Use Committee.

AUTHOR CONTRIBUTIONS

HS performed the initial characterization of loss of CEP3 phenotype, which is confirmed by MK. MK further examined the activity of CEP3 in somite segmentation with live imaging and examined the interaction between CEP3 and Cdc42. SN designed and guided the experiments, and prepared the manuscript.

FUNDING

This work is supported by startup fund from Georgia Institute of Technology to SN. This work has been approved by Georgia Institute of Technology's Institutional Animal Care and Use Committee.

SUPPLEMENTARY MATERIAL

The Supplementary Material for this article can be found online at: https://www.frontiersin.org/articles/10.3389/fphys.2019.00542/full#supplementary-material

Supplementary Movie 1 | Somite segmentation in Wilson explants was affected by CEP3-MO. Wilson explants receiving EGFP-CAAX on the left and EGFP-CAAX plus CEP3-MO on the right were imaged for 10 h at 10-min intervals. CEP3-MO affected cell shape changes and somite segmentation.

REFERENCES

Afonin, B., Ho, M., Gustin, J. K., Meloty-Kapella, C., and Domingo, C. R. (2006). Cell behaviors associated with somite segmentation and rotation in *Xenopus laevis*. *Dev. Dyn.* 235, 3268–3279. doi: 10.1002/dvdy.20979

Benink, H. A., and Bement, W. M. (2005). Concentric zones of active rhoa and Cdc42 around single cell wounds. *J. Cell Biol.* 168:429–439. doi: 10.1083/jcb.200411109

Burbelo, P. D., Snow, D. M., Bahou, W., and Spiegel, S. (1999). MSE55, a Cdc42 effector protein, induces long cellular extensions in fibroblasts. *Proc. Natl. Acad. Sci. U.S.A.* 96, 9083–9088.

Calvo, F., Ranftl, R., Hooper, S., Farrugia, A. J., Moeendarbary, E., Bruckbauer, A., et al. (2015). Cdc42EP3/BORG2 and septin network enables mechano-transduction and the emergence of cancer-associated fibroblasts. *Cell Rep.* 13, 2699–2714. doi: 10.1016/j.celrep.2015.11.052

Choi, S. C., and Han, J. K. (2002). Xenopus Cdc42 regulates convergent extension movements during gastrulation through Wnt/Ca^{2+} signaling pathway. *Dev. Biol.* 244, 342–357. doi: 10.1006/dbio.2002.0602

Christ, B., and Ordahl, C. P. (1995). Early stages of chick somite development. *Anat. Embryol. (Berl)* 191, 381–396.

Cohen, S., Kovari, D. T., Wei, W., Keate, R., Curtis, J. E., and Nie, S. (2018). Cdc42 regulates the cellular localization of Cdc42ep1 in controlling neural crest cell migration. *J. Mol. Cell Biol.* 10, 376–387. doi: 10.1093/jmcb/mjx044

Della Gaspera, B., Armand, A. S., Sequeira, I., Chesneau, A., Mazabraud, A., Lecolle, S., et al. (2012). Myogenic waves and myogenic programs during xenopus embryonic myogenesis. *Dev. Dyn.* 241, 995–1007. doi: 10.1002/dvdy.23780

Dubrulle, J., and Pourquie, O. (2004). Coupling segmentation to axis formation. *Development* 131, 5783–5793. doi: 10.1242/dev.01519

Farrugia, A. J., and Calvo, F. (2016). The borg family of Cdc42 effector proteins Cdc42EP1-5. *Biochem. Soc. Trans.* 44, 1709–1716. doi: 10.1042/BST20160219

Farrugia, A. J., and Calvo, F. (2017). Cdc42 regulates Cdc42EP3 function in cancer-associated fibroblasts. *Small GTPases* 8, 49–57. doi: 10.1080/21541248.2016.1194952

Fernandez-Sauze, S., Grall, D., Cseh, B., and Van Obberghen-Schilling, E. (2009). Regulation of fibronectin matrix assembly and capillary morphogenesis in endothelial cells by rho family GTPases. *Exp. Cell Res.* 315, 2092–2104. doi: 10.1016/j.yexcr.2009.03.017

Hidalgo, M., Sirour, C., Bello, V., Moreau, N., Beaudry, M., and Darribere, T. (2009). *In vivo* analyzes of dystroglycan function during somitogenesis in *Xenopus laevis*. *Dev. Dyn.* 238, 1332–1345. doi: 10.1002/dvdy.21814

Hirsch, D. S., Pirone, D. M., and Burbelo, P. D. (2001). A new family of Cdc42 effector proteins, CEPs, function in fibroblast and epithelial cell shape changes. *J. Biol. Chem.* 276, 875–883. doi: 10.1074/jbc.M007039200

Hollway, G. E., Bryson-Richardson, R. J., Berger, S., Cole, N. J., Hall, T. E., and Currie, P. D. (2007). Whole-somite rotation generates muscle progenitor cell compartments in the developing zebrafish embryo. *Dev. Cell.* 12, 207–219. doi: 10.1016/j.devcel.2007.01.001

Joberty, G., Perlungher, R. R., and Macara, I. G. (1999). The borgs, a new family of Cdc42 and TC10 GTPase-interacting proteins. *Mol. Cell Biol.* 19, 6585–6597.

Joberty, G., Perlungher, R. R., Sheffield, P. J., Kinoshita, M., Noda, M., Haystead, T., et al. (2001). Borg proteins control septin organization and are negatively regulated by Cdc42. *Nat. Cell Biol.* 3, 861–866. doi: 10.1038/ncb1001-861

Keller, R. (2000). The origin and morphogenesis of amphibian somites. *Curr. Top Dev. Biol.* 47, 183–246. doi: 10.1016/S0070-2153(08)60726-7

Kragtorp, K. A., and Miller, J. R. (2007). Integrin alpha5 is required for somite rotation and boundary formation in xenopus. *Dev. Dyn.* 236, 2713–2720. doi: 10.1002/dvdy.21280

Lango Allen, H., Estrada, K., Lettre, G., Berndt, S. I., Weedon, M. N., Rivadeneira, F., et al. (2010). Hundreds of variants clustered in genomic loci and biological pathways affect human height. *Nature* 467, 832–838. doi: 10.1038/nature09410

Liu, Z., Vong, Q. P., Liu, C., and Zheng, Y. (2014). Borg5 is required for angiogenesis by regulating persistent directional migration of the cardiac microvascular endothelial cells. *Mol. Biol. Cell* 25, 841–851. doi: 10.1091/mbc.E13-09-0543

Moreno, T. A., and Kintner, C. (2004). Regulation of segmental patterning by retinoic acid signaling during *xenopus* somitogenesis. *Dev. Cell* 6, 205–218. doi: 10.1016/S1534-5807(04)00026-7

Nakaya, Y., Kuroda, S., Katagiri, Y. T., Kaibuchi, K., and Takahashi, Y. (2004). Mesenchymal-epithelial transition during somitic segmentation is regulated by differential roles of Cdc42 and Rac1. *Dev. Cell* 7, 425–438. doi: 10.1016/j.devcel.2004.08.003

Nalbant, P., Hodgson, L., Kraynov, V., Toutchkine, A., and Hahn, K. M. (2004). Activation of endogenous Cdc42 visualized in living cells. *Science* 305, 1615–1619. doi: 10.1126/science.1100367

Nelson, K. K., and Nelson, R. W. (2004). Cdc42 effector protein 2 (XCEP2) is required for normal gastrulation and contributes to cellular adhesion in *Xenopus laevis*. *BMC Dev. Biol.* 4:13. doi: 10.1186/1471-213X-4-13

Pourquie, O. (2001). The vertebrate segmentation clock. *J. Anat.* 199, 169–175. doi: 10.1046/j.1469-7580.2001.19910169.x

Pourquie, O. (2003). The segmentation clock: converting embryonic time into spatial pattern. *Science* 301, 328–330. doi: 10.1126/science.1085887

Saga, Y., and Takeda, H. (2001). The making of the somite: molecular events in vertebrate segmentation. *Nat. Rev. Genet.* 2, 835–845. doi: 10.1038/35098552

Sanchez, R. S., and Sanchez, S. S. (2015). Paraxis is required for somite morphogenesis and differentiation in *Xenopus laevis*. *Dev. Dyn.* 244, 973–987. doi: 10.1002/dvdy.24294

Sato, Y., Yasuda, K., and Takahashi, Y. (2002). Morphological boundary forms by a novel inductive event mediated by lunatic fringe and notch during somitic segmentation. *Development* 129, 3633–3644.

Shifley, E. T., and Cole, S. E. (2007). The vertebrate segmentation clock and its role in skeletal birth defects. *Birth Defects Res. C Embryo Today* 81, 121–133. doi: 10.1002/bdrc.20090.

Turnpenny P. D. (2008). "Defective somitogenesis and abnormal vertebral segmentation in man," in *Somitogenesis. Advances in Experimental Medicine and Biology, Vol 638*, eds M. Maroto and N. V. Whittock (New York, NY: Springer), 164–189. doi: 10.1007/978-0-387-09606-3_9

Vong, Q. P., Liu, Z., Yoo, J. G., Chen, R., Xie, W., Sharov, A. A., et al. (2010). A role for borg5 during trophectoderm differentiation. *Stem Cells* 28, 1030–1038. doi: 10.1002/stem.428.

Watanabe, T., Sato, Y., Saito, D., Tadokoro, R., and Takahashi, Y. (2009). EphrinB2 coordinates the formation of a morphological boundary and cell epithelialization during somite segmentation. *Proc. Natl. Acad. Sci. U.S.A.* 106, 7467–7472. doi: 10.1073/pnas.0902859106.

Wilson, P. A., Oster, G., and Keller, R. (1989). Cell rearrangement and segmentation in xenopus: direct observation of cultured explants. *Development* 105, 155–166.

Youn, B. W., and Malacinski, G. M. (1981a). Comparative analysis of amphibian somite morphogenesis: cell rearrangement patterns during rosette formation and myoblast fusion. *J. Embryol. Exp. Morphol.* 66, 1–26.

Youn, B. W., and Malacinski, G. M. (1981b). Somitogenesis in the amphibian *Xenopus laevis*: scanning electron microscopic analysis of intrasomitic cellular arrangements during somite rotation. *J. Embryol. Exp. Morphol.* 64, 23–43.

Conflict of Interest Statement: The authors declare that the research was conducted in the absence of any commercial or financial relationships that could be construed as a potential conflict of interest.

frontiers in Physiology

ORIGINAL RESEARCH
published: 08 May 2019
doi: 10.3389/fphys.2019.00502

Using the *Xenopus* Developmental Eye Regrowth System to Distinguish the Role of Developmental Versus Regenerative Mechanisms

*Cindy X. Kha†, Dylan J. Guerin† and Kelly Ai-Sun Tseng**

School of Life Sciences and Nevada Institute of Personalized Medicine, University of Nevada, Las Vegas, Las Vegas, NV, United States

A longstanding challenge in regeneration biology is to understand the role of developmental mechanisms in restoring lost or damaged tissues and organs. As these body structures were built during embryogenesis, it is not surprising that a number of developmental mechanisms are also active during regeneration. However, it remains unclear whether developmental mechanisms act similarly or differently during regeneration as compared to development. Since regeneration is studied in the context of mature, differentiated tissues, it is difficult to evaluate comparative studies with developmental processes due to the latter's highly proliferative environment. We have taken a more direct approach to study regeneration in a developmental context (regrowth). *Xenopus laevis*, the African clawed frog, is a well-established model for both embryology and regeneration studies, especially for the eye. *Xenopus* eye development is well-defined. *Xenopus* is also an established model for retinal and lens regeneration studies. Previously, we demonstrated that *Xenopus* tailbud embryo can successfully regrow a functional eye that is morphologically indistinguishable from an age-matched control eye. In this study, we assessed the temporal regulation of retinal differentiation and patterning restoration during eye regrowth. Our findings showed that during regrowth, cellular patterning and retinal layer formation was delayed by approximately 1 day but was restored by 3 days when compared to eye development. An assessment of the differentiation of ganglion cells, photoreceptor cells, and Müller glia indicated that the retinal birth order generated during regrowth was consistent with that observed for eye development. Thus, retina differentiation and patterning during regrowth is similar to endogenous eye development. We used this eye regrowth model to assess the role of known mechanisms in development versus regrowth. Loss-of-function studies showed that Pax6 was required for both eye development and regrowth whereas apoptosis was only required for regrowth. Together, these results revealed that the mechanisms required for both development and regrowth can be distinguished from regrowth-specific ones. Our study highlights this developmental model of eye regrowth as a robust platform to systematically and efficiently define the molecular mechanisms that are required for regeneration versus development.

Keywords: eye, apoptosis, retina, *Xenopus*, development, stem cells, regrowth, neural regeneration and repair

OPEN ACCESS

Edited by:
Emily Sempou,
Yale University, United States

Reviewed by:
Katia Del Rio-Tsonis,
Miami University, United States
Tamira Elul,
Touro University California, United States

***Correspondence:**
Kelly Ai-Sun Tseng
kelly.tseng@unlv.edu

†These authors have contributed equally to this work

Specialty section:
This article was submitted to Embryonic and Developmental Physiology, a section of the journal Frontiers in Physiology

Received: *18 December 2018*
Accepted: *08 April 2019*
Published: *08 May 2019*

Citation:
Kha CX, Guerin DJ and Tseng KA-S (2019) Using the Xenopus Developmental Eye Regrowth System to Distinguish the Role of Developmental Versus Regenerative Mechanisms. Front. Physiol. 10:502. doi: 10.3389/fphys.2019.00502

INTRODUCTION

Many animals have the ability to undergo regeneration, the successful restoration of tissues and organs after injury, but some animals lack this ability. Even though there is now considerable knowledge regarding the cellular and molecular pathways that regulate regeneration, the basic question of why the same tissues and organs from diverse (or even closely related) species often respond differently to injury and damage remains largely unanswered. To address this question, an area of focus has been to understand the role of developmental mechanisms in regeneration.

As regeneration requires the restoration of lost body structures generated during development, it is not surprising that a number of pathways involved in development are also active during regeneration (Schaefer et al., 1999; Lin and Slack, 2008; Malloch et al., 2009; Martinez-De Luna et al., 2011; Halasi et al., 2012; Meyers et al., 2012). However, it has been a challenge to effectively identify which developmental mechanisms are required for regeneration and to assess whether the roles of these mechanisms are similar or different during embryogenesis versus regeneration.

A second challenge in understanding the role of developmental mechanisms in regeneration is that existing models largely seek to examine regeneration in adult or mature differentiated tissues. The mature tissues are in contrast to a developmental environment where proliferation is high and cellular differentiation is low or just beginning. Furthermore, recent studies indicate that stem cells may have different functions in developing versus adult tissues (Wang and Conboy, 2010). Thus, it remains difficult to pinpoint the developmental mechanisms that can be successfully manipulated for inducing adult regeneration.

To address these challenges, a model to study regenerative mechanisms in the context of development is needed. This approach can reduce some of the complexities in comparing developmental processes to regenerative processes in mature tissues. For such a model to be valuable, two important characteristics would be needed: a high regenerative ability coupled with well-understood developmental events. *Xenopus laevis,* the South African clawed frog, fulfills these criterion as it is an animal that is an established and well-studied regenerative and developmental model (Beck et al., 2009; Sater and Moody, 2017). In particular, *Xenopus* eye development has been studied extensively (Perron and Harris, 1999; Rapaport, 2006; Henry et al., 2008; Viczian and Zuber, 2015). *Xenopus* can also regenerate mature eye tissues including the retina and lens [reviewed in Araki (2007), Vergara and Del Rio-Tsonis (2009), Henry et al. (2013), Tseng (2017)]. Additional advantages of the *Xenopus* system include: external development of embryos–facilitating developmental eye studies, amenability to molecular and cellular manipulations, and strong genetic similarity to humans. Using *Xenopus*, we established an embryonic model to study developmental eye regrowth (defined here as the ability of an embryo to compensate for missing tissues by restoring normal organ structures and function) (Kha and Tseng, 2018; Kha et al., 2018).

Our recent study showed that the *Xenopus* tailbud embryo at developmental stage (st.) 27 successfully regrew its eye after significant tissue loss (Kha et al., 2018). The completion of eye regrowth occurred by 4–5 days as overall development progressed without delay. Importantly, the regrown eye was age and size-appropriate with the expected complement of structures including the lens, retina, and pigmented epithelium. It was connected to the brain via the optic nerve and functional, displaying visual preference. Furthermore, the function of the regrown eye was dependent upon successful growth of new tissues since remnant eye cells in the regrowth-inhibited eyes lacked the ability to restore visual function (Kha and Tseng, 2018). To facilitate the use of this model to understand the role of developmental mechanisms in regrowth, we sought to determine whether eye formation during regrowth is comparable to endogenous eye development. Here, we show that while induction of regrowth delayed retinal differentiation and patterning, the overall retinogenesis process was consistent with a recapitulation of normal eye development. Furthermore, loss-of-function studies using our model showed that Pax6, a gene that is required for eye development, is also required for regrowth. In contrast, apoptosis is not required for eye development but is required for regrowth.

RESULTS

Restoration of Cellular Patterning During Regrowth

In our previous study, histological analyses showed that retinal layer formation in a regrowing eye was delayed during the first 2 days post surgery (dps) even though overall development proceeded normally (Kha et al., 2018). The cellular patterning of the regrowing eye during this period was more similar to embryos at younger developmental stages. Notably, the regrowing eye regained overall size and cellular patterning comparable to an uninjured age-matched eye within 3–5 days post surgery (Kha et al., 2018). To better understand eye regrowth and assess this process as compared to normal eye development, we examined the temporal regulation of eye formation during regrowth at three successive 24-h timepoints.

First, we assessed the overall cellular structure and patterning of the regrowing eye as compared to its uninjured contralateral eye. Here, we used the contralateral eye as the control to ensure that the comparative studies were made at the same developmental stages. Our previous work confirmed that the uninjured contralateral control was equivalent to the eye of age-matched sibling embryos [(Kha et al., 2018) and data not shown]. The lens and retina of the developing eye are surrounded by the basement membrane found in the extracellular matrix. To examine the basement membrane structure of the embryonic eye, a marker recognizing the basement membrane (an anti-Laminin antibody) was used (Kha et al., 2018). At st. 34/35 in the control embryonic eye, the basement membrane outlined the eye cup and the lens vesicle as it proceeds through development (**Figures 1A4–6,A4'–6'**). Induction of eye regrowth required tissue removal surgery, which also disrupted the basement

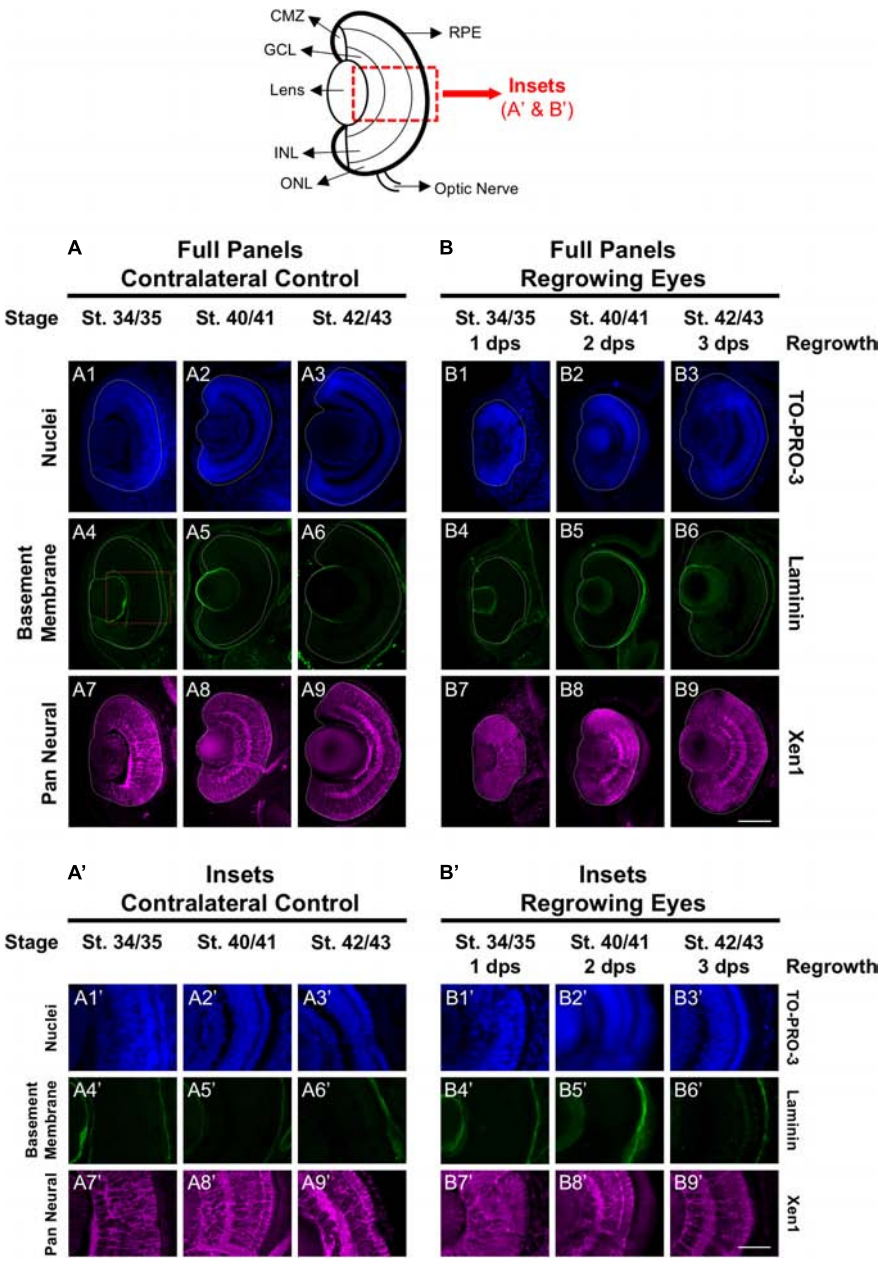

FIGURE 1 | Regrown eyes regain cellular patterning by 3 dps. Images shown are immunostained, transverse sections at three developmental timepoints corresponding to 1, 2, and 3 days post surgery (dps). The top schematic is a diagram of a section through a mature, differentiated tadpole eye. **(A,B)** Regrowing eyes display retinal patterning comparable to the contralateral control eyes (unoperated) by 3 days. White dashed lines delineate each eye. **(A',B')** Representative images shown in panels **A'** and **B'** correspond to the region shown in the inset box in panel A4 for the corresponding A or B panel at high magnification. Blue color indicates nuclear staining (TO-PRO-3). Green color indicates the basal lamina (anti-Laminin), which is expressed in all basement membranes and outlines the optic vesicle. Magenta color indicates neural tissues (Xen1). Sample sizes: 1 day, $n = 6$; 2 days, $n = 5$; and 3 days, $n = 5$. **(A,B, A',B')** Up = dorsal, down = ventral, lens is on the left. Scale bar: **A,B** = 100 μm and **A',B'** = 50 μm.

membrane and showed lack of laminin expression (Kha et al., 2018). At 1 dps (st. 34/35), the basement membrane structure was restored as it surrounded the regrowing eye entirely. Similar to the control eye, the basement membrane surrounding the regrowing eye was maintained through to st. 42/43 as normal size is restored (**Figures 1B4–6,B4–6'**).

The Xen1 antibody recognizes neural tissues in the *Xenopus* embryo and is a reliable marker for visualizing retinal layers in the developing eye (Ruiz i Altaba, 1992; Kha et al., 2018). During *Xenopus* eye development, retinal layer formation begins at st. 33/34 and is completed by st. 41 (Holt et al., 1988). Consistent with previous studies, Xen1 expression showed that at st. 34/35,

retinal layering was visible in the developing eye but not fully organized. Proper patterned retinal layers are seen by st. 40/41 (**Figures 1A8, A8'**). In contrast, a delay is observed during regrowth as Xen1 expression in the regrowing eye at st. 34/35 (1 dps) showed a lack of organization (**Figures 1B7,B7'**). By st. 40/41, the patterning in the regrowing eye is more similar to that of a younger control eye at st. 34/35 (compare **Figures 1B8,B8'** with **Figures 1A7, A7'**). The retinal layer patterning in the regrowing eye was restored by 3 dps (st. 42/43) (**Figures 1B9,B9'**). Together, our data indicated that the basement membrane of the regrowing eye was fully restored by 1 dps, whereas retinal layer formation was delayed and then restored by 3 dps.

Restoration of Retinal Differentiation During Regrowth

The mature vertebrate retina is composed of the retinal pigmented epithelium (RPE) and the neural retina. For *Xenopus* eye development, retinal differentiation (retinogenesis) begins at st. 24 at the ventral midline and increasingly spreads toward the periphery along the presumptive retina (Holt et al., 1988). The process is completed by st. 41, when the differentiated structures found in a mature eye are present (Holt et al., 1988). This is a short window representing an overall period of approximately 2 days. The Xen1 expression patterns during regrowth indicated an initial delay in differentiation (**Figure 1**). We thus assessed the formation of the RPE and neural retina during regrowth. To assess RPE differentiation, we used an antibody against RPE65, a protein that is expressed in the mature RPE (Yoshii et al., 2007; Vergara and Del Rio-Tsonis, 2009). During eye development at st. 34/35, RPE65 was first expressed in a short segment extending from the ventral midline (**Figures 2A4,A4'**, white dashed lines demarcate the neural retina and lens). It was previously shown that retinal differentiation demonstrated a dorsal bias in maturity – dorsal cells in the central region differentiate slightly earlier than ventral ones (Holt et al., 1988). Indeed, RPE65 expression also showed a dorsal bias (**Figure 2A4**). By st. 40/41, RPE65 expression reached both the dorsal and ventral peripheries and remained the same at st. 42/43 (**Figures 2A5–6,A5'–6'**). During regrowth, RPE65 showed a similar expression pattern at 1 dps as the control (albeit larger) eye at the same stage (compare **Figures 2B4,B4'** with **Figures 2A4,A4'**). This observation is consistent with our earlier finding that the black pigment of the RPE is morphologically visible by 1 dps in a regrowing eye (Kha et al., 2018). Unlike a control eye, RPE65 expression in the 2 dps regrowing eye failed to reach the periphery by st. 40/41 (compare **Figure 2A5** with **Figure 2B5**). An additional day is required for the RPE65 expression to reach the periphery (**Figure 2B6**). Together, the data indicate that RPE differentiation was delayed as compared to the control eye. However, RPE differentiation was restored by 3 days as the embryo reached the mature eye stage (st. 42/43).

Next, we examined retinal differentiation during regrowth. The neural retina consists of three nuclear layers and two plexiform layers (**Figure 1**: schematic shows the 3 nuclear layers). Photoreceptor cells (rods and cones) are located in the outer nuclear layer (ONL). Bipolar, horizontal, and amacrine cells are found in the inner nuclear layer (INL). The retinal ganglion cells are located in the ganglion cell layer (GCL). The birth order of retinal cell types occur in a consistent yet overlapping temporal order with the retinal ganglion cells (RGCs) being the first to be specified, followed by horizontal cells, cone photoreceptor cells, rod photoreceptor cells, amacrine cells, bipolar cells, and lastly the Müller glial cells (Wong and Rapaport, 2009). Using known antibody markers that identify retinal cell types, we assessed the timing of retinogenesis.

Islet1 is a marker of vertebrate RGCs including *Xenopus* (Dorsky et al., 1997). The Islet1 antibody that we used also identified additional cells in the INL including subsets of amacrine, bipolar, and horizontal cells (Álvarez-Hernán et al., 2013). At st. 34/35, the presumptive GCL was readily apparent and somewhat patterned in the control eye (**Figures 2A10,A10'**). At this stage, a small number of differentiated cells in the presumptive INL showed Islet1 expression. The number of Islet1-positive cells in the INL increased with increasing age (**Figures 2A10–12,A10'–12'**). At 1 dps (st. 34/35) in the regrowing eye, the presumptive RGC layer is apparent but was poorly patterned and remained incomplete at the periphery as compared to the control eye (compare **Figures 2B10,B10'** with **Figures 2A10,A10'**). At 2 dps (st. 40/41), the RGC layer has reached the periphery with some Islet1-positive cells found in the INL but remained less patterned than the same stage control (compare **Figures 2B11,B11'** with **Figures 2A11,A11'**). At 3 dps, the Islet1 expression pattern was largely comparable to the control eye (compare **Figures 2B12,B12'** with **Figures 2A12,A12'**). Together, the data showed that retinal differentiation was delayed as compared to the control eye. However, retinal differentiation was restored by 3 days as the embryo reached the mature eye stage (st. 42/43).

Restoration of Cone Photoreceptor Differentiation

To further define the temporal delay in retinal differentiation during regrowth, we used an anti-Calbindin antibody to assess cone photoreceptor differentiation as we had done previously (Kha et al., 2018). In *Xenopus*, both cone and rod photoreceptors are generated at similar times in the middle of the retinal differentiation sequence. However, a close study of retinogenesis indicated that cone photoreceptors are generated just prior to rod photoreceptors and are the 3rd cell type to be specified (Wong and Rapaport, 2009). During eye development at st. 34/35, a few cone photoreceptor cells were detected by calbindin expression in the central region of the presumptive photoreceptor layer (**Figures 3A4,A4'**). By st. 40/41, cone photoreceptor differentiation reached the retinal periphery and appeared to be restored (**Figures 3A5,A5'**). This pattern was maintained in st. 42/43 (**Figures 3A6,A6'**). In contrast, cone photoreceptors were not observed in the regrowing eye at 1 dps (st. 34/35; **Figures 3B4,B4'**). As regrowth proceeded, cone photoreceptor differentiation was visible by 2 dps and showed patterning that is somewhat comparable to age-matched developing eye (compare **Figures 3B5,B5'** with **Figures 3A5,A5'**). By 3 dps, cone photoreceptor cells have expanded along the retina and showed

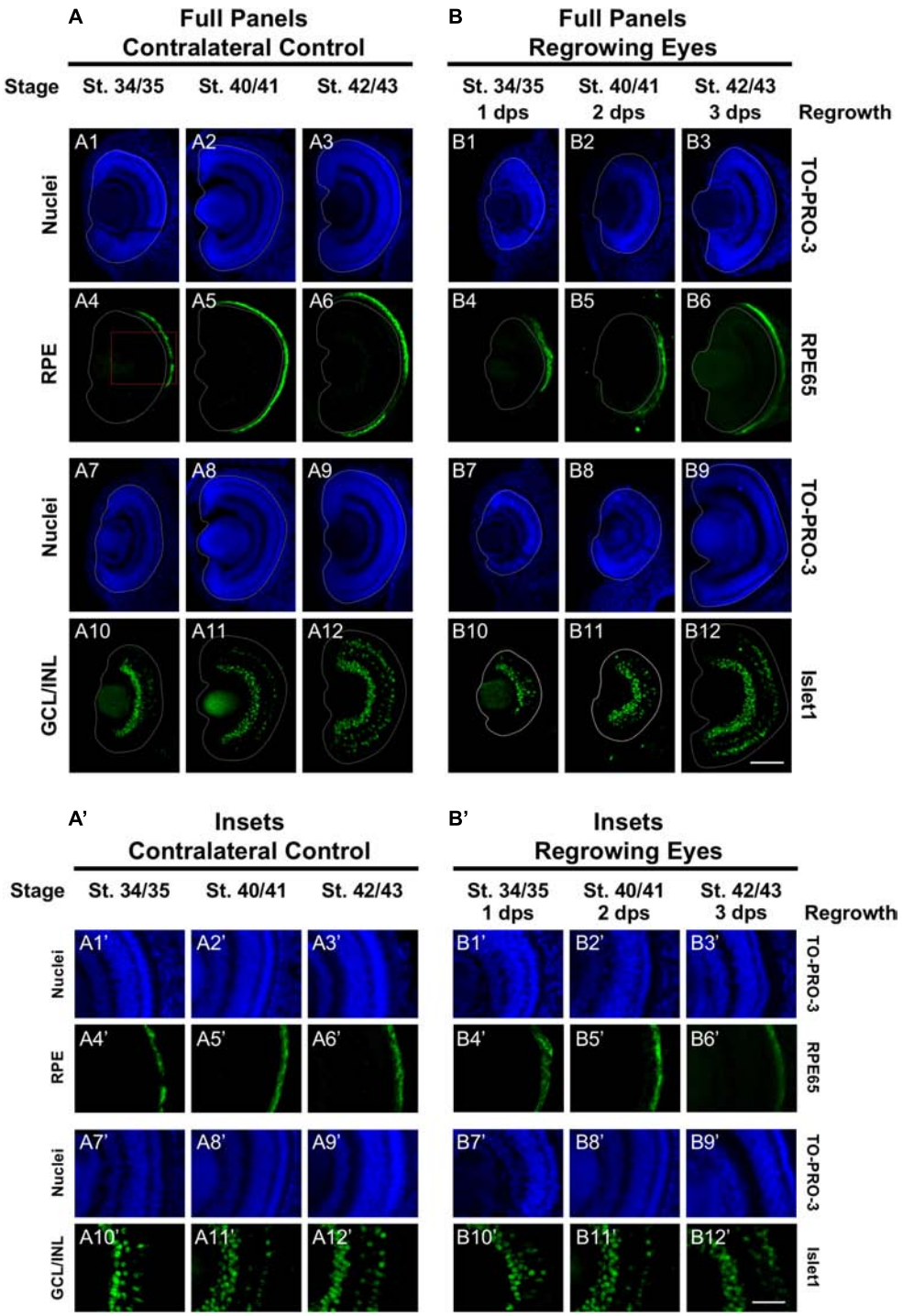

FIGURE 2 | Regrown eyes regain retinal differentiation by 3 dps. Images shown are immunostained, transverse sections at three developmental timepoints corresponding to 1, 2, and 3 days post surgery (dps). **(A,B)** The contralateral control eyes (unoperated) complete retinogenesis by st. 41. By 1 dps, RPE is already visible in the regrowing eye as shown by anti-RPE65 signal (retinal pigmented epithelium; green). By 3 dps, Islet1 expression (identifying subpopulations of retinal ganglion cells and subsets of amacrine cells, bipolar cells, and horizontal cells; green) show expected retinal patterning of a mature eye. White dashed lines delineate each eye. **(A',B')** Images shown in panels **A'** and **B'** correspond to the region shown in the inset box in panel **A4** for the corresponding **(A or B)** panel at high magnification. Blue color indicates nuclear staining (TO-PRO-3). Sample sizes: 1 day, $n = 5$; 2 days, $n = 7$; and 3 days, $n = 6$. **(A,B, A',B')** Up = dorsal, down = ventral, lens is on the left. Scale bar: **(A,B)** = 100 μm and **(A',B')** = 50 μm.

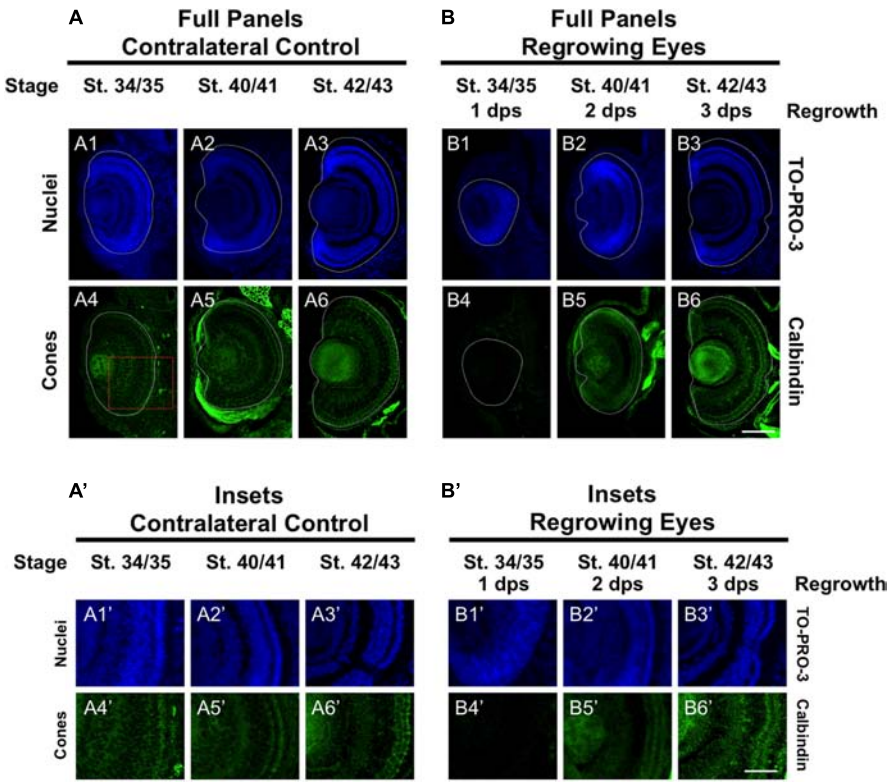

FIGURE 3 | Regrown eyes regain cone differentiation by 3 dps. Images shown are immunostained, transverse sections at three developmental timepoints corresponding to 1, 2, and 3 days post surgery (dps). **(A,B)** Differentiation of cone photoreceptor cells is delayed during 1, 2 dps but regains patterning that is comparable to contralateral control eyes (unoperated) by 3 days. White dashed lines delineate each eye. **(A',B')** Images shown in panels **A'** and **B'** correspond to the region shown in the inset box in panel **A4** for the corresponding **A or B** panel at high magnification. Blue color indicates nuclear staining (TO-PRO-3). Green color indicates anti-Calbindin signal (cone photoreceptors). Sample sizes: 1 day, $n = 6$; 2 days, $n = 5$; and 3 days, $n = 6$. **(A,B, A',B')** Up = dorsal, down = ventral, lens is on the left. Scale bar: **A,B** = 100 μm and **A',B'** = 50 μm.

a comparable pattern to the control eye at st. 42/43 (compare **Figures 3B6,B6'** to **Figures 3A6,A6'**). Our results indicated that in the regrowing eye, cone photoreceptor cell differentiation is delayed by 1 day but is restored by 3 days when the embryo reached the mature eye stage (st. 42/43).

Restoration of Rod Photoreceptor Differentiation

To further define the temporal delay in retinal differentiation during regrowth, we assessed rod photoreceptor differentiation using anti-Rhodopsin antibody (Kha et al., 2018). Rod photoreceptor cells are the fourth of seven retinal cell types to be specified (Wong and Rapaport, 2009). At st. 34/35, rod photoreceptor cells were first seen in a short segment extending from the ventral midline (**Figures 4A4,A4'**), reached the periphery by st. 40/41 and maintained at st. 42/43 (**Figures 4A5,6,A5',6'**). In contrast, there were very few rod photoreceptor cells seen in the ventral midline in the regrowing eye at 1 dps (st. 34/35; **Figures 4B4,B4'**). This was in contrast to the formation of GCL, which appeared to be more advanced at the same stage (compare **Figures 4B4,B4'** with **Figures 2B10,B10'**). As regrowth proceeded, rod photoreceptor differentiation expanded along the retina until it showed a similar pattern to the control eye by st. 42/43 (compare **Figures 4B6,B6'** with **Figures 4A6,A6'**).

To confirm our observations, we quantitated and compared the number of rod photoreceptor cells during development and regrowth (**Figure 4C**). At 1 dps, there were 28.3 ± 1.8 rod photoreceptor cells in the control eye whereas there were only 4.2 ± 0.8 rod photoreceptor cells in the regrowing eye ($n > 5$ per condition and timepoint, $p < 0.05$). At 2 dps, the number of rod photoreceptor cells in the control eye increased to 67.0 ± 2.7 whereas the number of rod photoreceptor cells in the regrowing eye only reached 31.3 ± 3.8. By 3 dps, there were 69.6 ± 5.4 rod photoreceptor cells in the control eye whereas there was a significant increase in the regrowing eye to 55.5 ± 5.4 rod photoreceptor cells. Measurements of the length of the rod differentiation zone supported the rod photoreceptor cell counts (**Figure 4D**). At 2 dps, the rod differentiation zone was shorter in the regrowing eye as compared to the control eye ($n > 5$ per condition, $p < 0.05$). However, by 3 dps, the rod differentiation zone in the regrowing eye reached comparable length to the uninjured control eye ($n > 6$ per condition, $p = 0.73$). Together, the data showed that rod photoreceptor differentiation and patterning was delayed as compared to the control eye. However,

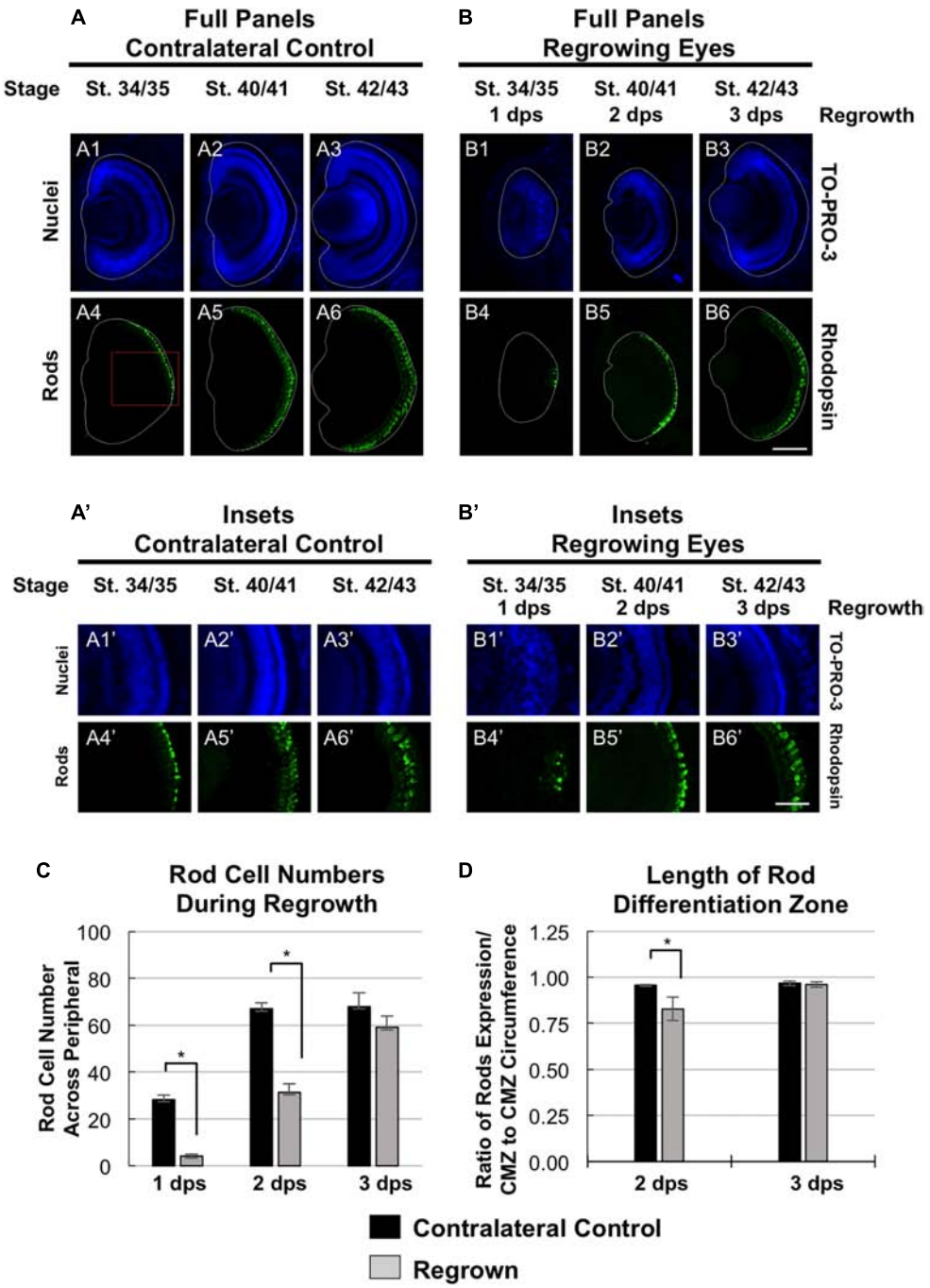

FIGURE 4 | Regrown eyes regain rod differentiation by 3 dps. Images shown are immunostained, transverse sections at three developmental timepoints corresponding to 1, 2, and 3 days post surgery (dps). **(A,B)** Differentiation of rod photoreceptor cells is delayed during 1, 2 dps but regains patterning that is comparable to contralateral control eyes (unoperated) by 3 days. White dashed lines delineate each eye. **(A',B')** Images shown in panels **A'** and **B'** correspond to the region shown in the inset box in panel **A4** for the corresponding **A or B** panel at high magnification. Blue color indicates nuclear staining (TO-PRO-3). Green color indicates anti-Rhodopsin signal (rod photoreceptors). Sample sizes: 1 day, $n = 5$; 2 days, $n = 7$; and 3 days, $n = 7$. **(A,B, A',B')** Up = dorsal, down = ventral, lens is on the left. Scale bar: **A,B** = 100 μm and **A',B'** = 50 μm. **(C)** Quantification of rod photoreceptor cells in the regrowing eye structure at three developmental timepoints corresponding to 1, 2, and 3 dps. The number of rod photoreceptors per 60 μm section in the regrown eye is comparable to number of rod photoreceptor cells in the contralateral control eyes by 3 dps. *denotes $p < 0.05$ ($n > 5$ per timepoint). Data are means ± SEM. **(D)** Rod photoreceptor cells expression pattern was measured and compared to the overall circumference of the retinal layer from one end of the ciliary margin zone (CMZ) to the end of the opposite CMZ in both regrowing and contralateral eyes. The ratio of rhodopsin expression in the retinal layer over the retinal layer circumference measurements is shown. By 3 dps, the rod photoreceptor cell expression is comparable to the contralateral control eye. *denotes $p < 0.05$ ($n > 6$ per timepoint). Data are means ± SEM.

rod photoreceptor differentiation was restored by 3 days as the embryo reached the mature eye stage (st. 42/43). Combined, the progress of RGC differentiation at 1 dps as compared to the initial lack of rod photoreceptor differentiation at the same timepoint also suggested that the developmental retinal birth order is maintained during regrowth.

Restoration of Müller Glial Cell Differentiation

In the retina, the Müller glial cells serve as neuronal support cells. They are typically the last retinal cell type to be specified (Holt et al., 1988). Our data on RGC and rod photoreceptor differentiation during regrowth were consistent with the maintenance of the developmental retinal birth order (**Figures 2**, **4**). We hypothesized that if retinal differentiation during regrowth is similar to developmental retinal differentiation, then the cellular patterning of Müller glial cells would be the last to be restored. To test our hypothesis, we used a Müller glial cell marker, an anti-glutamine synthetase antibody, to assess its differentiation pattern as we did previously (Kha et al., 2018). As expected for a cell type that is the last to be specified during retinogenesis, there was no detectable glutamine synthetase expression indicative of Müller glial differentiation in the control eye at st. 34/35 (**Figures 5A5,A5**'). The presence of Müller glial cell patterning was visible by st. 40/41 and full patterning was observed by st. 42/43 (**Figures 5A6,7,A6',7'**). In the regrowing eye, there was also no detectable Müller glial differentiation at st. 34/35 (**Figures 5B5,B5**'). By 2 dps (st. 40/41), only a small number of Müller glial cells were visible – much less when compared to the control eye (compare **Figures 5B6,B6**' with **Figures 5A6,A6**'). By 3 dps (st. 42/43), the pattern in the regrowing eye was similar to that of the pattern observed for st. 40/41 control eye (compare **Figures 5B7,B7**' with **Figures 5A6,A6**'). Müller glial differentiation was restored by st. 45/46 at 4 dps (**Figures 5B8, B8'**). Together, the data showed that Müller glial differentiation was delayed as compared to the control eye. However, Müller glial differentiation was restored by 4 days – a timepoint that was later than the restoration of patterning observed for other retinal cell types. These findings supported the hypothesis that Müller glial cells are specified later than other retinal cell types in the regrowing eye.

Changes in Pax6 Expression During Regrowth

Pax6 is an eye field transcription factor that is expressed in the presumptive eye primordium after gastrulation (st. 12.5) and specifies the eye field (Zuber et al., 2003). Prior to st. 33/34, Pax6 mRNA is expressed throughout the neural retina (Hirsch and Harris, 1997). By st. 33/34 and onward, Pax6 mRNA expression becomes more restricted to the presumptive GCL and INL of the retina so that by st. 42, Pax6 expression is observed only in those two layers (Hirsch and Harris, 1997). We used an anti-Pax6 antibody to assess its expression during regrowth (Rungger-Brändle et al., 2010). Consistent with previous reports, we observed that Pax6 expression in the control eye was mostly restricted to the presumptive GCL and INL and extended out to the periphery at st. 34/35 (**Figures 6A4,A4**'). By st. 40/41, Pax6 expression was tightly restricted to the GCL and INL (**Figures 6A5,A5**') and retained this expression pattern through st. 42/43 (**Figures 6A6,A6**'). In the 1 dps regrowing eye, the retinal layers were not apparent (as seen by Xen1 expression, **Figure 1B7**). At this timepoint, Pax6 expression was not localized and remained expanded, with apparent higher expression levels in the central region (**Figures 6B4,B4**'). This pattern was more reminiscent of Pax6 expression in embryos younger than st. 33 (Hirsch and Harris, 1997). By 2 dps (st. 40/41), Pax6 was largely restricted to the GCL and INL in the regrowing eye although expression near the retinal periphery is weaker than those cells located more centrally (**Figures 6B5,B5**'). By 3 dps, Pax6 patterning was restored as its expression became restricted to GCL and INL (**Figures 5B6,B6**'). Together, our data indicated that Pax6 expression was not restricted to the GCL and INL layers 1 dps in the regrowing eye. As regrowth continues, these Pax6-expressing cells changed and became restricted to the GCL and INL of the retina by 3 dps.

Assessment of the Roles of Pax6 and Apoptosis During Development and Regrowth

A key feature of this developmental eye repair model is that it can facilitate a rapid assessment of development and regenerative mechanisms. Our previous work and current data combined suggest that eye formation and differentiation during regrowth is delayed but largely followed the normal developmental process, resulting in an eye that was indistinguishable to a normal one (**Figures 1–6**; Kha et al., 2018). This model now provides the opportunity to use the same developmental context to ask whether specific molecular mechanisms are required in development and/or regeneration for the eye. Therefore, we assessed the roles of Pax6 (which is required for eye development) and apoptosis (which is required for eye regrowth) in both eye development and regrowth.

Pax6 is required for proper vertebrate eye development. In *Xenopus tropicalis*, loss-of-function Pax6 mutations reduced eye size and shows additional eye defects (Nakayama et al., 2015). *X. laevis* embryos injected with a Pax6 morpholino showed reduced or absent eyes (Rungger-Brändle et al., 2010). We also examined Pax6 loss-of-function effects on the eye. We injected either a published Pax6 morpholino or a control morpholino into the dorsal blastomere at the 4-cell stage and assessed for eye defects at a tadpole stage (st. 46). Consistent with previous studies, Pax6 morpholino expression resulted in eye defects in the majority of embryos (57.1%, $n = 91$) as compared to embryos expressing a control morpholino (0%, $n = 30$, $p < 0.05$) (**Figure 7A**). The eye defects included reduced or absent eyes (**Figure 7C**, compare top panels).

In *X. laevis*, apoptosis can be detected in embryos starting at gastrulation (st. 10.5) and was observed in the anterior region throughout neurulation (Hensey and Gautier, 1998). For apoptosis inhibition during development, we used M50054, a known apoptosis inhibitor that blocks caspase activity and successfully inhibited both *Xenopus* tadpole tail regeneration

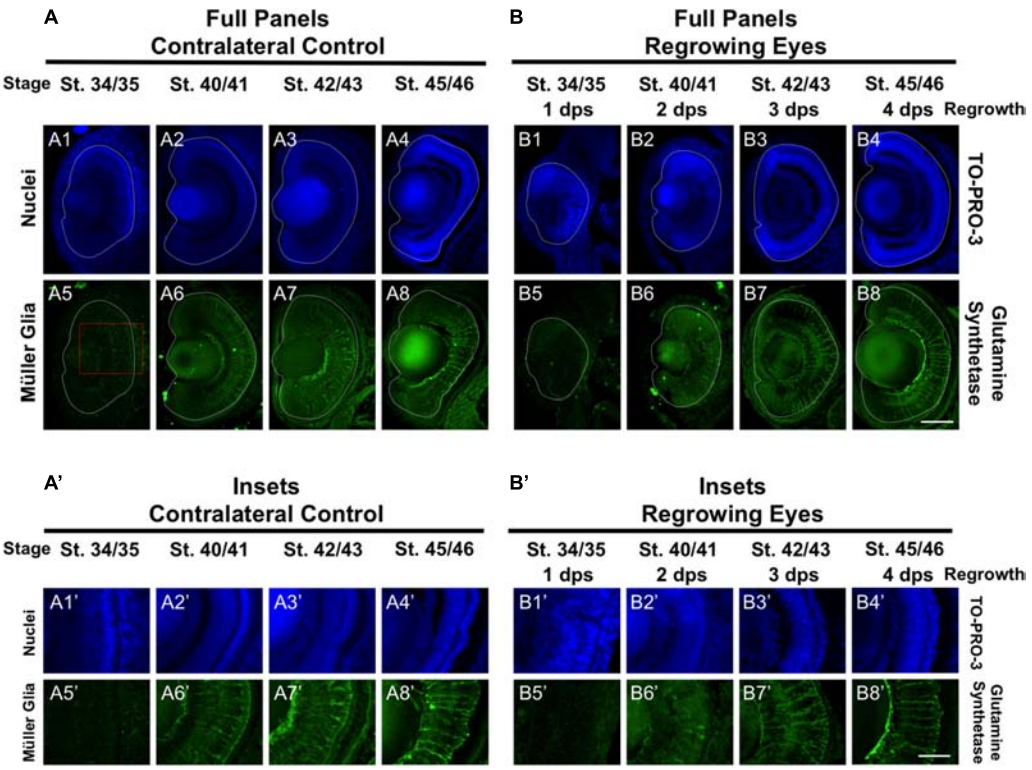

FIGURE 5 | Regrown eyes regain Müller glia differentiation by 4 dps. Images shown are immunostained, transverse sections at four developmental timepoints corresponding to 1, 2, 3, and 4 days post surgery (dps). **(A,B)** Regrown eyes show differentiation of Müller glial cells beginning at 2 dps. However, proper patterning of Müller glial cells is delayed in the regrowing eyes when compared to the contralateral control eyes until 4 dps. White dashed lines delineate each eye. **(A',B')** Images shown in panels **A'** and **B'** correspond to the region shown in the inset box in panel **A5** for the corresponding **A or B** panel at high magnification. Blue color indicates nuclear staining (TO-PRO-3). Green color indicates anti-Glutamine Synthetase (identifies Müller glial). Sample sizes: 1 day, $n = 5$; 2 days, $n = 5$; and 3 days, $n = 5$. **(A,B, A',B')** Up = dorsal, down = ventral, lens is on the left. Scale bar: **A,B** = 100 μm and **A'-B'** = 50 μm.

and eye regrowth (Tsuda et al., 2001, Tseng et al., 2007; Kha et al., 2018). Embryos were treated with 28 μM of M50054 from st. 10 (gastrulation) to st. 27 (tailbud embryo) and scored at st. 46 (tadpole). Embryos treated with either M50054 ($n = 30$) or DMSO (vehicle only, $n = 30$), did not display any morphological eye defects (**Figures 7A,C**, compare bottom panels). Our previous study also showed that M50054 treatment from st. 27 to st. 34/35 did not induce eye defects (Kha et al., 2018). These data were also consistent with a previous study showing that overexpression of the anti-apoptotic gene, BcL-xL, during embryogenesis did not induce eye defects (Johnston et al., 2005). Thus, apoptosis does not appear to be required for eye development.

To assess the role of Pax6 in eye regrowth, the same Pax6 morpholino injection was carried out using a reduced concentration so as to enable normal overall development. This is to ensure that eye tissue removal surgery can be performed on embryos with normal eyes. 81.8% of embryos expressing the control morpholino in the eye region at st. 27 fully regrew eyes (**Figure 7B**, RI = 278, $n = 22$; and **Figure 7D**, compare top panels). In contrast, only 13.7% of embryos expressing the Pax6 morpholino in the eye region at st. 27 showed full eye regrowth whereas 86.3% failed (**Figure 7B**, RI = 168, $n = 51$, $p < 0.01$ when compared to control; and **Figure 7D** compare top panels). Thus, Pax6 morpholino successfully blocked eye regrowth. For apoptosis, we confirmed our previous study showing that inhibition of apoptosis using M50054 blocked eye regrowth [**Figure 7B**, $n = 41$, $p < 0.01$, and **Figure 7D**; compare bottom panels, and (Kha et al., 2018)]. Our data indicate that Pax6 is required for successful *Xenopus* eye regrowth. Although this is not an unexpected result, this data showed that at least one key eye development gene is used for eye regrowth.

DISCUSSION

In this study, we showed that eye formation during regrowth was delayed but generally followed the endogenous retinal differentiation and cellular patterning process to generate a regrown eye that is age and size appropriate (summarized in **Figure 8A**). Consistent with this data, the formation of the ciliary margin zone (CMZ) was also delayed. The CMZ is located at the periphery of the retina and produces all retinal cell types for eye growth post-embryonically (Hollyfield, 1971). It can be visualized by its distinct spatial cellular organization in eye sections and was formed by st. 34/34 (**Supplementary Figures S1A,A'**). In the regrowing eye, the formation of the CMZ was delayed until st. 40/41 (2 dps; **Supplementary Figures S1B,B'**).

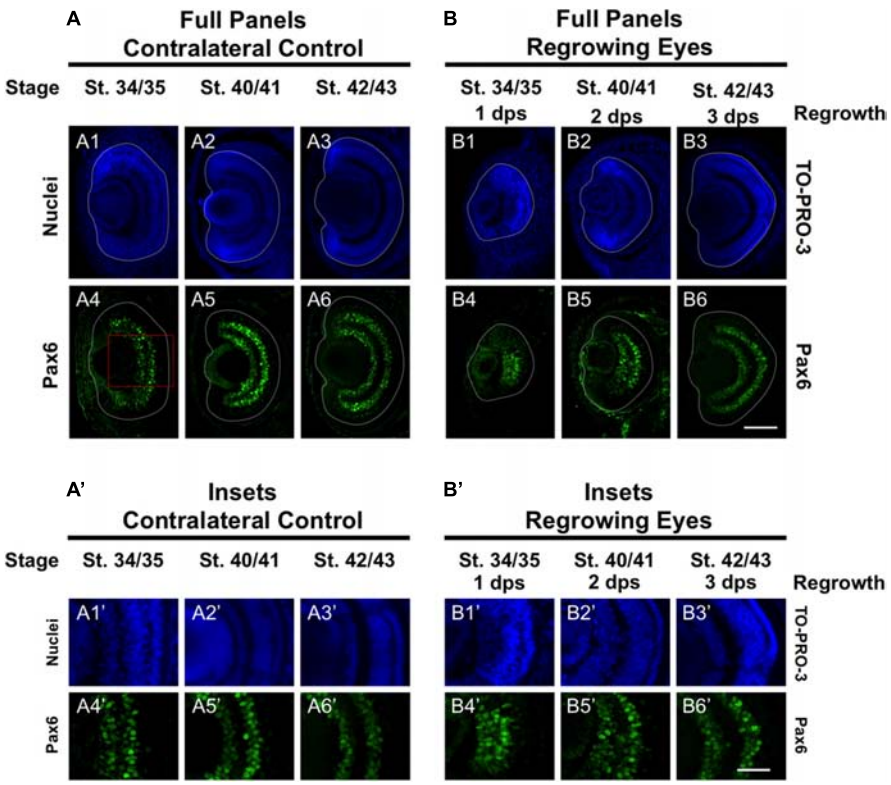

FIGURE 6 | Regrown eyes regain Pax6 patterning by 3 dps. Images shown are immunostained, transverse sections at three developmental timepoints corresponding to 1, 2, and 3 days post surgery (dps). **(A,B)** Pax6 expression in the regrowing eye is less organized at 1 dps but regains patterning similar to contralateral control eyes (unoperated) by 3 dps. White dashed lines delineate each regrowing eye. **(A',B')** Images shown in panels **A'** and **B'** correspond to the region shown in the inset box in panel **A4** for the corresponding **A or B** panel at high magnification. Blue color indicates nuclear staining (TO-PRO-3). Green color indicates anti-Pax6 signal. Sample sizes: 1 day, $n = 5$; 2 days, $n = 7$; and 3 days, $n = 6$. **(A,B, A',B')** Up = dorsal, down = ventral, lens is on the left. Scale bar: **A,B** = 100 μm and **A',B'** = 50 μm.

A distinct characteristic of retinogenesis is that it contains an intrinsic timer for initiating differentiation. In *X. laevis*, retinogenesis timing remained the same and began by st. 24 even when there was a significant reduction of retinal progenitors cells by chemical inhibition of proliferation during embryogenesis (Harris and Hartenstein, 1991). In our eye regrowth model, a significant reduction of retinal progenitors (average loss is approximately 83%) is achieved by tissue removal surgery at st. 27 (Kha et al., 2018). Here, we examined the temporal regulation of the regrowth process in more detail. Endogenous retinogenesis is initiated at st. 24 and completes by st. 41, a time period of about 2 days (Holt et al., 1988). Our previous work showed there was a significant increase in proliferation at the injury site during the first 24 h of regrowth (Kha et al., 2018). Here, we report that reparative retinogenesis showed a delay and started at 1 dps (st. 34/35) with completion occurring by 3 dps (st. 42/43). Like the endogenous process, reparative retinogenesis needed a time period of about 2 days. These results suggest that while retinogenesis can be re-induced at a developmental stage later than st. 24, the overall time required to complete the differentiation process was maintained as for development. Even though the eye formation time window can be re-started past the endogenous timeframe, there was no shortening of the eye formation period to catch up as quickly as possible.

As the first differentiated retinal cells are generated starting at st. 24, there is a continual decrease in the mitotic index of the retinal progenitor cells (RPCs) until most cells have exited the cell cycle by st. 37/38 (Holt et al., 1988). During this time, the estimated cell doubling time increases from 8.6 to 56 h (Rapaport, 2006). In contrast, there is significantly increased mitotic activity in the first 24 h during eye regrowth that continues until the regrown eye reached the expected age-appropriate size by 3 dps (Kha et al., 2018). The proliferative burst of RPCs in eye regrowth is counter to the endogenous process at the same developmental stages where cells are becoming postmitotic. Moreover, the increase in RPC proliferation, coupled with the delay of retinal differentiation suggests that induction of regrowth temporarily inhibited retinogenesis. There is no specific cell number required for retinogenesis as the initiation of *Xenopus* retinogenesis is not affected by greatly reduced retinal cell divisions during embryogenesis (Harris and Hartenstein, 1991). One possibility is that the sudden loss of RPCs at st. 27 via tissue removal surgery triggers a signal that extends the stem cell multipotency of RPCs in order to restore normal size. (It is also possible that

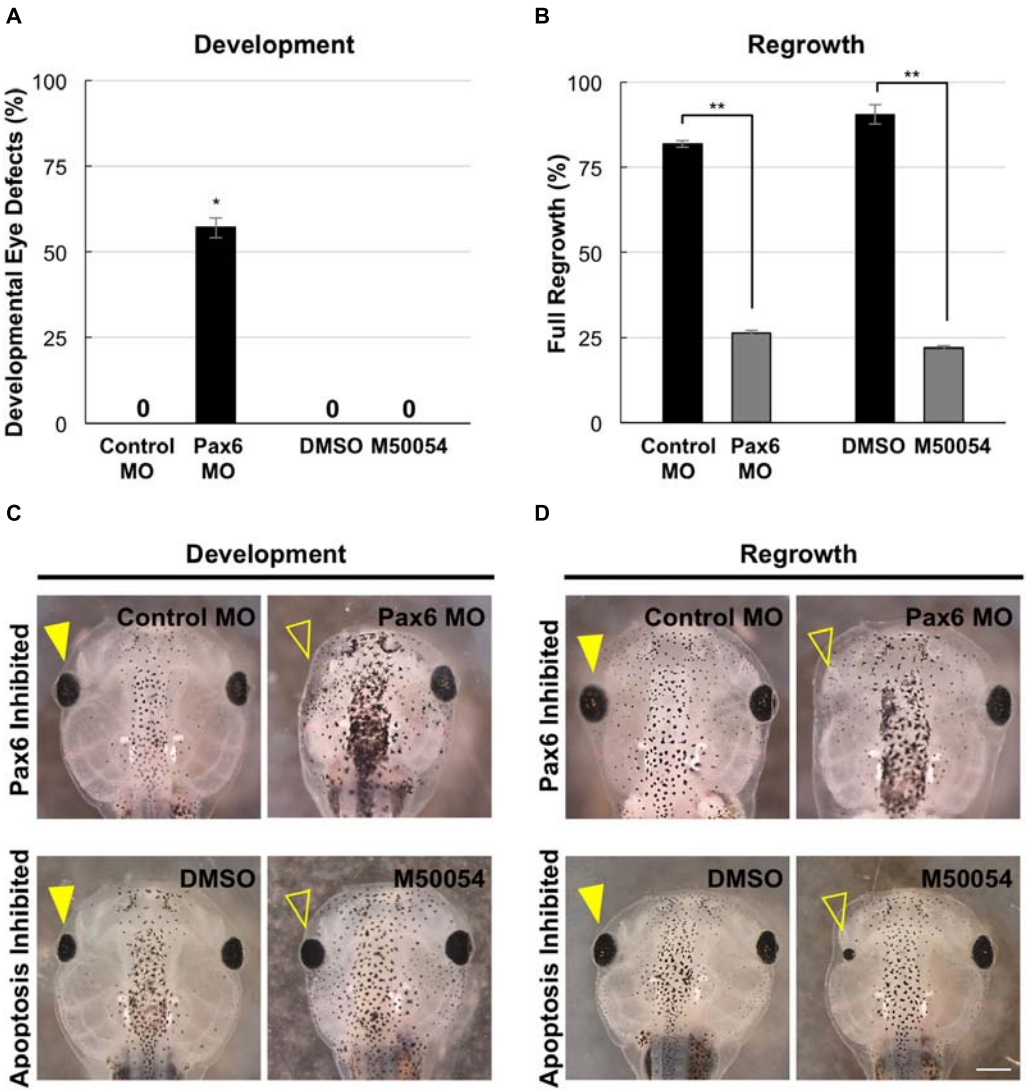

FIGURE 7 | Development and regrowth require Pax6, but only regrowth requires apoptosis. **(A)** Comparison of developmental eye defects percentage from embryos injected at the 4-cell stage (1 blastomere) with either the control or Pax6 morpholino or treated with DMSO control or M50054 at st. 10. A zero denotes no abnormal phenotype in the control by st. 27. *denotes $p < 0.05$ ($n > 90$). Data are means ± SEM. **(B)** Graphical representation of tadpoles achieving full eye regrowth at 5 dps (st. 46) with morpholino injection or apoptosis inhibitor treatment. **denotes $p < 0.01$ ($n > 20$). Data are means ± SEM. **(C,D)** Comparison of requirements for eye development and regrowth. **(C)** Pax6 morpholino injected tadpoles show reduced eyes when compared to the control by st. 46 in development. Apoptosis inhibitor show no effect on eye development ($n > 30$ per condition). Closed yellow arrowhead indicates eye of control, untreated tadpole. Open yellow arrowhead indicates eye of treated tadpole. **(D)** Pax6 morpholino and apoptosis inhibitor affects eye regrowth ($n > 30$). Closed yellow arrowhead indicates the eye of a control, untreated tadpole. Open yellow arrowhead indicates the eye of an inhibitor treated tadpole. **(C,D)** Up = anterior, down = posterior. Scale bar: **C,D** = 500 μm.

the source cells may be non-retinal in origin.) Although we used Pax6 as a differentiation marker in this study, it is also required for maintaining the multipotent state of RPCs prior to retinogenesis (Marquardt et al., 2001). The absence of restricted Pax6 expression in the regrowing eye at 1 dps (compare **Figures 6B4,A4**) is reminiscent of its expression at the younger, proliferative, developmental stages (Hirsch and Harris, 1997). It will be highly informative to identify the molecular mechanisms that regulate RPC proliferation during regrowth as this model has the potential to become a useful system to study endogenous RPC expansion.

During eye regrowth (st. 27 to st. 42/43), the embryo is changing rapidly as it proceeds from being a tailbud embryo with unformed organs toward becoming a tadpole with differentiated body structures (Nieuwkoop and Faber, 1994). Once eye regrowth is initiated after tissue loss, it appears to follow the endogenous developmental program and remain unaffected by rapid changes in the surrounding tissues during development. Indeed, the overall retinal birth order that was observed for the cell types examined was consistent with the described order for *Xenopus* retinogenesis. Of note, our study of retinal differentiation during regrowth did not specifically

examine each individual retinal cell type that is generated during eye formation. It is possible that there may exist some differences in formation of the regrown eye as compared to eye development that was not detected by the retinal markers used in this study.

Our findings revealed that successful eye development during regrowth induced similar cellular events as for eye development. This model now provides the opportunity to directly examine the role of developmental mechanisms in eye regrowth. We used this model to compare the role of two mechanisms, Pax6 and apoptosis, in development and regrowth (summarized in **Figure 8B**). Given the role of Pax6 as a "master regulator" of eye formation, it was not surprising that Pax6 was found to be also required for eye regrowth. In contrast, we found that apoptosis appears to be a regrowth-specific mechanism. Thus we have successfully used this model to define an initial similarity and an initial difference between eye development and regrowth. As there is a wealth of knowledge on the role of Pax6 (and other known regulators) during eye development, it will be highly feasible to distinguish any differences in the function of Pax6 and other genes in regrowth. For further comparison to developmental eye regrowth, follow-up studies can then be performed to examine the role of these genes in tadpole and adult retinal regeneration using established *Xenopus* models (Yoshii et al., 2007; Vergara and Del Rio-Tsonis, 2009; Araki, 2014). Potentially, developmental mechanisms that are not required for eye regrowth can also be identified. In summary, this developmental eye regrowth model will serve as a robust platform for systematically examining the common view that regeneration is a recapitulation of development.

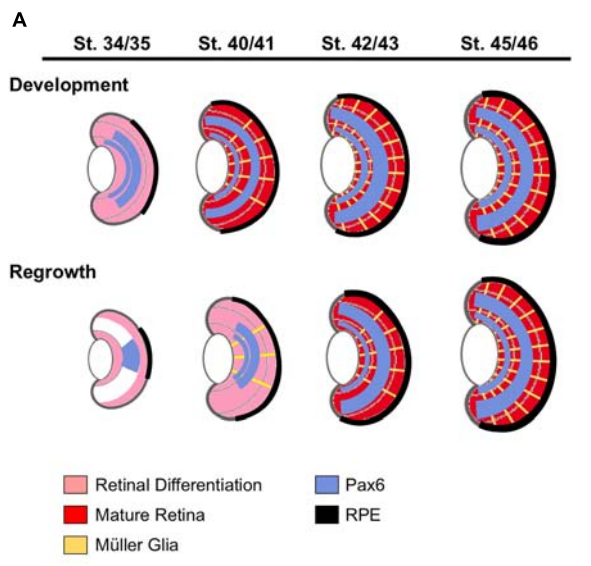

B

Summary of Requirements

	Development	Regrowth
Retinal Differentiation	YES	YES
Pax6	YES	YES
Apoptosis	NO	YES

FIGURE 8 | Summary. **(A)** A summary of retinal cell differentiation during regrowth as compared to development. The stages correspond to 1, 2, 3, and 4 days post surgery (dps), respectively. **(B)** Summary of required processes identified in eye development and regrowth.

MATERIALS AND METHODS

Embryo Culture and Surgery

Embryos were obtained via *in vitro* fertilization and raised in 0.1× Marc's Modified Ringer (MMR: 1 mM $MgSO_4$, 2.0 mM KCl, 2 mM $CaCl_2$, 0.1 M NaCl, 5 mM HEPES, pH 7.8) medium (Sive et al., 2000). The eye removal surgery and the regrowth assay were performed as described previously (Kha et al., 2018). Embryos at stage (st.) 27 (Nieuwkoop and Faber, 1994) were anesthetized with MS222 (Sigma) prior to surgery. Surgery was performed using fine surgical forceps (Dumont No. 5). An initial cut is first made in the skin surrounding the protruding eye cup and overlying lens placode. The cut is continued around the raised outline of the eye and the protruding tissues are removed. After surgery, embryos were transferred into 0.1× MMR, allowed to recover, and then cultured at 22°C for 1–5 days.

Embryo Sectioning and Immunofluorescence Microscopy

For agarose embedding and sectioning, animals were fixed overnight at 4°C in MEMFA (100 mM MOPS (pH 7.4), 2 mM EGTA, 1 mM $MgSO_4$, 3.7% (v/v) formaldehyde) (Sive et al., 2000) and processed according to Kha et al. (2018). Embryos and tadpoles were embedded in 4–6% low-melt agarose and sectioned into 60 μm slices using a Leica vt1000s vibratome. Sections were stained with primary antibodies including: Xen1 (pan-neural antibody, clone 3B1, 1:50 dilution, Developmental Studies Hybridoma Bank, **RRID: AB_531871**), anti-Islet1 (retinal ganglion cells and inner nuclear cell layer, clone 40.2D6, 1:200 dilution, Developmental Studies Hybridoma Bank, **RRID: AB_528315**), anti-Glutamine Synthetase (Müller glia, 1:200 dilution, Sigma-Aldrich, **RRID: AB_259853**), anti-Laminin (basal lamina, 1:300 dilution, Sigma-Aldrich, **RRID: AB_477163**), anti-Rhodopsin (rod photoreceptor cells, clone 4D2, 1:200 dilution, EMD Millipore, **RRID: AB_10807045**), anti-Calbindin-D-28 K (cone photoreceptor cells, 1:500 dilution, Millipore Sigma, **RRID: AB_258818**), anti-Pax6 (clone Poly19013, 1:500 dilution, BioLegend, **RRID: AB_291612**), anti-RPE65 (retinal pigment epithelium, 1:500 dilution, ThermoFisher Scientific, **RRID: AB_2181003**). Alexa fluor conjugated secondary antibodies were used at 1:1000 dilution (ThermoFisher Scientific). TO-PRO-3 (Molecular Probes) was used for DNA staining. The contralateral eye was used as the control. For each timepoint, at least 5 embryos were analyzed. In all embryos examined, the observed cellular

patterns were consistent for each antibody that was used. Quantification of rod photoreceptor cell numbers was performed using sections stained with an anti-Rhodopsin antibody. The number of rod photoreceptor cells was counted per 60 μm sections ($n > 5$ per timepoint). Rod photoreceptor cells expression pattern was measured in pixels as a drawn line along the outer nuclear layer and compared to the overall circumference of the retinal layer from one end of the ciliary margin zone (CMZ) to the other end of the CMZ ($n > 5$ per timepoint). The ratio of rhodopsin expression in the retinal layer over corresponding the retinal layer circumference measurement was calculated.

Microscopy

A Nikon A1R confocal laser scanning microscope (UNLV Confocal and Biological Imaging Core) was used to image immunostained tissue sections. Images of whole animals were obtained using a ZEISS SteREO Discovery V20 microscope with an AxioCam MRc camera. ZEN Image Analysis software and/or the open-source FIJI imaging software (Schindelin et al., 2012) were used to analyze and/or process all acquired images.

Chemical Treatments and Morpholino Injections

For apoptosis inhibition, embryos were treated with 28 μM of M50054 (Millipore, EMD Biosciences, Burlington, MA, United States, CAS number 54135-60-3). For vehicle control, dimethyl sulfoxide (DMSO) was used at the same concentration as for M50054 treatment (0.1%). For the developmental assay, age-matched embryos were raised in 0.1× MMR medium containing the inhibitor starting at st. 10 until st. 27. Eye development was assayed by st. 46. To assay for regrowth, eye surgery was performed on st. 27 tailbud embryos. The embryos were allowed to briefly recover, and then transferred into 0.1× MMR medium containing the inhibitor. After 1 day, embryos were washed with two changes of 0.1× MMR. Eye regrowth was assayed between 1 and 5 days post-surgery.

For morpholino injections, the following morpholinos (MO) were purchased from Gene Tools LLC (Philomath, Oregon): Pax6MO: 5′-GCTGTGACTGTTCTGCATGTCGAG-3′ (Li et al., 1997; Rungger-Brändle et al., 2010); and the non-specific standard control oligomer: 5′-CCTCTTACCTCAGTTACAATTTATA-3′. Each morpholino was modified with 3′ fluorescein. Morpholinos were resuspended in sterile water to a concentration of 1 mM. For both developmental and regrowth studies, morpholinos were injected separately into a dorsal blastomere of a 4-cell embryo using a microinjector (Harvard Apparatus, Holliston, MA)– targeting only one side of the embryo. Embryos with fluorescent signal in the eye region were selected for further analysis. A previously published concentration of 30 ng/embryo (Rungger-Brändle et al., 2010) was used for verification of published phenotypes. The titrated dosages for morpholino injections were: 27 ng/embryo (developmental assay) and 15 ng/embryo (eye regrowth assay). Lethality was observed in st. 27 tailbud embryos that were injected with 35.7 ng of Pax6 morpholino at the 4-cell stage.

Assessment of Eye Regrowth

The regrowth of the operated eyes as compared to unoperated contralateral eyes was assessed using the Regrowth Index (RI) as previously described (Kha et al., 2018). The quality of eye regrowth was scored based on 4 phenotype categories: full, good, weak, and none. Full, RI = 300; Partial, RI = 200; Weak, RI = 100; None, RI = 0. The RI ranges from 0 to 300, where 0 indicates no eye regrowth of all embryos in a given condition, 100 if all embryos achieve weak regrowth, 200 if all embryos achieve good regrowth, and 300 indicates that all embryos achieve full regrowth. Raw data from scoring was used to compare eye regrowth experiments. The unoperated contralateral eyes of embryos showed no difference from unoperated control eye of age-matched sibling embryos.

Statistical Analysis

To compare eye regrowth, raw data from scoring was used. Comparison of two treatments was analyzed with Mann-Whitney *U* test for ordinal data with tied ranks, using normal approximation for large sample sizes. Multiple treatments were compared using a Kruskal-Wallis test, with Dunn's Q corrected for tied ranks. All other experiments were analyzed using a Student's *t*-test.

ETHICS STATEMENT

This study was carried out in accordance with the recommendations of the University of Nevada, Las Vegas Institutional Animal Care and Use Committee (IACUC). The protocol was approved by the UNLV IACUC.

AUTHOR CONTRIBUTIONS

KT contributed the conception and design of the study. CK and DG performed the experiments. CK, DG, and KT analyzed the data, wrote, revised, and approved the manuscript.

FUNDING

This work was supported by grants from the National Institute of General Medical Sciences (GM103440), National Science Foundation (1726925), and University of Nevada, Las Vegas (Top Tier doctoral dissertation graduate assistantship) to KT. The publication fees for this article were supported in part by the UNLV University Libraries Open Article Fund.

ACKNOWLEDGMENTS

We thank Michael E. Zuber and members of the Tseng lab for helpful discussions. Confocal imaging was performed at the

UNLV Confocal and Biological Imaging Core, with assistance of Sophie Choe. Some antibodies used in this study were obtained from the Developmental Studies Hybridoma Bank, a resource created by the NICHD of the NIH and maintained at The University of Iowa, Department of Biology, Iowa City, IA.

SUPPLEMENTARY MATERIAL

The Supplementary Material for this article can be found online at: https://www.frontiersin.org/articles/10.3389/fphys.2019.00502/full#supplementary-material

REFERENCES

Álvarez-Hernán, G., Bejarano-Escobar, R., Morona, R., González, A., Martín-Partido, G., and Francisco-Morcillo, J. (2013). Islet-1 immunoreactivity in the developing retina of *Xenopus laevis*. *Sci. World J.* 2013:740420. doi: 10.1155/2013/740420

Araki, M. (2007). Regeneration of the amphibian retina: role of tissue interaction and related signaling molecules on RPE transdifferentiation. *Dev. Growth Differ.* 49, 109–120. doi: 10.1111/j.1440-169x.2007.00911.x

Araki, M. (2014). "A model for retinal regeneration in *Xenopus*," in *Xenopus Development*, eds M. Kloc and J. Z. Kubiak (New York, NY: Oxford University Press), 346–367. doi: 10.1002/9781118492833.ch18

Beck, C. W., Izpisúa Belmonte, J. C., and Christen, B. (2009). Beyond early development: *Xenopus* as an emerging model for the study of regenerative mechanisms. *Dev. Dyn.* 238, 1226–1248. doi: 10.1002/dvdy.21890

Dorsky, R. I., Chang, W. S., Rapaport, D. H., and Harris, W. A. (1997). Regulation of neuronal diversity in the *Xenopus retina* by Delta signalling. *Nature* 385, 67–70. doi: 10.1038/385067a0

Halasi, G., Søviknes, A. M., Sigurjonsson, O., and Glover, J. C. (2012). Proliferation and recapitulation of developmental patterning associated with regulative regeneration of the spinal cord neural tube. *Dev. Biol.* 365, 118–132. doi: 10.1016/j.ydbio.2012.02.012

Harris, W. A., and Hartenstein, V. (1991). Neuronal determination without cell division in *Xenopus* embryos. *Neuron* 6, 499–515. doi: 10.1016/0896-6273(91)90053-3

Henry, J. J., Thomas, A. G., Hamilton, P. W., Moore, L., and Perry, K. J. (2013). "Cell signaling pathways in vertebrate lens regeneration," in *New Perspectives in Regeneration*, eds E. Heber-Katz and D. L. Stocum (Berlin: Springer), 75–98. doi: 10.1007/82_2012_289

Henry, J. J., Wever, J. M., Natalia Vergara, M., and Fukui, L. (2008). "*Xenopus*, an ideal vertebrate system for studies of eye development and regeneration," in *Animal Models in Eye Research*, ed. P. A. Tsonis (San Diego, CA: Academic Press), 57–92. doi: 10.1016/b978-0-12-374169-1.00006-0

Hensey, C., and Gautier, J. (1998). Programmed cell death during *Xenopus* development: a spatio-temporal analysis. *Dev. Biol.* 203, 36–48. doi: 10.1006/dbio.1998.9028

Hirsch, N., and Harris, W. A. (1997). *Xenopus* Pax-6 and retinal development. *J. Neurobiol.* 32, 45–61. doi: 10.1002/(sici)1097-4695(199701)32:1<45::aid-neu5>3.0.co;2-e

Hollyfield, J. G. (1971). Differential growth of the neural retina in *Xenopus laevis* larvae. *Dev. Biol.* 24, 264–286. doi: 10.1016/0012-1606(71)90098-4

Holt, C. E., Bertsch, T. W., Ellis, H. M., and Harris, W. A. (1988). Cellular determination in the *Xenopus retina* is independent of lineage and birth date. *Neuron* 1, 15–26. doi: 10.1016/0896-6273(88)90205-x

Johnston, J., Chan, R., Calderon-Segura, M., McFarlane, S., and Browder, L. W. (2005). The roles of Bcl-xL in modulating apoptosis during development of *Xenopus laevis*. *BMC Dev. Biol.* 5:20. doi: 10.1186/1471-213X-5-20

Kha, C. X., Son, P. H., Lauper, J., and Tseng, K. A.-S. (2018). A model for investigating developmental eye repair in *Xenopus laevis*. *Exp. Eye Res.* 169, 38–47. doi: 10.1016/j.exer.2018.01.007

Kha, C. X., and Tseng, K. A.-S. (2018). Developmental dependence for functional eye regrowth in *Xenopus laevis*. *Neural Regen. Res.* 13, 1735–1737.

Li, H., Tierney, C., Wen, L., Wu, J. Y., and Rao, Y. (1997). A single morphogenetic field gives rise to two retina primordia under the influence of the prechordal plate. *Development* 124, 603–615.

Lin, G., and Slack, J. M. W. (2008). Requirement for Wnt and FGF signaling in *Xenopus tadpole* tail regeneration. *Dev. Biol.* 316, 323–335. doi: 10.1016/j.ydbio.2008.01.032

Malloch, E. L., Perry, K. J., Fukui, L., Johnson, V. R., Wever, J., Beck, C. W., et al. (2009). Gene expression profiles of lens regeneration and development in *Xenopus laevis*. *Dev. Dyn.* 238, 2340–2356. doi: 10.1002/dvdy.21998

Marquardt, T., Ashery-Padan, R., Andrejewski, N., Scardigli, R., Guillemot, F., and Gruss, P. (2001). Pax6 is required for the multipotent state of retinal progenitor cells. *Cell* 105, 43–55. doi: 10.1016/s0092-8674(01)00295-1

Martinez-De Luna, R. I., Kelly, L. E., and El-Hodiri, H. M. (2011). The Retinal Homeobox (Rx) gene is necessary for retinal regeneration. *Dev. Biol.* 353, 10–18. doi: 10.1016/j.ydbio.2011.02.008

Meyers, J. R., Hu, L., Moses, A., Kaboli, K., Papandrea, A., and Raymond, P. A. (2012). β-catenin/Wnt signaling controls progenitor fate in the developing and regenerating zebrafish retina. *Neural Dev.* 7:30. doi: 10.1186/1749-8104-7-30

Nakayama, T., Fisher, M., Nakajima, K., Odeleye, A. O., Zimmerman, K. B., Fish, M. B., et al. (2015). Xenopus pax6 mutants affect eye development and other organ systems, and have phenotypic similarities to human aniridia patients. *Dev. Biol.* 408, 328–344. doi: 10.1016/j.ydbio.2015.02.012

Nieuwkoop, P. D., and Faber, J. (1994). *Normal Table of Xenopus laevis (Daudin) : A Systematical and Chronological Survey of the Development from the Fertilized Egg Till the End of Metamorphosis*. New York, NY: Garland Publishing.

Perron, M., and Harris, W. A. (1999). "Cellular determination in amphibian retina," in *Cell Lineage and Fate Determination*, 1st Edn, ed. S. A. Moody (New York: Academic Press), 353–368. doi: 10.1016/b978-012505255-9/50024-9

Rapaport, D. H. (2006). "Retinal neurogenesis," in *Retinal Development*, eds E. Sernagor, S. Eglen, B. Harris, and R. Wong (Cambridge, MA: Cambridge University Press), 30–58. doi: 10.1017/cbo9780511541629.005

Ruiz i Altaba, A. (1992). Planar and vertical signals in the induction and patterning of the *Xenopus* nervous-system. *Development* 116, 67–80.

Rungger-Brändle, E., Ripperger, J. A., Steiner, K., Conti, A., Stieger, A., Soltanieh, S., et al. (2010). Retinal patterning by Pax6-dependent cell adhesion molecules. *Dev. Neurobio* 70, 764–780. doi: 10.1002/dneu.20816

Sater, A. K., and Moody, S. A. (2017). Using *Xenopus* to understand human disease and developmental disorders. *Genesis* 55:e22997. doi: 10.1002/dvg.22997

Schaefer, J. J., Oliver, G., and Henry, J. J. (1999). Conservation of gene expression during embryonic lens formation and cornea-lens transdifferentiation in *Xenopus laevis*. *Dev. Dyn.* 215, 308–318. doi: 10.1002/(sici)1097-0177(199908)215:4<308::aid-aja3>3.3.co;2-9

Schindelin, J., Arganda-Carreras, I., Frise, E., Kaynig, V., Longair, M., Pietzsch, T., et al. (2012). Fiji: an open-source platform for biological-image analysis. *Nat. Methods* 9, 676–682. doi: 10.1038/nmeth.2019

Sive, H. L., Grainger, R. M., and Harland, R. M. (2000). *Early Development of Xenopus laevis: A Laboratory Manual*. Cold Spring Harbor, NY: Cold Spring Harbor Laboratory Press.

Tseng, A.-S. (2017). Seeing the future: using *Xenopus* to understand eye regeneration. *Genesis* 55:e23003. doi: 10.1002/dvg.23003

Tseng, A.-S., Adams, D. S., Qiu, D., Koustubhan, P., and Levin, M. (2007). Apoptosis is required during early stages of tail regeneration in *Xenopus laevis*. *Dev. Biol.* 301, 62–69. doi: 10.1016/j.ydbio.2006.10.048

Tsuda, T., Ohmori, Y., Muramatsu, H., Hosaka, Y., Takiguchi, K., Saitoh, F., et al. (2001). Inhibitory effect of M50054, a novel inhibitor of apoptosis, on anti-Fas-antibody-induced hepatitis and chemotherapy-induced alopecia. *Eur. J. Pharmacol.* 433, 37–45. doi: 10.1016/s0014-2999(01)01489-3

Vergara, M. N., and Del Rio-Tsonis, K. (2009). Retinal regeneration in the *Xenopus laevis* tadpole: a new model system. *Mol. Vis.* 15, 1000–1013.

Viczian, A. S., and Zuber, M. E. (2015). "Retinal development," in *Principles of Developmental Genetics*, ed. S. A. Moody (London: Elsevier), 297–313.

Wang, J., and Conboy, I. (2010). Embryonic vs. adult myogenesis: challenging the "regeneration recapitulates development" paradigm. *J. Mol. Cell Biol.* 2, 1–4. doi: 10.1093/jmcb/mjp027

Wong, L. L., and Rapaport, D. H. (2009). Defining retinal progenitor cell competence in *Xenopus laevis* by clonal analysis. *Development* 136, 1707–1715. doi: 10.1242/dev.027607

Yoshii, C., Ueda, Y., Okamoto, M., and Araki, M. (2007). Neural retinal regeneration in the anuran amphibian *Xenopus laevis* post-metamorphosis: transdifferentiation of retinal pigmented epithelium regenerates the neural retina. *Dev. Biol.* 303, 45–56. doi: 10.1016/j.ydbio.2006.11.024

Zuber, M. E., Gestri, G., Viczian, A. S., Barsacchi, G., and Harris, W. A. (2003). Specification of the vertebrate eye by a network of eye field transcription factors. *Development* 130, 5155–5167. doi: 10.1242/dev.00723

Conflict of Interest Statement: The authors declare that the research was conducted in the absence of any commercial or financial relationships that could be construed as a potential conflict of interest.

frontiers in Physiology

REVIEW
published: 26 June 2019
doi: 10.3389/fphys.2019.00817

The Many Faces of *Xenopus*: *Xenopus laevis* as a Model System to Study Wolf–Hirschhorn Syndrome

*Micaela Lasser†, Benjamin Pratt†, Connor Monahan, Seung Woo Kim and Laura Anne Lowery**

Department of Biology, Boston College, Chestnut Hill, MA, United States

Wolf–Hirschhorn syndrome (WHS) is a rare developmental disorder characterized by intellectual disability and various physical malformations including craniofacial, skeletal, and cardiac defects. These phenotypes, as they involve structures that are derived from the cranial neural crest, suggest that WHS may be associated with abnormalities in neural crest cell (NCC) migration. This syndrome is linked with assorted mutations on the short arm of chromosome 4, most notably the microdeletion of a critical genomic region containing several candidate genes. However, the function of these genes during embryonic development, as well as the cellular and molecular mechanisms underlying the disorder, are still unknown. The model organism *Xenopus laevis* offers a number of advantages for studying WHS. With the *Xenopus* genome sequenced, genetic manipulation strategies can be readily designed in order to alter the dosage of the WHS candidate genes. Moreover, a variety of assays are available for use in *Xenopus* to examine how manipulation of WHS genes leads to changes in the development of tissue and organ systems affected in WHS. In this review article, we highlight the benefits of using *X. laevis* as a model system for studying human genetic disorders of development, with a focus on WHS.

Keywords: Wolf–Hirschhorn syndrome, *Xenopus*, development, craniofacial, neural crest cells

OPEN ACCESS

Edited by:
John Noel Griffin, Duke University, United States

Reviewed by:
Engin Deniz, Yale University, United States
Sandra Guadalupe González Malagón, Foundation for Research and Technology Hellas, Greece

***Correspondence:**
Laura Anne Lowery
Laura.lowery@bc.edu

†These authors have contributed equally to this work

Specialty section:
This article was submitted to Embryonic and Developmental Physiology, a section of the journal Frontiers in Physiology

Received: *10 October 2018*
Accepted: *11 June 2019*
Published: *26 June 2019*

Citation:
Lasser M, Pratt B, Monahan C, Kim SW and Lowery LA (2019) The Many Faces of Xenopus: Xenopus laevis as a Model System to Study Wolf–Hirschhorn Syndrome. Front. Physiol. 10:817. doi: 10.3389/fphys.2019.00817

INTRODUCTION

Wolf–Hirschhorn syndrome (WHS) is a developmental disorder characterized by craniofacial malformations, intellectual disability, microcephaly, seizures, growth retardation, and developmental delays, though the severity of these symptoms varies from patient to patient (Fisch et al., 2010; Hannes et al., 2010; Sheth et al., 2012; Battaglia et al., 2015; Rutherford and Lowery, 2016). The core phenotype of WHS is the "Greek warrior helmet" appearance, defined by a prominent forehead, widely spaced eyes (hypertelorism), and an unusually wide and protrusive nasal bridge (Engbers et al., 2009). Other craniofacial abnormalities include an undersized jaw (micrognathia), a short philtrum, and cleft lip (Engbers et al., 2009). Most patients present with microcephaly and, less frequently, with skeletal defects, renal and urogenital defects, heart defects, hearing loss, and ocular irregularities (Andersen et al., 2014; Paradowska-Stolarz, 2014).

The chromosomal basis of WHS has been linked to a telomeric heterozygous microdeletion on the short arm of chromosome 4, though the nature and size of this deletion differs between patients (Zollino et al., 2014; Battaglia et al., 2015; Bi et al., 2016). The central phenotypes of WHS

are most strongly associated with the deletion of two adjacent, non-overlapping critical regions at 4p16.3, WHS critical region 1 (WHSCR1) and WHS critical region 2 (WHSCR2) (Battaglia et al., 2015). These regions are comprised of the primary candidate genes WHSC1, WHSC2, and LETM1 (**Figure 1**; Battaglia et al., 2015; Derar et al., 2018). However, most WHS patients harbor mutations that extend beyond these critical regions, affecting several flanking genes such as TACC3, FGFR3, SLBP, CTBP1, CPLX1, PIGG, MSX1, and FGFRL1, demonstrating that deletions encompassing these genes may also contribute to the presentation of WHS symptoms (Hannes et al., 2010; Endele et al., 2011; Battaglia et al., 2015; Ho et al., 2016; Rutherford and Lowery, 2016).

Due to the clinical and genetic variability of WHS, the pathology underlying the disorder has been difficult to determine. However, the characteristic facial and cardiac phenotypes of WHS suggest a particular cell population may be affected by mutations of WHS-associated genes. Vertebrate facial features are derived from or influenced by neural crest cells (NCCs), which are a group of multipotent stem cells that are born along the neural tube and migrate long distances toward their final destination (Mayor and Theveneau, 2013). Additionally, some WHS-associated genes have defined roles in epigenetic modifications or signaling pathways that are integral for proper embryonic development and cell-motility related processes (Rutherford and Lowery, 2016). Therefore, it is possible that some of the developmental defects associated with WHS may be due to abnormalities in signaling pathways that affect NCC motility or migration.

While some animal models of WHS do exist, most of these studies have focused on the cellular and molecular functions of singular WHS-associated genes, specifically WHSC1 and LETM1 (Battaglia et al., 2015). However, the link between haploinsufficiency of most WHS-associated genes to specific vertebrate developmental processes such as brain, craniofacial, and heart development, has not been carefully examined. Furthermore, clinical studies of WHS patients have provided clear evidence that the syndrome is multigenic (Battaglia et al., 2015); yet, we still lack a mechanistic understanding of how the depletion of WHS-associated genes combinatorially contributes to the phenotypic spectrum of the disorder.

The model organism, *Xenopus laevis,* has been used extensively in the research community for decades to examine fundamental developmental and cellular biological processes, making it an ideal system for investigating human genetic disorders, such as WHS. *X. laevis* offers a number of benefits, as they are inexpensive and easy to culture, maintain, manipulate, and image, compared to other vertebrates (Erdogan et al., 2016; Slater et al., 2017). Thus, *Xenopus* is well-suited to examine the role of WHS-associated genes during vertebrate development, and can be used to test whether abnormal NCC migration may be one mechanism by which mutations of these genes contribute to phenotypes of the disease.

In this review, we provide a brief overview of the known functions of WHS-associated genes and how they may be linked to developmental processes, such as NCC migration. We also highlight how *Xenopus* is an advantageous system to study WHS as a multigenic disorder, and we discuss ways in which it can be used to investigate how WHS-associated genes individually and combinatorially affect both proper embryonic development and the phenotypes linked to WHS.

WHS CRITICAL REGION AND ASSOCIATED CANDIDATE GENES

Wolf–Hirschhorn syndrome is a contiguous gene syndrome associated with small heterozygous deletions of the 4p chromosomal region. Following the initial characterization of the disorder in the 1960s, research has focused on generating a consensus of the core WHS phenotype, which includes intellectual disability, growth delay, seizures, and the typical craniofacial dysmorphisms, as well as defining the critical genomic region that gives rise to this core phenotype (Battaglia et al., 2015). The first critical region to be described, WHSCR1, consisted of a small 165 kb region encompassing two candidate genes, WHS Candidates 1 and 2 (WHSC1, WHSC2), and is deleted in all traditional cases of the disorder (Battaglia et al., 2015).

However, further clinical studies of children with WHS detected an even larger 1.9 Mb deletion that extends distally beyond WHSCR1, sufficient to produce the full WHS core phenotype (Battaglia et al., 2015). This newly described region is referred to as WHSCR2 and encompasses a more telomeric region of WHSC1, as well as a new candidate gene, leucine zipper and EF-hand containing transmembrane protein 1 (LETM1) (Battaglia et al., 2015). Moreover, many WHS patients harbor mutations of genes that flank these critical regions, providing increasing evidence that the manifestation of the disorder is not due to a single gene, but rather due to the haploinsufficiency of several closely linked genes (Battaglia et al., 2015; Rutherford and Lowery, 2016). Thus, WHS is largely considered to be a true multigenic disorder. In the subsequent sections, we describe the current known functions of the primary WHS candidate genes, as well as other WHS-associated genes, their potential roles during embryonic development, and how they may contribute to the spectrum of WHS phenotypes.

WHSC1

WHSC1 is a histone methyltransferase, belonging to a family of nuclear receptor SET domain (NSD) proteins that possess a SET domain encoding lysine melthyltransferase activity (Nimura et al., 2009; Ezponda et al., 2013; Liu et al., 2015). Specifically, WHSC1 is associated with trimethylation of histone H3K36, a mark that is highly correlated with active transcription. WHSC1 is partially or fully deleted in nearly all cases of WHS and is thought to be responsible for many of the core WHS phenotypes, including growth delay and facial irregularities (Andersen et al., 2014; Battaglia et al., 2015; Boczek et al., 2018; Derar et al., 2018); yet, the mechanism behind which its depletion leads to these phenotypes remains to be elucidated.

The spatial and temporal expression of WHSC1, as well as its transcriptional regulation activity, suggests that it plays an important role during development

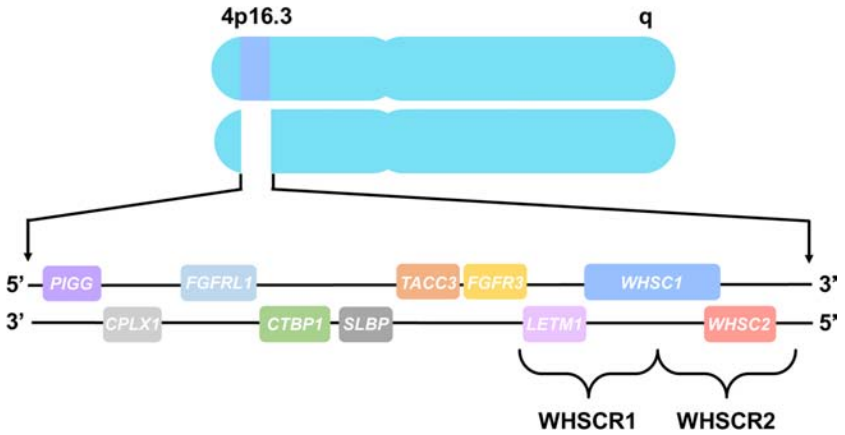

FIGURE 1 | Chromosome 4 and WHS-associated genes. All genes are represented in their order from left to right, telomeric to centromeric orientation, located on the distal arm of chromosome 4p16.3. Brackets delineate WHS critical region 1 (WHSCR1), comprised of *LETM1* and *WHSC1*, and WHS critical region 2 (WHSCR2), comprised of *WHSC1* and *WHSC2*. Genes that are also mutated in WHS patients consist of *PIGG*, *CPLX1*, *FGFRL1*, *CTBP1*, *SLBP*, *TACC3*, and *FGFR3*, which flank the WHS critical regions.

(Rutherford and Lowery, 2016). WHSC1 is a known regulator of TWIST, a key player in both the epithelial-to-mesenchymal transition (EMT) and cell migration (Ezponda et al., 2013). Moreover, WHSC1 is expressed in the developing nervous system, pharyngeal arches, and frontal facial region in both mice and *Xenopus laevis*, as well as jaw and heart in mice (Stec et al., 1998; Nimura et al., 2009; Yamada-Okabe et al., 2010; Liu et al., 2015; Mills et al., 2019), which is significant, given that many of these structures are both derived from the neural crest and are affected in WHS.

However, until recently, WHSC1 function had not been directly associated with NCC migration. To gain further insight into the role of WHSC1, specifically during processes that govern craniofacial morphogenesis, Mills et al. (2019) sought to observe the effects of reducing WHSC1 dosage levels in *Xenopus laevis* during embryonic development. They found that WHSC1 KD results in reduced length and area of the pharyngeal arches, as well as reduced NCC migration speed. Depletion of WHSC1 also causes severe craniofacial and brain morphology defects including widening of the facial width and area, and reduction of forebrain size. Together, these results are the first to demonstrate that reduced levels of WHSC1 cause aberrant NCC migration, which may lead to some of the craniofacial abnormalities seen in WHS patients. These results are consistent with other studies showing that WHSC1 depletion leads to irregularities in brain, cartilage, and bone formation, specifically incomplete motor neuron development in zebrafish, deficiencies in midline fusion and cleft palate in mice, as well as delayed bone ossification in both zebrafish and mice (Nimura et al., 2009; Yamada-Okabe et al., 2010; Ezponda et al., 2013; Liu et al., 2015), indicating a conserved developmental role for WHSC1 among various species.

An important question still remains as to which signaling pathways are affected by WHSC1 reduction and how they contribute to abnormal NCC migratory patterns and WHS phenotypes. A promising possibility is the Wnt signaling pathway, which has already been connected to WHSC1 dysregulation in the context of cancer (Toyokawa et al., 2011). Toyokawa et al. (2011) suggests that WHSC1 dosage may impact canonical Wnt signaling by affecting nuclear levels of beta-catenin through transcriptional regulation. Moreover, in *Xenopus*, canonical Wnt signaling has been shown to be important for NCC specification and migration during development, as well as subsequent craniofacial morphogenesis (Maj et al., 2016; Li et al., 2018). Thus, further experiments are necessary to examine whether alterations in WHSC1 dosage impact the Wnt signaling pathway, potentially leading to abnormal NCC migration and the spectrum of defects observed in WHS.

WHSC2

The WHSC2 gene, also known as NELF-A, encodes a component of the negative elongation factor complex, which negatively regulates RNA polymerase II progression during elongation, subsequently altering the expression of its target genes (Kerzendorfer et al., 2012). Though WHSC2 is commonly deleted in most WHS patients, it has not emerged as a primary contributor to any specific WHS phenotype (Battaglia et al., 2015). However, the cellular and molecular roles of WHSC2 have begun to be illuminated and functionally linked to other WHS-affected genes.

Depletion of WHSC2 in both cell culture and in *Drosophila* has been shown to reduce cellular proliferation and lead to irregularities in cell cycle progression (Gilchrist et al., 2008; Yung et al., 2009). Interestingly in breast cancer cell lines, reduction of the NELF-E component of the NELF complex is associated with lower levels of trimethylated H3K36 on promoters of NELF-regulated genes (Sun and Li, 2010). As previously mentioned, levels of trimethylated H3K36 are influenced by the activity of WHSC1, highlighting a potential link between WHSC1 and WHSC2 (NELF-A) in altering gene expression, although this remains to be examined.

WHSC2 also functions to recruit stem-loop binding protein (SLBP) to the 3′ ends of histone pre-mRNAs (Narita et al., 2007). SLBP lies telomeric to WHSC2 and mutations of this gene have been found in some WHS patients, though the functional impact of SLBP haploinsufficiency is unclear. SLBP is critical for the correct processing of histone pre-mRNAs and regulating histone degradation. Histone biogenesis is essential for epigenetic gene regulation through histone post-translational modifications and maintenance of chromatin structure (Margueron and Reinberg, 2010). Thus, it is possible that there is a functional connection between WHSC1, WHSC2, and SLBP, and reduced activity of these genes may have impacts on histone levels and transcriptional regulation, which could adversely affect normal development in the context of WHS.

Until recently, WHSC2 function during vertebrate tissue and organ development had not been carefully studied. Mills et al. (2019) found that WHSC2 expression in *Xenopus* is enriched in the developing nervous system, pharyngeal arches, and frontal facial region. Additionally, altered levels of WHSC2 lead to abnormalities in craniofacial, cartilage, and brain development. Specifically, reduction of WHSC2 causes smaller facial width and area, smaller cartilage elements, as well as smaller brain size (Mills et al., 2019), indicating that WHSC2 may play a larger role regarding WHS phenotypes than what was previously thought. It is possible that these phenotypes arise as a consequence of decreased cellular proliferation, as WHSC2 has already been linked to this process (Sun and Li, 2010), though this connection still needs to be tested. Moreover, it would be interesting to examine whether reduced dosage levels of WHSC2 in combination with WHSC1 or SLBP enhances these phenotypes, providing further evidence that these genes are functionally linked to one another.

LETM1

LETM1 is localized to the inner mitochondrial membrane and is important for maintaining normal mitochondrial function by participating in Ca^{2+}/H^{+} exchange and regulating Ca^{2+} homeostasis within the matrix (Dimmer et al., 2008; Jiang et al., 2013). LETM1 has been proposed as the candidate gene for seizures in WHS patients (Endele et al., 1999; McQuibban et al., 2010; Andersen et al., 2014; Battaglia et al., 2015). Heterozygous deletion of LETM1 in mice led to altered glucose metabolism and impaired control of ATP levels in the brain, which could explain the increased susceptibility to seizures observed in these animals (Jiang et al., 2013). However, some WHS patients with LETM1 deletions lack seizures and conversely, some WHS patients have seizures, yet have no detectable mutations in LETM1 (Battaglia et al., 2015). Therefore, it is likely that LETM1 is not solely responsible for the occurrence of seizures and that deletion of additional genes are required for the full expression of the phenotype.

In *Xenopus*, LETM1 is expressed ubiquitously during early embryonic development. As development progresses, more defined expression is observed in the pharyngeal arches, craniofacial and brain regions (Mills et al., 2019). Reduced dosage of LETM1 in *Xenopus* revealed that it is critical for proper craniofacial morphology and may contribute to some of the facial defects associated with WHS, which had not been previously demonstrated (Mills et al., 2019). Interestingly, knocking down LETM1 did not have a significant effect on NCC migration or motility, which is surprising, given the robust craniofacial phenotype observed. However, it is possible that LETM1 may play an entirely different role in these cells. Proper mitochondrial function and regulation of energy metabolism is critical for determining cell fate and maintaining cell survival (Khacho et al., 2019). Therefore, while reduced dosage of LETM1 may not directly affect NCC migration, it may greatly impact the metabolic homeostasis of NCCs and lead to downstream effects on differentiation, proliferation, or apoptosis during craniofacial morphogenesis. As LETM1 depletion in fibroblasts derived from WHS patients has already been associated with decreased cellular proliferation (Doonan et al., 2014), this seems a promising avenue of future research to understand the precise molecular mechanisms of LETM1 involvement in the pathogenesis of WHS.

Additional WHS-Associated Genes

While all WHS patients harbor full or partial deletions of the WHSCRs, most have mutations that affect multiple genes flanking these regions. It is widely accepted that haploinsufficiency of the WHS critical region genes alone cannot account for the full spectrum of WHS phenotypes (Battaglia et al., 2015). Thus, it is likely that these flanking genes, including TACC3, FGFR3, FGFRL1, SLBP, CTBP1, CPLX1, and PIGG, and MSX1 also contribute to WHS in some capacity.

Fibroblast growth factor receptor 3 (FGFR3) and fibroblast growth factor receptor like 1 (FGFRL1) are both involved in signaling pathways that influence cell division and differentiation. Both FGFR3 and FGFRL1 have been proposed as candidate genes responsible for the skeletal and craniofacial malformations of WHS patients (Battaglia et al., 2015). Homozygous null mouse lines for Fgfrl1 recapitulate many WHS phenotypes such as hypoplasia of skeletal elements, delayed fusion and bone ossification, abnormal forebrain development, and congenital heart defects (CHD) (Catela et al., 2009). Conversely, Fgfr3 null mice display severe kyphosis, abnormally long tails and femurs, which is indicative of prolonged bone growth (Simon and Bergemann, 2008). With opposing phenotypes, it is possible that these two genes antagonize each other to regulate chondrocyte proliferation and may genetically interact to control bone growth. Moreover, FGFR3 has been shown to directly affect NCC migration in chick, with its loss leading to slower NCC migration velocity and increased neural crest death close to the neural tube (Sato et al., 2011). However, it remains unclear whether the loss of either FGFR3 or FGFRL1 is directly linked to abnormal NCC migration in the WHS phenotypes.

Transforming acidic coiled-coil protein 3 (TACC3) is a microtubule plus-end tracking (+TIP) protein that resides on the end of polymerizing microtubules and has been shown to regulate microtubule dynamics during neural development (Nwagbara et al., 2014; Bearce et al., 2015; Cammarata et al., 2016; Erdogan et al., 2017). The ways in which TACC3 dosage levels affect gross morphological phenotypes reflected in WHS patients was recently examined and provides a strong link to abnormal NCC migration. In *Xenopus*, TACC3 expression is enriched in

the pharyngeal arches, as well as the frontal brain and facial regions (Mills et al., 2019). Knockdown of TACC3 led to overt craniofacial and cartilage defects, including smaller facial width, area and angle, which are likely due to overall smaller cartilage elements (Mills et al., 2019). Furthermore, *in vivo* migration of NCCs was affected as a consequence of reduced TACC3 levels. This manipulation also severely affected forebrain development, reflecting the microcephaly phenotype commonly associated with WHS. This is interesting given that TACC3 is also known to be an essential centrosome adaptor that is critical for proper cell division, and almost all microcephaly associated genetic defects involve proteins that maintain centrosomes and regulate the mitotic spindle (Peset and Vernos, 2008; Lasser et al., 2018). Thus, it is likely that TACC3 contributes to some WHS phenotypes, possibly by adversely altering the mitotic spindle such that it has downstream effects that influence cell fate and cell migration.

It has been suggested that C-terminal binding protein 1 (CTBP1), complexin 1 (CPLX1), and phosphatidylinositol glycan anchor biosynthesis class G (PIGG) are possible candidates for developmental delay, intellectual disabilities, and seizures in WHS patients (Zollino et al., 2014). CTBP1 is a transcriptional co-repressor known to mediate E-cadherin repression and play a key role in EMT (Zhang et al., 2013). Increased Ctbp activity has been shown to reduce epileptic behavior in rats following a ketogenic diet by forcing energy production via the TCA cycle and oxidation of NADH (Garriga-Canut et al., 2006). Reduced levels of NADH stimulates Ctbp activity and could be a mechanism by which loss of CTBP1 contributes to seizures. Ctbp1 mutant mice also exhibit defects in skeletal and muscle development (Hildebrand and Soriano, 2002). As CTBP1 is known to be involved in EMT (Zhang et al., 2013), it seems plausible that mutations of this gene may result in these phenotypes by influencing NCC migration.

CPLX1 is a cytosolic protein that is important for synaptic vesicle exocytosis and regulation of neurotransmitter release (Glynn et al., 2005). Mutations of CPLX1 have been associated with epilepsy and intellectual disability, and Cplx1 knockout mice exhibit pronounced motor and social deficits (Glynn et al., 2005; Drew et al., 2007; Redler et al., 2017). Pathogenic variants of PIGG are associated with intellectual disability, hypotonia, and seizures (Makrythanasis et al., 2016). PIGG localizes to the endoplasmic reticulum and is responsible for the biogenesis of GPI anchor proteins in zebrafish, which is critical for expression of voltage-gated sodium channels in a subset of neurons (Nakano et al., 2010). However, it is clear that further research is needed to determine how these genes are distinctly contributing to the development of organs and tissues that are affected in WHS.

MSX1 (Msh homeobox 1) functions as a transcriptional repressor during embryogenesis and has been suggested as a candidate gene for the oral and dental malformations seen in some WHS patients (Nieminen et al., 2003). Mutations of MSX1 have been associated with non-syndromic cleft palate and tooth agenesis in humans, and Msx1-deficient mice exhibit severe craniofacial abnormalities, cleft palate, and absence of teeth (Satokata and Maas, 1994; Zhang et al., 2002; Nieminen et al., 2003). In *Xenopus*, MSX1 has been shown to be critical for NCC induction and regulates the expression of genes that are necessary for proper NCC migration (Monsoro-Burq et al., 2005; Bonano et al., 2008; Macrì et al., 2016). Thus, it is likely that haploinsufficiency of MSX1 contributes to some craniofacial and dental defects associated with WHS by affecting NCC induction, as well as having downstream regulatory effects on genes that influence their subsequent migration.

USING *XENOPUS LAEVIS* AS A MODEL TO STUDY WHS

In an effort to answer some outstanding questions regarding the pathogenesis of WHS, it is critical to choose a model organism that is ideal for studying human genetic diseases. Every model system has its benefits and limitations; however, *X. laevis* has emerged as a particularly advantageous model for studying human genetic diseases, like WHS. While mouse models are an excellent mammalian system due to the similarity between the mouse and human genomes and the large genetic toolkit available, they are very costly to house and maintain. Moreover, litter sizes are small, embryonic development occurs *in utero*, and creating genetic lines that harbor mutant alleles is time-consuming. While zebrafish produce many offspring and have well-developed genetic manipulation strategies, their genome has lost a great deal of synteny with mammals and many relevant disease-related genes do not perform the same function (Garcia de la Serrana et al., 2014). Zebrafish also lack organ systems, such as limbs, digits, and lungs, that are involved in many human congenital syndromes. Additionally, the zebrafish heart only has one atrium and one ventricle, and cannot fully model developmental heart abnormalities, like those associated with WHS.

However, using *Xenopus* as a system to investigate human genetic diseases of development has enormous potential, and can complement more established systems, like mouse or zebrafish, to enhance our knowledge about the function of understudied genes and the underlying mechanisms by which developmental abnormalities arise. In the following sections, we highlight why *X. laevis* is an advantageous model to choose for investigating developmental disorders, with a specific focus on how it can be used to examine multiple aspects of WHS.

Advantages of *Xenopus laevis* as a Model Organism

Xenopus is an excellent system for relatively high throughput analysis of genetic manipulation on vertebrate embryonic development. *Xenopus* shares a high degree of synteny with humans and a majority of disease-associated genes are conserved between these species (Hellsten et al., 2010; Session et al., 2016). Despite *X. laevis* having a duplicated genome, genetic manipulation strategies can still be utilized. However, *X. tropicalis* may be more suitable, depending on the number of genes being studied, as they are diploid, making genetic manipulation much easier and more rapid. The *Xenopus* genome is widely available to the research community through the efforts of *Xenbase*, an online resource that has organized current annotated genetic information, protocols, *Xenopus* anatomy and development,

scientific literature, and provides useful sequencing tools, such as the genome browser and *Xenopus* specific BLAST (James-Zorn et al., 2018).

A key characteristic of the *Xenopus* model is the ease of acquiring large amounts of high quality embryos by inducing females to lay eggs via hormone priming (Sive et al., 2007a,b; Erdogan et al., 2016; Slater et al., 2017). Hundreds of embryos can be obtained in a single clutch, enabling numerous embryos to be manipulated and observed in a single experiment. *Xenopus* development occurs rapidly and externally, with gastrulation and neurulation occurring between 9 and 26 h post fertilization, and organogenesis almost complete by 5 days post fertilization (Nieuwkoop and Faber, 1994; Zahn et al., 2017). *Xenopus* organ development and morphology have been well-characterized and is comparable to those of mammalian systems, including orofacial (Dickinson, 2016), heart (Hempel and Kühl, 2016), kidney (Getwan and Lienkamp, 2017), and nervous system development (Pratt and Khakhalin, 2013; Lee-Liu et al., 2017), all of which are affected in WHS patients. Moreover, *Xenopus* is being used extensively as a model to understand a number of different human genetic diseases that lead to defects in these systems, such as congenital heart disorders (Boskovski et al., 2013; Sojka et al., 2014; Duncan and Khokha, 2016; Deniz et al., 2017), kidney disease (Lienkamp, 2016), ciliopathies (Brooks and Wallingford, 2015; Wallmeier et al., 2016), orofacial defects (Tahir et al., 2014; Dickinson, 2016), and neurodevelopmental disorders (Pratt and Khakhalin, 2013; Tandon et al., 2017; Willsey et al., 2018).

In order to characterize WHS-associated gene functions in relation to development and disease, *Xenopus* embryos can be injected with a variety of materials to manipulate gene expression, such as CRISPR/cas9 or morpholino oligonucleotides (MOs), in either the whole embryo or selected blastomeres (up to the 64-cell stage) (Mimoto and Christian, 2011; Tandon et al., 2012, 2017; Bestman and Cline, 2014; Bhattacharya et al., 2015; Wang et al., 2015; DeLay et al., 2016; Feehan et al., 2017; Moody, 2018a,b). As the lineage of individual cells has been well-documented, injections can be precisely targeted to specific tissues and organs that are affected in WHS, such as the heart, kidney, or brain. A unique feature of *Xenopus* compared to other models is the ability to perform one-sided embryo injections, wherein only one side of the embryo is experimentally manipulated and the opposite side serves as an internal control (**Figure 2**; Willsey et al., 2018; Mills et al., 2019). Thus, assessing phenotypic consequences that arise as a result of genetic manipulation can be compared side-by-side to wild-type gene expression.

Morpholino oligonucleotides are particularly useful in modeling genetic diseases, like WHS, as they can be easily titrated to reduce gene dosage levels similar to that in human patients (Tahir et al., 2014; Blum et al., 2015; McCammon and Sive, 2015). Because WHS-associated mutations result in haploinsufficiency, a full knockout of the candidate genes would not appropriately model the disease, and simultaneous knockdown of genes can be achieved by injecting multiple MOs at once, allowing for concurrent knockdown of genes that are often deleted together in WHS (Blum et al., 2015). While it is certainly possible to produce mouse lines with mutations in multiple genes (Simon and Bergemann, 2008), this is a costlier and more time-consuming process than the equivalent in *X. laevis*. As with all manipulation strategies, the appropriate controls must be used to account for off-target effects, such as generating more than one MO, dose dependency, and rescuing phenotypes by co-injecting mRNA that is not targeted by the MO (Blum et al., 2015; Gentsch et al., 2018).

The CRISPR/cas9 system has also been used as an extremely effective method to knock out target genes in both *X. tropicalis* and *X. laevis* (Bhattacharya et al., 2015; Wang et al., 2015; Tandon et al., 2017). While the off-target effects of CRISPR/cas9 are generally minimal, the use of proper controls is critical by carefully designing multiple sgRNAs and performing rescue experiments to confirm that any phenotypes observed are due to the knockout of a particular gene (Nakayama et al., 2013; Wang et al., 2015). The CRISPR/cas9 system can be employed to validate phenotypes that arise as a result of MO-mediated gene knockdown by comparing phenotypes generated by both methods (Bhattacharya et al., 2015; Willsey et al., 2018). Overall, *Xenopus* is an excellent system for investigating developmental disorders, such as WHS, and for elucidating the mechanism by which manipulation of WHS-associated genes alters proper embryonic development.

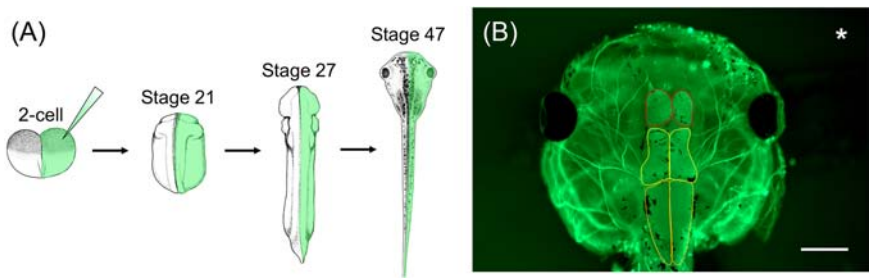

FIGURE 2 | *Xenopus* one-sided injections allow for side-by-side comparison to wild-type gene expression following genetic manipulation. **(A)** *Xenopus* embryos can be injected in one cell at the 2-cell stage with genetic manipulation macromolecules and fluorescent mRNA. At stage 21, embryos can be sorted depending on the side that was injected (left vs. right) and used for various assays throughout development. **(B)** Representative image of stage 47 *X. laevis* tadpole immunolabeled for acetylated tubulin. Asterisk represents the side that was injected with MO and fluorescent mRNA. Brain morphology, such as forebrain size (red outline), midbrain size (yellow outline), and hindbrain size (orange outline), of the manipulated side can be compared to the unaltered, wild-type side. Scale bar: 500 μm.

Xenopus laevis as a Model for Studying Neural Crest Cell Migration

As the underlying cellular and molecular mechanisms that cause WHS are unknown, it is essential to investigate the basis behind the disorder. One particularly promising avenue of research in this regard is the migration of the NCC population in the developing embryo (Rutherford and Lowery, 2016). As stated previously, NCCs are a multipotent stem cell population that originate along the neural tube, delaminate, and migrate throughout the developing embryo to their final destinations. Once at their proper locations, NCCs differentiate and contribute to various tissues and organ systems, including craniofacial cartilage and bone, smooth muscle of the heart, peripheral and enteric neurons, melanocytes, and glia (Bronner and LeDouarin, 2012). Considering craniofacial abnormalities are one of the defining phenotypes of WHS, the link to potential aberrations in NCC migration is strong. Moreover, almost all WHS-associated genes are connected with NCC migration or signaling pathways that may influence NCC differentiation or proliferation in some capacity. Therefore, research into NCC migration in relation to WHS is of great interest.

Xenopus laevis is an ideal model organism for studying NCC migration, as both *in vivo* and *in vitro* NCC migration can be tracked through multiple methods. NCC migration can be observed *in vivo* by performing transplantation assays, whereby NCCs are dissected from GFP-injected *Xenopus* embryos and transplanted to wild-type host embryos (Borchers et al., 2000; Cousin, 2018). These embryos can then be imaged using time-lapse confocal microscopy and NCC migration can be analyzed by measuring the number, width, and migration distance of the GFP-marked cranial segments. Additionally, two transgenic *X. laevis* frog lines, PAX3-GFP and SOX10-GFP, are available through the National *Xenopus* Resource (NXR) to study the *in vivo* development and migration of NCCs (Alkobtawi et al., 2018). *In vivo* NCC migration can also be analyzed through whole-mount *in situ* hybridization by observing the morphology of the pharyngeal arches using a marker for NCCs, such as TWIST or SOX9 (**Figure 3**; Devotta et al., 2016; Szabó et al., 2016).

Neural crest cell motility can be examined *in vitro* by dissecting NCCs from stage 16 *Xenopus* embryos and culturing explants on fibronectin-coated coverslips (Cousin and Alfandari, 2018). Migratory behavior of NCC explants can be observed using time-lapse confocal microscopy and multiple parameters of migration can be measured including velocity and dispersion (DeSimone et al., 2005; Milet and Monsoro-Burq, 2014; Cousin and Alfandari, 2018). Moreover, chemotaxis assays can be performed *in vitro* to assess the directional migration of NCCs toward an external, soluble factor by coating beads with a chemoattractant cue, such as SDF-1 (Theveneau and Mayor, 2011; Theveneau et al., 2013; Shellard and Mayor, 2016; Szabó et al., 2016). Recently, these methods were successfully used in *X. laevis* to test whether knockdown of particular WHS genes led to changes in NCC migration both *in vivo* and *in vitro* (Mills et al., 2019), demonstrating how *X. laevis* can provide a unique and varied approach to study how alterations in NCC migratory behavior may contribute to phenotypes of the disease.

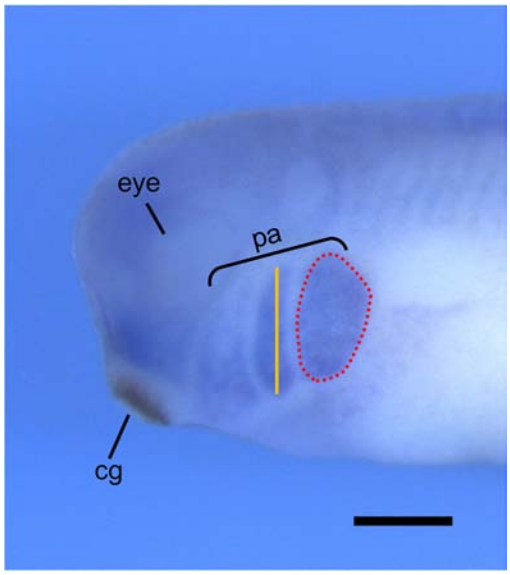

FIGURE 3 | Analysis of *in vivo* NCC migration using whole-mount *in situ* hybridization. Representative image of stage 30 *X. laevis* embryo labeled for xTWIST, a marker for NCCs. Measurements of the length (orange line) and area (red dotted line) of each individual pharyngeal arch can be done using ImageJ. Pharyngeal arch length is measured from the most dorsal point to the most ventral point of each individual arch. Pharyngeal arch area is measured as the area around the periphery of each individual arch. cg, cement gland; pa, pharyngeal arches. Scale bar: 500 μm.

Xenopus laevis as a Model for Studying Other Aspects of WHS

Craniofacial abnormalities are one of the defining phenotypes of WHS and *X. laevis* has emerged as an excellent system for determining which WHS-associated genes are important for craniofacial morphogenesis. As orofacial development is highly conserved between *Xenopus* and other mammalian species, craniofacial abnormalities in *Xenopus* often resemble phenotypes present in human patients (Dickinson and Sive, 2007, 2006; Tahir et al., 2014; Dubey and Saint-Jeannet, 2017). Various techniques to assess changes in *Xenopus* orofacial development have already been developed and used to study craniofacial defects associated with human genetic disorders (Tahir et al., 2014; Gonzalez Malagon et al., 2018; Mills et al., 2019). Similar to NCC transplant assays, facial transplant assays can be performed in *Xenopus* (Jacox L. A. et al., 2014; Jacox L. et al., 2014; Jacox et al., 2016; Gonzalez Malagon et al., 2018). This technique allows for the examination of gene or protein function in particular cell types involved in facial development, eliminating non-specific effects in the whole embryo, and can be used to study signaling mechanisms or mechanical forces that are involved in orofacial development (Dickinson, 2016).

More robust quantitative methods to examine alterations of orofacial development have also been adapted for use in *Xenopus*.

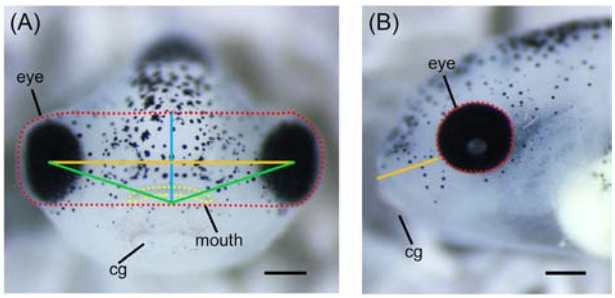

FIGURE 4 | Measurements of *Xenopus* craniofacial features. **(A)** Representative frontal view image of stage 42 *X. laevis* tadpole. Measurements of facial features include facial height (blue line), facial width (orange line), facial area (red dotted line), facial angle (green line), and mouth roundness (yellow dotted line). Facial height is measured from the top of the middle of the eyes to the top of the cement gland. Facial width is measured from the middle of one eye to the middle of the opposite eye. Facial area is measured as the area around the top of the eyes to the top of the cement gland. Facial angle is measured as the angle between the middle of the eyes and the top of the cement gland. Mouth roundness is measured as the area around the periphery of the mouth. **(B)** Representative lateral view image of stage 42 *X. laevis* tadpole. Measurements of facial features include eye area (red dotted line) and snout length (orange line). Eye area is measured as the area around the periphery of the eye. Snout length is measured from the most anterior part of the face to the bottom of the eye. All measurements can be performed using ImageJ. cg, cement gland. Scale bar: 100 μm.

Measurements of various craniofacial features such as facial width, height, angle, and area can be done on embryos at different developmental stages using ImageJ (**Figure 4**; Kennedy and Dickinson, 2014a; Tahir et al., 2014). These measurements can be combined with geometric morphometrics in order to detect subtle differences in face shape and size throughout development (Kennedy and Dickinson, 2014b; Dickinson, 2016). Furthermore, techniques for visualizing cartilage morphology, such as Alcian blue staining, can be used to determine whether craniofacial abnormalities arise as a result of defects in cartilage development (**Figure 5**; Tahir et al., 2014; Devotta et al., 2016).

It is important to note that there are some craniofacial and cartilage morphological differences between *Xenopus* and humans that will prevent some direct correlations to disease pathology. For example, Meckel's cartilage will eventually become a component of the lower jaw in both *Xenopus* and humans, however in humans, it will also become part of the middle ear skeletal structures. Nevertheless, using these techniques in *Xenopus* has provided evidence that some WHS-associated genes are required for proper craniofacial development and contribute to the signature craniofacial dysmorphisms seen in WHS patients (Mills et al., 2019).

Individuals with WHS display a variety of other symptoms such as microcephaly, heart defects, and renal defects. Whether WHS-associated genes are required for proper development of these organ and tissue systems in relation to WHS still remains unknown. However, many techniques exist in *Xenopus* to study brain, heart, and kidney development. *Xenopus* neurodevelopment has been explored extensively using both *in vitro* and *in vivo* methods (Erdogan et al., 2016; Slater et al., 2017). Due to the large size of its growth cones, *X. laevis* is an excellent model to study cytoskeletal dynamics in axon outgrowth and guidance during early development. Moreover, live imaging can be done on both retinal and spinal axonal tracts *in vivo* (Erdogan et al., 2016; Slater et al., 2017). Additionally, changes in brain morphology can be quantified simply by measuring the area of the forebrain, midbrain, and hindbrain (**Figure 2B**), and used as a technique to reflect the microcephaly phenotype associated with WHS (Willsey et al., 2018; Mills et al., 2019).

Congenital heart defects have emerged as the most life-threatening birth defect in newborn patients across different developmental disorders, including WHS (Duncan and Khokha, 2016; Garfinkel and Khokha, 2017). Early heart development is highly conserved between *Xenopus* and mammalian systems, and assays to analyze CHD candidate genes have been created for use in *Xenopus* (Sojka et al., 2014; Duncan and Khokha, 2016; Hempel and Kühl, 2016; Deniz et al., 2017; Garfinkel and Khokha, 2017; Tandon et al., 2017). The effect of genetic manipulation on heart development can be explored at early tadpole stages using whole-mount *in situ* hybridization, immunohistochemistry with anti-tropomyosin (Tmy) antibody, scanning electron microscopy (SEM), transmission electron microscopy (TEM), or optical coherence tomography (OCT) (Sojka et al., 2014; Hempel and Kühl, 2016; Deniz et al., 2017). These assays help to visualize and detect improperly looped

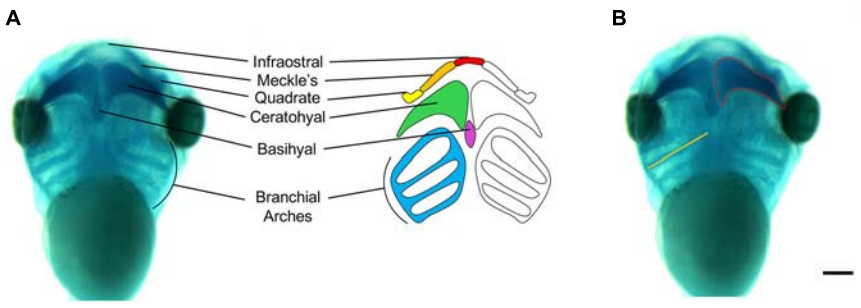

FIGURE 5 | Measurements of *Xenopus* cartilage elements. **(A)** *Xenopus* cartilage anatomy with all major cartilage elements labeled in various colors. **(B)** Representative ventral view image of stage 45 *X. laevis* tadpole stained for Alcian blue. Measurements of cartilage elements include branchial arch length (orange line) and ceratohyal area (red dotted line), which can be performed using ImageJ. Scale bar: 300 μm.

hearts, failed chamber formation, and abnormal structure of the adjacent connective tissue, and can be used to elucidate how mutations of WHS genes lead to CHD (Sojka et al., 2014; Duncan and Khokha, 2016).

In vitro explant, transplant, and ablation techniques can be used to derive insight into how mutations of genes associated with renal disease affect the progression of kidney development in *Xenopus* (Getwan and Lienkamp, 2017). *In vivo* experiments of kidney development range from optogenetic manipulations of physiological parameters (calcium, pH) to characterizations of electrophysiological recordings (Lienkamp, 2016; Getwan and Lienkamp, 2017). Together, *X. laevis* can be used as a powerful system to study how mutations of WHS-associated genes affect the development of multiple tissue and organ systems.

CONCLUSION

Xenopus laevis has emerged as an effective model organism for studying human genetic disorders of development, such as WHS. *Xenopus* embryos can be collected in large numbers and are easy to maintain, manipulate, and image. Genetic manipulation strategies are straightforward, allow for the concurrent KD or KO of multiple genes at once, and can be titrated to reduce gene dosage levels similar to that in human patients with WHS. Numerous techniques exist in *Xenopus* to study a variety of tissue and organ systems in order to understand the function of WHS-associated genes during embryonic development. Most importantly, *Xenopus* provides a system in which phenotypes of WHS, including craniofacial abnormalities, brain defects, heart defects, and kidney defects can be easily examined. Moreover, the mechanism by which mutations of WHS-associated genes affects embryonic development can be studied in *Xenopus*, such as changes in NCC migration. Thus, *X. laevis* is an excellent model system for investigating the underlying pathology of WHS, as well as many other human genetic diseases.

AUTHOR CONTRIBUTIONS

BP and LL contributed to the conception and design of the manuscript. BP and ML wrote the first draft of the manuscript. CM and SK wrote the sections of the manuscript. LL edited the manuscript. All authors contributed to the revision, read, and approved the final version of the manuscript for submission.

FUNDING

This work was supported by Charles H. Hood Foundation, NIH R03 DE025824 and NIH R01 MH109651 (to LL), and NIH R01 GM121907 (to ML). American Cancer Society (RSG-16-144-01-CSM) to the funding list for LL.

ACKNOWLEDGMENTS

We thank members of the Lowery Lab for helpful discussions, suggestions, and editing. We also thank the National Xenopus Resource RRID:SCR_013731 and Xenbase RRID:SCR_003280 for their support.

REFERENCES

Alkobtawi, M., Ray, H., Barriga, E. H., Moreno, M., Kerney, R., Monsoro-Burq, A.-H., et al. (2018). Characterization of Pax3 and Sox10 transgenic *Xenopus laevis* embryos as tools to study neural crest development. *Dev. Biol.* 444(Suppl. 1), S202–S208.

Andersen, E. F., Carey, J. C., Earl, D. L., Corzo, D., Suttie, M., Hammond, P., et al. (2014). Deletions involving genes WHSC1 and LETM1 may be necessary, but are not sufficient to cause Wolf-Hirschhorn Syndrome. *Eur. J. Hum. Genet.* 22, 464–470. doi: 10.1038/ejhg.2013.192

Battaglia, A., Carey, J. C., and South, S. T. (2015). Wolf-Hirschhorn syndrome: a review and update. *Am. J. Med. Genet. C Semin. Med. Genet.* 169, 216–223. doi: 10.1002/ajmg.c.31449

Bearce, E. A., Erdogan, B., and Lowery, L. A. (2015). TIPsy tour guides: how microtubule plus-end tracking proteins (+TIPs) facilitate axon guidance. *Front. Cell. Neurosci.* 9:241. doi: 10.3389/fncel.2015.00241

Bestman, J. E., and Cline, H. T. (2014). Morpholino studies in Xenopus brain development. *Methods Mol. Biol.* 1082, 155–171. doi: 10.1007/978-1-62703-655-9_11

Bhattacharya, D., Marfo, C. A., Li, D., Lane, M., and Khokha, M. K. (2015). CRISPR/Cas9: an inexpensive, efficient loss of function tool to screen human disease genes in Xenopus. *Dev. Biol.* 408, 196–204. doi: 10.1016/j.ydbio.2015.11.003

Bi, W., Cheung, S. W., Breman, A. M., and Bacino, C. A. (2016). 4p16.3 microdeletions and microduplications detected by chromosomal microarray analysis: new insights into mechanisms and critical regions. *Am. J. Med. Genet. A* 170, 2540–2550. doi: 10.1002/ajmg.a.37796

Blum, M., De Robertis, E. M., Wallingford, J. B., and Niehrs, C. (2015). Morpholinos: antisense and sensibility. *Dev. Cell* 35, 145–149. doi: 10.1016/j.devcel.2015.09.017

Boczek, N. J., Lahner, C. A., Nguyen, T.-M., Ferber, M. J., Hasadsri, L., Thorland, E. C., et al. (2018). Developmental delay and failure to thrive associated with a loss-of-function variant in WHSC1 (n.d.). *Am. J. Med. Genet. A* 176, 2798–2802. doi: 10.1002/ajmg.a.40498

Bonano, M., Tríbulo, C., De Calisto, J., Marchant, L., Sánchez, S. S., Mayor, R., et al. (2008). A new role for the Endothelin-1/Endothelin-A receptor signaling during early neural crest specification. *Dev. Biol.* 323, 114–129. doi: 10.1016/j.ydbio.2008.08.007

Borchers, A., Epperlein, H. H., and Wedlich, D. (2000). An assay system to study migratory behavior of cranial neural crest cells in *Xenopus*. *Dev. Genes Evol.* 210, 217–222. doi: 10.1007/s004270050307

Boskovski, M. T., Yuan, S., Pedersen, N. B., Goth, C. K., Makova, S., Clausen, H., et al. (2013). The heterotaxy gene GALNT11 glycosylates Notch to orchestrate cilia type and laterality. *Nature* 504, 456–459. doi: 10.1038/nature12723

Bronner, M. E., and LeDouarin, N. M. (2012). Development and evolution of the neural crest: an overview. *Dev. Biol.* 366, 2–9. doi: 10.1016/j.ydbio.2011.12.042

Brooks, E. R., and Wallingford, J. B. (2015). *In vivo* investigation of cilia structure and function using *Xenopus*. *Methods Cell Biol.* 127, 131–159. doi: 10.1016/bs.mcb.2015.01.018

Cammarata, G. M., Bearce, E. A., and Lowery, L. A. (2016). Cytoskeletal social networking in the growth cone: how +TIPs mediate microtubule-actin cross-linking to drive axon outgrowth and guidance. *Cytoskeleton* 73, 461–476. doi: 10.1002/cm.21272

Catela, C., Bilbao-Cortes, D., Slonimsky, E., Kratsios, P., Rosenthal, N., and Te Welscher, P. (2009). Multiple congenital malformations of Wolf-Hirschhorn syndrome are recapitulated in Fgfrl1 null mice. *Dis. Model. Mech.* 2, 283–294. doi: 10.1242/dmm.002287

Cousin, H. (2018). Cranial neural crest transplants. *Cold Spring Harb. Protoc.* 2018:db.rot097402. doi: 10.1101/pdb.prot097402

Cousin, H., and Alfandari, D. (2018). Cranial neural crest explants. *Cold Spring Harb. Protoc.* 2018:db.rot097394. doi: 10.1101/pdb.prot097394

DeLay, B. D., Krneta-Stankic, V., and Miller, R. K. (2016). Technique to target microinjection to the developing *Xenopus* kidney. *J. Vis. Exp.* 111:e53799. doi: 10.3791/53799

Deniz, E., Jonas, S., Hooper, M., N Griffin, J., Choma, M. A., and Khokha, M. K. (2017). Analysis of craniocardiac malformations in *Xenopus* using optical coherence tomography. *Sci. Rep.* 7:42506. doi: 10.1038/srep42506

Derar, N., Al-Hassnan, Z. N., Al-Owain, M., Monies, D., Abouelhoda, M., Meyer, B. F., et al. (2018). De novo truncating variants in WHSC1 recapitulate the Wolf-Hirschhorn (4p16.3 microdeletion) syndrome phenotype. *Genet. Med.* 21, 185–188. doi: 10.1038/s41436-018-0014-8

DeSimone, D. W., Davidson, L., Marsden, M., and Alfandari, D. (2005). The *Xenopus* embryo as a model system for studies of cell migration. *Methods Mol. Biol.* 294, 235–245.

Devotta, A., Juraver-Geslin, H., Gonzalez, J. A., Hong, C.-S., and Saint-Jeannet, J. -P. (2016). Sf3b4-depleted *Xenopus* embryos: a model to study the pathogenesis of craniofacial defects in Nager syndrome. *Dev. Biol.* 415, 371–382. doi: 10.1016/j.ydbio.2016.02.010

Dickinson, A., and Sive, H. (2007). Positioning the extreme anterior in *Xenopus*: cement gland, primary mouth and anterior pituitary. *Semin. Cell Dev. Biol.* 18, 525–533. doi: 10.1016/j.semcdb.2007.04.002

Dickinson, A. J. G. (2016). Using frogs faces to dissect the mechanisms underlying human orofacial defects. *Semin. Cell Dev. Biol.* 51, 54–63. doi: 10.1016/j.semcdb.2016.01.016

Dickinson, A. J. G., and Sive, H. (2006). Development of the primary mouth in *Xenopus laevis*. *Dev. Biol.* 295, 700–713. doi: 10.1016/j.ydbio.2006.03.054

Dimmer, K. S., Navoni, F., Casarin, A., Trevisson, E., Endele, S., Winterpacht, A., et al. (2008). LETM1, deleted in Wolf-Hirschhorn syndrome is required for normal mitochondrial morphology and cellular viability. *Hum. Mol. Genet.* 17, 201–214. doi: 10.1093/hmg/ddm297

Doonan, P. J., Chandramoorthy, H. C., Hoffman, N. E., Zhang, X., Cárdenas, C., Shanmughapriya, S., et al. (2014). LETM1-dependent mitochondrial Ca^{2+} flux modulates cellular bioenergetics and proliferation. *FASEB J.* 28, 4936–4949. doi: 10.1096/fj.14-256453

Drew, C. J. G., Kyd, R. J., and Morton, A. J. (2007). Complexin 1 knockout mice exhibit marked deficits in social behaviours but appear to be cognitively normal. *Hum. Mol. Genet.* 16, 2288–2305. doi: 10.1093/hmg/ddm181

Dubey, A., and Saint-Jeannet, J.-P. (2017). Modeling human craniofacial disorders in *Xenopus*. *Curr. Pathobiol. Rep.* 5, 79–92. doi: 10.1007/s40139-017-0128-8

Duncan, A. R., and Khokha, M. K. (2016). *Xenopus* as a model organism for birth defects-Congenital heart disease and heterotaxy. *Semin. Cell Dev. Biol.* 51, 73–79. doi: 10.1016/j.semcdb.2016.02.022

Endele, S., Fuhry, M., Pak, S. J., Zabel, B. U., and Winterpacht, A. (1999). LETM1, a novel gene encoding a putative EF-hand Ca^{2+}-binding protein, flanks the Wolf-Hirschhorn syndrome (WHS) critical region and is deleted in most WHS patients. *Genomics* 60, 218–225. doi: 10.1006/geno.1999.5881

Endele, S., Nelkenbrecher, C., Bördlein, A., Schlickum, S., and Winterpacht, A. (2011). C4ORF48, a gene from the Wolf-Hirschhorn syndrome critical region, encodes a putative neuropeptide and is expressed during neocortex and cerebellar development. *Neurogenetics* 12, 155–163.

Engbers, H., van der Smagt, J. J., van 't Slot, R., Vermeesch, J. R., Hochstenbach, R., and Poot, M. (2009). Wolf-Hirschhorn syndrome facial dysmorphic features in a patient with a terminal 4p16.3 deletion telomeric to the WHSCR and WHSCR 2 regions. *Eur. J. Hum. Genet.* 17, 129–132. doi: 10.1038/ejhg.2008.168

Erdogan, B., Cammarata, G. M., Lee, E. J., Pratt, B. C., Francl, A. F., Rutherford, E. L., et al. (2017). The microtubule plus-end-tracking protein TACC3 promotes persistent axon outgrowth and mediates responses to axon guidance signals during development. *Neural Dev.* 12:3.

Erdogan, B., Ebbert, P. T., and Lowery, L. A. (2016). Using *Xenopus laevis* retinal and spinal neurons to study mechanisms of axon guidance in vivo and in vitro. *Semin. Cell Dev. Biol.* 51, 64–72. doi: 10.1016/j.semcdb.2016.02.003

Ezponda, T., Popovic, R., Shah, M. Y., Martinez-Garcia, E., Zheng, Y., Min, D.-J., et al. (2013). The histone methyltransferase MMSET/WHSC1 activates TWIST1 to promote an epithelial-mesenchymal transition and invasive properties of prostate cancer. *Oncogene* 32, 2882–2890. doi: 10.1038/onc.2012.297

Feehan, J. M., Chiu, C. N., Stanar, P., Tam, B. M., Ahmed, S. N., and Moritz, O. L. (2017). Modeling dominant and recessive forms of retinitis pigmentosa by editing three rhodopsin-encoding genes in *Xenopus laevis* using Crispr/Cas9. *Sci. Rep.* 7:6920.

Fisch, G. S., Grossfeld, P., Falk, R., Battaglia, A., Youngblom, J., and Simensen, R. (2010). Cognitive-behavioral features of Wolf-Hirschhorn syndrome and other subtelomeric microdeletions. *Am. J. Med. Genet. C Semin. Med. Genet.* 154C, 417–426. doi: 10.1002/ajmg.c.30279

Garcia de la Serrana, D., Mareco, E. A., and Johnston, I. A. (2014). Systematic variation in the pattern of gene paralog retention between the teleost superorders Ostariophysi and Acanthopterygii. *Genome Biol. Evol.* 6, 981–987. doi: 10.1093/gbe/evu074

Garfinkel, A. M., and Khokha, M. K. (2017). An interspecies heart-to-heart: using *Xenopus* to uncover the genetic basis of congenital heart disease. *Curr. Pathobiol. Rep.* 5, 187–196. doi: 10.1007/s40139-017-0142-x

Garriga-Canut, M., Schoenike, B., Qazi, R., Bergendahl, K., Daley, T. J., Pfender, R. M., et al. (2006). 2-Deoxy-D-glucose reduces epilepsy progression by NRSF-CtBP-dependent metabolic regulation of chromatin structure. *Nat. Neurosci.* 9, 1382–1387. doi: 10.1038/nn1791

Gentsch, G. E., Spruce, T., Monteiro, R. S., Owens, N. D. L., Martin, S. R., and Smith, J. C. (2018). Innate immune response and off-target mis-splicing are common morpholino-induced side effects in *Xenopus*. *Dev. Cell* 44, 597–610.e10. doi: 10.1016/j.devcel.2018.01.022

Getwan, M., and Lienkamp, S. S. (2017). Toolbox in a tadpole: *Xenopus* for kidney research. *Cell Tissue Res.* 369, 143–157. doi: 10.1007/s00441-017-2611-2

Gilchrist, D. A., Nechaev, S., Lee, C., Ghosh, S. K. B., Collins, J. B., Li, L., et al. (2008). NELF-mediated stalling of Pol II can enhance gene expression by blocking promoter-proximal nucleosome assembly. *Genes Dev.* 22, 1921–1933. doi: 10.1101/gad.1643208

Glynn, D., Drew, C. J., Reim, K., Brose, N., and Morton, A. J. (2005). Profound ataxia in complexin I knockout mice masks a complex phenotype that includes exploratory and habituation deficits. *Hum. Mol. Genet.* 14, 2369–2385. doi: 10.1093/hmg/ddi239

Gonzalez Malagon, S. G., Lopez Muñoz, A. M., Doro, D., Bolger, T. G., Poon, E., Tucker, E. R., et al. (2018). Glycogen synthase kinase 3 controls migration of the neural crest lineage in mouse and *Xenopus*. *Nat. Commun.* 9:1126.

Hannes, F., Drozniewska, M., Vermeesch, J. R., and Haus, O. (2010). Duplication of the Wolf-Hirschhorn syndrome critical region causes neurodevelopmental delay. *Eur. J. Med. Genet.* 53, 136–140. doi: 10.1016/j.ejmg.2010.02.004

Hellsten, U., Harland, R. M., Gilchrist, M. J., Hendrix, D., Jurka, J., Kapitonov, V., et al. (2010). The genome of the Western clawed frog *Xenopus tropicalis*. *Science* 328, 633–636. doi: 10.1126/science.1183670

Hempel, A., and Kühl, M. (2016). A matter of the heart: the African clawed frog *Xenopus* as a model for studying vertebrate cardiogenesis and congenital heart defects. *J. Cardiovasc. Dev. Dis.* 3:21. doi: 10.3390/jcdd3020021

Hildebrand, J. D., and Soriano, P. (2002). Overlapping and unique roles for C-terminal binding protein 1 (CtBP1) and CtBP2 during mouse development. *Mol. Cell. Biol.* 22, 5296–5307. doi: 10.1128/MCB.22.15.5296-5307.2002

Ho, K. S., South, S. T., Lortz, A., Hensel, C. H., Sdano, M. R., Vanzo, R. J., et al. (2016). Chromosomal microarray testing identifies a 4p terminal region associated with seizures in Wolf-Hirschhorn syndrome. *J. Med. Genet.* 53, 256–263. doi: 10.1136/jmedgenet-2015-103626

Jacox, L., Chen, J., Rothman, A., Lathrop-Marshall, H., and Sive, H. (2016). Formation of a "Pre-mouth Array" from the extreme anterior domain is directed by neural crest and Wnt/PCP signaling. *Cell Rep.* 16, 1445–1455. doi: 10.1016/j.celrep.2016.06.073

Jacox, L., Sindelka, R., Chen, J., Rothman, A., Dickinson, A., and Sive, H. (2014). The extreme anterior domain is an essential craniofacial organizer acting through Kinin-Kallikrein signaling. *Cell Rep.* 8, 596–609. doi: 10.1016/j.celrep.2014.06.026

Jacox, L. A., Dickinson, A. J., and Sive, H. (2014). Facial transplants in *Xenopus laevis* embryos. *J. Vis. Exp.* 85:e50697. doi: 10.3791/50697

James-Zorn, C., Ponferrada, V., Fisher, M. E., Burns, K., Fortriede, J., Segerdell, E., et al. (2018). Navigating xenbase: an integrated *Xenopus* genomics and gene expression database. *Methods Mol. Biol.* 1757, 251–305. doi: 10.1007/978-1-4939-7737-6_10

Jiang, D., Zhao, L., Clish, C. B., and Clapham, D. E. (2013). Letm1, the mitochondrial Ca^{2+}/H^{+} antiporter, is essential for normal glucose metabolism and alters brain function in Wolf-Hirschhorn syndrome. *Proc. Natl. Acad. Sci. U.S.A.* 110, E2249–E2254. doi: 10.1073/pnas.1308558110

Kennedy, A. E., and Dickinson, A. J. (2014a). Quantification of orofacial phenotypes in *Xenopus*. *J. Vis. Exp*. 93:e52062. doi: 10.3791/52062

Kennedy, A. E., and Dickinson, A. J. (2014b). Quantitative analysis of orofacial development and median clefts in *Xenopus laevis*. *Anat. Rec.* 297, 834–855. doi: 10.1002/ar.22864

Kerzendorfer, C., Hannes, F., Colnaghi, R., Abramowicz, I., Carpenter, G., Vermeesch, J. R., et al. (2012). Characterizing the functional consequences of haploinsufficiency of NELF-A (WHSC2) and SLBP identifies novel cellular phenotypes in Wolf-Hirschhorn syndrome. *Hum. Mol. Genet.* 21, 2181–2193. doi: 10.1093/hmg/dds033

Khacho, M., Harris, R., and Slack, R. S. (2019). Mitochondria as central regulators of neural stem cell fate and cognitive function. *Nat. Rev. Neurosci.* 20, 34–48. doi: 10.1038/s41583-018-0091-3

Lasser, M., Tiber, J., and Lowery, L. A. (2018). The role of the microtubule cytoskeleton in neurodevelopmental disorders. *Front. Cell. Neurosci.* 12:165. doi: 10.3389/fncel.2018.00165

Lee-Liu, D., Méndez-Olivos, E. E., Muñoz, R., and Larraín, J. (2017). The African clawed frog *Xenopus laevis*: a model organism to study regeneration of the central nervous system. *Neurosci. Lett.* 652, 82–93. doi: 10.1016/j.neulet.2016.09.054

Li, J., Perfetto, M., Neuner, R., Bahudhanapati, H., Christian, L., Mathavan, K., et al. (2018). *Xenopus* ADAM19 regulates Wnt signaling and neural crest specification by stabilizing ADAM13. *Development* 145:dev158154. doi: 10.1242/dev.158154

Lienkamp, S. S. (2016). Using *Xenopus* to study genetic kidney diseases. *Semin. Cell Dev. Biol.* 51, 117–124. doi: 10.1016/j.semcdb.2016.02.002

Liu, S., Higashihori, N., Yahiro, K., and Moriyama, K. (2015). Retinoic acid inhibits histone methyltransferase Whsc1 during palatogenesis. *Biochem. Biophys. Res. Commun.* 458, 525–530. doi: 10.1016/j.bbrc.2015.01.148

Macrì, S., Simula, L., Pellarin, I., Pegoraro, S., Onorati, M., Sgarra, R., et al. (2016). Hmga2 is required for neural crest cell specification in *Xenopus laevis*. *Dev. Biol.* 411, 25–37. doi: 10.1016/j.ydbio.2016.01.014

Maj, E., Künneke, L., Loresch, E., Grund, A., Melchert, J., Pieler, T., et al. (2016). Controlled levels of canonical Wnt signaling are required for neural crest migration. *Dev. Biol.* 417, 77–90. doi: 10.1016/j.ydbio.2016.06.022

Makrythanasis, P., Kato, M., Zaki, M. S., Saitsu, H., Nakamura, K., Santoni, F. A., et al. (2016). Pathogenic variants in PIGG cause intellectual disability with seizures and hypotonia. *Am. J. Hum. Genet.* 98, 615–626. doi: 10.1016/j.ajhg.2016.02.007

Margueron, R., and Reinberg, D. (2010). Chromatin structure and the inheritance of epigenetic information. *Nat. Rev. Genet.* 11, 285–296. doi: 10.1038/nrg2752

Mayor, R., and Theveneau, E. (2013). The neural crest. *Development* 140, 2247–2251. doi: 10.1242/dev.091751

McCammon, J. M., and Sive, H. (2015). Addressing the genetics of human mental health disorders in model organisms. *Annu. Rev. Genomics Hum. Genet.* 16, 173–197.

McQuibban, A. G., Joza, N., Megighian, A., Scorzeto, M., Zanini, D., Reipert, S., et al. (2010). A *Drosophila* mutant of LETM1, a candidate gene for seizures in Wolf-Hirschhorn syndrome. *Hum. Mol. Genet.* 19, 987–1000. doi: 10.1093/hmg/ddp563

Milet, C., and Monsoro-Burq, A.-H. (2014). Dissection of *Xenopus laevis* neural crest for *in vitro* explant culture or *in vivo* transplantation. *J. Vis. Exp*. 85:e51118. doi: 10.3791/51118

Mills, A., Bearce, E., Cella, R., Kim, S. W., Selig, M., Lee, S., et al. (2019). Wolf-Hirschhorn Syndrome-associated genes are enriched in motile neural crest and affect craniofacial development in *Xenopus laevis*. *Front. Physiol.* 10:431. doi: 10.3389/fphys.2019.00431

Mimoto, M. S., and Christian, J. L. (2011). Manipulation of gene function in *Xenopus laevis*. *Methods Mol. Biol.* 770, 55–75. doi: 10.1007/978-1-61779-210-6_3

Monsoro-Burq, A. -H., Wang, E., and Harland, R. (2005). *Msx1* and *Pax3* cooperate to mediate FGF8 and WNT signals during *Xenopus* neural crest induction. *Dev. Cell* 8, 167–178. doi: 10.1016/j.devcel.2004.12.017

Moody, S. A. (2018a). Lineage tracing and fate mapping in *Xenopus* embryos. *Cold Spring Harb. Protoc*. 2018:db.rot097253.

Moody, S. A. (2018b). Microinjection of mRNAs and oligonucleotides. *Cold Spring Harb. Protoc*. 2018:db.rot097261.

Nakano, Y., Fujita, M., Ogino, K., Saint-Amant, L., Kinoshita, T., Oda, Y., et al. (2010). Biogenesis of GPI-anchored proteins is essential for surface expression of sodium channels in zebrafish Rohon-Beard neurons to respond to mechanosensory stimulation. *Development* 137, 1689–1698. doi: 10.1242/dev.047464

Nakayama, T., Fish, M. B., Fisher, M., Oomen-Hajagos, J., Thomsen, G. H., and Grainger, R. M. (2013). Simple and efficient CRISPR/Cas9-mediated targeted mutagenesis in *Xenopus tropicalis*. *Genesis* 51, 835–843. doi: 10.1002/dvg.22720

Narita, T., Yung, T. M. C., Yamamoto, J., Tsuboi, Y., Tanabe, H., Tanaka, K., et al. (2007). NELF interacts with CBC and participates in 3' end processing of replication-dependent histone mRNAs. *Mol. Cell* 26, 349–365. doi: 10.1016/j.molcel.2007.04.011

Nieminen, P., Kotilainen, J., Aalto, Y., Knuutila, S., Pirinen, S., and Thesleff, I. (2003). *MSX1* gene is deleted in Wolf-Hirschhorn syndrome patients with oligodontia. *J. Dent. Res.* 82, 1013–1017. doi: 10.1177/154405910308201215

Nieuwkoop, P. D., and Faber, J. (1994). *Normal Table of Xenopus Laevis (Daudin): A Systematical and Chronological Survey of the Development From the Fertilized Egg Till the End of Metamorphosis*. (New York, NY: Garland Pub).

Nimura, K., Ura, K., Shiratori, H., Ikawa, M., Okabe, M., Schwartz, R. J., et al. (2009). A histone H3 lysine 36 trimethyltransferase links Nkx2-5 to Wolf-Hirschhorn syndrome. *Nature* 460, 287–291. doi: 10.1038/nature08086

Nwagbara, B. U., Faris, A. E., Bearce, E. A., Erdogan, B., Ebbert, P. T., Evans, M. F., et al. (2014). TACC3 is a microtubule plus end-tracking protein that promotes axon elongation and also regulates microtubule plus end dynamics in multiple embryonic cell types. *Mol. Biol. Cell* 25, 3350–3362. doi: 10.1091/mbc.E14-06-1121

Paradowska-Stolarz, A. M. (2014). Wolf-Hirschhorn syndrome (WHS) - literature review on the features of the syndrome. *Adv. Clin. Exp. Med.* 23, 485–489. doi: 10.17219/acem/24111

Peset, I., and Vernos, I. (2008). The TACC proteins: TACC-ling microtubule dynamics and centrosome function. *Trends Cell Biol.* 18, 379–388. doi: 10.1016/j.tcb.2008.06.005

Pratt, K. G., and Khakhalin, A. S. (2013). Modeling human neurodevelopmental disorders in the *Xenopus* tadpole: from mechanisms to therapeutic targets. *Dis. Model. Mech.* 6, 1057–1065. doi: 10.1242/dmm.012138

Redler, S., Strom, T. M., Wieland, T., Cremer, K., Engels, H., Distelmaier, F., et al. (2017). Variants in CPLX1 in two families with autosomal-recessive severe infantile myoclonic epilepsy and ID. *Eur. J. Hum. Genet.* 25, 889–893. doi: 10.1038/ejhg.2017.52

Rutherford, E. L., and Lowery, L. A. (2016). Exploring the developmental mechanisms underlying Wolf-Hirschhorn Syndrome: evidence for defects in neural crest cell migration. *Dev. Biol.* 420, 1–10. doi: 10.1016/j.ydbio.2016.10.012

Sato, A., Scholl, A. M., Kuhn, E. N., Kuhn, E. B., Stadt, H. A., Decker, J. R., et al. (2011). FGF8 signaling is chemotactic for cardiac neural crest cells. *Dev. Biol.* 354, 18–30. doi: 10.1016/j.ydbio.2011.03.010

Satokata, I., and Maas, R. (1994). Msx1 deficient mice exhibit cleft palate and abnormalities of craniofacial and tooth development. *Nat. Genet.* 6, 348–356. doi: 10.1038/ng0494-348

Session, A. M., Uno, Y., Kwon, T., Chapman, J. A., Toyoda, A., Takahashi, S., et al. (2016). Genome evolution in the allotetraploid frog *Xenopus laevis*. *Nature* 538, 336–343. doi: 10.1038/nature19840

Shellard, A., and Mayor, R. (2016). Chemotaxis during neural crest migration. *Semin. Cell Dev. Biol.* 55, 111–118. doi: 10.1016/j.semcdb.2016.01.031

Sheth, F., Akinde, O. R., Datar, C., Adeteye, O. V., and Sheth, J. (2012). Genotype-phenotype characterization of Wolf-Hirschhorn syndrome confirmed by FISH: case reports. *Case Rep. Genet.* 2012:878796. doi: 10.1155/2012/878796

Simon, R., and Bergemann, A. D. (2008). Mouse models of Wolf-Hirschhorn syndrome. *Am. J. Med. Genet. C Semin. Med. Genet.* 148C, 275–280. doi: 10.1002/ajmg.c.30184

Sive, H. L., Grainger, R. M., and Harland, R. M. (2007a). Inducing ovulation in *Xenopus laevis*. *CSH Protoc.* 2007:db.rot4734.

Sive, H. L., Grainger, R. M., and Harland, R. M. (2007b). *Xenopus laevis* in vitro fertilization and natural mating methods. *CSH Protoc.* 2007:db.rot4737. doi: 10.1101/pdb.prot4737

Slater, P. G., Hayrapetian, L., and Lowery, L. A. (2017). *Xenopus laevis* as a model system to study cytoskeletal dynamics during axon pathfinding. *Genesis* 55:e22994. doi: 10.1002/dvg.22994

Sojka, S., Amin, N. M., Gibbs, D., Christine, K. S., Charpentier, M. S., and Conlon, F. L. (2014). Congenital heart disease protein 5 associates with CASZ1 to maintain myocardial tissue integrity. *Development* 141, 3040–3049. doi: 10.1242/dev.106518

Stec, I., Wright, T. J., van Ommen, G. J., de Boer, P. A., van Haeringen, A., Moorman, A. F., et al. (1998). WHSC1, a 90 kb SET domain-containing gene, expressed in early development and homologous to a *Drosophila* dysmorphy gene maps in the Wolf-Hirschhorn syndrome critical region and is fused to IgH in t(4;14) multiple myeloma. *Hum. Mol. Genet.* 7, 1071–1082. doi: 10.1093/hmg/7.7.1071

Sun, J., and Li, R. (2010). Human negative elongation factor activates transcription and regulates alternative transcription initiation. *J. Biol. Chem.* 285, 6443–6452. doi: 10.1074/jbc.M109.084285

Szabó, A., Melchionda, M., Nastasi, G., Woods, M. L., Campo, S., Perris, R., et al. (2016). In vivo confinement promotes collective migration of neural crest cells. *J. Cell Biol.* 213, 543–555. doi: 10.1083/jcb.201602083

Tahir, R., Kennedy, A., Elsea, S. H., and Dickinson, A. J. (2014). Retinoic acid induced-1 (Rai1) regulates craniofacial and brain development in *Xenopus*. *Mech. Dev.* 133, 91–104. doi: 10.1016/j.mod.2014.05.004

Tandon, P., Conlon, F., Furlow, J. D., and Horb, M. E. (2017). Expanding the genetic toolkit in *Xenopus*: approaches and opportunities for human disease modeling. *Dev. Biol.* 426, 325–335. doi: 10.1016/j.ydbio.2016.04.009

Tandon, P., Showell, C., Christine, K., and Conlon, F. L. (2012). Morpholino injection in *Xenopus*. *Methods Mol. Biol.* 843, 29–46. doi: 10.1007/978-1-61779-523-7_4

Theveneau, E., and Mayor, R. (2011). Beads on the run: beads as alternative tools for chemotaxis assays. *Methods Mol. Biol.* 769, 449–460. doi: 10.1007/978-1-61779-207-6_30

Theveneau, E., Steventon, B., Scarpa, E., Garcia, S., Trepat, X., Streit, A., et al. (2013). Chase-and-run between adjacent cell populations promotes directional collective migration. *Nat. Cell Biol.* 15, 763–772. doi: 10.1038/ncb2772

Toyokawa, G., Cho, H.-S., Masuda, K., Yamane, Y., Yoshimatsu, M., Hayami, S., et al. (2011). Histone lysine methyltransferase Wolf-Hirschhorn syndrome candidate 1 is involved in human carcinogenesis through regulation of the Wnt pathway. *Neoplasia* 13, 887–898.

Wallmeier, J., Shiratori, H., Dougherty, G. W., Edelbusch, C., Hjeij, R., Loges, N. T., et al. (2016). TTC25 deficiency results in defects of the outer dynein arm docking machinery and primary ciliary dyskinesia with left-right body asymmetry randomization. *Am. J. Hum. Genet.* 99, 460–469. doi: 10.1016/j.ajhg.2016.06.014

Wang, F., Shi, Z., Cui, Y., Guo, X., Shi, Y.-B., and Chen, Y. (2015). Targeted gene disruption in *Xenopus laevis* using CRISPR/Cas9. *Cell Biosci.* 5:15.

Willsey, H. R., Walentek, P., Exner, C. R. T., Xu, Y., Lane, A. B., Harland, R. M., et al. (2018). Katanin-like protein Katnal2 is required for ciliogenesis and brain development in *Xenopus* embryos. *Dev. Biol.* 442, 276–287. doi: 10.1016/j.ydbio.2018.08.002

Yamada-Okabe, T., Imamura, K., Kawaguchi, N., Sakai, H., Yamashita, M., and Matsumoto, N. (2010). Functional characterization of the zebrafish WHSC1-related gene, a homolog of human NSD2. *Biochem. Biophys. Res. Commun.* 402, 335–339. doi: 10.1016/j.bbrc.2010.10.027

Yung, T. M. C., Narita, T., Komori, T., Yamaguchi, Y., and Handa, H. (2009). Cellular dynamics of the negative transcription elongation factor NELF. *Exp. Cell Res.* 315, 1693–1705. doi: 10.1016/j.yexcr.2009.02.013

Zahn, N., Levin, M., and Adams, D. S. (2017). The Zahn drawings: new illustrations of Xenopus embryo and tadpole stages for studies of craniofacial development. *Development* 144, 2708–2713. doi: 10.1242/dev.151308

Zhang, X.-L., Huang, C.-X., Zhang, J., Inoue, A., Zeng, S.-E., and Xiao, S.-J. (2013). CtBP1 is involved in epithelial-mesenchymal transition and is a potential therapeutic target for hepatocellular carcinoma. *Oncol. Rep.* 30, 809–814. doi: 10.3892/or.2013.2537

Zhang, Z., Song, Y., Zhao, X., Zhang, X., Fermin, C., and Chen, Y. (2002). Rescue of cleft palate in Msx1-deficient mice by transgenic Bmp4 reveals a network of BMP and Shh signaling in the regulation of mammalian palatogenesis. *Development* 129, 4135–4146.

Zollino, M., Orteschi, D., Ruiter, M., Pfundt, R., Steindl, K., Cafiero, C., et al. (2014). Unusual 4p16.3 deletions suggest an additional chromosome region for the Wolf-Hirschhorn syndrome-associated seizures disorder. *Epilepsia* 55, 849–857. doi: 10.1111/epi.12617

Conflict of Interest Statement: The authors declare that the research was conducted in the absence of any commercial or financial relationships that could be construed as a potential conflict of interest.

frontiers in Physiology

MINI REVIEW
published: 30 July 2019
doi: 10.3389/fphys.2019.00953

Xenopus: Driving the Discovery of Novel Genes in Patient Disease and Their Underlying Pathological Mechanisms Relevant for Organogenesis

*Woong Y. Hwang†, Jonathan Marquez† and Mustafa K. Khokha**

Department of Pediatrics and Genetics, The Pediatric Genomics Discovery Program, Yale University School of Medicine, New Haven, CT, United States

OPEN ACCESS

Edited by:
Timothy J. Moss, Hudson Institute of Medical Research, Australia

Reviewed by:
Peter Walentek, Freiburg University Medical Center, Germany
André Brändli, Ludwig Maximilian University of Munich, Germany

***Correspondence:**
Mustafa K. Khokha
Mustafa.Khokha@yale.edu

†These authors have contributed equally to this work

Specialty section:
This article was submitted to Embryonic and Developmental Physiology, a section of the journal Frontiers in Physiology

Received: *30 October 2018*
Accepted: *09 July 2019*
Published: *30 July 2019*

Citation:
Hwang WY, Marquez J and Khokha MK (2019) Xenopus: Driving the Discovery of Novel Genes in Patient Disease and Their Underlying Pathological Mechanisms Relevant for Organogenesis. Front. Physiol. 10:953. doi: 10.3389/fphys.2019.00953

Frog model organisms have been appreciated for their utility in exploring physiological phenomena for nearly a century. Now, a vibrant community of biologists that utilize this model organism has poised *Xenopus* to serve as a high throughput vertebrate organism to model patient-driven genetic diseases. This has facilitated the investigation of effects of patient mutations on specific organs and signaling pathways. This approach promises a rapid investigation into novel mechanisms that disrupt normal organ morphology and function. Considering that many disease states are still interrogated *in vitro* to determine relevant biological processes for further study, the prospect of interrogating genetic disease in *Xenopus in vivo* is an attractive alternative. This model may more closely capture important aspects of the pathology under investigation such as cellular micro environments and local forces relevant to a specific organ's development and homeostasis. This review aims to highlight recent methodological advances that allow investigation of genetic disease in organ-specific contexts in *Xenopus* as well as provide examples of how these methods have led to the identification of novel mechanisms and pathways important for understanding human disease.

Keywords: *Xenopus*, gene discovery, organogenesis, disease model, mechanism discovery, genetics of congenital malformations, birth defects

INTRODUCTION

The frog has served as a powerful tool for understanding human physiology dating back to early efforts in biomedical research. Many researchers found this model appealing due to its prevalence as a pregnancy test (Elkan, 1938). Injected human chorionic gonadotrophin induces ovulation and facilitates fertilization of a large number of embryos for experimentation. Subsequently, there has been an ongoing effort to develop methods to interrogate biology in the *Xenopus* embryo. Recently,

next generation sequencing technologies have allowed researchers to rapidly amass a compendium of candidate gene variants that are putatively disease causing (Zaidi et al., 2013; Glessner et al., 2014; Homsy et al., 2015; Sifrim et al., 2016; Jin et al., 2017; Li et al., 2017; Manheimer et al., 2018). A major challenge is annotating these candidate genes with pathogenesis mechanisms. While statistical analysis of variants and computational approaches to predict mutational effect are necessary to identify putative disease-causing patient variants, many of the candidate genes have no known relevant biological function suggestive of its role in disease pathogenesis. Therefore, there is a pressing need for model systems to decipher these mechanisms. This is where patient driven gene discovery and disease modeling in *Xenopus* have proven fruitful.

SCREENING AND EVALUATION OF PATIENT VARIANTS

Xenopus tadpoles develop most organs in just 3 days and the cell fate map for each organ system is well defined, so rapid phenotyping in knockout animals is possible (Moody, 1987). In fact, several gene knockout *Xenopus* lines are available to researchers through the community resources Xenbase and the international *Xenopus* resource centers (**Table 2**). In addition, the ability to manipulate only one side of the embryos and use the un-injected side as an internal control by one of two cell injection strategy has rendered *Xenopus* as a useful model to decipher disease mechanisms of patient variants.

Also, advances in CRISPR/Cas9 technology allow screening genes for disease relevance rapidly and inexpensively. The efficiency of knockout through CRISPR/Cas9 targeting is sufficient for screening in the F0 population of *Xenopus* embryos (Blitz et al., 2013; Bhattacharya et al., 2015). These F0 mosaic knockouts can also be used as founders to establish mutant lines. Community created resources such as CRISPR Scan (Moreno-Mateos et al., 2015) which can facilitate targeting specific loci and avoiding off target effects (Doench et al., 2014) have greatly simplified CRISPR based gene depletion experiments. Various tools are available to assess CRISPR genome editing efficiency, such as tracking of indels by decomposition (Etard et al., 2017). Off target effects can also be further evaluated by designing multiple non-overlapping sgRNAs to verify that multiple gene disruptions lead to similar phenotypes. Alternatively, complementary methods such as the use of morpholino oligos can similarly validate the phenotypic effects of CRISPR in F0 knockout screens. Subsequently, to test the specificity of targeted gene depletion strategies, human derived mRNA can be co-injected to rescue a mutated phenotype.

While results for CRISPR based knock-in technologies look promising in *Xenopus* (Aslan et al., 2017), knock-ins of human gene variants have not yet been fully utilized. On the other hand, to test patient variants for pathology, gene depletion followed by rescue with either wildtype human mRNA or patient variant mRNA has been effective and highly efficient (Braun et al., 2018; Kulkarni et al., 2018). Another limitation of the *Xenopus* model is a lack of antibodies available to detect *Xenopus* proteins, and there is an on-going concerted effort to produce monoclonal antibodies which will be freely shared with the *Xenopus* research community (personal communication D. Alfandari).

EMERGING METHODS IN EVALUATING EFFECTS OF GENETIC MANIPULATIONS IN ORGANOGENESIS

Cardiac Morphogenesis

Xenopus is well suited for studying heart development as, unlike mice, *Xenopus* embryos do not require functional blood circulation for early cardiac development. This permits analysis of mutations that would prove embryonic lethal in mice. Additionally, the optical transparency which persists throughout early organogenesis enables assessment of morphological heart defects via multiple live imaging strategies (**Figure 1**).

Through targeted genome editing and a fate mapping, early heart developmental processes are well outlined in *Xenopus*. Similar to mammals, *Xenopus* heart development begins with pre-cardiac mesoderm formation during gastrulation (Sater and Jacobson, 1989). Cardiac precursor cells then migrate toward the ventral midline where they subsequently become specified as cardiac progenitor cells in two lineages: the first and second heart fields. These two heart fields undergo further remodeling to become two-atria/one ventricle and the outflow tract, respectively (Buckingham et al., 2005; Gessert and Kuhl, 2009). Several transgenic *Xenopus* lines have been engineered

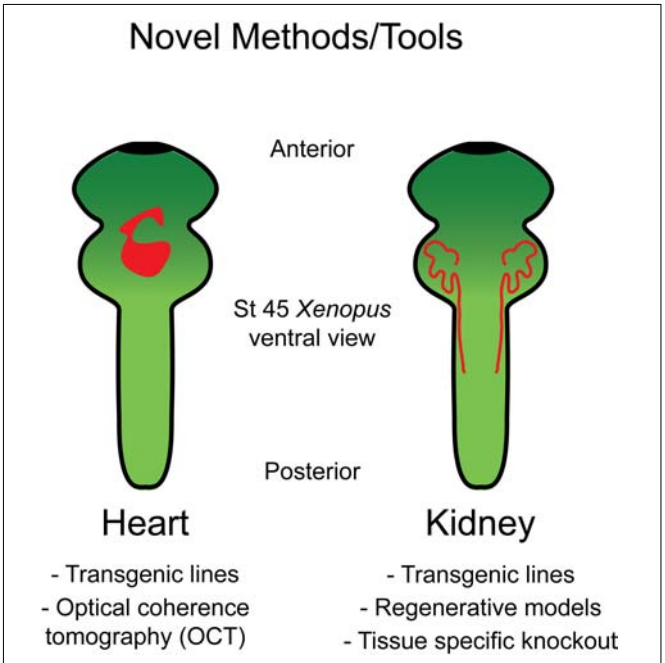

FIGURE 1 | Tools in *Xenopus* allow for the study of heart and kidney development. Schematic of the organ systems in *Xenopus* along with available tools to interrogate these systems.

TABLE 1 | Transgenic lines discussed in this review.

Transgenic line	Development	Proposed utility
Tg(nkx2.5:GFP)	Approx. 7.3 kb upstream of transcriptional start site of nkx2.5 (GU573788) fused to GFP. This region should contain the nkx2.5 promoter	Early heart field studies
Tg(mlc3:GFP)	8 kb of promoter of the *X. laevis* MLClv (myosin light chain 3) gene driving expression of EGFP (note MLClv synonym for = mlc3)	Myocardium studies
Tg(smad3:eGFP)	1.5 kb of promoter of the *X. laevis* smad3 gene driving expression of eGFP	Endocardium studies
Tg(WntREs:dEGFP)	7 copies of a TCF/LEF1 binding DNA element, a minimal TATA box and a reporter gene encoding destabilized eGFP and a polyA sequence	Wnt signaling in cardiogenesis
Tg(Dre.cdhl7:eGFP)	Approximately a 4.3 kb genomic fragment upstream of the Danio rerio cdhl7 driving expression of EGFP	Pronephric development

TABLE 2 | A subset of mutant lines of interest to disease processes in the National *Xenopus* Resource Database.

Organ of interest	Mutation	Species	Associated human disease
Kidney	Pkhd1L	*X. Laevis*	Autosomal Recessive Polycystic Kidney Disease
	pkd2.L	*X. Laevis*	Polycystic Kidney Disease 2
	wdpcp.L	*X. Laevis*	Bardet-Biedl syndrome (ciliopathic genetic disorder that affects many parts of body including kidney failure)
	eya1.L	*X. Laevis*	Branchio-oto-renal syndrome
Heart	tbx5	*X. Tropicalis*	Hold-Oram syndrome (cardiac-limb syndrome)
	gdf1	*X.Tropicalis*	Double outlet right ventricle, tetralogy of Fallot, Right atrial isomerism
	lmna	*X. Tropicalis*	dilated cardiomyopathy
	myh6	*X.Tropicalis*	familial hypertrophic cardiomyopathy, dilated cardiomyopathy, atrial septal defect

with fluorescent proteins fused to promotor regions of relevant cardiac markers to examine these developmental processes *in vivo*. One *Xenopus* line harbors the promoter of NKX2 fused to GFP and serves as a suitable marker for the early heart field (Sparrow et al., 2000), while MLC1v-GFP and SMAD3-GFP lines prove useful for labeling the myocardium and endocardium, respectively (Smith et al., 2005; Smith and Mohun, 2011; **Table 1**).

Another exciting model is the Wnt reporter line developed in *Xenopus* (7X LEF/TCF-GFP) (Tran et al., 2010; Tran and Vleminckx, 2014; **Table 1**). Both canonical and non-canonical Wnt signaling is spatiotemporally controlled to orchestrate proper cardiac development (Nakamura et al., 2003; Naito et al., 2006; Tzahor, 2007; Ueno et al., 2007; Gessert and Kuhl, 2010). In the context of left-right patterning, Wnt and serotonin signaling were found to be crucial for left-right organizer (LRO) specification and differentiation (Nascone and Mercola, 1997; Beyer et al., 2012). In particular, Wnt direct target gene, *foxj1,* expression is up-regulated in ATP4a dependent manner that consequently controls motile ciliogenesis in the LRO (Walentek et al., 2012). Left–right patterning in turn has far reaching consequences for cardiogenesis (Reviewed in Duncan and Khokha, 2016; Garfinkel and Khokha, 2017). Wnt action during cardiogenesis can be divided into four stages. First, high levels of Wnt/β-catenin activity is required for the formation of prospective heart mesoderm (Smith and Howard, 1992; Antin et al., 1994). Once cardiac mesodermal cells colonize the ventral midline, Wnt signaling is damped down allowing for cardiac specification and generation of multi-potent progenitor cells (Marvin et al., 2001; Schneider and Mercola, 2001). Shortly thereafter, Wnt signaling is up-regulated for the expansion and proliferation of cardiogenic progenitor cells and repressed again for terminal differentiation of cardiomyocytes (Ai et al., 2007; Kwon et al., 2007). As the role of Wnt signaling in cardiac development is both dynamic and complex, further investigation is warranted in this *Xenopus* Wnt reporter line. Exemplifying the utility of this model, recent work using this Wnt transgenic *Xenopus* line has comprehensively delineated the spatial and temporal dynamics of Wnt signaling through whole-mount *in situ* hybridization and cross-sectioning of embryos (Borday et al., 2018).

Lastly, optical coherence tomography (OCT) has recently been employed as a reliable and efficient imaging modality to assess cardiac structural anomalies in *Xenopus* tadpoles (Deniz et al., 2017). OCT uses coherent light waves to capture cross-sectional images of tissues in live embryos (Kagemann et al., 2008). OCT can thus comprehensively measure *Xenopus* cardiac structures including the atria, trabeculated ventricle, atrioventricular valve, and the diameter of outflow tract. As evidence of its utility, depletion of the myosin heavy chain 6 (myh6) gene which has been shown to have variants that cause human cardiomyopathy (Abu-Daya et al., 2009) was employed in *Xenopus* embryos. OCT imaging of these embryos yielded successful dynamic assessment of cardiac defects such as dysregulated AV valve excursion times (Deniz et al., 2017). Overall, OCT and cardiac fluorescent transgenic models maximize the power of the optical transparency in *Xenopus* embryos by allowing for dynamic live imaging and observation of cardiac development at both cellular and sub-cellular levels.

Kidney Morphogenesis

The embryonic kidney in *Xenopus* consists of a pronephros that is simplistic compared to human metanephroi (Fox and Hamilton, 1964; Vize et al., 1995); however, this provides a straightforward structure that can be readily interrogated (**Figure 1**). Additionally, regions of the pronephros correspond to regions of the human metanephros based on function and patterns of gene expression (Carroll and Vize, 1999; Carroll et al., 1999; Wild et al., 2000; Saulnier et al., 2002; Zhou and

Vize, 2004; Alarcon et al., 2008; Raciti et al., 2008; Buisson et al., 2015). Although the whole mount *in situ* hybridization has been used to interrogate the pronephros based on expression, new tools allow kidney research to observe changes *in vivo*. Among these is a transgenic line with GFP fused to Cdh17 that facilitates visualization of the entire pronephros (Corkins et al., 2018; **Table 1**).

Recent efforts in kidney research in *Xenopus* have also yielded models of pronephric regeneration that show great promise (Caine and McLaughlin, 2013). These studies build upon work that has addressed pronephroi as *in vitro* explants (Moriya et al., 1993; Osafune et al., 2002; Asashima et al., 2009). As kidney tissue is susceptible to damage from genetic as well as acquired renal disease, understanding its regenerative potential may allow us to identify methods of recovering tissue function in the context of disease. Additionally, observing regeneration as opposed to organogenesis of the pronephros facilitates uncoupling signaling relevant for the generation of this specific organ from generalized processes of development. Such an approach may be essential for understanding the mechanisms of dysfunction observed due to patient-derived candidate gene variants.

The ability to target specific regions of the developing embryo is a powerful avenue to home in on factors relevant for specific pathways and tissues. Screening candidate genes based on patient variants in the *Xenopus* kidney is no exception. Although F0 CRISPR based knockout of genes is a powerful tool, this has been deployed largely in whole embryo approaches. Developing a tissue-specific targeting strategy is an important next step to screen for organ-specific dysfunction. Fortunately, this has been evaluated precisely in the context of the *Xenopus* pronephros wherein CRISPR/Cas9 was injected in a targeted manner to demonstrate that this technology could be applied in a subset of embryonic blastomeres that give rise to the pronephric tissue (DeLay et al., 2018). This advance shows that despite the mosaicism observed via the targeted use of CRISPR/Cas9 in the F0 generation, this technology can be used to observe downstream consequences of loss of function in particular regions of F0 embryos without the need to raise mutant lines. This may be particularly useful for studying the pronephroi in the context of gene knockout scenarios in which embryonic development is so severely affected as to preclude the study of later organ development. By adopting this approach to limit candidate gene screening to the embryonic kidney, we may be better equipped to answer what role a novel gene is playing in patient disease affecting this organ.

RECENT PATIENT DRIVEN *XENOPUS* STUDIES IN ORGANOGENESIS

Novel Mechanisms in Congenital Heart Disease (CHD)

Congenital heart disease (CHD) is the most prevalent class of birth defects leading to high infant mortality in the United States and yet for the vast majority of cases, the underlying molecular mechanisms remain elusive (Van der Linde et al., 2011; Triedman and Newburger, 2016). However, by coupling cost-effective sequencing technologies to gene editing tools in animal model systems, novel genetic variants from patients can be quickly analyzed *in vivo* in a high-throughput manner. This has been a productive approach in *Xenopus* as candidate genes have been efficiently analyzed for their functional cardiac relevance in *Xenopus* embryos.

For example, *RAPGEF5* which encodes a guanine nucleotide exchange factor for Rap-GTPase was found to have an internal duplication which would likely lead to a null allele in a heterotaxy patient. Depletion of Rapgef5 in *Xenopus* recapitulates the left-right patterning phenotype found in the patient. Unexpectedly, mechanistic studies established that RAPGEF5 regulates left-right patterning via Wnt signaling by regulating the nuclear localization of β-catenin (Griffin et al., 2018). As previously noted, Wnt signaling is critical for proper induction of dorsal mesoderm including cardiac precursors and the LRO. As such, dysregulation of Wnt signaling caused by Rapgef5 knockdown resulted in abnormal LRO formation and cardiac looping phenotypes. Moving beyond CHD, dysregulation of Wnt signaling is implicated in many human diseases especially colorectal cancers (Morin et al., 1997; Cancer Genome Atlas Network, 2012). Therefore, elucidating this transport machinery may lead to novel therapeutic targets for a host of diseases.

Another successful example of modeling heterotaxy candidate genes in *Xenopus* was demonstrated by identifying a novel functional role of inner-ring nucleoporins, Nup188 and Nup93 in the context of cilia. Nup188 and its interactant Nup93 were discovered to localize to the base of cilia suggesting a role outside of the nuclear envelope. Knockdown of these components results in the loss of cilia in the LRO subsequently leading to abnormal heart patterning (Del Viso et al., 2016). Cilia are key cellular structures necessary to generate and sense unidirectional fluid flow and induce asymmetric gene expression for proper organ situs (Wallingford and Mitchell, 2011; Boskovski et al., 2013; Blum et al., 2014; Yoshiba and Hamada, 2014). These studies demonstrate the complex genetic etiology of CHD and the successful use of *Xenopus* to identify and characterize disease mechanisms of pathogenic human variants.

Novel Mechanisms in Congenital Disease of the Kidney

Work utilizing the developing *Xenopus* kidney has led to new roles and mechanisms for candidate genes in kidney development and disease. Congenital anomalies of the kidney and urinary tract (CAKUT) include a wide variety of patient presentations ranging from abnormal kidney and urinary tract size and morphology to tumor growth within this organ system (Rodriguez, 2014). As these anomalies comprise the most common cause of childhood renal failure, high throughout models for candidate CAKUT genes are useful for testing candidate genes and exploring pathogenesis mechanisms.

For example, variants of *NRIP1* were identified in patients with CAKUT (Vivante et al., 2017). These anomalies consisted

of renal hypodysplasia and either vesicoureteral reflux or ectopia. Prior to this work, the mechanism of NRIP1 function in kidney development or even developmental at large was not established. This study also highlights the potential to investigate novel therapeutic pathways for patients in which variants are identified. Since retinoic acid signaling was downregulated by *NRIP1* mutation in this instance, manipulation of retinoic acid dependent pathways is an appealing avenue for therapeutic studies.

Studies of ciliopathies are another excellent example of these efforts. Though ciliopathies affect a wide array of organ systems including the heart (Duncan and Khokha, 2016), the kidney is particularly susceptible to the loss of function of cilia-related proteins. Ciliopathies are a diverse array of diseases caused by disrupted formation and/or function of cilia (Bisgrove and Yost, 2006; Gerdes et al., 2009; Oh and Katsanis, 2012; Werner and Mitchell, 2013; Choksi et al., 2014). Cilia are cellular extensions that have been shown to serve as mediators of extracellular signals in the case of primary cilia (Nachury and Mick, 2019) or a means by which cells coordinate extracellular fluid flow in the case of motile cilia (Mitchison and Valente, 2017). In the kidney, cilia dysfunction often manifests itself as a cystic change in tissue morphology that renders the kidney unable to regulate the urine concentration and hemofiltration (Ma et al., 2017). The mechanisms by which cilia dysfunction leads to this tissue level dysfunction are still not well understood.

In another example of patient driven gene discovery, identifying a role for the DNA repair protein NME3 in cilia established another example for a growing list of ciliopathies (Hoff et al., 2018). Depletion of NME3 resulted in renal malformations and left–right patterning defects typical of ciliopathies in *Xenopus* along with a loss of cilia in complementary vertebrate and cell culture models. The association of NME3 with the ciliary nephronophthisis proteins NEK8, CEP164, and ANKS6 supports its role as a ciliopathy gene. This discovery adds to a growing number of ciliopathy related genes that have known roles away from the cilium but seem to also play an important role when recruited to the cilium. This has far reaching implications for kidney disease biology, as the discovery of new roles and/or localizations for gene products will allow us to harness previous knowledge about these components to understand the disease. Complementarily, subsequent discovery of the proteins' role in kidney morphogenesis may lead to understanding its function in other contexts. In the case of NME3, this work has led to a still evolving connection between primary cilia function and DNA damage repair, which may constitute an even broader pathway important for kidney development and homeostasis.

Similarly, recent studies have implicated mutations in several components of the outer-ring of the nuclear pore complex (NPC) in steroid resistant nephrotic syndrome (SRNS) (Braun et al., 2018). SRNS is a broad category of disease in which the body excessively excretes proteins in the urine thus leading to systemic fluid distribution imbalances and swelling which is most often linked to disruption of the renal vascular interface that functions in podocyte mediated fluid filtration (Dogra and Kaskel, 2017). Variants of outer-ring NUPs were tested in *Xenopus* knockdown models to verify their deleterious status (Braun et al., 2018). This study went on to determine that this effect on kidney morphogenesis is mediated through Cdc42 signaling important for filopodia (Nobes and Hall, 1995). These findings highlight that proteins essential for the function of every cell such as NPC components can still give tissue specific phenotypes suggesting that we have a great deal to learn about the pathogenesis mechanisms of human disease.

Though these studies demonstrate the power that patient driven gene discovery has for assigning disease causing variants in human kidney disease, they also begin to show how this approach aids in discovering novel mechanisms important for kidney morphogenesis and function. Moving forward, the many congenital kidney malformations that affect patients early in life may be an efficient source of genetic information to direct the study of kidney morphogenesis.

CONCLUSION

Sequencing technologies continue to improve in speed, accuracy, and cost. Consequently, rather than phenotype driven therapy, patient genotype can be included in decision-making and treatment options tailored to individuals. However, one major challenge to this approach is determining the biological relevance of each variant as many candidate genes have no known role in disease. Therefore, each variant offers the opportunity for molecular function discovery in animal models. Studying organogenesis in *Xenopus* including that of the heart and kidney will allow us to unravel mechanisms of disease pathogenesis. Analysis of candidate genes in *Xenopus* will not only allow for assessing allele pathogenicity, but also promises to expand our understanding of developmental biology.

AUTHOR CONTRIBUTIONS

All authors wrote and edited the manuscript.

FUNDING

WH and JM are supported by the Yale MSTP NIH T32GM07205 Training Grant, the Yale Predoctoral Program in Cellular and Molecular Biology T32GM007223 Training Grant, and the Paul and Daisy Soros Fellowship for New Americans. WH is also supported by the NIH F30HL143878. MK is supported by the NIH R01HD081379 and R01HL124402. MK was a Mallinckrodt Scholar.

ACKNOWLEDGMENTS

We thank the patients and families who are the inspiration for candidate gene and mechanism discovery. We also thank the many labs involved in developing *Xenopus* as an excellent model for human disease. We unfortunately lack sufficient space to cite all the great work carried out in this growing field.

REFERENCES

Abu-Daya, A., Sater, A. K., Wells, D. E., Mohun, T. J., and Zimmerman, L. B. (2009). Absence of heartbeat in the *Xenopus tropicalis* mutation muzak is caused by a nonsense mutation in cardiac myosin myh6. *Dev. Biol.* 336, 20–29. doi: 10.1016/j.ydbio.2009.09.019

Ai, D., Fu, X., Wang, J., Lu, M. F., Chen, L., Baldini, A., et al. (2007). Canonical Wnt signaling functions in second heart field to promote right ventricular growth. *PNAS* 104, 9319–9324. doi: 10.1073/pnas.0701212104

Alarcon, P., Rodriguez-Seguel, E., Fernandez-Gonzalez, A., Rubio, R., and Gomez-Skarmeta, J. L. (2008). A dual requirement for Iroquois genes during *Xenopus* kidney development. *Development* 135, 3197–3207. doi: 10.1242/dev.023697

Antin, P. B., Taylor, R. G., and Yatskievych, T. (1994). Precardiac mesoderm is specified during gastrulation in quail. *Dev. Dyn.* 200, 144–154. doi: 10.1002/aja.1002000206

Asashima, M., Ito, Y., Chan, T., Michiue, T., Nakanishi, M., Suzuki, K., et al. (2009). In vitro organogenesis from undifferentiated cells in Xenopus. *Dev. Dyn.* 238, 1309–1320. doi: 10.1002/dvdy.21979

Aslan, Y., Tadjuidje, E., Zorn, A. M., and Cha, S. W. (2017). High-efficiency non-mosaic CRISPR-mediated knock-in and indel mutation in F0 *Xenopus*. *Development* 144, 2852–2858. doi: 10.1242/dev.152967

Beyer, T., Danilchik, M., Thumberger, T., Vick, P., Tisler, M., Schneider, I., et al. (2012). Serotonin signaling is required for Wnt-dependent GTP specification and leftward flow in Xenopus. *Curr. Biol.* 22, 33–39. doi: 10.1016/j.cub.2011.11.027

Bhattacharya, D., Marfo, C. A., Li, D., Lane, M., and Khokha, M. K. (2015). CRISPR/Cas9: an inexpensive, efficient loss of function tool to screen human disease genes in *Xenopus*. *Dev. Biol.* 408, 196–204. doi: 10.1016/j.ydbio.2015.11.003

Bisgrove, B. W., and Yost, H. J. (2006). The roles of cilia in developmental disorders and disease. *Development* 133, 4131–4143. doi: 10.1242/dev.02595

Blitz, I. L., Biesinger, J., Xie, X., and Cho, K. W. (2013). Biallelic genome modification in F(0) *Xenopus tropicalis* embryos using the CRISPR/Cas system. *Genesis* 51, 827–834. doi: 10.1002/dvg.22719

Blum, M., Schweickert, A., Vick, P., Wright, C. V. E., and Danilchik, M. V. (2014). Symmetry breakage in the vertebrate embryo: when does it happen and how does it work? *Dev. Biol.* 393, 109–123. doi: 10.1016/j.ydbio.2014.06.014

Borday, C., Parain, K., Tran, H. T., Vleminckx, K., Perron, M., and Monsoro-Burq, A. H. (2018). An atlas of Wnt activity during embryogenesis in *Xenopus Tropicalis*. *PLoS One* 13:e0193606. doi: 10.1371/journal.pone.0193606

Boskovski, M. T., Yuan, S., Pedersen, N. B., Goth, C. K., Makova, S., Clausen, H., et al. (2013). The heterotaxy gene GALNT11 glycosylates Notch to orchestrate cilia type and laterality. *Nature* 504, 456–459. doi: 10.1038/nature12723

Braun, D. A., Lovric, S., Schapiro, D., Schneider, R., Marquez, J., Asif, M., et al. (2018). Mutations in multiple components of the nuclear pore complex cause nephrotic syndrome. *J. Clin. Invest.* 128, 4313–4328. doi: 10.1172/JCI98688

Buckingham, M., Meihac, S., and Zaffran, S. (2005). Building the mammalian heart from two sources of myocardial cells. *Nat. Rev. Genet.* 6, 826–835. doi: 10.1038/nrg1710

Buisson, I., Le Bouffant, R., Futel, M., Riou, J. F., and Umbhauer, M. (2015). Pax8 and Pax2 are specifically required at different steps of *Xenopus* pronephros development. *Dev. Biol.* 397, 175–190. doi: 10.1016/j.ydbio.2014.10.022

Caine, S. T., and McLaughlin, K. A. (2013). Regeneration of functional pronephric proximal tubules after partial nephrectomy in *Xenopus laevis*. *Dev. Dyn.* 242, 219–229. doi: 10.1002/dvdy.23916

Cancer Genome Atlas Network (2012). Comprehensive molecular characterization of human colon and rectal cancer. *Nature* 487, 330–337. doi: 10.1038/nature11252

Carroll, T. J., and Vize, P. D. (1999). Synergism between Pax-8 and lim-1 in embryonic kidney development. *Dev. Biol.* 214, 46–59. doi: 10.1006/dbio.1999.9414

Carroll, T. J., Wallingford, J. B., and Vize, P. D. (1999). Dynamic patterns of gene expression in the developing pronephros of *Xenopus laevis*. *Dev. Genet.* 24, 199–207. doi: 10.1002/(sici)1520-6408(1999)24:3/4<199::aid-dvg3>3.3.co;2-4

Choksi, S. P., Lauter, G., Swoboda, P., and Roy, S. (2014). Switching on cilia: transcriptional networks regulating ciliogenesis. *Development* 141, 1427–1441. doi: 10.1242/dev.074666

Corkins, M. E., Hanania, H. L., Krneta-Stankic, V., DeLay, B. D., Pearl, E. J., Lee, M., et al. (2018). Transgenic *Xenopus laevis* line for in vivo labeling of nephrons within the kidney. *Genes* 9:E197. doi: 10.3390/genes9040197

Del Viso, F., Huang, F., Myers, J., Chalfant, M., Zhang, Y., Reza, N., et al. (2016). Congenital heart disease genetics uncovers context-dependent organization and function of nucleoporins at Cilia. *Dev. Cell* 38, 478–492. doi: 10.1016/j.devcel.2016.08.002

DeLay, B. D., Corkins, M. E., Hanania, H. L., Salanga, M., Deng, J. M., Sudou, N., et al. (2018). Tissue-specific gene inactivation in *Xenopus laevis*: knockout of lhx1 in the kidney with CRISPR/Cas9. *Genetics* 208, 673–686. doi: 10.1534/genetics.117.300468

Deniz, E., Jonas, S., Hooper, M., Griffin, J. N., Choma, M. A., and Khokha, M. K. (2017). Analysis of craniocardiac malformations in *Xenopus* using optical coherence tomography. *Sci. Rep.* 7:42506. doi: 10.1038/srep42506

Doench, J. G., Hartenian, E., Graham, D. B., Tothova, Z., Hegde, M., Smith, I., et al. (2014). Rational design of highly active sgRNAs for CRISPR-Cas9-mediated gene inactivation. *Nat. Biotechnol.* 32, 1262–1267. doi: 10.1038/nbt.3026

Dogra, S., and Kaskel, F. (2017). Steroid-resistant nephrotic syndrome: a persistent challenge for pediatric nephrology. *Pediatr. Nephrol.* 32, 965–974. doi: 10.1007/s00467-016-3459-5

Duncan, A. R., and Khokha, M. K. (2016). Xenopus as a model organism for birth defects-congenital heart disease and heterotaxy. *Semin. Cell Dev. Biol.* 51, 73–79. doi: 10.1016/j.semcdb.2016.02.022

Elkan, E. R. (1938). The Xenopus pregnancy test. *Br. Med. J.* 2, 1253–1256, 1274–2.

Etard, C., Joshi, S., Stegmaier, J., Mikut, R., and Strahle, U. (2017). Tracking of indels by decomposition is a simple and effective method to assess efficiency of Guide RNAs in Zebrafish. *Zebrafish* 14, 586–588. doi: 10.1089/zeb.2017.1454

Fox, H., and Hamilton, L. (1964). Origin of the pronephric duct in *Xenopus Laevis*. *Arch. Biol.* 75, 245–251.

Garfinkel, A. M., and Khokha, M. K. (2017). An interspecies heart to heart: using *Xenopus* to uncover the genetic basis of congenital heart disease. *Curr. Pathobiol. Rep.* 5, 187–196. doi: 10.1007/s40139-017-0142-x

Gerdes, J. M., Davis, E. E., and Katsanis, N. (2009). The vertebrate primary cilium in development, homeostasis, and disease. *Cell* 137, 32–45. doi: 10.1016/j.cell.2009.03.023

Gessert, S., and Kuhl, M. (2009). Comparative gene expression analysis and fate mapping studies suggest an early segregation of cardiogenic lineages in *Xenopus laevis*. *Dev. Biol.* 334, 395–408. doi: 10.1016/j.ydbio.2009.07.037

Gessert, S., and Kuhl, M. (2010). The multiple phases and faces of Wnt signaling during cardiac differentiation and development. *Circ. Res.* 107, 186–199. doi: 10.1161/CIRCRESAHA.110.221531

Glessner, J. T., Bick, A. G., Ito, K., Homsy, J., Rodriguez-Murillo, L., Fromer, M., et al. (2014). Increased frequency of de novo copy number variants in congenital heart disease by integrative analysis of single nucleotide polymorphism array and exome sequence data. *Circ. Res.* 115, 884–896. doi: 10.1161/CIRCRESAHA.115.304458

Griffin, J. N., Del Viso, F., Duncan, A. R., Robson, A., Hwang, W., Kulkarni, S., et al. (2018). RAPGEF5 regulates nuclear translocation of beta-catenin. *Dev. Cell* 44, 248–260. doi: 10.1016/j.devcel.2017.12.001

Hoff, S., Epting, D., Falk, N., Schroda, S., Braun, D. A., Halbritter, J., et al. (2018). The nucleoside diphosphate kinase NME3 associates with nephronophthisis proteins, and is required for ciliary function during renal development. *J. Biol. Chem.* 293, 15243–15255. doi: 10.1074/jbc.RA117.000847

Homsy, J., Zaidi, S., Shen, Y., Ware, J. S., Samocha, K. E., Karczewski, K. J., et al. (2015). De novo mutations in congenital heart disease with neurodevelopmental and other congenital anomalies. *Science* 350, 1262–1266. doi: 10.1126/science.aac9396

Jin, S. C., Homsy, J., Zaidi, S., Lu, Q., Morton, S., DePalma, S. R., et al. (2017). Contribution of rare inherited and de novo variants in 2,871 congenital heart disease probands. *Nat. Genet.* 49, 1593–1601. doi: 10.1038/ng.3970

Kagemann, L., Ishikawa, H., Zou, J., Charukamnoetkanok, P., Wollstein, G., Townsend, K. A., et al. (2008). Repeated noninvasive high resolution spectral domain optical coherence tomography imaging of zebrafish embryos. *Mol. Vis.* 14, 2157–2170.

Kulkarni, S. S., Griffin, J. N., Date, P. P., Liem, K. F., and Khokha, M. K. (2018). WDR5 stabilizes actin architecture to promote multiciliated cell formation. *Dev. Cell* 46, 595–610. doi: 10.1016/j.devcel.2018.08.009

Kwon, C., Arnold, J., Hsiao, E. C., Taketo, M. M., Conklin, B. R., and Srivastava, D. (2007). Canonical Wnt signaling is a positive regulator of mammalian cardiac progenitors. *PNAS* 104, 10894–10899. doi: 10.1073/pnas.0704044104

Li, A. H., Hanchard, N. A., Furthner, D., Fernbach, S., Azamian, M., Nicosia, A., et al. (2017). Whole exome sequencing in 342 congenital cardiac left sided lesion cases reveals extensive genetic heterogeneity and complex inheritance patterns. *Genome Med.* 9:95. doi: 10.1186/s13073-017-0482-5

Ma, M., Gallagher, A. R., and Somlo, S. (2017). Ciliary mechanisms of cyst formation in polycystic kidney disease. *Cold Spring Harb. Perspect. Biol.* 9:a028209. doi: 10.1101/cshperspect.a028209

Manheimer, K. B., Richter, F., Edelmann, L. J., D'Souza, S. L., Shi, L., Shen, Y., et al. (2018). Robust identification of mosaic variants in congenital heart disease. *Hum. Genet.* 137, 183–193. doi: 10.1007/s00439-018-1871-6

Marvin, M. J., Di Rocco, G., Gardiner, A., Bush, S. M., and Lassar, A. B. (2001). Inhibition of Wnt activity induces heart formation from posterior mesoderm. *Genes Dev.* 15, 316–327. doi: 10.1101/gad.855501

Mitchison, H. M., and Valente, E. M. (2017). Motile and non-motile cilia in human pathology: from function to phenotypes. *J. Pathol.* 241, 294–309. doi: 10.1002/path.4843

Moody, S. A. (1987). Fates of the blastomeres of the 16-cell stage Xenopus embryo. *Dev. Biol.* 119, 560–578. doi: 10.1016/0012-1606(87)90059-5

Moreno-Mateos, M. A., Vejnar, C. E., Beaudoin, J. D., Fernandez, J. P., Mis, E. K., Khokha, M. K., et al. (2015). CRISPRscan: designing highly efficient sgRNAs for CRISPR-Cas9 targeting in vivo. *Nat. Methods* 12, 982–988. doi: 10.1038/nmeth.3543

Morin, P. J., Sparks, A. B., Korinek, V., Barker, N., Clevers, H., Vogelstein, B., et al. (1997). Activation of beta-catenin-Tcf signaling in colon cancer by mutations in beta-catenin or APC. *Science* 275, 1787–1790. doi: 10.1126/science.275.5307.1787

Moriya, N., Uchiyama, H., and Asashima, M. (1993). Induction of pronephric tubules by activin and retinoic acid in presumptive ectoderm of *Xenopus laevis*. *Dev. Growth Differ.* 35, 123–128. doi: 10.1111/j.1440-169x.1993.00123.x

Nachury, M. V., and Mick, D. U. (2019). Establishing and regulating the composition of cilia for signal transduction. *Nat. Rev. Mo. Cell Biol.* 20, 389–405. doi: 10.1038/s41580-019-0116-4

Naito, A. T., Shiojima, I., Akazawa, H., Hidaka, K., Morisaki, T., Kikuchi, A., et al. (2006). Developmental stage-specific biphasic roles of Wnt/beta-catenin signaling in cardiomyogenesis and hematopoiesis. *PNAS* 103, 19812–19817. doi: 10.1073/pnas.0605768103

Nakamura, T., Sano, M., Songyang, Z., and Schneider, M. D. (2003). A Wnt and beta-catenin dependent pathway for mammalian cardiac myogenesis. *PNSA* 100, 5834–5839. doi: 10.1073/pnas.0935626100

Nascone, N., and Mercola, M. (1997). Organizer induction determines left-right asymmetry in *Xenopus*. *Dev. Biol.* 189, 68–78. doi: 10.1006/dbio.1997.8635

Nobes, C. D., and Hall, A. (1995). Rho, rac and cdc42 GTPases: regulators of actin structures, cell adhesion and motility. *Biochem. Soc. Trans.* 23, 456–459. doi: 10.1042/bst0230456

Oh, E. C., and Katsanis, N. (2012). Cilia in vertebrate development and disease. *Development* 139, 443–448. doi: 10.1242/dev.050054

Osafune, K., Nishinakamura, R., Komazaki, S., and Asashima, M. (2002). In vitro induction of the pronephric duct in *Xenopus* explants. *Dev. Growth Differ.* 44, 161–167. doi: 10.1046/j.1440-169x.2002.00631.x

Raciti, D., Reggiani, L., Geffers, L., Jiang, Q., Bacchion, F., Subrizi, A. E., et al. (2008). Organization of the pronephric kidney revealed by large-scale gene expression mapping. *Genome Biol* 9:R84. doi: 10.1186/gb-2008-9-5-r84

Rodriguez, M. M. (2014). Congenital anomalies of the kidney and the urinary tract (CAKUT). *Fetal Pediatr. Pathol.* 33, 293–320. doi: 10.3109/15513815.2014.959678

Sater, A. K., and Jacobson, A. G. (1989). The specification of heart mesoderm occurs during gastrulation in *Xenopus laevis*. *Development* 105, 821–830.

Saulnier, D. M., Ghanbari, H., and Brandli, A. W. (2002). Essential function of Wnt-4 for tubulogenesis in the *Xenopus* pronephric kidney. *Dev. Biol.* 248, 13–28. doi: 10.1006/dbio.2002.0712

Schneider, V. A., and Mercola, M. (2001). Wnt antagonism initiates cardiogenesis in *Xenopus laevis*. *Genes Dev.* 15, 304–315. doi: 10.1101/gad.855601

Sifrim, A., Hitz, M. P., Wilsdon, A., Breckpot, J., Turki, S. H., Thienpont, B., et al. (2016). Distinct genetic architectures for syndromic and nonsyndromic congenital heart defects identified by exome sequencing. *Nat. Genet.* 48, 1060–1065. doi: 10.1038/ng.3627

Smith, J. C., and Howard, J. E. (1992). Mesoderm-inducing factors and the control of gastrulation. *Development* 116, 127–136.

Smith, S. J., Ataliotis, P., Kotecha, S., Towers, N., Sparrow, D. B., and Mohun, T. J. (2005). The MLC1v gene provides a transgenic marker of myocardium formation within developing chambers of the *Xenopus* Heart. *Dev. Dyn.* 232, 1003–1012. doi: 10.1002/dvdy.20274

Smith, S. J., and Mohun, T. J. (2011). Early cardiac morphogenesis defects caused by loss of embryonic macrophage function in *Xenopus*. *Mech. Dev.* 128, 5–6. doi: 10.1016/j.mod.2011.04.002

Sparrow, D. B., Cai, C., Kotecha, S., Latinkic, B., Cooper, B., Towers, N., et al. (2000). Regulation of the tinman homologues in *Xenopus* embryos. *Dev. Biol.* 227, 65–79. doi: 10.1006/dbio.2000.9891

Tran, H. T., Sekkali, B., Imschoot, G. V., Janssens, S., and Vleminckx, K. (2010). Wnt/beta-catenin signaling is involved in the induction and maintenance of primitive hematopoiesis in the vertebrate embryo. *PNAS* 107, 16160–16165. doi: 10.1073/pnas.1007725107

Tran, H. T., and Vleminckx, K. (2014). Design and use of transgenic reporter strains for detecting activity of signaling pathways in *Xenopus*. *Methods* 3, 422–432. doi: 10.1016/j.ymeth.2013.06.028

Triedman, J. K., and Newburger, J. W. (2016). Trends in congenital heart disease: the next decade. *Circulation* 133, 2716–2733. doi: 10.1161/circulationaha.116.023544

Tzahor, E. (2007). Wnt/beta-catenin signaling and cardiogenesis: timing does matter. *Dev. Cell* 13, 10–13. doi: 10.1016/j.devcel.2007.06.006

Ueno, S., Weidinger, G., Osugi, T., Kohn, A. D., Golob, J. L., Pabon, L., et al. (2007). Biphasic role for Wnt/β-catenin signaling in cardiac specification in zebrafish and embryonic stem cells. *PNAS* 104, 9685–9690. doi: 10.1073/pnas.0702859104

Van der Linde, D., Konings, E. E., Slager, M. A., Witsenburg, M., Helbing, W. A., Takkenberg, J. J., et al. (2011). Birth prevalence of congenital heart disease worldwide: a systematic review and metaanalysis. *J. Am. Coll. Cardiol.* 58, 2241–2247. doi: 10.1016/j.jacc.2011.08.025

Vivante, A., Mann, N., Yonath, H., Weiss, A. C., Getwan, M., Kaminski, M. M., et al. (2017). A dominant mutation in nuclear receptor interacting protein 1 causes urinary tract malformations via dysregulation of retinoic acid signaling. *J. Am. Soc. Nephrol.* 28, 2364–2376. doi: 10.1681/ASN.2016060694

Vize, P. D., Jones, E. A., and Pfister, R. (1995). Development of the *Xenopus* pronephric system. *Dev. Biol.* 171, 531–540. doi: 10.1006/dbio.1995.1302

Walentek, P., Beyer, T., Thumberger, T., Schweickert, A., and Blum, M. (2012). ATP4a is required for Wnt-dependent Foxj1 expression and leftward flow in Xenopus left-right development. *Cell Rep.* 1, 516–527. doi: 10.1016/j.celrep.2012.03.005

Wallingford, J. B., and Mitchell, B. (2011). Strange as it may seem: the many links between Wnt signaling, planar cell polarity, and cilia. *Genes Dev.* 25, 201–213. doi: 10.1101/gad.2008011

Werner, M. E., and Mitchell, B. J. (2013). Using Xenopus skin to study cilia development and function. *Methods Enzymol.* 525, 191–217. doi: 10.1016/B978-0-12-397944-5.00010-9

Wild, W., Pogge von Strandmann, E., Nastos, A., Senkel, S., Lingott-Frieg, A., Bulman, M., et al. (2000). The mutated human gene encoding hepatocyte nuclear factor 1beta inhibits kidney formation in developing Xenopus embryos. *Proc. Natl. Acad. Sci. U.S.A.* 97, 4695–4700. doi: 10.1073/pnas.080010897

Yoshiba, S., and Hamada, H. (2014). Roles of cilia, fluid flow, and Ca2+ signaling in breaking of left right symmetry. *Trends Genet.* 30, 10–17. doi: 10.1016/j.tig.2013.09.001

Zaidi, S., Choi, M., Wakimoto, H., Ma, L., Jiang, J., Overton, J. D., et al. (2013). De novo mutations in histone-modifying genes in congenital heart disease. *Nature* 498, 220–223. doi: 10.1038/nature12141

Zhou, X., and Vize, P. D. (2004). Proximo-distal specialization of epithelial transport processes within the *Xenopus* pronephric kidney tubules. *Dev. Biol.* 271, 322–338. doi: 10.1016/j.ydbio.2004.03.036

Conflict of Interest Statement: The authors declare that the research was conducted in the absence of any commercial or financial relationships that could be construed as a potential conflict of interest.

frontiers in Physiology

BRIEF RESEARCH REPORT
published: 20 September 2019
doi: 10.3389/fphys.2019.01197

Quantitative Phenotyping of *Xenopus* Embryonic Heart Pathophysiology Using Hemoglobin Contrast Subtraction Angiography to Screen Human Cardiomyopathies

Engin Deniz[1]*, *Stephan Jonas*[2], *Mustafa K. Khokha*[1,3] and *Michael A. Choma*[1,4,5,6]

[1] Department of Pediatrics, Yale University, New Haven, CT, United States, [2] Department of Informatics, Technical University of Munich, Munich, Germany, [3] Department of Genetics, Yale University, New Haven, CT, United States, [4] Department of Diagnostic Radiology, Yale University, New Haven, CT, United States, [5] Department of Biomedical Engineering, Yale University, New Haven, CT, United States, [6] Department of Applied Physics, Yale University, New Haven, CT, United States

Congenital heart disease (CHD) is a significant cause of mortality in infants and adults. Currently human genomic analysis has identified a number of candidate genes in these patients. These genes span diverse categories of gene function suggesting that despite the similarity in cardiac lesion, the underlying pathophysiology may be different. In fact, patients with similar CHDs can have drastically different outcomes, including a dramatic decrease in myocardial function. To test these human candidate genes for their impact on myocardial function, we need efficient animals models of disease. For this purpose, we paired *Xenopus tropicalis* with our microangiography technique, hemoglobin contrast subtraction angiography (HCSA). To demonstrate the gene-teratogen-physiology relationship, we modeled human cardiomyopathy in tadpoles. First we depleted the sarcomeric protein myosin heavy chain 6 (myh6) expression using morpholino oligos. Next, we exposed developing embryos to the teratogen ethanol and in both conditions showed varying degrees of cardiac dysfunction. Our results demonstrate that HCSA can distinguish biomechanical phenotypes in the context of gene dysfunction or teratogen. This approach can be used to screen numerous candidate CHD genes or suspected teratogens for their effect on cardiac function.

Keywords: Xenopus tadpole, hemoglobin subtraction angiography, human cardiomyopathy, animal model cardiovascular system, videomicroscopy

OPEN ACCESS

Edited by:
Theresia Kraft,
Hannover Medical School, Germany

Reviewed by:
Rebecca Maree Dyson,
University of Otago, New Zealand
Helen Willsey,
University of California, San Francisco, United States

***Correspondence:**
Engin Deniz
engin.deniz@yale.edu

Specialty section:
This article was submitted to Embryonic and Developmental Physiology, a section of the journal Frontiers in Physiology

Received: *28 November 2018*
Accepted: *03 September 2019*
Published: *20 September 2019*

Citation:
Deniz E, Jonas S, Khokha MK and Choma MA (2019) Quantitative Phenotyping of Xenopus Embryonic Heart Pathophysiology Using Hemoglobin Contrast Subtraction Angiography to Screen Human Cardiomyopathies. Front. Physiol. 10:1197. doi: 10.3389/fphys.2019.01197

INTRODUCTION

Congenital heart disease (CHD) occurs in ∼8 out of 1,000 live births and effects 1.3 million newborns per year worldwide (Marelli et al., 2007; van der Linde et al., 2011). Currently the prevalence of adults with CHD exceeds the pediatric population, shifting the burden of disease to adulthood, and enlarging the cohort of CHD patients. Despite the early corrective measures and close, multidisciplinary care, adults with CHD still have a significantly higher mortality rate (Pierpont et al., 2007). Sudden death and early onset congestive heart failure remains the most common causes of mortality suggesting that premature myocardial failure may be associated

with adult CHD (Sabatine et al., 2006; O'Donnell and Nabel, 2011; Kathiresan and Srivastava, 2012). Currently very little is known about the interactions between the malformed heart and biomechanical function which ultimately affects life expectancy and the quality of life.

Human genomics technologies are now enabling genetic analyses of patients with CHD (Fakhro et al., 2011; Sanders et al., 2012; Zaidi and Brueckner, 2017; Pierpont et al., 2018). Based on the diversity of the genes identified in similar phenotypic patients, we suggest that genetic heterogeneity may explain the differences seen in patient outcomes. To better understand this relationship between a candidate gene and the biomechanical phenotype, we need to develop efficient animal models to evaluate the effect of candidate CHD genes on cardiac function. This would be the first step to investigate the functional variability seen in CHD patients.

Imaging small animal cardiovascular system remains to be a challenge because of the small heart sizes as well as the fast heart rates requiring high resolution, high speed imaging. Cardiac MRI with gating has been used for imaging anesthetized mice and rat cardiovascular system yet image acquisition time reaching to hours making it difficult to use for any screening purposes (Ramirez and Bankson, 2007; Ramirez et al., 2007; Esparza-Coss et al., 2008). Alternatively micro-CT systems are designed to provide fast (1–2 s) imaging. Combined with the cardio-respiratory gating and laborious segmentation, 4D data sets can be formed to measure cardiac function (Yushkevich et al., 2006; Clark et al., 2013). Both of these modalities have limited utilization for rapid, high-throughput screening since they require extensive image processing. As an alternative modality our group and the others have implemented Optical Coherence Tomography (OCT) imaging for small animal cardiovascular imaging (Tearney et al., 1996; Luo et al., 2006; Männer et al., 2009; Yoo et al., 2011; Wang et al., 2016; Deniz et al., 2017; Grishina et al., 2017). Principally OCT imaging is similar to the ultrasound but light is utilized instead of sound and provides cross-sectional images. With scan rates of ∼100 2D frames/s and implemented Doppler technology, OCT imaging has been evolving in functional analysis of cardiovascular system in small animal models (Davis et al., 2008; Jenkins et al., 2010). The main disadvantages of OCT are the expense of the commercially available products and the limitations of Doppler application. For accurate quantification of blood flow by doppler application requires high speed systems to prevent phase-wrapping artifacts and also relies on laminar flow. This is very difficult to obtain from motile, trabeculated embryonic ventricle, limiting Doppler OCT application at its current state for accurately quantifying cardiac ventricle function.

We previously demonstrated that hemoglobin contrast subtraction angiography (HCSA) can exploit the wavelength-sensitive absorption of hemoglobin as a molecular-specific source of endogenous flow contrast and can be applied to *Xenopus* tadpole hearts in a straightforward manner (Deniz et al., 2012) using an EOS camera. HCSA can quantify changes in the embryonic cardiac function after perturbation with a calcium channel blocker. In this brief report, we demonstrate that *Xenopus* can be a fast gene-teratogen-function assay and when coupled with HCSA, can be used to quantify physiological cardiac phenotypes over a short period of time. *Xenopus,* as a model of cardiac development, has a favorable balance between human modeling and cost/efficiency that is required for high throughput screening (Warkman and Krieg, 2007; Khokha, 2012). The tadpole cardiovascular system develops within 72 h and remains optically accessible throughout the early stages of development. Importantly, during this period of development, tadpoles can survive with severely malformed hearts since nutrient and O_2 delivery is not dependent on blood circulation. Here, we capitalized on these advantages to model human cardiomyopathy in *Xenopus* in two ways, first by reducing the expression of the sarcomeric protein myosin heavy chain 6 (MYH6) using morpholino oligonucleotides (MO) and, in a separate set of experiments, by exposing them to the known teratogen ethanol (EtOH).

Cardiac muscle myosin consists of two heavy chain subunits, two light chain subunits, and two regulatory subunits. We used MYH6 morpholino to block the translation start site of the mRNA encoding the alpha heavy chain. It has been shown that mutations in MYH6 gene cause cardiomyopathy both in humans (Hershberger et al., 2010) and *Xenopus* suggesting a well-conserved disease mechanism (Abu-Daya et al., 2009). One substantial advantage of MOs is that gene dosage can be titrated based on the amount of MO injected providing fine dosage control. This is important since most cardiomyopathy patients are heterozygous (Zaidi and Brueckner, 2017) and therefore gene dosage may play a critical role.

In parallel to the knockdown approach, we exposed the developing embryo to EtOH, a known cardiac teratogen, affecting one in eight pregnant women (Floyd and Sidhu, 2004) and leading to fetal alcohol syndrome (FAS). Worldwide FAS affects many children with a prevalence of 23 per 1,000 (Roozen et al., 2016). Patients with FAS also present with structural birth defects including cardiac defects (Jones et al., 2010). To investigate the effects of EtOH on the developing cardiovascular system, studies in zebrafish found increased heart volumes, decreased thickness of the ventricular wall, and decreased basal heart rates (Dlugos and Rabin, 2010). Similarly, in *Xenopus* embryos exposed to EtOH, a reduction in trabeculae formation was found (Yelin et al., 2007). More elaborate work in chick suggested that ethanol-induced alterations in early cardiac function may potentially lead to late-stage valve and septal defects (Karunamuni et al., 2014). Together, EtOH appears to alter myocardial formation and pump function.

In this report we show that HCSA imaging can detect changes in embryonic cardiac function using several different anatomic and physiological metrics, establishing a rapid, non-destructive, low-cost method to investigate cardiac gene-function relationship.

MATERIALS AND METHODS

Xenopus Husbandry

Xenopus tropicalis were housed and cared for in our aquatics facility according to established protocols that were approved by the Yale Institutional Animal Care and Use Committee

(IACUC) in accordance with NIH guidelines. Female and male mature *Xenopus tropicalis* were obtained from National Xenopus Resource.

MYH6 Knockdown

In vitro fertilization and microinjections were done as previously described (del Viso and Khokha, 2012). In order to deplete *myh6*, we injected fertilized eggs with either 1 or 2 ng of MYH6-MOs and the tracer dye Alexa488 (Invitrogen) at one cell stage. Controls were injected with only tracer dye Alexa488. The advantage of MOs is that "gene dosage" can be titrated based on amount of MO injected providing fine dosage control. We used a translational-blocking start site morpholino oligo (MO) (Morcos, 2007) to deplete the alpha heavy chain, MYH6 (sequence 5′ AGTCTGCCATCAGGGCATCACCCAT-3′–Gene-Tools, LLC) which was previously utilized and verified in *Xenopus* (Abu-Daya et al., 2009). Embryos were injected at the one cell stage with borosilicate glass needles. Post-injections, embryos were incubated in 1/9 Modified Ringer's solution supplemented with 50 μg/ml of gentamycin at 25°C. Injections were confirmed by fluorescent lineage tracing with a Zeiss Lumar fluorescence stereomicroscope at stage 28 and tadpoles further raised at until stage 45 (Nieuwkoop—Faber staging. ∼ post-fertilization day 4 at 25°C Nieuwkoop and Faber, 1994) for imaging.

EtOH Treatment

We incubated *Xenopus* embryos in 1% EtOH in 1/9 Modified Ringer's solution at 25°C following mid-blastula stage (stage 9, Nieuwkoop—Faber staging Nieuwkoop and Faber, 1994) as described previously (Yelin et al., 2007) until stage 45 to determine the effects on the myocardium using HCSA imaging. EtOH solution refreshed daily for 4–5 days until tadpoles reached stage 45.

Imaging and Image Processing

We used a Nikon SMZ800 stereomicroscope equipped with Canon EOS 5D Mark II digital camera and Sugar CUBE—LED (4,000 Lumens) with ring illuminator. Image acquisition setup: Zoom 6.2/Gain: 0/Depth 14 bit/LED 4,000 Lumens. Fifty RAW images acquired with 0.2 s intervals. High Speed color movie obtained with Motion Xtra N4-IDT, Inc. N4 Camera. For cardiac functional analysis, we embedded Stage 44–45 (post fertilization day 3 at 28°C) tadpoles in low melt agarose and positioned ventral surface exposed to the imaging plane (**Supplemental Figure 1A**). First, we obtained a scout image to record the tadpole stage, tadpole position and overall development. Next, we imaged the cardiac sac and confirmed that ventricle borders were clearly delineated. We obtained 50 still images (14-bit frames in RAW format) in the time lapse mode with a 0.2 s interframe interval using a Canon EOS 5D Mark II digital camera (**Supplemental Figure 1B**). Acquiring 50 images effectively captured end-systolic and end-diastolic stages of the cardiac cycle. Next, we processed the images and calculated various metrics using our custom image processing and analysis software. The custom software was developed in Matlab (The Mathworks, Natick, USA) Version 2012B. The application allows the user to load a high-bit depth image series in PNG format, sort, and select images of systole or diastole, segment the outline of the ventricle and store results as comma-separated value files. The software is available open-source[1].

Matlab Interface

The graphical user interface allows the user to browse through the acquired images and select the frames corresponding to the maximal end-systole and end-diastole (**Supplemental Figure 1C**—Right Panel). Then on the selected images the ventricle is manually segmented (**Supplemental Figure 1C**—white dots). Using an Otsu-based thresholding function in MATLAB, we classified pixels into those that contain hemoglobin and those that do not. Finally, we quantified the number of hemoglobin-containing pixels (referred as Hb blush) within a manually segmented ventricle at the end of systole and diastole (**Supplemental Figure 1D**).

Measurements

Based on hemoglobin pixel counts and the total ventricular area delineated by manual segmentation, we estimated the total ventricular end-diastolic area (*tEDA*), the total ventricular end-systolic area (*tESA*), percent change in the total ventricular area ($\Delta_{\%}tA = 100^{*}(tEDA\text{-}tESA)/tEDA$), end-diastolic blood area (*EDBA*), end-systolic blood area (*ESBA*), the stroke area ($SA = EDBA\text{-}ESBA$), and ejection fraction ($EF = 100^{*}SA/EDBA$). We also derived a "myocardial fraction" metric where we estimated the myocardial area and referred to that as the myocardial mass index (MMI). To derive MMI, we assumed that during peak systole, where the myocardium is at its maximal contraction, most of the blood is ejected minimizing this confounding volume. We then subtracted the end-systolic blood area from the total ventricular end-systolic area assuming that the remainder of the segmented area would be a rough estimate of the myocardial mass at maximal contraction.

Dye Injection

Tadpole raised and positioned in 1% agar as described above. Using microinjector (Harvard Apparatus PLI-100 Pico-Injector Microinjection System) Brilliant Blue FCF (Sigma-Aldrich) dye injected to the cardinal vein. Movie obtained with Redlake/IDT Y4 Lite grayscale camera.

Statistics

For comparison we utilized the Mann-Whitney test (non-parametric and not paired) and used a scatter plot with the bar showing the median and 95% confidence interval. We also included before-after graph including standard error of the mean. All significant differences between groups indicated in the figure legends. Significance was determined when the *p*-value is lower than 0.05.

[1]http://mhealthgroup.net/software (Note to editors and reviewers: the software will be made available upon publication of the manuscript).

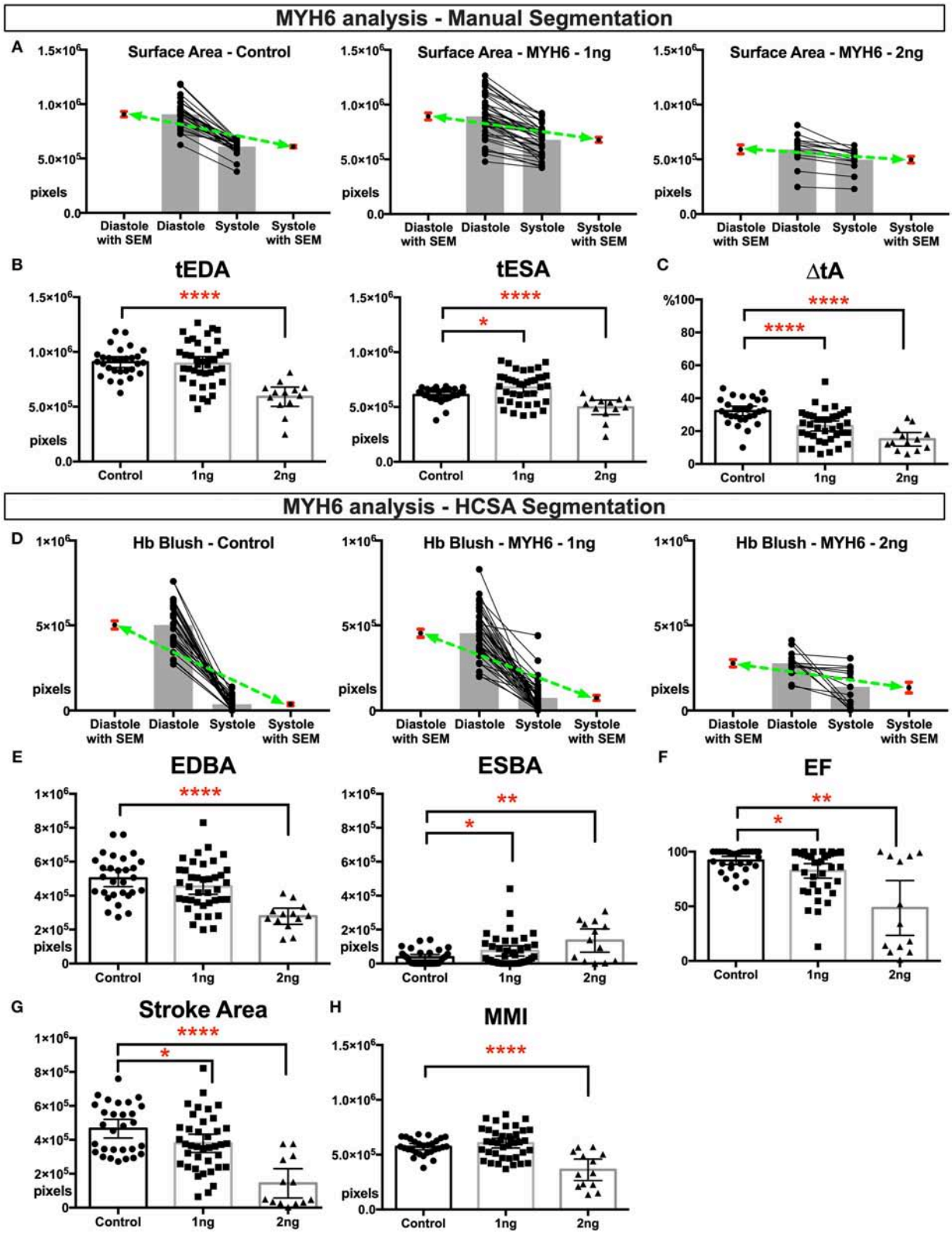

FIGURE 1 | Physiological quantification of embryo heart function in MYH6 morphants. For this experiment 29 control, 39 morphants-–1 ng morpholino injected and 13 morphants-–2 ng morpholino injected analyzed. Measurements derived from manual segmentation include surface area at the end of diastole and systole and

(Continued)

FIGURE 1 | the change in ventricle area. **(A)** Before-after graph presented with extra columns pointing mean with SEM in red. Green line between means flattens as change in surface area diminishes with increasing MO dose. **(B,C)** As the MO dose is increased, the change in ventricle area is reduced, and the ventricle sizes are smaller. **(D)** Measurements derived from HCSA application include Hb blush at the end of diastole and systole and the change in blush area. Before-after graph presented with extra columns pointing mean with SEM in red. Green line between means flattens as change in blush area diminishes with increasing MO dose. **(E,F)** Following HCSA application, Hb blush is quantified at the end of diastole and systole. Ejection Fraction is derived from these measurments. Morphants demonstrated a dose dependent diminished ejection fraction and **(G)** stroke area. **(H)** Myocardial mass index estimates the amount of cardiac mass within the manually segmented heart. Myocardial mass index is affected in 2 ng morphants but remains within normal limits in 1 ng morphants. SEM, standard error of the mean; Hb Blush, Hemoglobin-containing pixels; tEDA, total end-diastolic area; tESA, total end-systolic area; ΔtA, change in total area; EDBA, end diastolic blood area; ESBA, end-systolic blood area; EF, ejection fraction; MMI, myocardiac mass index; HCSA, Hb contrast subtraction angiography. $^{****}p < 0.0001$, $^{**}p < 0.01$, and $^{*}p < 0.05$.

RESULTS

HCSA Imaging Can Detect Cardiac Dysfunction in the Setting of Sarcomere Perturbation

We first analyzed cardiac function in MYH6 morphant group. We analyzed HCSA images from 29 control embryos, 39 embryos injected with 1 ng MYH6 morpholino, and 13 embryos injected with 2 ng MYH6 morpholino. Overall, the 2 ng-morphant hearts were smaller in size as ascertained using total ventricular end-diastolic area (*tEDA)* (**Figures 1A,B**), whereas 1 ng-morphants had similar end diastolic area but slightly larger end systolic area when compared to the controls. The percent change in the ventricle area during contraction ($\Delta_{\%}tA$) was significantly reduced in both morphants suggesting myocardial dysfunction (**Figure 1C**). We derived these measurements with manual segmentation as described in methods. Then we applied HCSA, where we were able to quantify end-diastolic and end-systolic Hb blush (*EDBA*: end-diastolic blood area; *ESBA*: end-systolic blood area), which is a surrogate for blood area. In end-diastole, due to their overall smaller cardiac size, 2 ng morphants filled with less blood whereas 1 ng morphants, given their normal cardiac size, filled with a similar amount of blood when compared to the controls (**Figures 1D,E**). Importantly, at the end of systole, they both showed a significant failure in emptying the ventricle leading to an increase in end systolic blood area (**Figures 1D,E**). Therefore, the ejection fraction and the stroke area diminished, so we concluded that the magnitude of the dysfunction was worse in 2 ng morphants (**Figures 1F,G**). Then we estimated MMI at maximal ventricular contraction. As shown in **Figure 1H**, 1 ng *myh6* morphants did not have a significant reduction in myocardial mass in contrast to 2 ng morphants where MMI was significantly reduced. In conclusion, 2 ng morphants showed both structural loss of myocardium size and functional loss of contractility. Nevertheless, even without a change in MMI in 1 ng *myh6* morphants, HCSA imaging could still delineate changes in myocardial function.

Next we analyzed the ethanol exposed tadpoles. In the ethanol group, we analyzed HCSA images from 30 control and 30 exposed tadpoles. Grossly dysmorphic embryos were excluded. In this group, ventricles were smaller than the control group (**Figures 2A,B**) and the change in ventricle area was diminished (**Figure 2C**), suggesting that EtOH exposed ventricle can't shorten appropriately. Aslo *ESBA*, a surrogate for blood volume at the end of systole, was significantly higher than controls (**Figures 2D,E**) which is also likely due to the reduced ability to generate adequate ventricular force, shown as reduced ejection fraction and stroke area (**Figures 2F,G**). Therefore, together these tadpoles had slightly smaller looking ventricles with reduced myocardial pump function. Furthermore, "myocardial fraction" in systole shows a significant reduction suggesting a loss of myocardial mass (**Figure 2H**).

DISCUSSION

The incidence of CHD is staggering: ∼1% of live births and 10% of aborted fetuses have CHD worldwide (Bernier et al., 2010; van der Linde et al., 2011; Jorgensen et al., 2014). New genomics technologies are enabling genetic analyses of CHD patients and identifying sequence variations in patients with CHD (Fakhro et al., 2011; Zaidi et al., 2013; Glessner et al., 2014; Homsy et al., 2015; McKean et al., 2016; Priest et al., 2016; Jin et al., 2017; Hoang et al., 2018; Manheimer et al., 2018). Genes identified in genomic studies are many but their role in cardiac development and function is uncertain; therefore, functional assays must be relatively rapid and inexpensive. We have previously shown that *Xenopus tropicalis* with the CRISPR/Cas9 system enables the analysis of hundreds of different genes in cardiac development (Deniz et al., 2018) and in this brief report we demonstrate that HSCA imaging can be used to screen for types of CHDs that present with sarcomeric dysfunction, for example cardiomyopathies.

The advantage of our HCSA method is that we can quantitate different metrics across multiple embryos to identify statistically significant differences between groups rather than relying on a qualitative assessment of function. In *myh6* morphants with increasing doses of morpholino we showed worsening cardiac function, yet 1 ng morphants didn't show differences in EDA, EDBA, and MMI suggesting that even subtle changes in sarcomeric function can be demonstrated with HCSA imaging. Similarly EtOH treated hearts were smaller overall and failed to eject adequate blood, again suggesting sarcomeric dysfunction that was easily quantified with HCSA imaging.

As a major advantage HCSA imaging is non-destructive, reproducible, faster, and most importantly non-lethal to the tadpole enabling multiple viewing session at various stages. This is important in analyzing numerous candidate genes. Fluoroscopy-based angiography requires microinjection in tadpoles, is fatal preventing subsequent imaging, and is difficult to reproduce limiting its utility for screening

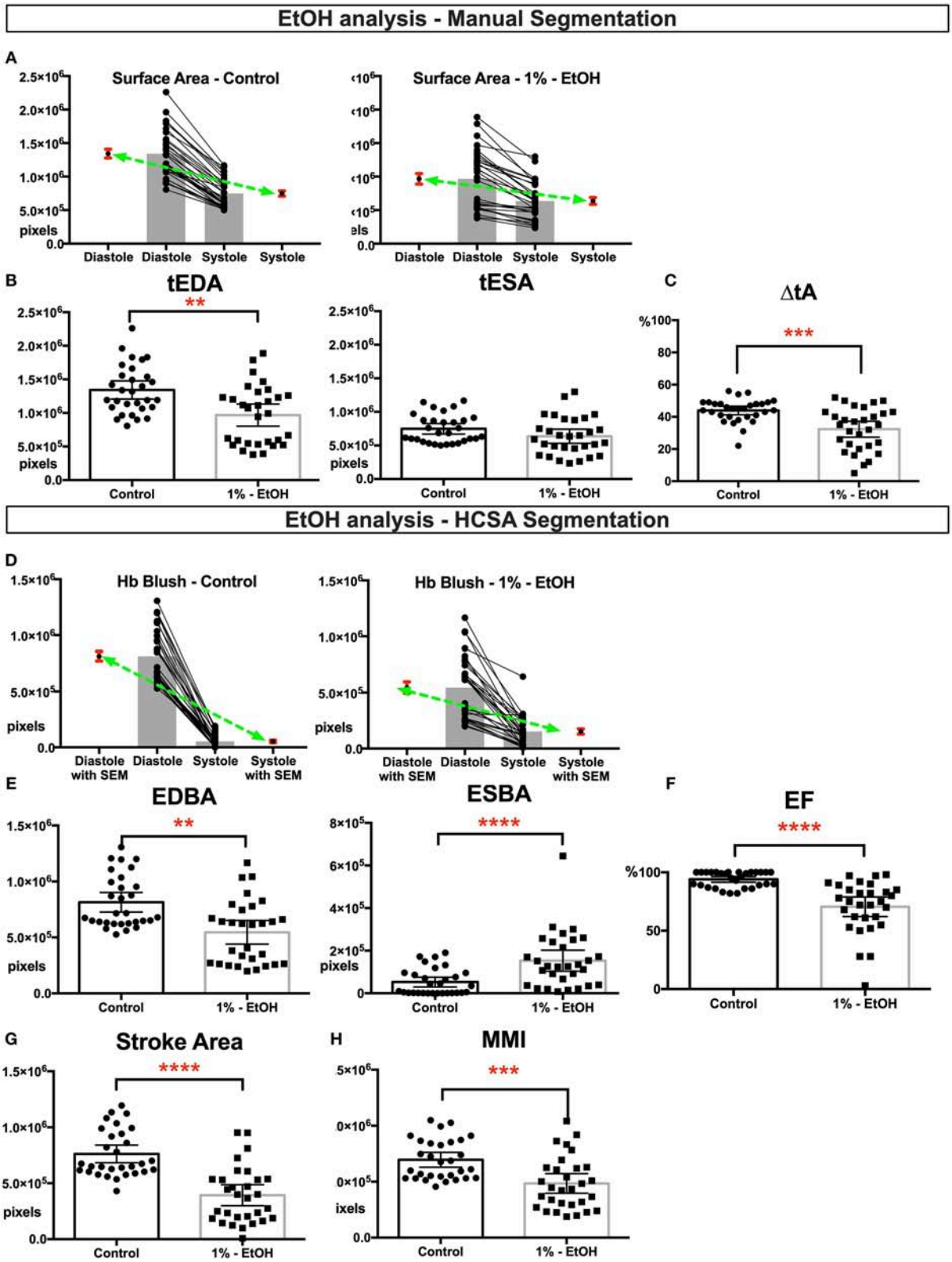

FIGURE 2 | Physiological quantification of embryo heart function in EtOH treated tadpoles. For this experiment 30 controls and 30 EtOH exposed tadpoles analyzed. Measurements derived from manual segmentation includes surface area at the end of diastole and systole and the change in ventricle area. **(A)** Before-after graph

(Continued)

FIGURE 2 | presented with extra columns pointing mean with SEM in red. Green line between means flattens as change in surface area diminishes in EtOH group. **(B,C)** Ventricles of the ethanol exposed tadpoles were slightly smaller in size but had diminished change in the ventricle area. Following HCSA application, Hb blush quantified at the end of diastole and systole. Ejection fraction is derived from these measurements. **(D)** Before-after graph presented with extra columns pointing mean with SEM in red. Green line between means flattens as change in blush area diminishes in EtOH group. **(E,F)** Ethanol exposed tadpoles had less blood at the end of diastole and blood is not propelled efficiently leading an increase in end systolic Hb blush, diminished ejection fraction, and diminished **(G)** stroke area. **(H)** Myocardial Mass Index. In ethanol exposed tadpoles myocardial mass is diminished. SEM, standard error of the mean; Hb Blush, Hemoglobin-containing pixels; tEDA, total end-diastolic area; tESA, total end-systolic area; ΔtA, change in total area; EDBA, end diastolic blood area; ESBA, end-systolic blood area; EF, ejection fraction; MMI, myocardiac mass index; HCSA, Hb contrast subtraction angiography. $^{****}p < 0.0001$, $^{***}p < 0.001$, and $^{**}p < 0.01$.

purposes (**Movie 1**). As the high-speed color cameras (>250 fps) are more available and cheaper, more detailed functional analysis including simultaneous assessment for cardiac and peripheral vasculature structures will be more feasible (**Movie 2**) providing structural details comparable to angiography images.

Clinical cardiology has demonstrated that imaging modalities (e.g., echocardiography and cardiac angiography) are essential to identify abnormal heart structures and heart function (Cua and Feltes, 2012; Roest and de Roos, 2012). Current advances in optical imaging are enabling comprehensive, high-resolution cardiac imaging in small animal models, which facilitates studying gene-phenotype and teratogen-phenotype relationships (Choma et al., 2010). *Xenopus* is ideal for these studies given the ease of *in vivo* optical access to the cardiac structures as well as the optimal balance between human modeling and cost/efficiency (Warkman and Krieg, 2007). In this report we showed the effects of a human cardiomyopathy gene (MYH6) and a known teratogen, EtOH (known to cause Fetal Alcohol Syndrome) on early cardiac development using HCSA imaging. Broadly our results support the utility of HCSA imaging, when paired with *Xenopus*, to screen the impact of novel candidate CHD genes or potential teratogens on cardiac function.

DATA AVAILABILITY STATEMENT

All datasets generated for this study are included in the manuscript/**Supplementary Files**.

ETHICS STATEMENT

Xenopus tropicalis were housed and cared for in our aquatics facility according to established protocols that were approved by the Yale Institutional Animal Care and Use Committee (IACUC) in accordance with NIH guidelines. Female and male mature Xenopus tropicalis were obtained from National Xenopus Resource.

AUTHOR CONTRIBUTIONS

ED, SJ, MK, and MC designed the study. ED and SJ acquired and analyzed the data. ED wrote the first draft of the article. SJ, MK, and MC contributed to the interpretation of the results and the writing of the manuscript. All authors have approved the final manuscript.

FUNDING

This work was supported by NIH 5R33HL120783 to MK. MK is a Mallinckrodt scholar.

ACKNOWLEDGMENTS

The authors would like to thank all the members of the Khokha Lab and Choma Lab their support.

SUPPLEMENTARY MATERIAL

The Supplementary Material for this article can be found online at: https://www.frontiersin.org/articles/10.3389/fphys.2019.01197/full#supplementary-material

Supplemental Figure 1 | Experimental and quantitative analysis workflow. **(A)** For *myh6* experiments, one cell *Xenopus* embryos are injected with either MOs and the tracer dye (Alexa488) or only the tracer dye (control group). In ethanol exposure experiments, we incubated post-midblastula stage embryos in1% EtOH. On day five, NF Stage 44 tadpoles are embedded in low melt agarose (1%) for non-pharmacological immobilization to facilitate imaging. **(B)** Scout Image and Magnified Images acquired. **(C)** Custom software interface. Right panel allows the user navigate through the acquired images and adjust the brightness and the contrast. Once maximal end-diastolic and maximal-end-systolic frames are identified, the ventricle is manually segmented. **(D)** Images processed and Hb blush is quantified within the segmented area using the HCSA software interface. IVF, *in vitro* fertilization; lta, left truncus arteriosus; rta, right truncus arteriosus; v, ventricle; oft, out flow tract; Hb, hemoglobin.

Movie 1 | Grayscale movie demonstrating injection of Brilliant Blue dye via cardinal tail vein and tracking of flow from the venous system sequentially to the atrium, ventricle, and outflow tract that eventually propagates to the systemic circulation.

Movie 2 | High speed (250 fps—color) color movie and processed HCSA movie.

REFERENCES

Abu-Daya, A., Sater, A. K., Wells, D. E., Mohun, T. J., and Zimmerman, L. B. (2009). Absence of heartbeat in the Xenopus tropicalis mutation muzak is caused by a nonsense mutation in cardiac myosin myh6. *Dev. Biol.* 336, 20–29. doi: 10.1016/j.ydbio.2009.09.019

Bernier, P. L., Stefanescu, A., Samoukovic, G., and Tchervenkov, C. I. (2010). The challenge of congenital heart disease worldwide: epidemiologic and demographic facts. *Semin. Thorac. Cardiovasc. Surg. Pediatr. Card. Surg. Annu.* 13, 26–34. doi: 10.1053/j.pcsu.2010.02.005

Choma, M. A., Suter, M. J., Vakoc, B. J., Bouma, B. E., and Tearney, G. J. (2010). Heart wall velocimetry and exogenous contrast-based cardiac flow imaging

in Drosophila melanogaster using Doppler optical coherence tomography. *J. Biomed. Opt.* 15:056020. doi: 10.1117/1.3503418

Clark, D., Badea, A., Johnson, G. A., and Badea, C. T. (2013). Constructing a 4D murine cardiac micro-CT atlas for automated segmentation and phenotyping applications. *Med. Imag. 2013 Image Process.* 8669:86691P. doi: 10.1117/12.2007043

Cua, C. L., and Feltes, T. F. (2012). Echocardiographic evaluation of the single right ventricle in congenital heart disease. *Circ. J.* 76, 22–31. doi: 10.1253/circj.CJ-11-1267

Davis, A. M., Rothenberg, F. G., Shepherd, N., and Izatt, J. A. (2008). *In vivo* spectral domain optical coherence tomography volumetric imaging and spectral Doppler velocimetry of early stage embryonic chicken heart development. *J. Opt. Soc. Am. A Opt. Image Sci. Vis.* 25, 3134–3143. doi: 10.1364/JOSAA.25.003134

del Viso, F., and Khokha, M. (2012). Generating diploid embryos from Xenopus tropicalis. *Methods Mol. Biol.* 917:33–41. doi: 10.1007/978-1-61779-992-1_3

Deniz, E., Jonas, S., Hooper, M., Griffin, N. J., Choma, M. A., and Khokha, M. K. (2017). Analysis of craniocardiac malformations in Xenopus using optical coherence tomography. *Sci. Rep.* 7:42506. doi: 10.1038/srep42506

Deniz, E., Jonas, S., Khokha, M., and Choma, M. A. (2012). Endogenous contrast blood flow imaging in embryonic hearts using hemoglobin contrast subtraction angiography. *Opt. Lett.* 37, 2979–2981. doi: 10.1364/OL.37.002979

Deniz, E., Mis, E. K., Lane, M., and Khokha, M. K. (2018). CRISPR/Cas9 F0 screening of congenital heart disease genes in Xenopus tropicalis. *Methods Mol. Biol.* 1865, 163–174. doi: 10.1007/978-1-4939-8784-9_12

Dlugos, C. A., and Rabin, R. A. (2010). Structural and functional effects of developmental exposure to ethanol on the zebrafish heart. *Alcohol. Clin. Exp. Res.* 34, 1013–1021. doi: 10.1111/j.1530-0277.2010.01176.x

Esparza-Coss, E., Ramirez, M. S., and Bankson, J. A. (2008). Wireless self-gated multiple-mouse cardiac cine MRI. *Magn. Reson. Med.* 59, 1203–1206. doi: 10.1002/mrm.21562

Fakhro, K. A., Choi, M., Ware, S. M., Belmont, J. W., Towbin, J. A., Lifton, R. P., et al. (2011). Rare copy number variations in congenital heart disease patients identify unique genes in left-right patterning. *Proc. Natl. Acad. Sci. U.S.A.* 108, 2915–2920. doi: 10.1073/pnas.1019645108

Floyd, R. L., and Sidhu, J. S. (2004). Monitoring prenatal alcohol exposure. *Am. J. Med. Genet. C Semin. Med. Genet.* 127C, 3–9. doi: 10.1002/ajmg.c.30010

Glessner, J. T., Bick, A. G., Ito, K., Homsy, J., Rodriguez-Murillo, L., Fromer, M., et al. (2014). Increased frequency of *de novo* copy number variants in congenital heart disease by integrative analysis of single nucleotide polymorphism array and exome sequence data. *Circ. Res.* 115, 884–896. doi: 10.1161/CIRCRESAHA.115.304458

Grishina, O. A., Wang, S., and Larina, I. V. (2017). Speckle variance optical coherence tomography of blood flow in the beating mouse embryonic heart. *J. Biophotonics* 10, 735–743. doi: 10.1002/jbio.201600293

Hershberger, R. E., Norton, N., Morales, A., Li, D., Siegfried, J. D., and Gonzalez-Quintana, J. (2010). Coding sequence rare variants identified in MYBPC3, MYH6, TPM1, TNNC1, and TNNI3 from 312 patients with familial or idiopathic dilated cardiomyopathy. *Circ. Cardiovasc. Genet.* 3, 155–161. doi: 10.1161/CIRCGENETICS.109.912345

Hoang, T. T., Goldmuntz, E., Roberts, A. E., Chung, W. K., Kline, J. K., Deanfield, J. E., et al. (2018). The congenital heart disease genetic network study: cohort description. *PLoS ONE* 13:e0191319. doi: 10.1371/journal.pone.0191319

Homsy, J., Zaidi, S., Shen, Y., Ware, J. S., Samocha, K. E., Karczewski, K. J., et al. (2015). *De novo* mutations in congenital heart disease with neurodevelopmental and other congenital anomalies. *Science* 350, 1262–1266. doi: 10.1126/science.aac9396

Jenkins, M. W., Peterson, L., Gu, S., Gargesha, M., Wilson, D. L., Watanabe, M., et al. (2010). Measuring hemodynamics in the developing heart tube with four-dimensional gated Doppler optical coherence tomography. *J. Biomed. Opt.* 15:066022. doi: 10.1117/1.3509382

Jin, S. C., Homsy, J., Zaidi, S., Lu, Q., Morton, S., DePalma, S. R., et al. (2017). Contribution of rare inherited and *de novo* variants in 2,871 congenital heart disease probands. *Nat. Genet.* 49, 1593–1601. doi: 10.1038/ng.3970

Jones, K. L., Hoyme, H. E., Robinson, L. K., Del Campo, M., Manning, M. A., Prewitt, L. M., et al. (2010). Fetal alcohol spectrum disorders: Extending the range of structural defects. *Am. J. Med. Genet. A* 152A, 2731–2735. doi: 10.1002/ajmg.a.33675

Jorgensen, M., McPherson, E., Zaleski, C., Shivaram, P., and Cold, C. (2014). Stillbirth: the heart of the matter. *Am. J. Med. Genet. A.* 164A, 691–699. doi: 10.1002/ajmg.a.36366

Karunamuni, G., Gu, S., Doughman, Y. Q., Peterson, L. M., Mai, K., McHale, Q., et al. (2014). Ethanol exposure alters early cardiac function in the looping heart: a mechanism for congenital heart defects? *Am. J. Physiol. Heart Circ. Physiol.* 306, H414–H421. doi: 10.1152/ajpheart.00600.2013

Kathiresan, S., and Srivastava, D. (2012). Genetics of human cardiovascular disease. *Cell* 148, 1242–1257. doi: 10.1016/j.cell.2012.03.001

Khokha, M. K. (2012). Xenopus white papers and resources: folding functional genomics and genetics into the frog. *Genesis* 50, 133–142. doi: 10.1002/dvg.22015

Luo, W., Marks, D. L., Ralston, T. S., and Boppart, S. A. (2006). Three-dimensional optical coherence tomography of the embryonic murine cardiovascular system. *J. Biomed. Opt.* 11:021014. doi: 10.1117/1.2193465

Manheimer, K. B., Richter, F., Edelmann, L. J., D'Souza, S. L., Shi, L., Shen, Y., et al. (2018). Robust identification of mosaic variants in congenital heart disease. *Hum. Genet.* 137, 183–193. doi: 10.1007/s00439-018-1871-6

Männer, J., Thrane, L., Norozi, K., and Yelbuz, T. M. (2009). *In vivo* imaging of the cyclic changes in cross-sectional shape of the ventricular segment of pulsating embryonic chick hearts at stages 14 to 17: a contribution to the understanding of the ontogenesis of cardiac pumping function. *Dev. Dyn.* 238, 3273–3284. doi: 10.1002/dvdy.22159

Marelli, A. J., Mackie, A. S., Ionescu-Ittu, R., Rahme, E., and Pilote, L. (2007). Congenital heart disease in the general population: changing prevalence and age distribution. *Circulation* 115, 163–172. doi: 10.1161/CIRCULATIONAHA.106.627224

McKean, D. M., Homsy, J., Wakimoto, H., Patel, N., Gorham, J., DePalma, S. R., et al. (2016). Loss of RNA expression and allele-specific expression associated with congenital heart disease. *Nat. Commun.* 7:12824. doi: 10.1038/ncomms12824

Morcos, P. A. (2007). Achieving targeted and quantifiable alteration of mRNA splicing with Morpholino oligos. *Biochem. Biophys. Res. Commun.* 358, 521–527. doi: 10.1016/j.bbrc.2007.04.172

Nieuwkoop, P. D., and Faber, J. (1994). *Normal Table of Xenopus laevis (Daudin): A Systematical and Chronological Survey of the Development From the Fertilized Egg Till the End of Metamorphosis* (New York, NY: Garland Publisher), 252, 10 leaves of plates.

O'Donnell, C. J., and Nabel, E. G. (2011). Genomics of cardiovascular disease. *N. Engl. J. Med.* 365, 2098–2109. doi: 10.1056/NEJMra1105239

Pierpont, M. E., Basson, C. T., Benson, D. W., Gelb, B. D., Giglia, T. M., Goldmuntz, E., et al. (2007). Genetic basis for congenital heart defects: current knowledge: a scientific statement from the American Heart Association Congenital Cardiac Defects Committee, Council on Cardiovascular Disease in the Young: endorsed by the American Academy of Pediatrics. *Circulation* 115, 3015–3038. doi: 10.1161/CIRCULATIONAHA.106.183056

Pierpont, M. E., Brueckner, M., Chung, W. K., Garg, V., Lacro, R. V., McGuire, A. L., et al. (2018). Genetic basis for congenital heart disease: revisited: a scientific statement from the American Heart Association. *Circulation* 138, e653–711. doi: 10.1161/CIR.0000000000000631

Priest, J. R., Osoegawa, K., Mohammed, N., Nanda, V., Kundu, R., Schultz, K., et al. (2016). *De novo* and rare variants at multiple loci support the oligogenic origins of atrioventricular septal heart defects. *PLoS Genet.* 12:e1005963. doi: 10.1371/journal.pgen.1005963

Ramirez, M. S., and Bankson, J. A. (2007). A practical method for 2D multiple-animal MRI. *J. Magn. Reson. Imaging.* 26, 1162–1166. doi: 10.1002/jmri.21112

Ramirez, M. S., Ragan, D. K., Kundra, V., and Bankson, J. A. (2007). Feasibility of multiple-mouse dynamic contrast-enhanced MRI. *Magn. Reson. Med.* 58, 610–615. doi: 10.1002/mrm.21348

Roest, A. A., and de Roos, A. (2012). Imaging of patients with congenital heart disease. *Nat. Rev. Cardiol.* (2012). 9, 101–115. doi: 10.1038/nrcardio.2011.162

Roozen, S., Peters, G. J., Kok, G., Townend, D., Nijhuis, J., and Curfs, L. (2016). Worldwide prevalence of fetal alcohol spectrum disorders: a systematic literature review including meta-analysis. *Alcohol. Clin. Exp. Res.* 40, 18–32. doi: 10.1111/acer.12939

Sabatine, M. S., Seidman, J. G., and Seidman, C. E. (2006). Cardiovascular genomics. *Circulation* 113, e450–e455. doi: 10.1161/CIRCULATIONAHA.105.560151

Sanders, S. J., Murtha, M. T., Gupta, A. R., Murdoch, J. D., Raubeson, M. J., Willsey, A. J., et al. (2012). *De novo* mutations revealed by whole-exome sequencing are strongly associated with autism. *Nature* 485, 237–241. doi: 10.1038/nature10945

Tearney, G. J., Bouma, B. E., Boppart, S. A., Golubovic, B., Swanson, E. A., and Fujimoto, J. G. (1996). Rapid acquisition of *in vivo* biological images by use of optical coherence tomography. *Opt. Lett.* 21, 1408–1410. doi: 10.1364/OL.21.001408

van der Linde, D., Konings, E. E., Slager, M. A., Witsenburg, M., Helbing, W. A., Takkenberg, J. J., et al. (2011). Birth prevalence of congenital heart disease worldwide: a systematic review and meta-analysis. *J. Am. Coll. Cardiol.* 58, 2241–2247. doi: 10.1016/j.jacc.2011.08.025

Wang, S., Lakomy, D. S., Garcia, M. D., Lopez, A. L., Larin, K. V., and Larina, I. V. (2016). Four-dimensional live imaging of hemodynamics in mammalian embryonic heart with Doppler optical coherence tomography. *J. Biophotonics* 9, 837–847. doi: 10.1002/jbio.201500314

Warkman, A. S., and Krieg, P. A. (2007). Xenopus as a model system for vertebrate heart development. *Semin. Cell Dev. Biol.* 18, 46–53. doi: 10.1016/j.semcdb.2006.11.010

Yelin, R., Yelin, D., Oh, W. Y., Yun, S. H., Boudoux, C., Vakoc, B. J., et al. (2007). Multimodality optical imaging of embryonic heart microstructure. *J. Biomed. Opt.* 12:064021. doi: 10.1117/1.2822904

Yoo, J., Larina, I. V., Larin, K. V., Dickinson, M. E., and Liebling, M. (2011). Increasing the field-of-view of dynamic cardiac OCT via post-acquisition mosaicing without affecting frame-rate or spatial resolution. *Biomed. Opt. Express* 2, 2614–2622. doi: 10.1364/BOE.2.002614

Yushkevich, P. A., Piven, J., Hazlett, H. C., Smith, R. G., Ho, S., Gee, J. C., et al. (2006). User-guided 3D active contour segmentation of anatomical structures: significantly improved efficiency and reliability. *Neuroimage* 31, 1116–1128. doi: 10.1016/j.neuroimage.2006.01.015

Zaidi, S., and Brueckner, M. (2017). Genetics and genomics of congenital heart disease. *Circ. Res.* 120, 923–940. doi: 10.1161/CIRCRESAHA.116.309140

Zaidi, S., Choi, M., Wakimoto, H., Ma, L., Jiang, J., Overton, J. D., et al. (2013). *De novo* mutations in histone-modifying genes in congenital heart disease. *Nature* 498, 220–223. doi: 10.1038/nature12141.

Conflict of Interest: The authors declare that the research was conducted in the absence of any commercial or financial relationships that could be construed as a potential conflict of interest.

frontiers in Physiology

ORIGINAL RESEARCH
published: 18 February 2020
doi: 10.3389/fphys.2020.00075

Modeling Bainbridge-Ropers Syndrome in *Xenopus laevis* Embryos

Hava Lichtig[1], Artyom Artamonov[1], Hanna Polevoy[1], Christine D. Reid[2], Stephanie L. Bielas[3] and Dale Frank[1]†*

[1] Department of Biochemistry, Faculty of Medicine, The Rappaport Family Institute for Research in the Medical Sciences, Technion – Israel Institute of Technology, Haifa, Israel, [2] Department of Genetics, Stanford University, Stanford, CA, United States, [3] Department of Human Genetics, University of Michigan Medical School, Ann Arbor, MI, United States

The *Additional sex combs-like (ASXL1-3)* genes are linked to human neurodevelopmental disorders. The *de novo* truncating variants in ASXL1-3 proteins serve as the genetic basis for severe neurodevelopmental diseases such as Bohring-Opitz, Shashi-Pena, and Bainbridge-Ropers syndromes, respectively. The phenotypes of these syndromes are similar but not identical, and include dramatic craniofacial defects, microcephaly, developmental delay, and severe intellectual disability, with a loss of speech and language. Bainbridge-Ropers syndrome resulting from *ASXL3* gene mutations also includes features of autism spectrum disorder. Human genomic studies also identified missense *ASXL3* variants associated with autism spectrum disorder, but lacking more severe Bainbridge-Ropers syndromic features. While these findings strongly implicate *ASXL3* in mammalian brain development, its functions are not clearly understood. ASXL3 protein is a component of the polycomb deubiquitinase complex that removes mono-ubiquitin from Histone H2A. Dynamic chromatin modifications play important roles in the specification of cell fates during early neural patterning and development. In this study, we utilize the frog, *Xenopus laevis* as a simpler and more accessible vertebrate neurodevelopmental model system to understand the embryological cause of Bainbridge-Ropers syndrome. We have found that ASXL3 protein knockdown during early embryo development highly perturbs neural cell fate specification, potentially resembling the Bainbridge-Ropers syndrome phenotype in humans. Thus, the frog embryo is a powerful tool for understanding the etiology of Bainbridge-Ropers syndrome in humans.

Keywords: Bainbridge-Ropers syndrome, ASXL3 protein, *Xenopus laevis* embryos, neurodevelopmental disease model, neural crest

OPEN ACCESS

Edited by:
John Noel Griffin, University of East Anglia, United Kingdom

Reviewed by:
Elena Silva, Georgetown University, United States
Anna Philpott, University of Cambridge, United Kingdom
Jean-Pierre Saint-Jeannet, New York University, United States

***Correspondence:**
Dale Frank
dale@technion.ac.il

†***ORCID:***
Dale Frank
orcid.org/000-0002-1857-6820

Specialty section:
This article was submitted to Embryonic and Developmental Physiology, a section of the journal Frontiers in Physiology

Received: *31 January 2019*
Accepted: *23 January 2020*
Published: *18 February 2020*

Citation:
Lichtig H, Artamonov A, Polevoy H, Reid CD, Bielas SL and Frank D (2020) Modeling Bainbridge-Ropers Syndrome in Xenopus laevis Embryos. Front. Physiol. 11:75. doi: 10.3389/fphys.2020.00075

INTRODUCTION

Bainbridge-Ropers syndrome (BRS; OMIM 615485) is characterized by failure to thrive, craniofacial defects, feeding problems, global developmental delay, hypotonia, intellectual disability and delays in language acquisition (Bainbridge et al., 2013; Russell and Graham, 2013). *De novo* truncating mutations in *Additional sex combs-like 3* (*ASXL3*) have emerged as the cause of BRS, while missense mutations in ASXL3 have been identified in individuals with autism spectrum

disorder (ASD) (Dinwiddie et al., 2013; Russell and Graham, 2013; De Rubeis et al., 2014). Many *de novo* mutations disrupt chromatin remodeling genes, suggesting that chromatin perturbation and the subsequent misregulation of transcription is an important molecular mechanism in human genetic disease (Veltman and Brunner, 2012; Allen et al., 2013; Dinwiddie et al., 2013; Ku et al., 2013). *ASXL* genes are vertebrate homologs of the *Drosophila Additional sex combs* gene. Members of this gene family enhance transcription regulation by Polycomb-group and Trithorax-group complexes (Gaytán de Ayala Alonso et al., 2007; Baskind et al., 2009; Fisher et al., 2010). In vertebrates, the ASXL family consists of three members, the ASXL1, ASXL2, and ASXL3 proteins (Fisher et al., 2006; Aravind and Iyer, 2012; Gelsi-Boyer et al., 2012; Katoh, 2013, 2015). Germline mutations of ASXL proteins occur in patients with congenital disorders, whereas somatic mutations are seen in cancer (Gelsi-Boyer et al., 2012; Katoh, 2013; Srivastava et al., 2017).

Molecular functions have been predicted for ASXL3 based on its similarity to other ASXL family proteins, but its true function remains unknown. ASXL1 protein acts as a scaffold for ubiquitin C-terminal hydrolase (BAP1), histone lysine methyltransferase (EZH2) and nuclear receptors (Katoh, 2015). ASXL1 interacts with BAP1 protein to form the human Polycomb repressive deubiquitination (PR-DUB) complex, which removes mono-ubiquitin from lysine 119 of histone H2A (Di Croce and Helin, 2013). BAP1 alone cannot deubiquitinate H2A, so PR-DUB formation is critical for normal function. While BAP1 is a required component of a PR-DUB, other ASXL family members in addition to ASXL1 are likely interchangeable to form the active deubiquitinase complex (Scheuermann et al., 2010; Lai and Wang, 2013; Srivastava et al., 2016). In human cells, ASXL3 protein was shown to interact with BAP1 to form the PR-DUB complex (Srivastava et al., 2016).

In primary fibroblasts established from a BRS patient with a truncation mutation, *asxl3* mRNA underwent nonsense mediated decay, suggesting that BRS results from a reduction in ASXL3 activity (Srivastava et al., 2016). In these fibroblasts, H2A ubiquitination was increased, suggesting that either the reduced levels of endogenous ASXL3 protein and/or the ASXL3 truncated protein disrupt the normal PR-DUB complex activity. In primary human cells, the effect of elevated histone H2 ubiquitination on global transcription was examined by comparing gene expression levels in ASXL3 truncation versus normal individuals. This study found over five hundred genes had significant changes in expression in BRS derived cells versus controls, half increased while half decreased (Srivastava et al., 2016). Interestingly, the truncated ASXL3 protein interacts with BAP1 protein (Srivastava et al., 2016). Germline mutations in PRC1 complex components were shown to disrupt H2A mono-ubiquitination in ASD and primary microcephaly (Awad et al., 2013; Gao et al., 2014). BRS is the first single gene disorder shown to exhibit defects in deubiquitination of H2A (Srivastava et al., 2016). These findings highlight a role for dynamic regulation of H2A ubiquitination in neurodevelopmental disease.

Often, in human genetic disease, the path from mutation to function is not an easy one. Because of the complexities of human neurodevelopment, it remains unclear how the ASXL3 truncation mutation leads to BRS. Truncated ASXL3 protein could be dominant-negative, hypomorphic or dead. Not mutually exclusive, the protein could be functional (varying degrees of hypomorphy) and its activity could be rate-limited due to RNA mediated decay and overall reduced ASXL3 protein levels causing a haploinsufficiency phenotype. Understanding the correct temporal role of ASXL3 protein in early neural development will elucidate mechanisms underlying both BRS and autism syndromes caused by ASXL3 activity perturbation in early human embryonic development. Early *Xenopus* development offers an easy manipulable system for unraveling the etiology of the ASXL3 induced disease state. *Xenopus* is unique in offering the resolution of a changing organism with a disease phenotype/state and not a cell line to examine these questions. We examine the effects of ASXL3 knockdown through all stages of early neurodevelopment in a whole organism. We have found that knockdown of ASXL3 protein disturbs the earliest stages of neural cell fate specification, including early nervous system induction and anteroposterior (AP) patterning. ASXL3 morphant embryos express lower levels of genes required for correct formation of forebrain, hindbrain, primary neurons and neural crest. Analysis of patients and fetuses of BRS patients show similar defects in craniofacial, motor neuron and hindbrain development (Bainbridge et al., 2013; Balasubramanian et al., 2017; Bacrot et al., 2018). These results show that perturbation of ASXL3 function during early vertebrate development has devastating effects on formation of the early nervous system.

RESULTS

ASXL3 Knockdown Modulates Neural Cell Fate Formation

To determine a role for ASXL3 protein during early *Xenopus* development, we depleted endogenous ASXL3 protein by using a translation blocking morpholino oligonucleotide (MO). ASXL3 knockdown embryos show a modulated posterior neural structure, impeded neural plate elongation, with slowed and reduced neural folding (**Figure 1A**, see star). To characterize this phenotype in neurula stage embryos, neural markers were examined by both *in situ* hybridization (**Figure 1B**, compare left to right panels) and sqRT-PCR (**Figure 1C**, compare lanes 2–3). In ASXL3 knockdown embryos, expression of hindbrain (*krox20*), neural crest (*foxd3*), and primary neuron (*n-tub*) markers was severely reduced. The number of primary neurons was lower and their normal arrangement was also perturbed, as observed by *n-tub* expression (**Figure 1B**). Interestingly spinal cord marker (*cdx*) expression was not reduced (**Figures 1B,C**); *cdx1* expression was consistently increased slightly in ASXL3 morphant embryos (**Figure 1C**, compare lanes 2–3).

These results suggest that ASXL3 protein is a crucial regulator that balances the correct levels of early posterior neural cell fates. These observations also suggest that ASXL3 may function in the

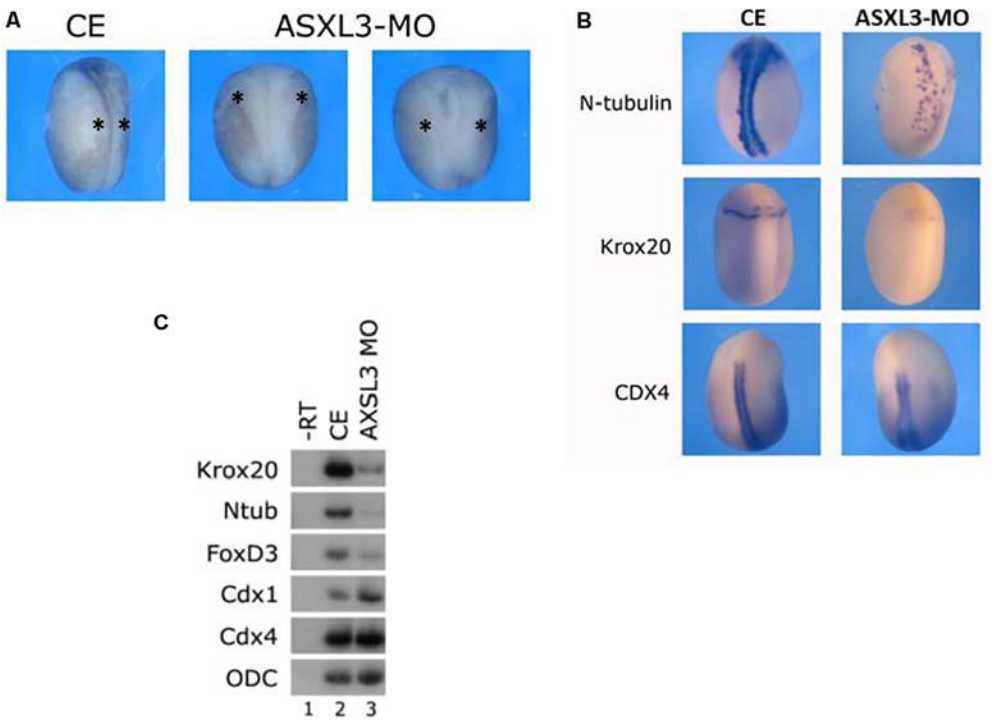

FIGURE 1 | ASXL3 knockdown causes neural tube defects and inhibits expression of posterior neural markers. **(A)** Neurula stage embryos were examined for neural tube defect phenotypes. Control embryos (CE – left panel) were injected with 15ng *ASXL3-MO* at the one cell stage (two right panels) The *ASXL3* morphant embryos are squat, less elongated, with poor neural folding and open neural plates. In the CE group 87% of the embryos had normal neural folds (n = 158) versus the *ASXL3-MO* groups in which 86% had an open neural plate phenotype (n = 603). This was repeated in six independent experiments. The star marks the neural folds regions in the embryos. **(B)** Control embryos (CE, left panel) were injected at the one-cell stage with *ASXL3-MO* (15 ng, right panel). *In situ* hybridization was carried out on late neurula (st.18) embryos to the markers: *n-tub* (primary neuron), *krox20* (hindbrain and lateral neural crest stripes) and *cdx4* (spinal cord). *Ntub* was weakly expressed in 68% (n = 19) of the embryos; *krox20* was weakly expressed in 85% (n = 20) of the embryos and *cdx4* expression was normal in 81% (n = 21) of the *ASXL3-MO* injected embryos. **(C)** Control embryos (lane 2) were injected at the one-cell stage with *ASXL3-MO* (15 ng, lane 3). sqRT-PCR was carried out on total RNA isolated from pools of eight neurula (st.16) embryos from each group to the genes: *krox20* (hindbrain) *ntub* (primary neuron), *foxd3* (neural crest) and *cdx1/4* (spinal cord). -RT was performed (lane 1) to total RNA isolated from the control uninjected embryos. The housekeeping gene *ODC* serves as positive control for RNA levels.

earliest network of genes regulating the specification of posterior-trunk neural tissue such as hindbrain, primary neurons and neural crest. This phenotype is quite similar to the knockdown phenotype for the Meis3 homeodomain protein (Dibner et al., 2001; Gutkovich et al., 2010) or embryos disrupted for early Wnt-signaling, where hindbrain, neural crest, and primary neuron cell fates are lost, but the spinal cord forms quite normally (Elkouby et al., 2010; Polevoy et al., 2019).

Ectopic Expression of Full-Length or Truncated Human ASXL3 Protein Rescues the Knockdown Phenotype

The wild-type full-length (FL) human ASXL3 protein (**Figure 2A**) functions during early *Xenopus* development. Ectopic expression of human ASXL3 protein rescued neural marker expression in ASXL3 morphant embryos (**Figure 2B**, compare lanes 3–6). As shown by *in situ* hybridization (**Figure 2D**), primary neuron (*ntub*, left panel) and neural crest (*twist*, right panel) marker expression is significantly rescued, more so resembling the normal uninjected embryos for both levels and pattern of gene expression. Ectopic expression of ASXL3 in normal embryos at the concentration described (**Figures 2B,C**) does not alter gene expression of neural markers or cause a significant phenotype (not shown). We also ectopically expressed a mutant/truncated form of the ASXL3 protein (**Figure 2A**) associated with BRS into ASXL3 morphant embryos (**Figure 2C**). This mutant ASXL3 protein has a severe truncation, having an ORF of 484 amino acids in comparison to the wildtype ASXL protein of 2248 amino acids (**Figure 2A**). This mutant protein has a functional N-terminal domain that interacts with the BAP1 hydrolase protein that removes mono-ubiquitin from histone H2A lysine 119 as a component of the PR-DUB complex, like wild type ASXL3 protein (Srivastava et al., 2016). Somewhat surprisingly, when compared to the wildtype protein, the truncated ASXL3 protein also robustly rescued neural marker expression in the morphant embryos (**Figure 2C**, compare lanes 3–5). This result suggests that the truncated protein has significant biological activity via its forced ectopic expression in *Xenopus* embryos. In BRS, it was suggested that nonsense mediated decay may affect *asxl3* mRNA and subsequent protein levels (Srivastava et al., 2016). This is

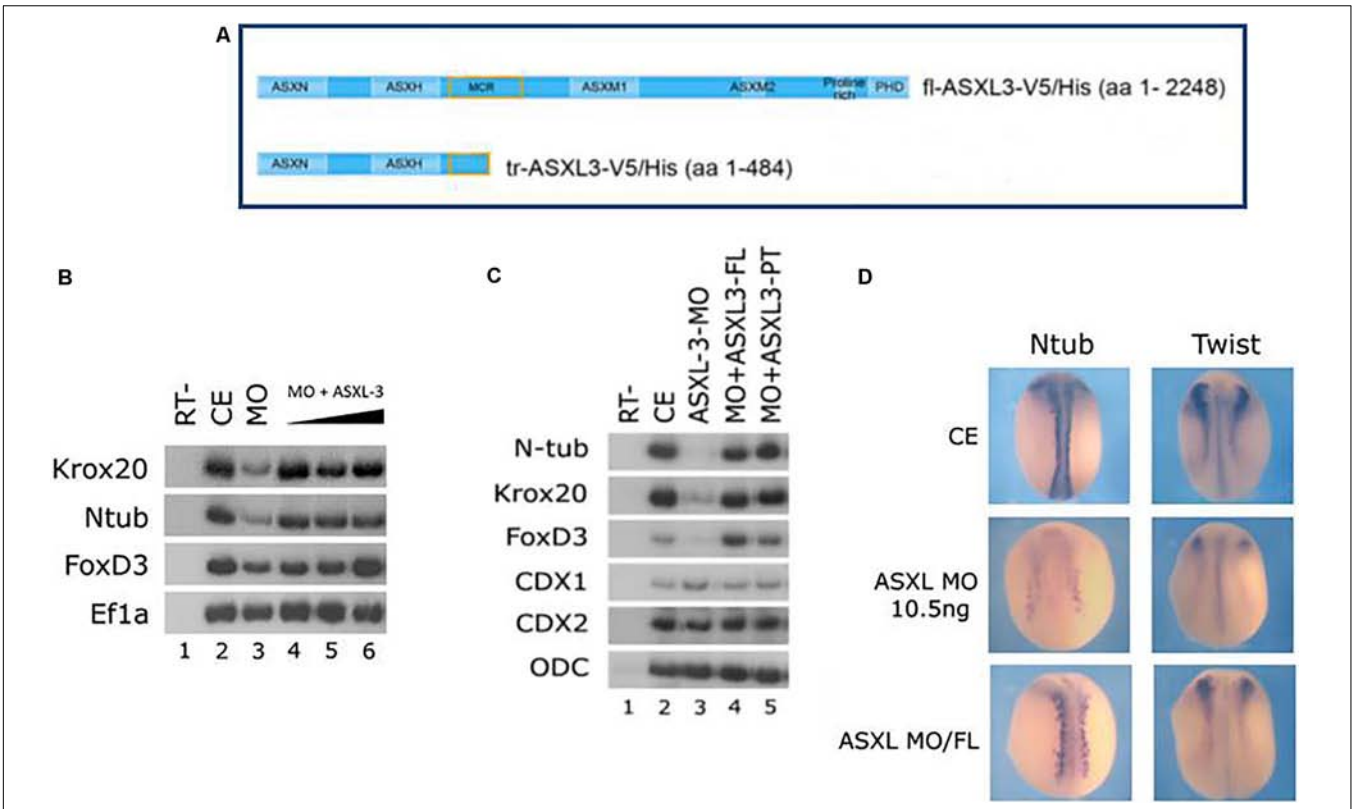

FIGURE 2 | Full-length and truncated/mutant human ASXL3 proteins rescue the *ASXL3-MO* Knockdown phenotype. **(A)** A schematic illustration of the main functional units of the full-length human and truncated/mutant ASXL3 proteins that were used in this study (Srivastava et al., 2016). **(B)** Control embryos (lane 2) were injected at the one-cell stage with *ASXL3-MO* (12.5 ng, lane 3) and increasing concentrations of the full-length mRNA (250–750 pg) encoding the human ASXL3 protein (lanes 4–6). sqRT-PCR was carried out on total RNA isolated from pools of seven neurula (st.16) embryos to the genes: *krox20*, *ntub,* and *foxd3*. -RT was performed (lane 1) to RNA isolated from the uninjected control embryos. The housekeeping gene *Ef1α* serves as positive control for RNA levels. **(C)** Control embryos (lane 2) were injected at the one-cell stage with *ASXL3-MO* (12.5 ng, lane 3) and the mRNAs (500 pg) encoding the full-length (FL – 2248 amino acids) or truncated/mutant (PT – 484 amino acids) human ASXL3 proteins (lanes 4–5). sqRT-PCR was carried out on total RNA isolated from pools of seven neurula (st.17–18) embryos to the genes: *ntub*, *krox20*, *foxd3*, *cdx1,* and *cdx2*. -RT was performed (lane 1) to RNA isolated from the uninjected control embryos. The housekeeping gene *ODC* serves as positive control for RNA levels. **(D)** Control embryos (CE, top panels) were injected at the one-cell stage with *ASXL3-MO* (middle panels) and mRNA (300 pg) encoding the full-length (FL) human ASXL3 protein (bottom panels). *In situ* hybridization was carried out in late neurula stage embryos to the markers: *ntub* (primary neuron) and twist (neural crest). *Ntub* was weakly expressed in 81% (n = 21) of the *ASXL3-MO* embryos versus controls (compare top/middle panels, left side); rescued expression was observed in 68% (n = 19) of the *ASXL3-MO* embryos (compare bottom/middle panels, left side). *Twist* was weakly expressed in 90% (n = 21) of the *ASXL3-MO* embryos versus controls (compare top/middle panels, right side); rescued expression was observed in 46% (n = 24) of the *ASXL3-MO* embryos (compare bottom/middle panels, right side).

a dilemma for human geneticists in trying to understand the etiology and mechanism of disease. However, in our assay of ectopic forced over-expression, the protein seems not to be dead or dominant-negative, but fairly functional.

ASXL3 Is Necessary to Induce Posterior Neural Cell Fates in Embryonic Explants

Xenopus offers an opportunity to use explant assays in real embryonic time to directly study induction of cell fate specification in pluripotential cells. We have utilized the animal cap (AC) assay to determine potential pathway interactions for ASXL3 in the embryo. We initially addressed ASXL3 interactions with the Meis3 homeodomain protein, since this protein is one of the most important early regulators of posterior neural cell fates (Dibner et al., 2001). In Meis3 morphant embryos, there is a loss of posterior neural cell fates (Dibner et al., 2001; Gutkovich et al., 2010), similar to the ASXL3 knockdown (**Figures 1B,C**, **2B,C**). To address this question, we co-injected one-cell stage embryos with mRNA encoding Meis3 protein and the *ASXL3-MO*. AC explants were removed at blastula stages and cultured to neurula stages, and posterior neural marker expression was examined. In this AC assay (Salzberg et al., 1999), Meis3 robustly induces expression (**Figure 3A**, compare lanes 3–4) of hindbrain (*krox20*, *hoxd1*) and spinal cord markers (*cdx1*). Co-expression of Meis3/*ASXL3-MO* led to a sharp decrease in hindbrain marker (*krox20*, *hoxd1*) expression, while the *cdx1* spinal cord marker expression levels were virtually unchanged (**Figure 3A**, compare lanes 4 and 6) or slightly increased. Thus in the absence of ASXL3, Meis3 protein is differentially perturbed, it cannot induce hindbrain but still efficiently activates expression of spinal cord markers. These results mimic the observation

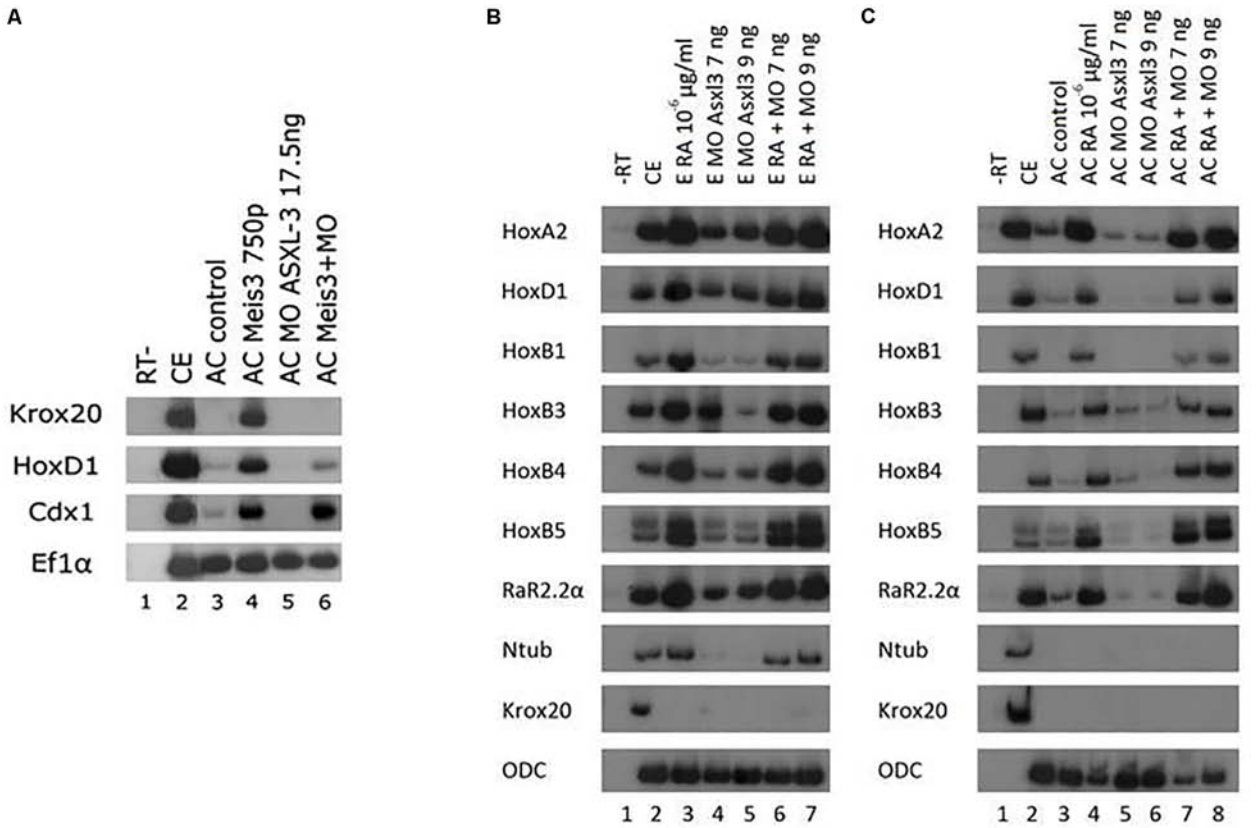

FIGURE 3 | ASXL3 is necessary to induce posterior neural cell fates via Meis3 but not via retinoic acid. **(A)** One-cell stage embryos (lane 2) were injected at the one-cell stage with *meis3* encoding RNA (750 pg, lane 4), *ASXL3-MO* (17.5 ng, lane 5) or both (lane 6). AC explants were removed from control (lane 3) and injected embryos (lanes 4–6) at blastula stage 9, and cultured to neurula stage 16. sqRT-PCR was carried out on total RNA isolated from five control embryos (lane 2), and from eighteen ACs from each group (lanes 3–6) to the genes: *krox20, hoxd1* (hindbrain), *cdx1* (spinal cord). -RT was performed for RNA levels. The housekeeping gene *Ef1*α serves as positive control for RNA levels. **(B)** Control embryos (lane 2) were injected at the one-cell stage with *ASXL3-MO* (7 and 9 ng, lanes 5 and 6, respectively). Upon reaching blastula stage 10 control embryos and the injected groups were placed in retinoic acid at 10^{-6} µg/ml (lanes 3, 6, 7). The Embryos were cultured to neurula stage 16. sqRT-PCR was carried out on total RNA isolated from five control embryos (lane 2), and from eighteen ACs from each group (lanes 3–8) to the genes: *hoxa2, hoxb1, hoxb3, hoxb4, hoxd1, rar2.2*α*, krox20* (hindbrain), *hoxb5* (spinal cord), and *ntub* (primary neuron). -RT was performed for RNA levels. The housekeeping gene *ODC* serves as positive control for RNA levels. **(C)** Control embryos (lane 2) were injected at the one-cell stage with *ASXL3-MO* 7 and 9 ng, (lanes 5 and 6, respectively). AC explants were removed from control (lane 3) and injected embryos (lanes 3–8) at blastula stage 9, and upon reaching blastula stage 10 AC controls and the injected groups were placed in retinoic acid at 10^{-6} µg/ml (lanes 4, 7, 8). The ACs were cultured to neurula stage 16. sqRT-PCR was carried out on total RNA isolated from five control embryos (lane 2), and from eighteen ACs from each group (lanes 3–8) to the genes: *hoxa2, hoxb1, hoxb3, hoxb4, hoxd1, rar2.2*α*, krox20* (hindbrain), *hoxb5* (spinal cord), and *ntub* (primary neuron). -RT was performed for RNA levels. The housekeeping gene *ODC* serves as positive control for RNA levels.

seen in ASXL3 morphant embryos where hindbrain formation is perturbed, but the spinal cord marker expression is fairly normal (**Figures 1B,C**). This result suggests that ASXL3 acts in parallel with Meis3 protein in hindbrain specification.

Retinoic acid (RA) signaling is crucial for formation and patterning the hindbrain during early embryonic development (rev. in Frank and Sela-Donenfeld, 2019). We examined if ASXL3 knockdown modified RA inducing activity in embryos or AC explants. Embryos were treated with RA at gastrula stages and examined for neural markers at neurula stages. Expression levels of genes activated by RA in embryos or explants, such as the hindbrain markers *hoxa2, hoxd1, hoxb1, hoxb3, hoxb4, rar2.2*α *krox20*, spinal cord marker *hoxb5,* were examined (**Figures 3B,C**). In the ASXL3 morphant embryos, there was a strong reduction in the expression of the *hoxb1, hoxb3,* and *krox20* hindbrain markers. An intermediate inhibitory effect was observed for the hindbrain markers *hoxa2* and *rar2.2*α. No significant inhibition was seen in ASXL3 morphant embryos for the more posterior *hoxb4* (hindbrain/spinal cord border) and *hoxb5* (spinal cord) expression. All of these markers are activated by RA, except for *krox20* which is repressed by both the *ASXL3-MO* and RA treatment (Dibner et al., 2004). In the *ASXL3-MO*/RA group, the genes repressed by the *ASXL3-MO* are re-activated to high levels by RA, similar to control embryos. Clearly RA canceled the negative effect on gene expression mediated by ASXL3 protein knockdown. Similar results were seen in animal caps, in which the expression of RA target genes was not inhibited by the *ASXL3-MO* (**Figure 3C**, compare lanes 3–4 to 7–8).

Thus RA signaling seems to act independently of ASXL3 protein activity during posterior neural cell fate specification.

Inhibition of ASXL3 Differentially Modifies Noggin Neural Inducing Activity

To further explore the role of ASXL3 protein in early neural development, we examined if initial anterior and general neural induction by a BMP antagonist (noggin) or one of its downstream mediators requires functional ASXL3 protein. We co-expressed the BMP-antagonist protein noggin and the *ASXL3-MO* in ACs (**Figure 4A**). Noggin alone robustly induces panneural (*nrp1*, *ncam*), cement gland (*xag*) and forebrain marker (*xanf*, *foxd1*, *foxg1*, *otx2*) expression in ACs (**Figure 4A**, compare lanes 3–5). In Noggin/*ASXL3-MO* co-expressing ACs, neural markers were not all inhibited to the same extent. The *ncam*, *foxd1*, *foxg1,* and *xag* markers were the most strongly inhibited (**Figure 4A**, compare lanes 3–5 to lanes 7–8). Moderate inhibition was observed for the *otx2* and *nrp1* markers (**Figure 4A**, compare lanes 3–5 to lanes 7–8), while expression of the most anterior *xanf1* marker was slightly stimulated (**Figure 4A**, compare lanes 3–5 to lanes 7–8). This observation suggests that ASXL3 is not acting as a simple permissive on/off switch for noggin activity. ASXL3 protein appears to be modifying noggin neural activity in a complex manner that may have implications for cell fate specification in the developing embryo. Interestingly, expression of the most anterior *xanf1* forebrain marker was slightly stimulated and not repressed by ASXL3 knock down (**Figure 4A**). Ectopic XANF1 protein levels were shown to repress expression of the adjacently expressed *otx2* and *foxg1* forebrain markers (Ermakova et al., 1999). Perhaps ASXL3 knockdown sets the stage for more efficient repression of forebrain genes by XANF1, by increasing its expression levels at the cost of more posterior forebrain regions.

ASXL3 also regulates gene expression downstream to noggin. To address this point, we examined the effect of ASXL3 knockdown on FoxD1 protein activity. FoxD1 is a transcriptional repressor protein, whose expression is induced by BMP-antagonism (noggin) in *Xenopus*, and it acts downstream to induce expression of panneural and forebrain markers (Mariani and Harland, 1998; Polevoy et al., 2017). FoxD1 is required as a mediator of early neural induction in the forebrain region in *Xenopus* (Mariani and Harland, 1998; Polevoy et al., 2017). In ACs, FoxD1 induces expression of a primary neuron marker (*ntub*) in a Wnt-dependent manner (Fonar et al., 2011; Polevoy et al., 2017). In ACs, FoxD1 protein induced panneural (*ncam*), forebrain (*otx2*) and *ntub* marker expression (**Figure 4B**, compare lanes 3–6). In FoxD1/*ASXL3-MO* co-expressing animal caps, similar to noggin, FoxD1 fails to efficiently induce these markers (**Figure 4B**, compare lanes 4–6 to lanes 8–10). Thus, activity of the BMP-antagonism downstream mediator, FoxD1 is inhibited by the absence ASXL3 protein. Interestingly, *ntub* expression is also inhibited, suggesting that Wnt-dependent processes are also affected. This result complements our observation in ASXL3 morphant embryos, where Wnt-dependent cell fates such as primary neurons, hindbrain and neural crest are all reduced (**Figures 1B,C**).

We also examined expression of anterior neural markers in ASXL3 morphant embryos. Interestingly, anterior neural expression in whole embryos recapitulated many of the observations seen in the previous AC experiment shown in **Figure 4A**. Expression of the most anterior forebrain marker, *xanf* is not significantly altered by ASXL3 knockdown (**Figure 4C**, lanes 2–4). However, expression of the forebrain specific *foxd1* and *foxg1* markers as well as the cement gland marker *xag* is highly reduced, whereas expression of the fore-midbrain marker *otx2* is only moderately perturbed (**Figure 4C**, lanes 2–4). The same was true for panneural markers, where expression of *nrp1* was fairly normal, but *ncam* expression was highly reduced (**Figure 4C**, lanes 2–4). As previously shown (**Figure 1**), expression of hindbrain (*krox20*, *hoxb3*), primary neuron (*ntub*) and neural crest (*snail2, foxd3*) markers was highly inhibited, but expression of the *cdx* genes in the spinal cord was normal or slightly increased (**Figure 4C**, lanes 2–4). Tailbud stage ASXL3 morphant embryos have a squat-body and perturbed head/trunk formation (**Figure 5A**), which is similar to phenotypes in which hindbrain and/or neural crest formation is perturbed (Dibner et al., 2001; Gutkovich et al., 2010).

The effects of ASXL3 knockdown are specific for neural tissue and are not a secondary result of a loss of mesoderm that regulates neural induction and patterning. Expression of dorsal (*gsc*, *xnot*, *chd*), dorsal-lateral (*myod*), ventral (*osr1/2*, *vent2*), and pan-mesodermal (*xbra*) markers in gastrula stage ASXL3 morphant embryos is normal (**Figure 4E**, compare lanes 2–4). In later stage sibling embryos, neural marker expression (*en2*, *krox20*, *ncam*, *ntub*, *foxd3*) is characteristically reduced (**Figure 4F**, compare lanes 2–4), while some markers are typically unaffected (*cdx2/4*, *sox2/3*). *Sox2/3* expression suggests that neural progenitor cell formation is not disrupted in the knockdown embryos (**Figure 4F**).

In ASXL3 morphants, we see abnormal head formation (**Figure 5A**), suggesting a disruption of more anterior neural tissue. The neural crest also seems atypical as seen by abnormal melanocyte patterning along the body axis and malformation of the dorsal fin (**Figure 5A**). In tailbud stage embryos, there is a strong reduction of *twist* marker expression (**Figure 5B**), which is specific for head/craniofacial neural crest cells (Figueiredo et al., 2017). Additionally, neural crest derived head cartilage formation is perturbed and reduced in ASXL3 morphant embryos (**Figure 5C**). The phenotypes seen in neurula (**Figures 1**, **2**) through tadpole stage embryos (**Figures 5A–C**) are supported by the *ASXL3* gene expression patterns. By *in situ* hybridization (**Figures 5D,E**), *ASXL3* mRNA transcripts are detected throughout the neural plate in neurula stage embryos (**Figure 5D**) and predominantly in the head and dorsal fin in later tadpole stages (**Figure 5E**), regions derived from neural crest. *ASXL3* transcripts were not significantly detected in the more anterior cement gland or in the developing eye regions (**Figure 5E**).

ASXL3 knockdown causes a multitude of differential AP patterning disruptions in nervous system development. In the posterior nervous system, hindbrain, primary neuron and neural crest formation is perturbed, yet the spinal cord appears normal. Neural marker expression in the more anterior forebrain is

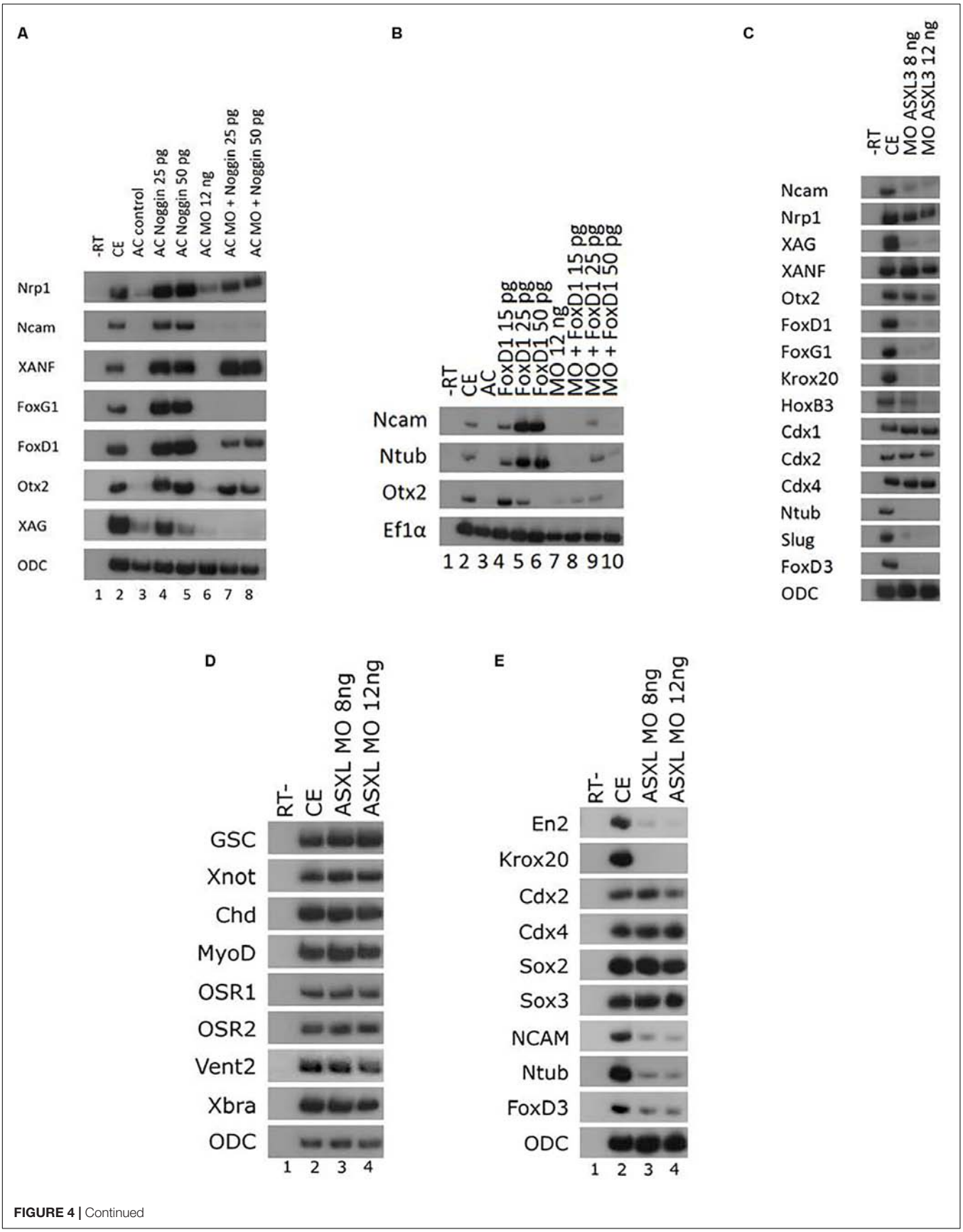

FIGURE 4 | Continued

FIGURE 4 | Inhibition of ASXL3 differentially modifies noggin neuralizing activity. **(A)** Control embryos (lane 2) were injected at the one-cell stage with noggin encoding RNA (25 and 50 pg, lanes 4 and 5), *ASXL3-MO* (12 ng, lane 6), or both (lanes 7 and 8). AC explants were removed from control (lane 3) and injected embryos (lanes 4–8) at blastula stage 9, and cultured to neurula stage 16. sqRT-PCR was carried out on total RNA isolated from five control embryos (lane 2), and from eighteen ACs from each group (lanes 3–8) to the genes: *nrp1, ncam* (panneural), *xanf1, foxg1, foxd1, otx2* (forebrain), and *xag* (cement gland). -RT was performed for RNA levels. The housekeeping gene *ODC* serves as positive control for RNA levels. **(B)** Control embryos (lane 2) were injected at the one-cell stage with *ASXL3-MO* (12 ng, lane 7) and mRNA (15, 25, 50 pg) encoding foxd1 (lanes 4–6), or both (lanes 8–10). AC explants were removed from control (lane 3) and injected embryos (lanes 4–10) at blastula stage, and cultured to neurula stage 16. sqRT-PCR was carried out on total RNA isolated from five control embryos (lane 2), and from eighteen ACs from each group (lanes 3–10). sqRT-PCR was carried out on total RNA isolated from pools of seven neurula (st.16) embryos to the genes: *ncam* (panneural), *ntub* (primary neurons), and *otx2* (forebrain). -RT was performed (lane 1) to RNA isolated from the uninjected control embryos. The housekeeping gene *Ef1*α serves as positive control for RNA levels. **(C)** Control embryos (lane 2) were injected at the one-cell stage with *ASXL3-MO* (8, 12 ng; lanes 3–4). sqRT-PCR was carried out on total RNA isolated from pools of five neurula (st.16) embryos from each group to the genes: *ncam*, *nrp1, xag*, *xanf*, *otx2*, *foxd1*, *foxg1*, *krox20*, *hoxb3*, *cdx1*, *cdx2*, *cdx4*, *ntub*, *snail2,* and *foxd3*. -RT was performed (lane 1) to total RNA isolated from the control uninjected embryos. The housekeeping gene *ODC* serves as positive control for RNA levels. **(D)** Control embryos (lane 2) were injected at the one-cell stage with *ASXL3-MO* (8, 12 ng; lanes 3–4). sqRT-PCR was carried out on total RNA isolated from pools of six gastrula (st.11.5) embryos from each group to the genes: *goosecoid* (*gsc*), *xnot*, *chordin* (*chd*), *myod*, *osr1*, *osr2*, *vent2,* and *brachyury* (*xbra*). -RT was performed (lane 1) to total RNA isolated from uninjected control embryos. The housekeeping gene *ODC* serves as positive control for RNA levels. **(E)** Sibling embryos from **(D)** were taken for sqRT-PCR. Total RNA was isolated from pools of six neurula (st.16) embryos to the genes: *engrailed2* (*en2*), *krox20*, *cdx2/4*, *sox2/3*, *ncam*, *ntub*, and *foxd3*. -RT (lane 1) to RNA isolated from the control embryos. The housekeeping gene *ODC* serves as positive control for RNA levels.

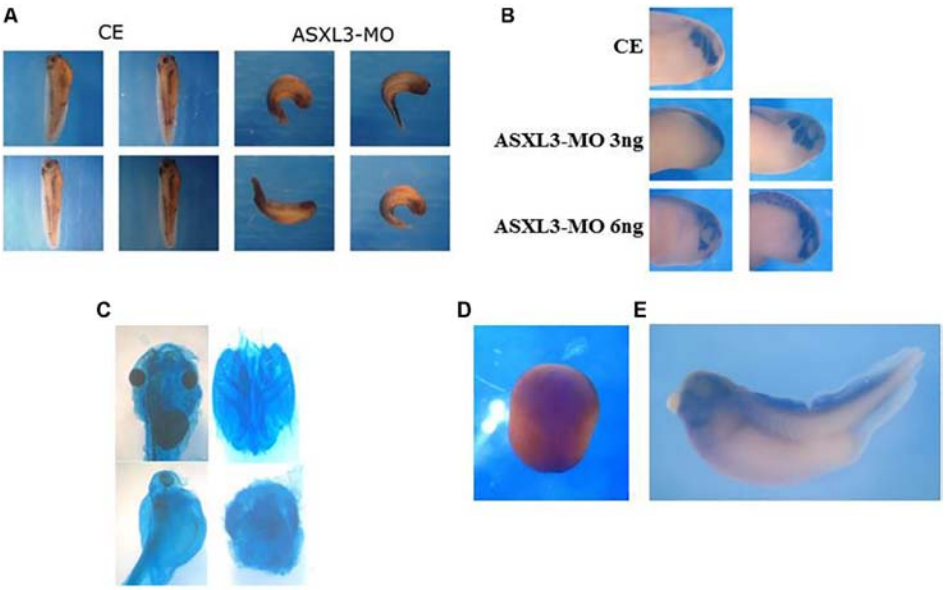

FIGURE 5 | ASXL3 knockdown disrupts head formation. **(A)** Stage 37 tadpole stage embryos were examined for axial defect phenotypes. Control embryos (CE – four left panels) were injected with 12 ng *ASXL3-MO* at the one-cell stage (four right panels) The *ASXL3* morphant embryos are squat, less elongated, with poor trunk and head development. In the CE group 100% of the embryos developed normally development (n = 41) versus the *ASXL3-MO* group in which 100% of the embryos had a disrupted axial phenotype (n = 41). Four representative embryos are shown for each group. **(B)** Embryos were microinjected with *ASXL3-MO* (3 or 6 ng) into one-blastomere at the two-cell stage, so only half the embryo is perturbed. At tailbud stage 22, *in situ* hybridization was performed to the *twist* gene; *twist* is a marker for craniofacial neural crest cells (top panel control embryo/CE, 100% normal; n = 30). In middle and bottom panel, left side is injected and right side is normal. *Twist* expression is inhibited and (asymmetric, 60%; n = 40) in the left panel (*ASXL3-MO*), but its expression is normal on the uninjected side of the embryo in the right panel. **(C)** Embryos were injected with *ASXL3-MO* (12 ng) at the one-cell stage. Embryos were stained for cartilage formation at tadpole stages. Control embryos (90%, n = 27; panel) normal head cartilage staining (upper panel, left: head shot; right: dissected head cartilage). All morphant embryos (100%, n = 14) had reduced and abnormal head cartilage staining (lower panel, left: head shot; right: dissected head cartilage). **(D,E)** *In situ* hybridization was performed with a *Xenopus laevis ASXL3* probe to neurula (**D**; dorsal view, anterior-posterior is top-bottom) and tadpole stage 35 **(E)** embryos.

also perturbed, but differentially and even panneural markers are not affected equally. These results suggest that ASXL3 acts downstream to a number of signaling pathways and transcription factors to differentially modulate chromatin in genes that respond to these cues. Perhaps, only a subset of neural-specific genes are affected in differing embryonic regions along the neural AP axis, which could be the trigger of the general nervous system defects seen in BRS.

DISCUSSION

In this study, we utilized *Xenopus laevis* as a platform to better understand the etiology of BRS during early embryonic development. BRS is caused by different truncations of the ASXL3 polycomb protein, and is heterozygous in nature. ASXL3 plays a role in H2A deubiquitination by binding the BAP1 protein to form the PR-DUB complex. This complex modifies

H2A ubiquitination to regulate chromatin structure and gene expression. Indeed, in fibroblast cells derived from BRS patients, H2A ubiquitination was increased and over five-hundred genes had altered gene expression levels (Srivastava et al., 2016).

Our initial goal was to examine how *ASXL3-MO* protein knockdown modulates early nervous system development. In embryos, we found a differential inhibition of posterior neural cell fates. Hindbrain, neural crest and primary neuron cell fates were perturbed in neurula through tadpole stage embryos. The embryos also had impeded neural plate elongation and folding which seem to be partially compensated for at later stages. The spinal cord seemed to form normally and ASXL3 morphant embryos had slightly increased expression of some spinal cord markers. Our experiments in explants suggest that there is a differential requirement for ASXL3 protein in the hindbrain versus spinal cord. It is clear that while not identical to BRS, the perturbation of neural crest formation in *Xenopus* development may give us clues as to the initial etiology of the craniofacial defects found in BRS (Bainbridge et al., 2013; Dinwiddie et al., 2013; Russell and Graham, 2013; Hori et al., 2016; Balasubramanian et al., 2017; Kuechler et al., 2017; Bacrot et al., 2018). Formation of hindbrain, primary neurons and neural crest tissues are perturbed in ASXL3 morphant embryos. While BRS patients do not have an apparent strong knockdown/out phenotype, they do display similar phenotypic defects in craniofacial, motor neuron and hindbrain organization (Bainbridge et al., 2013; Dinwiddie et al., 2013; Russell and Graham, 2013; Hori et al., 2016; Balasubramanian et al., 2017; Kuechler et al., 2017; Bacrot et al., 2018). Our experiments in embryos in explants also show that the loss of ASXL3 activity modulates initial neural induction by modulating early expression of anterior and panneural markers induced by BMP antagonism. Anterior forebrain marker expression is variably disrupted in the ASXL3 morphant embryos, suggesting that in the forebrain ASXL3 acts to differentially regulate levels of transcription factors crucial for correct forebrain development. In ASXL3 morphants, the increase in *xanf1* expression could trigger repression of other transcription factor genes required for proper forebrain formation (Ermakova et al., 1999). It is interesting that RA signaling appears unaffected by ASXL3 knockdown. RA triggers activation of the retinoic acid receptor (RAR) that binds RARE elements in target genes during nervous system development (Janesick et al., 2015). Presumably, these elements are not irreversibly modified by ASXL3 mediated chromatin changes, and RAR proteins act independently of ASXL3 to bind RARE elements and activate RA-target gene expression. Further experimentation needs to be carried out to examine how ASXL3 regulates other signaling pathways required for hindbrain, neural crest and primary neuron formation. FGF and canonical Wnt signaling are crucial for the induction and specification of these cell types (Dorey and Amaya, 2010; Elkouby and Frank, 2010; Gutkovich et al., 2010). We will need to examine how ASXL3 protein knockdown modulates these signaling pathways and how this effects gene expression and the specification of these early posterior neural cell fates.

The genetic etiology of BRS is unknown, but interestingly both full-length and mutant/truncated ASXL3 proteins rescued the ASXL3 knockdown phenotype, by re-activating expression of hindbrain, neural crest and primary neuron marker genes. This observation suggests that at least in the assay utilized, the truncated protein is not dead or dominant-negative. It could be hypomorphic, and the forced ectopic levels of expression could circumvent this problem. Early *Xenopus* embryos are an excellent experimental system to investigate whether the ASXL3 mutation causes a dominant-negative, hypomorph or haploinsufficiency phenotype. We have already developed embryo and explant assays to address ASXL3 function in normal development. In future experiments, we can inject the *ASXL3-MO* at low to high concentration ranges in order to induce hypomorphic phenotypes in embryos/explants at the lower MO concentrations. The hypomorph concentrations can mimic the BRS disease phenotypes induced by haploinsufficiency as a result of RNA mediated decay or the mutant/truncated ASXL3 protein being a hypomorph/null protein. We can co-express full-length and mutant ASXL3 proteins in our various assays on the morphant background. *Xenopus ASXL3-MO* embryos/explants co-expressing equal levels of the wild-type and mutant proteins could mimic the mechanism of BRS. Haploinsufficiency is a possible cause of BRS (Srivastava et al., 2016). For ASXL2 truncation mutations, the mRNA does not undergo nonsense mediated decay, suggesting but not proving that that the protein is acting in a dominant-negative manner (Shashi et al., 2016). Depending on our accumulated knowledge, we will decide which of these approaches will be the best platform for transcriptome analysis versus control embryos. *Xenopus laevis* is unique in offering the resolution of a changing organism with a disease phenotype/state and not a cell line to examine this question. Via the *Xenopus* embryo, these future experiments identifying the earliest expressed embryonic target genes modulated by ASXL3 knockdown could be the key to understanding the embryonic etiology of BRS in humans.

Besides the ASXL3 truncation mutations associated with BRS, genomic studies have uncovered missense *ASXL3* variants linked to ASD that lack the BRS phenotype. How these mutant ASXL3 proteins cause BRS or missense variant proteins participate in ASD is not understood. Thus, another future goal is to develop bioassay screens to address functional differences in wildtype ASXL3 versus protein variants causing BRS or ASD. Often, there are no available bioassays to screen functional differences between proteins causing diseases or syndromes versus the normal protein. *Xenopus* may offer a solution to this problem. Our system offers an opportunity to address real-time physiological function *in vivo* during early development to actually address how a "model" protein causing genetic neural disorders or autism modulates early cell fate decisions, gene expression and neuron formation in the developing brain. We can leverage this system to understand the changing activities of mutant proteins that trigger human disorders. By understanding the role of ASXL3 in normal neural development in our different explant and embryo assays, we will substitute the various mutant versions (truncated or missense versions associated with BRS or ASD) of the protein and assay them for specific functions. Using these techniques, we will develop bioassays based on embryological activity to identify different activities of the ASXL3

protein mutants and missense-isoforms in involved in BRS or ASD. Thus, we hope to utilize the *Xenopus* embryonic system as a powerful tool to understand the molecular regulation of human genetic neural developmental disorders.

MATERIALS AND METHODS

Xenopus Embryos and Explants

Ovulation, *in vitro* fertilization, culture, explant dissection and treatment were as described (Re'em-Kalma et al., 1995; Bonstein et al., 1998). Embryos were stained with Alcian Blue for cartilage detection at tadpole stages (Figueiredo et al., 2017).

RNA and MO Injections

Both the full-length and the truncated-mutant ASXL3 pcDNA3.1/V5-His-TOPO vector constructs used for making mRNA were described in Srivastava et al. (2016). Capped sense *in vitro* transcribed mRNA constructs of human full-length and mutant-truncated *asxl3*, *meis3*, *noggin,* and *foxd1* (Salzberg et al., 1999; Srivastava et al., 2016; Polevoy et al., 2017) were injected into the animal hemisphere of one-cell stage embryos, as was the antisense translational-blocking *ASXL3*-morpholino oligonucleotide (*ASXL3-MO*; GeneTools) 5′GTCTTTCATGTTTGCATCTCATTGA -3′.

In situ Hybridization

Whole-mount *in situ* hybridization was performed (Harland, 1991) with digoxigenin-labeled probes *neural-specific tubulin* (*n-tub*), *krox20*, *cdx4, twist* (Gutkovich et al., 2010; Fonar et al., 2011; Figueiredo et al., 2017), and *asxl3*. Two *Xenopus asxl3* probes were used. One was synthesized based on the *Xenopus asxl3* gene sequence (Syntezza Ltd.). The other probe was subcloned into a T-easy vector (Promega) from neurula stage mRNA by RT-PCR. Both probes gave identical *in situ* hybridization patterns. Control sense probes gave no specific expression pattern.

Semi-Quantitative (sq) RT-PCR Analysis

sqRT-PCR was performed (Snir et al., 2006). In all sqRT-PCR experiments, three to six independent experimental repeats were typically performed. In all experiments, samples are routinely assayed a minimum of two times for each marker. sqRT-PCR Primers: *efα*, *odc*, *ncam*, *nrp1*, *sox2*, *sox3*, *xanf1*, *foxd1*, *foxg1*, *otx2*, *xag1*, *en2*, *krox20*, *hoxd1*, *hoxb1*, *hoxa2*, *hoxb3*, *hoxb4*, *hoxb5*, *RARα2.2*, *cdx1*, *cdx2*, *cdx4*, *n-tub*, *foxd3*, *slug* (*snail2*), *gsc*, *xnot*, *chd*, *myod*, *osr1*, *osr2*, *vent2,* and *xbra* (Aamar and Frank, 2004; Fonar et al., 2011; Elkouby et al., 2012; Bin-Nun et al., 2014).

ETHICS STATEMENT

This study has been carried out under the guidelines of DF's animal ethics permit (IL-134-11-18). The above research proposal has been reviewed by the Animal Care and Use Committee of the Technion, Israel Institute of Technology, and found to confirm with the regulations of this institution for work with laboratory animals. The Technion holds a valid Assurance (#A5027-01) of the US Department of Health & Human Services for humane care and use of laboratory animals.

AUTHOR CONTRIBUTIONS

HL, AA, HP, CR, SB, and DF conceived and designed the research. HL, AA, and HP performed the experiments. HL, AA, HP, and DF wrote the manuscript with input from CR and SB.

FUNDING

DF was supported by grants from the Israel Science Foundation (658/15), the Israel Cancer Research Fund, and the Lester Aronberg Fund in Neurology, Technion.

REFERENCES

Aamar, E., and Frank, D. (2004). *Xenopus* Meis3 protein forms a hindbrain-inducing center by activating FGF/MAP kinase and PCP pathways. *Development* 131, 153–163. doi: 10.1242/dev.00905

Allen, A. S., Berkovic, S. F., Cossette, P., Delanty, N., Dlugos, D., Eichler, E. E., et al. (2013). De novo mutations in epileptic encephalopathies. *Nature* 501, 217–221. doi: 10.1038/nature12439

Aravind, L., and Iyer, L. M. (2012). The HARE-HTH and associated domains: novel modules in the coordination of epigenetic DNA and protein modifications. *Cell Cycle* 11, 119–131. doi: 10.4161/cc.11.1.18475

Awad, S., Al-Dosari, M. S., Al-Yacoub, N., Colak, D., Salih, M. A., Alkuraya, F. S., et al. (2013). Mutation in PHC1 implicates chromatin remodeling in primary microcephaly pathogenesis. *Hum. Mol. Genet.* 22, 2200–2213. doi: 10.1093/hmg/ddt072

Bacrot, S., Mechler, C., Talhi, N., Martin-Coignard, D., Roth, P., Michot, C., et al. (2018). Whole exome sequencing diagnoses the first fetal case of Bainbridge-Ropers syndrome presenting as pontocerebellar hypoplasia type 1. *Birth Defects Res.* 3, 538–542. doi: 10.1002/bdr2.1191

Bainbridge, M. N., Hu, H., Muzny, D. M., Musante, L., Lupski, J. R., Graham, B. H., et al. (2013). De novo truncating mutations in ASXL3 are associated with a novel clinical phenotype with similarities to Bohring-Opitz syndrome. *Genome Med.* 5:11. doi: 10.1186/gm415

Balasubramanian, M., Willoughby, J., Fry, A. E., Weber, A., Firth, H. V., Deshpande, C., et al. (2017). Delineating the phenotypic spectrum of Bainbridge-Ropers syndrome: 12 new patients with de novo, heterozygous, loss-of-function mutations in *ASXL3* and review of published literature. *J. Med. Genet.* 54, 537–543. doi: 10.1136/jmedgenet-2016-104360

Baskind, H. A., Na, L., Ma, Q., Patel, M. P., Geenen, D. L., and Wang, Q. T. (2009). Functional conservation of *Asxl2*, a murine homolog for the Drosophila enhancer of trithorax and polycomb group gene *Asx*. *PLoS One* 4:e4750. doi: 10.1371/journal.pone.0004750

Bin-Nun, N., Lichtig, H., Malyarova, A., Levy, M., Elias, S., and Frank, D. (2014). PTK7 modulates Wnt signaling activity via LRP6. *Development* 141, 410–421. doi: 10.1242/dev.095984

Bonstein, L., Elias, S., and Frank, D. (1998). Paraxial-fated mesoderm is required for neural crest induction in *Xenopus* embryos. *Dev. Biol.* 193, 156–168. doi: 10.1006/dbio.1997.8795

De Rubeis, S., He, X., Goldberg, A. P., Poultney, C. S., Samocha, K., Cicek, A. E., et al. (2014). Synaptic, transcriptional and chromatin genes disrupted in autism. *Nature* 515, 209–215.

Di Croce, L., and Helin, K. (2013). Transcriptional regulation by Polycomb group proteins. *Nat. Struct. Mol. Biol.* 20, 1147–1155. doi: 10.1038/nsmb.2669

Dibner, C., Elias, S., and Frank, D. (2001). XMeis3 protein activity is required for proper hindbrain patterning in *Xenopus laevis* embryos. *Development* 126, 3415–3426.

Dibner, C., Elias, S., Ofir, R., Souopgui, J., Kolm, P., Sive, H., et al. (2004). The Meis3 protein and retinoid signaling interact to pattern the *Xenopus* hindbrain. *Dev. Biol.* 271, 76–87.

Dinwiddie, D. L., Soden, S. E., Saunders, C. J., Miller, N. A., Farrow, E. G., Smith, L. D., et al. (2013). De novo frameshift mutation in *ASXL3* in a patient with global developmental delay, microcephaly, and craniofacial anomalies. *BMC Med. Genomics* 6:32. doi: 10.1186/1755-8794-6-32

Dorey, K., and Amaya, E. (2010). FGF signalling: diverse roles during early vertebrate embryogenesis. *Development* 137, 3731–3742. doi: 10.1242/dev.037689

Elkouby, M. Y., Elias, S., Casey, S. E., Blythe, A. S., Tsabar, N., Klein, S. P., et al. (2010). Mesodermal Wnt signaling organizes the neural plate via Meis3. *Development* 137, 1531–1541. doi: 10.1242/dev.044750

Elkouby, Y. M., and Frank, D. (2010). "Wnt/β-catenin-signaling in vertebrate posterior neural development," in *Colloquium Series on Developmental Biology*, Vol. 4, ed. D. S. Kessler, (San Rafael, CA: Morgan & Claypool Life Sciences), 1–79. doi: 10.4199/c00015ed1v01y201007deb004

Elkouby, Y. M., Polevoy, H., Gutkovich, Y. E., Michaelov, A., and Frank, D. (2012). A hindbrain-repressive Wnt3a/Meis3/Tsh1 circuit promotes neuronal differentiation and coordinates tissue maturation. *Development* 139, 1487–1497. doi: 10.1242/dev.072934

Ermakova, G. V., Alexandrova, E. M., Kazanskaya, O. V., Vasiliev, O. L., Smith, M. W., and Zaraisky, A. G. (1999). The homeobox gene, Xanf-1, can control both neural differentiation and patterning in the presumptive anterior neurectoderm of the *Xenopus laevis* embryo. *Development* 126, 4513–4523.

Figueiredo, A. L., Maczkowiak, F., Borday, C., Pla, P., Sittewelle, M., et al. (2017). PFKFB4 control of AKT signaling is essential for premigratory and migratory neural crest formation. *Development* 144, 4183–4194. doi: 10.1242/dev.157644

Fisher, C. L., Lee, I., Bloyer, S., Bozza, S., Chevalier, J., Dahl, A., et al. (2010). Additional sex combs-like 1 belongs to the enhancer of trithorax and polycomb group and genetically interacts with Cbx2 in mice. *Dev. Biol.* 337, 9–15. doi: 10.1016/j.ydbio.2009.10.004

Fisher, C. L., Randazzo, F., Humphries, R. K., and Brock, H. W. (2006). Characterization of *Asxl1*, a murine homolog of *Additional sex combs*, and analysis of the *Asx-like* gene family. *Gene* 369, 109–118. doi: 10.1016/j.gene.2005.10.033

Fonar, Y., Gutkovich, Y. E., Root, H., Malyarova, A., Aamar, E., Golubovskaya, V. M., et al. (2011). Focal adhesion kinase protein regulates Wnt3a gene expression to control cell fate specification in the developing neural plate. *Mol. Biol. Cell* 22, 2409–2421. doi: 10.1091/mbc.e10-12-0932

Frank, D., and Sela-Donenfeld, D. (2019). Hindbrain induction during early vertebrate development. *Cell. Mol. Life Sci.* 76, 941–960. doi: 10.1007/s00018-018-2974-x

Gao, Z., Lee, P., Stafford, J. M., von Schimmelmann, M., Schaefer, A., and Reinberg, D. (2014). An AUTS2-polycomb complex activates gene expression in the CNS. *Nature* 516, 349–354. doi: 10.1038/nature13921

Gaytán de Ayala Alonso, A., Gutiérrez, L., Fritsch, C., Papp, B., Beuchle, D., and Müller, J. (2007). A genetic screen identifies novel polycomb group genes in Drosophila. *Genetics* 176, 2099–2108. doi: 10.1534/genetics.107.075739

Gelsi-Boyer, V., Brecqueville, M., Devillier, R., Murati, A., Mozziconacci, M. J., and Birnbaum, D. (2012). Mutations in *ASXL1* are associated with poor prognosis across the spectrum of malignant myeloid diseases. *J. Hematol. Oncol.* 5:12. doi: 10.1186/1756-8722

Gutkovich, Y. E., Ofir, R., Elkouby, Y. M., Dibner, C., Gefen, A., Elias, S., et al. (2010). *Xenopus* Meis3 protein lies at a nexus downstream to Zic1 and Pax3 proteins, regulating multiple cell-fates during early nervous system development. *Dev. Biol.* 338, 50–62. doi: 10.1016/j.ydbio.2009.11.024

Harland, R. M. (1991). In situ hybridization: an improved whole-mount method for *Xenopus* embryos. *Methods Cell Biol.* 36, 685–695. doi: 10.1016/s0091-679x(08)60307-6

Hori, I., Miya, F., Ohashi, K., Negishi, Y., Hattori, A., Ando, N., et al. (2016). Novel splicing mutation in the ASXL3 gene causing Bainbridge-Ropers syndrome. *Am. J. Med. Genet. A* 170, 1863–1867. doi: 10.1002/ajmg.a.37653

Janesick, A., Wu, S. C., and Blumberg, B. (2015). Retinoic acid signaling and neuronal differentiation. *Cell. Mol. Life Sci.* 72, 1559–1576. doi: 10.1007/s00018-014-1815-9

Katoh, M. (2013). Functional and cancer genomics of *ASXL* family members. *Br. J. Cancer* 109, 299–306. doi: 10.1038/bjc.2013.281

Katoh, M. (2015). Functional proteomics of the epigenetic regulators ASXL1, ASXL2 and ASXL3: a convergence of proteomics and epigenetics for translational medicine. *Expert Rev. Proteomics* 12, 317–328. doi: 10.1586/14789450.2015.1033409

Ku, C. S., Polychronakos, C., Tan, E. K., Naidoo, N., Pawitan, Y., Roukos, D. H., et al. (2013). A new paradigm emerges from the study of de novo mutations in the context of neurodevelopmental disease. *Mol. Psychiatry* 18, 141–153. doi: 10.1038/mp.2012.58

Kuechler, A., Czeschik, J. C., Graf, E., Grasshoff, U., Hüffmeier, U., Busa, T., et al. (2017). Bainbridge-Ropers syndrome caused by loss-of-function variants in ASXL3: a recognizable condition. *Eur. J. Hum. Genet.* 25, 183–191. doi: 10.1038/ejhg.2016.165

Lai, H. L., and Wang, Q. T. (2013). Additional sex combs-like 2 is required for polycomb repressive complex 2 binding at select targets. *PLoS One* 8:e73983. doi: 10.1371/journal.pone.0073983

Mariani, F. V., and Harland, R. M. (1998). XBF-2 is a transcriptional repressor that converts ectoderm into neural tissue. *Development* 125, 5019–5031.

Polevoy, H., Gutkovich, Y. E., Michaelov, A., Volovik, Y., Elkouby, Y. M., and Frank, D. (2019). New roles for Wnt and BMP signaling in neural anteroposterior patterning. *EMBO Rep.* 20:e45842. doi: 10.15252/embr.201845842

Polevoy, H., Malyarova, A., Fonar, Y., Elias, S., and Frank, D. (2017). FoxD1 protein interacts with Wnt and BMP signaling to differentially pattern mesoderm and neural tissue. *Int. J. Dev. Biol.* 61, 293–302. doi: 10.1387/ijdb.160300df

Re'em-Kalma, Y., Lamb, T., and Frank, D. (1995). Competition between noggin and bone morphogenetic protein 4 activities may regulate dorsalization during *Xenopus* development. *Proc. Natl. Acad. Sci. U.S.A.* 92, 12141–12145. doi: 10.1073/pnas.92.26.12141

Russell, B., and Graham, J. M. (2013). Expanding our knowledge of conditions associated with the *ASXL* gene family. *Genome Med.* 5:16. doi: 10.1186/gm420

Salzberg, A., Elias, S., Nachaliel, N., Bonstein, L., Henig, C., and Frank, D. (1999). A Meis family protein caudalizes neural cell fates in *Xenopus*. *Mech. Dev.* 80, 3–13. doi: 10.1016/s0925-4773(98)00187-7

Scheuermann, J. C., de Ayala Alonso, A. G., Oktaba, K., Ly-Hartig, N., McGinty, R. K., Fraterman, S., et al. (2010). Histone H2A deubiquitinase activity of the Polycomb repressive complex PR-DUB. *Nature* 465, 243–247. doi: 10.1038/nature08966

Shashi, V., Pena, L. D., Kim, K., Burton, B., Hempel, M., Schoch, K., et al. (2016). De novo truncating variants in ASXL2 are associated with a unique and recognizable clinical phenotype. *Am. J. Hum. Genet.* 99, 991–999. doi: 10.1016/j.ajhg.2016.08.017

Snir, M., Ofir, R., Elias, S., and Frank, D. (2006). *Xenopus laevis* POU91 protein, an Oct3/4 homologue, regulates competence transitions from mesoderm to neural cell-fates. *EMBO J.* 25, 3664–3674. doi: 10.1038/sj.emboj.7601238

Srivastava, A., McGrath, B., and Bielas, S. L. (2017). Histone H2A monoubiquitination in neurodevelopmental disorders. *Trends Genet.* 33, 566–578. doi: 10.1016/j.tig.2017.06.002

Srivastava, A., Ritesh, K. C., Tsan, Y. C., Liao, R., Su, F., Cao, X., et al. (2016). De novo dominant *ASXL3* mutations alter H2A deubiquitination and transcription in Bainbridge-Ropers syndrome. *Hum. Mol. Genet.* 25, 597–608. doi: 10.1093/hmg/ddv499

Veltman, J. A., and Brunner, H. G. (2012). De novo mutations in human genetic disease. *Nat. Rev. Genet.* 13, 565–575. doi: 10.1038/nrg3241

Conflict of Interest: The authors declare that the research was conducted in the absence of any commercial or financial relationships that could be construed as a potential conflict of interest.

Advantages of publishing in Frontiers

OPEN ACCESS
Articles are free to read for greatest visibility and readership

FAST PUBLICATION
Around 90 days from submission to decision

HIGH QUALITY PEER-REVIEW
Rigorous, collaborative, and constructive peer-review

TRANSPARENT PEER-REVIEW
Editors and reviewers acknowledged by name on published articles

Frontiers
Avenue du Tribunal-Fédéral 34
1005 Lausanne | Switzerland

Visit us: www.frontiersin.org
Contact us: info@frontiersin.org | +41 21 510 17 00

REPRODUCIBILITY OF RESEARCH
Support open data and methods to enhance research reproducibility

DIGITAL PUBLISHING
Articles designed for optimal readership across devices

FOLLOW US
@frontiersin

IMPACT METRICS
Advanced article metrics track visibility across digital media

EXTENSIVE PROMOTION
Marketing and promotion of impactful research

LOOP RESEARCH NETWORK
Our network increases your article's readership